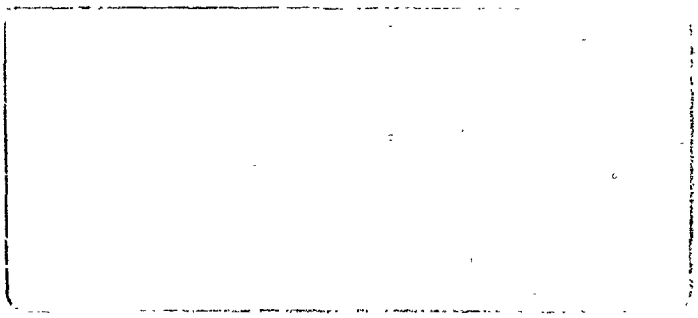
J Sherman





FACILITY FORM 602

N65-27875
(ACCESSION NUMBER) (THRU)

258 1
(PAGES) (CODE)

CR 63748 31
(NASA CR OR TMX OR AD NUMBER) (CATEGORY)

GPO PRICE $ _____

OTS PRICE(S) $ _____

Hard copy (HC) 8.58

Microfiche (MF) 2.75

LIBRARY COPY

LEWIS LIBRARY, NASA
CLEVELAND, OHIO

JET PROPULSION LABORATORY
CALIFORNIA INSTITUTE OF TECHNOLOGY
PASADENA, CALIFORNIA

ENGINEERING DOCUMENT

ENGINEERING PLANNING DOCUMENT
NO. 250

MARINER
MARS 1969 ORBITER
TECHNICAL FEASIBILITY STUDY

EPD-250

16 NOVEMBER 1964

APPROVED:

P. K. Eckman

P. K. ECKMAN
CHAIRMAN, MARS '69 ORBITER
TECHNICAL FEASIBILITY STUDY GROUP

JET PROPULSION LABORATORY
CALIFORNIA INSTITUTE OF TECHNOLOGY
PASADENA, CALIFORNIA

ACKNOWLEDGMENTS

Contributors to this document include the following:

DIVISION 16: Advanced Technical Studies Office	P. Eckman	DIVISION 34: Guidance and Control	J. Castleman*
			E. Cherniack
			R. Curry
			C. Fredrickson
			R. Ivanoff
DIVISION 24: Deep Space Network	N. Renzetti		R. Morris
			J. Nicklas
			G. Pace
			D. Rubin
DIVISION 29: Project Engineering	E. Pounder*		S. Szirmay
	M. Botta		
	P. Buwalda		
	H. Corbello	DIVISION 35: Engineering Mechanics	D. Spencer*
	E. Framan		R. Bamford
	T. Gottlieb		B. Carley
			M. Gayman
			W. Hagemeyer
DIVISION 31: Systems	C. Kohlhase*		J. Hasbrouck
	D. Grimes		J. Jodele
	J. Light		R. McCreary
	R Richard		
		DIVISION 38 Propulsion	A. Harper*
DIVISION 32: Space Sciences	C. Campen*		S. Horimoto
	G. Baker		T. Lance
	J. Haas		C. Robillard
	J. Martin		L. Sola
	J. Stallkamp		
DIVISION 33: Telecommunications	L. Nalaboff*		
	S. Aranyi		
	J. Boreham		
	R. Piereson		

*Division Representatives

CONTENTS

Section		Page
I	INTRODUCTION	1-1
II	SUMMARY	
	A. Significant Results	2-1
	B. Trajectories	2-2
	1. Type I vs Type II Trajectories	2-2
	2. Nominal Orbit	2-2
	3. Sterilization Requirements	2-2
	C. Communications Capability	2-3
	D. Weight Summary and Launching Vehicle Performance	2-3
	E. Pacing Items Requiring Early Attention	2-6
III	MISSION OBJECTIVES	3-1
IV	MISSION CONSTRAINTS AND DESIGN CRITERIA	4-1
V	ENVIRONMENTAL CONSTRAINTS	
	A. Launch Vehicle Environment	5-1
	1. Launch Vehicle System Technical Description	5-1
	2. Launch Vehicle Environment	5-10
	3. Typical Sequence of Events for Atlas/Centaur Parking Orbit Mission	5-13
	B. Solar Flare Activity	5-15
	C. Interplanetary Meteoroid Flux	5-16
	D. In-Orbit Parameters	5-17
	E. Mars High-Altitude Atmospheric Density	5-18
VI	SPACECRAFT CONSTRAINTS	
	A. Surveyor Nose Fairing	6-1
	B. Standardized Packaging	6-3
	1. Conceptual Design	6-3
	2. Structural Integration	6-3
	3. Proposed Configuration	6-3
	4. Packaging Techniques	6-5
	5. Octagon Size	6-6
	C. Temperature Limits of Subsystems	6-7

CONTENTS (cont)

Section		Page
VII	SYSTEM DESCRIPTION AND PERFORMANCE CAPABILITY	
	A. System Description	7-1
	B. System Elements	7-2
	1. Launch Vehicle	7-2
	2. Spacecraft System	7-2
	3. Operational Support Equipment	7-4
	4. Space Flight Operations System	7-4
	5. System Integration	7-5
	C. Performance Capabilities	7-7
	D. Alternate Design Approaches and Mechanization	7-7
VIII	SYSTEMS ANALYSIS	
	A. Earth-Mars Trajectories	8-1
	1. Basic Trajectory Characteristics	8-1
	2. Heliocentric Arrival Conditions	8-13
	3. Approach Aiming Diagrams	8-20
	B. Satellite Orbit Selection	8-25
	1. General Orbit Considerations	8-25
	2. Approach Geometry	8-32
	3. Orbit Lifetime Results	8-36
	4. Orbiter Payload Results	8-42
	5. General In-Orbit Motion Curves	8-50
	6. Potentially Attractive Satellite Orbits	8-50
	7. Type I vs Type II Trajectories	8-96
	8. Summarizing Remarks	8-97
	C. Orbit Determination	8-99
	1. Summary	8-99
	2. Assumptions	8-99
	3. Discussion of Results	8-100
	4. Concluding Remarks	8-106
	D. Midcourse Guidance	8-109
	1. Introduction to Guidance Policy	8-109
	2. Midcourse Velocity Allocation	8-110
	3. The First Maneuver and Its Execution Errors	8-110
	4. The Concept of Biasing	8-116
	5. Type I Trajectory Accuracies	8-118

CONTENTS (cont)

Section		Page
VIII (cont)	6. Type II Trajectory Accuracies	8-120
	7. Conclusions	8-121
	E. Orbit Insertion Guidance Analysis	8-123
	1. Introduction	8-123
	2. Guidance Law Propellant Efficiency Study	8-123
	3. Accuracy Study	8-128
IX	SPACECRAFT SYSTEM FUNCTIONAL REQUIREMENTS	
	A. Spacecraft Functional Requirements	9-1
	1. Minimum Case Functional Requirements	9-1
	2. Maximum and Nominal Cases Functional Requirements	9-4
	B. Spacecraft System Description	9-8
	1. Definition of Minimum, Nominal and Maximum Case Spacecraft	9-8
	2. Constraints Assumed for Purpose of the Study	9-8
	3. Spacecraft System Description	9-9
	C. Sequence of Events	9-15
	1. Sequence of Operations	9-15
	2. Design Constraints	9-19
	3. Detailed Sequence of Events	9-26
	D. Spacecraft Block Diagram	9-35
	E. Data Handling, Telemetry and RF Command Requirements	9-37
	1. Description	9-37
	2. RF Command Requirements	9-41
	3. Deviations from the Nominal Case	9-41
	4. Twenty-Watt Transmitter Alternate	9-48
	F. TV, Mars Scanner, Occultation-Probability of Success	9-50
	1. Introduction	9-50
	2. Restrictive Assumptions	9-53
	3. Reliability Model	9-53
	4. Conclusions	9-54
X	SPACECRAFT SYSTEM MECHANIZATION DESCRIPTION	
	A. Nominal Configurations	10-1
	1. Instruments and Subsystems	10-1
	2. Basic Configurations	10-2

CONTENTS (cont)

Section			Page
X (cont)	3.	Configuration 1 Science Instruments (Figure 10-1)	10-2
	4.	Spacecraft Bus	10-7
	5.	Configuration 2-Solid Rocket Propulsion System (Figure 10-2)	10-10
B.		Weight Summary	10-15
	1.	Spacecraft Summary	10-15
	2.	Cases	10-15
	3.	Weight Estimation	10-15
	4.	Additional Weight Entries	10-15
C.		Power Requirements	10-20
D.		Temperature Control	10-22
	1.	Spacecraft Bus Thermal Considerations	10-22
	2.	Planet Science Platform Thermal Considerations	10-24
	3.	Component Thermal Considerations	10-24
XI		SUBSYSTEM FUNCTIONAL DESCRIPTION, INTERFACE REQUIREMENTS AND POSSIBLE MECHANIZATION	
A.		Attitude Control	11-1
	1.	Cruise Attitude Control	11-1
	2.	The Midcourse Autopilot	11-8
	3.	The Retro Autopilot	11-13
	4.	Orbital Instrument Pointing	11-22
B.		Spacecraft Control	11-25
	1.	Central Computer and Sequencer (CC&S) Functional Description	11-25
	2.	Possible Mechanization	11-28
C.		Electrical Power	11-34
	1.	Study Summary	11-34
	2.	Solar Photovoltaic Power System for Mariner 1969	11-35
	3.	Sizing of Primary Power Sources	11-42
	4.	Energy Storage Source	11-55
	5.	Preliminary Design Study of Power Conversion System	11-58
	6.	Electrical Power System Problem Areas	11-93
D.		Scientific Measurements	11-95
	1.	Planetary Scan Experiments, General Characteristics and Requirements	11-95
	2.	Television Measurements	11-95

CONTENTS (cont)

Section			Page
XI (cont)		3. Infrared Interferometer Measurements	11-99
		4. Mars Scanner	11-99
		5. Ultraviolet Spectrometer	11-100
		6. Planetary Environment - Cruise Experiments	11-101
		7. Tabular Data	11-101
	E.	Spacecraft Data Handling	11-108
		1. Science System Data and Command Requirements	11-108
	F.	Propulsion Systems	11-120
		1. Introduction	11-120
		2. Mission Considerations	11-121
		3. Solid Propellant Retro Motor	11-123
		4. Midcourse Propulsion System	11-125
		5. Bipropellant Liquid System	11-130
		6. Small Correction Vernier System	11-134
		7. Nominal Case Propulsion System Conceptual Designs	11-135
		8. Summary	11-139
	G.	Structures and Dynamics	11-143
	H.	Spacecraft Mechanisms	11-144
	I.	Telecommunications	11-146
		1. Introduction	11-146
		2. Constraints, Assumptions, and Philosophy	11-148
		3. Functional Description and Mechanization	11-152
		4. Performance Capabilities	11-179
		5. Weight, Power and Volume	11-179
	J.	Environmental Control	11-188
		1. Functional Requirements for the Mars Orbiter Temperature Control System	11-188
		2. Description	11-189
		3. Temperature Limits	11-189
		4. Influence of Meteoroids on Propellant Tank Wall Thickness	11-189
	K.	Alternate Spacecraft Configurations	11-194

CONTENTS (cont)

Section		Page
	APPENDIXES	
A.	DEEP SPACE NETWORK CONFIGURATION MARS 1969 ORBITER STUDY	
	1. General DSN Configuration and Availability	A-1
	2. 85-Foot HA-Dec Antenna Network	A-1
	3. 210-Foot Az-El Antenna	A-2
	4. Tracking Capability	A-2
	5. Communications	A-4
	6. Space Flight Operations Facility	A-7
B.	ELECTRICAL POWER DATA	
	1. Preliminary System Sizing Analysis (Revised 9/17/64)	B-1
	2. Justification for Array Overcapacity	B-23

ILLUSTRATIONS

Number	Title	Page
2-1	1969 Mars Orbiter Performance	2-5
5-1	Atlas/Centaur Configuration	5-2
5-2	Centaur Stage Configuration	5-6
5-3	Ambient Pressure, Function of Flight Time, 0 to 150 Seconds	5-11
5-4	Ambient Pressure, Function of Flight Time, 150 to 250 Seconds	5-12
6-1	Clamshell Type Centaur/Surveyor Nose Fairing	6-2
6-2	Mariner 1969 Packaging and Cabling Conception	6-4
7-1	Atlas/Centaur/Mariner 1969 Configuration	7-3
8-1	Curves of Constant Orbiter Mass for Various Firing Periods (Variable Loading)	8-2
8-2	Hyperbolic Excess Velocity Relative to Mars	8-3
8-3	Basic Arrival Date vs Launch Date Trajectory Design Chart	8-4
8-4	Relationship of Mars-Earth Vector to Approach Asymptote	8-5
8-5	Relationship of Mars-Sun Vector to Approach Asymptote	8-6
8-6	Basic Arrival Date vs Launch Date Trajectory Design Chart	8-7
8-7	Limiting Launch Azimuth vs Outward Radial Declination for Cape Kennedy	8-8
8-8	Kill Probability vs Launch Azimuth for Assumed Centaur Reliability of 0 Percent	8-9
8-9	Definition of $\bar{R}$, $\bar{S}$, $\bar{T}$, Aiming Coordinates and Body Angles η and ζ	8-10
8-10	Heliocentric Arrival Geometry	8-14
8-11	Cone Angle of Earth vs Time from Injection for Transits I-A and I-C	8-15
8-12	Earth Cone Angle vs Time from Injection for Type II Trajectories II-Z and II-C	8-16
8-13	Clock Angle of the Earth vs Time from Injection for Trajectories I-A and I-C	8-17
8-14	Clock Angle of the Earth vs Time from Injection for Trajectories II-A and II-C	8-18
8-15	Earth-Mars Range, Cone and Clock of the Earth vs Calendar Date	8-20
8-16	Northward Progression of Wave of Darkening	8-21
8-17	Approach Aiming Diagram for Transit II-B	8-23
8-18	Approach Aiming Diagram for Transit I-A	8-23
8-19	Approach Aiming Diagram for Transit I-C	8-24

ILLUSTRATIONS (cont)

Number	Title	Page
8-20	Fundamental Orbit Parameters	8-26
8-21	Rotation of Possible Orbit Planes About Approach Asymptote	8-27
8-22	Approach Geometry for Trajectories I-A, I-C, II-B	8-33
8-23	Earth Occultation Aiming Regions	8-35
8-24	Log Density vs Altitude for JPL Atmosphere (Model I)	8-37
8-25	Log Density vs Altitude for NASA "Maximum" Atmosphere (Model II)	8-38
8-26	Lifetime vs Periapsis Altitude for Curves of Constant Orbit Eccentricity	8-39
8-27	Apoapsis Altitude vs Periapsis Altitude to Yield 50-Year Lifetime	8-40
8-28	Variable vs Fixed Propellant Loading	8-43
8-29	Separated Spacecraft Weight Requirements for Useful Orbiter Weight of 950 lbs (Type I and Type II Trajectories, Variable Propellant Loading)	8-45
8-30	Separated Spacecraft Weight Requirements for Useful Orbiter Weight of 800, 950, 1100 lbs (Type II Trajectories, Variable Loading)	8-46
8-31	Separated Spacecraft Weight Requirements for Useful Orbiter Weights of 800, 950, 1100 lbs (Type I Trajectories, Variable Loading)	8-47
8-32	Separated Spacecraft Weight Requirements for Useful Orbiter Weights of 600, 700, 800 lbs (Type I and Type II Trajectories, Variable Loading)	8-48
8-33	Orbiter Mass Ratio for Optimum Type II Trajectories with Variable Loading and 30-Day Launch Period	8-51
8-34	Orbiter Mass Ratio for Optimum Type II Trajectories (H_p = 1500 km, H_a = 20,000 km)	8-51
8-35	Orbiter Mass Ratio for Optimum Type II Trajectories (H_p = 1500 km, H_a = 50,000 km)	8-52
8-36	Maximum Hyperbolic Excess Velocity at Mars for Optimum Type II Trajectories with Variable Loading	8-52
8-37	Orbiter Mass Ratio for Type I Trajectories with Variable Loading and DLA ≥ -50 Degrees	8-53
8-38	Orbiter Mass Ratio for Type I Trajectories with Variable Loading (H_p = 1500 km, H_a = 20,000 km)	8-54
8-39	Maximum Hyperbolic Excess Velocity at Mars for Type I Trajectories with Variable Loading	8-54
8-40	Orbiter Altitude vs True Anomaly for H_p = 1500 km	8-55

ILLUSTRATIONS (cont)

Number	Title	Page
8-41	Time from Periapsis vs Orbiter True Anomaly for H_p = 1500 km (0 to 100 Degrees)	8-56
8-42	Time from Periapsis vs Orbiter True Anomaly for H_p = 1500 km (90 to 190 Degrees)	8-57
8-43	Horizontal Component of Orbiter Inertial Velocity vs Orbiter True Anomaly	8-58
8-44	Orbiter Altitude vs True Anomaly	8-59
8-45	Time from Periapsis vs Orbiter (0 to 100 Degrees) True Anomaly	8-59
8-46	Time from Periapsis vs Orbiter (100 to 180 Degrees) True Anomaly	8-60
8-47	Orbit Period vs Apoapsis Altitude	8-60
8-48	Nodal Regression Rate vs Orbit Inclination to Mars Equator	8-61
8-49	Apsidal Precession Rate vs Orbit Inclination to Mars Equator	8-62
8-50	Nodal Plus Apsidal Precession Rate vs Orbit Inclination to Mars Equator	8-63
8-51	Nodal Regression Rate vs Orbit Inclination to Mars Equator	8-63
8-52	Apsidal Precession Rate vs Orbit Inclination to Mars Equator	8-64
8-53	Nodal Plus Apsidal Precession Rate vs Orbit Inclination to Mars Equator	8-65
8-54	Type I Aiming Regions	8-67
8-55	Type II Aiming Regions	8-68
8-56	Type I-B Nominal 4000 by 50,000 km Orbit Profile (View Along Approach Asymptote)	8-73
8-57	Type I-B Nominal 1500 by 50,000 km Orbit Profile (General View)	8-74
8-58	Type I-B Nominal 4000 by 50,000 km Orbit Profile (View Along Sun-Mars Line)	8-75
8-59	Type I-B Nominal 4000 by 50,000 km Orbit Profile (View Along Earth-Mars Line)	8-76
8-60	Type I-B Nominal 1500 by 50,000 km Orbit Profile (View Normal to Orbit Plane)	8-77
8-61	Type I-B Nominal 4000 by 50,000 km Orbit Profile (View Normal to Orbit Plane)	8-78
8-62	Type II-B Nominal 4000 by 50,000 km Orbit Profile (View Along Approach Asymptote)	8-79
8-63	Type II-B Nominal 1500 by 50,000 km Orbit Profile (General View)	8-80

ILLUSTRATIONS (cont)

Number	Title	Page
8-64	Type II-B Nominal 4000 by 50,000 km Orbit Profile (General View)	8-81
8-65	Type II-B Nominal 4000 by 50,000 km Orbit Profile (View Along Sun-Mars Line)	8-82
8-66	Type II-B Nominal 4000 by 50,000 km Orbit Profile (View Along Earth-Mars Line)	8-83
8-67	Type II-B Nominal 1500 by 50,000 km Orbit Profile (View Normal to Orbit Plane)	8-84
8-68	Type II-B Nominal 4000 by 50,000 km Orbit Profile (View Normal to Orbit Plane)	8-85
8-69	Latitude/Lighting Coverage for Type I-B 1500 by 50,000 km Orbit Profile Inclined 45 Degrees Below Mars Equator	8-89
8-70	Latitude/Lighting Coverage for Type II-B 1500 by 50,000 km Orbit Profile Inclined 50 Degrees Below Mars Equator	8-89
8-71	Latitude/Lighting Coverage for Type II-B 1500 by 50,000 km Orbit Profile Inclined 50 Degrees Above Mars Equator	8-90
8-72	Sun-Spacecraft-Planet Near-Limb Angle vs Orbiter True Anomaly, Mars 1969 Type I-B, Nominal 4000 by 50,000 km, Inclination = -45 Degrees	8-91
8-73	Sun-Spacecraft Near-Limb Angle vs Orbiter True Anomaly, Mars 1969 Type II-B, Nominal 4000 by 50,000 km, Inclination = -50 Degrees	8-92
8-74	Earth-Spacecraft-Planet Near-Limb Angle vs Orbiter True Anomaly, Mars 1969 Type I-B, Nominal 1500 by 50,000 km, Inclination = -45 Degrees	8-93
8-75	Latitude of Spacecraft vs Orbiter True Anomaly, Mars 1969 Type II-B, Nominal 1500 by 50,000 km, Inclination = -50 Degrees	8-94
8-76	Sun-Spacecraft-Planet Angle vs Orbiter True Anomaly, Mars 1969 Type II-B, Nominal 1500 x 50,000 km, Inclination = -50 Degrees	8-95
8-77	Semi-Major Axis of Dispersion Ellipse	8-113
8-78	Basic Arrival Data vs Launch Data Trajectory Design Chart	8-114
8-79	Biasing Locus for Trajectory I-A	8-118
8-80	Biasing Locus for Trajectory I-B	8-119
8-81	Biasing Locus for Trajectory II-B	8-121
8-82	Minimum Retro-Velocity Decrement vs True Anomaly Along Ellipse for Various Thrust Programs	8-124
8-83	Periapsis Radius vs True Anomaly for Various Thrust Programs	8-125
8-84	Angle Variation with Time for Optimum Thrust Program	8-126
8-85	Conservative Velocity Losses for Various Thrust Programs vs Hyperbolic Periapsis Distance	8-127

ILLUSTRATIONS (cont)

Number	Title	Page
8-86	Orbiter Spacecraft Guidance System Functional Block Diagram	8-129
8-87	Orbiter Spacecraft Retro Maneuver Sequence Block Diagram	8-130
8-88	Apoapsis Altitude vs Orbit Insertion Errors for 1500 by 20,000 km Orbit	8-134
8-89	Periapsis Altitude Behavior with Orbit Insertion Errors for 1500 by 20,000 km Orbit	8-135
8-90	Orbit Period vs Insertion Errors for Nominal 1500 by 20,000 km Orbit	8-137
8-91	Orbit Rotation vs Orbit-Insertion Errors for 1500 by 20,000 km Orbit	8-138
8-92	Apoapsis Altitude vs Orbit-Insertion Errors for 1500 by 50,000 km Orbit	8-139
8-93	Periapsis Altitude Behavior with Orbit-Insertion Errors for 1500 by 50,000 km Orbit	8-140
8-94	Orbit Period vs Insertion Errors for 1500 by 50,000 km Orbit	8-141
8-95	Orbit Rotation vs Orbit-Insertion Errors for 1500 by 50,000 km Orbit	8-142
8-96	Apoapsis Altitude Which Results from Removing Nominal Velocity Decrement at Non-Nominal Periapsis Altitudes as a Function of Nominal	8-143
8-97	Velocity Increment at Apoapsis Required to Restore Periapsis Altitude to Nominal Value	8-143
8-98	Velocity Increment Required to Restore Periapsis and Apoapsis Altitude to Nominal Value	8-144
8-99	Maximum Apoapsis Altitude Which Can Be Nominally Selected and Still Guarantee Capture in the Presence of a Velocity Error at Periapsis Equal to k Times the Retro Velocity Increment (for Mars)	8-145
9-1	Mars 1969 Nominal Retro Maneuver	9-17
9-2	Mars 1969 (Maximum Case) Retro Maneuver	9-18
9-3	Mars 1969 Nominal Orbit Sequence	9-20
9-4	Type I-B, Inclination = 45 Degrees, Southerly Direct Aiming Point, Mars Orbit Geometry (0 Day)	9-22
9-5	Type II-B, Inclination = 50 Degrees, Southerly Direct Aiming Point, Mars Orbit Geometry (0 Day)	9-23
9-6	Mars 1969 Type I-B, Nominal 1500 by 50,000 km, Inclination = 45 Degrees, Southerly Direct; Time and Event Schedule for 6-month Orbit Mission	9-24
9-7	Mars 1969 Type II-B, Nominal 1500 by 50,000 km, Inclination = 50 Degrees, Southerly Direct; Time and Event Schedule for 6-month Orbit Mission	9-25

ILLUSTRATIONS (cont)

Number	Title	Page
9-8	Mars 1969 Spacecraft System Block Diagram (Nominal Case)	9-36
9-9	Telemetry Mode Functional Block Diagram	9-38
9-10	Telemetry Mode Sample Format	9-39
9-11	Mariner Mars 1969 Probability of One Spacecraft Operating for T Hours	9-51
10-1	Configuration 1 Using a Liquid Retro Propulsion System	10-3
10-1a	Boost Configuration	10-4
10-1b	Deployment Configuration	10-5
10-1c	Platform Actuation Axes	10-6
10-2	Configuration 2 Using a Solid Propulsion Retro System	10-11
10-2a	Boost Configuration	10-12
10-2b	Deployed Configuration	10-13
10-2c	Planet Oriented View	10-14
10-3	Power Profile Nominal Case	10-21
11-1	Basic Roll or Pitch-Yaw Attitude Control Block Diagram	11-2
11-2	Orbital Attitude Control Block Diagram	11-5
11-3	Average Torque Unbalance in Dyne-Cm	11-7
11-4	Autopilot Block Diagram	11-10
11-5	Rocket Thrust Vector in Spacecraft Coordinates	11-11
11-6	Placement of Jet Vanes on Rocket Motor	11-12
11-7	Antenna Position Control System	11-21
11-8	Timer-Oriented CC&S, Functional Block Diagram	11-29
11-9	Time-Keeping Routine	11-31
11-10	Memory-Oriented CC&S, Functional Block Diagram	11-32
11-11	Orbital Power Characteristics Using P/N Silicon Cells	11-40
11-12	Orbital Power Characteristics Using N/P Silicon Cells	11-40
11-13	Power Block Diagram with Redundant Regulator and Inverter 58 lb (Conversion Plus Case Plus Harness)	11-43
11-14	Solar Intensity as a Functional Distance from the Sun	11-44
11-15	Panel Degradation Expected from a Dose of Integrated Electron Flux	11-45
11-16	Decrease in Solar Panel Specific Energy as a Function of Sun Distance	11-47
11-17	Thermal Energy Available Per Unit of Solar Intensity	11-48
11-18	Thermal Energy Collected as a Function of Concentrator Diameter	11-49

ILLUSTRATIONS (cont)

Number	Title	Page
11-19	Thermal Energy as a Function of Generator Cavity Aperture	11-50
11-20	Solar Concentrator Weight as a Function of Diameter	11-51
11-21	Thermionic Generator Power Output as a Function of Energy Density of the Converters and the Total Emitter Area Available	11-52
11-22	Loss in Power as a Function of Angular Deviation from the True Sun Line	11-54
11-23	Functional Block Diagram for Mariner 1964 Power Subsystem	11-60
11-24	400 cps, Single Phase, Square Wave Inverter	11-66
11-25	400 cps, Three Phase, Quasi-Square Wave Inverter	11-66
11-26	2.4 kc Square Wave Inverter	11-67
11-27	4.8 kc Square Wave Inverter (400 Watt Peak)	11-68
11-28	4.8 kc Square Wave Inverter (220 Watt Peak)	11-69
11-29	2.4 kc Square Wave Inverter (Peak Power Capacity 110 Watts)	11-69
11-30	Booster Type Regulator	11-71
11-31	Booster Type Regulator (High Output Power)	11-71
11-32	Switching Type Regulator (260 Watt Unit)	11-73
11-33	Switching Type Regulator (400 Watt Unit)	11-73
11-34	Simplified Block Diagram for Mariner 1969 Electrical Conversion (for Use with Photovoltaic or RTG Power Sources)	11-83
11-35	Low Voltage Input Converter-Regulator	11-85
11-36	Simplified Block Diagram for Mariner 1969 Electrical Conversion (for Use with Thermionic Power Sources)	11-92
11-37	Scan Platform Instruments	11-96
11-38	Spacecraft Bus Instruments	11-97
11-39	Data Acquisition Requirements for Planet-Oriented Science Instruments	11-98
11-40	Data Requirements for Planet-Oriented Science Instruments	11-109
11-40a	Data Requirements for Planet-Oriented Science Instruments	11-110
11-41	Tape Storage Capabilities	11-113
11-42	Impulsive Velocity Increment for Martian Orbits	11-122
11-43	Ratio of Orbiter Mass to Injected Spacecraft Mass for Solid Propellant Retro System	11-126

ILLUSTRATIONS (cont)

Number	Title	Page
11-44	Regulated-Gas-Pressure-Fed Constant Thrust Spacecraft Propulsion System Monopropellant Hydrazine	11-127
11-45	Monopropellant Propulsion System Mass	11-129
11-46	State-of-the-Art Bipropellant System Schematic Cold Gas Pressurization System	11-131
11-47	Mass of State-of-the-Art Ablative Thrust Chamber Assemblies	11-132
11-48	Ratio of Orbiter Mass to Injected Spacecraft Mass for Liquid Bipropellant Retro System	11-133
11-49	Small Correction Propulsion System Mass	11-135
11-50	Typical Configuration for Solid Propellant Retro Motor	11-140
11-51	Bipropellant Liquid Stage Layout In-Line Tankage	11-141
11-52	Bipropellant Liquid Stage Layout Side-by-Side Tankage	11-142
11-53	Standard Deep Space Station for Mariner 1969 Support	11-149
11-54	Low Noise Listening Station Configuration	11-149
11-55	1969 Orbiter Telecommunications (Minimum Case) Block Diagram	11-153
11-56	1969 Orbiter Telecommunications (Nominal & Maximum) Block Diagram	11-154
11-57	Type I Trajectory Low-Gain Antenna Coverage vs. Cone Angle with Mariner Mars 1964 Low-Gain Antenna	11-156
11-58	Performance Margin vs Days After Launch (Mariner Mars 1964 Low-Gain Antenna, 10 w Spacecraft Transmitter, 85-Foot Diameter Ground Antenna, Communication Rate 8 1/3 bps, Launch 3-7-69)	11-158
11-59	Performance Margin vs Days After Launch (Mariner Mars 1964 Low-Gain Antenna, 10 w Spacecraft Transmitter, 85-Foot Diameter Ground Antenna, Communication Rate 8 1/3 bps, Launch 3-20-69)	11-158
11-60	Performance Margin vs Days After Launch (Mariner Mars 1964 Low-Gain Antenna, 10 w Spacecraft Transmitter, 85-Foot Diameter Ground Antenna, Communication Rate 8 1/3 bps, Launch 4-4-69)	11-159
11-61	Type II Trajectory Low-Gain Antenna vs Cone Angle with Mariner Mars 1964 Low-Gain Antenna	11-160
11-62	Performance Margin vs Days After Launch (Mariner Mars 1964 Low-Gain Antenna, 10 w Spacecraft Transmitter, 85-Foot Diameter Ground Antenna, Communication Rate 8 1/3 bps, Launch 1-9-69)	11-161
11-63	Performance Margin vs Days After Launch (Mariner Mars 1964 Low-Gain Antenna, 10 w Spacecraft Transmitter, 85-Foot Diameter Ground Antenna, Communication Rate 8 1/3 bps, Launch 1-24-69	11-161

ILLUSTRATIONS (cont)

Number	Title	Page
11-64	Performance Margin vs Days After Launch (Mariner Mars 1964 Low-Gain Antenna, 10 w Spacecraft Transmitter, 85-Foot Diameter Ground Antenna, Communication Rate 8 1/3 bps, Launch 2-7-69)	11-162
11-65	Type II Trajectory Low-Gain Antenna Coverage vs Cone Angle with Forward and Rear Looking Low-Gain Antennas	11-163
11-66	Type II Trajectory Low-Gain Antenna Coverage vs Cone Angle with Forward and Side Looking Low-Gain Antennas	11-164
11-67	Single Axis of Freedom High-Gain Antenna Spacecraft Orientation	11-167
11-68a	Earth Look Angles Relative to Spacecraft Coordinates for Early Type I Trajectory	11-168
11-68b	Earth Look Angles Relative to Spacecraft Coordinates for Late Type I Trajectory	11-169
11-68c	Earth Look Angles Relative to Spacecraft Coordinates for Early Type II Trajectory	11-170
11-68d	Earth Look Angles Relative to Spacecraft Coordinates for Late Type II Trajectory	11-171
11-69	Orbiter S-Band Transmitters	11-172
11-70	Radio and Antenna System Switching Arrangement	11-174
11-71	Command Performance Margin vs Range (Transmitter Power 100 kw, Transmitting Antenna 85-Foot Diameter)	11-182
11-72	Information Rate vs Range (85-Foot Diameter Ground Antenna, 36-Inch Diameter Spacecraft Single Degree of Freedom High-Gain Antenna)	11-182
11-73	Information Rate vs Range (210-Foot Diameter Ground Antenna, 36-Inch Diameter Spacecraft Single Degree of Freedom High-Gain Antenna)	11-183
11-74	Information Rate vs Range (210-Foot Diameter Ground Antenna, 48-Inch Diameter Spacecraft Two Degree of Freedom High-Gain Antenna)	11-183
11-75	Maneuver Telemetry Performance Margin vs Range (10-w Spacecraft Transmitter, 85-Foot Diameter Ground Antenna, 8-1/3 bps Information Rate)	11-184
11-76	Maneuver Telemetry Performance Margin vs Range (10-w Spacecraft Transmitter, 210-Foot Diameter Ground Antenna, 8-1/3 bps Information Rate)	11-184
11-77	Spacecraft Mars Orbiter, JPL Drawing 4300619, Sheet 17	11-195
11-78	Spacecraft Mars Orbiter, JPL Drawing 4300619, Sheet 13	11-196
11-79	Spacecraft Mars Orbiter, JPL Drawing 4300619, Sheet 19	11-197
11-80	Spacecraft Mars Orbiter, JPL Drawing 4300619, Sheet 18	11-198

ILLUSTRATIONS (cont)

Number	Title	Page
B-1	Boost Regulator Block Diagram	B-4
B-2	Series Regulator Block Diagram	B-5
B-3	Partial-Shunt Regulator Block Diagram	B-6
B-4	Typical Orbital Power Profile and List of Symbols	B-8
B-5	Array Overcapacity for Cases I and II	B-9
B-6	Battery Specific Weight (10 Hour Orbit)	B-12
B-7	Battery Cell Efficiency	B-14
B-8	System Specific Weight	B-16
B-9	Plot of Eclipse Function (Condition of Equal Weights)	B-18
B-10	Plot of Eclipse Functions (Normalized Versions)	B-19
B-11	General Power Profile	B-20
B-12	Array Overcapacity for 14-Hour (a= 0.07) and 50-Hour (a = 0.02) Orbits as a Function of Peak Load Duration	B-24
B-13	Array Overcapacity as in Figure B-12, Except Science (Peak) Loads are Turned Off For Every Other Orbit	B-24
B-14	Effect of Duty-Cycling By Orbit for a System Using Ag Cd Batteries	B-25
B-15	Normalized Voltage X Maximum Theoretical Array Requirement	B-25
B-16	Solution to Transcendental Equation (14)	B-26
B-17	Current Capacity Increase Due to Peak-Point Voltage Variation	B-26
B-18	Array Overcapacity Caused By Variation in the Regulation Start Voltage	B-27
B-19a	Increase in Operating Voltage Caused By Variation of the Regulation-Start Voltage	B-27
B-19b	Intersection of F (x) with 1/x for Various ε_v	B-28
B-20	Array and Load Characteristics in Relation to Battery Discharge	B-28
B-21	Discharge Circuit (Undervoltage) Implementation	B-35
B-22	SCR Turn-On Circuit	B-38
B-23	Undervoltage Trigger Circuit	B-39
B-24	Array Overcapacity Required as a Result of Battery Discharge Voltage Range or Undervoltage Trigger Level Range	B-40

TABLES

Number	Title	Page
1-1	"Maximum" Case Science	1-2
1-2	"Nominal" Case Science	1-2
2-1	Data Rates Resulting from 10 and 20 w Parameters	2-3
2-2	1969 Mars Orbiter Summary (Bipropellant System with Variable Loading	2-4
5-1	Atlas/Centaur Estimated Characteristics	5-1
5-2	Selected Ground Rules for Atlas/Centaur Performance	5-3
5-3	Atlas/Centaur Typical Event Times (Parking Orbit)	5-14
6-1	Temperature Limits of Mariner 1969	6-8
7-1	Major Technical Alternates	7-8
7-2	Implications of Technical Alternates	7-9
8-1	Trajectory Characteristics	8-12
8-2	Permissible Aiming Regions For Pointing High-Gain Antennas Towards Earth	8-34
8-3	Atmospheric Lifetime Results (Required Orbit Altitudes)	8-38
8-4	Launch Period Capability Matrix (1000-lb Orbiter)	8-49
8-5	Type I-A Orbits (1500 by 20,000 km; Period = 850 min)	8-70
8-6	Type I-C Orbits (1500 by 20,000 km; Period = 850 min)	8-71
8-7	Type II-B Orbits (1500 by 20,000 km; Period = 850 min)	8-72
8-8	Effect of Orbit Dispersions upon Occultation Times (Orbits I-B and II-B, 1500 by 50,000 km)	8-87
8-9	Orbit Orientation Angles to Ecliptic	8-88
8-10	Semi-Major Axis of Dispersion Ellipse (Kilometers)	8-101
8-11	Semi-Minor Axis (Kilometers)	8-102
8-12	Orientation Angle (Degrees) (Measured Clockwise from $\overline{T}$ to Major Axis	8-103
8-13	Flight Time Uncertainty (Seconds)	8-104
8-14	Trajectory II-B	8-106
8-15	Semi-Major Axis of Dispersion Ellipse (Kilometers)	8-107
8-16	Semi-Minor Axis (Kilometers)	8-107
8-17	Flight Time Uncertainty (Seconds)	8-107
8-18	Typical Dispersion Ellipses Due to First Maneuver Execution Errors of 0.1 meters/sec per Axis	8-112
8-19	Error Ellipses Resulting From Spherical Velocity Errors of 0.39 m/sec	8-116
8-20	Finite Burning Time and Guidance - Law Losses	8-125
8-21	Hyperbolic Energy and Elliptical Orbit Numbers	8-127
8-22	Worst-Case Conditions	8-136

TABLES (cont)

Number	Title	Page
9-1	Typical Flight Sequence--Mars 1969 Orbiter (Nominal Case)	9-27
9-2	Nominal Case Commutation Allocations	9-40
9-3	Mariner 1969 Orbiter Command List (Discrete Commands)	9-42
9-4	Mariner 1969 Orbiter Command List (Quantitative Commands)	9-46
9-5	Maximum Case Commutation Allocations	9-47
9-6	Additional Maximum Case Commands	9-47
9-7	Minimum Case Commutation Allocations	9-48
9-8	Probability of Obtaining TV/MS Data (Mars 1969 Spacecraft)	9-52
9-9	Mars 1969 Spacecraft Probability of Success for TV, MS Occultation Experiments	9-54
10-1	Mariner Mars 1969 Orbiter Weight in Pounds	10-16
10-2	Weight Breakdown of Nominal Case Using Dipropellant Liquid Propulsion System for Mariner 1969 Mars Orbiter	10-18
10-3	Weight Breakdown of Nominal Case Using A Solid Propellant Retro Propulsion System for Mariner 1969 Mars Orbiter	10-19
10-4	Temperature Control Subsystem Weight Breakdown and Power Requirements	10-23
11-1	Breakdown of Weight Total	11-6
11-2	Spacecraft Moments of Inertia Calculations	11-6
11-3	Power and Weight Estimates (Nominal Case)	11-9
11-4	Summary Retro Autopilot Characteristics	11-20
11-5	Comparison of Weight, Power and Volume	11-33
11-6	Spacecraft Electrical Power Constraints	11-35
11-7	User Power Requirements (Watts)	11-37
11-8	Solar Panel Sizing and Power Requirements	11-38
11-9	Optional Modes of Operation	11-39
11-10	Solar Panel Battery Subsystem Major Parameters	11-42
11-11	Contingency Factors in Panel Design	11-46
11-12	Summary List of Parameters	11-53
11-13	Characteristics of 400-Watt System	11-55
11-14	Battery Requirements and Comparisons	11-59
11-15	Weight Efficiency and Capability	11-59
11-16	Capabilities of Power Converter Modules	11-64

TABLES (cont)

Number	Title	Page
11-17	Raw Power Requirement, Photovoltaic or RTG Source Booster Regulator System	11-75
11-18	Weight Calculation, Photovoltaic or RTG Source Booster Regulator System	11-76
11-19	Regulated Power Requirements	11-77
11-20	Square Wave 2.4 kc, 4.8 kc Regulated Power Requirement	11-78
11-21	Raw Power Requirement, Photovoltaic or RTG Source Switching Regulator System	11-79
11-22	Weight Calculations, Photovoltaic or RTG Source Switching Regulator System	11-80
11-23	Regulator Power Requirement, Switching Regulator System	11-81
11-24	Raw Power Requirement, Photovoltaic or RTG Source, Switching Regulator System	11-82
11-25	Raw Power Requirements, Thermionic Battery Source Low Voltage Converter Regulator System	11-86
11-26	Raw Power Requirements, Thermionic Battery Source Booster Regulator System	11-87
11-27	Weight Calculations, Solar Thermionic Source Low Voltage Converter Booster Regulator	11-88
11-28	Regulated Power Requirement, Low Voltage Converter Regulator or Booster Regulator System, 260 Watt Peak Power	11-89
11-29	2.4 kc Regulator Power Requirements	11-90
11-30	Power Conversion System Weight Efficiency	11-91
11-31	Weight/Power/Volume Summary	11-102
11-32	Temperature Control Requirements	11-103
11-33	Science System Command Requirements	11-103
11-34	Science System Functional Design Parameters, Case A	11-104
11-35	Science System Functional Design Parameters, Case B	11-105
11-36	Power Profile Science Instruments (Case A)	11-106
11-37	Power Profile Science Instruments (Case B)	11-107
11-38	Science System Command Requirements (Mariner 1969)	11-115
11-39	Solid Propellant Retro Motor Characteristics for a Mariner 1969 Mars Orbiter Mission	11-118
11-40	Monopropellant Midcourse Propulsion System Characteristics For Mariner 1969 Mars Orbiter Mission	11-128
11-41	Summary of Parameters for Selected Trajectories and Orbits	11-136

TABLES (cont)

Number	Title	Page
11-42	Mass Breakdown of Solid Propellant Retro Propulsion Systems for Mariner 1969 Mars Orbiter	11-137
11-43	Mass Breakdown of Bipropellant Liquid Propulsion Systems for Mariner 1969 Mars Orbiter	11-138
11-44	Summary Comparison of Candidate Systems	11-142
11-45	Standard Deep Space Station Parameters	11-151
11-46	Low Noise Listen Station Parameters	11-151
11-47	DSIF Transmitting Parameters	11-180
11-48	Orbit Parameters, Earth to Orbiter Link	11-180
11-49	Orbiter Communication Parameters, High-Gain Antennas	11-181
11-50	Orbiter Communications Parameters, Low-Gain Antennas	11-181
11-51	Spacecraft Telecommunication Weight and Volume Estimates	11-185
11-52	Spacecraft Telecommunications Power Estimates	11-186
11-53	Aluminum Target Comparisons	11-190
11-54	Mission Probabilities of No Punctures	11-192
B-1	Mariner Block IV Power Profile (10 Watt RF System)	B-2
B-2	Mariner Block IV Power Profile (20 Watt RF System)	B-3
B-3	Battery Parameters	B-13
B-4	Margin Calculation Requirements Summary	B-41

SECTION I

INTRODUCTION

On 9 July 1964, the NASA Office of Space Science and Applications (OSSA) directed the office of Advanced Technical Studies at the Jet Propulsion Laboratory to assess the feasibility of performing a 1969 Mars Orbiter mission using the Atlas/Centaur launching vehicle. This Engineering Planning Document reports the results of this study.

The purpose of the study was to determine:

1) The gross capabilities and limitations of a 1969 Mars Orbiter launched by a floxed Atlas/Centaur vehicle.
2) The risks associated with such a system in this time-scale.
3) The pacing state-of-the-art and advanced development areas requiring immediate additional attention and support.

During the course of the study three spacecraft, with discrete levels of performance capability, complexity, and lifetime, were considered. These are referred to as Maximum, Nominal, and Minimum Cases and will be described in detail in Sections VII and IX.

Briefly, the Maximum Case was conceived to carry an extensive number of experiments (listed in Table 1-1) for an orbiting lifetime about Mars of 180 days. The capabilities of this spacecraft are not significantly less than those of the Voyager-type orbiter considered by the APSSC (Advanced Planetary Spacecraft Study Committee) in 1963; e.g., see EPD-139, Volumes II and III.

The Nominal Case considered carries a somewhat reduced number of experiments (listed in Table 1-2) for an orbiting lifetime of 90 days. This spacecraft, however, still represents an ambitious and significant Mars orbiting program, especially for a first attempt.

The Minimum Case considered is almost a trivial one; it represents a spacecraft making maximum use of Mariner 1964 subsystems which performs as an attitude-stabilized spacecraft in Mars orbit for 30 days, but carries no scientific instruments or science-related equipment. This concept does serve a useful purpose, however, because it does establish a minimum system upon which one must build and improve.

Table 1-1. "Maximum" Case Science

Item	Experiments (180-Day Orbit)	Weight (lb)
1	Magnetometer	4.5
2	Magnetometer Boom	10
3	Plasma Probe	10
4	Energetic Particles	2.5
5	Micrometeorite Detector	5
6	RF Occultation Receiver	5.5
7	RF Noise Detector	4.5
8	RF Noise Detector Antenna	2.5
9	IR Interferometer*	26
10	UV Spectrometer	24
11	TV*	23
12	Mars Scanner*	13
13	DAS	37
14	Scan Platform	41.5
15	Case Harness	8
16	Case	5
	Total Science Payload	221.5 lb

Table 1-2. "Nominal" Case Science

Item	Experiments (90-Day Orbit)	Weight (lb)
1	Magnetometer	4.5
2	Magnetometer Boom	10
3	Plasma Probe	10
4	Energetic Particles	2.5
5	Micrometeorite Detector	5
6	RF Occultation Receiver	5.5
7	RF Noise Detector	4.5
8	RF Noise Detector Antenna	2
9	TV*	23
10	Mars Scanner*	13
11	DAS	28
12	Scan Platform	23.5
13	Case Harness	6
14	Case	5.5
	Total Science Payload	143.2 lb

*Located on Scan Platform

SECTION II

SUMMARY

A SIGNIFICANT RESULTS

On the basis of this study, several important conclusions can be stated.

1) The Nominal mission (as defined in Section I) is feasible in 1969 if the revised 30% floxed Atlas/Centaur performance estimates (see Figure II-1) provided by Lewis Research Center can be demonstrated.
2) The Nominal mission is not feasible with the "original" 30% floxed Atlas/Centaur performance estimates, however it should be noted that even the Nominal payload is a rather ambitious one. It appears that some mission between the Minimum and Nominal Case is feasible with the original 30% floxed performance estimates.
3) No attractive fully-stabilized orbiter mission appears feasible without floxing of the Atlas/Centaur.
4) The in-orbit control and operation of the spacecraft appear to be the major technological developments required to accomplish this mission. Ground-based command capability of the orbiting part of the mission will be required, probably on an "around-the-clock basis" for the duration of the orbiter lifetime.
5) The ability to observe the same small area of Mars at high resolution over many months is doubtful for any mission considered.
6) Northeast launches (required for Type I trajectories) offer significant advantages in terms of short flight times, low communication distances, and in-orbit geometry. Northeast launches require special range-safety waivers; however, at this time, the potential advantages appear great enough that such launches should be considered.
7) Sterilization constraints require early selection of a Mars high-altitude atmospheric model. With the present uncertainties associated with such a model, the periapsis altitude of Mars orbiters must be kept large (on the order of 4000 km) with a resulting loss of approximately 125 pounds of active payload in orbit compared to that possible with lower periapsis altitude (1500 km).
8) A cylindrical extension of the Surveyor nose fairing should be seriously considered. The present nose fairing imposes major packaging problems such as requiring double-folding of the solar panels and limiting the spacecrafts high-gain antenna diameter to 4-feet.
9) The program to uprate the Centaur performance should be continued if the Atlas/Centaur is to be considered for Mars orbiting missions.

B. TRAJECTORIES

1. Type I vs Type II Trajectories

Type I transit trajectories appear particularly attractive. The trip times are from 80 to 100 days shorter than those for Type II trajectories, and the distance from Earth at encounter is about 70% of that for Type II trajectories. In addition, Type I trajectories provide several attractive geometric advantages over the Type II's; the Type I trajectories do not pass inside the Earth's orbit early in transit, and hence, reduce the associated communications gray-out. Orbit determination uncertainties and sensitivity to midcourse execution errors are significantly lower during the first several weeks of transit. Finally, Type I trajectories offer certain in-orbit mission advantages.

2. Nominal Orbit

A Nominal orbit with a periapsis altitude of 1500 km, an apoapsis altitude of 50,000 km and an orbital period of 42 hours has been examined in considerable detail. This Nominal orbit yields maximum in-orbit payload, consistent with the guidance capability provided by DSIF tracking and the spacecraft propulsion and control subsystems. With the proper choice of inclination, such an orbit minimizes Sun and Canopus occultation problems. The long orbital period appears to be advantageous because with periapsis passage occurring only once every 42 hr, there is "time to think" back at Earth where command and control decisions must be made. Sufficient data can be collected at each periapsis to fully utilize the entire orbital period for data transmission.

3. Sterilization Requirements

Present sterilization requirements will force the choice of a higher periapsis altitude so that an orbit of 4000 km by 50,000 km may be more realistic. If such is the case, approximately 1000 ft/sec additional velocity increment is required to establish this orbit, and therefore, an additional 300 pounds of vehicle performance is required at Earth injection to place the same payload in-orbit as was done for the Nominal 1500 by 50,000-km orbit.

C. COMMUNICATIONS CAPABILITIES

For the nominal case, with a 90-day in-orbit lifetime, a single degree-of-freedom, 36-inch diameter antenna is employed. Two RF power levels can be considered, 10 and 20 watts. Data rates resulting from these parameters are shown in Table 2-1.

Table 2-1. Data Rates Resulting from 10 and 20-w Parameters

Power Output	10 Watt	20 Watt
Cruise Data Rate	8 1/3 bit/sec	16 2/3 bit/sec
Orbit Data Rate		
Until 12/2/69	133 1/3 bit/sec	266 2/3 bit/sec
Until 2/1/70	66 2/3 bit/sec	133 1/3 bit sec
Note: Last day of arrival for Type I Trajectories		3 October 1969
Last day of arrival for Type II Trajectories		2 November 1969

D. WEIGHT SUMMARY AND LAUNCHING VEHICLE PERFORMANCE

Table 2-1 shows the propulsion requirements and separated spacecraft weights for both the 1500-km by 50,000-km and for 4000-km by 50,000-km orbits. The table also presents a brief weight statement for the Minimum, Nominal, and Maximum cases, in addition, where applicable, the weights for Mariner 1964 subsystems are also tabulated.

Figure 2-1 shows the performance capabilities required to inject the Nominal case payload into either of these two orbits.

It will readily be seen that the original 30-percent floxed vehicle cannot inject the Nominal payload into either orbit. The revised 30-percent floxed estimates will provide a 30-day launch window for the 4000-km by 50,000-km orbit and a much longer launch window (in excess of 60 days) for the 1500-km by 50,000-km orbit.

Table 2-2. 1969 Mars Orbiter Summary
(Bipropellant System with Variable Loading)

	Minimum (30 Day)	Nominal (90 Day)	Maximum (180 Day)	MA-1964
Science	0	143	221	71.1
Structure	65	88	100	73.0
Thermal Control	20	35	35	13.1
Communications	101	165	210	100.5
Power	179	294	384	157.2
Guidance and Control	78	104	133	71.2
Pyrotechnics	13	16	17	13.0
Cabling	10	20	26	19.8
	466	865	1126	518.9
Design Margin (15%)	70	130	169	10
Active Orbit Weight	536	995	1295	528.9
Orbit:	1500 by 50,000 km	4000 by 50,000 km		
ΔV Capability: (Including 330 ft/sec Midcourse and gt Loss)	6600 ft/sec	7570 ft/sec		
Dry Propulsion System	177	210		51.3
Design Margin (15%)	26	31		
Propellant	1085	1380		
Separated S/C Weight	2283	2616		579.3
Adapter	100	100		56
Gross System Weight	2383	2716		635

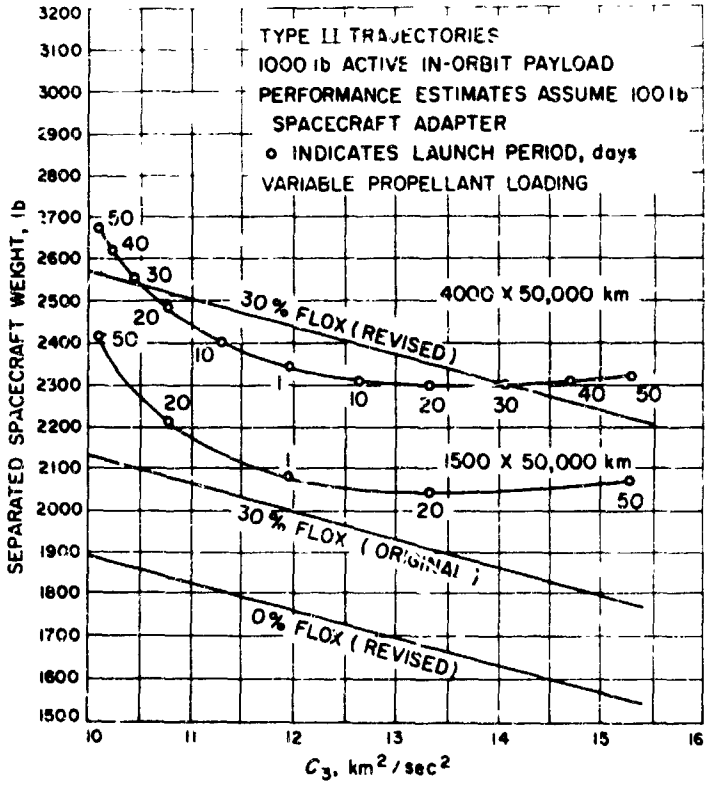


Figure 2-1. 1969 Mars Orbiter Performance

E. PACING ITEMS REQUIRING EARLY ATTENTION

On the basis of this study, several pacing state-of-the-art advanced development items appear to require early attention:

1) It is imperative that mission objectives and experiments be selected and agreed upon early in the preliminary design. This is particularly the case for an orbiting mission, because the in-orbit lighting, control, sequencing, etc., are affected so strongly by the requirements of the experiments themselves.
2) The propulsion system selected, while not a critical design problem, is a long lead-time development and requires intitiation at an early date
3) The in-orbit control and operation of the spacecraft and its planet-oriented experiments is the major new technological development required for this mission. The flexibility required for the experiments in the Nominal case requires versatility and sophistication in the command system to a degree that should be viewed with skepticism so far as early orbiter missions are concerned.
4) The CC&S requirements for an orbiter mission are such that it is desirable to utilize a memory-oriented sequencer (i.e. a digital computer) to provide in-orbit control, switching and sequencing.
5) The Date Automation System (DAS) elements to be employed for an orbiting mission will require considerable improvement over those used for Mariner-1964.
6) Storage devices with a capacity of at least 15 by 10^6 bits are required, and their development requires early initiation.
7) The missions considered in this study vary in lifetime from 220 days (Type I trajectories, 30 days in-orbit) to 460 days (Type II trajectories, 180 days in-orbit). It is readily apparent that a whole new technology of long-life performance of components and subsystems must be developed to accomplish such missions. Life tests, comparable to the mission duration, can probably never be performed on which to base confidence of demonstrated reliability. Hence, other techniques must be developed to provide statistical confidence and assurance that mission performance will be met.
8) Range safety discussions should begin at once to explore the possibility of utilizing Northeast launchings, down to an azimuth as low as 35 deg East of North.
9) Serious consideration should be given to a cylindrical extension of the Centaur nose fairing. An Extension on the order of 4 ft appears to be desirable.
10) The selection of a high-altitude Mars atmosphere model and the resolution of the associated sterilization policy should be done prior to the initiation of competitive Phase I design studies by industrial contractors.

SECTION III

MISSION OBJECTIVES

The objectives for the 1969 Mars orbit mission as defined at the beginning of the study are as follows:

1) Perform an orbiting mission about Mars in the 1969 opportunity.
2) Provide the capability for planet-oriented science; i.e., the capability of pointing scientific instruments toward the planet.
3) Ability to carry non-planet-oriented science in the vicinity of Mars; i.e., to carry certain body-fixed instruments.
4) A lifetime in orbit about the planet of at least 90 days, and if possible, a lifetime of 180 days.
5) Carry interplanetary scientific instruments which would function during the transit from Earth to Mars.
6) Provide an opportunity for technological development which would be compatible with an evolving planetary exploration program.
7) Be flexible enough to allow a repeat of the mission during the 1971 opportunity.

SECTION IV

MISSION CONSTRAINTS AND DESIGN CRITERIA

At the outset of this mission study, certain constraints and design criteria were assumed.

1) The use of a floxed Atlas-Centaur launching vehicle. The performance capability assumed was identical to that provided to Lockheed and to Avco earlier this year for their JPL-contracted studies of a 1969 Mars orbiter and a 1969 Fly-by Lander, respectively. Subsequently, the Lewis Research Center has provided JPL with new estimates of the floxed Atlas-Centaur performance. These performance estimates are shown in Figure 2-1. During the course of the study both performance estimates have been considered.
2) The use of the Centaur/Surveyor nose fairing, as shown in Figure 5-2.
3) The availability of two launching pads for the Atlas-Centaur so that simultaneous checkout and countdown can be performed.
4) A total of two spacecraft launching attempts for the 1969 opportunity.
5) A nominal 30-day launching period to assure a high probability of achieving two launchings.
6) Sterilization constraints such that there must be less than one chance in 10^4 that a single viable organism will enter the Mars atmosphere.
7) Consideration of both Type I and Type II transit trajectories. Type I trajectories would require Northeast launches from the Eastern Test Range.
8) Deep Space Network (DSN) capability which includes the availability of three 210-ft receiving antennas and command capability of 100 kilowatts over 85-ft antennas during the entire orbit phase of the mission. A discussion of these capabilities is presented in Appendix A.
9) No test launchings to be performed prior to the 1969 opportunity.
10) Hardware consistent with the state-of-the-art at the beginning of preliminary design on March 1, 1965.
11) Sufficient hardware and operational redundancy to handle most of the foreseeable nonstandard mission situations which might occur due to malfunctions of the launching vehicle, the spacecraft during transit, and the spacecraft during its orbit lifetime.
12) A typical instrumentation payload provided by NASA headquarters which consists of instruments which are planet-oriented and body-fixed:
    a) Scan Platform
        1) Infrared Spectrometer or Interferometer.
        2) Ultraviolet Spectrometer.

3) TV
4) Mars Scanner (visual, thermal, and water vapor).

b) Spacecraft Body

1) Magnetometer.
2) Plasma Probe.
3) Energetic Particle Detector.
4) Micrometeorite Detector.
5) Two-frequency Occultation Beacon.
6) Mars Radio-Noise Detector.

This preliminary list of instruments was provided by R. F. Fellows of NASA headquarters. (See Reference 1.)

Reference 1: NASA Memorandum, R. F. Fellows, 11 August 1964

To : SL/Project Manager, Mariner Mars '69 Mission
From : SL/Mariner Mars '69 Program Scientist
Subject: Preliminary payload to be used for feasibility and design studies for the Mariner Mars 1969 and 1971 orbital missions

The following payload is suggested as the preliminary one to be used for feasibility and design studies for the Mariner Mars 1969 and 1971 orbital missions.

1. Scan Platform
   A. Infrared Spectroscopy (Interferometer or Spectrometer)
   B. Ultraviolet Spectroscopy
   C. TV Pictures
   D. Mars Scanner - visual, thermal, and water vapor
2. Spacecraft Body
   A. Magnetometer
   B. Plasma Probe
   C. Energetic Particles
   D. Micrometeorite Detector
   E. Two-frequency Occultation Beacon
   F. Mars Radio-Frequency-Noise Detector

It is realized that this represents a more ambitious payload than has been possible to date. However, the basic reason for undertaking the mission is to accomplish a scientific exploration of the planet and its atmosphere. Therefore, it is felt that the initial payload considered for design studies should be one capable of performing a reasonable scientific survey. It may be necessary to decrease the size of this payload as a result of feasibility studies, but the studies should demonstrate the necessity for this, rather than starting with the premise that a smaller payload should be considered.

The importance of a scan platform capable of accommodating four major experiments cannot be overstressed. The most important information to be obtained concerns the nature of the changes occurring on the planetary surface and the composition and characteristics of the atmosphere. The four types of instruments recommended here hold great promise in obtaining this information. The visible, thermal and water vapor scanner is a very desirable addition to the other three scan experiments in that it

serves as an independent backup to some of their functions using a different type of instrument. In addition, it is an experiment with specific objectives aimed at answering some of the important unknowns concerning the atmosphere and surface.

Representative weights, power and telemetry requirements, and size are not included because it is believed that this information is available to JPL as a result of the Mars 66 deliberations earlier this year, and from experiments being carried on the Mars 64 mission and other space-probe missions. The occultation beacon and the radio-frequency-noise experiment are relative newcomers and I hope to furnish specific information on these in about two weeks. In any event, they will require specialized artennas, one pointing to the Earth and one surveying the planet.

Lifetime is an important consideration for this mission and it is realized that many compromises are involved. In the absence of specific information, it is hoped that communication with the spacecraft would be possible for at least three months and preferably six months.

SECTION V

ENVIRONMENTAL CONSTRAINTS

A. LAUNCH VEHICLE ENVIRONMENT

1. Launch Vehicle System Technical Description

The Atlas/Centaur launch vehicle consists of two stages: The first is a modified Atlas D, and the second (Centaur) is a liquid hydrogen/liquid oxygen, high-specific impulse stage. The principal features of the operational vehicle are listed in Table 5-1, and the configuration is illustrated in Figure 5-1.

The Atlas/Centaur is now in its flight-test phase; therefore, it is not possible at this time to precisely define the configuration and performance expected to be available for Mariner Mars 1969. However, selected ground rules for Atlas/Centaur performance are noted in Table 5-2.

Table 5-1. Atlas/Centaur Estimated Characteristics

Item	Stage 1	Stage 2
Vehicle	Atlas (Modified) - Stub D	Centaur
Engines	Rocketdyne Atlas Complex (2 boost, 1 sustainer, 2 vernier)	2 Pratt and Whitney, RL10-A-3
Nominal Thrust, lb	165,000 (per boost engine) 57,000 (sustainer) 1,000 (per vernier engine) 389,000 (total)	15,000 (per engine)
Fuel	RP-1	Liquid hydrogen
Oxidizer	Liquid oxygen	
Guidance	Minneapolis-Honeywell all-inertial	
Launch Gross Weight	299,729 lb	
Overall Dimensions	110 ft long x 10 ft diameter	

a. First Stage

(1) Vehicle Modifications. The first-stage vehicle is a modified version of the Atlas ICBM (SM-65) Series D missile. The principal modifications to the Atlas D missile are:

1) The forward conical section of the LOX tank has been enlarged to a 10 ft diameter cylindrical section.

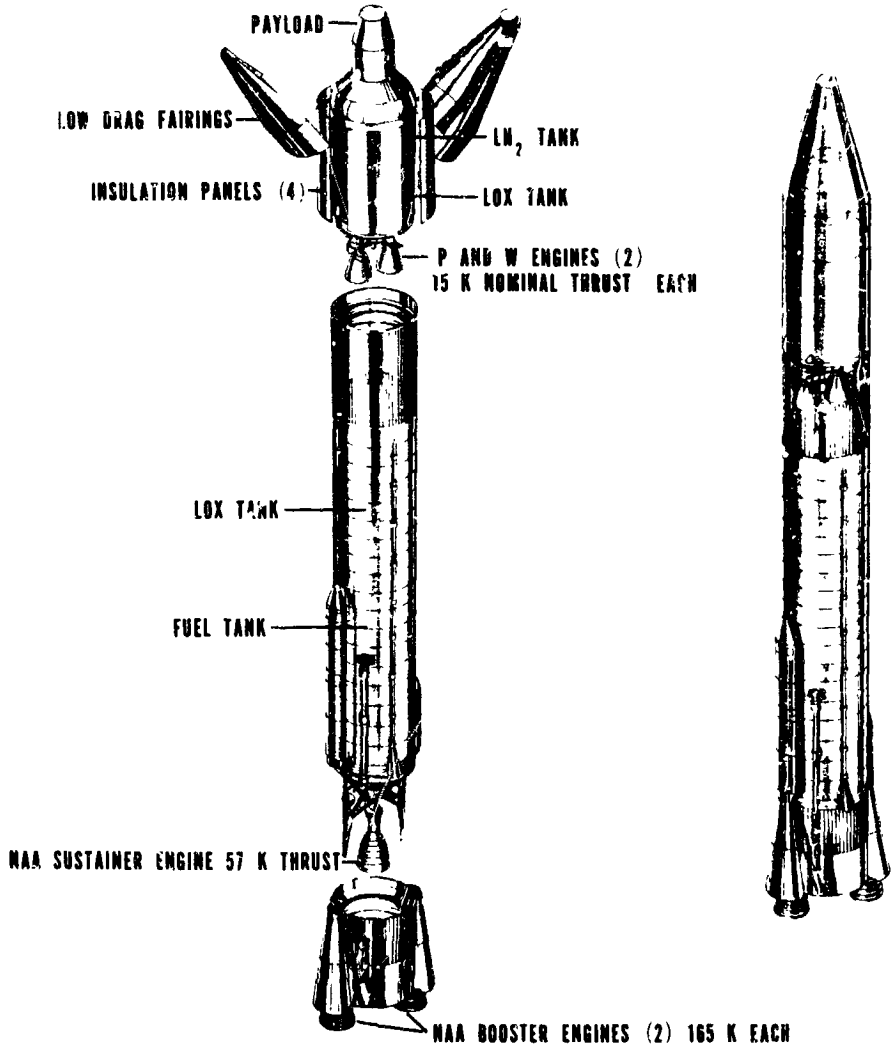


Figure 5-1. Atlas/Centaur Configuration

Table 5-2. Selected Ground Rules for Atlas/Centaur Performance

Item	Selections and Performance	Requirements
A	Trajectory Constraints	
	1. Launch Azimuth (σ_L), AFETR	90° to 114°
	2. Injection True Anomaly (η_i)	+2°
	3. Parking Orbit Altitude	90 nm
B	First Stage	
	1. Designation	Atlas Stub - D
	2. Propulsion System	MA-5 (165K)
	3. Baffled Injectors	Yes
	4. Retro Rockets	8
C	Second Stage	
	1. Designation	Alpha/Centaur
	2. Tank Material	301
	3. Nose Fairing	1520 lb*
	4. Insulation Panels	800 lb
	5. Propulsion	RL10-A-3
	6. Guidance System	MH-3
	7. Hydrogen Peroxide Attitude Control System	Yes
	8. Telemetry System	"TASC"
	9. Range Safety Receiver	Dual
	10. C-Band Beacon	Yes
	11. (Electrical) Battery	100 amp hr
	12. Jettison Weight	4000 lb
D	Performance Rules	
	1. Booster Engine Cutoff (BECO)	5.7 g's
	2. Insulation Staging	BECO +50 sec
	3. Fairing Staging	BECO +83 sec
	4. Sustainer Cutoff (SECO)	(minimum residuals sensor)
	5. Vernier Engine Cutoff (VECO)	at SECO
	6. Separation Sequence Atlas/Centaur	"Fast"
	7. Centaur Propellant Data Flight Performance Reserve (FPR)	3.0 sigma

*Weight figures presented in this table are approximate.

2) A 10 ft diameter sheet stringer cylindrical adapter to support the Centaur stage has been added.
3) An advanced propellant-utilization system will be incorporated.
4) The vehicle equipment pods have been modified to accommodate electronic equipment changes and to reduce gross weight.
5) The General Electric radio guidance system, the impact predicter the reentry vehicle separation system, and the high-intensity photoflash system have been removed.
6) The flight-control system is equipped to accommodate steering signals from the second-stage guidance system.

(2) Airframe. The first-stage airframe is composed of the main propellant tank section, the aft booster section, and the forward interstage-adapter section. Total length of the airframe is approximately 72.5 ft. The main propellant tank consists of two tandem compartments 10 ft in diameter jointed by ellipsoidal intermediate bulkhead. The tank is a thin wall, internally pressurized monocoque structure. The booster-section structure is a jettisonable compartment housing the dual-boost engines and their associated hydraulic and pneumatic subsystems. The forward adapter section is a 10 ft diameter sheet stringer aluminum cylindrical section approximately 1 ft long joining the Atlas and Centaur stages. This adapter is attached to the Atlas and is fitted with access doors and cutouts to provide for Centaur H_2O_2 system servicing, oxidizer (Atlas and Centaur) boiloff lines, the Centaur aft umbilical, the interstage heating and air-conditioning ducts, and the helium lines for Centaur engine chilldown. The Atlas/Centaur separation system is installed on the adapter. The Atlas/Centaur separation system utilizes a linear-shaped charge to effect separation of the Centaur from the interstage adapter. Inflight operation of the separation system is initiated by a signal from the first-stage flight-control programmer coincident with Atlas sustainer and vernier-engine cutoff. The sustainer retro rockets are installed at Station 1139 near the booster separation plane.

(3) Propulsion. The propulsion subsystem is composed of three assemblies: The booster-engine assembly, containing two engines, the vernier engines, for roll control during sustainer flight, and the sustainer engine. The total nominal thrust rating for the propulsion subsystem at liftoff is approximately 388,000 lb (Table 5-1).

(4) Flight Control. Flight control of the first stage is accomplished by an autopilot (located in the first stage) that is fed guidance or steering commands from the all-inertial missile guidance set, located in the second stage (Centaur). The autopilot contains displacement gyroscopes for attitude reference, rate gyroscopes for response damping, and a programmer for the initial vehicle roll command after liftoff, early pitch programming, and control sequencing. Vehicle attitude and steering control is accomplished in flight by the coordinated gimbaling of the five propulsion thrust chambers in response to the autopilot signals.

(5) Telemetry. The first-stage telemetry system, which is essentially the same as that used on Atlas-D R and D missiles, monitors first-stage functions from before launch to beyond Atlas/Centaur separation. The telemetry equipment, excluding the transducer and one of the two antennas, is located in the B-1 equipment pod. The antennas are mounted on opposite sides of the first stage at the forward end of the equipment pods.

(6) Range Safety. The Atlas employs a modified Mark II range-safety command system similar to that used on Atlas D-A/G and E missiles. A destructor mounted on the first stage, and a destructor-control-unit and destructor mounted on the second stage constitute the range-safety command system. The system provides the capability of manually cutting off the Atlas engines and/or destroying the composite vehicle at any time during first-stage flight. The complete system is inactive after normal Atlas/Centaur-staging is obtained.

b. Second Stage

(1) The Centaur configuration is shown in Figure 5-2. Centaur propulsion is provided by two gimbal-mounted Pratt and Whitney RL10-A-3 engines, providing approximately 15,000-lb thrust each. The second stage is bolted to the first stage (Atlas) adapter section. The length of the second stage is 47 ft from the aft end of the thrust chambers to the tip of the nose fairing.

(2) Nose Fairing (4-3-2). The 4-3-2 nose fairing, which has the following features, may be utilized:

1) The two upper portions, which are half-cones, are installed on the upper spacecraft adapter, with spacecraft attached, in the hangar at AFETR.
2) Following this installation, the encapsulated spacecraft is not physically accessible.
3) The encapsulated spacecraft, incuding upper spacecraft adapter, is then mated to the lower adapter section of the Centaur at the launch stand.
4) The two lower-half cylindrical sections of the nose fairing are then installed between the upper portions and the Centaur.
5) The inflight separation of the clamshell nose fairing is accomplished in two pieces.

(3) Airframe. The main propellants are contained within the second-stage airframe which also provides structural support for all second-stage airborne systems, as well as primary structural integrity for the Centaur vehicle.

THE SECOND-STAGE CENTAUR *is a high-energy space vehicle powered by two Pratt & Whitney RL-10 engines. Fully fueled, the vehicle weighs about 37,000 pounds. The tank structure is fabricated from thin-gauge stainless steel. On operational vehicles, skin thickness of the cylindrical portion of the tank is 0.014 inch.*

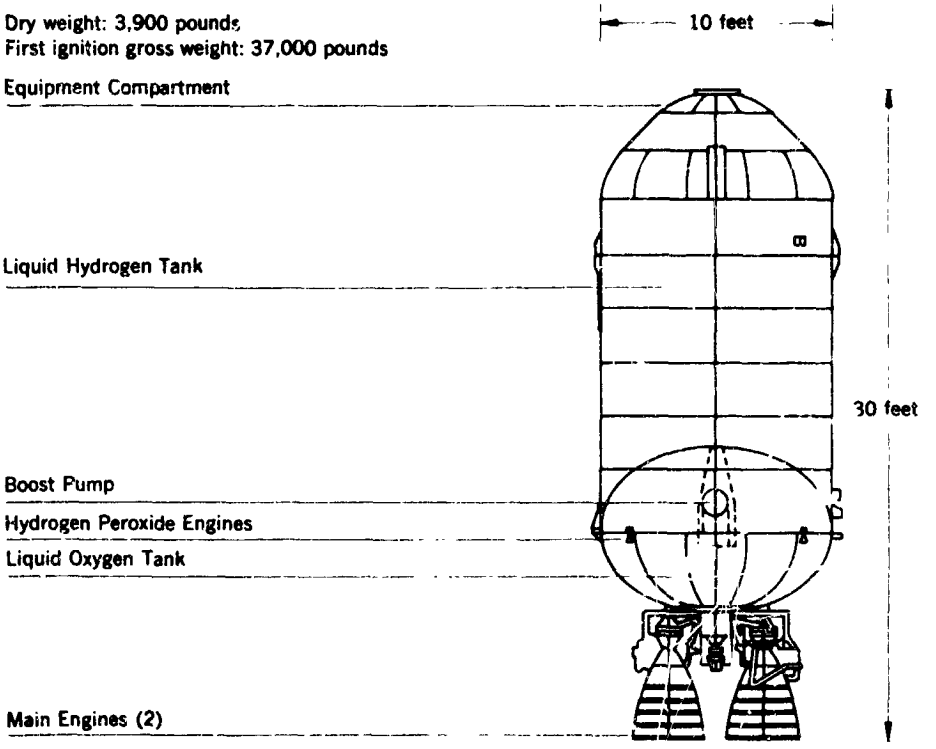


Figure 5-2. Centaur Stage Configuration

Mounted on the forward tank bulkhead and arranged around the periphery of the payload mounting-ring are the electrical and electronic equipment packages. These units are arranged in two tiers to maintain a favorable location of the center of gravity for the second-stage vehicle. The low-drag clamshell fairing, designed to reduce the drag of the two-stage vehicle and shield the spacecraft and second-stage electrical and electronic equipment from excessive aerodynamic heating during flight, encloses the equipment located forward of the tank adapter ring.

The midsection includes the main propellant tanks on which are located the electrical fairing, conduits, antennas, fuel-tank insulation, and attitude-control rocket engines.

The liquid-hydrogen and liquid-oxygen tanks are pressurized balloon tanks constructed of stainless steel. The liquid-hydrogen tank consists of a cylinder with an ellipsoidal bulkhead welded to each end, and with the cylindrical portion of the tank welded to the circumference of the liquid-oxygen tank to form the basic shape of the vehicle. The thrust structure is attached to the lower bulkhead of the liquid-oxygen tank and provides support for the main engines. The propellant tanks are self-pressurized, requiring no auxiliary pressurization.

Four removable insulation panels, with built-in fairings to accommodate antennas, conduits, and other basic tank protrusions, completely cover the liquid-hydrogen tank walls. These panels are jettisoned during ascent-flight phase just prior to nose-fairing jettison. The propellant-tank forward bulkhead is insulated on its entire exterior surface by 1 inch thick stafoam panels which are covered by a laminated aluminum and fiberglass sheet.

The airframe aft section, which is enclosed by the interstage adapter to the Atlas vehicle until Atlas/Centaur staging, consists of the main engine and boost-pump structure, the pneumatic control system (including gas storage bottles and associated equipment), and the mounting structure.

Upon actuation of the nose-fairing separation system and by command from the Atlas programmer, the explosive fittings fire to separate the nose fairing into two "clamshell" halves, and the gaseous nitrogen thrust bottles (one in each half) force the panels outward. This motion continues, with each panel rotating approximately 45 degrees about its hinge line. At this time, the hinges release and the two nose panels fall outward and away from the still-accelerating vehicle.

(4) Propulsion. The second-stage propulsion subsystem contains three individual elements: attitude control, main engines, and main-engine propellant feed.

The attitude-control unit consists of six monopropellant hydrogen peroxide rocket engines mounted on the periphery of the main propellant tanks at the interstage-adapter

separation plane. Two 3-lb thrust units are located 180 degrees apart and provide pitch attitude control. Each of these units is integrated with a pair of 1.5-lb thrust units. These smaller units provide yaw and roll control by firing in opposite directions along a plane tangent to the periphery of the tank. The six units may be fired individually or in any combination.

The main engine assembly consists of two Pratt and Whitney RL-10-A-3 fixed-thrust, single-chamber, regeneratively-cooled turbopump-fed engines rated at 15,000-lb thrust each at 200,000 ft. The engines are gimbal-mounted to permit a square pattern movement of ±3 degrees from the engine centerline. Each engine has its own integral propellant turbopump driven by a hydrogen-gas expansion turbine, prestart and start controls, thrust chamber, igniter system, valves, and interconnecting lines which provide multiple restart capability. The liquid-oxygen and liquid-hydrogen propellants are consumed at a nominal oxidizer/fuel ratio of 5:1 by weight. The total flight-duty-cycle operating time will be approximately 420 seconds.

Nor nal operating propellant-mixture ratio is controlled by means of a propellant-utilizatior system composed of fuel and oxidizer capacitance probes, an error ratio detector, and an oxidizer-boost-pump control unit. Engine-mixture ratio is adjusted by varying a mixture-ratio control valve in the box line.

(5) Guidance and Control. The guidance subsystem (or guidance set) consists of five major components:

1) The inertial platform
2) The platform electronics
3) The signal conditioner
4) The navigation computer
5) The pulse rebalance, gyro torquer and power supply

(a) Guidance Set. The guidance set performs the following functions:

1) Provides a gyro-stabilized three-axis orthogonal reference system for the measurement of vehicle thrust acceleration in inertial coordinates.
2) Provides continuous steering signals to the Agena type timer used on Centaur and to logic in the Atlas Autopilot.
3) Provides continuous coordinate transformation of the steering signals from platform coordinates to vehicle coordinates referenced to the vehicle pitch, yaw and roll axes.

4) Provides discrete signals (to the Agena type timer) for such commands as booster engine cutoff (BECO), booster separation, and main engine cutoff (MECO).
5) Accepts a steering alert signal from the Agena type timer.
6) Provides its own temperature control.
7) Provides its own power derived from the vehicle power supply system.
8) Provides analog and digital telemetry outputs.

(b) Inertial Platform. The inertial platform consists of an outer housing and a four-gimbal, all-attitude gimbal structure. The platform contains three single-degree-of-freedom rate integrating gyros and three pendulous pulse-rebalanced accelerometers. The platform incorporates provisions for optical determination of gyro drifts, accelerometer misalignment angles, and gyro compassing accuracy by means of three optical grade mirrors and a prism mounted on the inner-optical access to the mirrors and prism. The prism size and location permits prelaunch optical alignment of the inertial platform in azimuth to a specified accuracy.

(c) Platform Electronics. The platform electronics include the modulators, amplifiers, and other electronic components and circuitry required to stabilize the platform, to cage and align the gimbals, to isolate and amplify the coordinate-transformation signals, and to route the platform signals to and from the guidance-set components.

(d) Signal Conditioner. The signal conditioner provides demodulators scaling and other electronic circuitry to modify the guidance-set signals for acceptance by the Centaur telemeter.

(e) Navigation Computer. The navigation computer performs time-varying solutions of the guidance equations in flight and provides prelaunch outputs such as a semiautomatic calibration sequence from gyro drift and accelerometer scale factor, timing, and leveling and azimuth torquing commands. The computer, then, performs in the following specific modes:

1) Component calibration and platform alignment mode.
2) Computer and guidance system checkout.
3) The guidance mode (steering signals, gyro torquing and discrete commands).
4) Prediction and reset mode.
5) A self-order test routine during all phases of operation.

(f) Other Components. The pulse rebalance, gyro torquer, and power-supply component supplies precision voltages and currents necessary for the operation of the accelerometer-pulse rebalance electronics and of the remainder of the guidance-set electronics.

The control subsystem consists of an Agena type timer, a rate gyro package, a servo amplifier package, and the controllers for the main and attitude control engines described above.

The Agena type timer accepts the steering signals and discrete signals described above from the guidance set, provides a steering alert signal to the guidance set, provides signals and logic functions for the rate gyro and servo amplifier packages, accepts an engine alert signal from the Atlas programmer, and provides commands for such functions as engine start and payload separation.

c. Launch Facilities

ETR facilities at Cape Kennedy Florida, will be used for launch and prelaunch operations. Prelaunch assembly and checkout will be conducted in Hangar H or J for the Atlas and Centaur stages and at the Spacecraft Checkout Facility (Building AC) for the spacecraft. An Explosive Safe Facility will be used for propellant and gas loading, final spacecraft alignment, installation of the retro rocket and other hazardous components, and spacecraft encapsulation.

Launch operations will be conducted from ETR Complex 36A and 36B using facilities installed for the Centaur R and D Program. ETR launch-through-injection tracking and telemetry reception will be required for Mariner 1969 instrumentation and DSIF acquisition purposes.

2. Launch Vehicle Environment

a. Thermal Environment

Conditioned air circulated internally to the nose fairing is available for temperature control of the spacecraft. The air temperature, humidity, flow rate and direction of flow are [illegible]onal.

At launch when the air conditioning is disconnected, the air which is inside the nose fairing cavity escapes through small holes near the lower end of the nose fairing. The resulting ambient pressure is as defined on Figures 5-3 and 5-4.

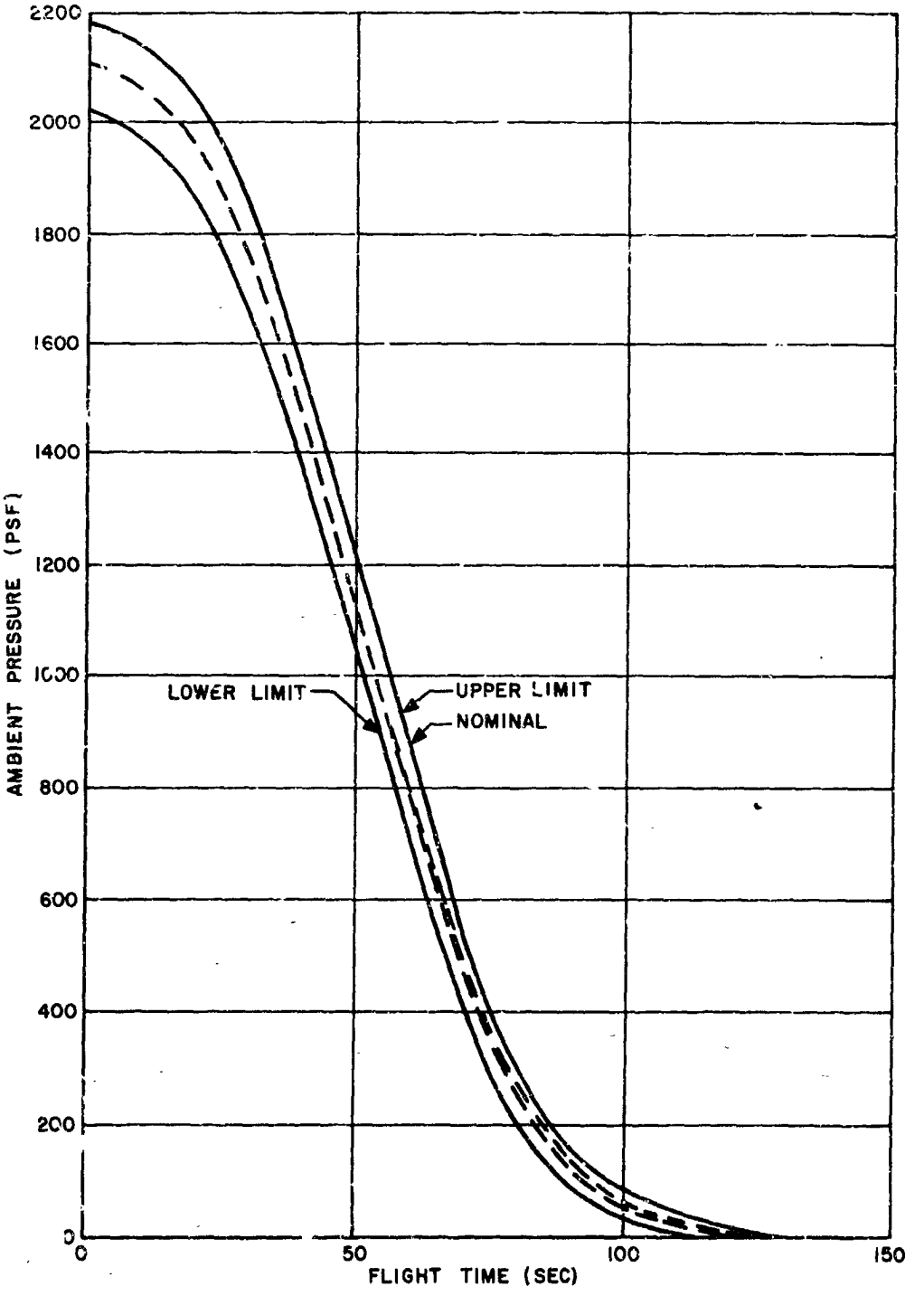


Figure 5-3. Ambient Pressure, Function of Flight Time, 0 to 150 Seconds

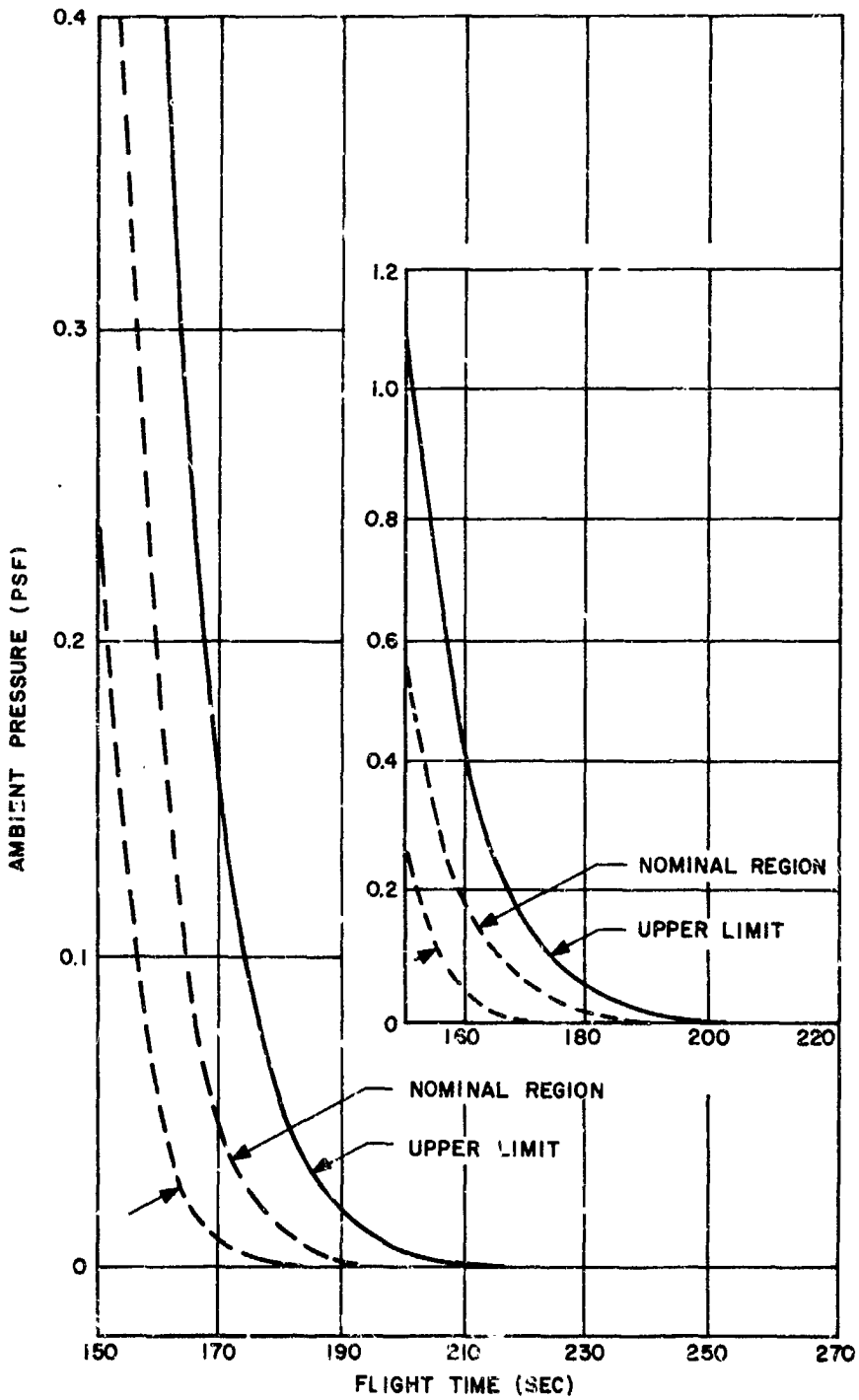


Figure 5-4. Ambient Pressure, Function of Flight Time, 150 to 250 Seconds

With regard to aerodynamic heating, the nose fairing on a worst case (that is, a 3 sigma maximum heating trajectory) has a heating rate of 157 BTU per hour per square foot. This is considered to be the average for the period of time from launch through nose fairing ejection.

b. Vibration and Acoustic Loads

Specification of these loads is not planned before early 1965.

c. Cleanliness Environment

Specification of cleanliness environment is not planned before early 1965.

d. Quasisteady-State Loads

Quasisteady-state accelerations at the separation plane imposed by the launch vehicle should not exceed:

1) 5.9 g longitudinal
2) 0.4 g lateral

3. Typical Sequence of Events for Atlas/Centaur Parking Orbit Mission

Sequence of events and event times for a typical Atlas/Centaur Parking Orbit Mission are given in Table 5-3.

Table 5-3. Atlas/Centaur Typical Event Times (Parking Orbit)

Item	Event	Time (Second)
1.	Liftoff	0
2.	Booster Cutoff (BECO)	135
3.	Booster Jettison	138
4.	Insulation Panel Jettison	185
5.	Nose Fairing Jettison	218
6.	Sustainer, Vernier Cutoff (SECO, VECO)	222
7.	Atlas-Centaur Separation	22
8.	Centaur Main Engine 1st Start (MES #1)	230
9.	Centaur Main Engine 1st Cutoff (MECO #1)	532
10.	Centaur Main Engine 2nd Start (MES #2)	2,032
11.	Centaur Main Engine 2nd Cutoff (MECO #2)	2,137
12.	Spacecraft Separation Command	2,143
13.	Start 180° Turn	2,148
14.	End 180° Turn and Start Retromaneuver	2,348

B. SOLAR FLARE ACTIVITY

From a direct time extrapolation of the solar Sun spot cycle and related flare data, it is predicted that the 1969 mission will occur during the declining portion of Sun spot cycle 20. During the equivalent portion of cycle 19 (roughly calendar year 1960) flare activity was extreme.

REFERENCES

1. Solar Proton Manual; Edited by Frank B. McDonald, NASA TR R-169; September 1963.

C. INTERPLANETARY METEOROID FLUX

The meteoroid environment in interplanetary space is a potential hazard to planetary spacecraft because of the length of time associated with the cruise phase of a planetary mission. The results of Explorer XVI and Mariner II (along with other data) show that the near-Earth flux is significantly greater than that in interplanetary space for particles of mass less than approximately 10^{-7} grams. Larger meteoroids are not expected to exhibit a greater concentration near the Earth; therefore, the near-Earth flux and interplanetary flux would be expected to be the same for meteoroids of mass greater than 10^{-7} grams. However, sufficient statistical data on interplanetary particle fluxes are not available. Whipple states (see Reference 1) that there is limited evidence that the meteoritic impact rates may be 10 to 100 times greater than predicted by his flux equation for particle masses of 10^{-4} gram and that it is necessary to allow for the possibility, not proved, "that there is an unobserved large flux of meteoritic material in the mass range 10^{-3} to 10^{-7} gram." It will be shown in Subsection XI.1 that the meteoroid size of interest to a Mars orbiter mission is approximately 10^{-4} to 10^{-5} grams; thus this aspect of the flux-mass distribution is very important.

It is now generally accepted that most meteoroids have average densities of approximately 0.4 gm/cc. Although the distribution of these particles in interplanetary space has not been defined, Whipple states (see Reference 1) that "It is safe to assume that the variation near the plane of the ecliptic will follow at least an inverse law of solar distance." This statement may not be realistic since, in the interplanetary space between Earth and Mars, the asteroid belt (mean distance = 2.6 A. U.) is a "source" of meteoroids with average densities of approximately 3 gm/cc. The flux-mass distribution of these meteoroids and their radial distribution in interplanetary space is completely unknown, except for the large asteroids, (minor planets) which have been observed visually and whose orbits have been determined. It is expected that the asteroidal meteoroid flux would be higher at Mars distance than at the Earth distance from the Sun. For the Mariner 1969 opportunity, encounter occurs at a Mars radial distance from the Sun of approximately 1.4 A.U.; therefore, the meteoroid hazard in 1969 would not be expected to be as severe as may result in years where the encounter occurs near 1.7 A.U.

REFERENCES

1. F. L. Whipple. "Meteoroids and Penetration," Journal of Geophysical Research, Vol. 68 No. 17, pp. 4929-4939, September 1, 1963.

D. IN-ORBIT PARAMETERS

1. Magnetic Fields

Fields up to the order of magnitude of the field of the Earth may be expected.

2. Radiant Flux-Martian Surface

Refer to Memorandum RM-4000-NASA (see Reference 1).

3. Meteoroid Flux

Use the interplanetary data of Subsection C.

REFERENCES

1. Geometric and Photometric Parameters of the Terrestial Planets. G. De Vancouleurs. Memorandum RM-4000-NASA, prepared by Rand Corporation, March 1964.

E. MARS HIGH-ALTITUDE ATMOSPHERIC DENSITY

The only estimates of high-altitude (thermosphere) atmospheric density for Mars are those of Chamberlain (Reference 1) and Vachon (Reference 2). In both cases, the atmospheric radiative balance was based on low (≈5 percent by volume) CO_2 content in the atmosphere. Recent evidence (References 3 and 4) from ground-based astronomical observations indicates that CO_2 may comprise 7 to 25 percent by volume of the Mars atmosphere. Therefore, application of either set of estimates is not strictly correct to model atmospheres with varying CO_2 content.

One of the model atmospheres used to predict minimum periapsis altitude consistent with a certain spacecraft orbit lifetime is the "maximum" model atmosphere given in "NASA Standard Engineering Models of the Mars Atmosphere" (Reference 5). This maximum model atmosphere is based on a Mars surface pressure of 40 mb. The high-altitude thermosphere thermal gradient used to estimate the high-altitude density profile is +2°K/km. This value "was based on a representative value given by Vachon." Although Vachon "prefers" a thermosphere thermal gradient of 1°K/km, there is inadequate evidence to state that the gradient should not be 2°K/km or higher. The higher the thermal gradient, the greater the scale height at any given altitude, therefore the greater the density at that altitude. As discussed in Section VIII B.3, this "maximum" model atmosphere requires approximately a 4000 km periapsis in order to achieve a 50-year spacecraft lifetime in Mars orbit.

REFERENCES

1. J. W. Chamberlain "Upper Atmospheres of the Planets," The Astrophysical Journal, V136, No. 2, pp 582-593, September 1962.

2. D. N. Vachon, "The Density of the Upper Atmosphere of Mars," General Electric Co., Space Sciences Lab., Report No. R62SD58, May 1962.

3. L. D. Kaplan, G. Munch, and H. Spinrad, "An Analysis of the Spectrum of Mars," Astrophysical Journal Vol. No. 139, No. 1, January 1964.

4. G. P. Kuiper, Private Communication, to be published as University of Arizona Lunar and Planetary Communications No. 31 and 32, 1964.

5. NASA Standard Engineering Models of the Mars Atmosphere. Ed by G. E. Levin, D. E. Evans, and V. Stevens to be published as a NASA Space Vehicle Criteria Document.

SECTION VI

SPACECRAFT CONSTRAINTS

A. SURVEYOR NOSE FAIRING

Figure 6-1 illustrates the clamshell-type Centaur/Surveyor nose fairing and available envelope. The spacecraft envelope is basically conical except for flats at the line of separation of the two nose fairing halves. A sterilization diaphragm extends from the Centaur adapter out to the nose fairing at the start of the conical shape. Although spacecraft sterilization is not a requirement for this mission, the nose fairing diaphragm is retained within the envelope to ensure spacecraft cleanliness.

The nose fairing separation is accomplished with cold gas jets located in the forward end. There has been no consideration given in this study to potential blast effects of the spacecraft from these gas jets. The two halves of the fairing hinge at their support points on the Centaur forebody, and at nose fairing separation, the clamshell rotates outward about these hinge points. As the nose fairing opens, the sterilization diaphragm moves upward into a region potentially available for spacecraft components. To avert contact of the nose fairing and the spacecraft, the spacecraft components must be packaged to allow for this motion.

Consideration should be given to extending the cylindrical section of the nose fairing. An extension of from 3 to 5 feet will facilitate packaging of the solar panels, antennae, and propulsion systems. The nominal configurations described in Section X.A are restricted by the available envelope and any increase in subsystem size is severely limited by the nose fairing.

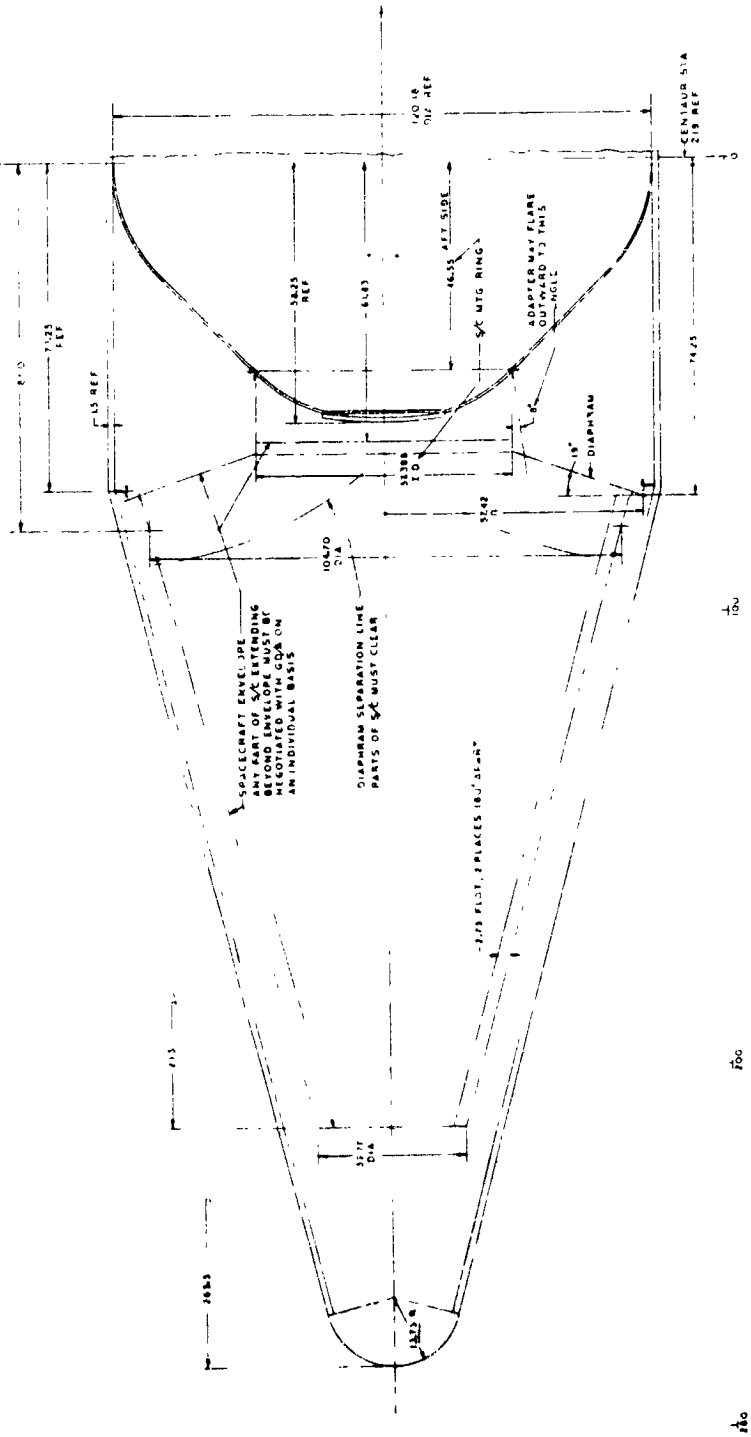


Figure 6-1. Clamshell Type Centaur/Surveyor Nose Fairing

B. STANDARDIZED PACKAGING

1. Conceptual Design

a. Standardization of Assemblies and Subassemblies

The arrangement of electronic subsystems in the spacecraft electronic equipment compartment (octagon) requires the following considerations:

1) Uniform heat distribution for temperature control.
2) Proper weight distribution for spacecraft center of gravity control.
3) Layout of subsystems for minimum cabling.
4) Meeting alignment or sensor-orientation requirements.

The use of standardized assemblies and subassemblies provides maximum flexibility to optimize equipment layout within the octagon compartment since an electronic subsystem can be located in any of the octagon bays.

2. Structural Integration

To improve spacecraft structural efficiency, electronic equipment assemblies are considered as load carrying members. This approach of integrally joining electronic subassemblies into one spacecraft compartment provides maximum stiffness with minimum weight. The structural design goal is to keep the resonances within the subassemblies above 400 cps frequency to minimize bending of components and interconnecting joints. Experience has shown that such a design goal is not too difficult to obtain and that such equipment, in general, is free of mechanical failures in vibration environment.

3. Proposed Configuration

A structurally well-integrated and highly flexible design configuration is proposed for Mariner 1969 as shown in Figure 6-2.

This configuration, which is typical in each of the eight electronic equipment bays, consists of three basic elements:

1) Chassis-harness assembly
2) Electronic equipment subassemblies
3) Outer panel

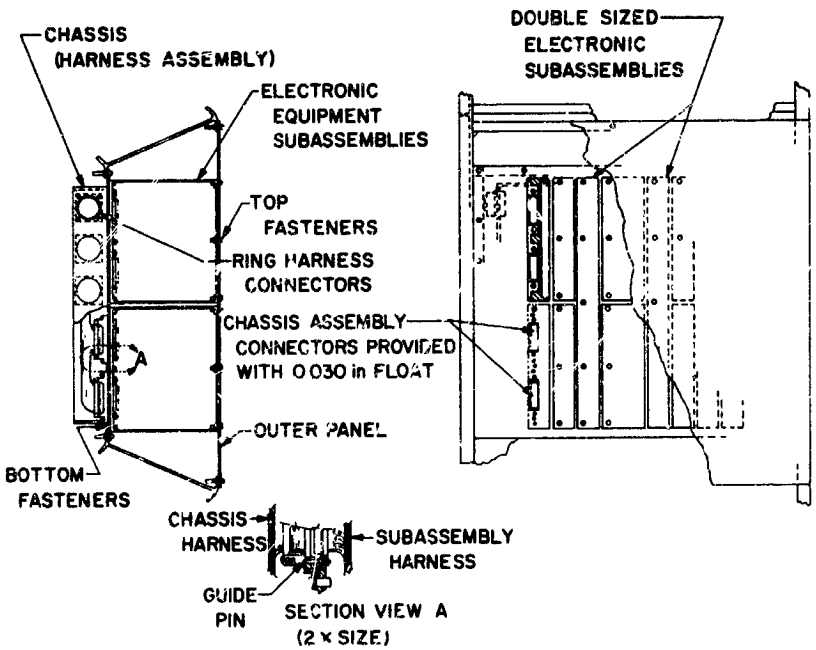


Figure 6-2. Mariner 1969 Packaging and Cabling Conception

a. Chassis-Harness Assembly

The chassis-harness assembly consists of a shallow tray which contains the interconnecting harness for that bay. All the connectors are mounted to the common plate and are provided with 0.030-inch float for free mating with the subassembly connectors. Since the connectors are fixed in their position, more direct wiring is obtainable. Furthermore, flexing of harnesses is not required, thus connectors need not be potted and the use of smaller gauge wire is possible.

b. Electronic Subassemblies

The electronic subassemblies are standardized to the basic size of 6.25 x 6.75 inches and are used in two columns in each bay. Wherever possible, to further reduce interconnecting cables, double sized (6.25 x 14 inches) subassemblies can be used.

The connectors for the electronic subassemblies are mounted with guide pins. These pins serve as both connector fasteners and as alignment pins for mating with cable connectors. This technique provides straight engagement and disengagement of connectors which reduces the possibility of bending the connector pins.

c. Outer Panel

The outer panel serves two purposes; it provides the outer shear panel for the spacecraft and it provides the temperature control plate. This panel would not be used during equipment electrical testing and checkout. The subassemblies would be mounted to the chassis-harness assembly by the bottom fasteners. The outer panel would be needed only for environmental testing and in the final spacecraft configuration.

4. Packaging Techniques

To obtain better fabrication and quality control and to reduce spacecraft complexity by using fewer processes and materials, as few packaging techniques as practical will be used.

a. Two Dimensional Flat Layout

Subassemblies, where large variation in component sizes is predominant and where component value changes are anticipated, are intended to be packaged in a flat layout configuration using single sided printed wiring boards and bifurcated terminals with externally visible solder joints. This technique is expected to be used in power converters and power supplies and some interface circuits. Wherever practical, repetitive circuits should be packaged in cordwood modules for better volume utilization.

b. Cordwood Packaging

An attempt will be made to standardize three-dimensional cordwood packaging for general electronic packaging. Welded cordwood packaging techniques are considered acceptable.

Interconnections of cordwood modules are expected to be standardized on two basic techniques: multi-layer and point-to-point soldered interconnect techniques.

c. Microelectronics

Packaging techniques for microelectronics are under study, and applications will be recommended as techniques are qualified.

5. Octagon Size

The present nominal spacecraft configuration shows the octagon height 1.25 times Mariner 1964 with resulting volume of 1.43 times Mariner 1964 since the midcourse bay is used for electronics (using the liquid propulsion system). If a solid propulsion system is used, the octagonal structure must be scaled up 1.43 times for the same packaging volume since the midcourse bay is not available for electronic equipment. This volume requirement came from an estimated increase in sizes of electronic subsystems as compared with Mariner 1964.

However, increased use of three-dimensional packaging could reduce the octagon size requirements to approximately that of Mariner 1964. This use of added three-dimensional packaging would not only decrease the size of the bus, but would also appreciably reduce the weight. An estimated 30 pounds could be saved by cordwood packaging which would come from smaller structures, fewer subchassis and shorter cables.

Spacecraft weight reduction could also be obtained using microelectronics. If spacecraft digital circuits were replaced with microelectronics, an additional 30 pound reduction could be readily realized.

C. TEMPERATURE LIMITS OF SUBSYSTEMS

The following bulk temperature limits represent the best estimate of the subsystem cognizant engineers. These temperature limits are to be used for gross design purposes only. A more detailed list will be generated during the design process, where the thermal problems associated with each component will be investigated. The detailed list will reflect the actual capabilities of the subsystem as well as the capabilities of the temperature control system.

This list is based on allowable values for Mariner 1964 where applicable. Temperature limits for the liquid propulsion system are based on anticipated lowest fill temperatures and maximum operating temperatures and are consistent with available ullage volume. Allowable temperature extremes for the solid propulsion system are consistent with required engine start and performance characteristics. Temperature limits for science instruments are those prescribed by the experimenter. Although the infrared (IR) spectrometer, IR interferometer and ultraviolet (UV) spectrometer are not part of the nominal science payload, allowable temperature limits for these instruments are included in Table 6-1.

Table 6-1. Temperature Limits of Mariner 1969

Subsystem	Operating		Non-Operating	
	Min °F	Max °F	Min °F	Max °F
1. Bus				
Power	14	167	*N/A	N/A
Propulsion				
Liquid (fuel tanks)	35	125	35	125
Solid	N/A	N/A	20	120
DAS	14	150	-67	257
Data Encoder	14	167	14	167
Command	0	185	0	185
Radio	14	167	N/A	N/A
Tape Recorder	14	150	14	167
Attitude Control	14	167	14	167
Gyros	30	131	30	131
Battery	40	140	14	140
2. External Components				
Solar Panels	-175	175	-175	200
Solar Panel Actuators	10	110	-100	130
Solar Pressure Vane	-400	300	-400	300
Solar Pressure Control	-65	175	-65	200
Cabling	-200	250	-200	250
A/C Nitrogen	40	140	0	200
Sun Sensors	30	130	-20	160
Canopus Sensor	-30	100	-30	125
High Gain Antenna	0	167	0	167
Low Gain Antennae	0	167	0	167
Louvers	-300	300	-300	300
Thermal Shields	-200	200	-200	200
Squibs	-70	167	-70	167
Pyro Arming Switch	-58	257	-58	257
Unlatch Motion Sensor	-70	167	-70	167
Separation Initiated Timer	20	140	20	140
3. Science				
IR Spectrometer	-110	50	-110	140
IR Interferometer	18	23	-58	140
UV Spectrometer	14	104	-22	140
TV	14	131	-22	176
Mars Scanner	-40	-4	-58	158
Magnetometer	14	131	-58	176
Plasma Probe	14	131	-58	176
Trapped Radiation Detector	14	131	-22	140
Cosmic Dust Detector	14	131	-58	176
Occultation Beacon	14	131	-58	176
RF Noise Detector	14	131	-58	176

*N/A - Not applicable

SECTION VII

SYSTEM DESCRIPTION AND PERFORMANCE CAPABILITY

A. SYSTEM DESCRIPTION

The complete system required for accomplishing the Mars-orbiter mission consists of a number of equipment elements and a series of operations which range from the testing of various portions of the system through the flight operations of the mission to the recovery and analysis of the mission data. The present study, and the bulk of this report, are concerned with the flight spacecraft and its characteristics. In Subsection B, the nature of the other equipments and operations of the mission are identified and briefly discussed. Subsection C summarizes the capabilities of the spacecraft systems described in this report, and Subsection D indicates possible alternate design approaches and mechanizations beyond the scope of the present study report.

B. SYSTEM ELEMENTS

1. Launch Vehicle

a. General

Two Atlas/Centaur launching vehicles are required for this mission. A two-burn Centaur stage was considered for this mission. Items involved in the spacecraft/Centaur interface area are shown in Figure 7-1.

b. Performance Capability

The launch vehicle capabilities as pertaining to the Mariner 1969 orbiter mission are graphically depicted in Figure 8-29 through 8-32 in Section VIII, Subsection B.4. Two launch vehicle performance estimates are considered; the original NASA numbers, and the relatively new Lewis Research Center performance figures. These figures show the parametric relationship between launch vehicle capability and injected spacecraft weight for the Mariner 1969 Orbiter Mission as considered in this EPD.

2. Spacecraft System

a. Spacecraft

The flight spacecraft consists of an integrated bus-orbiter spacecraft. The characteristics of these flight elements are given in other portions of this EPD.

The following types of orbiter spacecraft equipment are required:

1) Structural Test Model (STM)
2) Temperature Control Model (TCM)
3) Proof Test Model (PTM)
4) Type Approval Equipment (TA)
5) Flight Spacecraft
6) Spacecraft Spares

Three types of spacecraft configuration are presented in this study; a minimum, nominal, and maximum configuration. Each case has somewhat different capabilities and characteristics as described in Section X.

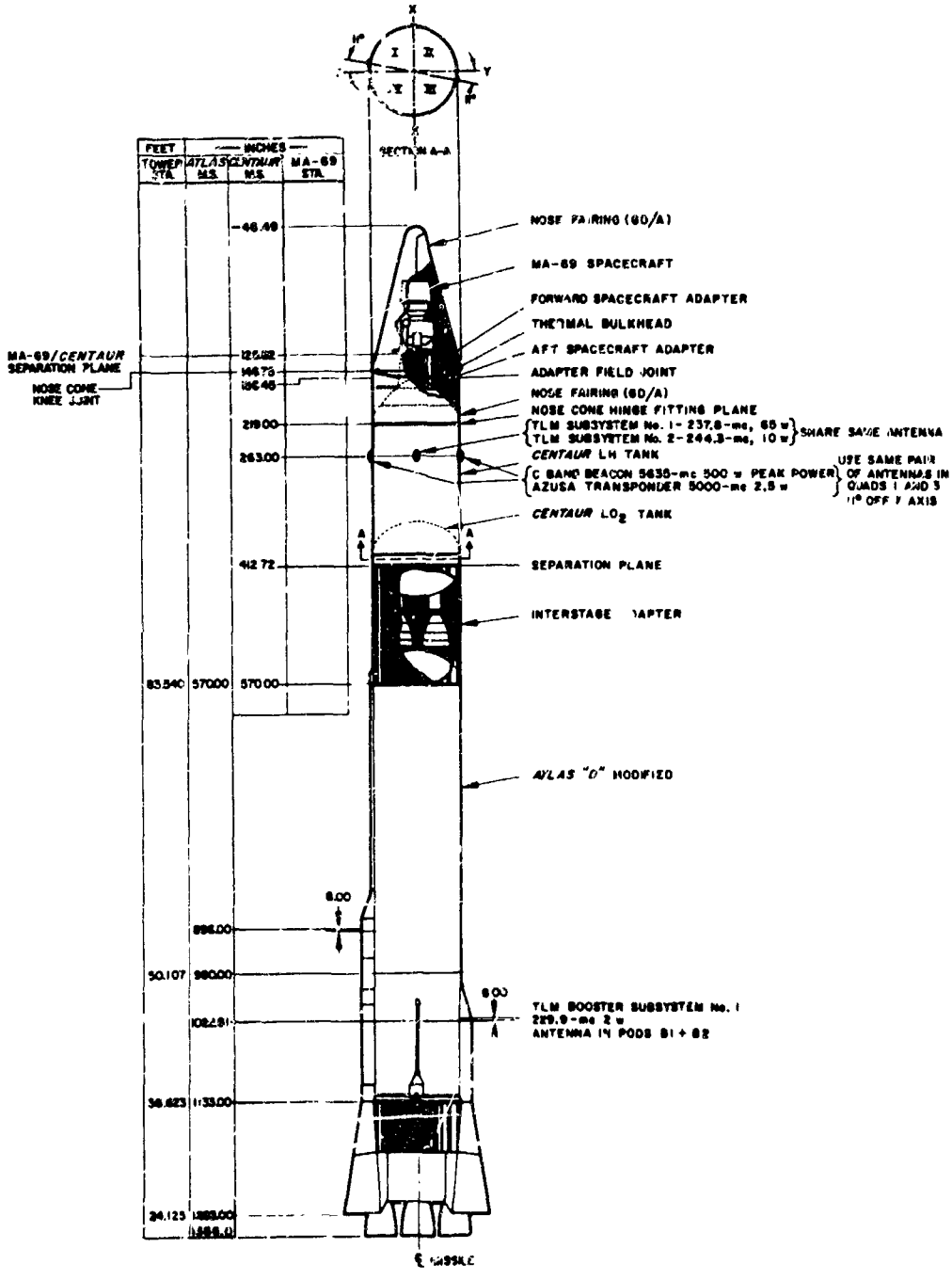


Figure 7-1. Atlas/Centaur/Mariner 1969 Configuration

3. Operational Support Equipment

a. System Test Complex (STC)

The Mariner 1969 System Test Complex shall include all elements, both electrical and mechanical, necessary to support subsystem and system testing of the spacecraft. It shall consist of a selected group of electronic test equipment and those mechanical fixtures necessary to assemble, handle and articulate the spacecraft during and in preparation for such testing.

The basic objective to be satisfied in the design of the Mariner 1969 Operational Support Equipment (OSE) is the generation of a tool which shall be capable of verifying the design and the flight readiness of the Mariner 1969 spacecraft. To accomplish this goal, the system test complex must be mechanized so that it is capable of exercising the spacecraft through all its standard and backup modes of operation. In addition, the STC must be sufficiently flexible to adapt to nonstandard conditions. The STC shall also be capable of supporting such troubleshooting as is necessary to locate spacecraft failures down to the provisioned spare level. To minimize troubleshooting time OSE shall be mechanized so that it can differentiate between OSE and spacecraft failures.

b. Launch Complex Equipment (LCE)

The Mariner 1969 Launch Complex Operational Support Equipment shall include all elements necessary for prelaunch operational support of the spacecraft.

The basic objective to be satisfied in the design of the Mariner 1969 LCE is the generation of equipment which will be capable of supporting spacecraft prelaunch operations, and verifying the flight readiness of the Mariner 1969 spacecraft. However, certain practical considerations exist around the OSE used with the launch complex which must be observed in the basic design. These considerations include compliance with JPL Spec 30505 requirements for equipment to be used in uncontrolled environments and size and weight limitations on the umbilical tower junction box.

4. Space Flight Operations System

a. U.S. Air Force Eastern Test Range (ETR) Tracking Network

The ETR Tracking Network covers the launch through Centaur separation phase of the mission. It provides tracking data for the initial spacecraft orbit determination and forwards information to the DSIF stations for initial spacecraft acquisition.

b. Space Flight Operations Facility (SFOF)

The SFOF will be utilized to conduct the flight operations of the mission. Any unique operations equipment requirements for the Mars 1969 mission will be incorporated and made operational within the SFOF.

c. Deep Space Instrumentation Facility (DSIF)

The DSIF will be utilized to communicate with the spacecraft during the space flight operations of the mission. It will incorporate any special equipment required for the mission and may have to provide the capability to communicate with two independent flight units simultaneously (2-orbiter spacecraft). The DSIF will provide an 85-foot 100 kw net for up and down link during cruise, an 85-foot 100 kw net for orbit uplink, and a 210 foot net downlink during orbit.

d. Compatibility Verification Equipment

This equipment will include all items required for maximum complete preflight systems tests which incorporate the spacecraft, OSE, Computer, SFOF, SDAT (Spacecraft Data Analysis Team), DSIF, either AFETR or SAF, and communications between these entities. The amount of equipment in this category will be small if the OSE (STC and LCE) are provided with SFOF and DSIF compatibility equipment.

5. System Integration

a. Interface

The complexity of the mission gives rise to a number of major interface areas. These interface areas will receive the same attention and control as is given to the design, development, and testing of the equipment elements of the mission. Interfaces exist between all of the equipment elements previously specified, and all of the operations entities of the mission (SFO, SDAT, testing, etc.).

b. System Reliability

A reliability program will be initiated during the study phase of effort, and will continue throughout the project period. The reliability program will include all reliability activities of the project and establish requirements to be met throughout the study, design and development processes. Elements of this program include:

1) Reliability Prediction and Estimation
2) Failure Mode, Effect, and Criticality Analyses
3) Maintainability and Elimination of Human-Induced Failure
4) Design Review Program
5) Failure Reporting and Correction
6) Standardization of Design Practices
7) Parts and Materials Program
8) Equipment Logs
9) Testing and Reliability Evaluation
10) Documentation Requirements
11) Relationship of Reliability Plan to Quality Control Activities

c. Testing and Operations

The testing and operations activities of the Mariner 1964 project will be required for the Mars 1969 mission. Test and operations requirements will be studied during the spacecraft design study period and established as soon as appropriate design data exist. Appropriate testing of the complete orbiter system will be carried out during the first SAF operations period.

d. Project Implementation

The Mars 1969 mission requires that all of the system elements described above be developed and integrated into a flight system ready for launching in 1969. In order to do this each element must undergo appropriate study, design, development, fabrication, and testing phases. A common approach for all elements of the mission is given here wherein each element is developed by performing the following tasks:

1) Prepare a set of objectives and design criteria for the mission element.
2) Examine the various means of meeting the objectives. Prepare design characteristics and restraints data for one or more approaches to meeting the objectives within the applicable restraints. This data shall provide a description of the system in sufficient detail so that the functions of the mission element can be identified and the interfaces between this and other mission elements can be described.
3) Prepare specifications of each system and subsystem within the mission element. Functional, design, or detail specifications will be required according to the nature of the mission element and the phase of effort.
4) Prepare a project plan including cost, manpower, and schedule information.

5) Carry out all fabrication, assembly, testing, operations, and analyses required by the project and the data developed under steps 1) through 4) above.

The emphasis among the several tasks given above will vary, as the project progresses from study through design and development phases, and according to the nature of the particular mission element under consideration. However, it is intended that operational and interface elements of the project be developed in this manner as well as the various equipment elements. The five areas of effort given above will also serve as major headings in documenting the nature of the project elements and their development.

C. PERFORMANCE CAPABILITIES

Three spacecraft systems have been considered within this study. These systems, designated as "maximum," "nominal," and "minimum" cases, are described in some detail in the following sections of this report. By comparing the spacecraft weight estimates for each of these cases with the launch vehicle capabilities shown in Figures 8-29 through 8-32, the following conclusions may be reached. In considering the original NASA figures, it may be observed that no mission considered in this study is feasible with zero-percent floxing. With 30-percent floxing, however, a nominal mission does exist for a 1500 km periapsis altitude, but not for a 4000 km periapsis altitude. In examining the more recent Lewis Research Center performance figures, it may be seen that a minimum mission exists for zero-percent floxing at 1500 km periapsis altitude only. The 30-percent LRC figures will support a nominal mission at both 1500 and 4000 km periapsis altitude. It is to be noted that none of those figures will support the maximum case as outlined in this EPD.

D. ALTERNATE DESIGN APPROACHES AND MECHANIZATIONS

The time scale of the present study precluded detailed examination of the alternate system design concepts for planetary orbiters. In order to illustrate the range of possibilities from which the spacecraft concepts of this report were selected, Tables 7-1 and 7-2 are included here. Table 7-1 shows alternate technical approaches for meeting the functional requirements of the orbiter mission. Some of the system implications and interactions implied by these alternate mechanizations are shown in Table 7-2. These possibilities in general suggest increased technical performance over the cases studied in detail, but involve considerable development, comparatively speaking, and therefore, are not as attractive from a project feasibility standpoint.

Table 7-1. Major Technical Alternates

Function	Alternate Technical Approaches				
	1	2	3	4	5
Supply Power	RTG power	Solar cells	Solar cell-Fuel cell system Fuel cells operate during limited orbiter life		
Track and Communicate (typical)					1. Spacecraft Antenna Diameter 2. Radiated Power 3. DSN Configuration
Control and Sequence	STD sequencer and RTC logic controller	As #1, but with some provision for onboard calculations for orbit retro	Onboard computer		
Guide	a) Launch, inject b) Near earth midcourse c) Heliocentric midcourse d) Orbit inject and trim	a) Launch, inject b) Near earth midcourse c) Terminal guidance d) Orbit inject	1 and 2 with variable fuel loading option		
Impart Impulse	Solid with storable liquid	One nozzle storable liquid system	Three nozzle storable liquid system	Cryogenic system	
Control Attitude	Reaction torque system	Cold gas	Hot gas	Solar pressure	
Control Environment	Sun stabilized	Earth stabilized, inertial	Planet stabilized, inertial	Earth-planet stabilized	
Handle Data (storage)	Magnetic tape recorder	Thermoplastic recorder	Magneto-optical storage		

Table 7-2. Implications of Technical Alternates

Functional Requirements	Alternate Technical Approaches										
	RTG Prime Power Source	Sola Panel Power Source	6 ft Antenna Dish High Power Xmitter	12 ft Ant Dish Low Power Xmitter	Onboard Orbit Adjust Calculation	Solid Retro Motor (Liquid Vernier)	Storable Liquid System	Sun-Inertial Stabilizatio.	Earth-Planet Stabilized	Planet-Inertial Stabilized	Magnetic Tape Recorder
Make Scientific Measurements	RTG radiation field might interfere with some experiments							Planetary scan platform with 2 degree of freedom required	No scan platform required	No scan platform required	Capacity for 10^8 bits storage
Make Engineering Measurements					Measurement of height above local planet vertical point required			Planet tracker			
Provide Data Handling Functions											
Supply Power		Fairly large power storage ability required for sun occultation periods						Solar Panel prime source may be used	Articulated solar panels required to use that power source	Articulated solar panels required to use that source	
Track and Communicate									Fixed high gain antenna may be used	Antenna must track Earth	10^8 bits implies high bit rate to transmit data
Control and Sequence		Switch front panel power to battery upon loss of sun	Sequence rough antenna pointing angle command adjust capability	Rough antenna pointing control							
Guide					Accurate orbit injection will not required further trim	Liquid vernier system used for midcourse and orbit trim (limited capability for latter)	Adaptable to terminal guide or orbit trim modes				
Impart Impulse					No orbit trim multiple restart capability required	Restartable liquid vernier No variable loading option	(Restartable) Variable loading possible to increase payload				
Control Attitude		Sun oriented cruise and orbital config required						Inertial stabilize spacecraft when sun is occulted	Provision for high total integrated torque requirement must be made	Provision for high total integrated torque must be made	
Control Environment	RTG provides thermal energy for active control	Fixed solar orientation						Easy to insulate bus from direct sunlight	Movable sun shade required if complete sun insulation is desired	Sun shielding capability for most fairly inclined orbits	Recorder must be pressurized and sealed
Extension		Solar panels must be extended after launch				Eject burn out solid casing after use					
Articulation		Solar orientation implies need for articulated science platform	Accuracy of open loop antenna pointing may be tolerated	Closed loop antenna pointing accuracy required	Altitude measuring instrument servo to local vertical			a) Science Platform, b) Point antenna at earth either by update or closed loop servo	a) Planet sensor b) Alternate orientation may be advisable during cruise	a) Planet sensor b) Point high gain at the Earth c) Alternate mode during cruise	

SECTION VIII

SYSTEMS ANALYSIS

A. EARTH-MARS TRAJECTORIES

1. Basic Trajectory Characteristics

In dealing with a Mars orbiter mission, care must be taken to distinguish between two kinds of trajectories. One is the interplanetary trajectory and is associated with the transfer of the spacecraft from Earth to Mars. The other trajectory is that one associated with the motion of the orbiter in a satellite orbit about Mars. The characteristics and selection criteria of the former will be discussed in this section and those of the latter in Subsection B.

There are two major types of interplanetary trajectories: Type I being defined as those for which the heliocentric central transfer angle from launch to encounter is less than 180 degrees, and Type II those for which the transfer angle is greater than 180 degrees. Some of the important characteristics of these trajectories for the Mars 1969 opportunity are presented in Figures 8-1 through 8-6. All of these figures are plots of particular parameters as a function of launch date and arrival date, with Type I in the lower right and Type II in the upper left region. The definitions of the parameters plotted in these six figures are given in the following paragraph, and the significance of these parameters with respect to the mission will be discussed in succeeding paragraphs.

Figure 8-1 depicts curves of constant optimum orbiter mass for 20, 30 and 50-day firing periods assuming continuous variable propellant loading, and also curves of constant declination (DLA) of the outgoing geocentric asymptote. Figure 8-2 presents curves of constant hyperbolic excess velocity at Mars (VPL), and Figure 8-3 curves of constant geocentric injection energy (C_3). Figures 8-4 and 8-5 include angles which define the location of Earth and Sun, respectively, with respect to the incoming Mars asymptote, and Figure 8-6 is a repeat of the basic Figure 8-3. It will be noted that Figures 8-1, 8-2, 8-4 and 8-5 are on transparent overlays for ease in comparing various requirements.

The curves of constant orbiter mass are derived from tradeoffs between C_3 and VPL; the higher C_3 becomes, the lower VPL must become in order to achieve the same orbiter mass. The DLA curves are included in Figure 8-1 because of the limitations which they place on the Type I trajectories.

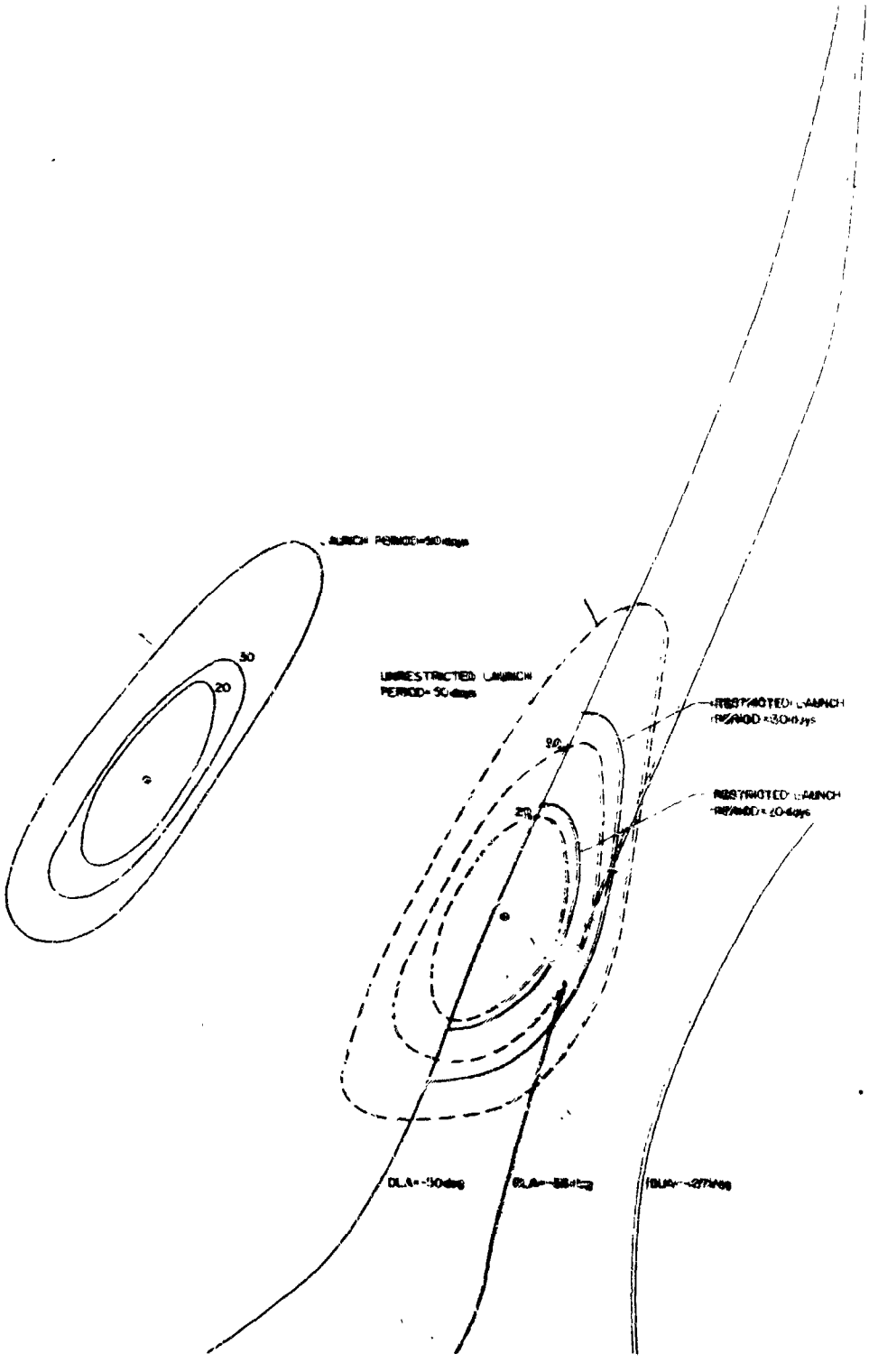
Specifically, the DLA restrictions are as follows: In past lunar and planetary missions, launch azimuths between 90 (due east) and 114 degrees (east-southeast) have been used. However, when, as in the case of the Mars 1969 Type I trajectories, the absolute magnitude of the declination of the outgoing asymptote becomes greater than that of the latitude of the launch site, there exists a band of launch azimuths symmetric about 90 degrees in which it is not possible to launch without performing prohibitive dog-leg maneuvers. The size of this band depends upon the declination of the outgoing asymptote and is depicted in Figure 8-7. From

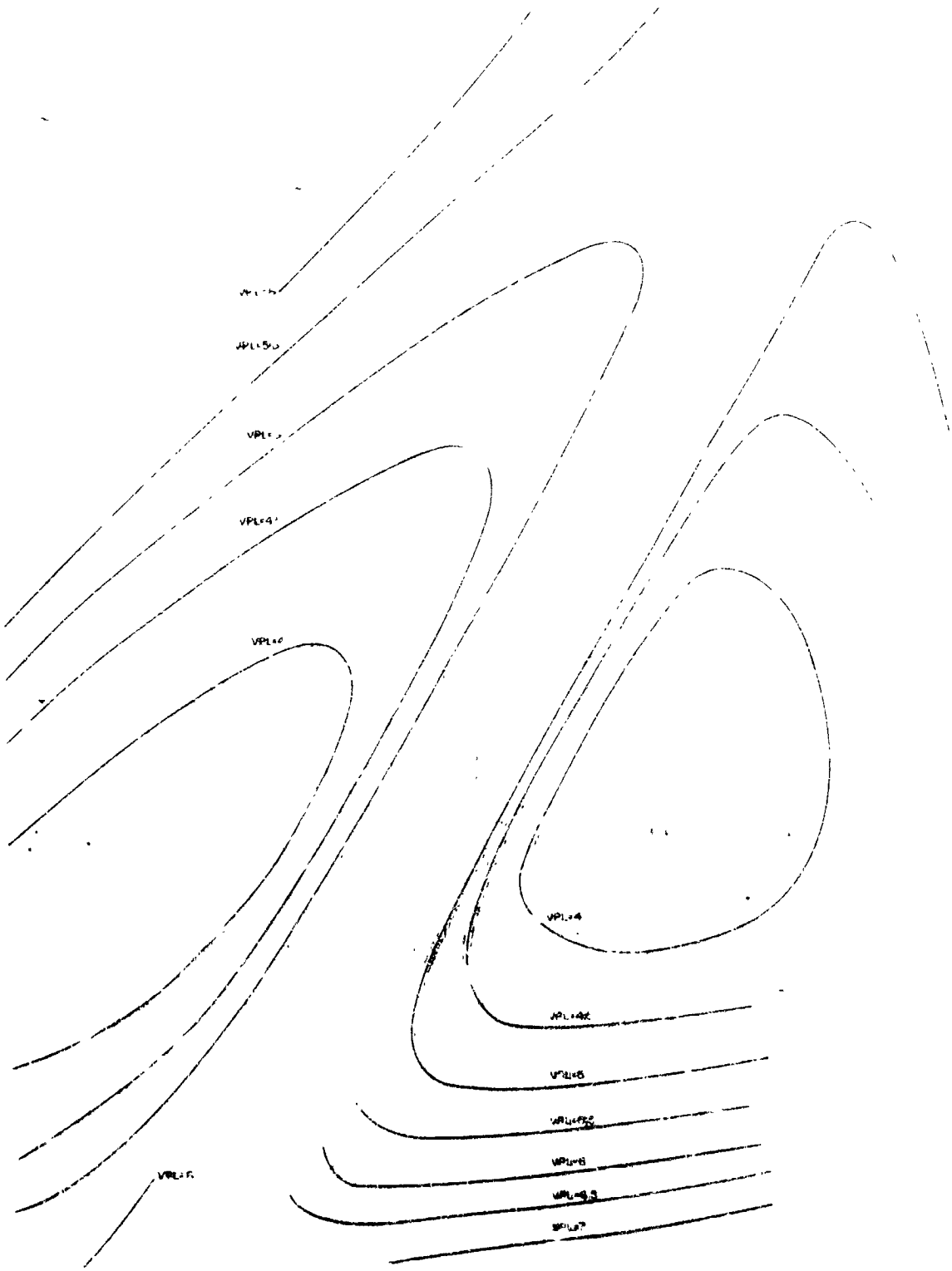
BLUE OVERLAY

Figure 8-1. Curves of Constant Orbiter Mass for Various Figure Periods (Variable Loading) p. 8-4

RED OVERLAY

Figure 8-2. Hyperbolic Excess Velocity Relative to Mars p. 8-5


30
20
UNRESTRICTED LAUNCH
PERIOD= 90 days
90
270


VPL=4
VPL=4x
VPL=5
VPL=5.5
VPL=6
VPL=6.5

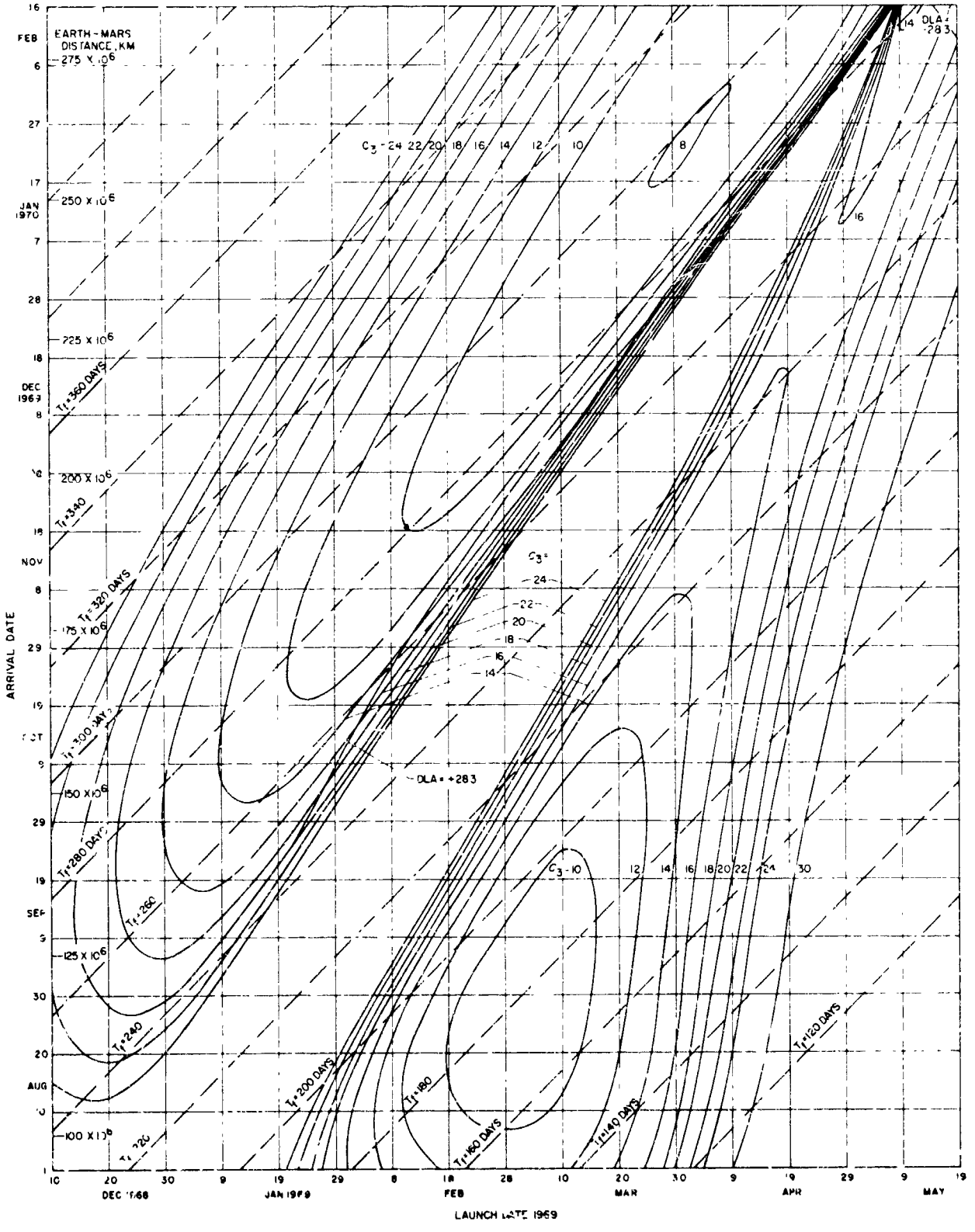


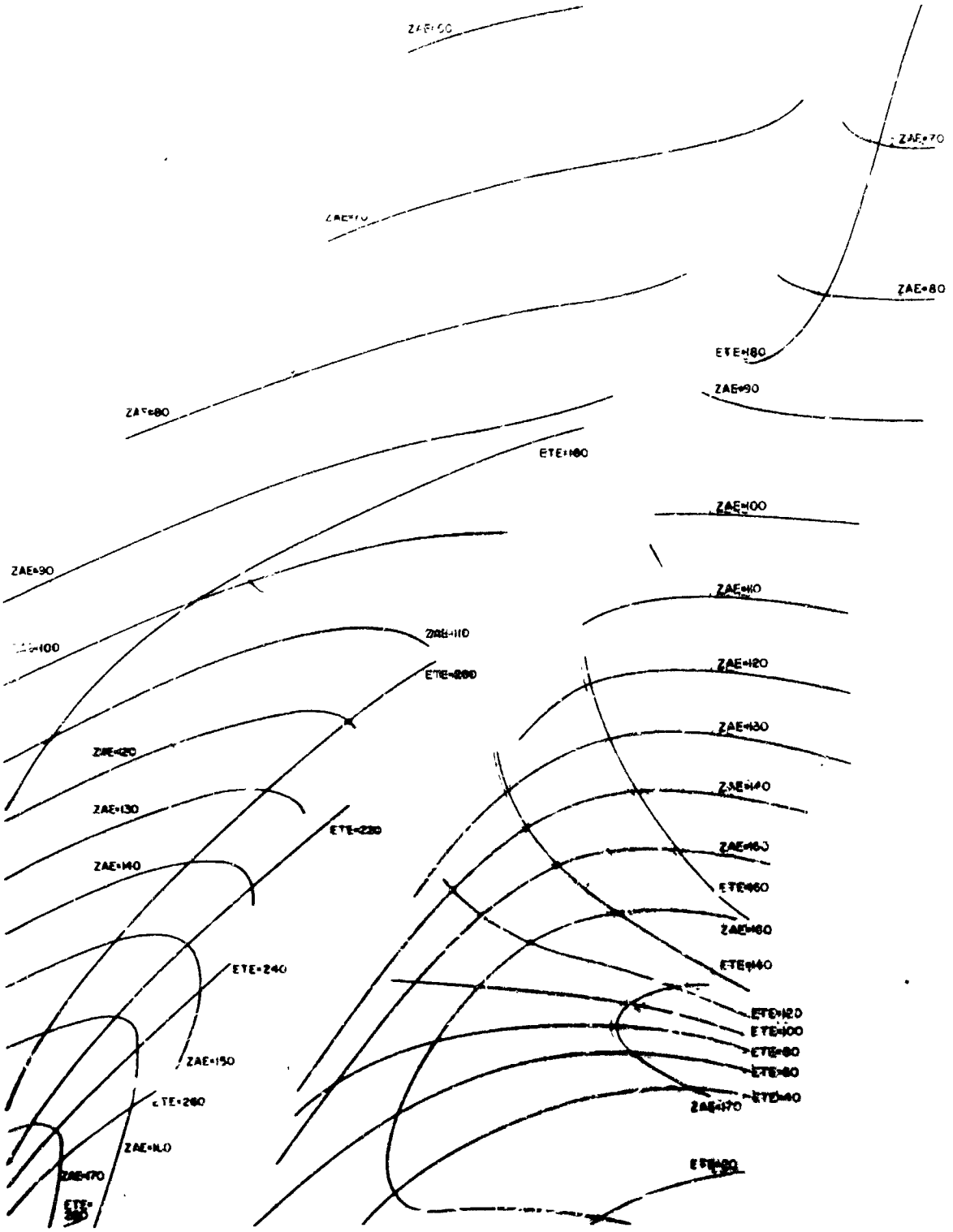
Figure 8-3. Basic Arrival Date vs Launch Date Trajectory Design Chart

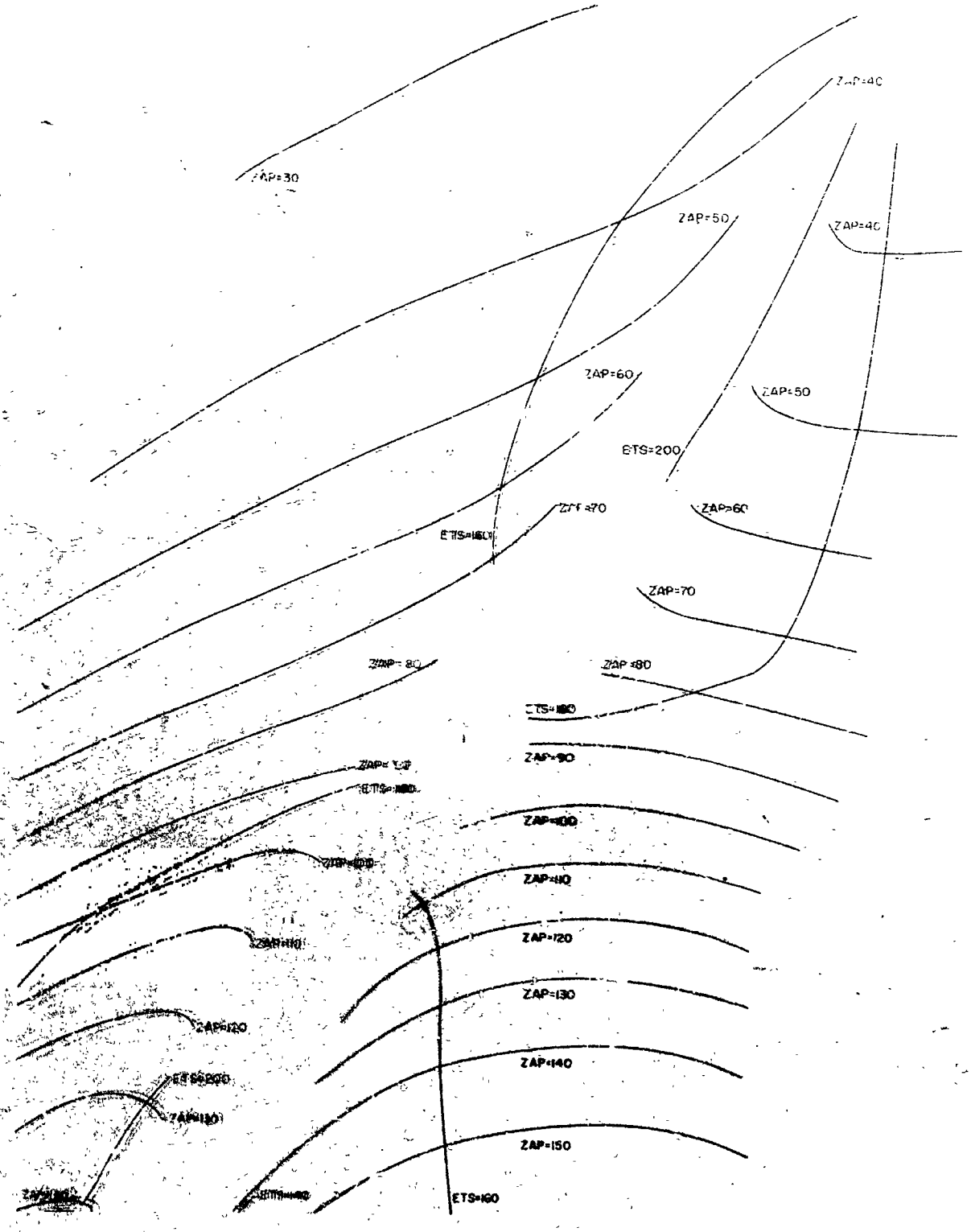
BLUE OVERLAY

Figure 8-4. Relationship of Mars-Earth Vector to Approach Asymptote p. 8-5

RED OVERLAY

Figure 8-5. Relationships of Mars-Sun Vector to Approach Asymptote p. 8-6


ZAE=50
ZAE=70
ZAE=80
ETE=180
ZAE=90
ETE=160
ZAE=90
ZAE=100
ZAE=110
ETE=200
ZAE=120
ZAE=130
ETE=220
ZAE=140
ETE=240
ZAE=150
ETE=260
ZAE=160
ZAE=170
ETE=
ZAE=100
ZAE=110
ZAE=120
ZAE=130
ZAE=140
ZAE=150
ETE=160
ZAE=160
ETE=140
ETE=120
ETE=100
ETE=80
ETE=60
ETE=40
ZAE=170
ETE=20


ZAP=30
ZAP=40
ZAP=50
ZAP=40
ZAP=60
ZAP=50
ETS=200
ZAP=70
ZAP=60
ETS=150
ZAP=70
ZAP=80
ZAP=80
ETS=180
ZAP=90
ZAP=100
ZAP=110
ZAP=120
ZAP=130
ZAP=140
ZAP=150
ETS=160

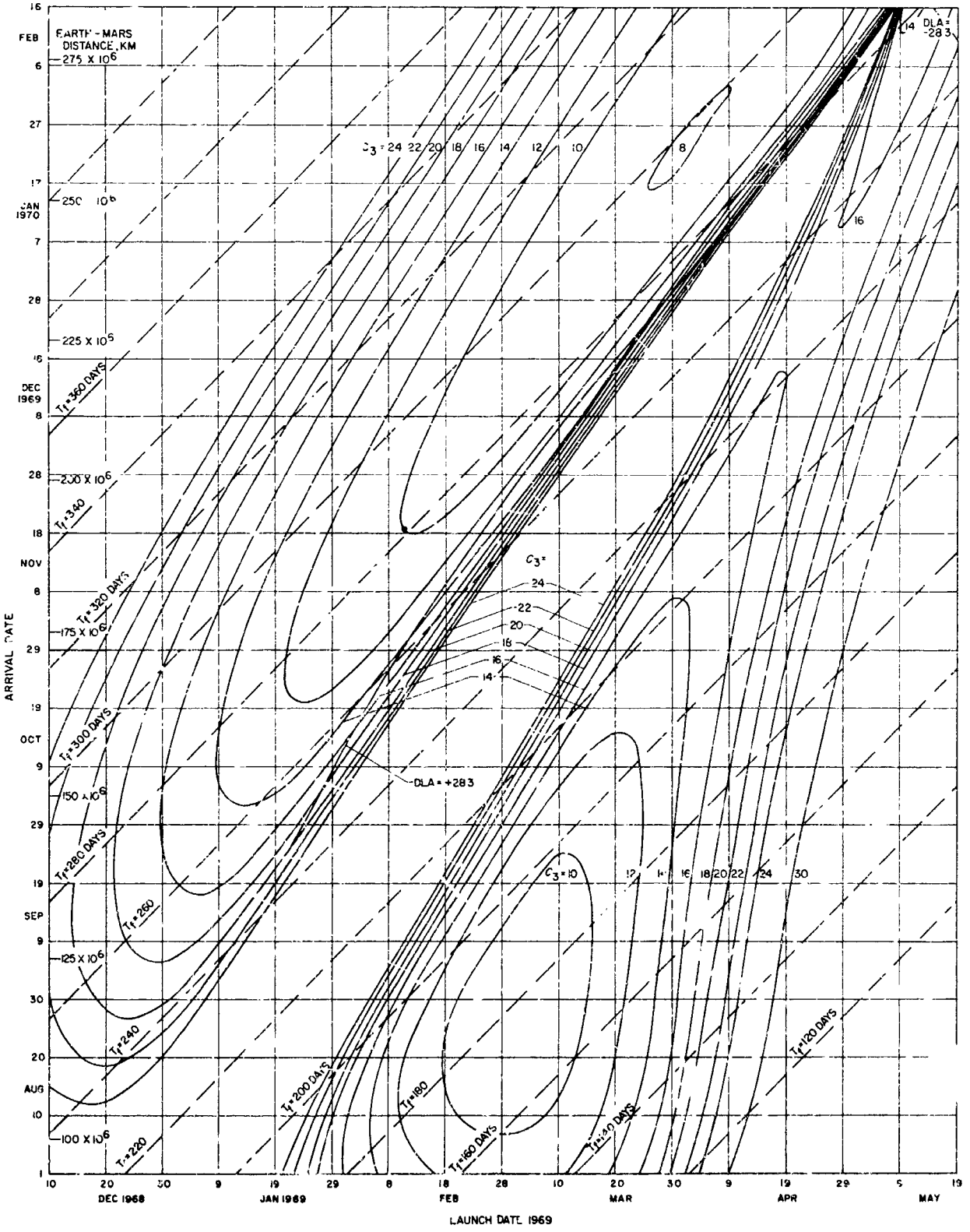


Figure 8-6. Basic Arrival Date vs Launch Date Trajectory Design Chart

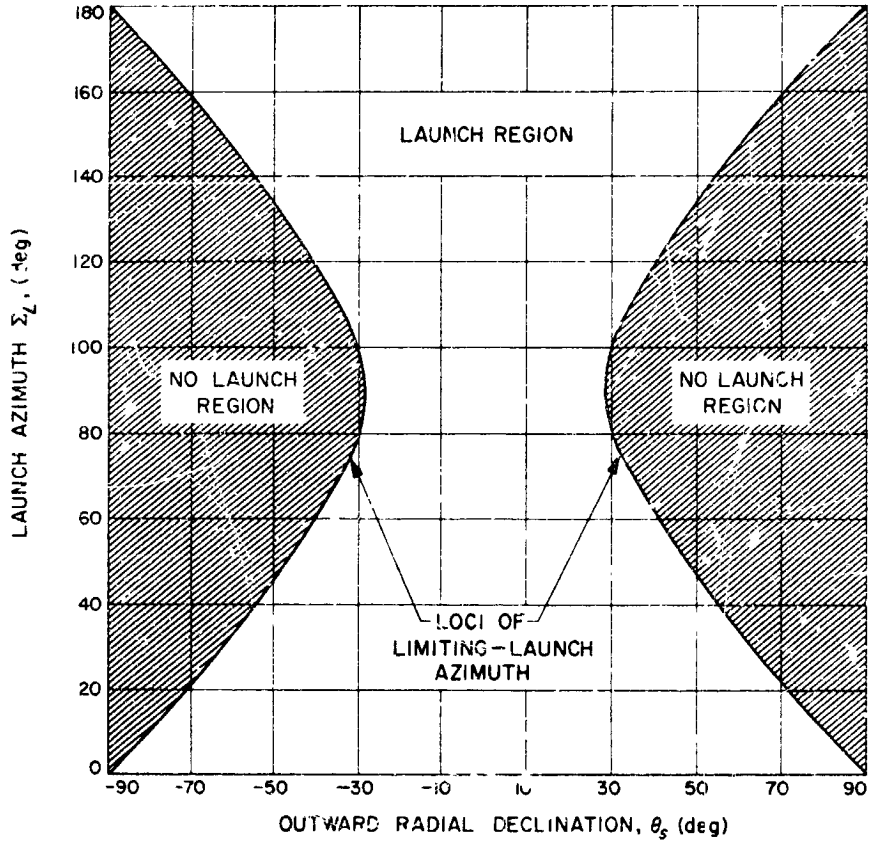


Figure 8-7. Limiting Launch Azimuth vs Outward Radial Declination for Cape Kennedy

this figure we see that for declinations greater in absolute magnitude than 36 degrees it is impossible to use launch azimuths between 66 degrees and 114 degrees, hence the traditional launch azimuths cannot be used. For DLA = -36 degrees and a launch azimuth of 114 degrees, extremely long coast times are required and would be particularly undesirable for Centaur. However, if it is possible to use launch azimuths as low as 45 degrees, then it is possible to achieve a two-hour launch window with short coast times if DLA $\geq$ - 50 degrees, (strictly speaking, $|DLA| \leq 50$ degrees), and a one-hour window if DLA $\geq$ -51 degrees. But, if launch azimuth is restricted to the 90 to 114 degree region in order to maintain minimum kill probability levels, then a one-hour window with a short coast arc can only be achieved if DLA $\geq$ -27 degrees. Because of the high injection energy required for such trajectories (see Figures 8-1 and 8-3) Type I trajectories are not useable if the traditional launch azimuths must be used, not even with the more powerful Saturn C1-B boost vehicle. Furthermore, direct ascent launches are not feasible for the 1969 mission because of the severe payload losses which occur whenever DLA is more than a few degrees away from -28.3 degrees.

The question of which launch azimuths can be used depends not only upon the required tracking and telemetry coverage but also upon the probability of the vehicle impacting an inhabited area due to a malfunction during boost. Allowable launch azimuths are specified by the range safety group at the Eastern Test Range, and involve a tradeoff between the mission requirements for a given launch azimuth and the impact probability for that particular azimuth. General Dynamics/Astronautics has performed a very thorough impact probability study for the basic Atlas/Centaur. Figure 8-8 shows the kill probability as a function of launch azimuth and has been taken from an unclassified page in the GD/A report (Reference 1). This curve is based upon an assumed reliability of 0 percent for the Centaur, so that if the reliability is actually R_c, then the kill probability for any azimuth is equal to $(1-R_c)$ times the number read off the curve. Therefore, if the Centaur has a reliability in 1969 of 90 percent, then the kill probabilities shown in Figure 8-8 will be reduced by an order of magnitude, thus resulting in a value of about 10^{-5} for a northeast launch at 45 degrees. Although the 45 degrees kill probability value is between one and two orders of magnitude higher than the 90 -114 degrees values, it is still a very small number. As a matter of fact it is roughly the same as the probability of tossing 17 consecutive heads with an unbiased coin. It would certainly be questionable to forbid the use of northeast launches and their associated short-flight-time Type I trajectories based upon a kill probability as low as 10^{-5}.

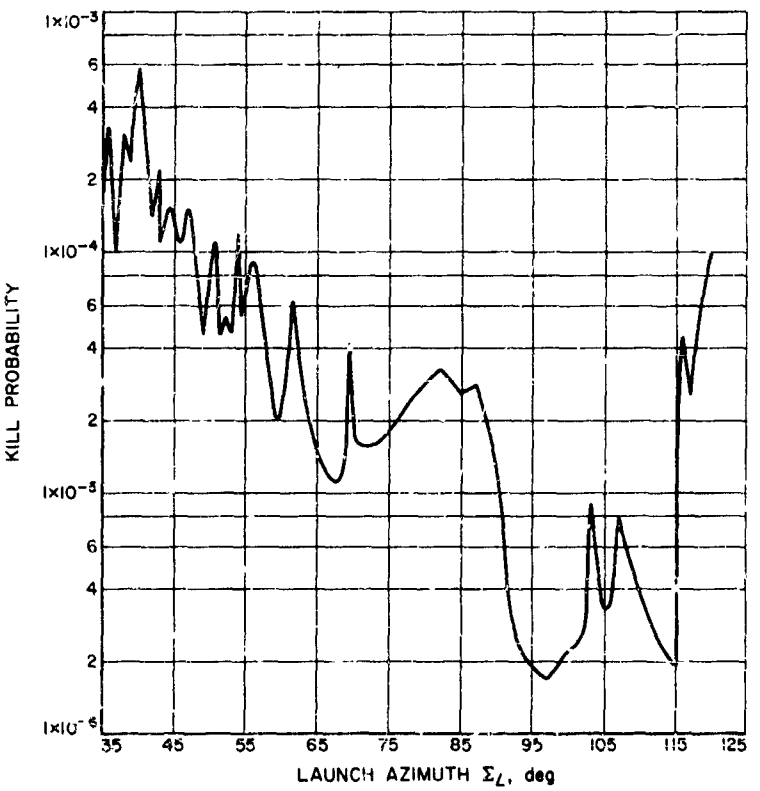


Figure 8-8. Kill Probability vs Launch Azimuth for Assumed Centaur Reliability of 0 Percent

Since the DLA = -50 degrees curve passes through the Type I maximum orbiter mass curves, some of the nominal launch period is lost. For this reason, 20 and 30-day launch period curves are also plotted for the constraint that DLA $\geq$ -50 degrees. It should be noted at this point that the DLA = -50 degrees value originated from its correspondence with a launch azimuth of about 46 degrees east of north, which was once believed to be a firm lower bound that could not be violated. Figure 8-8, however, shows launch azimuths down to 35 degrees. If these could be obtained, the Type I trajectory launch periods and achievable mass in orbit at Mars could be increased. A discussion of achievable orbiter mass is given in Subsection B.4.

As mentioned earlier, Figures 8-4 and 8-5 present orientation angles of Earth and Sun relative to the incoming asymptote at Mars. These angles are defined in Figure 8-9, where $\bar{S}$ is the incoming asymptote, $\bar{T}$ is normal to $\bar{S}$ and parallel to the ecliptic plane, and $\bar{R}$ is normal to $\bar{S}$ and $\bar{T}$. The coordinate origin is at the center of Mars. These figures are useful for determining the regions for which Earth and Mars are occulted for flyby and orbiter trajectories, and will be discussed further in Subsection A.3.

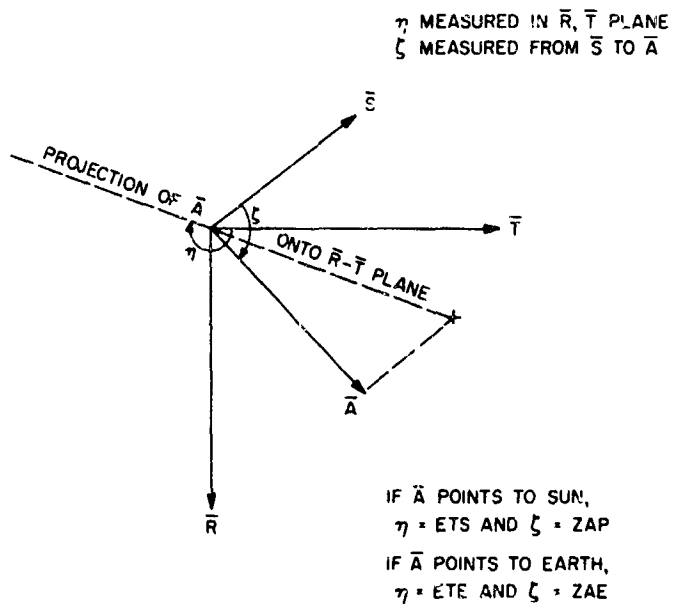


Figure 8-9. Definition of $\bar{R}$, $\bar{S}$, $\bar{T}$, Aiming Coordinates and Body Angles η and ζ

Quite generally, some of the main differences between the Type I and Type II trajectories giving near optimum orbiter mass for Mars 1969 are as follows: Type I's have flight times of about 185 days, arrive at Mars from early to late September, are always outside of the Earth's orbit, approach Mars from the sunlit side, and result in slightly less weight in orbit (than Type II) for firing periods in excess of about 15 days. The Type II's have flight times of about 270 days, arrive in middle to late October, dip inside the Earth's orbit during the early part of the flight (see Figure 8-11), and approach Mars near the terminator but slightly from the dark side. The fact that the Type II orbits dip inside the Earth's orbit introduces a difficulty in that the low-gain antenna is pointing away from the Earth during the early portion of the flight if it is in the Mariner 64 configuration. This will probably result in the need for a second low-gain antenna. A prohibitive decrease in payload would result from trying to correct this situation by going to different launch and arrival dates (i.e., a second antenna would weigh much less than the decrease in payload resulting from using trajectories which require only one antenna.

In order to perform a more detailed study of the characteristics and problems of the orbiter mission, six interplanetary trajectories were chosen for further study, three Type I and three Type II. These trajectories represent first, middle and last launch dates for the variable propellant loading, optimum mass in orbit, 30-day launch period (assuming the -50 degrees DLA constraint for Type I). An attempt was made to minimize the variation in arrival date so as to keep the approach geometry relatively constant. Important trajectory characteristics are presented in Table 8-1.

The explanation for the various columns is as follows:

LAUNCH DATE	Self-explanatory
ARRIVAL DATE	Self-explanatory
FLIGHT TIME	Self-explanatory
C_3	Twice the total geocentric injection energy per unit mass, km^2/sec^2
VPL, V_∞	Hyperbolic excess velocity at Mars, km/sec
ETE	Project the Mars-Earth vector onto the $\overline{R}$-$\overline{T}$ aiming plane. Then ETE is the angle measured clockwise from $\overline{T}$ to the negative of this projection
ZAE	Angle at Mars between the approach asymptote $\overline{S}$ and the Mars-Earth vector
ETS, ZAP	The same as for ETE and ZAE except for the Sun rather than the Earth

Table 8-1. Trajectory Characteristics

Launch Date (1969)	Arrival Date (1969)	Flight Time (days)	C_3 (km^2/sec^2)	VPL (km/sec)	ETE (deg) / ZAE (deg)	ETS (deg) / ZAP (deg)	CD_E (10^6 km) / CD_{E+90} / CD_{E+180}	SD_E (10^6 km) / SD_{E+90} / SD_{E+180}	GCE (deg) / EPS (deg)	SG1 (km) / SG2 (km) / θ (deg)	Type
1-9	10-14	278	14.0	3.74	186	176	159	207	279	5200	II-A
					125	80	245	213	46	520	
							340	231		25	
1-24	10-23	272	12.0	3.83	190	173	167	207	280	5900	II-B
					120	77	255	215	45	530	
							348	232		29	
2-7	11-2	268	11.7	4.05	190	169	176	207	281	6700	II-C
					113	73	267	216	45	560	
							357	233		29	
3-7	9-7	184	9.0	4.48	96	166	126	209	273	2200	I-A
					164	131	207	209	46	760	
							300	223		47	
3-20	9-24	188	11.0	3.85	143	172	141	207	276	1470	I-B
					156	114	227	211	46	800	
							320	225		129	
4-4	10-3	182	15.9	3.73	162	176	149	207	277	1940	I-C
					147	102	235	212	46	580	
							330	228		160	

CD_E, CD_{E+90}, CD_{E+180}	Earth-Mars distance at encounter, encounter plus 90 days, and encounter plus 180 days
SD_E, SD_{E+90}, SD_{E+180}	Same as above except for Sun-Mars distance rather than Earth-Mars distance
GCE	Clock angle of the Earth at encounter
EPS	Earth-probe-Sun angle at encounter
SG1	Semi-major axis of dispersion ellipse* in $\overline{R}$-$\overline{T}$ plane, assuming a spherically distributed 0.10-meter/sec velocity error in each of 3 orthogonal directions at a few days past injection
SG2	Semi-minor axis of dispersion ellipse in $\overline{R}$-$\overline{T}$ plane
θ	Angle between the $\overline{T}$-axis and SG1 axis measured clockwise from $\overline{T}$

One major item to be noticed in this table is the fact that the Earth and Sun positions relative to the incoming asymptote (ETE, ZAE, etc.) vary more rapidly for the Type I trajectories than for the Type II. However, it should also be noted that the Type I trajectories have flight times nearly 3 months shorter than the Type II. In addition, the distances from the Sun and the Earth are larger for the Type II. Although the dispersion ellipses are larger for Type II, the orientation angle of the ellipse is steady for Type II and varying for Type I.

It should perhaps be mentioned in connection with fixed propellant loading that although the payload would be decreased over the variable loading case, it would still be possible to keep the arrival date relatively constant, just as it would be possible with variable loading by decreasing the required payload, and hence the arrival geometry. Furthermore, the optimum launch period would not vary by much from the variable loading case.

2. Heliocentric Arrival Conditions

The heliocentric locations of the Earth and Mars for the Type I and Type II bands of arrival dates are presented in Figure 8-10. It is interesting to note that the Earth-Mars-Sun angle for all arrivals is around 45 to 46 degrees, thus simplifying the mechanization of the high-gain antenna. Figures 8-11 through 8-14 illustrate the variations during heliocentric transfer

*Projection of dispersion ellipsoid onto $\overline{R}$-$\overline{T}$ plane.

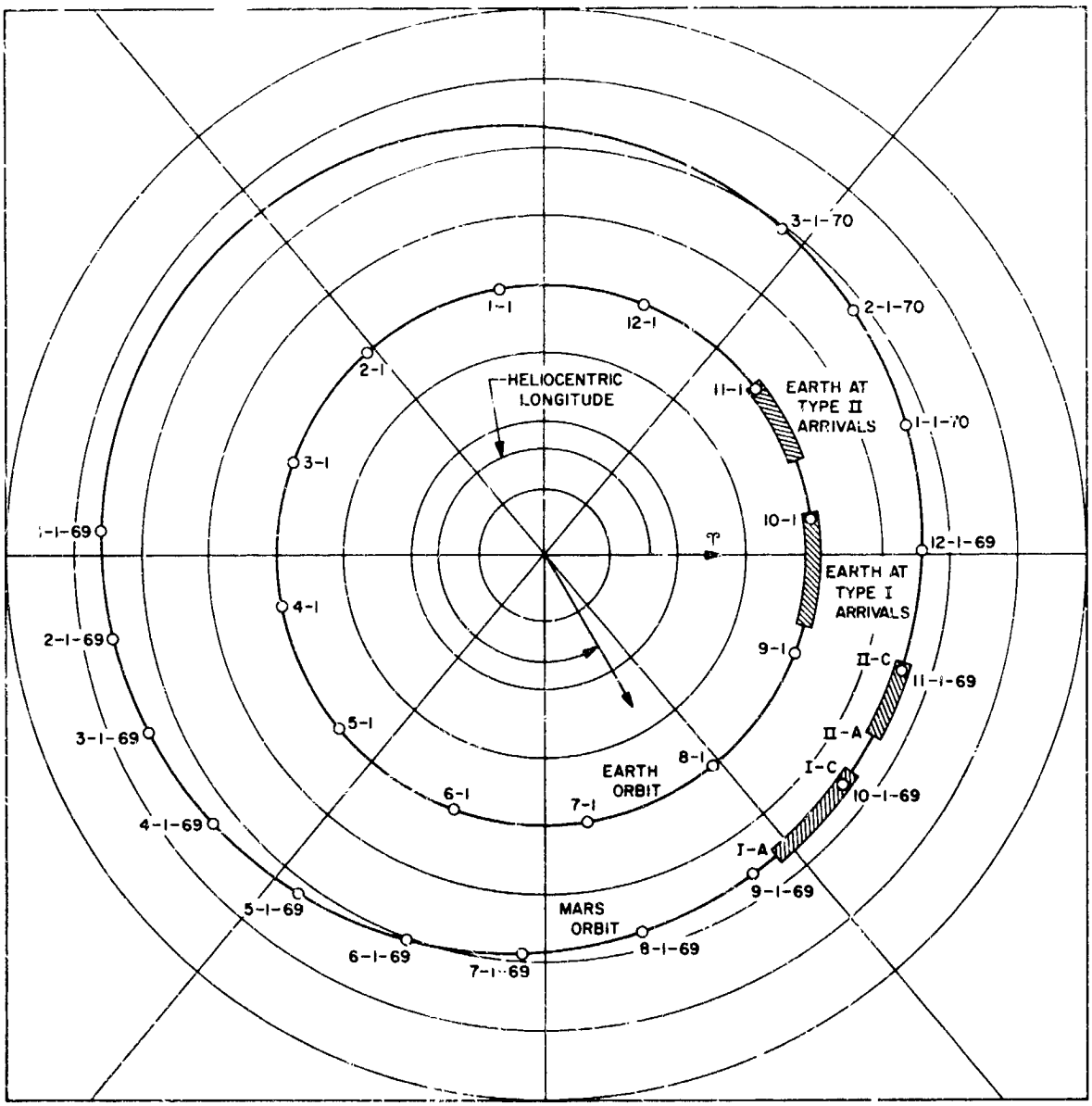


Figure 8-10. Heliocentric Arrival Geometry

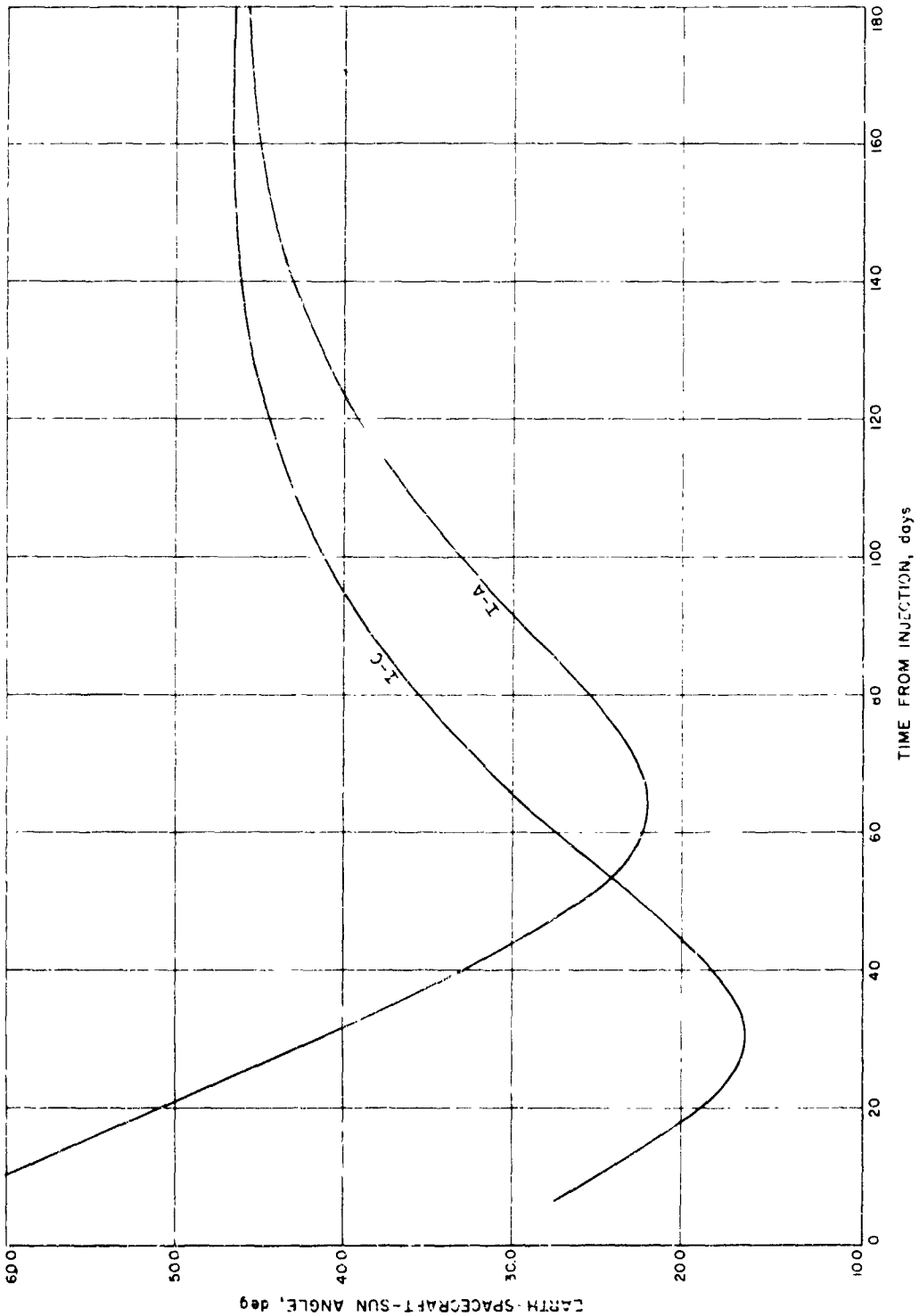


Figure 8-11. Cone Angle of Earth vs Time from Injection for Transits 1-A and 1-C

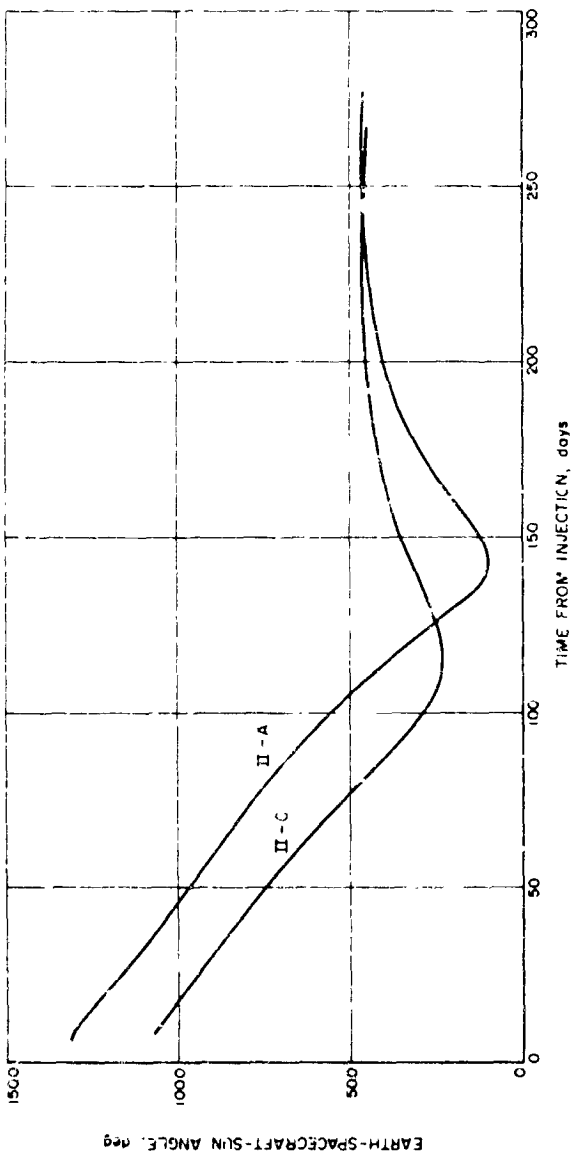


Figure 3-12. Earth Cone Angle vs Time from Injection for Type II Trajectories II-A and II-C

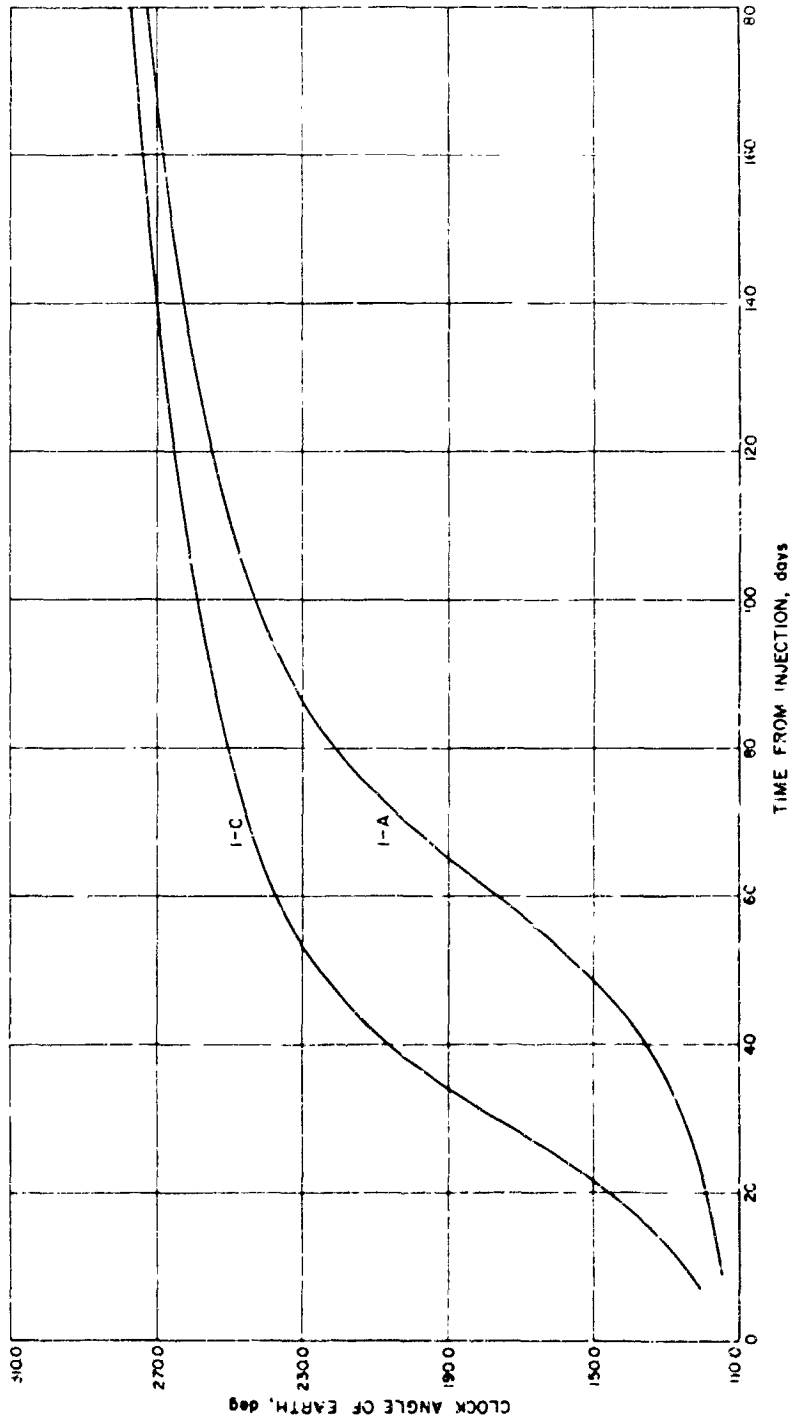


Figure 8-13. Clock Angle of the Earth vs Time from Injection for Trajectories I-A and I-C

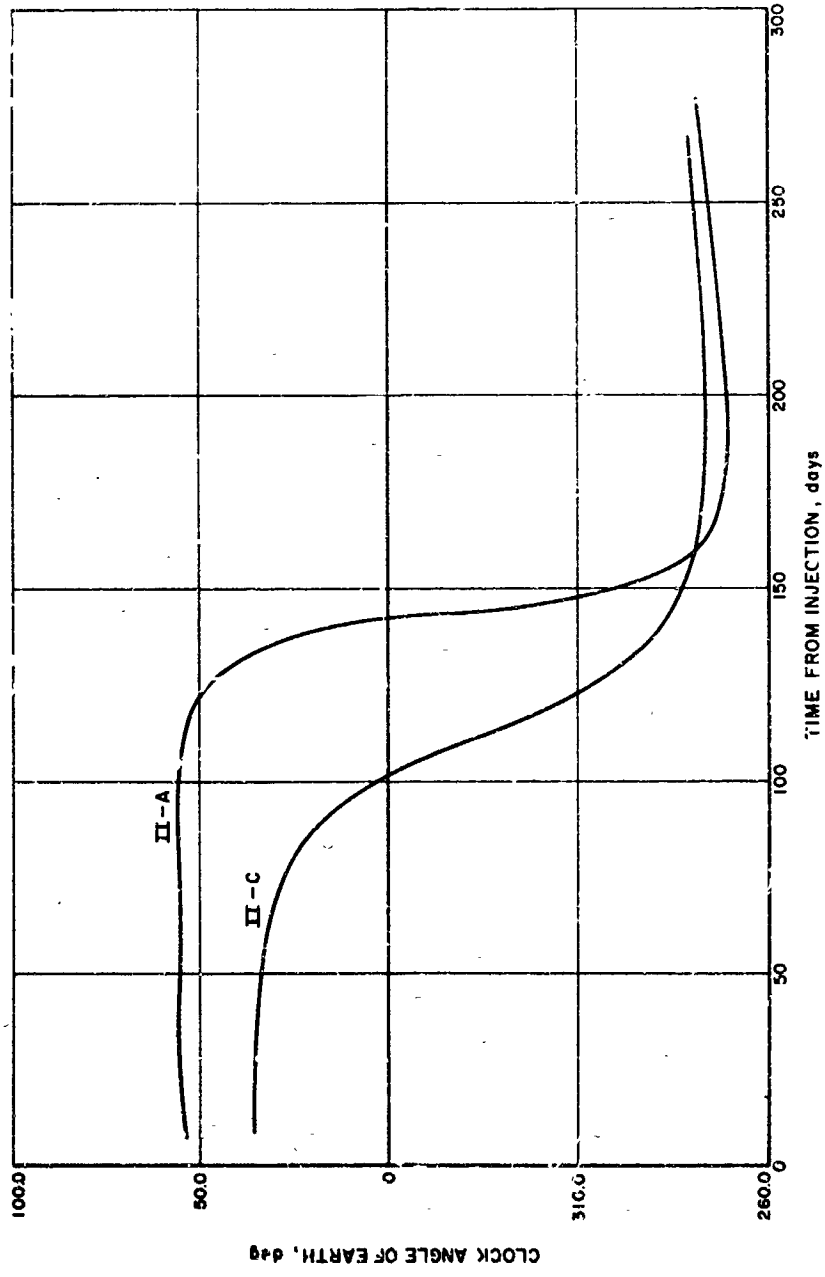


Figure 8-14. Clock Angle of the Earth vs Time from Injection for Trajectories II-A and II-C

of the Earth-spacecraft Sun angle (cone angle of Earth) and clock angle of the Earth for transits I-A, I-C, II-A, and II-C. Figure 8-15 shows the behavior of Earth-Mars distance and cone and clock angle of the Earth (as measured at Mars) as a function of calendar date.

It has been stated by NASA that the minimum mission (in orbit) lifetime should be about 3 months with a desired lifetime of 6 months. One might then logically ask when the major surface changes or "wave of darkening" occurs. In Reference 2, De Vaucouleurs makes the following remarks:

> "By marking the heliocentric longitude η_0 at which the upwards trend of the variation curves becomes noticeable (at some arbitrary level above the minimum intensity), i.e., by plotting the points of incipient darkening, it is even possible to trace with fair accuracy the propagation of the 'front' of a darkening wave progressing evenly northward from the south polar area.
>
> "This wave starts near the end of the southern winter (η_0 = 250 degrees) at about latitude ϕ = -60 degrees; it then spreads and crosses the equator before mid-spring (η_0 = 290 to 300 degrees), reaching latitude +40 degrees before the end of the southern spring (η_0 = 330 degrees). The front of the wave thus covers 100 degrees in latitude (6000 km) in about 130 days, travelling at some 45 km per day (or 0.5 m per sec). There is a possibility that the propagation might not be exactly synchronous at all longitudes around the globe, but the observational material is not yet sufficient to confirm this."

The heliocentric longitude of Mars for the currently assumed Type I transfer arrival dates varies from about 307 to 325 degrees, while for the Type II arrivals this range is 330 to 345 degrees. It would appear that only the Type I transfers arrive before the "end" of the northward progression of the wave of darkening. Even then, however, it may be questionable if these changes can be seen as the wave of darkening will be at roughly 15 degrees north latitude, but the orbit periapsis will be at some 40 degrees south with primary coverage in the southern hemisphere. It would seem wiser, however, to assure good photographic coverage of the interesting Mars latitudes just south of the equator and take "pot luck" on being able to see a change in a given surface feature as opposed to covering the less interesting northerly latitude region with the slim chance of seeing a given area twice and observing a change. Figure 8-16 has been extracted from Reference 2 and illustrates the northward progression of the wave of darkening as a function of the heliocentric longitude of Mars. This figure would seem to suggest the desirability of arriving earlier in 1969 when the rate of increasing darkening is a maximum in the southern hemisphere, in order to see the greatest difference in darkness intensity levels during a given orbit lifetime following encounter. It is important to note at this point, however, that other interpretations (by industry study groups) of the preferred arrival time have been proposed which suggest that the current arrival dates are attractive. Most of these points of view are based upon Figure 4 of Reference 3 by J.H. Focas of the National Observatory of Athens. Perhaps it is felt that if the orbit lifetime is as long as six months, the darkening intensity will have diminished in certain areas so that the

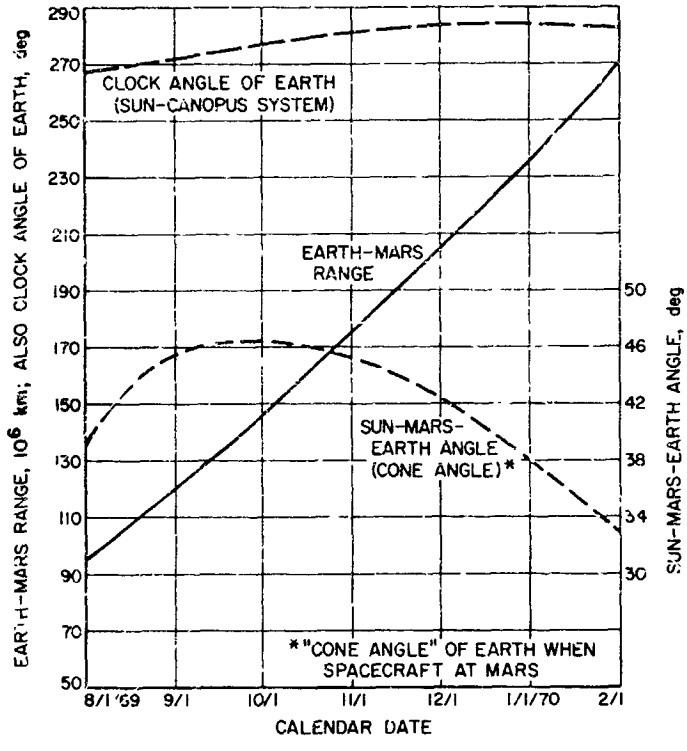
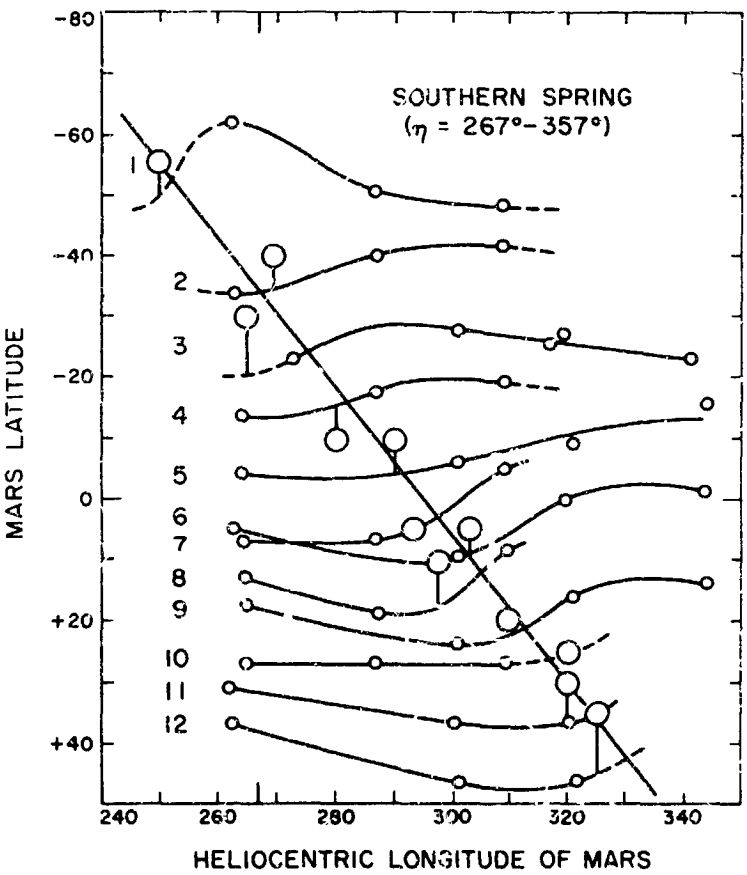


Figure 8-15. Earth-Mars Range, Cone and Clock Angles of the Earth vs Calendar Date

observation of a change might be possible. Before placing a requirement on the orbit lifetime of 3 to 6 months, however, this whole question involving the likelihood of "observing" a seasonal change should be carefully investigated. Such questions should be answered as (a) is the optimum arrival period at the time of maximum rate of increasing darkening, or after the level of greatest darkening has occurred? (b) what is the likelihood of observing the same area twice at a suitable interval? and (c) even if a given area is observed twice, does the probability of detecting a change depend upon also having similar lighting conditions and viewing angles for both observations?

3. Approach Aiming Diagrams

Figures 8-4 and 8-5 give the orientation angles of Earth and Sun with respect to the incoming asymptote. These angles determine the regions of Earth and Sun occultation for flyby trajectories, and ETE and ETS can be partially used for determining the occultation regions for orbiters. For example, if the Earth-Mars line lies in the orbit plane, the Earth will be occulted during part of the orbit. The factor which determines whether a body is occulted or not for an orbiter depends upon the size and orientation of the ellipse with respect



Seasonal variations of intensity in the dark areas of the surface of Mars at different latitudes during the southern spring in 1939, after G. DE VAUCOULEURS (Peridier Obs., 1945).

For greater clarity the curves are slightly displaced in latitude, but the circles marking the time at which each spot begins to darken are placed at the correct latitude.
The alignment of these circles demonstrates the existence and the propagation of a seasonal wave of darkening spreading northwards from the south polar region.
(1): Depressio Hellespontica; (2): Hellespontus; (3): Mare Sirenum; (4): Aurorae Sinus; (5): Sinus Sabaeus; (6): Ganges; (7): Euphrates (south); (8): Syrtis Major; (9): Lunae Lacus; (10): Euphrates (north); (11): Nilokeras; (12): Niliacus Lacus.

Figure 8-16. Northward Progression of Wave of Darkening

to the Body-Mars line. Figures 8-17, 8-18, and 8-19 give the occultation zones of Earth, Sun and Canopus for the trajectories II-B, 1-A, and I-C, as defined in Table 8-1. Only the middle Type II trajectory is included because the arrival geometry variation is sufficiently small that this plot is representative of the other Type II trajectories. Since Type I approach geometry varies much more rapidly, the first and last days are plotted. In these figures EPM is the Earth-probe-near-limb of Mars angle, SPM is the same for the Sun, and CPM the same for Canopus. As was stressed before, these figures really only give the occultation zones for flyby trajectories; however, for an orbiter passing through a particular occultation zone, the body associated with that zone will probably be occulted, assuming no plane change is made at orbit injection.

REFERENCES

A-1. GD/A Report No. BTD 64-145 entitled "Impact Probability Study for Atlas/Centaur Missions" (CONFIDENTIAL), dated September 23, 1964.

A-2. "Physics of the Planet Mars," Gerald De Vaucouleurs, Faber and Faber Limited, pages 243-248.

A-3. Planetary and Space Science, Volume 9, July 1962, "Seasonal Evolution of the Fine Structure of the Dark Areas of Mars," J.H. Focas, pages 371-381.

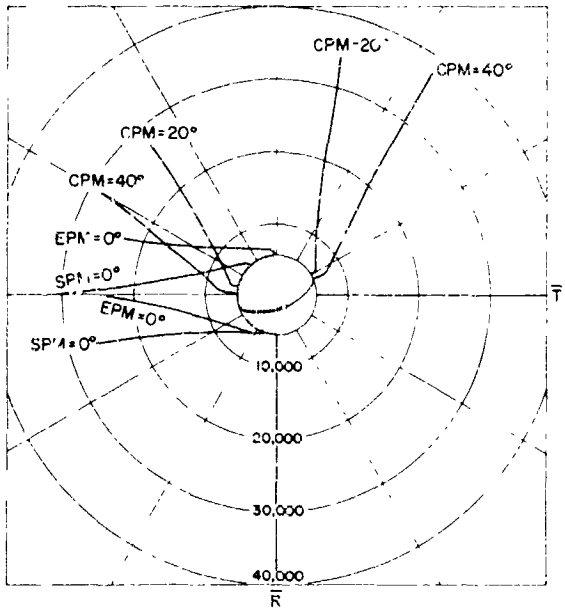


Figure 8-17. Approach Aiming Diagram for Transit II-B

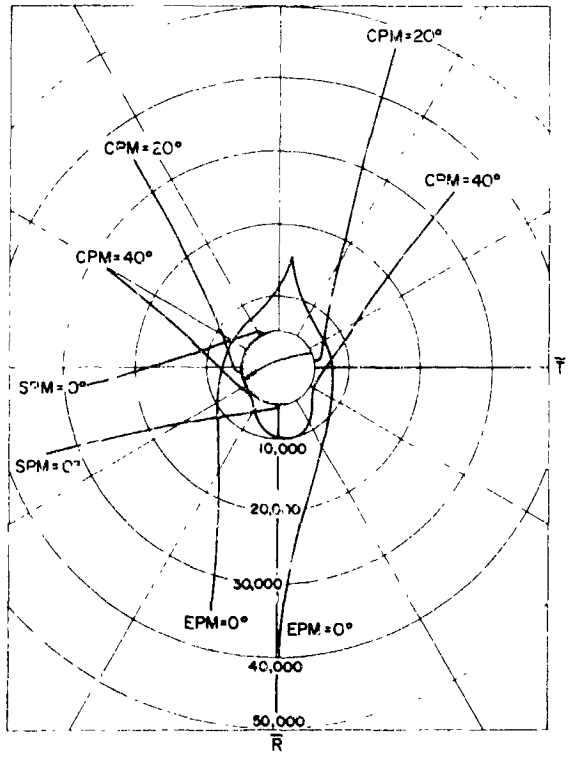


Figure 8-18. Approach Aiming Diagram for Transit I-A

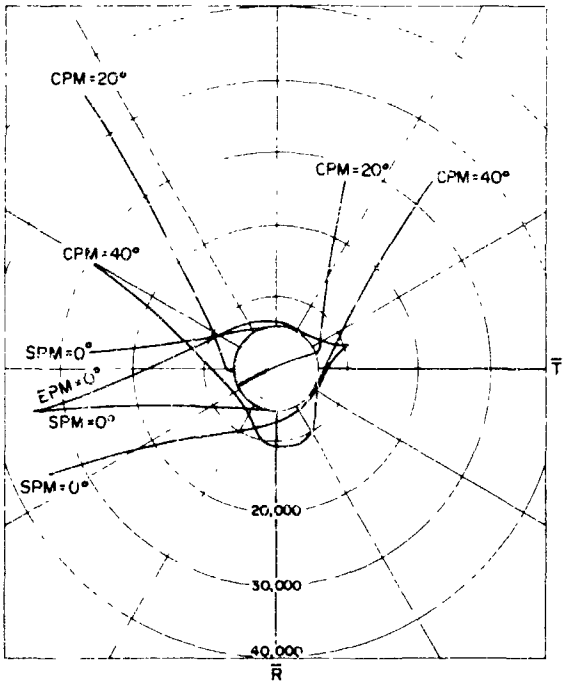


Figure 8-19. Approach Aiming Diagram for Transit I-C

B. SATELLITE ORBIT SELECTION

1. General Orbit Considerations

A large number of considerations are involved in attempting to select the optimum parameter values for a satellite orbit about Mars. This section will describe the most important parameters and indicate those factors which most strongly influence their selection. During the discussion, it will be noted that one of the most significant constraints in designing an orbiter mission about Mars involves the selection of a periapsis altitude which is felt to be of sufficient height as to ensure a probability of 10^{-4} that an unsterile orbiter will decay into the Mars atmosphere prior to contamination by a later mission. Depending upon the assumed high-altitude density model, practically any value of periapsis altitude from about 1000 km to 5000 km would be necessary to provide a lifetime of the order of 50 years. This subject will be covered in more detail in Subsection B. 3.

Figure 8-20 illustrates the basic parameters that are customarily used to define the shape and orientation of a planetary satellite orbit or capture orbit. It should be noted, however, that periapsis altitude has been shown rather than periapsis radius or distance from the planet center. This has been done because such considerations as drag effects upon orbit lifetime, instrument height above the surface, and photographic resolution make altitude a more useful parameter than distance from the planet center. In this study a value of 3400 km has been assumed for the Mars radius, although a more recent value of around 3378 km has been proposed. In Figure 8-20, the assumed value for the oblateness coefficient, J, is 0.00292 for Mars. Referring to the generalized situation shown in Figure 8-21, it can be seen that a variety of aiming points might be considered which result in different orbit inclinations with respect to the Mars equator, different latitudes for the location of the sub-periapsis point, different lighting conditions near periapsis, different orbit precession rates due to Mars oblateness, different occultation times for other bodies, and several other varying characteristics. In the absence of yaw or out-of-plane maneuvers in performing the orbit insertion, the family of all possible satellite orbit planes contains the approach asymptote vector $\overline{S}$.

a. Orbit Selection Constraints

In order to obtain preliminary orbit profiles, an attempt was made to achieve as many of the following conditions as possible:

1) It is desirable that Sun occultation be avoided for as long as possible.
2) In order to perform a useful Earth occultation experiment, it is desired that the Earth be occulted during each orbit for several days (up to perhaps a month) following initial orbit establishment, but the occultation time per orbit must not be large enough to reduce in any significant manner that portion of the orbit period needed for data transmission.

3) It is desirable that the angle (measured at the spacecraft) between Canopus and the near planet limb remain above some prespecified value (region of perhaps 20 to 50 degrees, depending upon adjustment policy or tradeoff between limiting field-of-view clock and cone angle values).

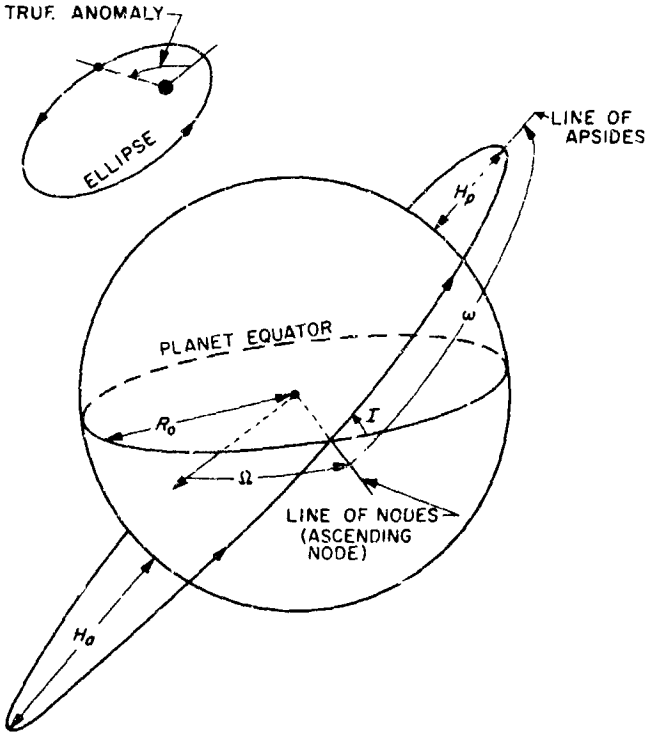
4) It is desirable that the following lighting and planetary coverage conditions exist simultaneously somewhere "reasonably" near periapsis:

   a) The Sun-orbiter planet angle should lie between about 100 and 140 degrees.

   b) The orbiter should be at a Mars latitude of between about 40 degrees south and 10 degrees north.

   c) The orbiter altitude should preferably not exceed about 2 to 3 times the periapsis altitude.

   The last condition is met as long as the orbiter true anomaly (in-plane angle from periapsis) is within about 60 to 80 degrees from periapsis ($2 \times H_p$) or about 80 to 100 degrees from periapsis ($3 \times H_p$).



SECULAR RATES

$\dot{a} \approx \dot{e} \approx \dot{I} \approx 0$

$\dot{\Omega} = -\frac{nJ}{p^2}\cos I$

$\dot{\omega} = \frac{nJ}{p^2}\left(2 - \frac{5}{2}\sin^2 I\right)$

$p = a(1-e^2)/R_0$

Figure 8-20. Fundamental Orbit Parameters

5) It is desirable that nodal and apsidal precession rates due to Mars oblateness tend to improve as many of the above conditions as reasonably possible.

6) The currently required orbit lifetime must be at least 50 years to satisfy the contamination constraint. The actual orbit lifetime will depend primarily upon estimates of atmospheric drag and secondarily upon third-body gravitational effects and other possible perturbations. The possibility of reducing the orbit lifetime requirement to below 50 years is discussed in Subsection B.3.

b. Periapsis Altitude Consideration

The selection of values for the key orbit parameters is influenced by many considerations. For example, the following factors govern the choice of a nominal periapsis altitude:

1) The strongest factor is probably the required orbit lifetime which depend primarily upon the high-altitude density profile and secondarily upon the apoapsis altitude. Another factor which must be considered in the prediction of orbit lifetime is the long-term effect of the Sun (third-body influence) upon the orbit periapsis altitude. During the short course of

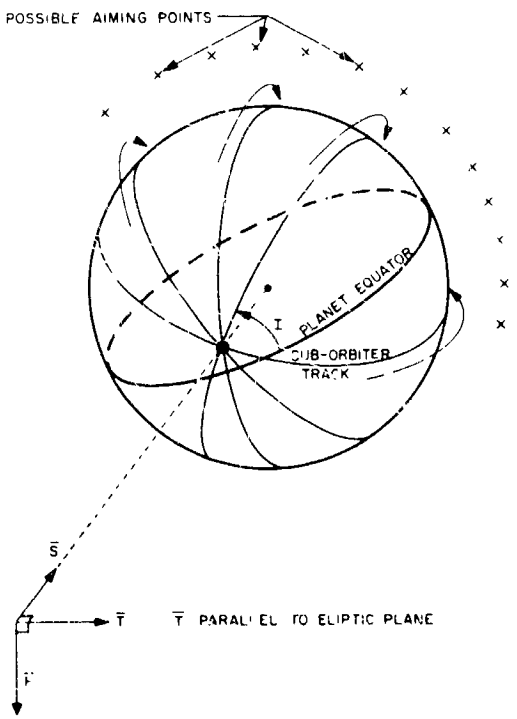


Figure 8-21. Rotation of Possible Orbit Planes About Approach Asymptote

this study, there has not been sufficient time to complete an adequate analysis in this area. Cursory consideration has indicated, however, that third-body effects can cause the periapsis altitude to diminish by as much as 50 to 200 km during a 50 year period for orbits with large semi-major axes. Finally, the question has been asked whether the moons of Mars could perturb the orbit path significantly. This problem has not been studied but it is expected that the probability of occurrence of such a perturbation is extremely small.

2) Another important factor which influences the choice of periapsis altitude is the estimated dispersion in this parameter due to orbit determination errors, midcourse guidance errors, and orbit insertion guidance errors. The importance of obtaining accurate estimates for these errors increases with the desire to achieve as low a periapsis altitude as possible consistent with the orbit lifetime requirements. Current estimates for the combined 3σ error in periapsis altitude due to the above sources are in the region of 500 to 1000 km. Assuming aiming point biasing and two midcourse corrections, the lower number could be associated with the Type I 1969 Mars trajectories and the higher number with the more sensitive Type II transits.

3) For a given apoapsis altitude, the in-orbit payload capability can be increased by lowering the periapsis altitude. This can become very important whenever the mission performance capability is marginal, as is the case for this study which has assumed a fixed Atlas/Centaur launch vehicle with an in-orbit active payload requirement on the order of 1000 lbs.

4) The scientific desire to orbit close to the Mars surface in order to obtain high resolution coverage obviously affects the selection of the nominal periapsis altitude. Do we want to get as close as guidance accuracy permits? What percentage error in controlling periapsis altitude is acceptable? For small H_p and large H_a, does the relatively high periapsis velocity cause image blur problems?

5) Any consideration of orbit trim affects the selection of both the initial and final periapsis altitudes. When mission orbiter weight capability is not marginal and can afford the luxury of additional retro fuel, an orbit-trim adjustment policy offers certain clear advantages. By choosing initially a conservative periapsis altitude, the danger of impact is minimized. Further, after determining the initial orbital elements accurately, an orbit trim maneuver can be utilized to achieve better control of the final periapsis altitude. An orbit trim policy has not been seriously considered for this study due to the tight weight situation which exists between the launch vehicle performance and desired orbiter weight estimates.

6) For a given orbit inclination and apoapsis distance, the periapsis altitude can be selected so as to increase the chances that certain bodies will or

will not be occulted to the orbiter by Mars. For the 1969 orbit profiles which currently appear the most attractive, lowering H_p improves the chances of ensuring Earth occultation but, at the same time, brings Canopus closer to the limb of Mars.

7) If it should be required to point a fixed or partially restricted high-gain antenna towards the Earth while in the orbit insertion attitude, such a constraint can be met with less difficulty if the added trajectory bending associated with lower periapsis altitudes can be utilized.

c. Apoapsis Altitude Consideration

The following factors influence the selection of an acceptable apoapsis altitude:

1) In-orbit payload requirements may require the use of a large apoapsis altitude. This appears to be the case for the current study but could of course change given a larger booster vehicle.
2) Orbit sensitivity (variations in apoapsis altitude, orbit period, etc.) to orbit insertion errors increases as the nominal apoapsis altitude is raised. Until a detailed error analysis has been completed, it would probably not be wise at this time to consider nominal apoapsis altitudes much higher than about 50,000 km in order to ensure capture.
3) For a given orbit inclination and periapsis altitude, the selection of a high apoapsis altitude reduces the likelihood of occultation of certain bodies. Also, a high value for H_a permits a lower value of H_p to be chosen which will still result in the prescribed orbit lifetime in the presence of atmospheric drag. As orbit period obviously increases with higher values of H_a, this gives ground facilities more time to prepare for each major scientific data collection sequence near periapsis.
4) Orbit precession rates (nodal regression $\dot{\Omega}$ and apsidal precession $\dot{\omega}$) due to Mars oblateness depend strongly upon the semi-major axis and therefore upon the apoapsis altitude. With careful planning, this orbit precession can usually be used to advantage by either causing the sub-periapsis point to move into more favorable latitude regions, by trying to delay Sun occultation, or by trying to reduce certain third-body effects. With very high apoapsis altitudes, however, the precession rates are too low to be of any significant value. Although there is no magic apoapsis altitude above which the rates can be disregarded, for apoapsis altitudes above about 20,000 km the precession rates are less than the apparent motion of the Sun of about 0.5 deg/day (due to Mars motion about Sun).
5) If it were possible to achieve the exact nominal H_p and H_a values, it would be possible to select an orbital period which results in evenly mapping the

planet surface as well as returning to the same area after a given period of time such as one month, for example, in order to increase the chances of observing a seasonal change. Guidance errors would in general preclude the accurate establishment of a preselected orbit period, but it still might be worthwhile to try nominally to achieve certain orbit periods. It can be shown that if the orbital period, P, is related to the planet period of rotation, T, by

$$P = (I \pm KN^{-1})^{-1} T$$

where I is any integer and K is any integer such that K and N are not both divisible by a common integer, then the orbital tracks will be equally spaced (in longitude) and will return to the same point on the Mars surface at the completion of exactly N planet days. In the presence of orbit plane precession due to oblateness, an effective planet period should actually be used and would be given by

$$T = 2\pi (\alpha - \dot{\Omega})^{-1}$$

where α is the planetary sidereal angular velocity and $\dot{\Omega}$ is the nodal precession rate of the orbit plane.

d. Orbit Inclination Considerations

The selection of orbit inclination to the Mars equator depends upon such considerations as:

1) From a scientific coverage standpoint, it is desirable that the orbit inclination not be less than about 30 degrees to the Mars equator. Although advanced surveillance orbiter missions with high data rate capabilities might well require much higher inclinations in order to map a larger portion of the Martian surface, the lower inclinations appear more favorable for the current study for the following reasons. First of all, given that only a reasonable number of pictures can be returned, these should presumably concentrate on the most interesting surface feature regions which lie within 30 to 40 degrees of the Mars equator (to the south). By using orbit inclinations close to these latitude regions, longer dwell times over these preferred latitudes can be achieved thus increasing the chances of being able to find some point along the orbit path which exhibits both a reasonable altitude and attractive lighting conditions. Also, the probability is increased of being able to observe a given area twice during the mission lifetime in order to look for possible changes.

2) The choice of orbit inclination obviously affects the occultation geometry with other bodies such as the Sun, Earth, and Canopus. Low inclinations increase the chances of occulting the former two bodies but leaving Canopus well in view, while high inclinations tend to have the opposite effect. We have to select low inclinations carefully so that Earth occultation will be achieved for some period of time but with no Sun occultation. Also, it must be remembered that, as the Mars equator is inclined some 25 degrees to the ecliptic plane, orbits having equal north and south inclinations to the Mars equator have quite different inclinations to the ecliptic plane, and it is this latter reference plane which more appropriately governs the occultation geometry with the Sun, Earth, and Canopus.

3) The orbit inclination affects the nodal and apsidal precession rates due to Mars oblateness. To first order, there is no movement of the line of apsides within the orbit plane for I = 63.4 degrees. For I > 63.4 degrees, apsidal movement is opposite to that of the orbiter and, for I < 63.4 degrees, apsidal movement is in the same direction as the orbiter. The nodal regression rate is zero for I = 90 degrees and increases as I decreases. Of possible importance is evaluating third-body effects, the sum $\dot{\Omega} + \dot{\omega}$ approaches zero for I = 46.4 degrees.

4) The desire to point a fixed or partially restricted high-gain antenna towards Earth during the orbit insertion orientation of the spacecraft places certain constraints on the selection of the orbit inclination. This subject is discussed later in more detail.

5) At this time, it appears that the only constraints which should be placed upon the choice of orbits from the standpoint of Earth-based determination of the satellite orbit are: (a) it is desirable that the angular rate of the orbit plane with respect to the Earth-planet line-of-sight be nonzero, (b) the orbit inclination with respect to the plane generated by the Earth-planet line-of-sight should be nonzero (this latter plane is very close to the ecliptic plane), and (c) the orbit plane should not be perpendicular to the Earth-Mars line. There is a very low probability that either of these situations would occur exactly, and slight departures from the above situations are generally acceptable.

e. Periapsis Location Consideration

The location of periapsis is clearly important for very elliptical orbits and is influenced by such considerations as:

1) It is desirable that periapsis occur on the Earth-side of Mars so that the entire orbit insertion maneuver can be covered. The 1969 Mars approach

geometry and aiming regions satisfy this condition for both the Type I and Type II orbits.

2) The location of the sub-periapsis point should preferably occur in the Mars latitude band between about 40 degrees south to 10 degrees north. In order to avoid orbits which exhibit Sun occultation, however, aiming points usually have to be chosen which result in initial periapsis latitudes slightly outside of this desired band. The orbits selected for this study (see Section B. 6) have $i < 63.4$ degrees, and, therefore, produce a movement of the sub-periapsis point towards the desired region. One must, however, trade off the sub-periapsis latitude location against the desired lighting conditions beneath the orbiter.

3) It should be noted that this study has assumed that the orbit periapsis coincides with the natural periapsis of the approach of hyperbola In the actual case, however, either the orbit insertion guidance mode employed or errors in the insertion maneuver can result in rotating this apsidal line by several degrees in the plane of motion. With extra retro fuel, one could consider an intended rotation of the apsidal line for the purpose of initially locating the sub-periapsis point over some preferred region. For the marginal mission (from a weight viewpoint) being considered, however, rotations in excess of about 10 to 20 degrees are probably not feasible.

2. Approach Geometry

Flyby approach aiming diagrams have been presented previously in Figures 8-17, 8-18, and 8-19 for some of the 1969 transfer trajectories. As can be seen from these figures, the Type I trajectories approach Mars from the lighted side while the Type II trajectories approach from slightly on the dark side Figure 8-22 illustrates the basic approach geometry (plan view and along $\bar{S}$) for transits I-A, I-C, and II-B. The Type I approach asympotes are inclined some 9 to 14 degrees to the ecliptic plane (coming from below), while the Type II trajectories approach Mars from 15 to 26 degrees above the ecliptic plane. Figures 4-58 through 4-60 of EPD-139, Volume III, illustrate the Type II approach geometry, although the actual orbit profiles selected to satisfy the ground rules of the current study differ significantly from those shown in EPD-139.

As the Type I trajectories approach Mars from the lighted side (relative motion with respect to Mars), aiming points also on this side result in direct motion of the orbiter about Mars and periapsis occurs on the lighted side but initially closer to the evening terminator. As the Type II trajectories approach from slightly on the dark side of the morning terminator, direct orbits result in periapsis being located about halfway between the two terminators. After a period of a few weeks, however, the motion of Mars about the Sun moves the morning terminator closer to the sub-periapsis point. Most of this information is covered in more detail in Subsection B. 6.

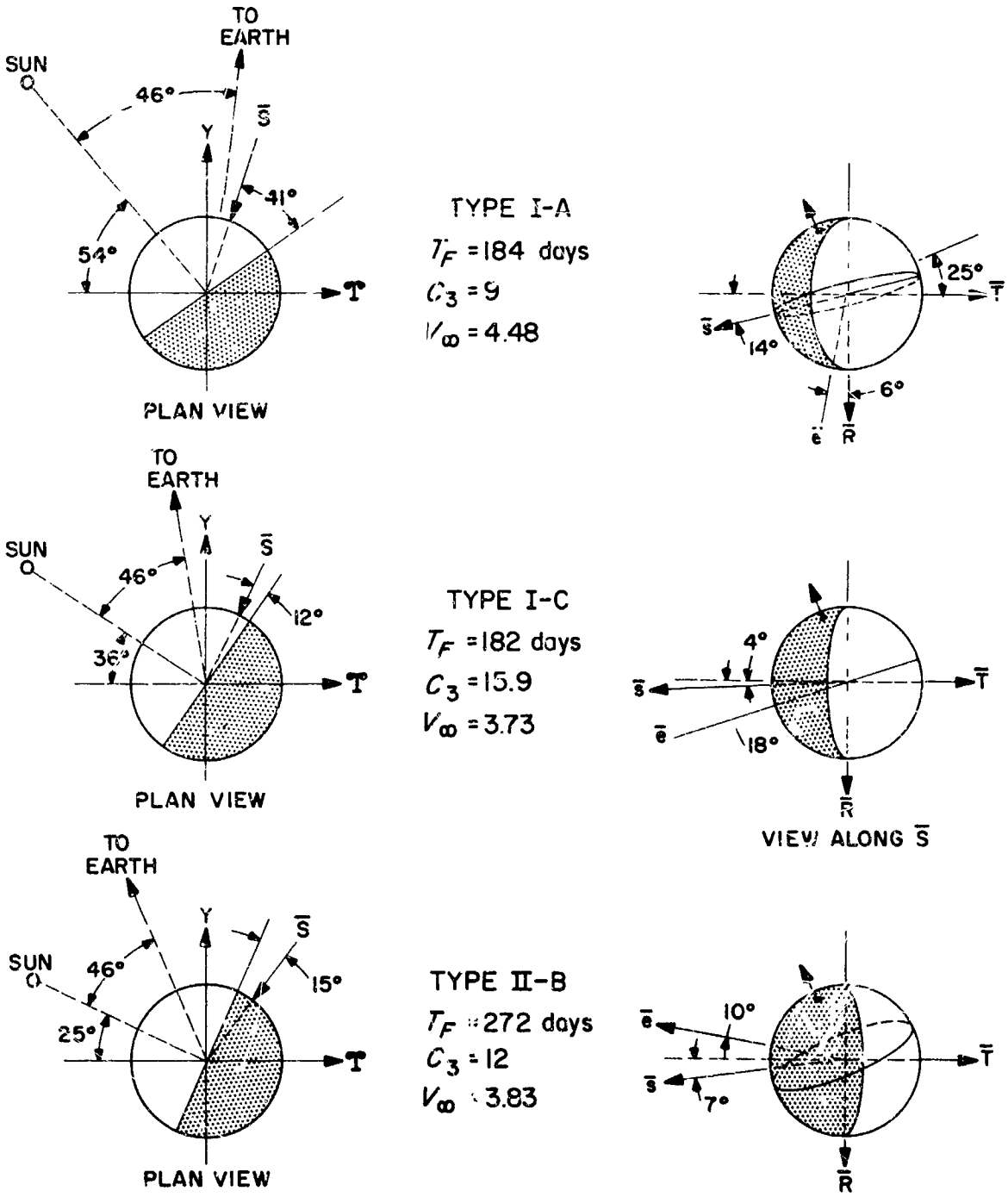


Figure 8-22. Approach Geometry for Trajectories I-A, 1-C, II-B

A short study was made to determine the effect upon the selection of orbiter aiming points of requiring that the high-gain antenna point towards the Earth during the orbit insertion orientation of the spacecraft. The ground rules assumed for this study were as follows.

1) The retro motor has its axis along the spacecraft roll axis.
2) The retro velocity decrement is removed in a direction opposite to that of the velocity vector at periapsis of the approach hyperbola.
3) The feed axis of the high-gain antenna can lie on a cone of 10° half angle, and the axis of this cone is 38° off the spacecraft roll axis.
4) The antenna pattern has a useful half-beam width of 6 degrees.
5) Periapsis altitude = 1500 km.

The six reference trajectories were investigated and the results are presented in Table 8-2 Generally speaking, the Type II trajectories are more favorable in satisfying the antenna-pointing constraint. It can be seen from Table 8-2 that, if the antenna feed axis can lie anywhere on the 10-degree conical surface, then both the Type I and Type II desired aiming regions satisfy the antenna-pointing constraint, although the Type I cases are just barely acceptable. If the antenna must be left in its encounter position, then the desired Type I aiming points are not acceptable whereas some of the later-launched Type II cases are acceptable. However, if the periapsis altitude is increased to 4000 km as a result of more recent atmospheric lifetime calculations, the reduced trajectory bending will degrade somewhat the above results. If the mission weight situation was not marginal and if extra retro fuel was available, one could consider less efficient orbit insertion attitudes which did not apply the retro velocity parallel to the periapsis velocity vector in order to point the antenna more closely in the direction of the Earth.

Table 8-2
Permissible Aiming Regions For
Pointing High-Gain Antenna Towards Earth

Trajectory	I-A	I-B	I-C	II-A	II-B	II-C
Desired Aiming Region Boundaries (deg)	15→25	15→25	12→25	5→20	5→20	5→20
Permissible Boundaries For Any Position On Cone (deg)	0→192	22→264	24→300	-72→88	-57→77	-36→55
Permissible Boundaries For High-Gain Antenna In Encounter Position Only (deg)	No	90→196	75→250	-66→-32 48→82	-52→-4 24→72	-28→48
All angles measured clockwise from T.						

Changing now to the subject of Earth occultation with an orbiter, Figures 8-17 through 8-19 are primarily intended for use in selecting aiming regions for a flyby trajectory. Therefore, it was necessary to use a different program to generate Earth occultation aiming zones for various satellite orbits about Mars. Assuming an orbit apoapsis altitude of 50,000 km, Figure 8-23 illustrates a portion of the Earth occultation aiming regions for certain of the reference trajectories. Of the Type II trajectories, only II-B has been shown as it is representative of II-A and II-C. In Subsection B.3, atmospheric lifetime calculations indicate that it may be necessary to maintain the orbit periapsis altitude as high as 1000 km above the Mars surface in order to guarantee a lifetime of 50 years. Therefore, if we must choose aiming points which lie outside of this altitude limit yet inside of the Earth occulation regions shown in Figure 8-23, tight control of the aiming point will be required. As a matter of fact, for 4000 by 50,000-km orbits, no Earth occultation is achieved for trajectories I-B and I-C unless the aiming points are moved to the less desirable northerly direct orbit profiles. Thus we find again that the atmospheric model assumed has a strong influence not only upon the science desires to get close to Mars, but also upon the possibility of performing Earth occultation related experiments.

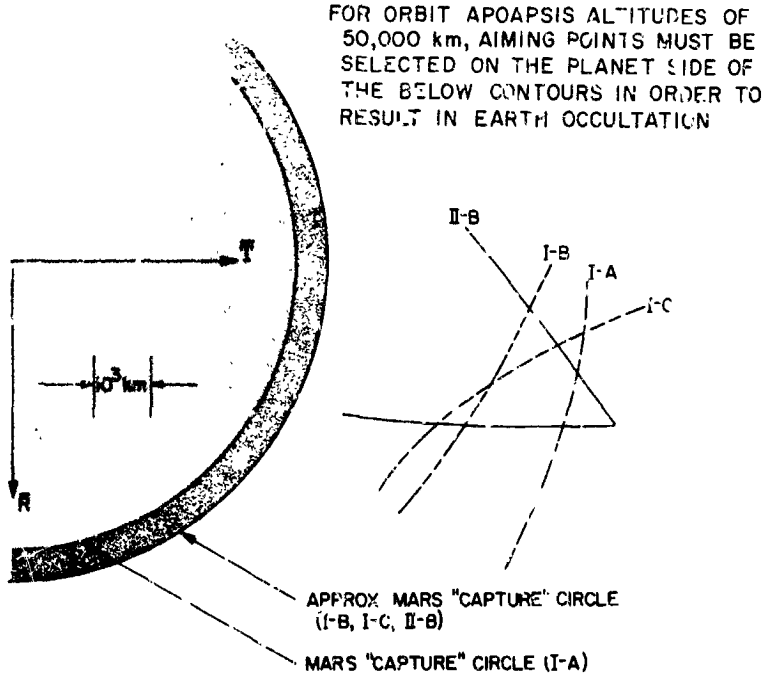


Figure 8-23. Earth Occultation Aiming Regions

3. Orbit Lifetime Results

Several factors can cause the periapsis altitude of a satellite orbit to vary:

1) atmospheric drag
2) solar gravitation
3) planet oblateness
4) solar radiation pressure

When the satellite is at low altitudes, the dominant effect is atmospheric drag. Although estimates of the near-surface atmospheric densities are believed known to a factor of perhaps two or three, the high altitude densities are uncertain by several orders of magnitude. In order to demonstrate the effect of these large uncertainties, two atmospheric models were chosen for this study. Model I (Figure 8-24) was generated at JPL (Reference B-1) and corresponds to a more or less nominal density profile, whereas Model II (Figure 8-25) was generated by the NASA Mars Standard Atmospheric Committee (Reference B-2) and corresponds to a "maximum" density profile. The results of this study are summarized in Table 8-3 and Figures 8-26 and 8-27. From Table 8-3, it can be seen that for a 50-year lifetime, a ballistic coefficient $m/C_DA = .18$ slugs/ft^2, and $H_a = 50,000$ km, H_p can vary from 750 to 3700 km, or a factor of five, depending upon the atmospheric model assumed. Clearly, it is therefore essential to define a specific upper atmospheric density profile and an orbiter sterilization policy which are acceptable to the scientific community, particularly to the biologists. It is also important to specify a particular atmospheric model in order to help standardize orbit lifetime computations which will be obtained by the various agencies or companies who participate in Mars orbiter studies.

The orbit lifetime results were generated by using two IBM-1620 computer programs (Reference B-3) written at JPL. The first program computes the time required for an elliptical orbit to decay into a circular orbit, while the second program then calculates the additional time required for the circular orbit to decay to the Mars surface. In addition to the atmospheric density, the orbit lifetime also depends upon the ballistic coefficient of the orbiter. The ballistic coefficient is defined by

$$k = \frac{m}{C_D A}$$

where C_D is the drag coefficient (assumed equal to 2 for the high altitude regime), A is the effective area, and m is the orbiter mass. Orbit lifetime varies directly with the ballistic coefficient, and doubling k doubles the orbit lifetime, etc. If we let k_r be the ballistic coefficient of the orbiter as viewed along the roll axis and k_n that normal to the roll axis, then a long-term effective value for the ballistic coefficient is given approximately by

$$k_{eff} = \frac{\pi}{2}\left[\frac{2}{\pi}\left(k_r^{-1} + k_n^{-1}\right) + k_n^{-1}\right]^{-1}$$

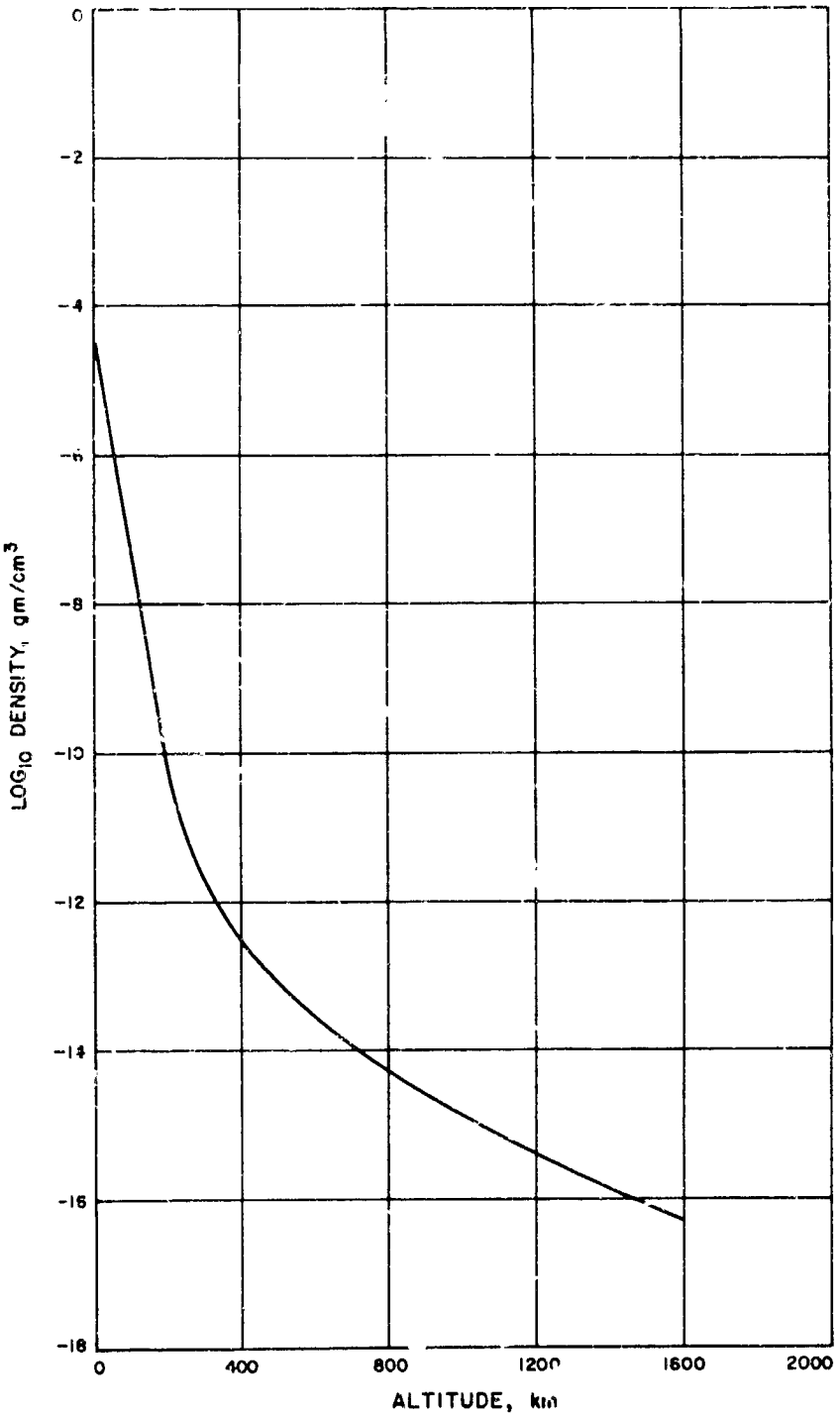


Figure 8-24. Log Density vs Altitude for JPL Atmosphere (Model 1)

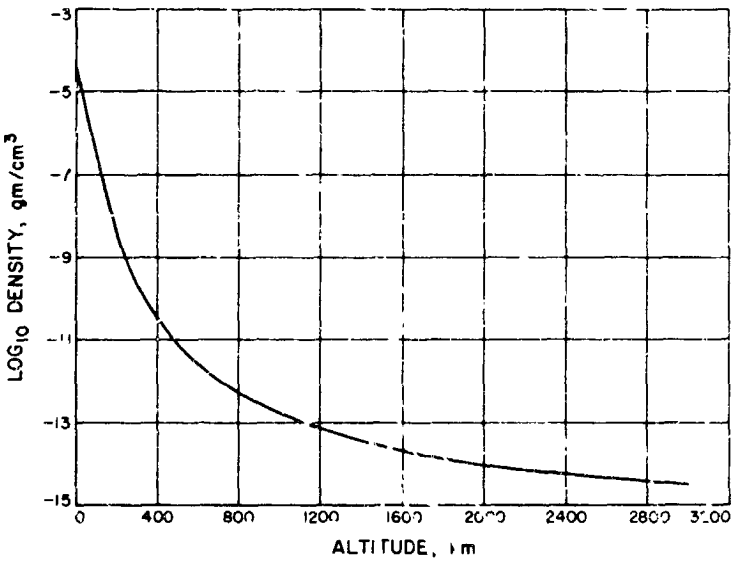


Figure 8-25. Log Density vs Altitude for NASA "Maximum" Atmosphere (Model II)

Table 8-3 Atmospheric Lifetime Results (Required Orbit Altitudes)

Atmosphere Model	Lifetime (years)	k_{eff} = 15 slugs/ft^2		k_{eff} = 18 slugs/ft^2	
		H_p (km)	H_a (km)	H_p (km)	H_a (km)
JPL (Model I)	50	1550	10,000	1250	10,000
		1150	20,000	1000	20,000
		825	50,000	750	50,000
		750	100,000	650	100,000
NASA (Model II)	50	4500	20,000	4350	20,000
		3850	50,000	3700	50,000
		3500	100,000	3350	100,000
	20			4000	10,000
				3500	20,000
				3100	50,000
				2800	100,000

Original estimates for k_r and k_n resulted in $k_{eff} = 0.15$ slugs/ft^2, which appears in several of the results. However, more recent values of $k_r = 0.112$ slugs/ft^2 and $k_n = 0.558$ slugs/ft^2 resulted in a slightly different value of $k_{eff} = 0.18$ slugs/ft^2. The required periapsis and apoapsis altitudes for this more recent value are given in Table 8-3. At one point in the study, it was thought that lower periapsis altitudes would be allowable if the solar panels could be reliably folded in after several weeks following initial orbit establishment. However, it turned out that if the panels were retracted in their full-length position (not multiple folded) k_{eff} was only increased to 0.204 slugs/ft^2 and was, therefore, not worthwhile.

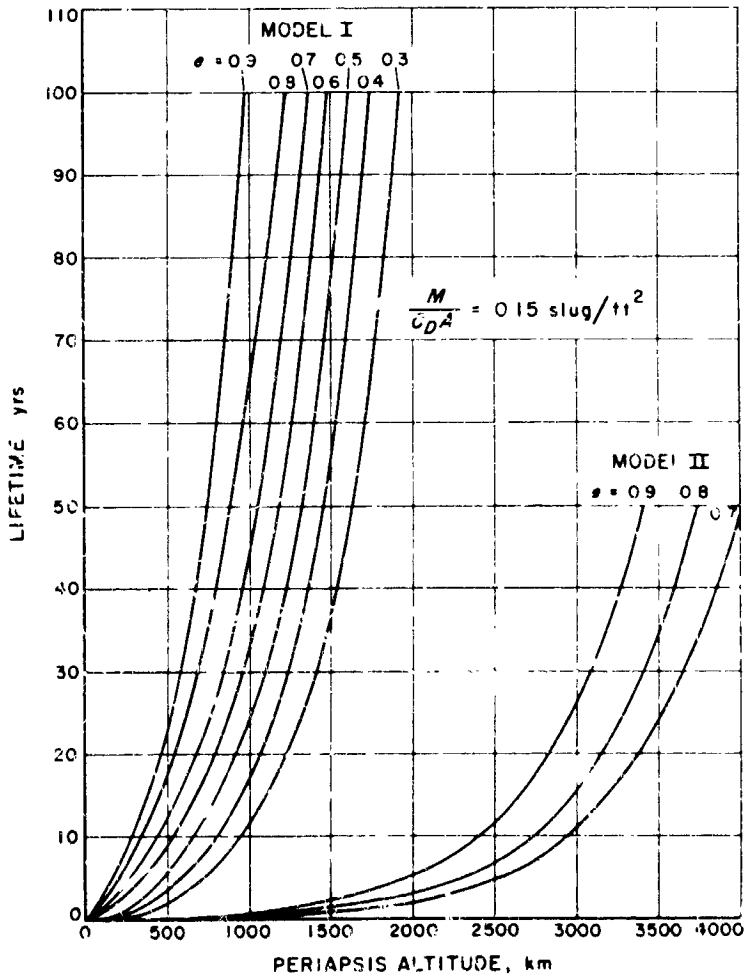


Figure 8-26. Lifetime vs Periapsis Altitude for Curves of Constant Orbit Eccentricity

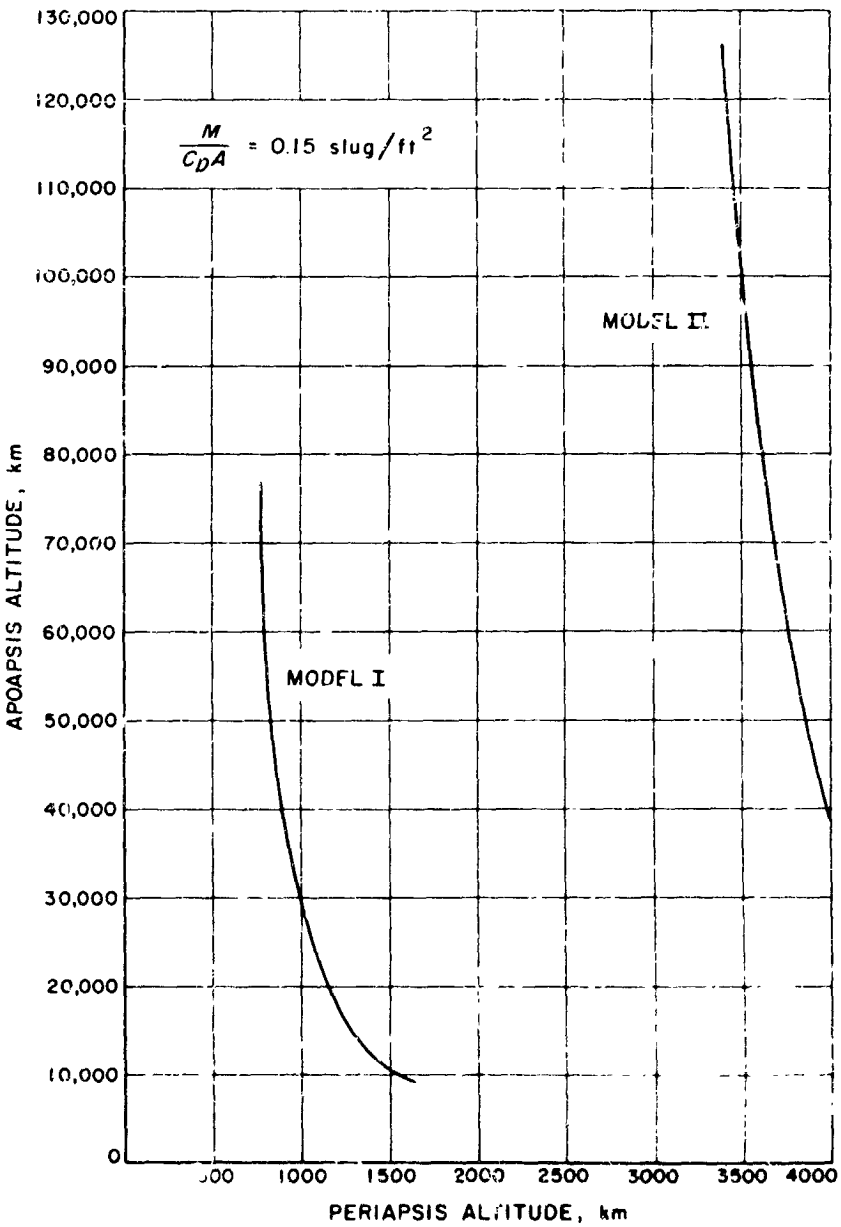


Figure 8-27. Apoapsis Altitude vs Periapsis Altitude to Yield 50-year Lifetime

In using Figure 8-26, apoapsis altitude, orbit eccentricity, and periapsis altitude are related by:

$$H_a = \left(R_o + H_p\right)\left(\frac{1+e}{1-e}\right) - R_o$$

where R_o is the planet radius which has been assumed as 3400 km for Mars.

After observing the effect upon periapsis altitude of requiring a 50-year orbit lifetime with the NASA "maximum" atmosphere model, one might logically ask if as long as 50 years would really be necessary to guarantee a probability of 0.9999 that Mars will have been contaminated by other means before the orbiter falls into the surface. There has not been sufficient time during the short course of this study to evaluate this question rigorously; however, a simple approach is outlined below. In order to arrive at a relatively short lifetime requirement, let us assume that unmanned missions are flown to Mars at every opportunity from 1969 through 1983, and that manned missions are flown at every opportunity from 1985 on. Let us also assume that the probability of at least one (out of two launches) successful unmanned mission at each opportunity is 0.5, while the probability of success for each manned mission is 0.8. Let us also assume that the unmanned as well as manned missions are trying to reach the Mars surface such that, given that a mission has been successful, we will assume a probability of unity that Mars has been "contaminated." If x represents the number of manned-mission opportunities, then

$$P\text{ (at least one contamination)} = 0.9999 = 1 - \left(\frac{1}{2}\right)^8 \left(\frac{1}{5}\right)^x$$

Solving for x, we find that the orbiter must not come down until about 1989, or some 20 years after orbit establishment. Table 8-3 indicates that reducing the lifetime requirement from 50 to 20 years permits the periapsis altitude to be lowered by only 600 km for the 50,000 km apoapsis orbit.

Suppose that we now alter the above assumptions so as to arrive at a safer lifetime requirement. Let unmanned missions be attempted only at every other opportunity from 1969 through 1985, and let manned attempts be also made at every other opportunity from 1987 on. Also let us assume that, if an unmanned mission is successful in the sense that it places something in the Martian environment, the probability that Mars is contaminated is only 0.1. But we will still assume that, if man lands on Mars, there is a probability of unity that the planet will be contaminated. These assumptions result in

$$P\text{ (at least one contamination)} = 0.9999 = 1 - \left(\frac{19}{20}\right)^5 \left(\frac{1}{5}\right)^x$$

Solving for x now results in requiring that the orbiter stay up until the year 2007, or a lifetime of roughly 37 years. Obviously, any change in the above assumptions will result in a different lifetime requirement.

Because of the relatively large ballistic coefficient of the orbiter as well as the larger Sun-orbiter distance, solar pressure effects are negligible for the currently desired orbiter lifetime span of tens of years. Solar gravitational effects, however, are not negligible. Depending upon the orientation of the orbit plane with respect to the Sun, solar gravitational effects (often referred to as third-body effects) can cause the periapsis altitude to vary by as much as a few hundred kilometers if the orbit plane remains in certain undesirable orientations. Fortunately, the oblateness of Mars can be put to good advantage by causing sufficient continuous change in the orbit plane orientation such that solar gravitational effects will have a much lower chance of being accumulative. The result is that periapsis altitude alternately rises and falls over fairly short periods of time (order of one hundred days or so). An attempt has been made to investigate the long-term effects of solar gravitation and planetary oblateness by utilizing a variation-of-parameters program for the IBM-7094. The program uses equations that have been averaged over one satellite orbit (see References B-4 and B-5). Some of the 1969 orbit profiles were run on the above program with a simulated lifetime of 50 years and net periapsis altitude reductions of 50 to 200 km were obtained, but it is very important to state at this point that the program has not been adequately checked out. Although the orbit periapsis altitudes which are indicated as a result of this study may seem unreasonably high, it may be of interest to note that a recent article by G. F. Schilling (Reference B-6) discusses the possibility that secular accelerations of the inner Moon Phobos may be due to exospheric drag. Schilling states that the actual existence of these orbital accelerations is in doubt; however, he still proposes that reasonable assumptions about the physical state of the equatorial exosphere of Mars can lead to values of atmosphere density which could exert observable drag effects upon Phobos without its being a hollow sphere. The orbit of Phobos is roughly circular at an altitude of almost 6000 km from the Mars surface.

Summarizing, it appears that oblateness and solar gravitational effects are, by themselves, not too serious; however, they can cause the periapsis altitude to diminish to regions where the atmospheric drag effects are significant. These latter effects depend upon the assumptions employed in defining a high-altitude density profile, and with the current large uncertainties involved, it is very important that the formulation of a standard high-altitude density model receive more attention. Finally, if one attempts to select a nominal periapsis altitude which is conservatively based upon (a) requiring a 50-year orbit lifetime with the NASA "maximum" atmosphere model, and (b) adding on an additional margin to accommodate solar gravitational effects as well as guidance and orbit determination errors, it is not at all unlikely that a nominal periapsis altitude as high as nearly 5000 km might be indicated. An altitude requirement of this magnitude certainly begins to reduce some of the attractive features of performing an orbiter mission.

4. Orbiter Payload Results

Throughout this section, the terms "fixed" and "variable" propellant loading are used. Fixed loading implies that the amount of retro fuel aboard the spacecraft will not be altered

at any time during the launch period. Whereas, in the variable loading situation, the amount of retro fuel will be varied (on-load for Type II and off-load for Type I) as one progresses through the firing period. Practical considerations will limit the actual number of times that the fuel load can be varied, thus the actual gain in orbiter mass will be somewhat less than that gain which could be realized if the propellant load is varied continuously during the firing period. This gain in orbiter mass which is made possible by varying the propellant load can be understood conceptually by referring to Figure 8-28. The variable loading scheme is optimized if the amount of fuel which is off-loaded is precisely equal to the reduction in injected weight capability associated with the increased injection energy. If the fixed-weight spacecraft can only weigh a total amount, W, and yet must have sufficient fuel to establish an acceptable capture orbit on launch day 1 when the approach speed, V_{∞}, at Mars is very high, then the retro fuel and payload must both shrink such that F'<F and P'<P. It turns out that, for both Type I and Type II trajectories, the gain in useful (active) orbiter mass (P - P') is about 70 lbs for a 30-day launch period. The term "useful orbiter mass" refers to all non-propulsion-system mass in orbit and therefore excludes the dry weight of the propulsion system.

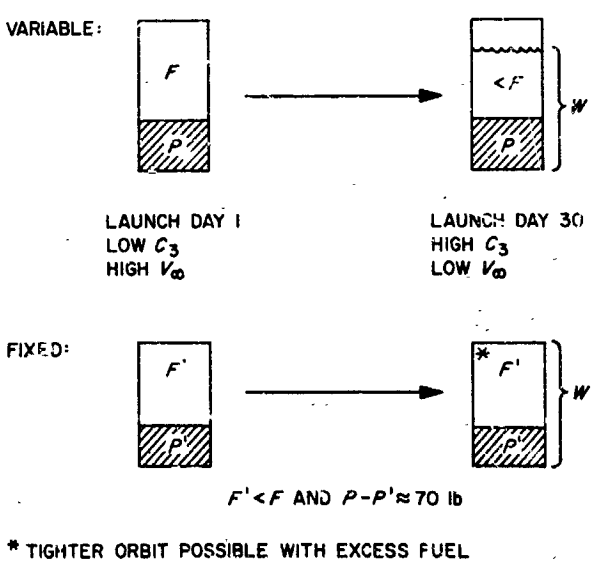


Figure 8-28. Variable vs Fixed Propellant Loading

Figures 8-29 through 8-32 illustrate the key results of this study. The required separated spacecraft weight curves were computed in the following manner. Given V_∞, R_a, and R_p, the impulsive retro velocity decrement, ΔV, necessary to establish the desired orbit with a periapsis-to-periapsis transfer is given by

$$\Delta V = \sqrt{V_\infty^2 + \frac{2\mu}{R_p}} - \sqrt{\frac{2\mu R_a}{R_p (R_a + R_p)}}$$

where $\mu = 4.29778 \times 10^4$ km^3/sec^2 for Mars. A polynomial relating initial spacecraft mass (prior to orbit retro) to useful mass in orbit was supplied by the Propulsion Division and is given by

$$\frac{\text{useful orbiter mass}}{\text{initial spacecraft mass}} = 0.0025625x^2 - 0.09325x + 0.952$$

where x is equal to ΔV (plus an allowance for midcourse corrections and gravity burning time losses) expressed in units of thousands of feet per second. Figures 8-29 through 8-32 were generated by using the following steps:

1) Obtain the C_3 and V_∞ values associated with the first and last launch days for the curves of constant orbiter mass shown in Figure 8-1.
2) Given V_∞, H_a, and H_p, compute ΔV and add an additional 100 meters/second to allow for midcourse corrections plus gravity burning time losses.
3) For any required useful orbiter mass, use the polynomial to compute the required total spacecraft mass.
4) Adjust the total spacecraft mass associated with the low-V_∞ launch day to reflect the same dry propulsion system mass as that computed for the high-V_∞ launch day.
5) Plot the required spacecraft mass above that value of C_3 associated with the particular V_∞ used.
6) Plot the actual separated payload capability of the booster vehicle as a function of C_3 and compare with the above-required separated spacecraft weight curves to determine mission feasibility.

A detailed discussion of the methods used to locate optimum regions of constant orbiter mass (such as shown in Figure 8-1 of this report, for example) may be found in EPD-139, Volume II. Figures 8-29 through 8-31 indicate an assumed nominal useful orbiter mass of 950 lbs. After these curves were completed, however, the nominal orbiter mass was increased to about 1000 lbs. This recent increase is shown in Table 8-4, which indicates the available launch periods for different assumptions. Before discussing the implication of the results shown in Table 8-4, the utilization of Figures 8-29 through 8-32 should be explained.

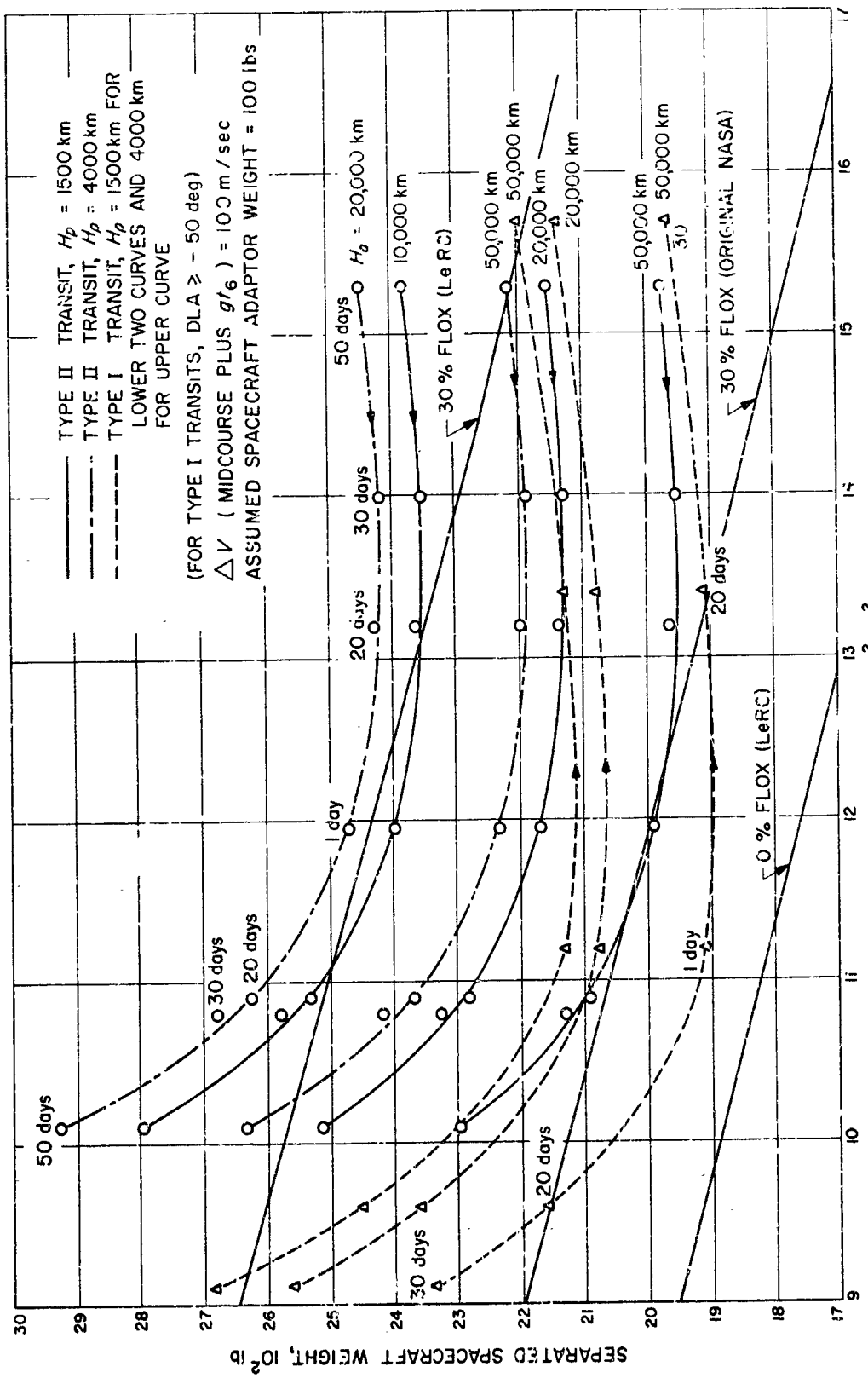


Figure 8-29. Separated Spacecraft Weight Requirements for Useful Orbiter Weight of 950 lbs (Type I and Type II Trajectories, Variable Propellant Loading)

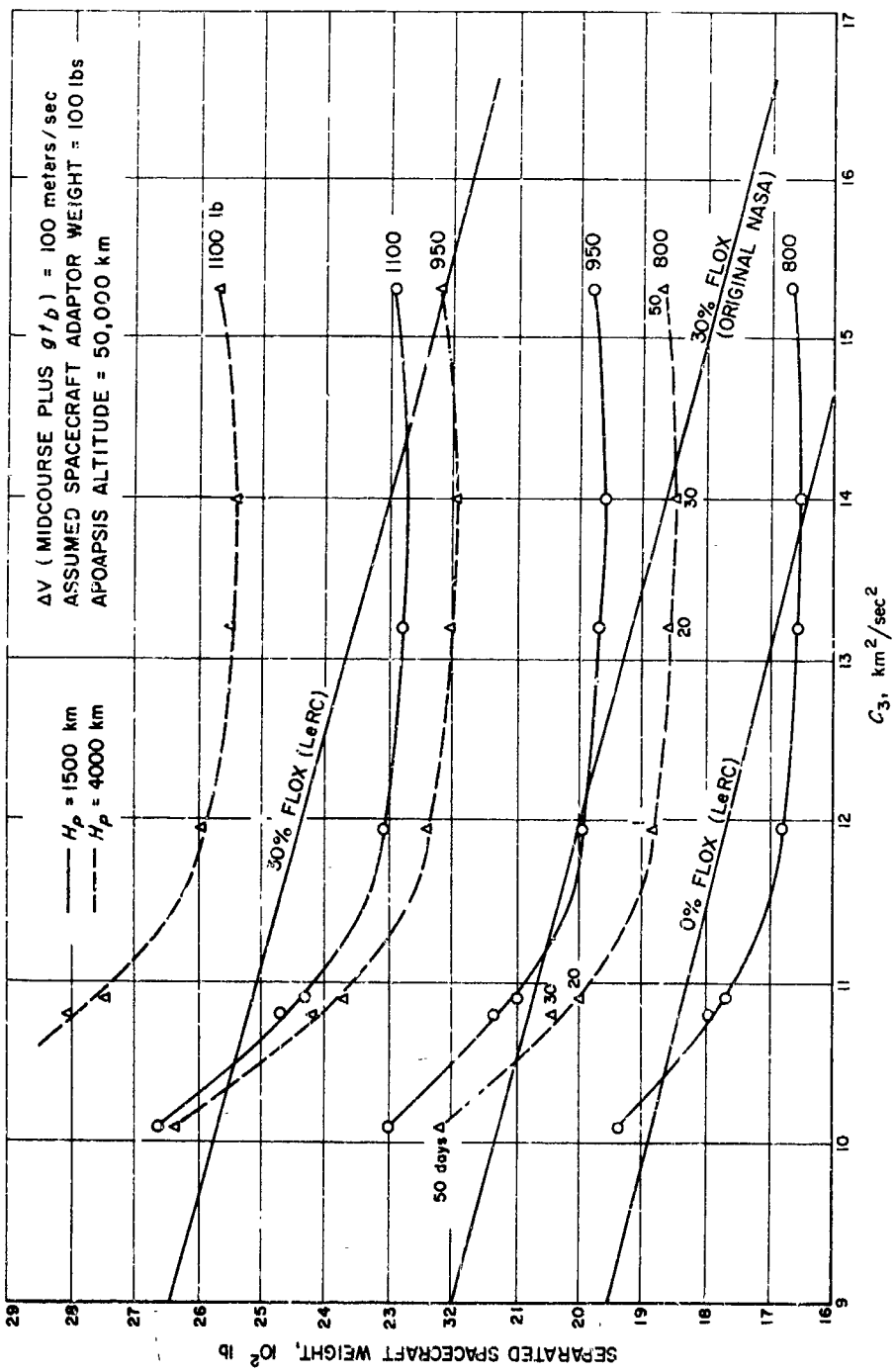


Figure 8-30. Separated Spacecraft Weight Requirements for Useful Orbiter Weight of 800, 950, 1100 lbs (TypeII Trajectories, Variable Loading)

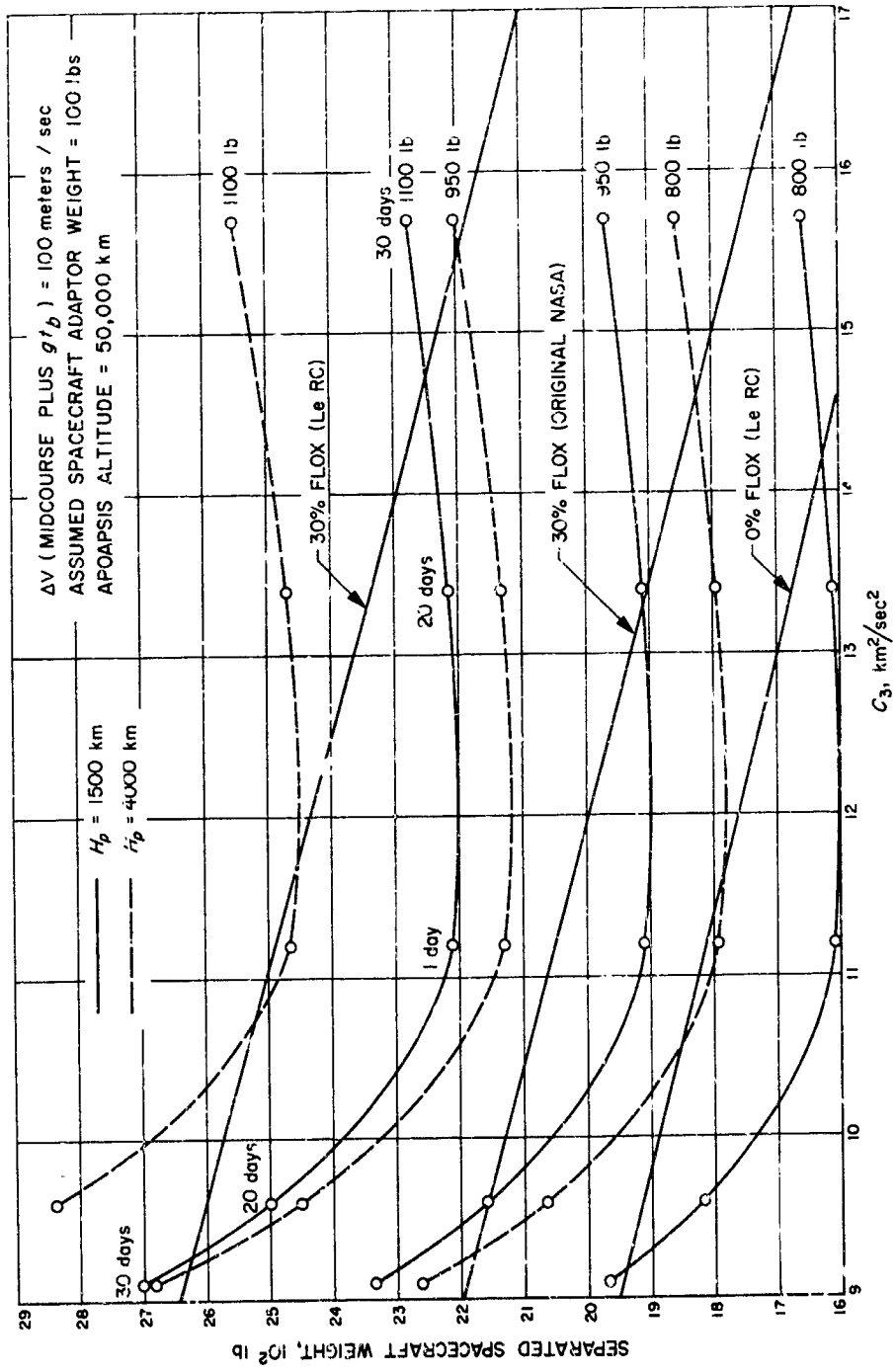


Figure 8-31. Separated Spacecraft Weight Requirements for Useful Orbiter Weights of 800, 950, 1100 lbs (Type I Trajectories, Variable Loading)

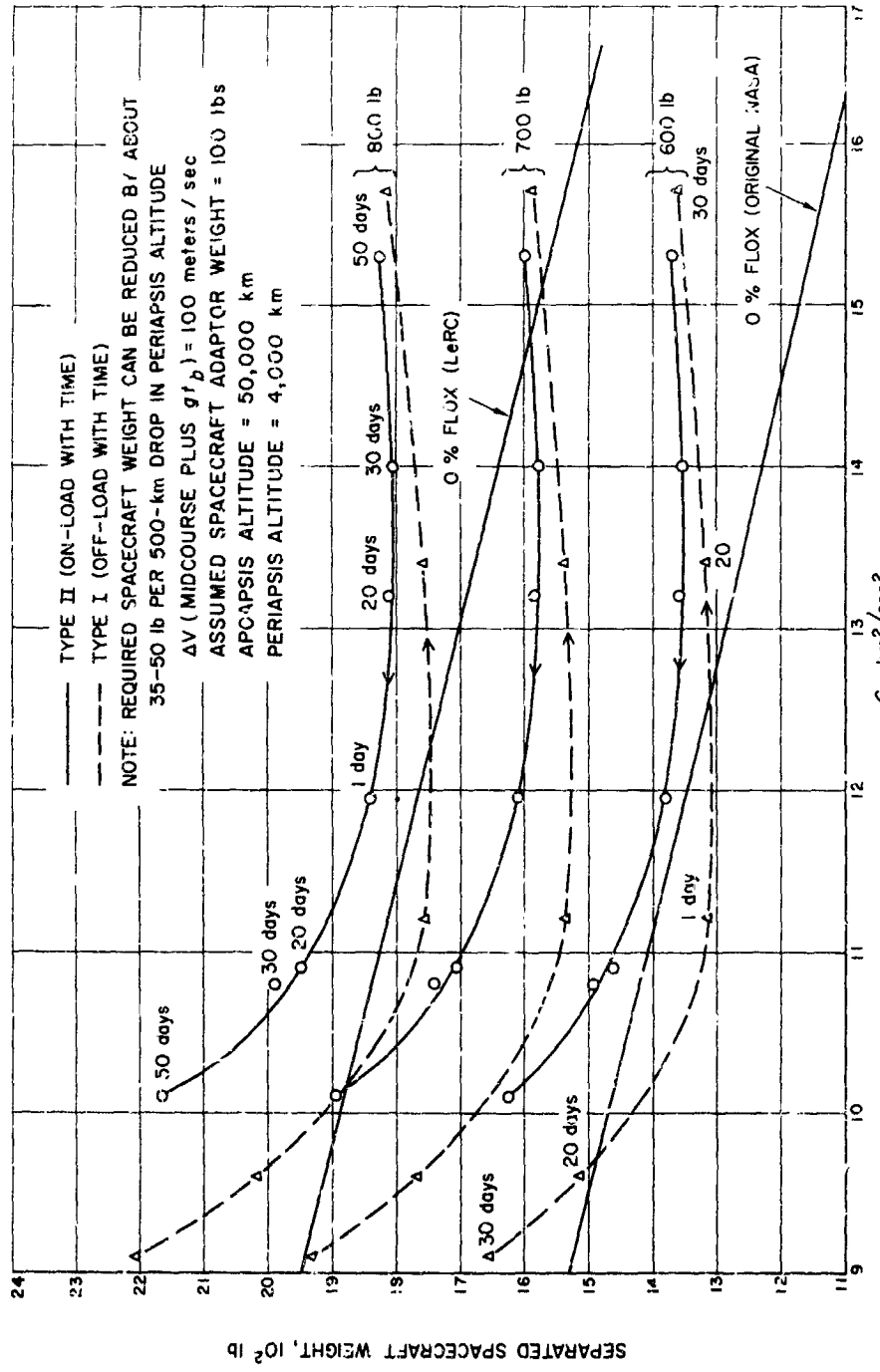


Figure 8-32. Separated Spacecraft Weight Requirements for Useful Orbiter Weights of 600, 700, 800 lbs (Type I and Type II Trajectories, Variable Loading)

Table 8-4. Launch Period Capability Matrix (1000-lb Orbiter)

30% Atlas Centaur FLOX Estimates From	H_p (10^3 km)	H_a (10^3 km)	Launch Period (Type II)	Launch Period (Type I)
NASA	1.5	50	0	8
NASA	4.0	50	0	0
LeRC	1.5	50	60	35
LeRC	1.5	20	40	25
LeRC	4.0	50	30	23

Note: Variable loading assumed. DLA ≥ - 50 degrees (Type I).

Referring to Figure 8-31, for example, suppose we wished to determine the available launch period for a Type I mission with a useful orbiter mass of 950 lbs and a 1500 x 50,000 km orbit. Using the 30 percent FLOX NASA (original) performance curve, we would find the required spacecraft weight is below the performance curve for a launch period of about 20 days. If periapsis altitude is raised to 4000 km, there would be no available launch period (hence no mission) for the NASA performance estimates. By going to the 30 percent FLOX LeRC (revised) performance curve, however, we could achieve a launch period of slightly less than 30 days. The implication of Figures 8-29 through 8-31 and Table 8-4 is simply this. Assuming a 30 percent floxed Atlas/Centaur and a nominal useful orbiter mass of 1000 lbs, a 1969 Mars orbiter mission is feasible (from an adequate weight and launch period standpoint) if we use the LeRC performance estimates and is not feasible for the original NASA performance estimates. Clearly, we are operating in a very critical region where it is very important to understand and define all of the assumptions associated with the Atlas/Centaur performance estimates. Referring to Figure 8-32, and depending again upon the launch vehicle performance estimates it would appear that a useful orbiter mass of between 600 and 750 lbs might be possible for a nonfloxed orbiter mission in 1969. In a previous section of this EPD, the Centaur performance estimates have been referred to as "original" and "revised." In this Subsection, the text and figures have used the terminology "NASA" and "LeRC."

It is very important to point out the effect of changing periapsis altitude upon the required separated spacecraft weight at injection. Referring to Figures 8-29 through 8-31, it can be seen that an additional weight of about 250 to 300 lbs is required if periapsis is raised from 1500 to 4000 km. At the beginning of the study, existing orbit lifetime results indicated that a 1500 x 50,000 km orbit (and dispersed orbits) would exhibit the necessary 50-year lifetime. Near the end of the study, however, a more dense atmospheric model (see Subsection B.3) was obtained and new lifetime calculations indicated that the periapsis altitude

should be increased to the vicinity of at least 4000 km. Therefore, in order to utilize Figures 8-29 through 8-32 in a conservative fashion, the higher periapsis altitude value should be assumed.

Figures 8-33 through 8-39 were generated during the early portion of the study when the 1500 km periapsis altitude was felt to be adequate. These curves may be used, however, to indicate the behavior of certain orbiter-mass-related parameters under various assumptions. Referring to Figure 8-33, for example, and assuming a separated spacecraft weight of 2000 lbs (NASA 30 percent FLOX and C_3 = 12 km^2/sec^2), the useful orbiter mass is increased from (0.411) (2000) = 822 lbs to (0.450) (2000) = 900 lbs by raising the apoapsis altitude from 20,000 km to 50,000 km for an orbit periapsis altitude of 2000 km. Figure 8-34 illustrates the cost of fixed vs variable propellant loading, Figure 8-35 shows the reduction in useful orbiter mass as the launch period is increased, etc. Figure 8-38 demonstrates the strong dependency of the achievable mass in orbit upon DLA for the Type I transits. In fact, there are almost an unlimited number of ways to present the interdependency of all of the parameters which affect the achievable mass in orbit. Figures 8-29 through 8-39 have illustrated several of these dependencies, but there has not been sufficient time or manpower available to prepare a more complete analysis and discussion of all of the problems and considerations.

5. General In-Orbit Motion Curves

This Subsection presents several curves which should be useful in performing various quantitative calculations related to orbiter altitude, true anomaly, time from periapsis, speed, orbit-plane precession, orbital period, etc. Figures 8-40 through 8-43 illustrate the behavior of altitude, time from periapsis, and horizontal velocity as a function of true anomaly for H_p = 1500 km and various apoapsis altitudes. Orbiter "true anomaly" (see Figure 8-20) is the angle measured in the orbit plane from periapsis to the position of the orbiter. Figures 8-44 through 8-46 depict altitude and time behavior with true anomaly for H_p = 4000 km. Figure 8-44 shows that the orbit altitude is twice the periapsis altitude for a true anomaly of about 80 degrees for H_a = 50,000 km) and is three time H_p for a true anomaly of 102 degrees. Figure 8-45 can be used to determine the available time between particular values of true anomaly. Figure 8-47 shows the behavior of orbit period with apoapsis altitude, for periapsis altitude values of 1500 and 4000 km. And finally, using the equations shown in Figure 8-20, orbit nodal and apsidal precession rate magnitudes are given in Figures 8-48 through 8-53.

6. Potentially Attractive Satellite Orbits

In Subsection A.1, three Type I and three Type II reference trajectories were described for the 1969 opportunity. All trajectories were selected so as to achieve closely maximum mass in orbit about Mars for a 30-day launch period. These six basic transit trajectories

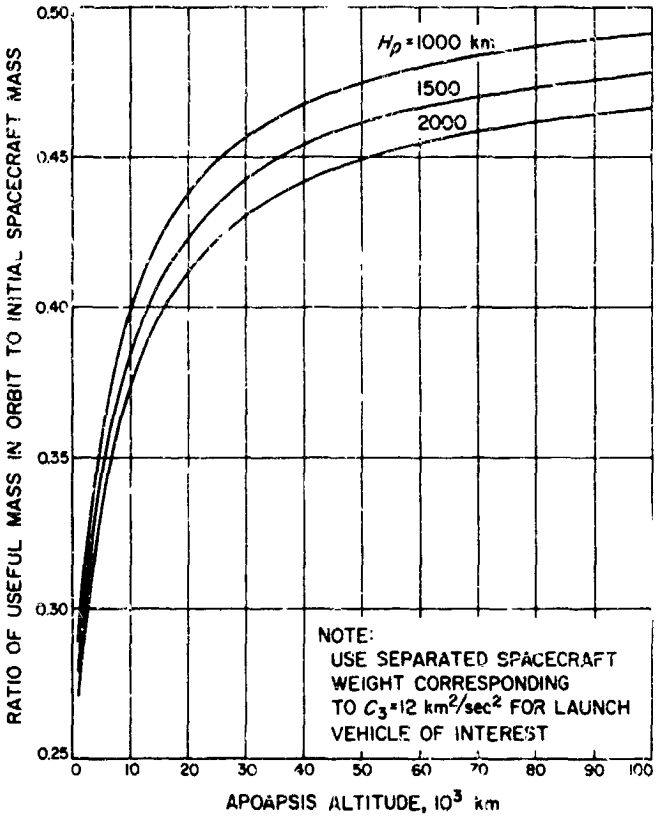


Figure 8-33. Orbiter Mass Ratio for Optimum Type II Trajectories with Variable Loading and 30-Day Launch Period

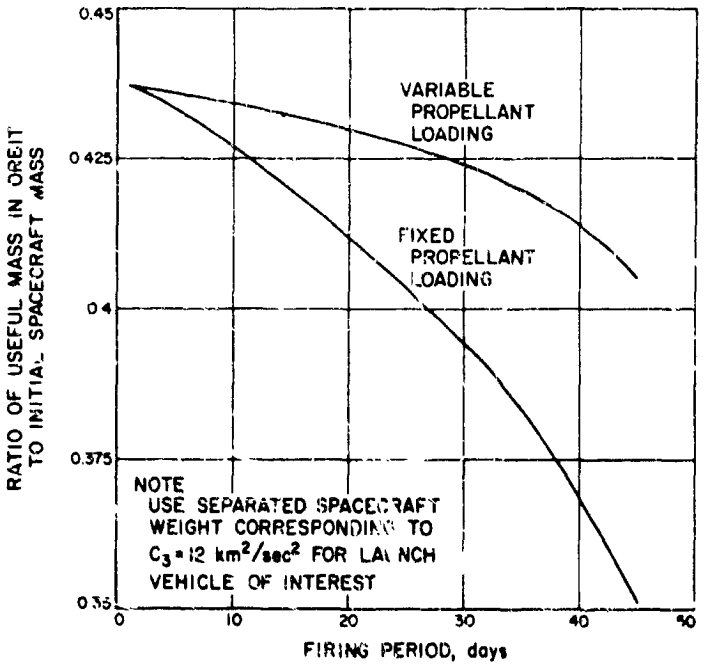


Figure 8-34. Orbiter Mass Ratio for Optimum Type II Trajectories (H_p = 1500 km, H_a = 20,000 km)

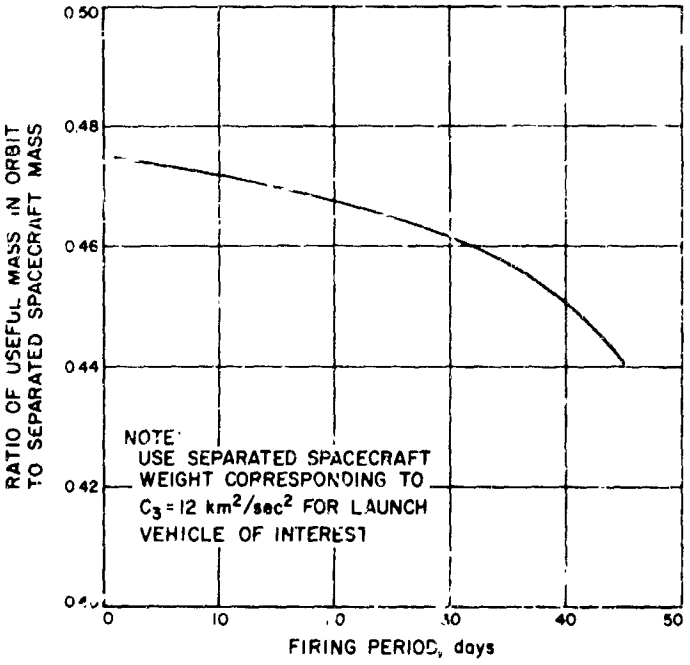


Figure 8-35. Orbiter Mass Ratio for Optimum Type II Trajectories (H_p = 1500 km, H_a = 50,000 km)

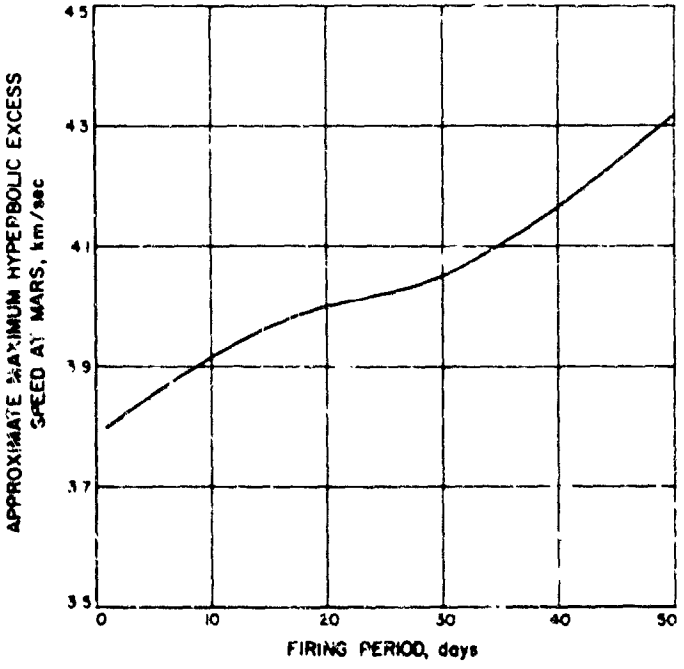


Figure 8-36. Maximum Hyperbolic Excess Velocity at Mars for Optimum Type II Trajectories with Variable Loading

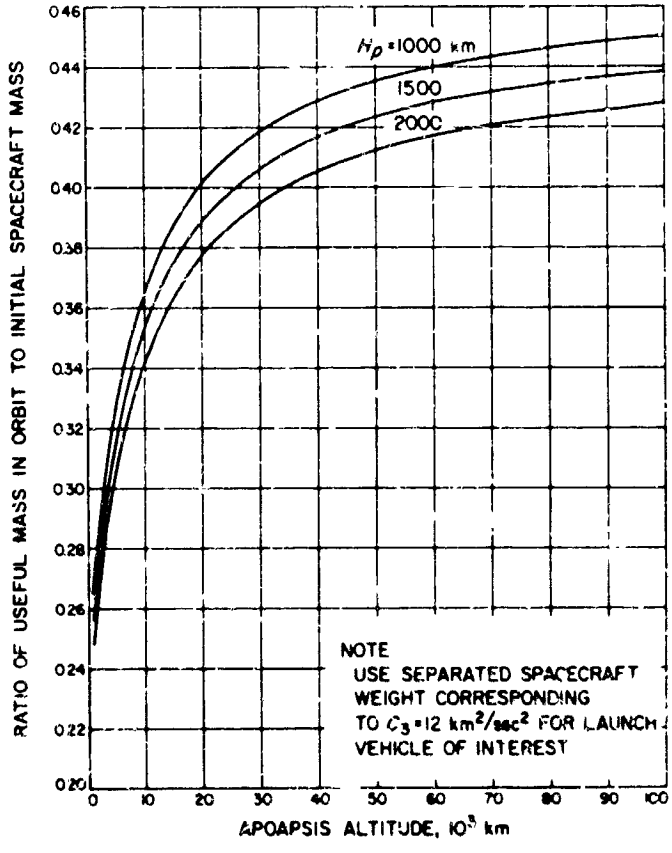


Figure 8-37. Orbiter Mass Ratio for Type I Trajectories with Variable Loading and DLA ≥ -50 Degrees

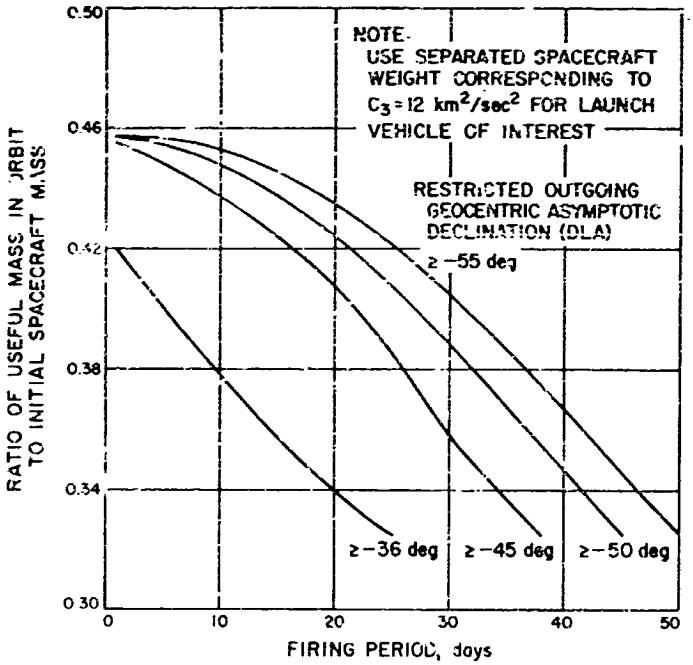


Figure 8-38. Orbiter Mass Ratio for Type I Trajectories with Variable Loading (H_p = 1500 km, H_a = 20,000 km)

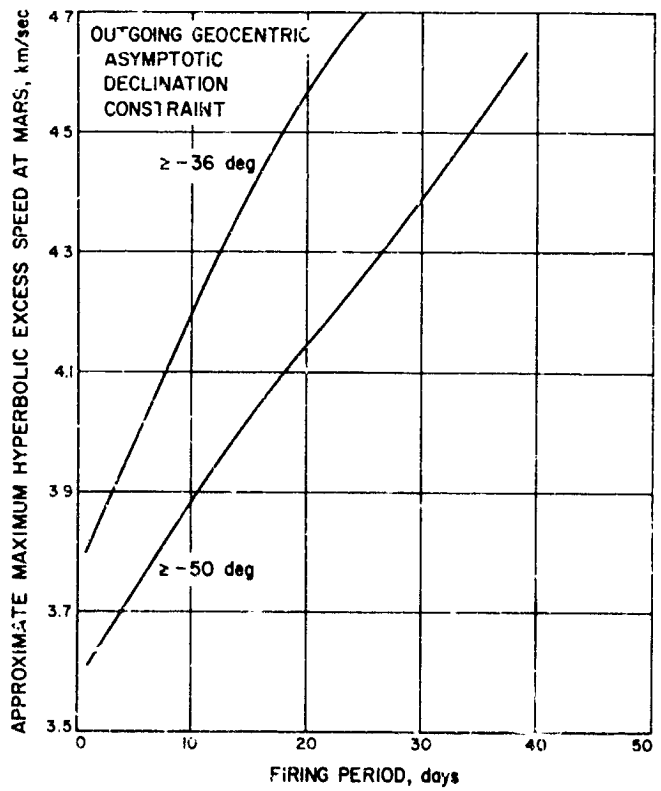


Figure 8-39. Maximum Hyperbolic Excess Velocity at Mars for Type I Trajectories with Variable Loading

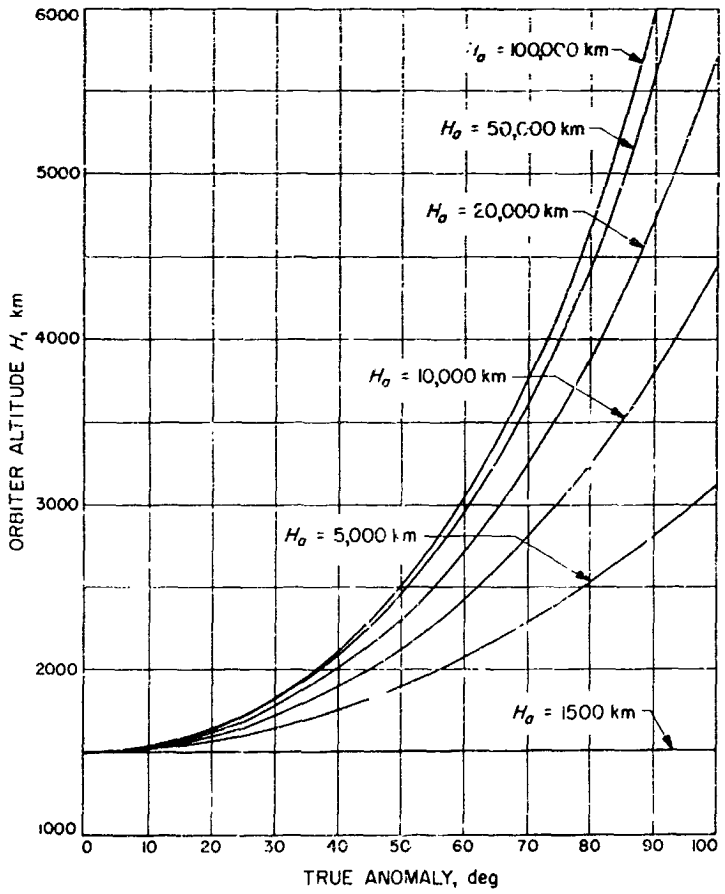


Figure 8-40. Orbiter Altitude vs True Anomaly for H_p = 1500 km

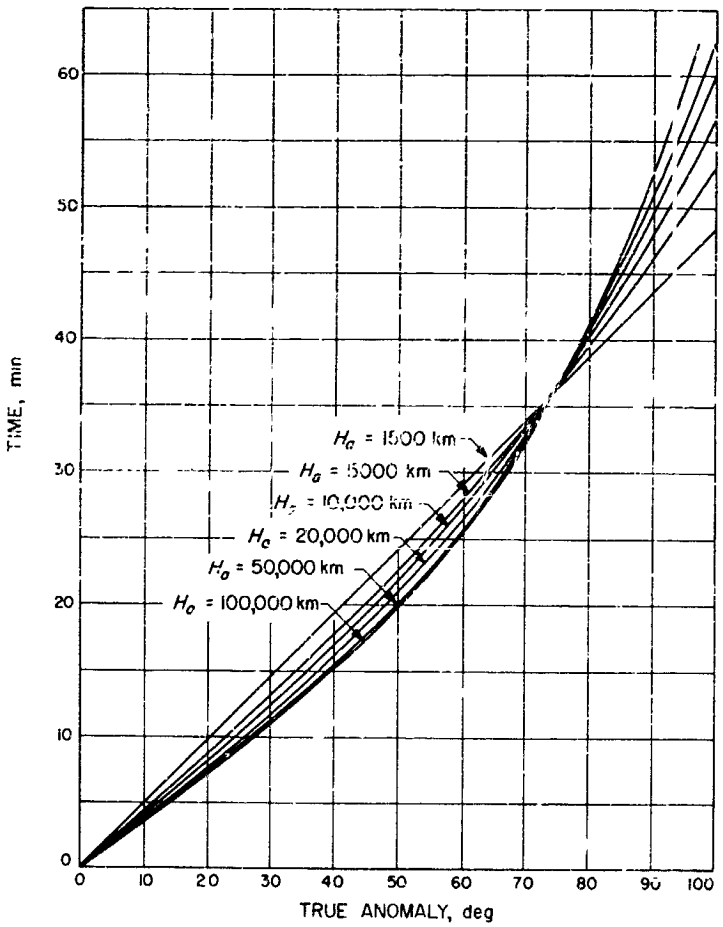


Figure 8-41. Time from Periapsis vs Orbiter True Anomaly for H_p = 1500 km

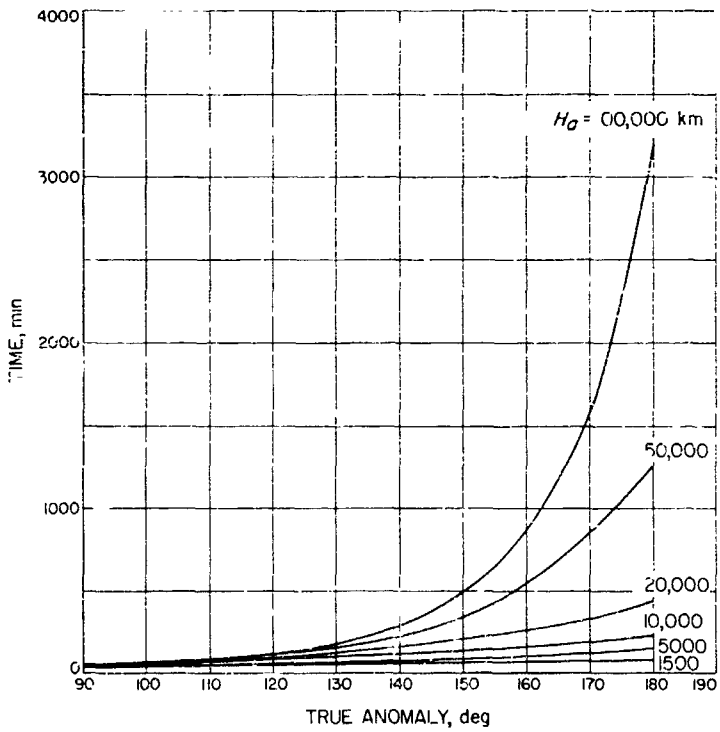


Figure 8-42. Time from Periapsis vs Orbiter True Anomaly for H_p = 1500 km

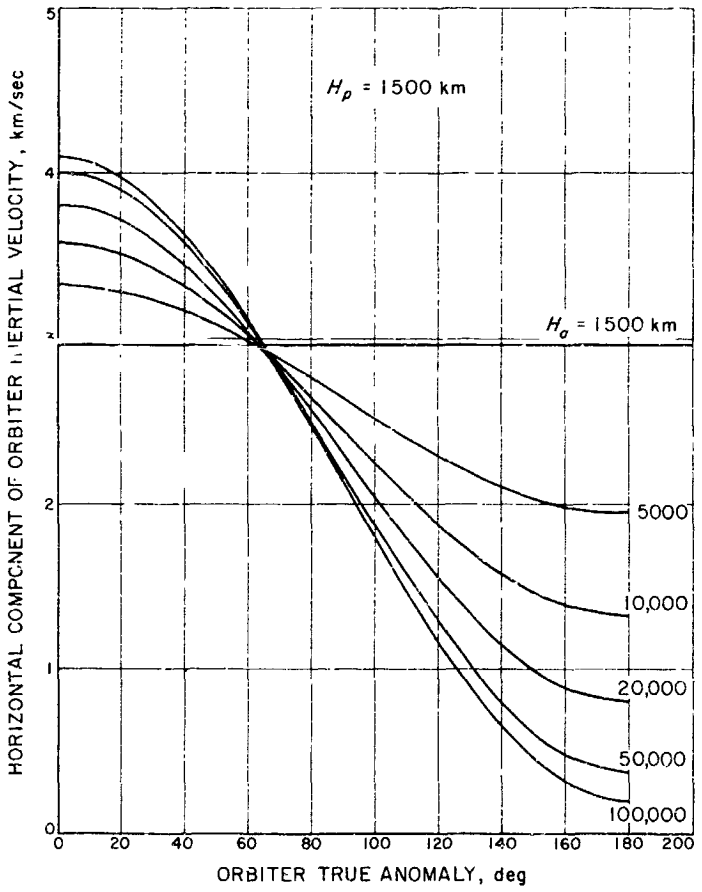


Figure 8-43. Horizontal Component of Orbiter Inertial Velocity vs Orbiter True Anomaly Degrees

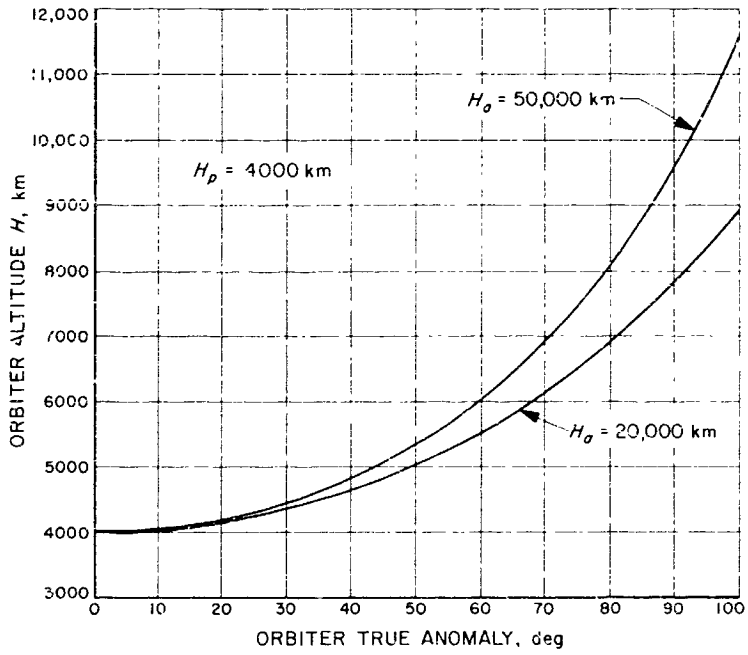


Figure 8-44. Orbiter Altitude vs True Anomaly

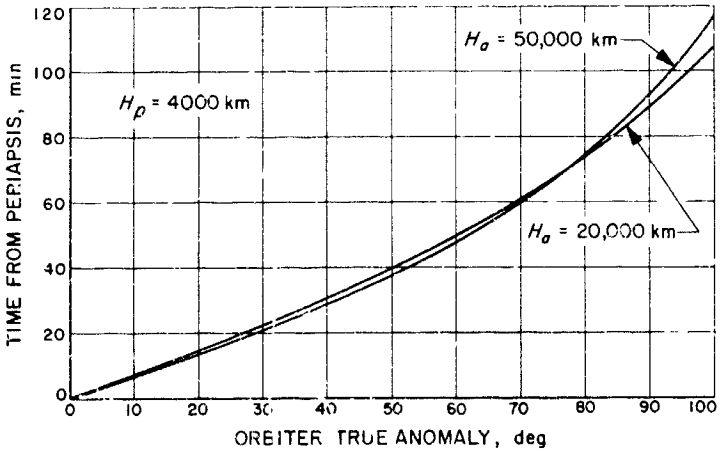


Figure 8-45. Time from Periapsis vs Orbiter True Anomaly

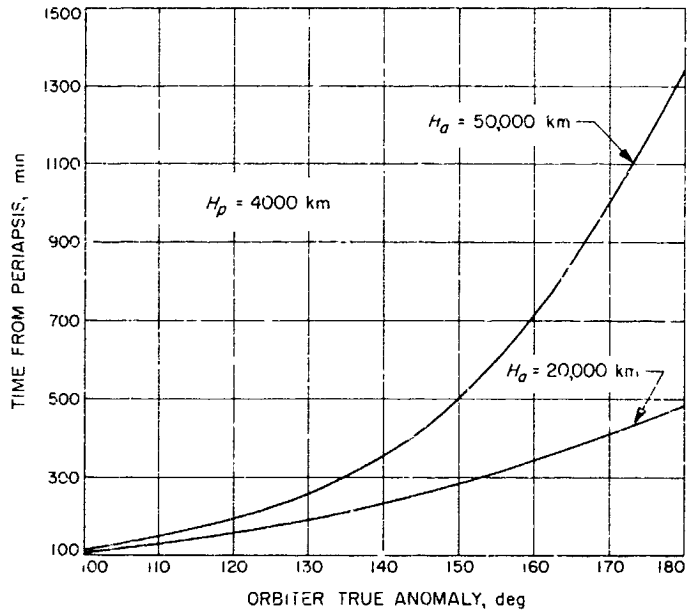


Figure 8-46. Time from Periapsis vs Orbiter True Anomaly

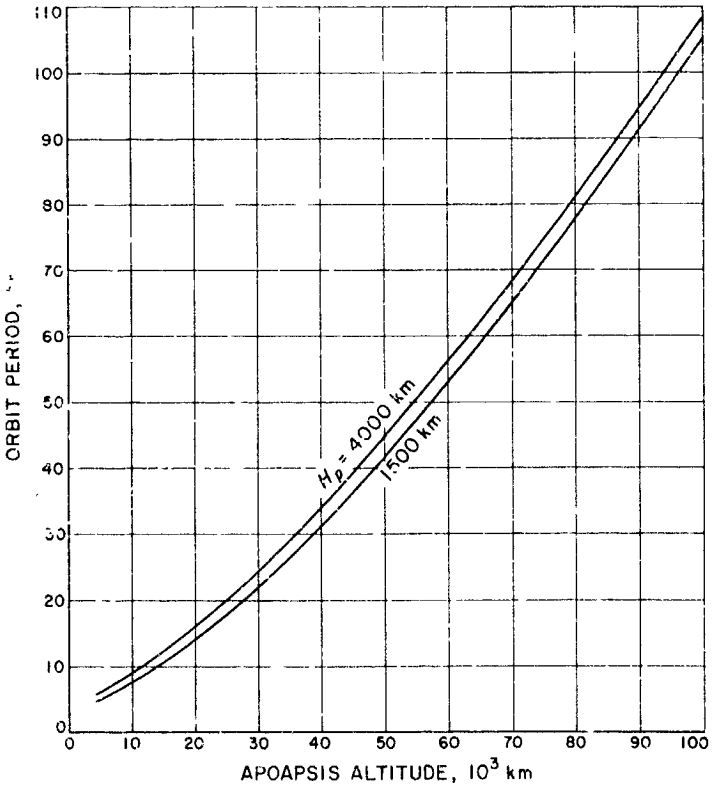


Figure 8-47. Orbit Period vs Apoapsis Altitude

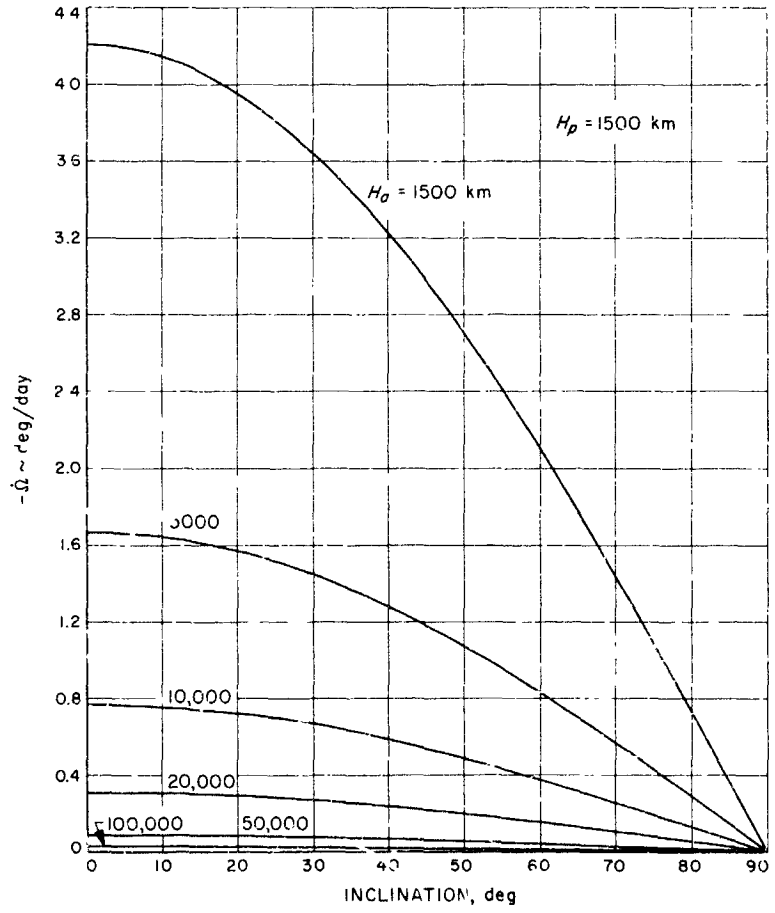


Figure 8-48. Nodal Regression Rate vs Orbit Inclination to Mars Equator

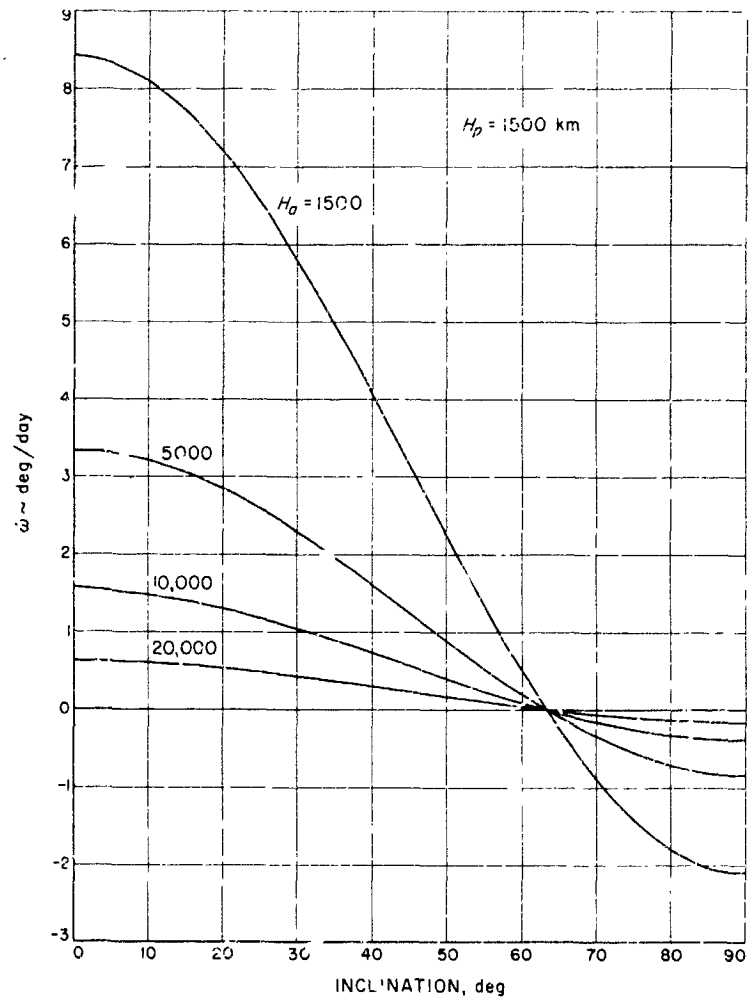


Figure 8-49. Apsidal Precession Rate vs Orbit Inclination to Mars Equator

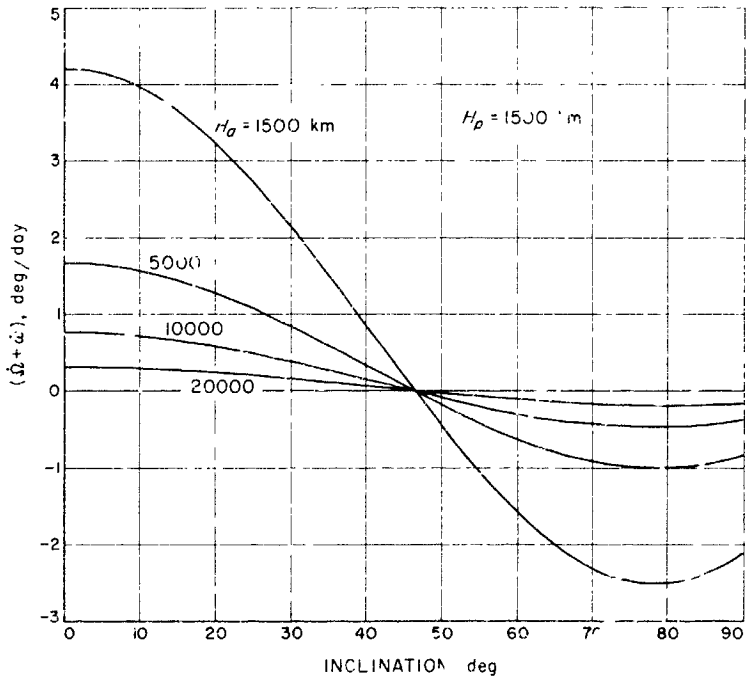


Figure 8-50. Nodal Plus Apsidal Precession Rate vs Orbit Inclination to Mars Equator

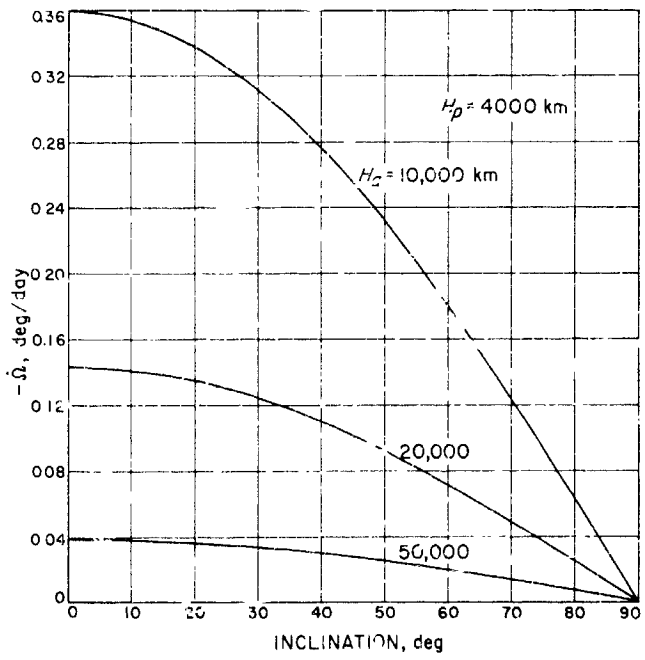


Figure 8-51. Nodal Regression Rate vs Orbit Inclination to Mars Equator

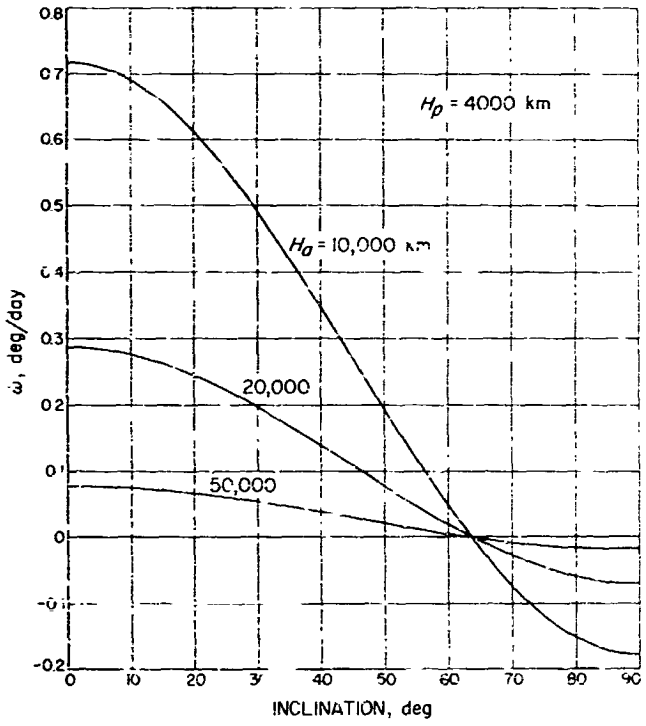


Figure 8-52. Apsidal Precession Rate vs Orbit Inclination to Mars Equator

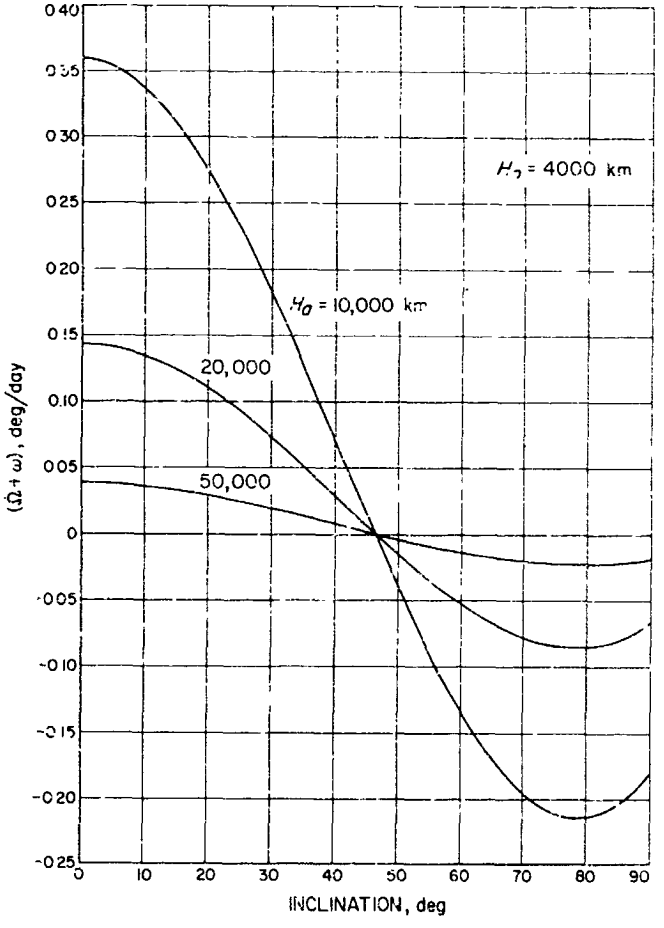


Figure 8-53. Nodal Plus Apsidal Precession Rate vs Orbit Inclination to Mars Equator

have been referred to by the symbols I-A, I-B, I-C, II-A, II-B, and II-C (see also Table 8-...), with the A, B, C designation simply in order of increasing launch date. As the three Type II approach characteristics are similar, only II-B was selected for generating orbit profiles. The three Type I approach geometries (see Figure 8-22 for I-A and I-C) exhibit reasonable differences, however, such that information has sometimes been included in this subsection for each of the three reference Type I trajectories.

Orbit selection considerations have already been covered in Subsection B. 1, and the approach geometry has been discussed in Subsection B. 2. Recalling this information and referring now to Figures 8-54 and 8-55, the following comments can be made concerning the selection of preferred aiming regions about Mars which should result in satisfying the largest number of constraints.

1) Region A is forbidden as a result of the contamination constraint which requires an adequate periapsis altitude to ensure a 50-year orbit lifetime for an unsterile orbiter. The size of Region A cannot be shown exactly due to the large uncertainties in the high-altitude atmospheric densities: however, the general size shown is intended to indicate that acceptable periapsis altitudes may be at least one planet radius from the surface of Mars.
2) Region B is undesirable as orbit periapsis occurs on the dark side of Mars.
3) Region C is sufficiently near the ecliptic as to result in solar occultation at some time during each orbit.
4) Region D results in the location of periapsis occurring at too extreme a northerly or southerly latitude, and the previously mentioned planetary coverage conditions (refer to Subsection B. 1) are not met satisfactorily.
5) We are thus left with regions E and F. Referring specifically to the Type I situation shown in Figure 8-54, region F is preferred over region E for the following reasons:
    a) Region E does not cover the interesting latitude areas just south of the Mars equator; also, Canopus comes very near the Mars limb.
    b) Region E does result, however, in a better Earth-occultation situation as can be concluded from Figure 8-23.
    c) Region F results in excellent coverage of the southern latitudes as well as no danger of Canopus loss due to the near Mars limb.
    d) Region F has therefore been selected for the nominal Type I aiming region.

Referring now to the Type II situation shown in Figure 8-55, regions E, E', and F all result in fairly good planetary coverage conditions. However, Canopus is occulted for aiming points in region E, thus this region may be eliminated. Canopus is above the near Mars limb in region E', but Earth occultation does not occur, thus region E' may be eliminated.

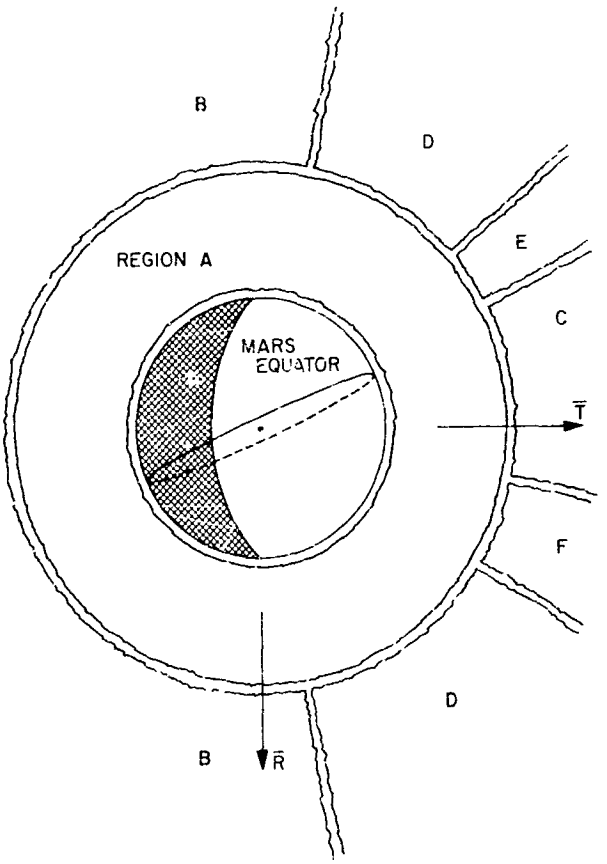


Figure 8-54. Type I Aiming Regions

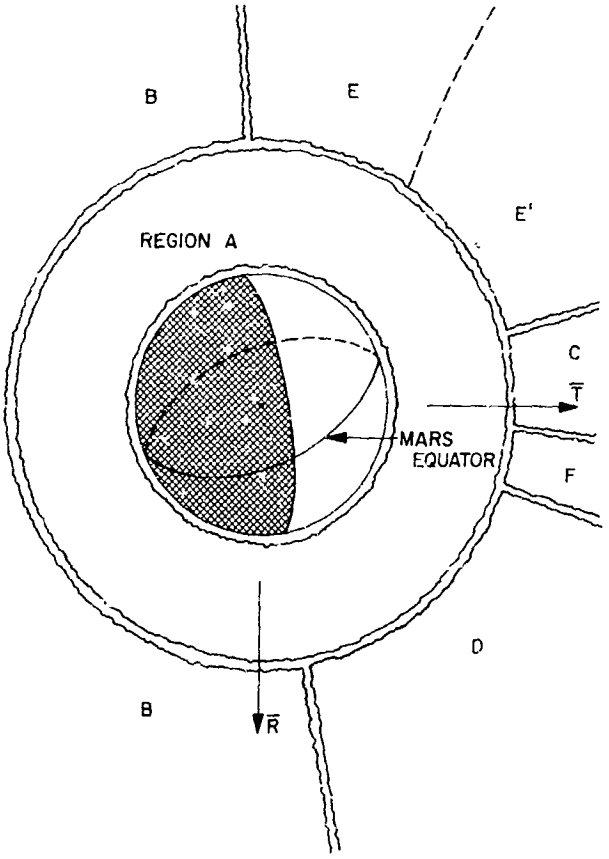


Figure 8-55. Type II Aiming Regions

Region F has therefore been selected for the nominal Type II aiming region. Having region F favorable for both Type I and Type II missions simplifies the design of a spacecraft which could be launched on both types of transit should the need arise.

Much of the information which was used to generate the forbidden aiming regions shown in Figures 8-54 and 8-55 is listed in Tables 8-5 through 8-7. These tables were compiled during the early phase of the study when it was thought that 1500 by 20,000 km orbits might be possible. Later in the study, however, increased orbiter weight estimates forced an increase in the apoapsis altitude, while increased atmospheric density estimates forced the periapsis altitude to be raised. From this point on in this section, only 1500 by 50,000 km and 4000 by 50,000 km orbits will be discussed. The nominal Type I orbit is inclined 45 degrees below the Mars equator, while the nominal Type II orbit is inclined 50 degrees below the Mars equator. Both of the nominal orbits may therefore be described as southerly direct orbits with aiming points in region F. At various places in this EPD, the nominal orbit inclinations are sometimes referred to as -45 degrees and -50 degrees in order to stress that the aiming points are below the Mars equator. Strictly speaking, however, direct orbits should have positively defined inclinations between zero and 90 degrees. The negative sign convention has, therefore, been used to distinguish between northerly and southerly aiming points from which the orbit profiles are established. Figures 8-56 through 8-68 illustrate the appearance of the nominal orbits as viewed from certain key directions. The geometry shown applies to the encounter geometry for transits I-B and II-B. The taped boundaries or "windows" shown on the Mars sphere indicate the desired TV coverage conditions in that (a) the upper and lower boundaries refer to the desired latitude band from 10 degrees N to 40 degrees S, while (b) the remaining two boundaries refer to the desired lighting conditions between 10 to 50 degrees from the terminator. As can be seen from Figure 8-58, two acceptable coverage regions exist, one near the morning terminator and the second near the evening terminator. In all of the figures, $\overline{Y}$ refers to the vernal equinox direction, $\overline{C}$ points to Canopus, $\overline{E}$ points to the Earth, and $\overline{S}$ is along the approach asymptote at Mars. The model is oriented in such a manner that the supportive rod is normal to the ecliptic plane.

Referring to Figures 8-56 through 8-61, we will now discuss the features of the nominal Type I orbit profile. Figure 8-56 illustrates the view along the approach asymptote and shows that the orbit is inclined 45 degrees to the Mars equator. The orbit shown is the 4000 by 50,000 km orbit. Most of the figures do show the larger orbit, although the 1500 by 50,000 km orbit is also shown in some of the figures. Figure 8-57 simply illustrates a general view of the 1500 km orbit, and it can be seen that periapsis is located over the evening terminator coverage zone. The small bands along the orbit ellipse mark the $2xH_p$ and $3xH_p$ points. Figure 8-58 shows the very interesting view as seen along the Sun-Mars line, and it can be seen that no solar occultation occurs. Figure 8-59 shows the view along the Earth-Mars line, and it can be seen that the Earth is occulted for a short time during the orbit. This occultation ends after several days. Figures 8-60 and 8-61 illustrate views normal to the 1500 km

Table 8-5. Type I-A Orbits (1500 x 20,000 km; Period = 850 min)

Aiming Θ Clockwise from ♈ (deg)	Orbit Inclination to Mars Equator (deg)	Minimum Angle from Sun to Near Planet Limb During First Orbit (deg)	Sun Occultation: Start (days), Finish (days), Max Time per Orbit (min)	Time of Sun Occultation from Periapsis (min)	Earth Occultation: Start, Finish, T_{max}/orbit	Time of Earth Occultation from Periapsis (min)	Return of Earth Occultation: Start, Finish, T_{max}	Canopus Situation
279	55	19	150, 180† 60	770-820	0, 35, 50	25-75	NO	-10-20
306	30	10	165, 180† 110	610-720	0, 45, 50	25-75	NO	- 3-12
316	20	3	180, NA, NA	550-600	0, 40, 50	25-75	NO	Canopus Barely Above Planet Limb
13	-40	2	70, 110, 90	240-330	0, 40, 35	15-50	NO	34° - 5°
18	-45	6	90, 120, 110	350-460	0, 35, 35	12-47	130, 160, 120	33° - 7°
24	-50	9	100, 130, 120	480-600	0, 30, 35	10-45	150, 170, 120	31° - 9°

Ordinary numbers indicate time (minutes) from Periapsis when Canopus is occulted; degree numbers refer to minimum near-limb angle to Canopus at 0 and 180 days.

Table 8-6. Type I-C Orbits (1500 x 20,000 km; Period = 850 min)

Aiming ● Clockwise from $\overline{T}$ (deg)	Orbit Inclination to Mars Equator (deg)	Minimum Angle from Sun to Near Planet Limb During First Orbit (deg)	Sun Occultation: Start (days), Finish (days), Max Time per Orbit (min)	Time of Sun Occultation from Periapsis (min)	Earth Occultation: Start, Finish, T_{max}/orbit	Time of Earth Occultation from Periapsis (min)	Return of Earth Occultation: Start, Finish, T_{max}	Canopus Situation
281	55	46	110, 170, 60	750-810	Fringe Case at 0 Days	NA	150, 180†, 60	-15- 15
306	30	35	120, 170, 40	660-700	0, 5, 30	30-60	160, 180†, 90	10m/orbit at 0 days no occult after 30 days
321	15	22	140, 180, 120	530-650	0, 20, 50	30-80	180, NA, NA	12° - 28°
336	1.3 (min)	8	160, 180†, 30	540-570	0, 50, 60	30-90	NO	24° - 24°
11	-35	2	40, 90, 120	340-460	0, 130, 90	See Note	NO	40° - 8°
16	-40	7	60, 100, 120	420-540	0, 20, 35	30-65	100, 130, 120	38° - 9°
21	-45	12	75, 110, 90	540-630	0, 10, 35	30-65	110, 140, 90	36° - 10°

Note: Earth occultation starts at 30 min past Periapsis at 0 days, almost disappears from 40 to 80 days, and starts at 270 min past Periapsis by 120 days after Encounter.

Table 8-7. Type II-B Orbits (1500 x 20,000 km; Period = 850 min)

Aiming θ Clockwise from ♈ (deg)	Orbit Inclination to Mars Equator (deg)	Minimum Angle from Sun to Near Planet Limb During First Orbit (deg)	Sun Occultation: Start (days), Finish (days), Max Time per Orbit (min)	Time of Sun Occultation from Periapsis (min)	Earth Occultation: Start, Finish, T_{max}/orbit	Time of Earth Occultation from Periapsis (min)	Return of Earth Occultation: Start, Finish, T_{max}	Canopus Situation
277	63.4 (ω = 0)	58	80, 125, 90	680-770	130, 160, 90	680-770	NO	-25- 5
288	55	53	70, 110, 90	680-770	120, 150, 60	680-710	NO	25- 0
311	40	34	50, 90, 90	580-670	110, 130, 120	500-620	NO	10° - 39°
335	32.7 (mi)	10	25, 75, 120*	425-545	70, 120, 90	360-450	180, NA, NA	34° - 53°
345	-34	1	5, 40, 120*	360-480	35, 100, 120	205-325	145, 180, 90	44° - 47°
351	-36	-3	0, 30, 100*	360-460	10, 75, 110	140-250	140, 180, 90	50° - 44°
359	-40	-1	0, 10, 80*	300-380	0, 60, 90	100-190	140, 180, 90	57° - 40°
15	-50	13	90, 180, 60	740-800	0, 20, 80	80-160	130, 180, 70	53 - 35°

*Repeat Sun occultation occurs for these orbits with 150, 180, 60; 120, 180, 120; 110, 180, 80; 100, 180, 60



Figure 8-56. Type I-B Nominal 4000 by 50,000-km Orbit Profile (View Along Approach Asymptote)



Figure 8-57. Type I-B Nominal 1500 by 50,600-km Orbit Profile (General View)



Figure 3-58. Type I-B Nominal 4000 by 50,000-km Orbit Profile (View Along Sun-Mars Line)

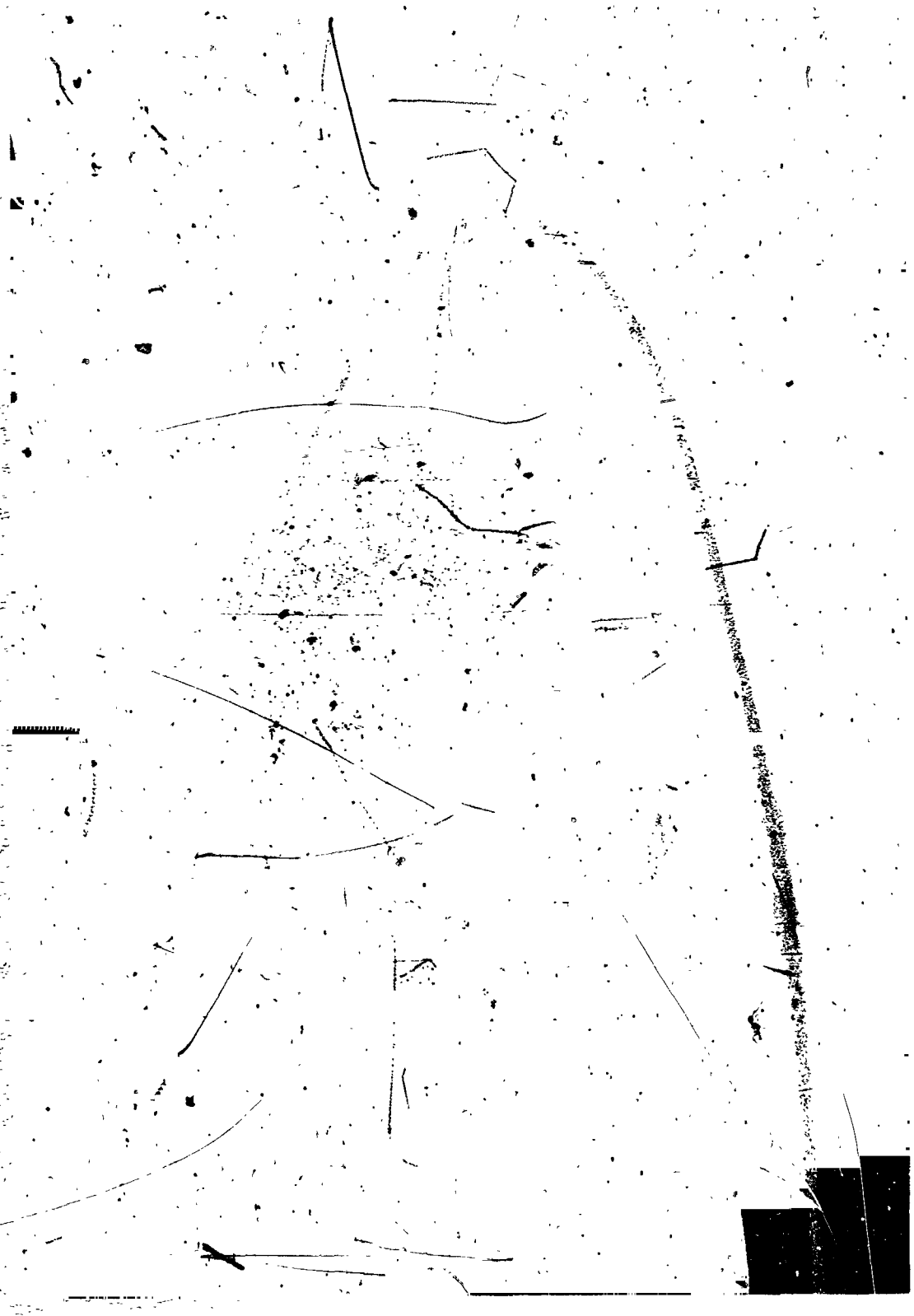


Figure 8-59. Type I-B Nominal 4000 by 50, 000-km Orbit Profile (View Along Earth-Mars Line)

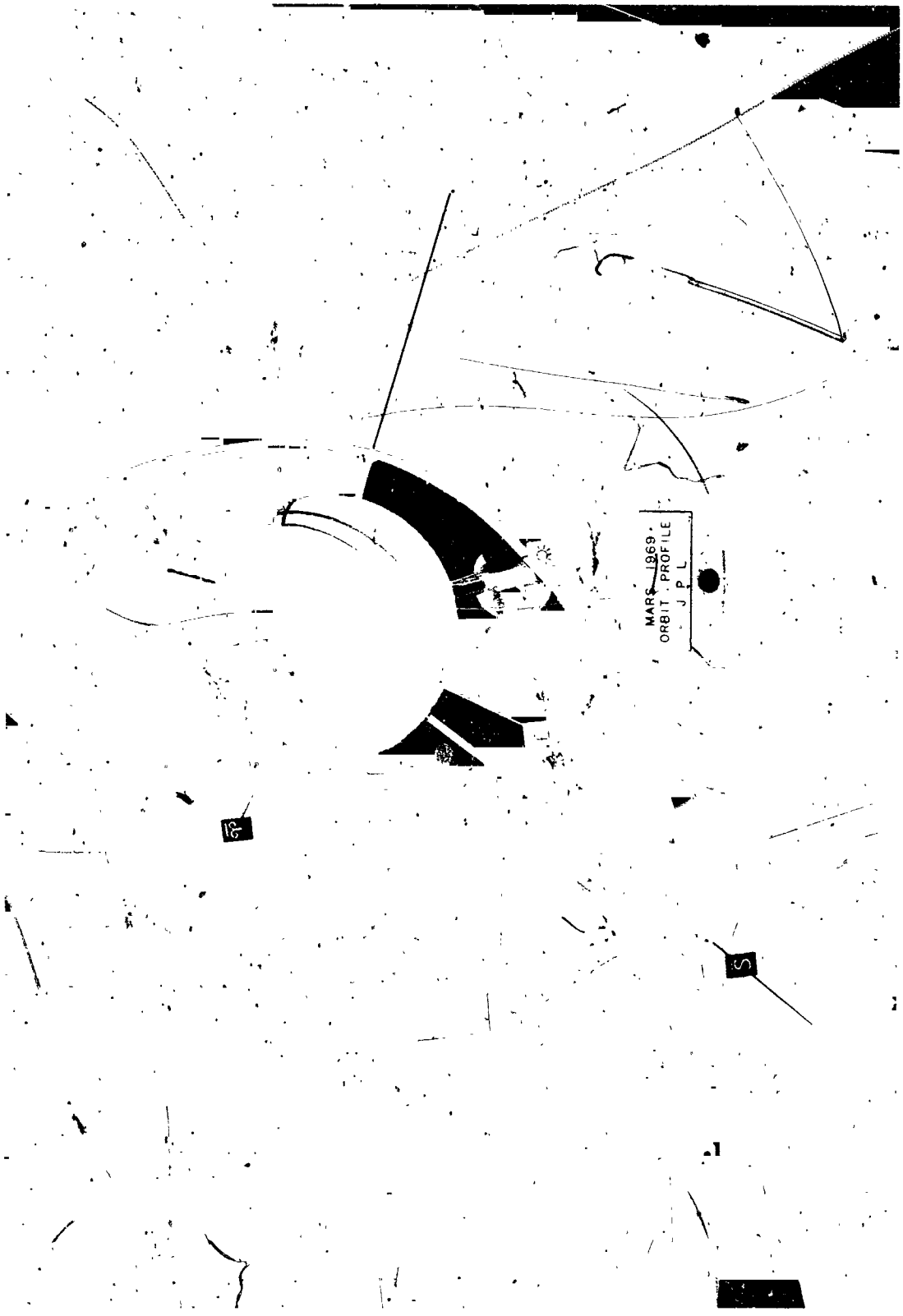


Figure 8-60. Type I-B Nominal 1500 by 50, 000-km Orbit Profile (View Normal to Orbit Plane)

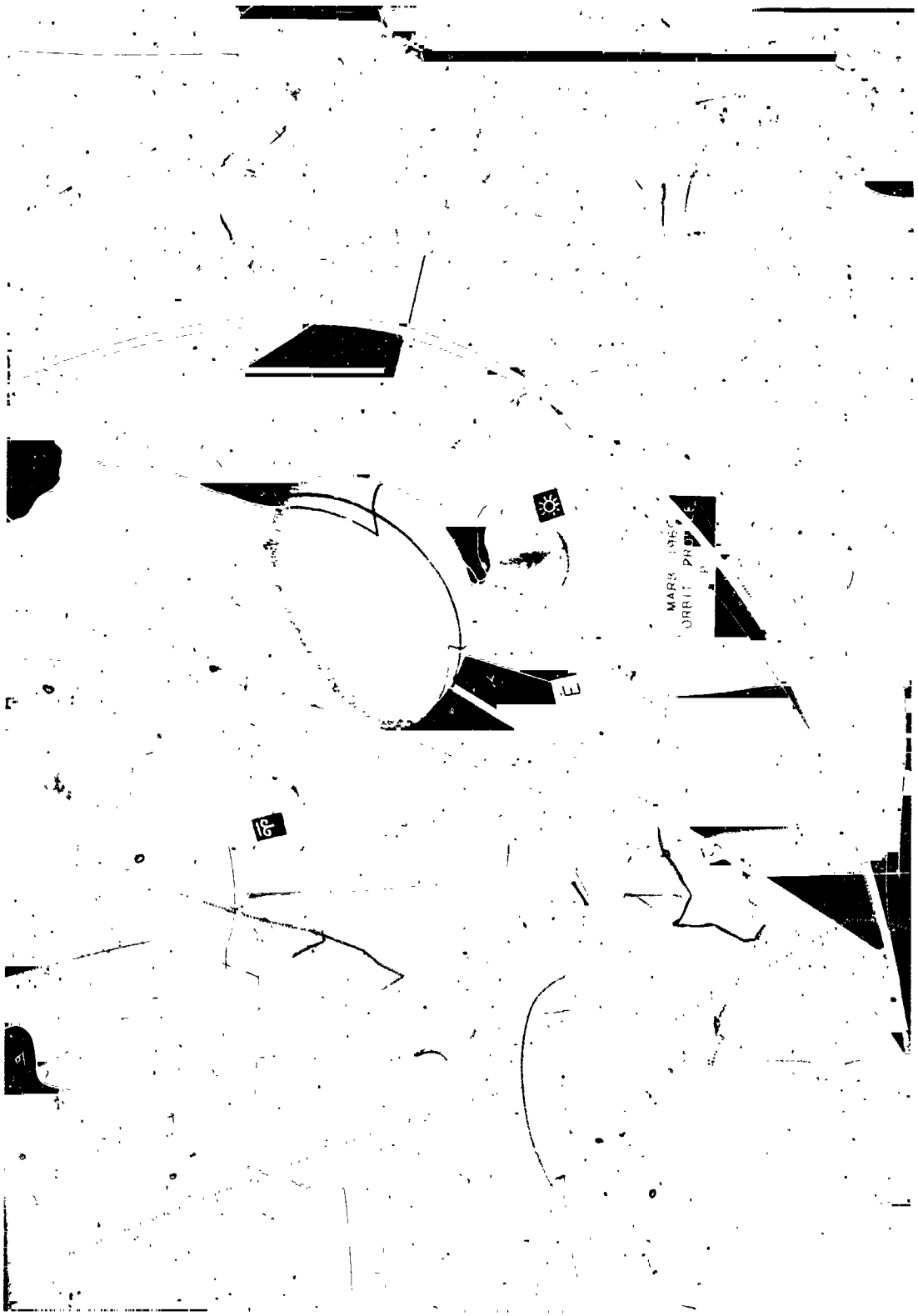


Figure 8-61. Type I-B Nominal 4000 by 50,000-km Orbit Profile (View Normal to Orbit Plane)



Figure 8-62. Type II-B Nominal 4000 by 50, 000-km Orbit Profile (View Along Approach Asymptote)



Figure 8-63. Type II-B Nominal 1500 by 50, 000-km Orbit Profile (General View)



Figure 8-64. Type II-B Nominal 4000 by 50, 000-km Orbit Profile (General View)



Figure 8-65. Type II-B Nominal 4000 by 50,000-km Orbit Profile (View Along Sun-Mars Line)



Figure 8-66. Type II-B Nominal 4000 by 50,000-km Orbit Profile (View Along Earth-Mars Line)

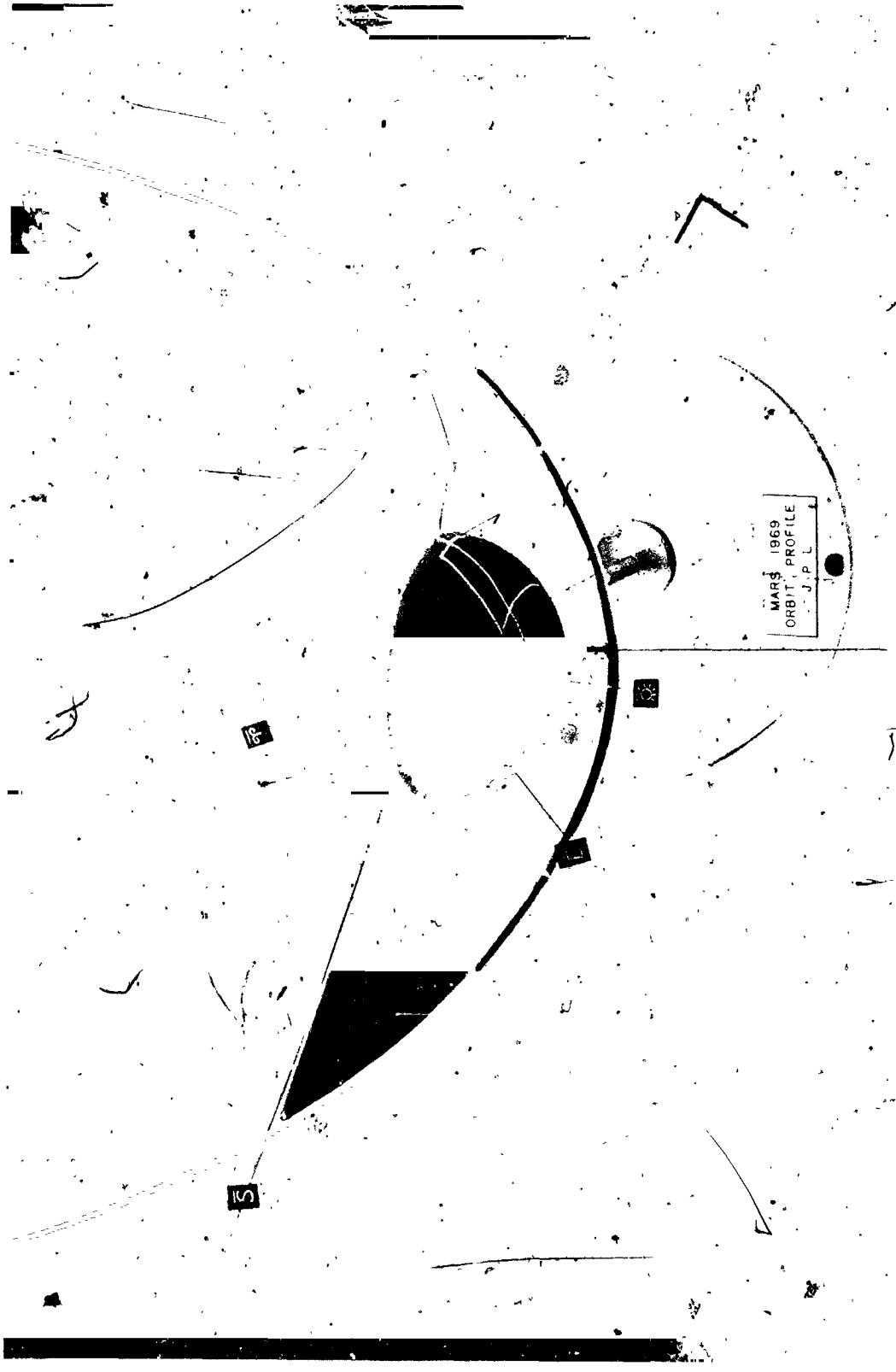


Figure 8-67. Type II-B Nominal 1500 by 50,000-km Orbit Profile (View Normal to Orbit Plane)



Figure 8-68. Type II-B Nominal 4000 by 50, 000-km Orbit Profile (View Normal to Orbit Plane)

and 4000 km orbits. These views show again the Type I coverage being preferred near the evening terminator.

Referring to Figures 8-62 through 8-68, the Type II orbit features will now be discussed: Figure 8-62 shows the view along the approach asymptote, and the orbit plane is inclined about 50 degrees to the Mars equatorial plane. The excellent view situation to Canopus (regarding the limb of Mars) is shown clearly in this figure. As mentioned earlier, however, the orbiter would pass periodically over the Moons of Mars which are travelling in near-circular orbits in the plane of the Mars equator. Figure 8-63 depicts a general view of the orbit profile, and the smaller-H_p orbit has been shown to better illustrate the geometry of features beneath the orbital path. Figure 8-64 illustrates the general view of the larger-H_p orbit. Figure 8-65 illustrates the view along the Sun-Mars line for the larger orbit and clearly displays the avoidance of Sun occultation. As will be discussed later, Sun occultation does not first occur until at least three months following initial orbit establishment. Figure 8-66 illustrates the view along the Earth-Mars line and indicates that Earth occultation does occur for a short time during the orbit. As in the case of the Type I orbit, Earth occultation terminates in less than one month following orbit establishment. Finally, Figures 8-67 and 8-68 illustrate views normal to the orbit plane. It can be seen that the initial location of the Type II orbit periapsis really favors neither terminator. However, the orbit precession rates due to Mars oblateness are much lower than the motion of the terminator (due to Mars' motion around the Sun) such that the morning terminator moves at about 0.5 deg/day towards the sub-periapsis point. In this sense, the Type II orbit profile does tend to favor coverage near the morning terminator by several weeks following initial orbit establishment.

More detailed information is given in Tables 8-8, 8-9, and Figures 8-69 through 8-76 concerning the nominal orbit profiles. Table 8-8 illustrates the effect of a 500 km dispersion at periapsis for a 1500 by 50,000 km orbit. Removal of the nominal retro velocity for the inner dispersion results in a 1000 by 35,000 km orbit (period = 26 hrs), while a 500 km outer dispersion would result in a 2000 by 80,000 km orbit (period = 78 hrs). As shown in Table 8-8, Sun occultation does not occur for at least 90 days. With a more probable orbit periapsis altitude of 4000 km, Sun occultation would occur even later. The higher periapsis altitude would also increase the minimum near-limb angles to Canopus but would reduce the chances for Earth occultation. Table 8-9 gives certain orbit orientation angles referenced to the Mars-Sun line and the ecliptic plane. Figures 8-69 through 8-71 illustrate the general TV coverage situation for various orbits. In Figure 8-69, for example, it can be seen that pictures would be taken within 30 degrees past periapsis during the early orbits but would move farther past periapsis in the following weeks. Figure 8-70 shows the Type II southerly-direct orbit coverage situation, and it can be seen that periapsis is not near the acceptable region at encounter, but conditions improve in the following weeks from the standpoint of being able to cover the region near the morning terminator at reasonable orbiter

Table 8-8. Effect of Orbit Dispersions Upon Occultation Times
(Orbits I-B and II-B, 1500 x 50,000 km)

Dispersed Orbit	Minimum Angle From Near Limb To Sun During First Orbit	Sun Occultation; Start (days), End (days), True Anomaly Range (deg)	Earth Occultation, Start (days), End (days), True Anomaly Range (deg)	Minimum Angle From Near Limb To Canopus At 0, 90, 180 Days
-40°	10	95, 125, 192-198	0, 20, 55- 92	36, 31, 27
NOM	14	110, 140, 198-210	0, 15, 54- 92	35, 31, 27
-50°	18	120, 160, 210-224	0, 15, 52- 88	34, 30, 26
INNER	12	90, 125, 188-196	0, 25, 40- 94	31, 22, 14
NOM	14	110, 140, 198-210	0, 15, 54- 92	35, 31, 27
OUTER	16	120, 160, 216-223	0, 8, 64- 88	38, 36, 35
-45°	0	125, 180+, 260-312	0, 30, 114-138	63, 63, 60
NOM	17	120, 180+, 260-320	0, 15, 116-136	58, 56, 54
-55°	24	115, 180+, 260-320	0, ϵ, ≈ 125	51, 50, 48
INNER	16	110, 180+, 256-320	0, 18, 108-136	56, 52, 46
NOM	17	120, 180+, 260-320	0, 15, 116-136	58, 56, 54
OUTER	18	130, 180+, 264-312	0, 10, 120-136	≈ 58

Table 8-9. Orbit Orientation Angles to Ecliptic

Type Transit	$H_p \times H_a$ (km)	Inclination to Mars Equator (deg)	Ω, Angle from Mars-Sun Line to Ascending Node in Ecliptic Plane (deg)	ω, Angle from Ascending Node to Periapsis Measured in Orbit Plane (deg)	I, Inclination of Orbit Plane to Ecliptic Plane (deg)
I-E	1500 x 50,000	-45	84, 39, 357, 320	325, 331, 337, 343	23, 24, 26, 27
I-A	1500 x 20,000	-45	100, 41, 347, 300	324, 346, 5, 21	23, 27, 32, 38
II-B	1500 x 50,000	-50	127, 83, 43, 6	237, 243, 249, 255	25, 25, 25, 25
II-B	1500 x 20,000	-50	127, 67, 11, 372	237, 259, 281, 300	25, 25, 26, 29
II-B	1500 x 50,000	34	227, 187, 150, 117	145, 150, 155, 160	40, 38, 37, 35

Angle values are given for 0, 60, 120, and 180 days following intial orbit establishment

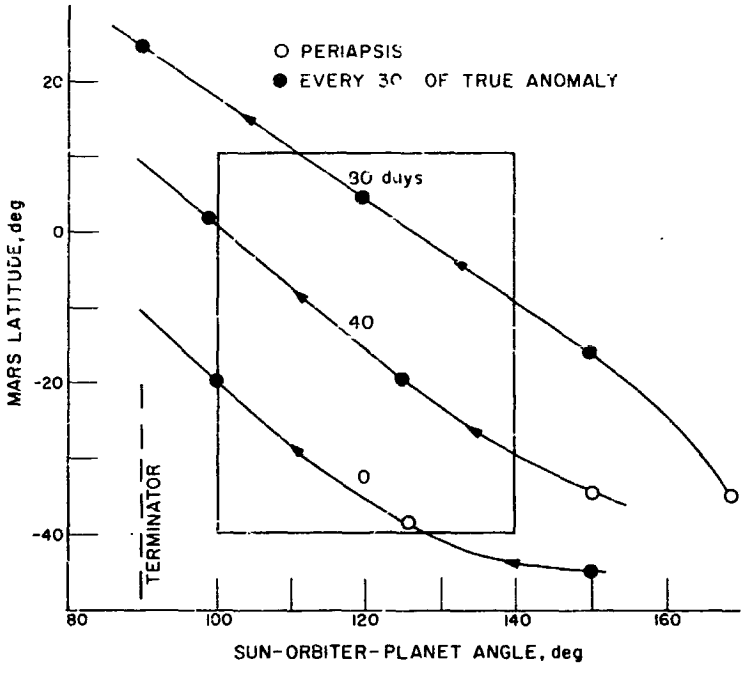


Figure 8-69. Latitude/Lighting Coverage for Type I-B, 1500 by 50,000 km Orbit Profile Inclined 45 Degrees Below Mars Equator

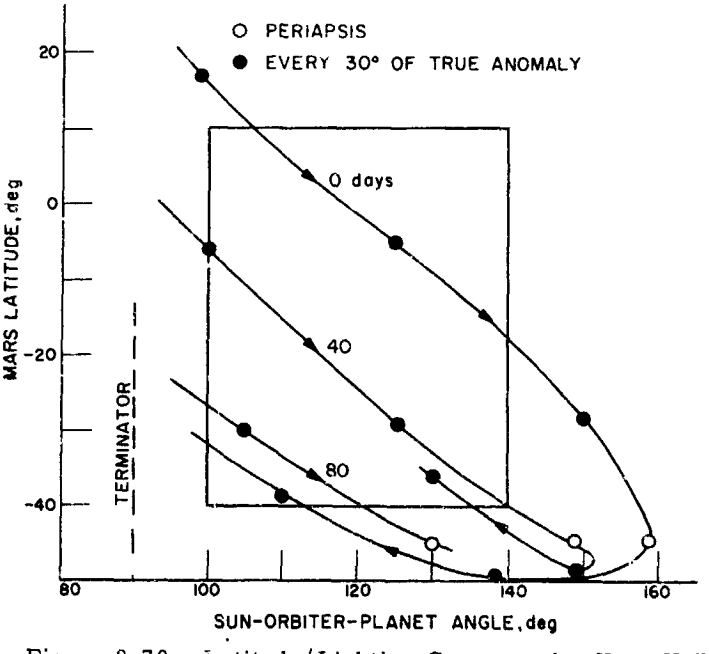


Figure 8-70. Latitude/Lighting Coverage for Type II-B 1500 by 50,000 km Orbit Profile Inclined 50 Degrees Below Mars Equator

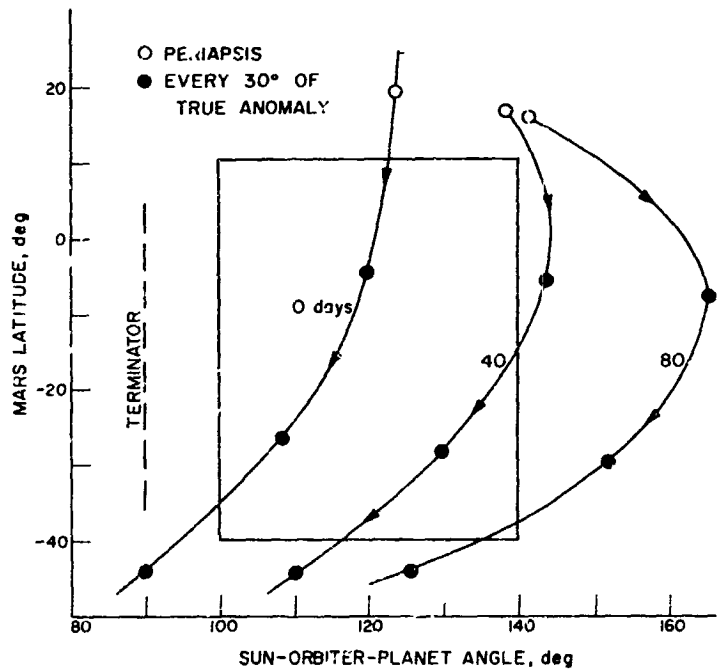


Figure 8-71. Latitude/Lighting Coverage for Type II-B 1500 by 50,000 km Orbit Profile Inclined 50 Degrees Above Mars Equator

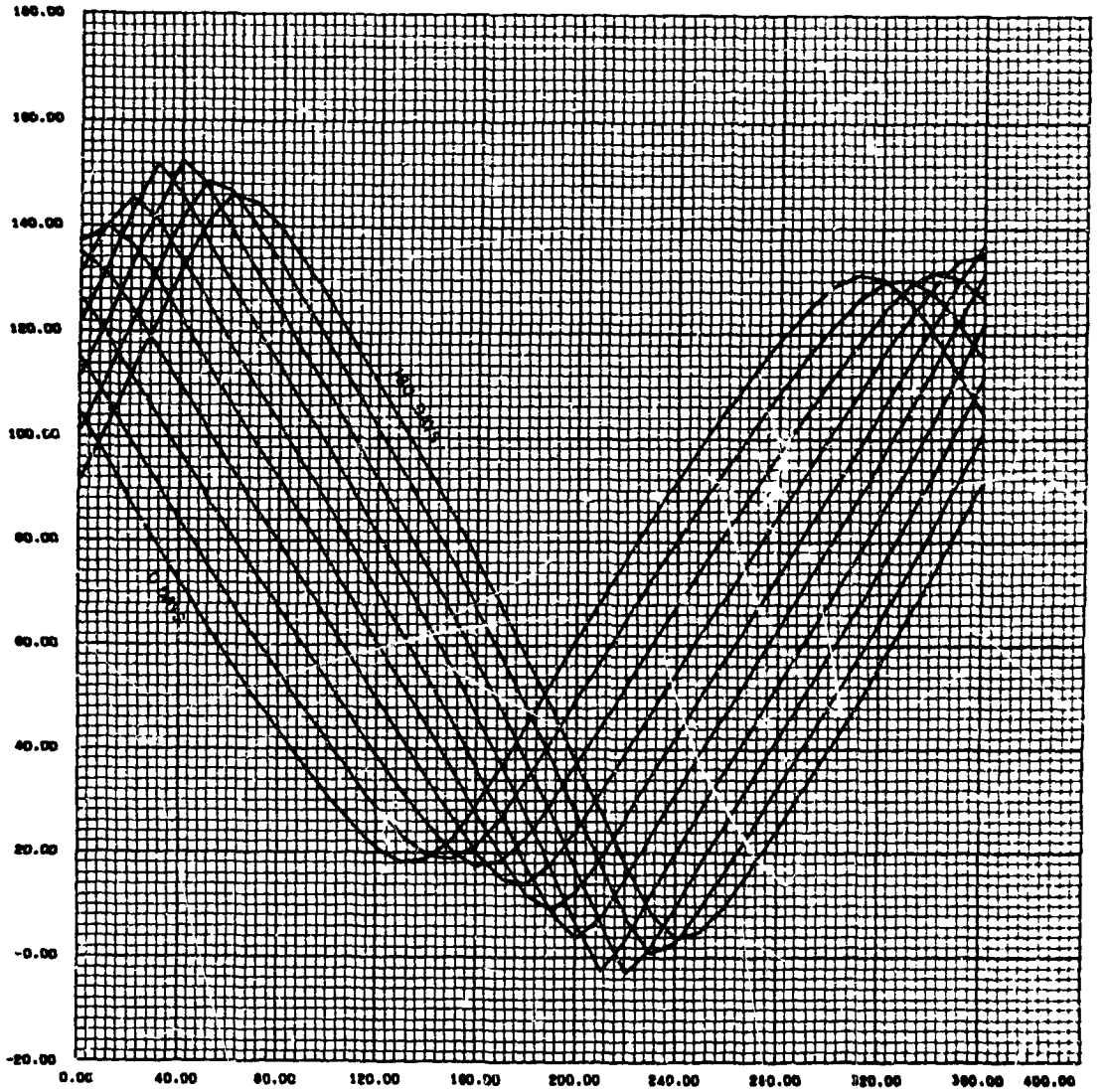


Figure 8-72. Sun-Spacecraft-Planet Near-Limb Angle vs Orbiter True Anomaly, Mars 1969 Type I-B, Nominal 4000 by 50,000 km, Inclination = -45 Degrees

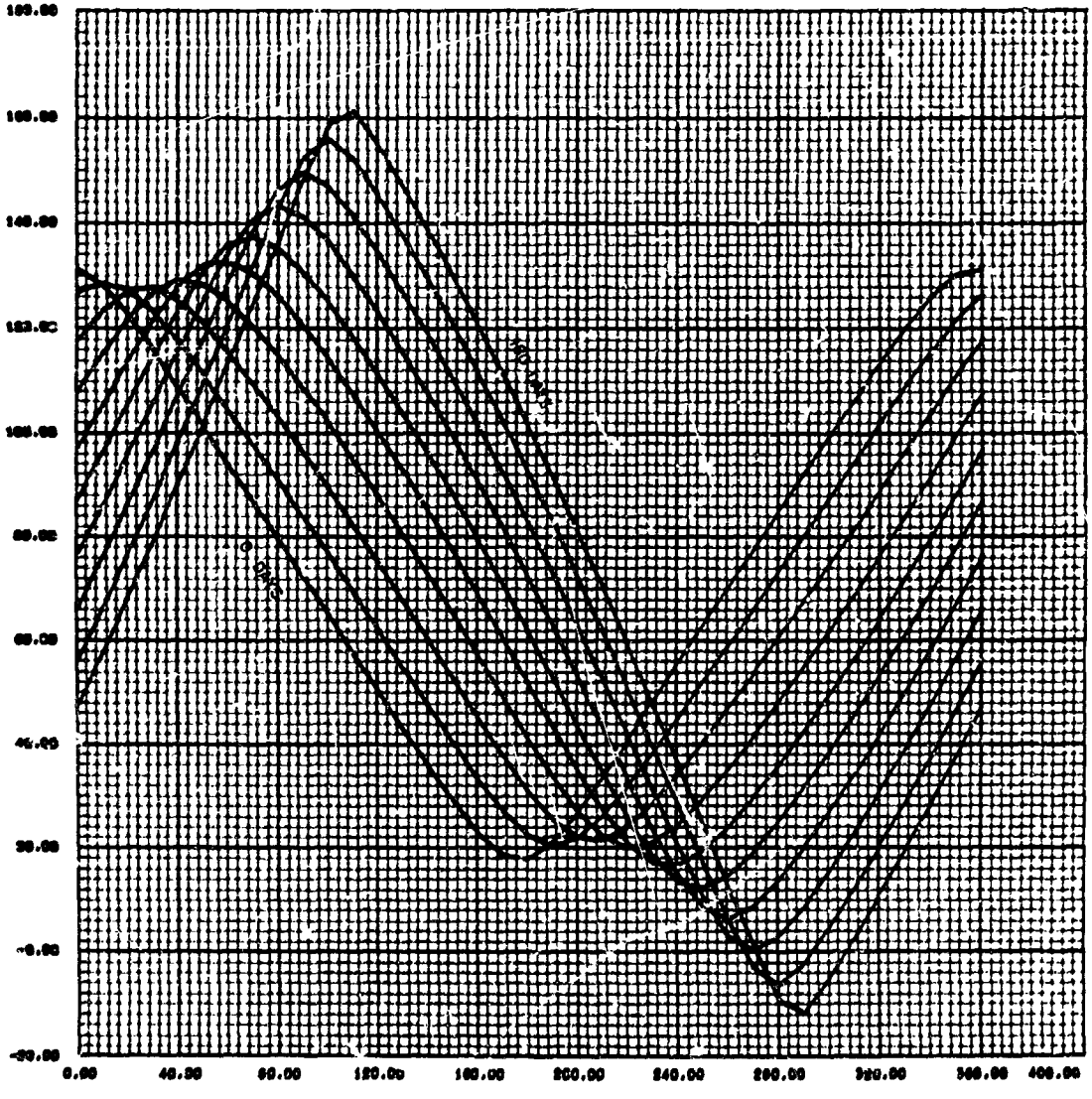


Figure 8-73. Sun-Spacecraft Near-Limb Angle vs Orbiter True Anomaly, Mars 196º Type II-B, Nominal 4000 by 50,000 km, Inc. = -50 Degrees

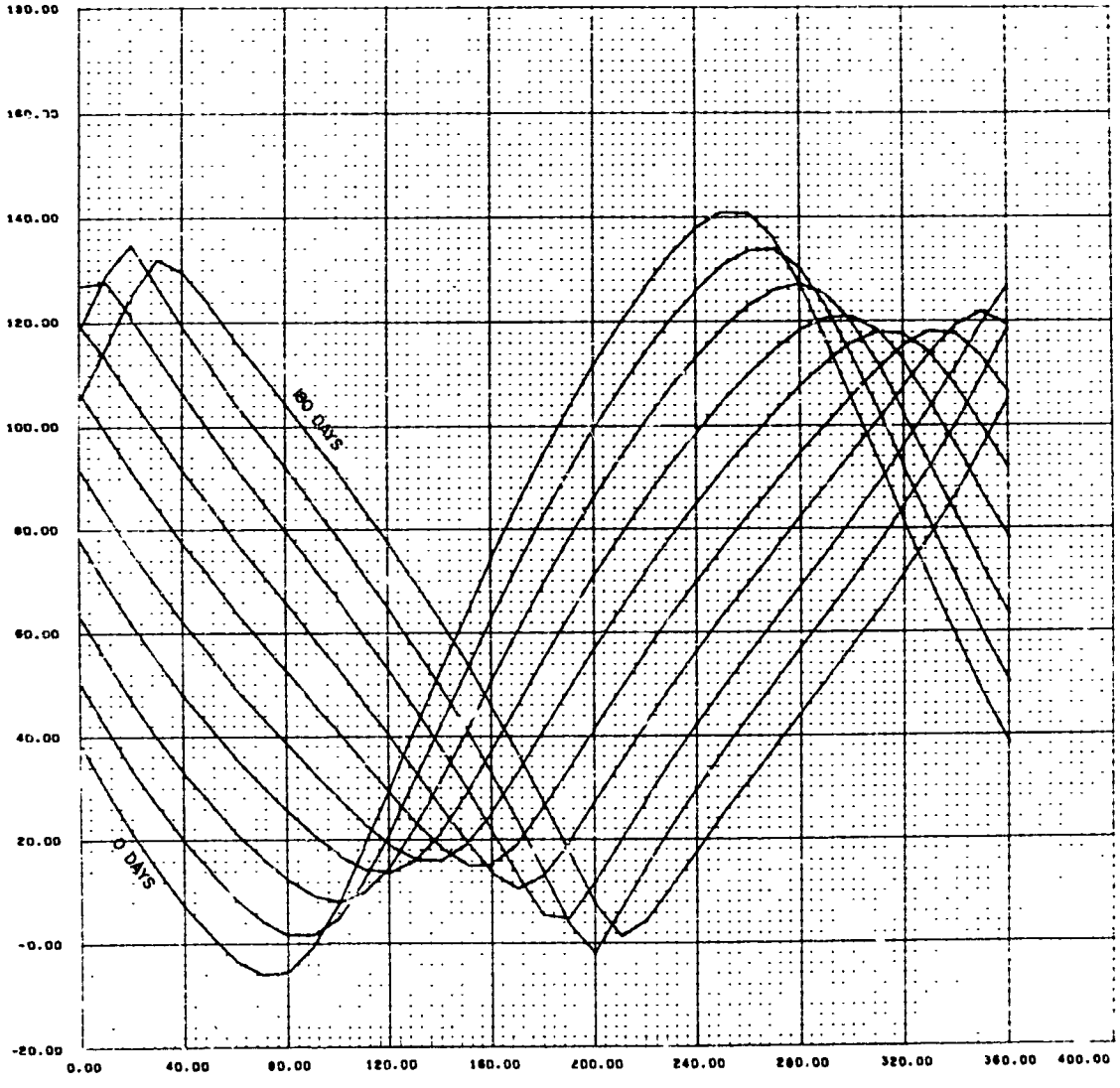


Figure 8-74. Earth-Spacecraft-Planet Near-Limb Angle vs Orbiter True Anomaly, Mars 1969 Type I-B, Nominal 1500 by 50,000 km, Inc. = -45 Degrees

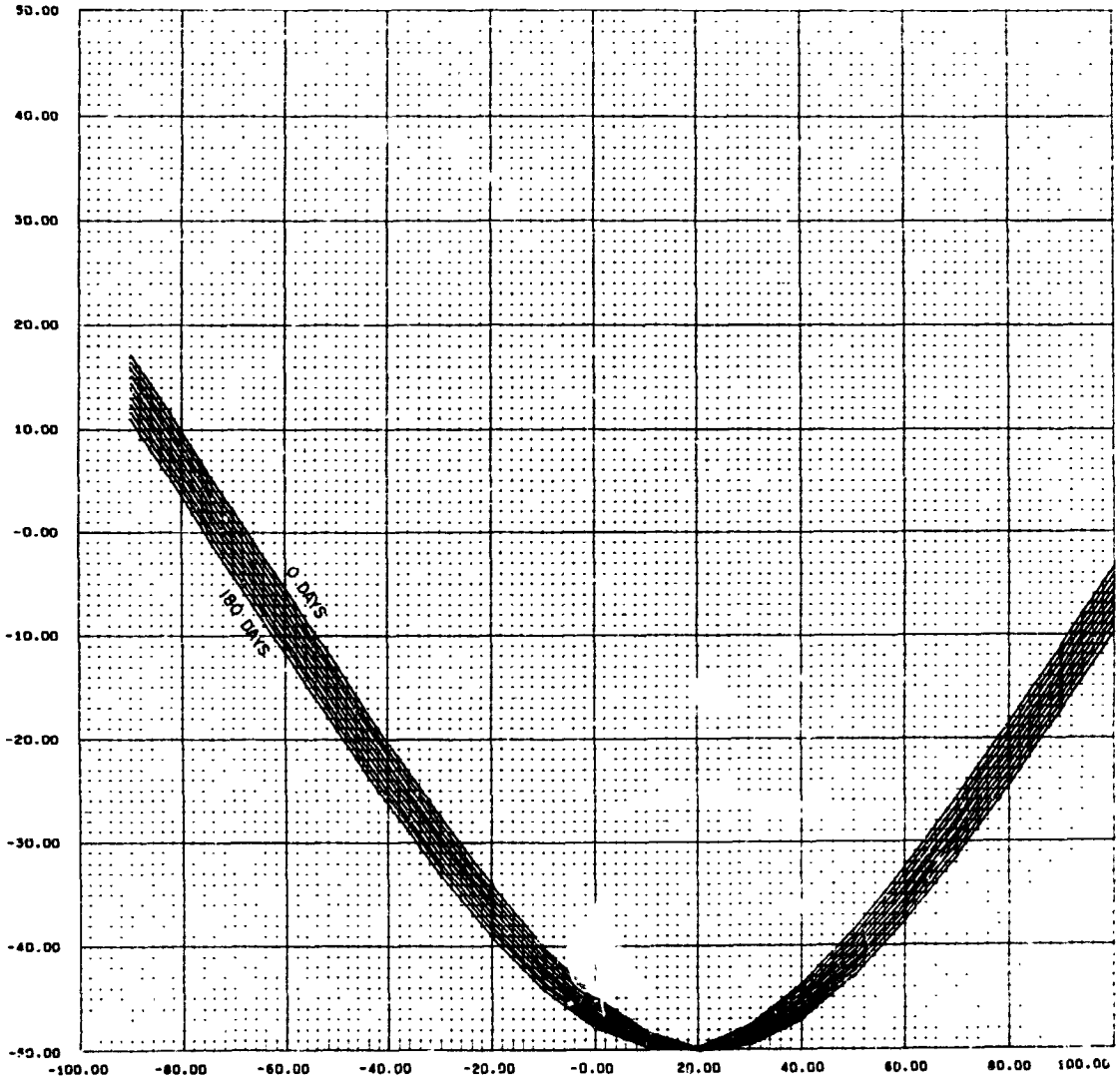


Figure 8-75. Latitude of Spacecraft vs Orbiter True Anomaly, Mars 1969 Type II-B, Nominal 1500 by 50,000 km, Inc. = -50 Degrees

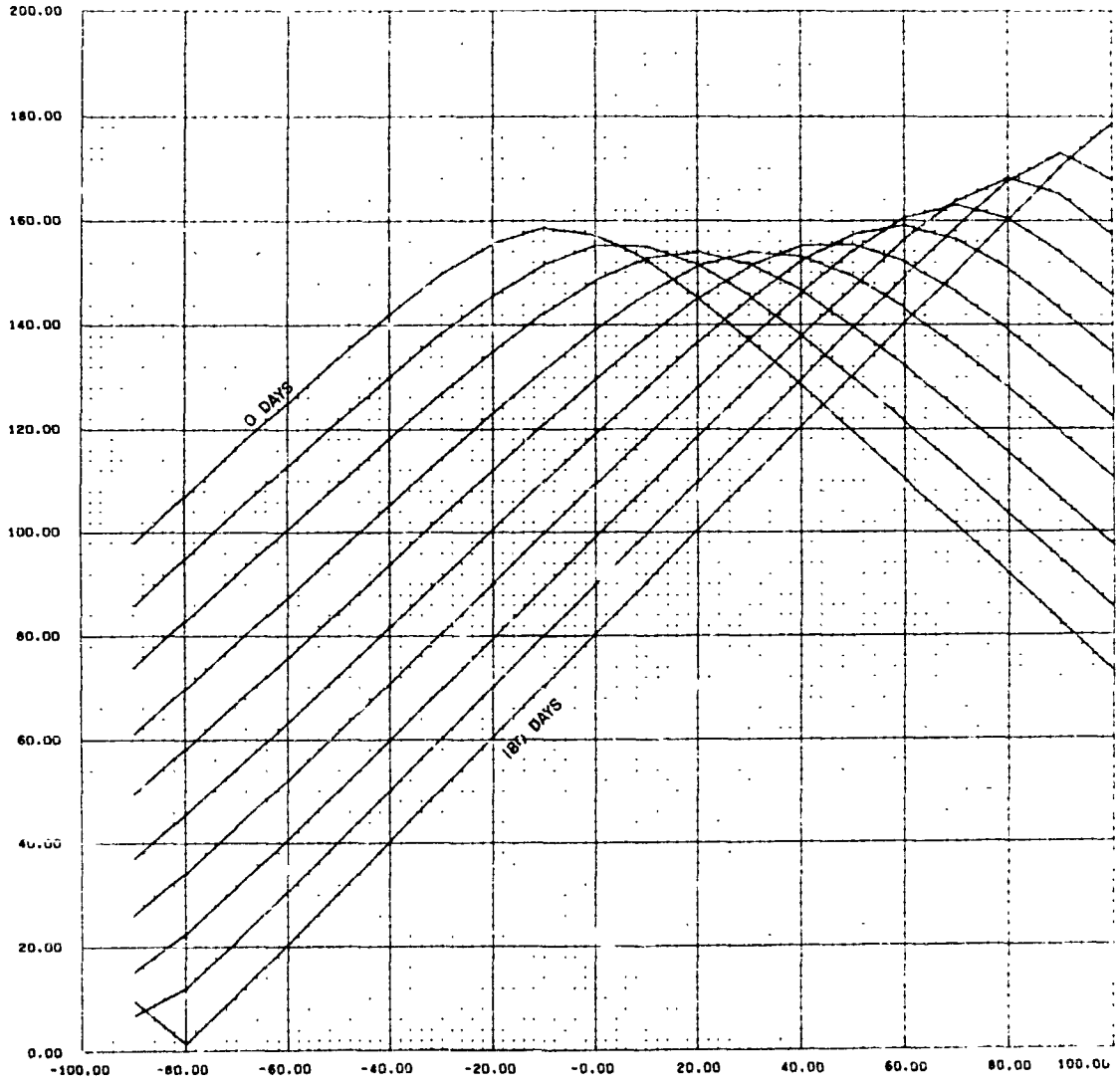


Figure 8-76. Sun-Spacecraft-Planet Angle vs Orbiter True Anomaly, Mars 1969 Type II-B, Nominal 1500 by 50,000 km, Inc. = -50 Degrees

altitudes. Figure 8-71 illustrates the coverage geometry for a northerly-direct Type II orbit. There is excellent north-to-south coverage for about the first 40 or 50 days, but these northerly orbits were not selected because of the less attractive Canopus situation and also because of the absence of Earth occultation. It would not be unlikely, however, that a change in emphasis or certain assumptions could make these northerly-direct shots (upper portion of region E' of Figure 8-55) possibly more attractive than the southerly-direct orbits.

Figures 8-72 through 8-76 are automatic plots from the Planetary Orbiter Study Program and demonstrate typical methods which are available for the presentation of the long-term behavior of certain key-orbit parameters. The curves of Figure 8-72 represent single orbits at 0, 20, ... 180 days following initial orbit establishment. It can be seen that Sun occultation does not first occur until about 110 days after encounter, and ends approximately 160 days after encounter. As the plot program connects data points with straight lines, some of the curves are not as smooth as they should be. The length of Sun occultation during an orbit at, say, 120 days after encounter can be determined by noting the true anomaly values which bound the occultation and then referring to Figure 8-46. The time required to go from a true anomaly of 207 to 215 degrees is the same (because of symmetry) as the time between 145 degrees and 153 degrees. From Figure 8-46 this time would be about 140 minutes. Figures 8-75 and 8-76 were used jointly to obtain the coverage information displayed in Figure 8-70.

7. Type I vs Type II Trajectories

The Type I trajectories exhibit the following advantages over the Type II trajectories:

1) The flight times are shorter by about 3 months.
2) The orbit-determination accuracies (Subsection 8.C) are significantly better during the early portion of the flight, and trajectory dispersions at Mars are much less sensitive to maneuver execution errors.
3) The Type I trajectories arrive before the "wave of darkening" has completed its northward progression.
4) The earlier arrival dates result in shorter Earth-Mars distances at given times after encounter.
5) The low-gain antenna geometry is better during the early part of the flight.
6) The coast times are shorter, hence less Centaur boil-off losses.
7) Except for the fact that the morning terminator may be slightly preferred over the evening terminator, the Type I satellite orbit profile exhibits better planetary coverage (latitude, lighting angle, and low altitudes near periapsis) during the first month following initial orbit establishment.

The Type II trajectories exhibit the following advantages over the Type I trajectories:

8) For launch periods in excess of about 15 to 20 days, the Type II trajectories realize a slightly larger mass in orbit. Or, equivalently, for values of orbiter mass less than a certain value, much longer launch periods (see Table 8-4) can be achieved by using the Type II transits.
9) The Type II trajectories can utilize the conventional southeast launch azimuths, thus maintaining minimum kill probability levels.
10) With respect to variable propellant loading, the Type II mission would not need to on-load fuel until the latter portion of the launch period, whereas the Type I mission would require off-loading early during the period.
11) In the event that variable loading is not feasible and fixed loading must be assumed, the Type II mission exhibits more flexibility in terms of being able to establish tighter orbits at Mars for launches during the early portion of the firing period, as the Type II trajectories start out with the lowest approach speeds at Mars.
12) The geometry is more favorable for pointing the high-gain antenna towards the Earth during the orbit-insertion attitude.
13) The potential exists for obtaining good north-to-south coverage (see Figure 8-71) for northerly-direct orbits if Canopus can be allowed to come near the Mars limb. Also, the currently selected Type II orbits favor the morning terminator by a month of so after encounter.
14) The Earth-occultation geometry is slightly better for the southerly-direct Type II orbit profiles.

8. Summarizing Remarks

The significant points covered in Subsection VIII.B may be summarized as follows:

1) Paragraph B.1 discussed the many factors which must be carefully considered in order to arrive at an acceptable orbit profile. One of the strongest factors involves the selection of a nominal periapsis altitude which is of sufficient height to ensure an orbit lifetime of 50 years.
2) Paragraph B.3 concluded that, if the NASA "maximum" atmospheric density model is assumed, the periapsis altitude must be in the region of 4000 km. It was also noted in this subsection that it is extremely important to agree upon and define a standard high-altitude density model to be used in future orbiter studies.
3) Paragraph B.4 concluded that a 1000-lb orbiter mission is feasible with the 30 percent FLOX LeRC (revised) estimates, but not with the 30 percent FLOX original NASA performance estimates. These two sets of performance

estimates differ in injected payload capability by nearly 410 lbs. We are operating in a very critical region, and slight changes in various assumptions have strong effects upon mission feasibility. The Type I achievable mass in orbit is a very strong function of the DLA assumed, and no theast launches must be used. Increasing the periapsis altitude from 1500 km to 4000 km requires an additional injected weight of 250 lbs in order to achieve the same final useful mass in orbit. Assuming a 30-day launch period for either Type I or Type II trajectories, the use of variable propellant loading (as opposed to fixed loading) results in a gain of 60 to 70 lbs of useful mass in orbit.

4) Paragraph B.6 illustrates potentially attractive orbit profiles which satisfy most of the desired constraints. Increasing the periapsis altitude from 1500 km to 4000 km improves the Canopus geometry and delays Sun occultation, but the chances of performing an Earth occultation experiment are diminished. Southerly-direct orbit profiles appear the most attractive and result in good coverage of the preferred southerly Mars latitude regions.

REFERENCES

B-1. JPL IOM from R.A. Mecklatchey to R.J. Richard entitled "Estimate of Atmospheric Parameters in the Upper Atmosphere of Mars", dated September 29, 1964.

B-2. "NASA Standard Engineering Models of the Mars Atmosphere" (Unpublished Preliminary Draft), Edited by G.M. Levin, D.E. Evans, V. Stevens.

B-3. JPL T.M. 312-307 entitled "The Effect of Atmospheric Drag on the Lifetime of Mars Orbiters", by A. Kliore, dated May 6, 1963.

B-4. JPL T.M. 312-161 entitled "Precession Rates of a Satellite Due to the J-Term in the Gravity Field", by J. Lorell, dated January 29, 1962.

B-5. JPL T.M. 312-162 entitled "Long-Term Perturbations of a Moon Satellite By the Earth and Sun", by J. D. Anderson, dated February 8, 1962.

B-6. Journal of Geophysical Research, Vol. 69, No. 9, "On Exospheric Drag as the Cause of the Supposed Secular Accelerations of Phobos", by G. F. Schilling, May 1, 1964.

C. ORBIT DETERMINATION

1. Summary

From a preliminary analysis of three 1969 Mars orbiter trajectories, it appears that there is a significant difference in the orbit determination accuracy between the Type II trajectory and the two Type I trajectories. This difference is especially noticeable in the earlier portion of the flight. The discrepancies are much less pronounced in the later portions of the trajectories.

2. Assumptions

This section presents the results of a preliminary orbit determination accuracy study made using three representative trajectories for the Mars 1969 orbiter mission. Two typical Type I trajectories are compared with a Type II. Each of these was used to investigate the improvement in orbit determination accuracy to be expected from using a smaller assumed noise on the data.

TRAJECTORIES

Designation:	I-A	I-C	II-B
Type:	I	I	II
Launch date:	March 7, 1969	April 4, 1969	January 24, 1969
Arrival date:	Sept. 7, 1969	Oct. 3, 1969	Oct. 23, 1969
Flight time (days):	184	182	272
Inclination of orbit to ecliptic (degrees):	2.93	2.41	3.34
ction energy C_3 km^2/sec^2):	8.87	16.11	11.98

The trajectories were run using the following spacecraft constants:

$$\text{mass} = 908 \text{ kg}$$
$$\text{area} = 13 \text{ m}^2$$
$$\gamma_B = 0.096$$

CONDITIONS USED

Range-rate data were taken from Goldstone and Johannesburg, using an uncertainty first 0.01 meter/second, then of 0.001 meter/second in the measurements, corresponding to a one-minute sample rate and count time.

The following a priori uncertainties were assumed on the values of the physical constants estimated:

$\sigma G = .055$
$\sigma AU = 300$ km

Station locations:

$\sigma RI = 5$ meters (radius)
$\sigma LO = 5 \times 10^{-5}$ degrees (longitude)

The trajectories were started at five days from injection, at which point it was assumed that a midcourse maneuver had resulted in a spherical dispersion of 50 km in position (to simulate earth ephemeris errors) and 15 meters/second in velocity. Subsequent maneuvers were introduced at injection +30 days and at encounter -10 days. The orbit corruptions due to these maneuvers were taken, respectively, as 50 km in position and 5 m/sec in velocity for the second maneuver, and 50 km in position and 0.1 m/sec in velocity for the third maneuver. The velocity perturbations assumed for the first and second midcourse corrections are very pessimistic, as the expected midcourse velocity errors will be about two orders of magnitude smaller.

3. Discussion of Results

Upon examination of Tables 8-10 through 8-13, one first notices that there are significant differences between the trajectories, particularly in the semi-major axis and the flight-time uncertainty. The most striking difference is that of the Type II trajectory compared to the two Type I's. There is, however, a smaller but still noteworthy discrepancy between the two Type I trajectories. The orientation angle shown in Table 8-12 is measured clockwise from the $\bar{T}$ axis to the major axis of the uncertainty ellipse.

These differences have not as yet been fully explained. One reason that the Type II trajectory dispersions are so much larger than those for the Type I trajectories is that the longer flight time for the Type II magnifies the effect of the uncertainty in the solar pressure.

Another factor that must be taken into consideration is the approach geometry. For trajectory I-A the incoming asymptote lies very near the Earth-Mars line, while that of I-C is approximately 33 degrees away from this line, and II-B approaches about 60 degrees away from the Earth-Mars line. This indicates that astronomical unit uncertainties should map primarily into position errors along $\bar{S}$ (equivalently, flight-time errors) as opposed to dispersions normal to $\bar{S}$ (errors in the $\bar{R}$-$\bar{T}$ plane).

Table 8-10. Semi-Major Axis of Dispersion Ellipse (Kilometers)

Trajectory		II-B		I-A		I-C	
σ_R (m/sec)		0.01	0.001	0.01	0.001	0.01	0.001
Injection	+10 d	4363	1669	193	87	642	180
	20	1,018	525	90	82	189	117
	30	711	428	84	81	152	109
	30*	262,565	262,563	50,369	50,369	85,125	85,248
	50	855	374			215	115
	100	259	180	87	63	116	45
	150	237	77	71	14	82	12
	200	85	9.3				
	250	32	3.3				
Encounter	-10 d	28	2.9	51	8.6	73	11
	-10*	104	101	112	100	118	94
	-2	83	38	103	33	112	43
	-2 h	75	19	94	29	99	34
	-1 h	72	19	92	22	98	27
	-30 m	63	9.7	35	4	38	4.5
	10 m	16	1.9	2.9	0.44	3.5	0.39
Encounter E		6.2	0.68	0.43	0.06	0.49	0.05

*After maneuver. The preceding values (at the same time) refer to the accuracy immediately before the maneuver.

Table 8-11. Semi-Minor Axis (Kilometers)

Trajectory		II-B		I-A		I-C	
$\sigma_{\dot{R}}$ (m/sec)		0.01	0.001	0.01	0.001	0.01	0.001
Injection	+10 d	221	62	121	22	139	75
	20	62	30	38	12	73	23
	30	51	28	23	8.0	37	6.9
	30*	26,833	26,818	42,952	42,952	35,728	35,724
	50	114	22			90	20
	100	54	7.9	16	1.9	52	11
	150	37	4.2	12	1.4	43	78
	200	28	3.1				
	250	23	2.4				
Encounter	-10 d	21	2.2	12	1.3	32	4.6
	-10*	102	100	101	100	98	93
	-2	46	26	46	22	52	31
	-2 h	4.4	0.76	8.8	1.4	5.0	0.87
	-1 h	1.4	0.20	2.0	0.26	1.2	0.16
	-30 m	0.52	0.08	0.50	0.06	0.38	0.05
	-10 m	0.17	0.04	0.13	0.02	0.06	0.01
Encounter E		0.17	0.04	0.07	0.01	0.01	0.00

*After maneuver. The preceding values (at the same time) refer to the accuracy immediately before the maneuver.

Table 8-12. Orientation Angle (Degrees)
(Measured Clockwise from $\overline{T}$ to Major Axis)

Trajectory		II-B		I-A		I-C	
σ_R (m/sec)		0.01	0.001	0.01	0.001	0.01	0.001
Injection	+10 d	34	34	15	64	10	178
	20	31	30	62	65	171	150
	30	30	29	66	65	156	149
	30*	26	26	86	86	167	167
	50	24	25			141	150
	100	18	22	71	69	142	161
	150	19	22	69	68	126	113
	200	10	11				
	250	150	149				
Encounter	-10 d	130	128	72	70	112	109
	-10*	142	175	72	4	113	156
	-2	102	4	92	88	101	108
	-2 h	97	98	92	90	90	89
	-11 h	98	98	92	91	89	89
	-30 m.	97	97	93	94	90	91
	-10 m.	96	96	98	96	94	94
Encounter E		96	97	112	116	98	98

*After maneuver. The preceding values (at the same time) refer to the accuracy immediately before the maneuver.

Table 8-13. Flight Time Uncertainty (Seconds)

Trajectory		II-B		I-A		I-C	
$\sigma_{\dot{R}}$ (m/sec)		0.01	0.001	0.01	0.001	0.01	0.001
Injection	+10 d	1229	504	123	53	341	104
	20	274	128	74	49	98	75
	30	186	106	57	48	82	71
	30*	68,706	68,661	31,624	31,624	31,219	21,159
	50	212	88			85	74
	100	61	44	54	39	75	33
	150	57	19	41	7.0	45	0.2
	200	20	2.2				
	250	6.2	0.64				
Encounter	-10 d	48	0.50	24	3.1	28	3.1
	-10*	26	26	33	22	37	25
	-2	9.8	8.0	3.8	1.1	5.7	2.6
	-2 h.	1.2	0.26	2.7	0.90	2.1	0.69
	-1 h	0.89	0.22	2.7	0.64	2.0	0.55
	-30 m	0.80	0.12	0.94	0.11	0.77	0.09
	-10 m	0.19	0.02	0.04	0.01	0.07	0.01
Encounter E		0.13	0.01	0.01	0.00	0.05	0.01

*After maneuver. The preceding values (at the same time) refer to the accuracy immediately before the maneuver.

Pending an investigation of the relative effects of the separate error sources, it appears that the most promising explanation of the large differences in accuracy is to be found in the geometry of the trajectories relative to the Earth. That is, the direction of the range rate measurements with respect to the critical plane must be examined. If it is found that the range rate measurements are being taken nearly perpendicular to this plane, the dispersions will be larger than the uncertainties corresponding to a case where the measurements are taken closer to the plane.

As a result of the unusually large Type II orbit determination uncertainties early in flight, it was decided to assume a more optimistic midcourse velocity corruption of 0.1 meters/second. For this case, range-rate data ($\sigma\dot{R}$ = 0.01 m/sec) were fitted for the period from injection to injection plus thirty days, with a maneuver at five days introducing corruptions of 50 km in position and 0.1 meters/second in velocity. The Earth's gravitational constant was estimated in addition to the other parameters, since the near-Earth portion of the trajectory was included. The a priori uncertainties used were:

$\sigma X = \sigma Y = \sigma Z = 1000$ km
$\sigma \dot{X} = \sigma \dot{Y} = \sigma \dot{Z} = 100$ km/sec
$\sigma KE = 4$ km^3/sec^2
$\sigma G = 0.055$
$\sigma AU = 300$ km
$\sigma RI = 5$ meters
$\sigma LO = 5 \times 10^{-5}$ degrees

} essentially no a priori knowledge

the same case was also run using a reduced AU uncertainty of 100 km, and the results are given in Table 8-14.

Comparing these results with the earlier tables, it can be seen that the use of the smaller maneuver uncertainty results in an improvement by a factor of almost three at I + 10 days, but that this difference has virtually disappeared by I + 30 days. It should be noted at this point that standard orbit determination policy is to make no assumptions regarding the accuracy of the maneuver and, instead, to let the orbit determination techniques re-establish the orbit.

It is very important to note that no significant improvement is achieved by using the smaller uncertainty in the astronomical unit.

The same case (with σAU = 300) was used to examine the relative effects of the various error sources. To do this, the set of estimated parameters was varied, all other factors being held constant. The sets used are as follows:

Case Designation	A	B	C	D	E	F
Position and Velocity	X	X	X	X	X	X
Earth Gravitational Constant			X	X	X	X
Solar Pressure Constant		X		X	X	X
Astronomical Unit		X	X		X	X
Station Locations		X	X	X		X

Table 8-14. Trajectory II-B

Time	Semi-Major Axis (km)		Semi-Minor Axis (km)		Orientation of Major Axis (deg)		Flight Time Uncertainty (sec)	
σAU (km)	300	100	300	100	300	100	300	100
Injection + 2 d	1009	985	70	58	33	34	307	302
5	724	690	46	28	32	33	213	206
5 (M/C)	5848	5844	622	622	31	31	1743	1742
10	1679	1665	78	68	33	32	483	480
15	1029	1006	52	38	32	33	283	278
20	830	802	43	2	32	32	219	212
25	749	718	39	22	31	32	193	185
30	697	664	37	20	31	32	178	169

Case F, with all the parameters being estimated, is the case tabulated above; it is included here and in Tables 8-15 through 8-17 in order to facilitate comparison. Orientation angle has not been shown in the tables, as it was between 30 and 35 degrees for all of the cases.

4. Concluding Remarks

It is apparent from the results in Tables 8-15 through 8-17 that until about the time of the maneuver, solar pressure uncertainty is the largest contributor to the semi-major axis and flight-time uncertainty. After the maneuver, however, station location errors become increasingly important, soon dominating the other error sources even though the assumed uncertainties in station locations were quite small. It is interesting to note that the contributions due to the astronomical unit and the Earth's gravitational constant are relatively minor.

Table 8-15. Semi-Major Axis of Dispersion Ellipse (Kilometers)

Case	A	B	C	D	E	F
Injection + 2 d	697	999	787	982	969	1009
5	336	648	462	686	681	724
5(M/C)	5813	5840	5822	5844	5843	5848
10	1528	1651	1610	1663	1607	1679
15	841	1016	977	1003	907	1029
20	590	820	783	798	660	830
25	460	737	689	714	551	749
30	376	684	622	659	490	697

Table 8-16. Semi-Minor Axis (Kilometers)

Case	A	B	C	D	E	F
Injection + 2 d	47	66	70	56	70	70
5	20	46	44	24	45	46
5(M/C)	621	622	622	622	622	622
10	64	78	78	67	76	78
15	30	52	50	36	50	52
20	17	43	42	24	41	43
25	14	39	39	19	36	39
30	12	37	37	16	33	37

Table 8-17. Flight Time Uncertainty (Seconds)

Case	A	B	C	D	E	F
Injection + 2 d	211	307	230	301	301	307
5	96	190	124	205	206	213
5(M/C)	1732	1740	1734	1742	1742	1743
10	440	473	459	479	467	483
15	238	280	272	277	255	283
20	163	217	210	211	180	219
25	125	191	180	184	148	193
30	101	174	160	168	130	178

The question will undoubtedly arise as to whether the extremely small dispersions near encounter are to be trusted. At present, this cannot be answered with any degree of confidence. The model presently in use includes the effect of astronomical unit uncertainty on the target planet's ephemeris, but does not take into account other uncertainties in the ephemeris. These are currently estimated as about 50 km in each of three coordinate directions. Adding a 50-km spherical dispersion to the probe's covariance matrix at the time of the final maneuver is an attempt to account for this ephemeris uncertainty. This problem will be handled much more readily when the planetary ephemerides are added to the orbit determination program as parameters to be estimated. The target date for this addition is June, 1965.

Referring again to Table 8-10, it can be seen that the semi-major axis is determined to better than 100 km (1σ) by several weeks before encounter. If willing to perform a sufficient number of midcourse corrections (two or sometimes three) so as to approach the orbit determination knowledge, it should therefore be possible to achieve 3σ accuracies at Mars of the order of 300 km. Practical considerations, however, such as the number of maneuvers performed, required trajectory biasing, maneuver execution times, etc., may prevent the actual accuracy from being quite this good, but perhaps 500 km is a reasonable value which can be realized.

D. MIDCOURSE GUIDANCE

1. Introduction to Guidance Policy

The premission analysis of midcourse guidance must attempt to provide concepts and data which relate to the following:

1) The number of necessary midcourse maneuvers.
2) The times that these maneuvers should be executed.
3) The acceptable bounds for midcourse execution errors.
4) The degree of accuracy that may be expected at the target.

In premission studies, the velocity errors which will be corrected by the first midcourse maneuver must be formulated in terms of a random variable. The errors introduced in the execution of this maneuver will consist, in part, of random errors proportional to the magnitude of the maneuver. Consequently, the errors remaining after the first maneuver will be partially composed of execution errors proportional to the product of random variables, a decidedly non-Gaussian distribution of errors. The consideration of further maneuvers only aggravates the already complex probability distribution. Analysis of the multiple maneuver problem must therefore utilize either a complex technique such as Monte Carlo analysis, or a series of tractable approximations to the actual probability distribution. The latter technique will be employed in this discussion of the midcourse guidance policy for a 1969 Mars orbiter mission.

Any acceptable maneuver policy must satisfy the currently specified NASA constraint that the probability of an unsterile spacecraft impacting Mars must not be greater than 10^{-4}. This constraint will necessitate a translation of the aiming point for the first midcourse maneuver, because of the possibility that later maneuvers may fail due to deterioration of the spacecraft. The translation of any maneuver aiming point away from the final aiming point will be referred to as "biasing" of the aiming point. As we shall subsequently demonstrate, this biasing will have a degrading effect upon the resultant accuracies at the target.

Relative to the above considerations, the maneuver policy for a typical multiple maneuver mission would entail the following sequence of events: The first maneuver would be executed when a sufficient quantity of orbit determination data had been accumulated and processed, typically within a few days after injection. The approximate size of the necessary maneuver would be calculated, and thus the approximate execution errors could be expressed in simple Gaussian form. The actual aiming point would then be determined such that the overall probability of impacting the planet (including the estimated reliability of subsequent maneuvers) would not exceed 10^{-4}. The first maneuver would then be executed, and tracking of the spacecraft would continue. The second maneuver, which would remove the bias and execution errors of the first maneuver, could be made when the orbit determination

uncertainties had diminished sufficiently to ensure the desired final accuracy. This might occur as early as 20-30 days after injection, or as late as a few weeks prior to encounter. If the errors in the second maneuver were still too great, a third maneuver might be required. The execution of the second and, if required, the third maneuver would be determined by an adaptive policy, i.e., the times of execution would be decided during the evolution of the flight.

2. Midcourse Velocity Allocation

The 1σ first midcourse velocity requirement to correct for Centaur injection guidance errors should be on the order of 10-15 meters/second. In order to maintain a sufficient correction capability to handle certain non-standard errors (in addition to the expected random errors) that do not abort the mission and that can be corrected, given additional midcourse fuel, it is usually wise to carry more nearly 5σ than 3σ correction capability. This allowance would be particularly important if the midcourse propulsion system was separate from the main retro propulsion system. This would then say we should allow some 50-75 meters/second to handle the first midcourse correction.

The performance of a second midcourse correction (to handle dispersions and adjust for biasing of the aiming point) should require at most only a few meters/second if applied earlier than about a month or so before encounter. Corrective velocity requirements would only begin to increase appreciably if a "moderate" correction was planned during the last few days prior to encounter. Even in the unlikely situation of attempting to change the aiming point by as much as 10,000 km with a maneuver as late as E-5 days, still only some 25 meters/second would be required. In summary, then, the total correction velocity capability which should be allocated for the 1969 mission has a minimum value of about 50 meters/second and a maximum value of 100 meters/second. For planning purposes, the lower figure of 50 meters/second may be used when the midcourse fuel is taken from a single large tank which supplies the retro fuel necessary for orbit establishment. On the other hand, in the event that a separate midcourse propulsion system is required (as a result of using a solid retro motor, for example), it is mandatory that an adequate allowance be carried. In this latter situation, 100 meters/second is recommended. If a very tight payload situation should exist, however, it may be possible to back off on the 100 meter/second figure down to perhaps 75 meters/second.

3. The First Maneuver and its Execution Errors

The magnitude of the first midcourse maneuver will be determined by the accuracy of injection. Recent estimates of the Centaur injection errors have placed the "figure of merit," i.e., the RMS velocity magnitude needed to correct injection errors, in the region of about 10 meters/second.

$$FOM = \sqrt{\overline{V^2}} = \sqrt{\overline{V_x^2} + \overline{V_y^2} + \overline{V_z^2}} = 10 \text{ meters/second}$$

If the injection errors are assumed to be spherically distributed,* i.e., equally distributed in all directions, then:

$$\overline{V_x^2} = \overline{V_y^2} = \overline{V_z^2} = 33.3 \text{ meters}^2/\text{second}^2$$

The performance of the first maneuver will be accompanied by errors due to imperfect execution. Estimates for typical execution errors are:

Proportional errors:

σ_s = .01 = standard deviation of proportional shutoff error

σ_p = .01 radians - standard deviation of per axis pointing error

Non-Proportional errors:

σ_r = .05 m/s = standard deviation of shutoff resolution error

In JPL T.M. 312-155, C.R. Gates has described a method for computing the second moment of the resultant non-Gaussian execution errors. He has shown that the covariance matrix of execution errors is given by:**

$$\Lambda_{V\text{-exec}} = (\sigma_s^2 - \sigma_p^2)\,\Lambda_V + \sigma_r^2\,\Gamma + \sigma_p^2\,\overline{V^2}\,I$$

Where:

σ_s = standard deviation of proportional shutoff error

σ_p = standard deviation of per axis pointing error

σ_r = standard deviation of shutoff resolution error

Λ_V = covariance matrix of midcourse corrections

$\overline{V^2}$ = mean square velocity magnitude = $(FOM)^2$

Γ = covariance matrix of direction cosines of the midcourse correction

If we assume that the velocity corrections are spherically distributed, the above equation reduces to:

$$\Lambda_{V\text{-exec}} = \sigma_{exec.}^2\, I$$

*Recent studies have demonstrated that this is a reasonable approximation.

**The effect of autopilot errors has been excluded for the purposes of this study.

where:

$$\sigma_{exec.} = \sqrt{1/3 \left[(\sigma_s^2 + 2\sigma_p^2)(FOM)^2 + \sigma_r^2 \right]}$$

$\sigma_{exec.}$ = second moment of per axis execution error.

Using the values of σ_s, σ_p, σ_r and FOM we have quoted earlier, we conclude that:

$$\sigma_{exec.} = 0.104 \text{ meters/second}$$

The resolution error, σ_r, contributes only 0.004 meters/second to this total. We may, therefore, approximate the total second moment by 0.10 meters/second and, effectively, ignore the contribution of the resolution error for the first midcourse correction.

Velocity errors at the midcourse time (a few days after injection) may be mapped into coordinate dispersions at the target using the JPL Heliocentric Conic Program, which computes the partials of target miss with respect to velocity deviations along the standard trajectory. The result of this mapping is a dispersion ellipsoid at the target, which may be projected on to the $\overline{R}$-$\overline{T}$ plane to ascertain the magnitude of the miss components. Table 8-18 presents the resultant ellipses, which are obtained by mapping a spherically symmetric velocity covariance matrix of .10 meters/second (each axis) to the target for each of the six trajectories being studied. Figure 8-77 illustrates the behavior of this mapping (semi-major axis dispersion only) over the entire Mars 1969 Type I and Type II trajectory space. The Type II trajectories exhibit sensitivities (in the semi-major axis) to velocity errors (applied a few days past injection) of 3 to 4 times those of the shorter flight time Type I trajectories.

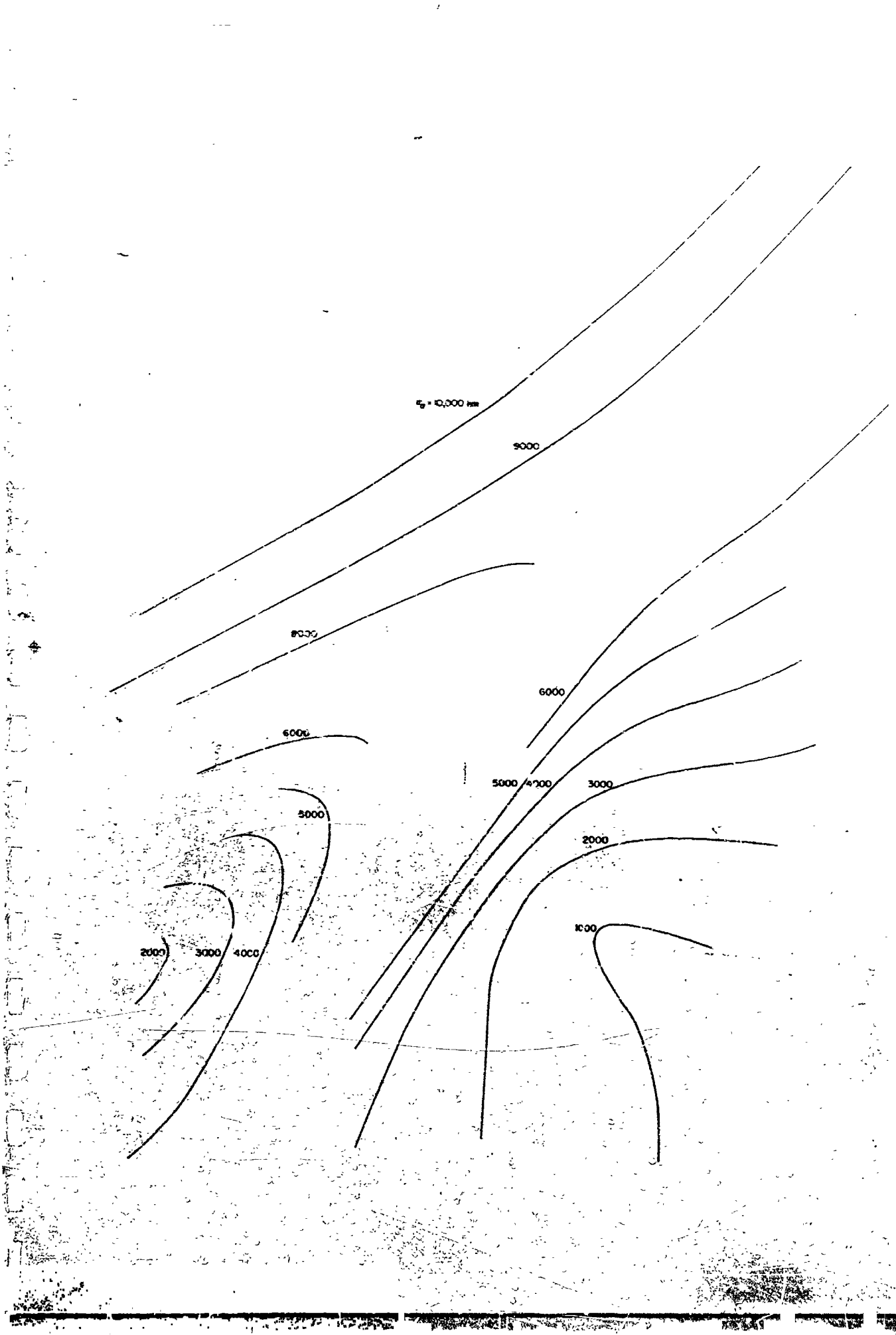
Table 8-18. Typical Dispersion Ellipses Due to First Maneuver Execution Errors of 0.1 meters/second per Axis

Trajectory	I-A	I-B	I-C	II-A	II-B	II-C
Semi-major axis (km)	2200	1470	1940	5200	5900	6700
Semi-minor axis (km)	760	800	580	520	530	560
Orientation clockwise from $\overline{T}$ (deg)	47	129	160	25	29	29

It is important to emphasize that the execution error distribution calculated in this premission analysis is decidedly non-Gaussian. The second moment of the distribution that we have calculated above is the second moment of the actual distribution. The usual conclusions about Gaussian probabilities cannot be extended to other properties of this distribution. In particular, we cannot construct simple 3σ ellipsoids and expect them to describe the usual percentage of all possible misses.

RED OVERLAY

Figure 8-77. Semi-Major Axis of Dispersion Ellipse


ϵ_p = 10,000 mm
9000
8000
6000
6000
5000
5000
4000
3000
2000
2000
3000
4000
1000

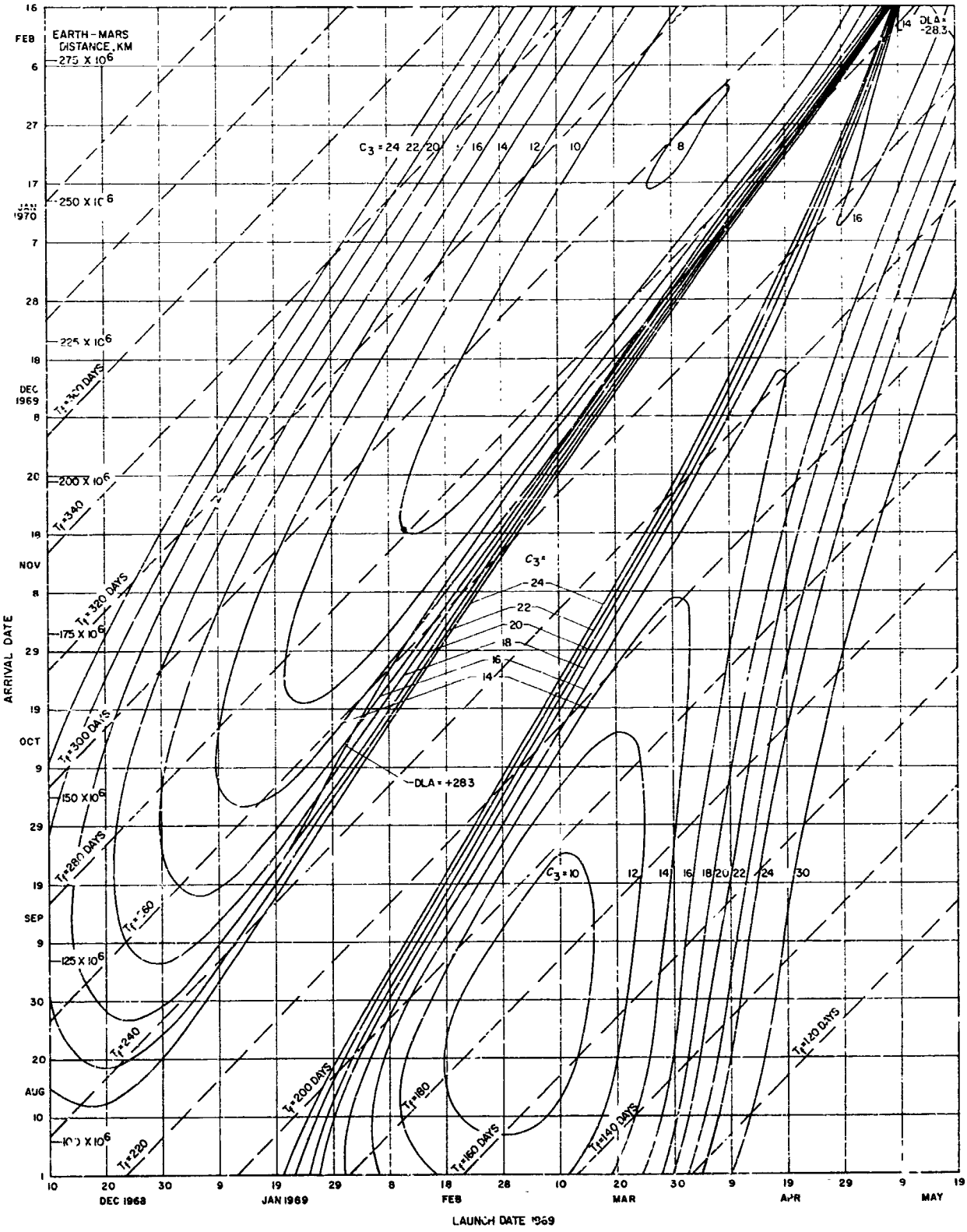


Figure 8-78. Basic Arrival Date vs Launch Date Trajectory Design Chart

A brief general investigation of this non-Gaussian probability distribution is presented here. The distribution of execution errors, produced when random proportional errors are multiplied by random velocity corrections, forms a Bessel function of the K_o type, which possesses significantly larger probabilities at the extremes of the distribution. In particular let us consider the one-dimensional case where $\delta V = \varepsilon V$, and ε and V are both Gaussian variables. ε describes the proportional error, V describes the magnitude of the maneuver, and δV the resultant magnitude of the error. We can show that:

$$\Pr(\delta V) = \frac{1}{\pi \sigma_\varepsilon \sigma_V} K_o\left(\frac{\delta V}{\sigma_\varepsilon \sigma_V}\right)$$

where K_o is the Bessel function described above.

And:

$$\Pr(\delta V > \delta V_o) = \int_{\delta V_o}^{\infty} \frac{1}{\pi \sigma_\varepsilon \sigma_V} K_o\left(\frac{\delta V}{\sigma_\varepsilon \sigma_V}\right) d(\delta V)$$

The value of the $\int_x^\infty K_o(t)\,dt$ are tabulated in various tables. In particular, from these tables we may conclude that if:

$$\frac{\delta V_o}{\sigma_\varepsilon \sigma_V} > 6.7,$$

then:

$$\Pr(\delta V > \delta V_o) < 10^{-4}$$

Therefore, in the one-dimensional case, we may pick a limit, δV_o, such that the probability of δV being greater than this δV_o is less than some prescribed value, for example, 10^{-4}.

This one-dimensional case may be extended to the three-dimensional spherically distributed case in the following manner: If we assume spherically symmetric velocity increments and error sources, the probability of any one component of the resultant product of random variables being greater than δV_o is less than 10^{-4}. Geometrically, we may say that δV_o is the radius of a sphere such that, if a plane is constructed tangent to this sphere at any point, the probability of the vector $\overline{\delta V}$ extending beyond this plane is less than 10^{-4}.

We may now extend this concept of the non-Gaussian probability limits to the problem of the execution errors resulting from a maneuver. For the present, we will assume that the dominant execution errors are the proportional errors, and neglect the effect of the smaller resolution errors. (This is, in fact, the case for a typical first midcourse maneuver.) With a spherically-distributed velocity correction, and a spherically-distributed

proportional error, we may construct a sphere in velocity space which represents the execution errors resulting from the first maneuver. In particular:

Since: FCM = 10/meters/second,

$$\sigma_v^2 \text{ per axis} = \overline{V_1^2} = 1/3\,(\overline{V_x^2} + \overline{V_y^2} + \overline{V_z^2}) = 1/3\,(FOM)^2$$

Then:

$$\sigma_v \text{ per axis} = \sqrt{\frac{(FOM)^2}{3}} = 5.8 \text{ m/sec}$$

And, of σ_ϵ equals .01 (corresponding to $\sigma_s = .01$, $\sigma_p = .01$ radians), and if:

$$\frac{\delta V_o}{\sigma_v \sigma_\epsilon} \text{ must be} > 6.7 \text{ if we require Pr } (\delta V > \delta V_o) < 10^{-4},$$

Then:

$$\delta V_o > (6.7)\,(.01)\,(5.8)$$

$$\delta V_o > .39 \text{ meters/second}$$

Therefore, if we construct a sphere of radius .39 m/sec in velocity space, the probability that an execution error will extend beyond a plane drawn tangent to this sphere is less than 10^{-4}. This sphere in velocity space may be mapped to the target yielding the ellipsoid of resultant dispersions at the target. The probability that an error at the target extends beyond a tangent plane to the ellipsoid is similarly less than 10^{-4}. The important dimensions of the $\overline{R}$-$\overline{T}$ ellipses are tabulated in Table 8-19 for each of the six trajectories under consideration.

Table 8-19. Error Ellipses Resulting From Spherical Velocity Errors of .39 m/sec

Trajectory	I-A	I-B	I-C	II-A	II-B	II-C
Semi-major axis (km)	8600	5730	7550	20,300	23,000	26,100
Semi-minor axis (km)	2960	3120	2260	2030	2070	2180
Orientation clockwise from $\overline{T}$ (deg)	47	129	160	25	29	29

With these two sets of spheres, and their respective mapped ellipsoids, we have partially characterized the distribution of first-manuever execution errors. To review, assuming spherically distributed first maneuvers and execution errors, the second moment per axis of the resultant spherically distributed execution errors will be about .1 meters/second. In addition, the probability that the error in a particular direction will exceed .39 meters/second is less than 10^{-4}.

4. The Concept of Biasing

The problem of biasing arises when we must select the exact aiming point for the first maneuver. The aiming point must be chosen such that the overall probability of impacting the planet (including the possible failure of subsequent maneuvers) is less than 10^{-4}. The

dispersions in the velocity after the first maneuver will include the orbit determination uncertainties as well as the execution errors of the first maneuver. In general, both sources must be considered before the bias can be determined. We have already shown that the second moment of typical execution errors will map to the target as shown in Table 8-18. Comparing these dispersion ellipses with the magnitudes of orbit determination uncertainties after 5 days (these can be extrapolated from the orbit determination section of this document) it appears that on typical Type I and Type II trajectories the execution errors will be the dominant errors. We will therefore assume that the velocity errors after the first maneuver can be attributed primarily to the execution errors in that maneuver.

To ascertain the size of a typical biasing distance, let us consider a typical 10 meters/second velocity correction on a Type I trajectory: Once the size of this velocity correction is known, the execution errors can be expressed as a three-dimensional Gaussian distribution. Assuming as before that $\sigma_p = .01$, $\sigma_s = .01$, and that shutoff resolution errors are negligible, we obtain a spherical Gaussian distribution of execution errors with $\sigma_{exec.} = .1$ meters/second. Let us now assume that the probability of a second maneuver failure due to deterioration of the spacecraft is .2. Then, to ensure less than 10^{-4} total chance of impacting the planet, we must locate the aiming point such that the probability of the spacecraft impacting the planet without a second maneuver is less than 5×10^{-4}. (The total probability of impact is now less than $.2 \times 5 \times 10^{-4}$.) It must be remembered that the probability of the spacecraft impacting Mars should actually be less than 10^{-4} in order that the total probability of either the booster last stage or the spacecraft impacting Mars does not exceed 10^{-4}. The probability of a Gaussian variable, X, being greater than some X_o is just the integrated distribution from X_o to infinity. In particular, if we choose $X_o = 3.3\sigma$, the probability of X being greater than X_o is less than 5×10^{-4}. We may thus construct a sphere in velocity space with radius equal to $3.3\sigma_{exec.} = .33$ m/s, such that if a plane is drawn tangent to the sphere at any point, the chance of the execution errors extending beyond this plane is less than 5×10^{-4}. If a sphere of radius .33 meters/second is mapped to Mars, the resulting dispersion ellipses will be about 85% as large as the numbers shown in Table 8-19 for the Type I trajectories. Referring to Figure 8-79, we want to choose an aiming point (the center of the ellipse) such that no part of the ellipse overlaps the planet. We have taken the "critical" radius of Mars equal to 3500 km, which is the actual radius of Mars plus an additional 100-kilometer atmospheric region which we wish to avoid. The locus of the centers of all ellipses of this shape and orientation, which are tangent to the sphere representing the forbidden region, is an oval as shown by the dotted curve in Figure 8-79. If the desired final aiming point is outside this oval, e.g., point A, no bias is necessary. If the final aiming point lies inside the oval, e.g., point B, then we must bias the actual aiming point out to some point on the oval. It is not obvious, in general, whether there is some optimum direction for the bias, and this should be a problem for future investigation. Intuitively, one would tend to select the off-radial bias direction for a midcourse guidance system which was expected to exhibit large ΔV magnitude errors, whereas the radial bias direction would be preferred in the presence of large pointing

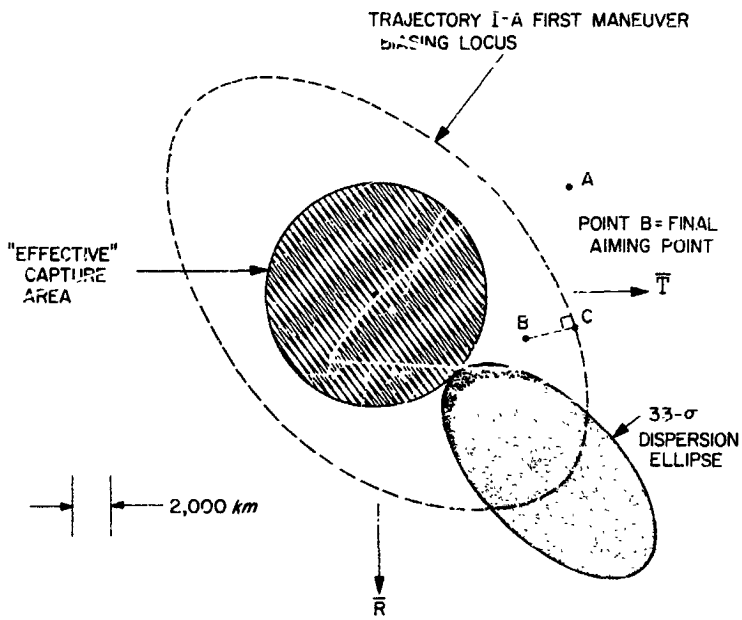


Figure 8-79. Biasing Locus for Trajectory I-A

errors. For a "balanced" system, the minimum bias distance (point C) may be optimum. Also, the selection of the first maneuver aiming point will be influenced by such alternate mission success questions as:

1) What is the preferred fly-by aiming region in the event that only one mid-course correction can be performed
2) Should the first maneuver aiming point be selected as close to Mars as possible in order to increase the probability of having adequate retro velocity capability to establish some type of a capture orbit in the absence of subsequent mid-course corrections, etc.

5. Type I Trajectory Accuracies

The final dispersions at the planet after a two-maneuver mission will consist of the following:

1) Orbit determination uncertainty at the time of the second maneuver
2) Execution errors in the second maneuver

The execution errors will consist of nonproportional resolution errors, and errors whose magnitude are proportional to the magnitude of the maneuver. The magnitude of the second maneuver is obviously influenced by the biasing policy described earlier. Figures 8-79 and 8-80 illustrate the biasing locus for trajectories I-A and I-B. It can be seen that the distance between the first and second maneuver aiming points can vary from zero to possibly 5000 km, depending upon the orientation of the biasing locus with respect to the final aiming point. Combining the biasing correction with the random dispersions from the first maneuver could result in having to correct a miss of typically 2000-8000 km. Assuming 1σ proportional errors of 1% in the second maneuver, the correction of such a miss could result in 3σ dispersions of 60-240 km due to execution errors in performing the second maneuver. The second maneuver would only be this accurate if proportional execution errors dominated the fixed errors. In order for this to be the case for very small second maneuvers, a vernier correction system capable of applying a meter/second or less with a 3σ accuracy of 3% may be required. The 60-240-km dispersion is based upon a first midcourse correction of 10 meters/second. If, however, a larger first midcourse correction is required as a result of certain nonstandard errors, the necessary biasing distance as well as the dispersions which result from first-maneuver execution errors will be larger. Consequently, the dispersions due to second-maneuver execution errors may be doubled.

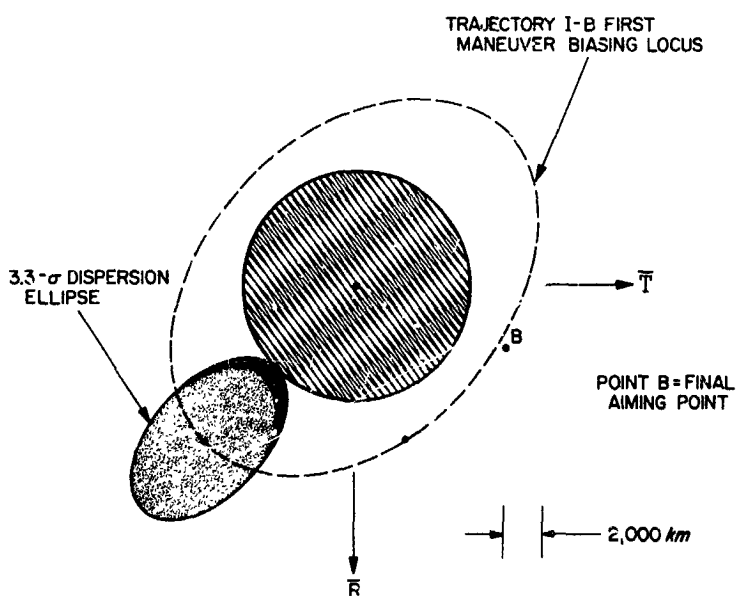


Figure 8-80. Biasing Locus for Trajectory I-B

Summarizing then, it should be possible to achieve 3σ accuracies of perhaps 500 km (this number includes orbit-determination uncertainties) for Type I trajectories with two midcourse corrections. The term "3σ" is now being used in a loose sense to mean a high

percentage of the cases. It is very important to note, however, that it may be necessary to extend the sigma bounds significantly to really "ensure" that all but 10^{-4} of the trajectories will pass through a given region. As a matter of fact, one might argue that the confidence level on the A. U. being known to better than say 500 km is hardly as high as 99.99%. Or, to generalize the argument, is not the probability higher than 10^{-4} that fallible man will overlook some detail which violates the contamination constraint?

6. Type II Trajectory Accuracies

The Type II trajectories exhibit a somewhat degraded accuracy situation when compared with the Type I trajectories. Several factors contribute to this degradation: As shown in subsection C, the orbit-determination knowledge is considerably worse during the early portion of the flight. In addition, as shown in Table 8-18, first midcourse velocity errors map into ellipsoids with considerably larger semi-major axes at Mars. And, finally, the required biasing distance is greater both because of the larger dispersion ellipsoids and the reduced reliability of performing a late second maneuver. Regarding the above remarks concerning the degraded Type II accuracy situation, it is very important to make the following distinction: This degraded accuracy primarily applies to a one or possibly two-maneuver mission. Obviously, if a sufficient number of midcourse corrections are performed such that the final accuracy approaches the orbit determination uncertainty when near Mars, then Type I and Type II achievable accuracies will be comparable.

Figure 8-81 illustrates the first-maneuver biasing locus for trajectory II-B. It can be seen that the distance between possible bias points and the final aiming point can vary from 6000 to 18,000 km. A 3.5σ dispersion ellipse (instead of 3.3σ for Type I) has been shown in order to allow for a later second maneuver whose probability of failure has increased to 0.4. Except for a midcourse guidance system with dominant pointing errors, biasing point C in Figure 8-81 appears the most desirable. Combining the biasing distance with the random dispersions in the first maneuver could result in the second maneuver having to remove a miss as large as perhaps 6000-25,000 km. This could result in a 3σ second maneuver execution error of 130-750 km. Combining this error with the orbit determination uncertainty, one might expect a total 3σ dispersion of 500-1000 km for a two-maneuver Type II mission.

In Subsection VIII. B, which discussed the selection of various orbit profiles about Mars, it was mentioned that a northerly-direct Type II orbit exhibited good planetary coverage but would not realize Earth occultation and also Canopus would come very near the Mars limb when the orbiter was near periapsis. For these reasons and also to achieve similarity (to permit the use of a more or less identical spacecraft for both Type I and Type II transits) with the clearly favorable southerly-direct Type I orbit profiles, a final aiming point in the vicinity of point B (Figures 8-79 through 8-81) was selected. Due to the orientation of the

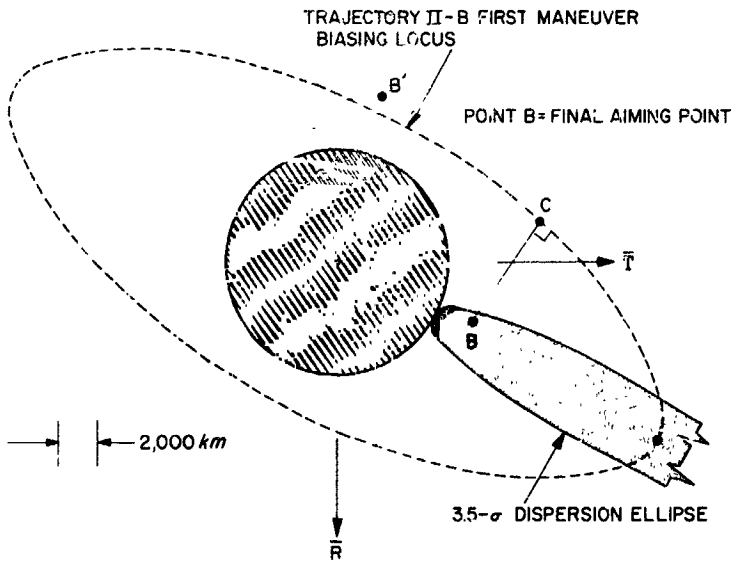


Figure 8-81. Biasing Locus for Trajectory II-B

Type II dispersion ellipse, however, point B' (northerly-direct Type II) would be preferable from a guidance-accuracy standpoint.

7. Conclusions

Precise premission analysis of the multiple-maneuver guidance policy requires a complex technique such as a Monte-Carlo simulation. In the absence of such a formulation, this study has attempted to arrive at approximate accuracy estimates for the 1969 Mars mission. Assuming the orbit determination errors shown in section C, a 1σ first-midcourse velocity of the order of 10-15 meters/second, and midcourse execution errors equal to 1% (1σ) of the required velocity increment, it should be possible to achieve final 3σ dispersions in the aiming point at Mars in the region of 500-1000 km. Such a region would contain perhaps as much as 99% of the dispersions but would have to be enlarged to contain 99.99%. If we are willing to occasionally perform as many as three midcourse corrections, it should be possible to control the final aiming point to better than 500 km (3σ) for Type II as well as Type I trajectories. This level of accuracy appears very desirable, if not necessary, for the currently conceived 1969 Mars orbiter mission which requires (a) maintaining a low periapsis altitude in order to achieve the necessary weight in orbit, (b) ensuring no Sun occultation for at least 3 months, and (c) achieving Earth occultation without violating the lower periapsis altitude limit for maintaining a 50-year lifetime. If the 1969 orbiter mission was not

marginal from a weight-in-orbit standpoint and could afford the luxury of extra retro fuel, the accuracy requirements on the approach trajectory could be reduced with the adoption of an orbit-trim policy.

The assumption that the midcourse guidance system can execute maneuvers to an accuracy of 1% (1σ) will probably necessitate the addition of a small vernier correction motor (can be cold gas) if it is desired to have such an accuracy capability over that large portion of the total flight during which the second maneuver would be less than a few meters/second. For the Type I trajectories, the vernier system would often permit the achievement of a 500-km accuracy by performing the second midcourse correction within as early as 30 days past injection. Whereas, for those Type II trajectories whose initial dispersions were large enough to suggest utilizing three midcourse corrections, the second and third corrections could be more optimumly spaced by being able to perform the second maneuver before getting too close to encounter. For either a two or three-maneuver Type II mission, the second maneuver would probably not be performed earlier than about 150-200 days after injection.

E. ORBIT INSERTION GUIDANCE ANALYSIS

1. Introduction

This subsection defines the guidance requirements for transferring a spacecraft from its hyperbolic approach trajectory to an elliptical orbit about Mars. For the initial consideration of orbiter feasibility, two principal questions were investigated:

1) Whether easily mechanized guidance laws are feasible in terms of propellant-weight requirements for orbital injection?
2) Do easily mechanized guidance laws provide the necessary accuracy for the mission?

Results obtained to date indicate that application of Ranger and Mariner midcourse guidance techniques to the orbiter retro guidance problem will result in a feasible system with reasonable accuracy and sufficient propellant efficiency. Control of the magnitude of the retro-velocity increment has been simulated by using both a timer and an accelerometer. For the loose nominal orbits covered in Section VIII. B. 6 with apoapsis altitudes as high as 50, 000 km, velocity magnitude errors associated with the timer control can be sufficiently large to prevent capture. For these large semi-major axes, very sensitive orbits, it is recommended that an accelerometer be used to control the magnitude of the retro-velocity increment.

The above conclusions are substantiated by the material in the remainder of this section. The material is organized into two parts: a comparison of several possible guidance laws in terms of propellant requirements, and an analysis of the accuracy characteristics of the system configuration resulting from application of Ranger-Mariner midcourse techniques to orbital injection guidance.

2. Guidance Law Propellant Efficiency Study

The first phase in a study to determine what guidance laws are feasible in terms of propellant-weight requirements for orbital injection has been completed with the following results:

1) The absolute minimum velocity requirements which inject a spacecraft into a 1, 500 by 20, 000 km altitude orbit from a hyperbolic orbit with $V_\infty = 4.0$ km/sec were found. Four guidance laws were investigated, and the initial thrust to weight ratio was 0. 3.
2) The values of hyperbolic periapsis distance, r_{ph}, which correspond to the minimum transfers were determined for future reference in computing the minimum maneuver as a function of this distance.

3) The ΔV losses due to guidance laws and finite burning time were found for the "gravity turn", and a conservative estimate for the other laws was computed.

The curves in Figures 8-82 and 8-83 were generated by integrating backward from various points on the ellipse, and terminating the integration when the energy per unit mass corresponding to the hyperbola was reached. The thrust-to-weight ratio was constrained to be 0.3 at this hyperbolic energy.

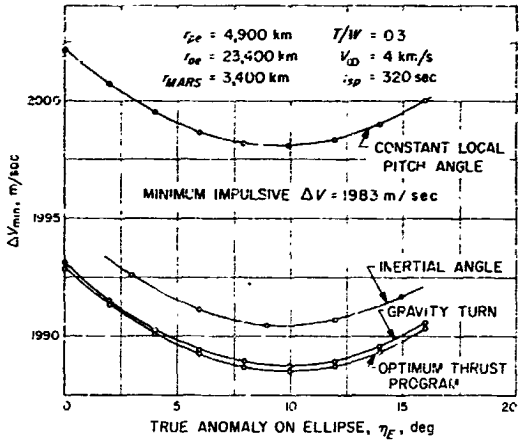


Figure 8-82. Minimum Retro-Velocity Decrement vs True Anomaly along Ellipse for Various Thrust Programs

Figure 8-82 shows the minimum velocity required to transfer to the true anomaly on the ellipse for four thrust-vector pointing laws:

1) The overall optimum thrust program
2) Gravity turn, or thrust-vector colinear to the velocity vector
3) Constant direction in inertial space
4) Constant local-pitch angle, or a constant thrust direction with respect to the local horizontal.

Figure 8-84 depicts the optimum thrust program as a function of time for the minimum transfer to the ellipse. The thrust orientation is given with respect to 1) the periapsis of the preburn hyperbola (ψ), 2) the local vertical (Γ), and 3) the velocity vector (β).

The following table (see Table 8-20) may be constructed from Figure 8-82. The finite burning time and guidance-law losses are defined to be the minimum velocity transfer minus the impulsive periapsis-to-periapsis velocity requirement. The guidance-law losses are defined to be the minimum velocity transfer minus the minimum velocity required for the optimum thrust program.

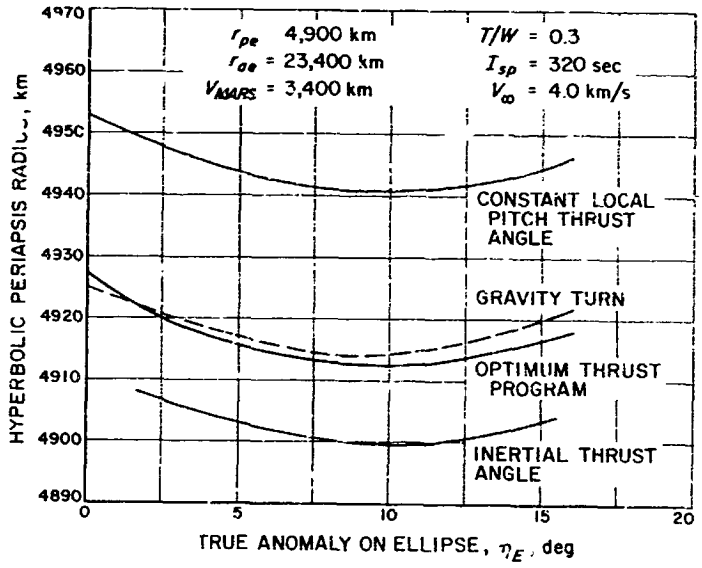


Figure 8-83. Periapsis Radius vs True Anomaly for Various Thrust Programs

Table 8-20. Finite Burning Time and Guidance-Law Losses

Guidance Law	Minimum Transfer (m/s)	Finite Burning Time & Guidance-Law Losses (m/s)	Guidance-Law Losses (m/s)
Impulsive	1983.1	0	N/A
Opt Thrust Prg	1988.5	5.4	0
Gravity Turn	1988.7	5.6	0.2
Const Inertial	1990.4	7.3	1.9
Const Local Pitch	1998.1	15.0	9.6

Figure 8-83 shows the values of hyperbolic periapsis distance which are required for the transfers to the true anomaly on the ellipse. A cross plot of minimum ΔV vs r_{ph} cannot be made from these figures because they are made for constant true anomaly on the ellipse and not constant r_{ph}. When r_{ph} is fixed, the choice of angle in the thrust program may be varied (except for the gravity turn, where the angle is specified) to minimize the velocity requirements; thus, the losses obtained from curves like Figure 8-82 are conservative estimates.

Figure 8-85 shows the minimum impulsive maneuver and the finite burning time and guidance-law losses as a function of r_{ph}. These losses are conservative estimates for the

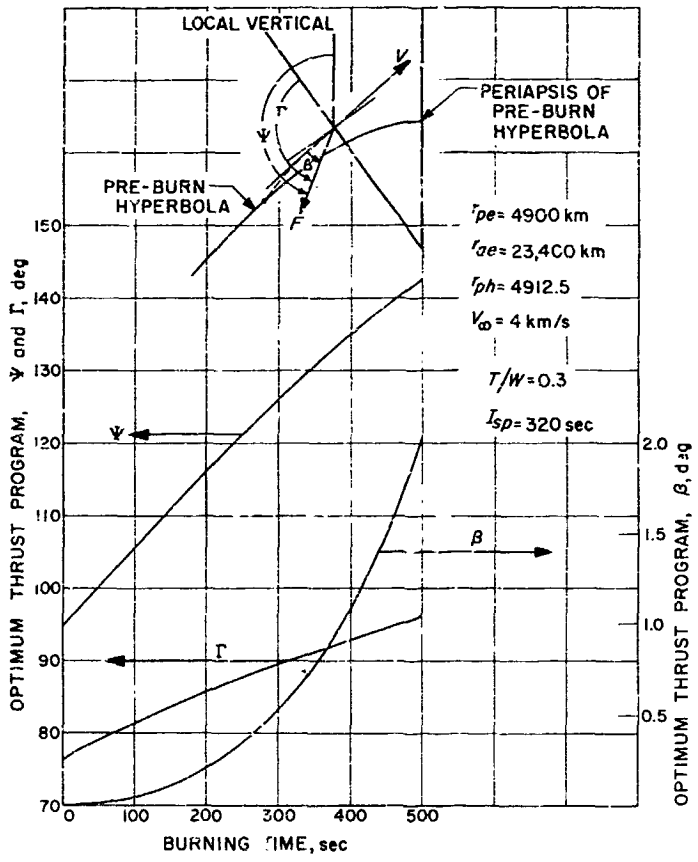


Figure 8-84. Angle Variation with Time for Optimum Thrust Program

inertial and constant local-pitch guidance laws. Because no choice of thrust angle exists with the gravity turn law, the gravity-turn losses in Figure 8-85 are the minimum values. The losses for the optimum thrust program are, of course, bounded by these gravity-turn losses.

Table 8-21 may be made from Figure 8-85. These numbers apply to the hyperbolic energy and elliptical orbit previously mentioned.

The results indicate that acceptable propellant efficiency may be achieved with an easily mechanized guidance law. The optimum thrust program gives the best guidance law but is very difficult to mechanize with exactness. The gravity-turn results are very close to optimum, but are difficult to mechanize since the direction of the instantaneous velocity vector in inertial space must be known. From Table 8-20, the constant inertial direction guidance law gives the next best results. This is the most easily mechanized system and is similar to the current Ranger and Mariner midcourse guidance techniques. The constant

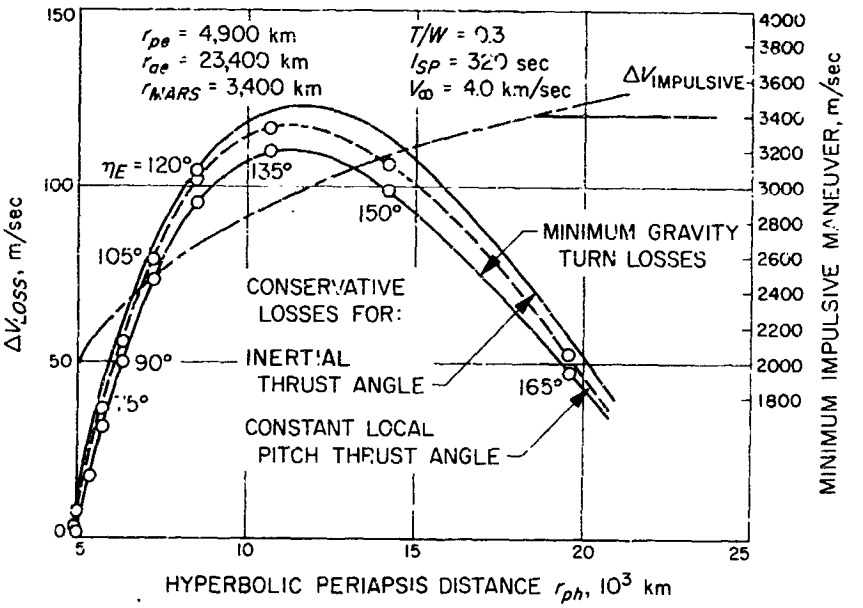


Figure 8-85. Conservative Velocity Losses for Various Thrust Programs vs Hyperbolic Periapsis Distance

Table 8-21. Hyperbolic Energy and Elliptical Orbit Numbers

Guidance Law	Max. Finite Burn Time and Guidance-Law Losses (m/s)	Maximum % Loss
Optimum Thrust Prg	≤ 111	≤ 3.6%
Gravity Turn	111	3.6%
Const. Local Pitch Thrust Angle	≤ 118	≤ 3.9%
Const. Inertial Thrust Angle	≤ 123	≤ 4.1%

local-pitch law gives the highest losses at the minimum transfer. This law, although more easily mechanized than the gravity turn, would be more difficult to mechanize than the constant inertial law due to the need for a planetary horizon scanner. Because of the previously stated considerations, the constant inertial law was chosen as the system to be used in the first accuracy study.

3. Accuracy Study

The system mechanization studied for accuracy capabilities uses the following:

1) Earth-based radio tracking for pre-maneuver orbit determination and maneuver computation
2) A series of single-axis gyro-controlled turns for initial spacecraft alignment
3) Ignites the retro rocket on the basis of time-to-go until periapsis passage on the hyperbola
4) Thrusts in a fixed inertial direction, and shuts off the rocket either on the integral of thrust acceleration or on the basis of time after ignition.

A block diagram of the guidance system is shown in Figure 8-86 and an operating sequence is shown in Figure 8-87.

a. Nominal Orbits

Numerical values used in determining the nominal transfer maneuvers include:

1)	Gravitational Constant of Mars:	42977.8 km^3/sec^2
2)	Radius of Mars:	3415 km
3)	Force-to Mass Conversion Constant (g_o):	0.00978 km/sec^2
4)	Hyperbolic Excess Velocity of Approach Trajectory:	4.0 km/sec
5)	Desired Periapsis Altitude of Ellipse:	1500 km
6)	Desired Apoapsis Altitudes of Ellipse:	
	Orbit A	20,000 km
	Orbit B	50,000 km
7)	Initial Thrust-to-Weight Ratio:	0.3 (600 lbf thrust, 2000 lbm S/C)
8)	Specific Impulse:	320 lbf-sec/ibm

The transfer maneuver is characterized by four parameters. These are listed in the table for the two ellipses.

Conditions	Orbit A	Orbit B	
Time-to-Periapsis at Ignition, t_i	292	272	second
Thrust Attitude with respect to local vertical at periapsis of approach trajectory, ψ_I (positive forward)	-90.0	-90.0	degree

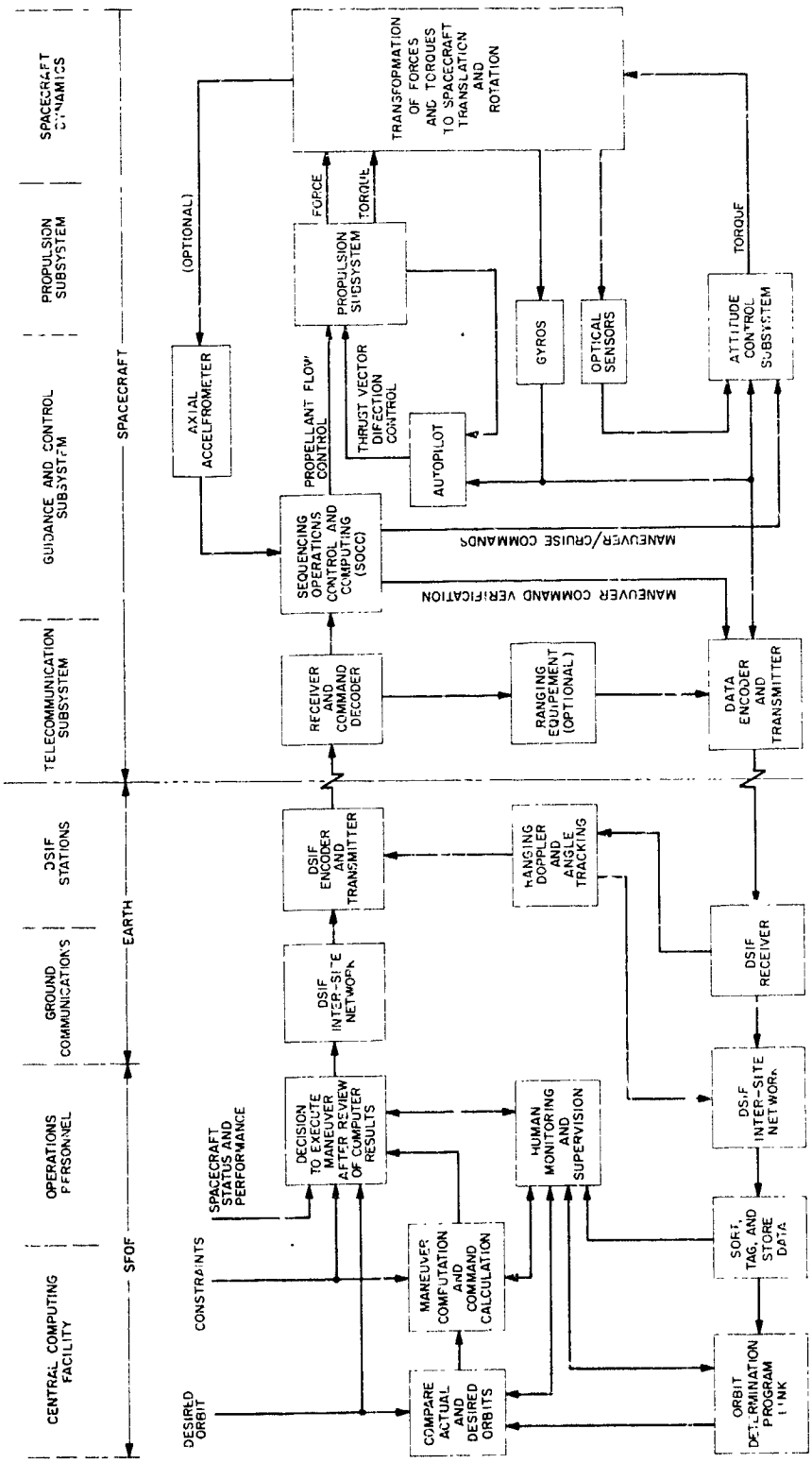


Figure 8-86. Orbiter Spacecraft Guidance System Functional Block Diagram

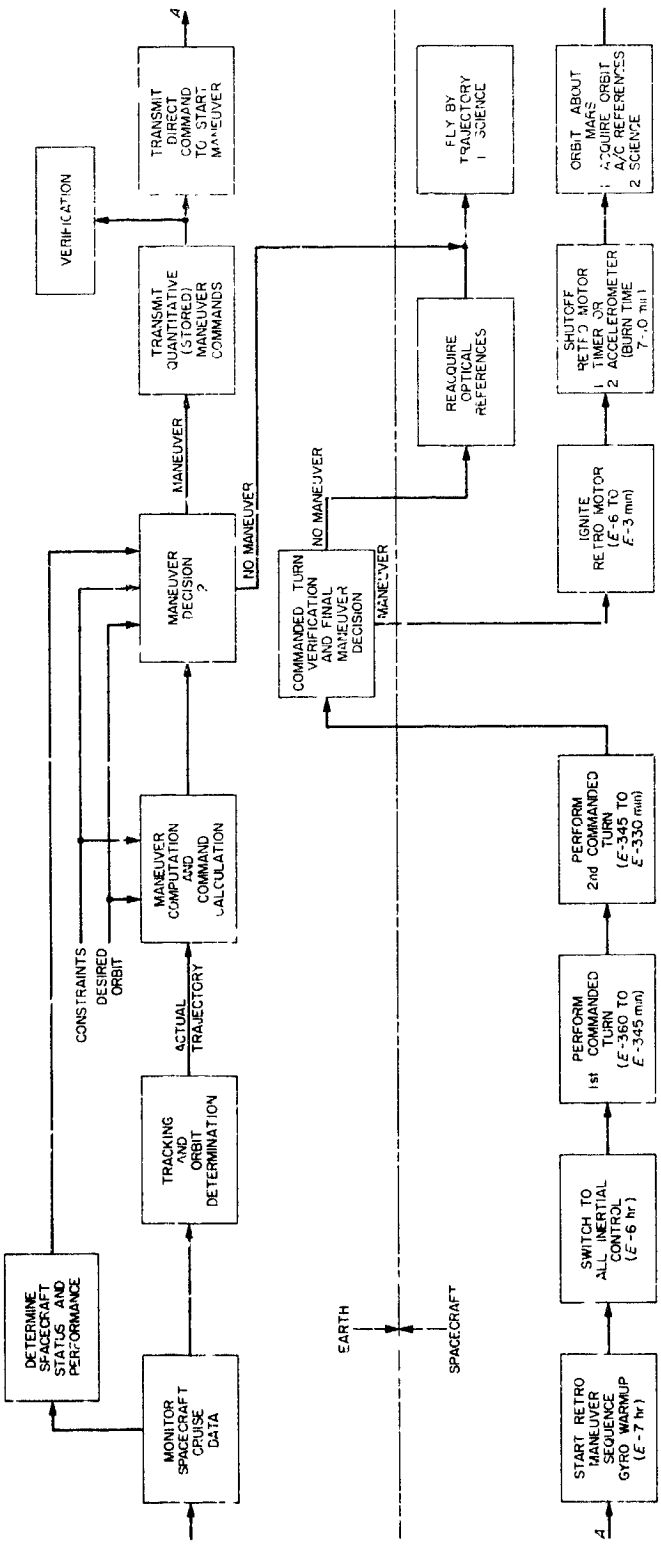


Figure 8-87. Orbiter Spacecraft Retro Maneuver Sequence Block Diagram

Conditions	Orbit A	Orbit B	
Velocity Increment, V	1.99250	1.79088	km/sec
Nominal Burning Time, t_B	502.330	464.778	second

b. Error Sources

Four major categories of error sources were considered and are as follows:

1) Periapsis altitude of the approach trajectory, h_p, (the hyperbolic excess velocity can be determined to an accuracy sufficiently great that errors do not visibly affect the resultant ellipse)
2) Starting time of the maneuver
3) Direction of the maneuver
4) Magnitude of the velocity increment. The velocity increment is affected by accelerometer errors when an accelerometer is used and by timing errors, specific impulse, flow rate, and initial weight errors when a timer is used.

Typical values of these error sources are listed below:

1)	Variation in control and knowledge of approach periapsis altitude	±200 to ±500 km
2)	Variation in knowledge of time of periapsis passage	±30 to ±90 sec
3)	SOCC timing resolution	1 sec
4)	SOCC frequency error	±.01%
5)	Command-transmission accuracy	unknown, but small based on past experience
6)	Pointing error accumulated during execution of commanded turns and execution of maneuver (Mariner performance)	±4 deg
7)	Drift rate on gyro control during waiting period and commands turns	less than 0.4 deg/hr
8)	Specific impulse error	±5 lbf-sec/lbm
9)	Flow rate error	±5% of nominal
10)	Initial spacecraft weight error	±2% of nominal
11)	Accelerometer scale factor error	±0.25%
12)	Accelerometer null offset	±0.0075 m/sec^2

These error-source values may be used to determine reasonable ranges over which the variations in the four primary quantities (periapsis altitude, time-to-go to periapsis, maneuver direction, and velocity increment) should be studied. The selection of these ranges is discussed in the following paragraphs.

The altitude of periapsis is determined directly from error source No. 1 in the table above. A range of ±200 km was selected for initial study.

Error sources 2, 3, 4 and 5 affect the time-to-go at which ignition is commanded. A range of ±120 seconds was selected for initial study on the basis of being reasonable bounds for the range of variations.

Errors 6 and 7 affect the direction of the maneuver. The total maneuver period under gyro control may be about 6 hours long, which yields a drift of about 2.5 degrees for the drift rate of error source No. 6. The pointing error due to gyro drift during the burning period has not been determined. However, for a mass unbalance of 1 deg/hr/g and a poor gyro orientation where drift occurred about the two control axes perpendicular to the thrust line, a total error of less than 0.25 degree would accumulate from this source. Other drifts such as anisoelasticity are expected to contribute even less to the pointing error. If all the above errors are linearly combined, the total pointing error remains less than 7 degrees. For this study, a range of ±10 deg was selected as reasonable bounds.

If a timer shutoff is used, the fractional error in maneuver velocity is given to the first order by the following equation:

$$\frac{\Delta V}{V} = \frac{\Delta I_{sp}}{I_{sp}} + \left[\frac{a_f}{\bar{a}}\right]\left[\frac{\Delta t_B}{t_B} + \frac{\Delta r}{r} - \frac{\Delta m_o}{m_o}\right]$$

where Δ's indicate variations from the nominal, and

V	= velocity increment	t_B	= burning time
I_{sp}	= specific impulse	a_f	= final acceleration
r	= flow rate	$\bar{a}$	= average acceleration, $\bar{a} = V/t_B$

Second-order effects increase the value by less than 10 percent of the linear approximation. For the numbers given in the error source table, the maximum error in velocity increment with a timer shutoff is less than ±12.5 percent. A range of ±15 percent was selected for the initial study.

If an accelerometer shutoff is used, the fractional error in maneuver velocity is given to the first order by the equation:

$$\frac{\Delta V}{V} = k + \frac{\eta}{\bar{a}}$$

where k = scale factor error

η = null offset

For the numbers given in the table of error sources, the maximum error in velocity is less than ±10 m/sec.

The SCCC currently studied has a resolution of approximately 1 part in 4000, resulting in timing or velocity resolution errors of less than .0125 percent of the maximum maneuver capability or approximately .25 m/sec. The motor velocity tailoff error is unknown, but is assumed to be small based on past experience. The total resolution errors are insignificant compared to the proportional errors previously listed.

c. Explanation of Figures

The accuracy capabilities for typical error magnitudes are summarized in the following figures for the two nominal orbits. These curves were prepared by integrating the equations of motion for the spacecraft in a 2-dimensional (planar) inverse-square central force field.

These plots show the variation of apoapsis altitude, periapsis altitude, orbit period, and orbit rotation, for errors in a nominal periapsis-to-periapsis transfer maneuver. The orbit rotation is defined as the amount the periapsis of the ellipse is rotated from the periapsis of the hyperbola with positive rotation in the direction of the velocity vector at the periapsis of the hyperbola. A periapsis-to-periapsis impulsive maneuver (zero burn time) would have a zero rotation. Major errors considered include errors in orbit determination, affecting the periapsis altitude of the approach trajectory and the time of periapsis passage; errors in ignition time due to timer inaccuracy; errors in the pointing of the thrust vector during the maneuver; and errors in the magnitude of the maneuver due to accelerometer, timer, specific impulse, flow rate, and initial-weight errors. The ranges covered are typical of conditions that may exist in an easily mechanized system.

The figures represent an attempt to display a large amount of information concisely, and deserve some explanation. For example, the ordinate of Figure 8-88 is the actual apoapsis altitude achieved. The main abcissa of all the plots is the error in maneuver magnitude. Curves are drawn for zero and ±200 km orbit-determination error in the periapsis altitude of the approach trajectory. The small parabolic curves intersecting the main apoapsis altitude vs. velocity-error curves show the effects of errors in pointing and start time at particular values of velocity and altitude-of-periapsis errors. The pointing error is displayed along the subsidiary abcissa above, and the starting-time error is the parameter differentiating the several curves at a particular combination of velocity and altitude-of-periapsis errors. In a sense, the parabolic curves are "cross-sections" of the 5-dimensional "surface" of possible apoapsis altitudes. The Δ's represent the actual value of the parameter minus the nominal value.

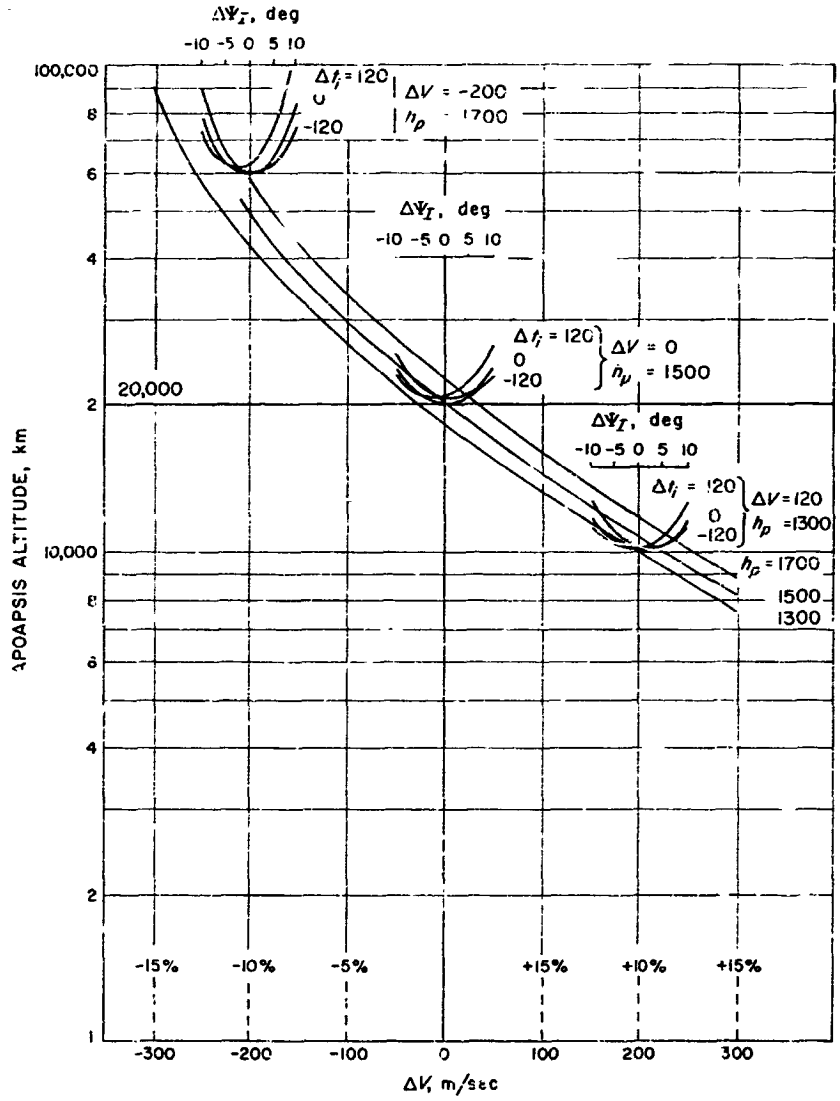


Figure 8-88. Apoapsis Altitude vs Orbit Insertion Errors for 1500 by 20,000 km Orbit

d. Results

The results indicate that a satisfactory orbit may be achieved with the guidance law studied. From a scientific point of view, the plots of orbit period and rotation are probably of most interest. These along with the plots of apoapsis and periapsis altitude are discussed in the following:

Figures 8-88 and 8-92 show the variation of apoapsis altitude with various errors. For the range of velocity errors considered with a timer shutoff, this variation is significant. The variations are greater with a more eccentric orbit as in Figure 8-92 (orbit B). The variation in apoapsis is the prime contributor to the variation in orbit period discussed below.

Figures 8-89 and 8-93 show the variation of periapsis altitude with the various errors. The error in the periapsis altitude of the hyperbola is the main source of this variation, although combinations of pointing and ignition time errors will also have an effect. The velocity error has no affect on the periapsis altitude except to change the variations slightly when pointing and ignition time errors are present. A combination of worst-case conditions for the errors considered yields variations in periapsis altitude from 1100 to 1750 km from the nominal 1500 km.

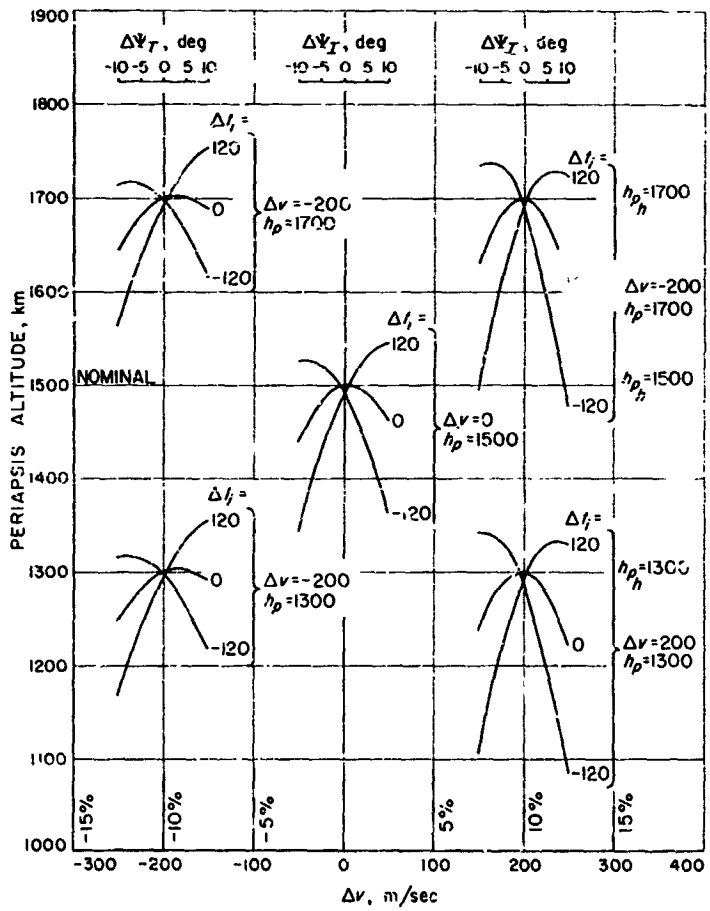


Figure 8-89. Periapsis Altitude Behavior with Orbit Insertion Errors for 1500 by 20,000 km Orbit

The variations in orbit period are shown in Figures 8-90 and 8-94. This variation is similar to that of the apoapsis altitude. A table of worst-case conditions (see Table 8-22) can be made from the figures. Note that the timer error used is only 10 percent, an optimistic estimate when referred to the timer-error discussion previously.

Table 8-22. Worst-Case Conditions

Conditions	Orbit period in hours	
	Orbit A	Orbit B
Worst-case low ($t_i = 0$, $\psi_i = 0$, $h_p = 1300$)		
1. Timer ($\Delta V/V = 10\%$)	7.2	13.5
2. Accelerometer ($\Delta V = 10$ m/s)	12.2	31.8
Nominal	14.19	41.93
Worst-case high ($t_i = 120$ sec, $\psi_i = -10^\circ$, $h_p = 1700$)		
1. Timer ($\Delta V/V = -10\%$)	120.	Fail to capture
2. Accelerometer ($\Delta V = -10$ m/s)	23.2	112.

The variations in period are significant for the range of velocity errors possible with a timer shutoff. This wide variation in period may require a greater flexibility in the timing of the orbital experiments. Also, with a highly eccentric orbit as in Figure 8-94 (orbit B) and a velocity error of -10 to -15 percent the spacecraft would fail to go into orbit. The use of an accelerometer for motor shutoff would significantly reduce this period variation and reduce the possibility of the spacecraft failing to go into orbit.

Figures 8-91 and 8-95 show the variation in orbit rotation with the error sources. It is observed that rotation varies linearly with pointing error and that this is the major contributor to the rotation. The error in the periapsis altitude of the hyperbola has relatively no effect on the rotation and the velocity and ignition time errors have only a small effect. Worst case combinations of all errors considered would yield a rotation of periapsis in the range of minus 20 to plus 20 degrees.

Some additional information of interest is presented in Figures 8-96 - 8-98, which are based upon the higher nominal periapsis altitude of 4000 km, which was suggested during the latter part of this study. Figure 8-96 illustrates the effect of removing the nominal retro velocity at the wrong altitude. The contribution to apoapsis dispersions due to this error source can be lowered by transmitting the retro velocity magnitude as late as possible, thus obtaining the maximum amount of near-Mars orbit determination information. Figures 8-97 and 8-98 should be used in conjunction with Figure 8-96 to indicate the size of orbit-trim

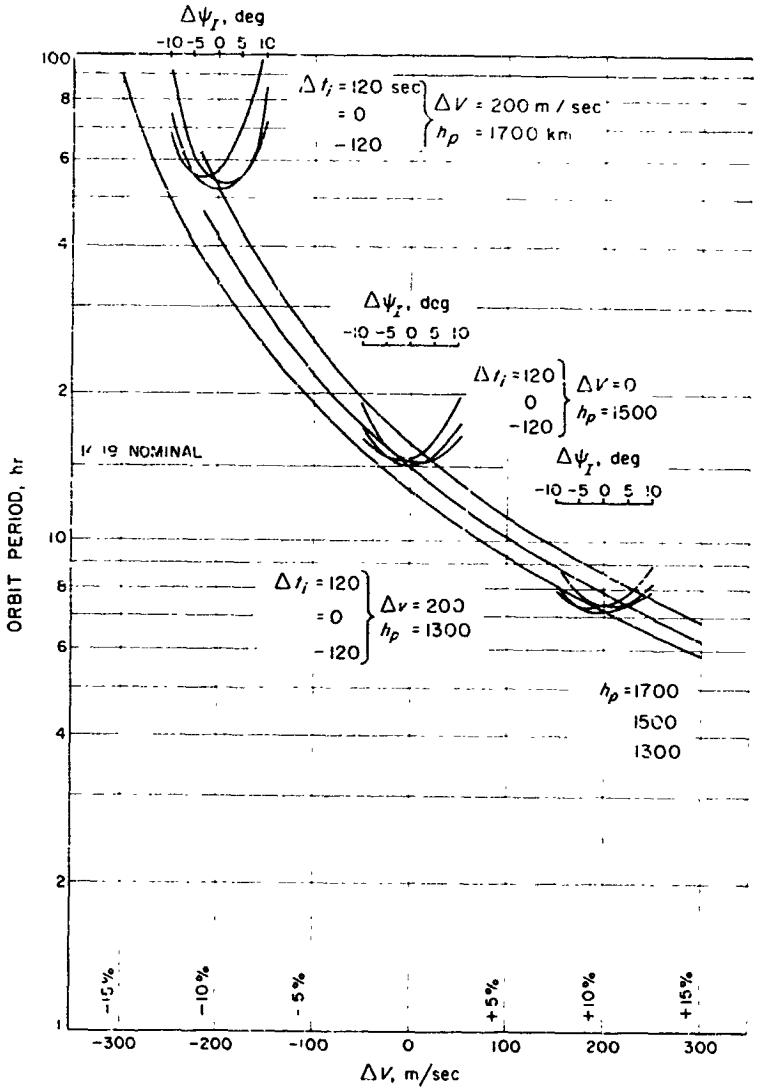


Figure 8-90. Orbit Period vs Insertion Errors for Nominal 1500 by 20,000 km Orbit

velocity requirements to restore the periapsis and apoapsis altitudes to their nominal values. An orbit-trim policy has not been assumed for the current study as a result of the marginal weight situation, but such a policy may be considered for future orbiter missions.

Finally, Figure 8-99 illustrates the maximum apoapsis altitude which can be nominally selected and still result in capture in the presence of a velocity error equal to k times the hyperbolic velocity decrement. For k = .10 and V_∞ in the region of 4 km/sec, it can be seen that the nominal apoapsis altitude should not be selected larger than about 50,000 km in order to ensure capture.

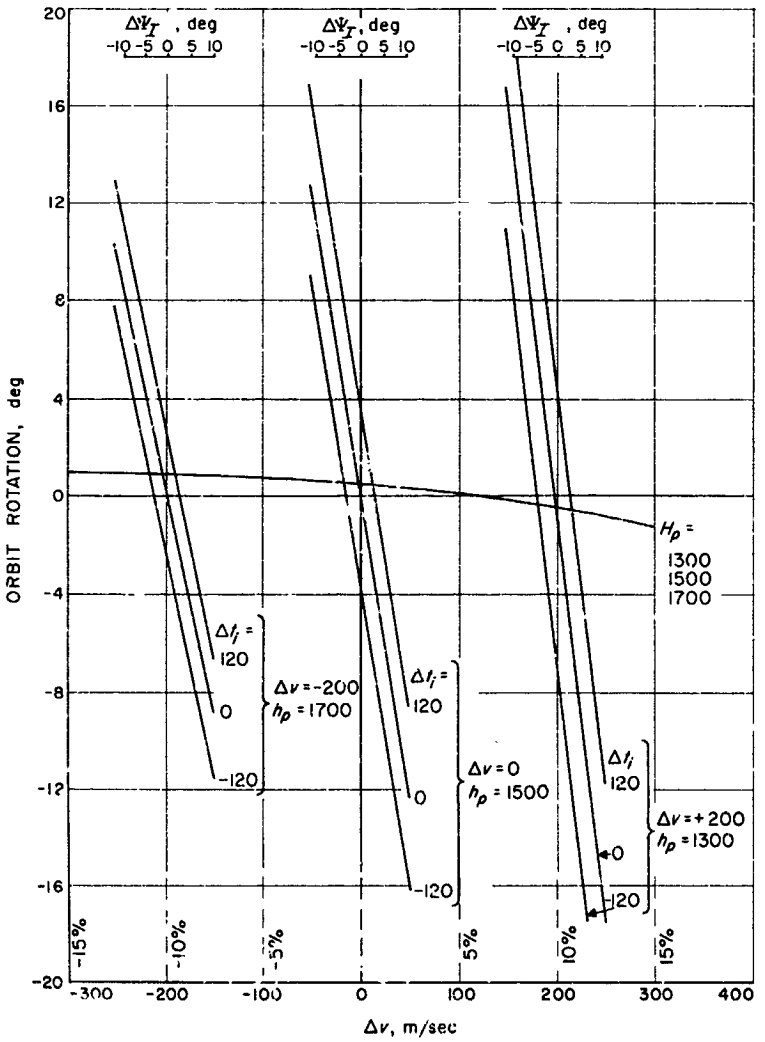


Figure 8-91. Orbit Rotation vs Orbit-Insertion Errors for 1500 by 20,000 km Orbit

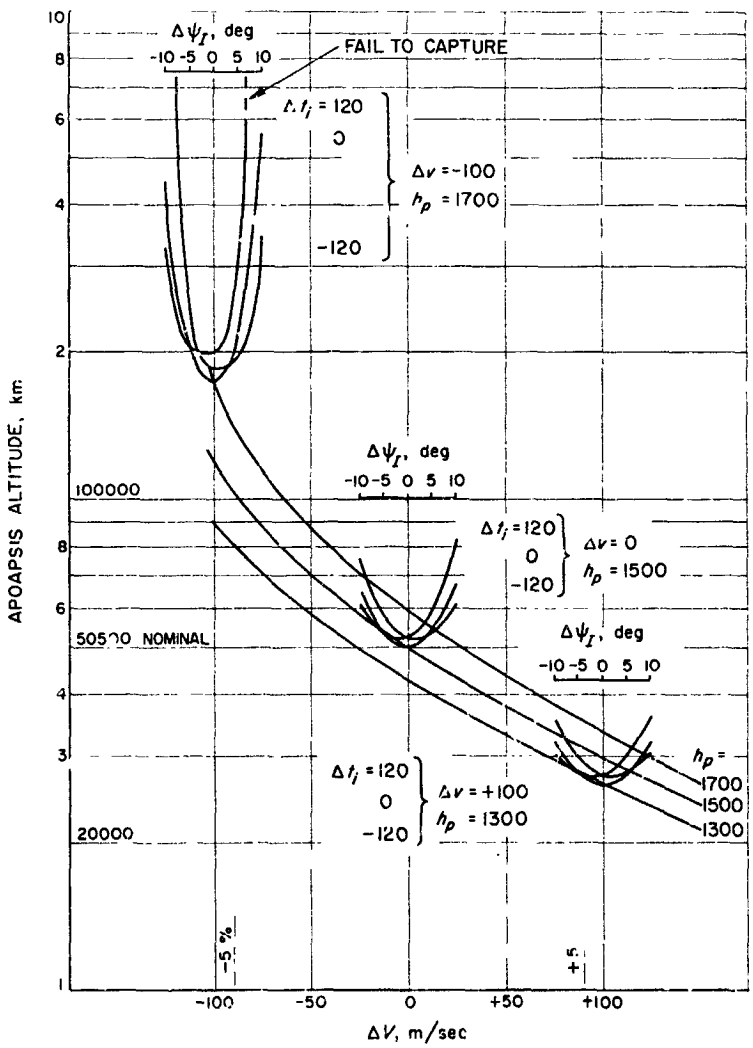


Figure 8-92. Apoapsis Altitude vs Orbit-Insertion Errors for 1500 by 50,000 km Orbit

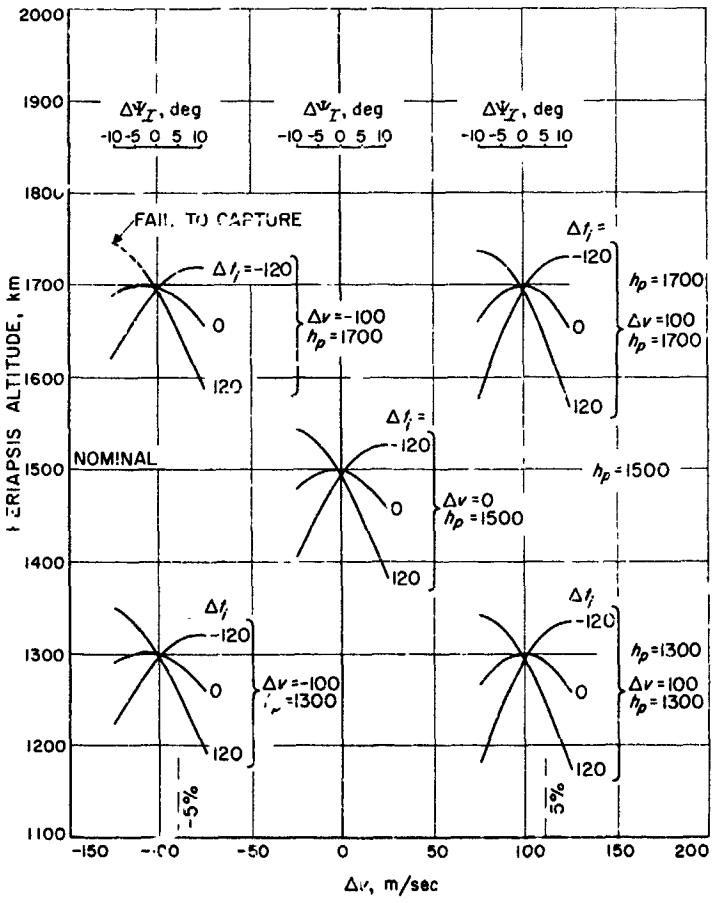


Figure 8-93. Periapsis Altitude Behavior with Orbit-Insertion Errors for 1500 by 50,000 km Orbit

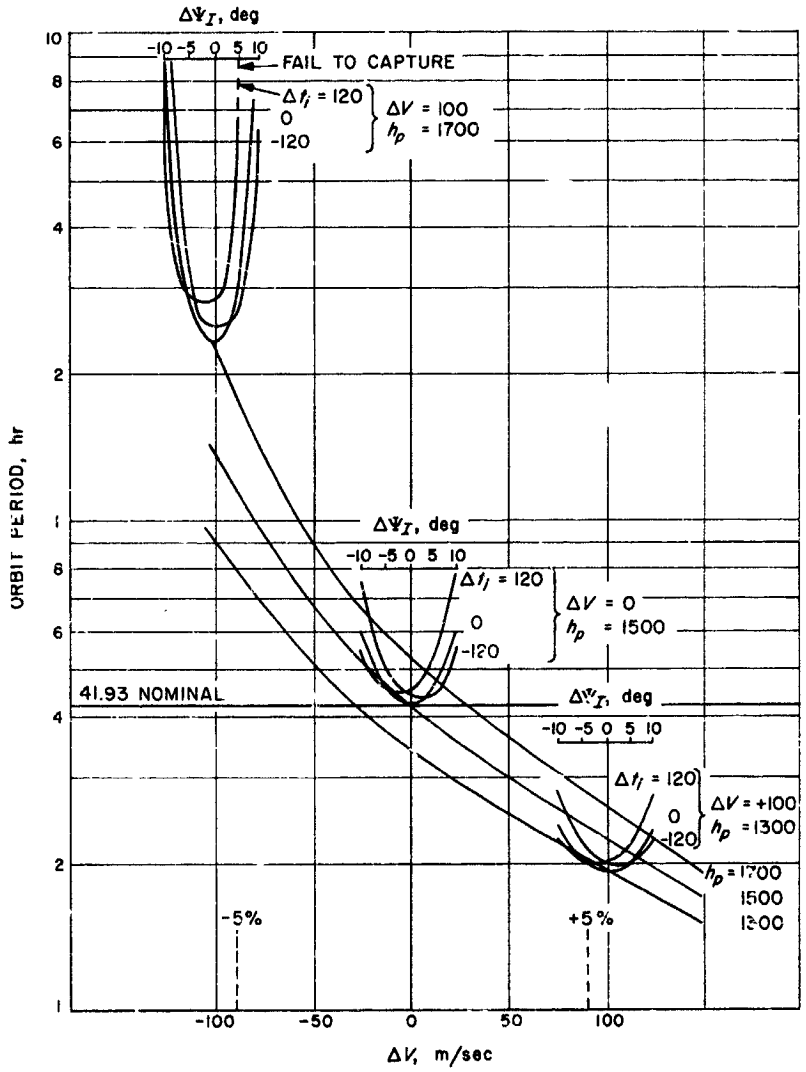


Figure 8-94. Orbit Period vs Insertion Errors for 1500 by 50,000 km Orbit

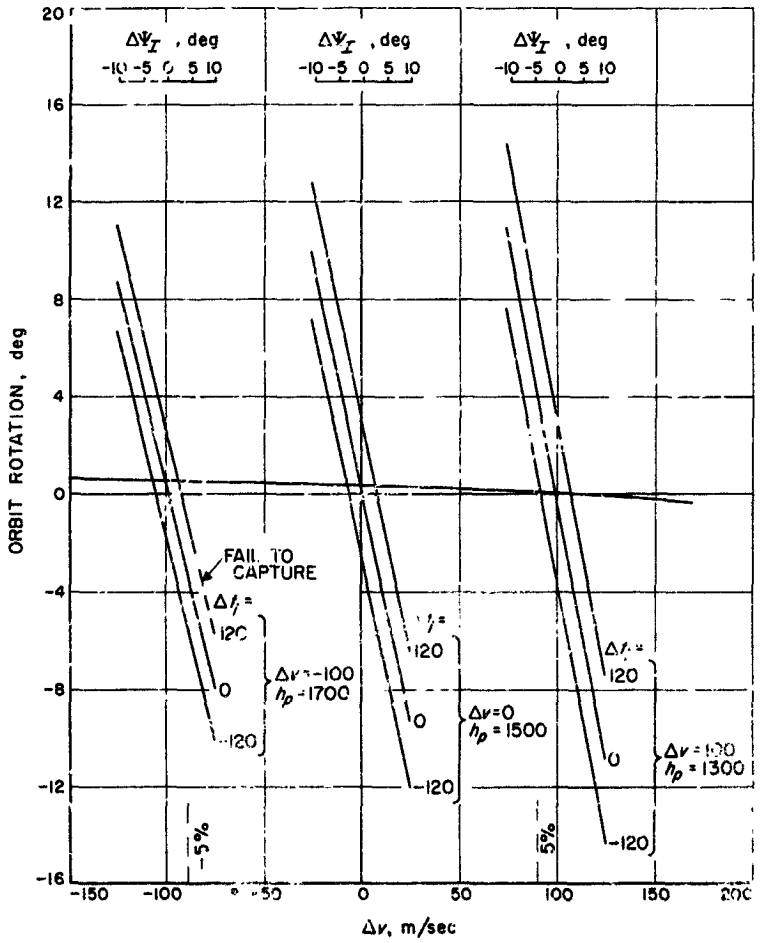


Figure 8-95. Orbit Rotation vs Orbit-Insertion Errors for 1500 by 50,000 km Orbit

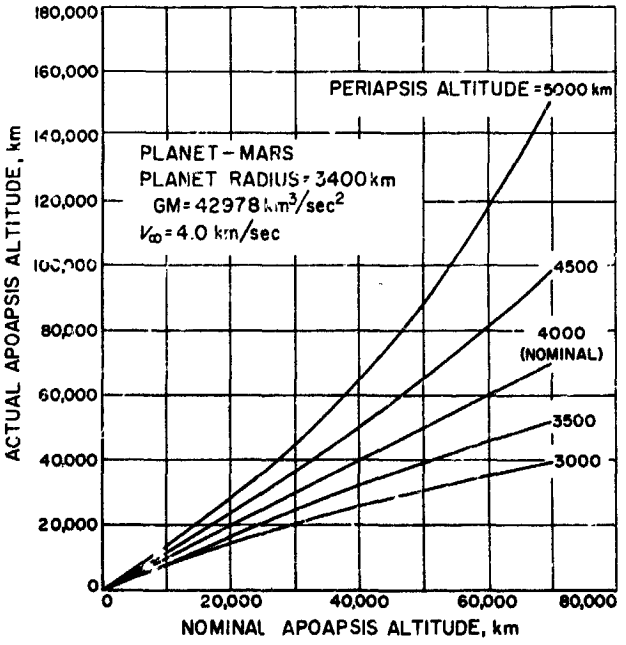


Figure 8-96. Apoapsis Altitude Which Results from Removing Nominal Velocity Decrement at Non-nominal Periapsis Altitudes as a Function of Nominal Apoapsis Altitude

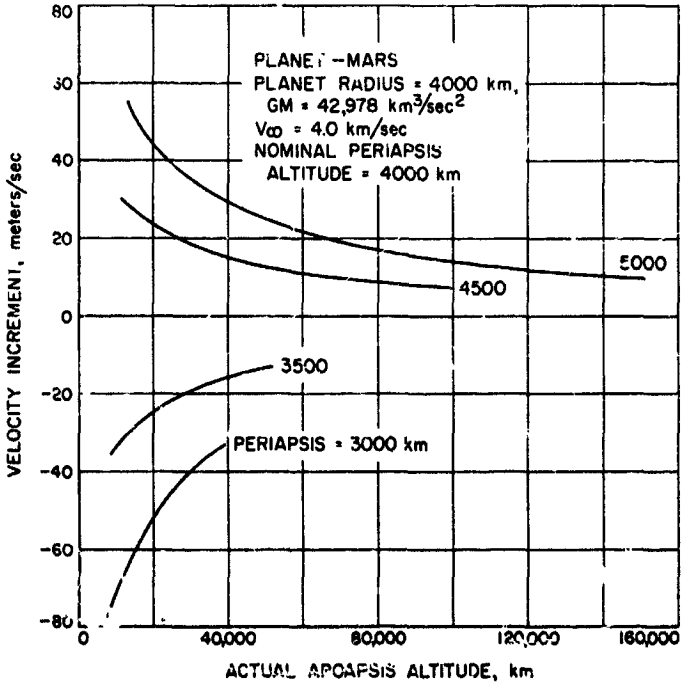


Figure 8-97. Velocity Increment at Apoapsis Required to Restore Periapsis Altitude to Nominal Value

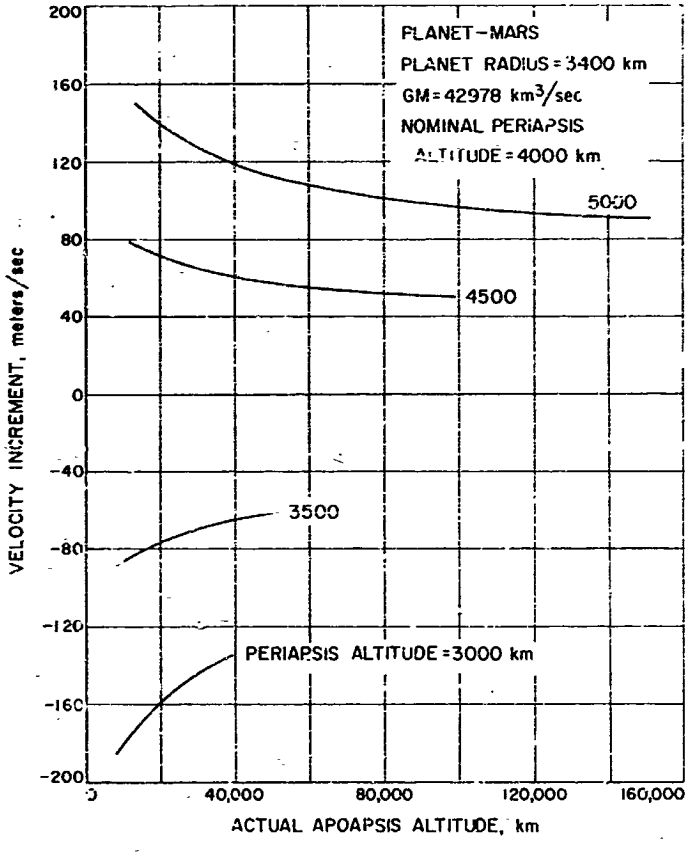


Figure 8-98. Velocity Increment Required to Restore Periapsis and Apoapsis Altitude to Nominal Value

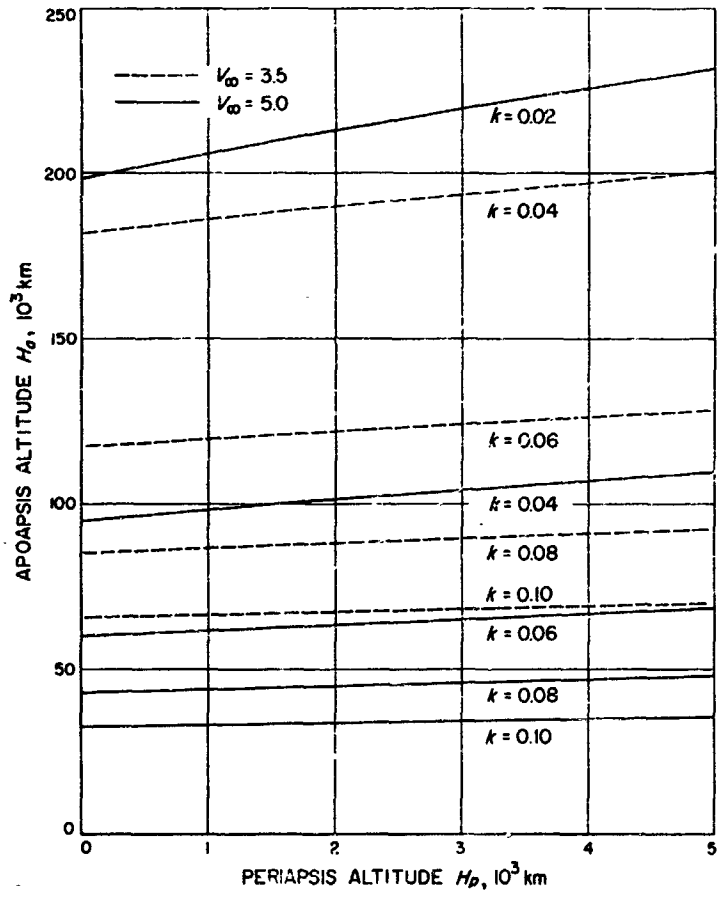


Figure 8-99. Maximum Apoapsis Altitude Which Can Be Nominally Selected and Still Guarantee Capture in the Presence of a Velocity Error at Periapsis Equal to k Times the Retro Velocity Increment (for Mars)

SECTION IX

SPACECRAFT SYSTEM FUNCTIONAL DESCRIPTION

A. SPACECRAFT FUNCTIONAL REQUIREMENTS

The following requirements describe in a general form the functional capability the spacecraft requires. These capabilities are required to satisfy the mission objectives, the constraints, and the performance capability. Compliance with these criteria shall be within the available trajectories and DSIF capability.

The following procedures provide an outline of spacecraft functional requirements for the three study cases, assuming Sun-Star references. The minimum case is covered in one set and the nominal and maximum are considered jointly in a second set.

1. Minimum Case Functional Requirements

   a. Engineering Measurements

      1) Direct the measurement of engineering quantities
         a) For normal operation
         b) For failure modes (diagnostic)
         c) For verification of spacecraft design to support development
      2) Condition data to T/M format

   b. Provide Data-Handling Functions

      1) Digitize, encode, and synchronize data
      2) Modulate the transmitted (down-link) signal with the T/M signals

   c. Supply Power

      1) Provide electrical power from a charged battery when primary source will not handle the load.
      2) Provide electrical power from primary power source for on-line spacecraft operation.
      3) Provide power from primary source to recharge battery.
      4) Condition power to a fixed format for spacecraft use; voltage, frequency, waveform, phase, noise level.
      5) Distribute power.
      6) Condition power to individual requirements.

d. Track and Communicate

1) Receive DSIF radio signal and retransmit a frequency-coherent signal to provide two-way doppler data.
2) Demodulate command signals, establish synchronization, detect the information, establish word organization, and route as appropriate.
3) Demodulate ranging signals, reconstruct the proper code, and remodulate the transponder output.
4) Provide a transmitter carrier signal which can be modulated by the coded telemetry information.
5) Transmit discrete and quantative commands from Earth to the spacecraft.

e. Control and Sequence

1) Generate timing frequencies and pulse trains on spacecraft.
2) Provide a timing capability for specific fixed intervals and events.
3) Provide a timing capability for specific commanded intervals (including in-orbit sequencer).
4) Provide control signals based on 1), 2), and 3).
5) Provide control signals based on direct commands.
6) On-board sequences may include the following:
   a) Prelaunch
   b) Launch
   c) Automatic acquisition
   d) Early maneuver (T/M on omni)
   e) Late maneuver (T/M on high-gain beyond the range of the omni antenna)
   f) Cruise, cyclics
   g) Retro maneuver (T/M on high-gain if possible)

Some of these may be identical, but each item has a separate initiation time, and in some cases several possible sources of starting signal.

f. Guide

1) Make measurements of the spacecraft position using two-way doppler, ranging and angular observation as appropriate, both in transit and in orbit.
2) Process data on Earth to obtain guidance commands (stored commands and start times)
3) Align the spacecraft attitude in accordance with stored commands, using inertial sensors.
4) Control the starting time and magnitude of the velocity impulse for the correction maneuvers in accordance with stored commands.
5) Control the starting time and magnitude of the velocity impulse for the orbit insertion maneuver in accordance with stored commands.

NOTE

The starting time is much more critical for Item 5) than for Item 4). The magnitude may be more critical also, but the difference in requirement is certainly much smaller than that for the starting time.

6) Control the spacecraft attitude using inertial sensors during any period when optical sensors are off, including propulsion maneuvers.

g. Impart Impulse

Provide velocity impulses for three in-transit trajectory corrections and one planetary orbital insertion in accordance with command signals.

h. Control Attitude

1) Acquire external attitude references for spacecraft and stabilize spacecraft with roll axis on Sun line and solar panels in Sun direction, except when inertial control is specifically commanded.
2) Acquire the secondary reference (Star Canopus), except when inertial control or reacquisition is specifically commanded.
3) Maintain or modify spacecraft attitude under control of inertial devices.

i. Control Articulated Subsystems

1) Separate spacecraft from ground launch facilities and launch vehicle.
2) Control the pointing of the high-gain antenna as required.
3) Control and pointing update of celestial attitude reference as required.
4) Extend and/or erect stowed members, i.e., solar panels, protective covers, etc.

j. Control Environment

1) Provide an acceptable thermal environment for all spacecraft subsystems as required. This control is supplied by passive and/or active techniques.
2) Provide Sun-shading for those items requiring protection from direct solar radiation.
3) Provide radiation shielding if required.
4) Provide magnetic shielding as required.
5) Provide RF shielding as required.

2. Maximum and Nominal Cases Functional Requirements

a. Scientific Measurement

1) Collect science data
2) Condition data to T/M format
3) Calibration of instrumentation as required

b. Engineering Measurements

1) Collect engineering data
   a) For normal operation
   b) For failure modes (diagnostic)
   c) For verification of spacecraft design to support spacecraft development
2) Condition data to T/M format

c. Provide Data-Handling Functions

1) Store scientific data of planet-oriented instruments, and corresponding calibration data.
2) Read out stored data.
3) Digitize, encode, and synchronize data.
4) Modulate the transmitted (down-link) signal with the T/M signals.

d. Supply Power

1) Provide electrical power from a charged battery when primary source will not handle the load.
2) Provide electrical power from primary power source for on-line spacecraft operation.
3) Provide power from primary source to recharge battery.
4) Condition power to a fixed format for spacecraft use; voltage, frequency, waveform, phase, noise level.
5) Distribute power.
6) Condition power to individual requirements.

e. Track and Communicate

1) Receive DSIF radio signal and retransmit a frequency-coherent signal to provide two-way doppler data.
2) Demodulate command signals, establish synchronization, detect the information, establish word organization, and route as appropriate.
3) Demodulate ranging signals, reconstruct the proper code, and remodulate the transponder output.
4) Provide a transmitter carrier signal which can be modulated by the coded telemetry information.
5) Transmit discrete and quantative commands from Earth to the spacecraft.

f. Control and Sequence

1) Generate timing frequencies and pulse trains on spacecraft.
2) Provide a timing capability for specific fixed intervals and events.
3) Provide a timing capability for specific commanded intervals (including in-orbit sequencer).
4) Provide control signals based on 1), 2) and 3).
5) Provide control signals based on direct commands.
6) On-board sequences may include the following:
   a) Prelaunch
   b) Launch
   c) Automatic acquisition
   d) Early maneuver (T/M on omni)
   e) Late maneuver (spacecraft beyond range of omni-antenna)
   f) Cruise, cyclics
   g) Retro maneuver (nominal no-flyby, max.,with flyby)
   h) No solar occultation for nominal, solar occultation compatibility required for maximum case.
   i) Orbital operation sequence
   j) Planetary Observation sequence

Some of these may be identical, but each item has a separate initiation time, and in some cases several possible sources of starting signal.

g. Guide

1) Make measurements of the spacecraft position using two-way doppler, ranging and angular observation as appropriate, both in transit and in orbit.
2) Process data on Earth to obtain guidance commands (stored commands and start times).

3) Align the spacecraft attitude in accordance with stored commands, using inertial sensors.
4) Control the starting time and magnitude of the velocity impulse for the correction maneuvers in accordance with stored commands.
5) Control the starting time and magnitude of the velocity impulse for the orbit insertion maneuver in accordance with stored commands.

NOTE

The starting time is much more critical for Item 5) than for Item 4). The magnitude may be more critical also, but the difference in requirement is certainly much smaller than that for the starting time.

6) Control the spacecraft attitude using inertial sensors during any period when optical sensors are off, including propulsion maneuvers.

h. Impart Impulse

Provide velocity impulses for three in-transit trajectory corrections and one planetary orbital insertion in accordance with command signals.

i. Control Attitude

1) Acquire external attitude references for spacecraft and stabilize spacecraft with roll axis on Sun line and solar panels in Sun direction, except when inertial control is specifically commanded.
2) Acquire the secondary reference (Star Canopus), except when inertial control or reacquisition is specifically commanded.
3) Maintain or modify spacecraft attitude under control of inertial devices.

j. Control Articulated Subsystems

1) Separate spacecraft from ground launch facilities and launch vehicle (umbilical).
2) Control the pointing of the high-gain antenna as required.
3) Control the pointing update of celestial attitude reference as required.
4) Control the pointing of the planetary directed instruments during a period of time-near-orbit periapsis. Functions required are platform pointing, lock, and update as required for each orbit or group of orbits.
5) Extend and/or erect stowed members, i.e., solar panels, protective covers, instrument supports, etc.

k. Control Environment

1) Provide an acceptable thermal environment for all spacecraft subsystems as required. This control is supplied by passive and/or active techniques.
2) Provide Sun-shading for those items requiring protection from direct solar radiation.
3) Provide radiation shielding if required.
4) Provide magnetic shielding as required.
5) Provide RF shielding as required.

B. SPACECRAFT SYSTEM DESCRIPTION

1. Definition of Minimum, Nominal and Maximum Case Spacecraft

The three spacecraft cases described are called the minimum case, the nominal case, and the maximum case. The nominal case, which received the primary consideration in this study, is described briefly by subsystem. The purpose of the minimum case without science capability is to supply a weight and capability lower limit. The maximum case is based on the total scientific payload suggested by NASA headquarters at the beginning of the study. The estimation of capability versus weight is facilitated within the range defined by the two cases. Only the differences from the nominal case are described for the minimum and maximum cases. The minimum and maximum differences follow the nominal case description for each subsystem.

2. Constraints Assumed for Purpose of the Study

The spacecraft will be launched by a 30 percent flexed Atlas-Centaur. The launch dates will be between 9 January 1969 and 4 April 1969 which includes both Type I and Type II opportunities. Two launchings are planned during this period. Two midcourse maneuvers are required, and the nominal and maximum cases have a capability of three. Orbit insertion will require 2.5 hours for the minimum case, 3 hours for the nominal case and 6.5 hours for the maximum case. Only the maximum case has the flyby option capability as a failure mode option.

The orbit life for the minimum case is 30 days, for the nominal case is 90 days, and for the maximum case is 180 days. The nominal orbit chosen will provide Earth occultation for a few weeks early in the orbit life. For the orbits selected, Sun occultation will not occur for at least 90 days after encounter. In addition the Canopus tracker should receive no light interference from the near limb of Mars. The noncontamination constraint is met by selecting a periapsis altitude consistent with a 50 year life and the Mars atmosphere model referred to in Section V.E. Two periapsis altitudes, 1500 km and 4000 km are considered for the nominal case. An apoapsis of 50,000 km was selected (see VIII. B).

For this study it was assumed that the three 85-foot DSN stations are available for the cruise phase of the mission, and that the orbit phase is additionally supported by the 210-foot receiving antenna capability and 85-foot 100 kw transmission capability at all three DSN sites.

3. Spacecraft System Description

a. System Functional Description

The system consists of the following subsystems interconnected to provide the functions listed in functional requirements:

1) Science Subsystem
2) Telecommunications Subsystem
3) Guidance and Attitude Control Subsystem
4) Central Computer and Sequencer (CC&S)
5) Power Subsystem
6) Propulsion Subsystem
7) Thermal Control Subsystem

For subsystem relationship, refer to the spacecraft nominal case of Figure 9-8 (see Subsection D). The appearance of the spacecraft is illustrated in Figure 10-2b of Section X.

The subsystem functions are as follows: 1) The science subsystem sequences the collection of scientific data, encodes it and supplies it to the telecommunications subsystem. The data is then recorded and/or transmitted to Earth. 2) The telecommunications subsystem supplies command receiving capability, engineering and scientific data transmission capability, and transponding capability. The latter is employed in spacecraft tracking by Earth for trajectory determination. 3) The guidance and attitude control subsystem supplies the attitude control and guidance control required to direct the spacecraft on the mission. 4) Decoded commands are directed to the CC&S and the science subsystem for execution. The CC&S receives and stores the commands and supplies appropriate signals for the execution of those commands. The CC&S also sequences the routine operations of the various mission phases. Timing reference signals are supplied by the CC&S to the science subsystem for the data retrieval and processing sequencing. 5) The power subsystem converts solar energy to power suitable for the spacecraft subsystems. It also supplies limited energy storage in batteries for off Sun intervals. 6) The propulsion system provides the required velocity environment corrections and changes required for the respective midcourse corrections and orbit insertion. The propulsion subsystem provides a means of thrust vector control. 7) The thermal control subsystem provides an acceptable thermal environment for all other spacecraft subsystems.

b. Subsystem Description

The nominal spacecraft system is described below on a subsystem basis and differences in the minimum and maximum cases follow each of these descriptions:

(1) Science Subsystem. The science subsystem consists of six cruise instruments, two planet oriented instruments, a data automation system (DAS) and a science platform. The subsystem collects scientific data and supplies it to the telecommunications subsystem for transmission to Earth.

(a) Cruise Instruments. The cruise instruments are the magnetometer, the plasma probe, the energetic particle detector, the micrometeoroid detector, the two-frequency occultation beacon, and the Mars radio noise experiment. The cruise instruments are operational for the entire mission and send cruise instrument data to Earth continuously during the cruise phase. However, cruise science data is not sent during maneuvers and diagnostic modes. Cruise science and engineering is time-shared with planetary science data while in orbit. (See IX. E.)

(b) Planet Oriented Instruments. The planet oriented experiments are the television camera, and the Mars scanner. The planet experiment data is taken during an interval included in a 2-hour period about periapsis. As the data is taken, it is stored in a tape recorder located in the telecommunications subsystem. The instrument performance data is transmitted in real time. During the remainder of the orbit, the stored data is played back and transmitted to Earth.

(c) Earth Occultation. At each occurrence of Earth occultation the two-frequency occultation beacon data is recorded at the DSN.

(d) Platform Pointing. The two planet experiments are mounted on the science platform which points the instruments. Platform pointing (about the scan axis, which is nearly perpendicular to the orbit plane) is set once per orbit. The direction of the scan axis can be updated once during the orbiting life of the mission. This update is used to keep the scan axis close to perpendicular to the orbit plane. The spacecraft orbit motion provides an instrument track across the planet.

(e) DAS Functions. The data automation subsystem, (DAS) controls the instruments and programs the data. The execution of these functions are facilitated by commands from the telecommunications subsystem and by control and timing signals from the CC&S.

(f) Minimum/Maximum Case Comparisons. The minimum case has no science capability and no facilities for handling scientific equipment or data. The maximum case has two planet instruments in addition to the nominal case complement; the infrared interferometer, and the ultraviolet spectrometer. Only the interferometer is added to the science platform, thereby making a total of three instruments on the main scan platform. Additional requirement of the platform is the stepping or setting during the orbit in the orbit

plane, and the setting of the platform axis for each orbit to allow for local vertical tracking and other options. The UV spectrometer has a separate (additional) pointing mechanization.

(2) Telecommunications Subsystem. Telecommunications consists of the telemetry subsystem, the radio subsystem, the command subsystem, and the antennas. The telecommunications subsystem receives and decodes commands, transmits scientific and engineering data to the DSN stations, and provides transponding capability that enables the Earth-based stations to determine the spacecraft position and velocity.

(a) Telemetry Subsystem. The telemetry subsystem accepts serial binary scientific data measurements and 130 engineering data channels. The analogue engineering samples are conditioned and converted to binary words. The scientific and digital data is time-multiplexed or commutated, and modulate a subcarrier. The modulated data subcarrier is added to a synchronization subcarrier to form composite signals which modulate the RF carrier of the spacecraft-to-Earth channel. Three bit rates are available; typical data rates are 133 1/3, 66 2/3 and 8 1/3 bps. A tape recorder with 15×10^6 bit capacity is furnished.

(b) Command Subsystem. The command subsystem recognizes commands in the receiver outputs, and converts them into digital form acceptable by the CC&S and the subsystems which execute the commands.

(c) Radio Subsystem. The radio consists of redundant receivers and redundant 10 watt transmitters. Twenty watt transmitters are considered as an alternative. The RF signals from the antennas are supplied to the receiver. Signals are amplified, phase locked, and demodulated into modulated signal outputs. The two demodulated signals, the commands subcarrier and the synchronization signal subcarrier are supplied to the command subsystem. The modulation signal output is supplied to the turnaround ranging unit, which demodulates the ranging signal, and supplies the demodulated signal to the transmitter for modulation at the transmitter frequency.

The transmitter modulates input signals at the spacecraft to Earth channel frequency, amplifies the signals, and radiates an effective 10 watts. The transmitter signal inputs are the scientific and engineering digital encoded data supplied by the telemetry subsystem, and the demodulated ranging signal supplied by the receiver.

(d) Antenna Subsystem. A single axis, steppable 3 foot diameter high-gain antenna and two low-gain antennas are furnished for receiving radio signals from Earth and transmitting radio signals to Earth. The spacecraft three axis attitude control subsystem supplies the base-reference for pointing the high-gain antenna. The high-gain antenna is pointed 9 degrees off the axis of its movement to provide incremental changes in pointing, thereby providing a circular coverage with the main lobe of the antenna pattern. The axis of

movement of the antenna is at an angle of 38 degrees to the -Z (roll) axis, on the end that faces the Sun. One low-gain antenna is mounted on the Z roll axis and a second low-gain antenna is mounted on the end of one of the solar panels.

(e) Minimum/Maximum Case Comparisons. The minimum case has a single receiver, and capacity for receiving only 30 discrete commands (D. C.) and one quantitative command (Q. C.). The data encoder handles 90 engineering measurements, and the 3-foot antenna is fixed. Only one Mariner 1964 type low gain antenna is supplied. No tape recorder is included and only one data mode is considered. Finally, only two data rates are incorporated; 33 1/3 and 8 1/3 bps.

The maximum case requires 45 D. C., 5 Q. C., and 150 engineering measurements. A 48 inch diameter two-axis steerable antenna provides increased data rates, which are 226 2/3, 122 1/3 and 16 2/3 bps. The increased data rates and science payload requires a larger tape recorder capacity of about 50 million bits. The transmitter has 20 watt power output capability.

(3) Guidance and Attitude Control Subsystem. The guidance and attitude control subsystem supplied attitude control, attitude references, and guidance control for all mission phases and maneuvers with one exception. The pitch and yaw thrust vector control hardware is supplied by the propulsion subsystem.

(a) Attitude Control. The cruise and orbit attitude control torque is supplied by a cold gas system consisting of a nitrogen tank, with plumbing to the ends of all of the solar panels, 12 jets, and 12 solenoid valves. Solar pressure torques on the spacecraft are reduced by adjustable fan shaped solar vanes mounted on the end of the four solar panels. Maneuver attitude control is supplied by the same cold gas system that supplies cruise and orbit attitude control. Roll control during powered flight is supplied by a separate cold gas system with jets on two solar panels tips.

(b) Attitude Reference. Primary attitude reference is supplied by Sun sensors which supply 4π steradian coverage, and a sharp pitch and yaw null detection. The null is aligned on the roll axis. A Canopus detector supplies roll reference. Attitude search and maneuvers require an inertial reference which is supplied by gyros. The velocity increment for midcourse maneuvers and the insertion maneuver are determined from measurements taken by a roll axis accelerometer.

(c) Minimum/Maximum Case Comparisons. The minimum case uses a timer to measure thrust duration because a higher periapsis altitude orbit is used and therefore a lower accuracy requirement is permissible for the trajectory corrections and orbit insertion.

The maximum case is no different from the nominal case in function, but the guidance and attitude equipment has an increased capacity to handle the larger spacecraft and to accommodate an additional three months orbit lifetime.

(4) Central Computer and Sequencer (CC&S). The central computer and sequencer (CC&S), consists of a frequency reference, and a memory oriented timing capability. The CC&S provides sequences for acquisition, maneuvers, cruise, and the orbit phase. In addition, timing signals are provided for the DAS. The maneuver sequence is supplied to the CC&S for storage in the form of quantitative command (Q. C.) No. 1 and the orbit sequencer is supplied in the form of Q. C. No. 2. A Mariner 1964 type timer CC&S is considered as an alternative.

(a) CC&S Capabilities. The CC&S has a random access memory, comparison registers, and simple addition and subtraction capability. The commands directed to the CC&S are stored in the memory and are then executed with signals produced by memory bit accumulation (counting), comparison, and signal output generation.

(b) Maximum/Minimum Case Comparisons. The minimum case CC&S utilizes timer and is similar to the Mariner 1964 CC&S. The CC&S consists of a frequency reference, a master timer, and a maneuver sequencer. The master timer provides the routine control timing for updates antenna switching, automatic searches, etc. The maneuver sequencer stores the maneuver, Q. C. No. 1, and then on an execute command, the sequencer provides the signals needed to carry out the necessary time and the thrust interval.

The maximum case is similar to the nominal case in function, but includes greater control capability.

(5) Power Subsystem. The power subsystem consists of solar panels, storage batteries, a battery charger, and conversion equipment. The subsystem supplies 2400 cps regulated, 400 cps 3 ϕ regulated and DC unregulated power. (See Section XI. C for the power profile.)

(a) Solar Panels. The four solar panels are unfolded after separation and face the Sun in the cruise and orbit phase spacecraft attitude. The four panels convert solar energy into electrical energy by means of 100 square feet of N on P silicon photovoltaic cells.

(b) Silver Cadmium Battery. The silver cadmium battery is in three 700-watt-hour-sections, each with an isolation diode. The battery supplies all of the power required to supplement the solar panels, for normal peak loads, and for maneuver and other off Sun intervals such as might be caused by a meteoric impact. The batteries are recharged when the roll axis is back on the Sun, and peak loads are not present.

(c) Power Conversion. Redundant 2400 cps regulated converters are included to convert solar panel dc to 2400 cps ac for general spacecraft power. A single 400 cps 3 ϕ ac regulator converts the same dc source to 400 cps and supplies gyro power. Some equipment such as the transmitter strip heater and the gimbaled motor actuators will use unregulated dc direct from the panels or battery.

(d) Minimum/Maximum Case Comparisons. The minimum case is similar to the nominal case in function, but requires less power. The maximum case is also similar to the nominal case in function, but requires more power. However, the maximum case has a flyby option, and Sun occultation late in the mission. As a result of the six and one-half hour injection maneuver, the battery requirement on the maximum case is increased considerably.

(6) Propulsion Subsystems. The two propulsion subsystems considered for orbit insertion are a solid propellant system and a liquid bipropellant system. The solid propellant system is supplemented by a liquid monopropellant system for midcourse maneuvers, whereas the liquid bipropellant system supplies the midcourse correction thrust as well as the insertion retro capability. Roll control is supplied as an attitude control function and is not included in the propulsion description.

(a) Liquid Bipropellant Subsystem. The liquid bipropellant subsystem consists of an oxidizer tank, a fuel tank and a gimbaled motor in line on the roll axis. Plumbing and valves are also included. The gimbaled motor supplies pitch and yaw attitude control for the thrust intervals.

(b) Solid Propulsion Subsystem. The solid propulsion subsystem consists of a spherical tank containing the solid propellant, a built in nozzle, and a nozzle injection liquid tank. The thrust is directed along the roll axis and pitch and yaw attitude control is supplied by nozzle injection thrust vector control.

(c) Liquid Monopropellant Subsystem. The liquid monopropellant subsystem for midcourse corrections occupies one octagonal bay. The system consists of one tank and a motor side by side, and the necessary plumbing, valves, and jet vanes. The motor supplies thrust at 90 degrees to the roll axis, and the jet vanes are used for thrust vector control.

(d) Maximum/Minimum Case Comparisons. The minimum and maximum case propulsion subsystems are the same in function with the nominal case. The minimum case requires a smaller capability, and the maximum case requires a larger capability than the nominal case.

(7) Thermal Control Subsystem. This subsystem is described in Section XI. D.

C. SEQUENCE OF EVENTS

1. Sequence of Operations

The nominal sequence of operations performed by the spacecraft is described from the Launch phase through the Orbit Sequence phase. The sequence is a function of many variables and those variables considered of major interest are discussed in detail. The events 1 through 5 are basically similar to those associated with the Mariner 1964. The second midcourse maneuver may be performed at any time up to a few weeks prior to encounter. This decision is a function of the spacecraft mechanization (i.e., liquid versus solid propellant) and the accuracy of orbit determination. The Retro Maneuver Sequence and the Orbit Sequence are unique to the Mars 1969 mission and are discussed to greater depth. A detailed sequence of events is described in Paragraph 3.

a. Launch

Launchings for the Mariner Mars 1969 Spacecraft will take place at AFETR using the 30 percent Floxed Atlas/Centaur launch vehicle.

b. Boost

From liftoff until nose fairing ejection the spacecraft will be radiated through a parasitic antenna located on the nose fairing. After nose fairing ejection, communication will be via the spacecraft low-gain antenna. At spacecraft separation, full power will be supplied to the transmitter and the low power amplifier stage will be switched off.

c. Initial Acquisition

Upon separation from the Centaur, the spacecraft will eject the solar panels, turn on the cruise science instruments and initiate the attitude stabilization and acquisition process.

Power during the launch and solar stabilization phases is provided by a battery. After solar stabilization, power will be provided by the solar panels. Solar acquisition will nominally be completed within 20 minutes after injection. Canopus acquisition will begin 932 minutes after initiation of the launch sequence (which is at liftoff -3 minutes), and nominally will require 75 minutes to complete.

d. Cruise

During the majority of the transit time, the spacecraft remains attitude stabilized and transmits continuously. The transmitted information will consist of commutated engineering data frames alternated with science data frames.

At preselected times throughout the trajectory, several discrete events will occur, as follows:

1) The Canopus sensor cone angle will be updated.
2) The bit rate will be switched from 66 2/3 to 8 1/3 bits per second.
3) The transmitter will be switched from the low-gain to the high-gain antenna and the high-gain antenna position updated.

These events will be initiated by on-board logic with ground command backups.

e. Midcourse Maneuver

In an interval from 2 to 10 days after injection, the cruise phase will be interrupted and a trajectory correction maneuver will be performed. A second maneuver will be required to improve the aiming point dispersion. During the maneuver sequence, only engineering data will be transmitted. The total maneuver period is 932 minutes with events possible in 0.91 minute increments from 0.91 minutes to 233 minutes (similar to Mariner 1964).

f. Retro Maneuver Sequence

This sequence is essentially known and established prior to launch. It is possible therefore, to insert into the CC&S two time intervals (i.e., 249 min and 215 min) to establish the start of Retro Motor Burn. This sequence is started by the insertion of Q.C. No. 1 which establishes Pitch and Roll duration and polarity and Retro Motor Burn duration. Figure 9-1 illustrates this sequence. A number of events of this sequence are of special interest:

1) A discrete command is sent to execute the start of the retro maneuver. This command must initiate the present time sequence of 249 minutes at R-249 plus a known tolerance. If it does not, then it may be sent again to attempt a more accurate start at R-215 minute.
2) After both Pitch and Roll turns have been completed and verified* the decision to start the Retro Motor Burn must be made. This decision is based upon the established probability of planet contamination of 10^{-4} as related to the orbit life of the spacecraft. The orbit life has been established at 50 years. The decision to inject into orbit requires that another discrete command be sent.
3) This discrete command may be mechanized to meet either:
   a) Sterilization requirements
   b) No sterilization requirements
4) The nominal Retro Maneuver sequence requires approximately 3 hours off Sun for the spacecraft. Figure 9-2 shows the Retro Maneuver sequence

*The Verification Problem requires further consideration.

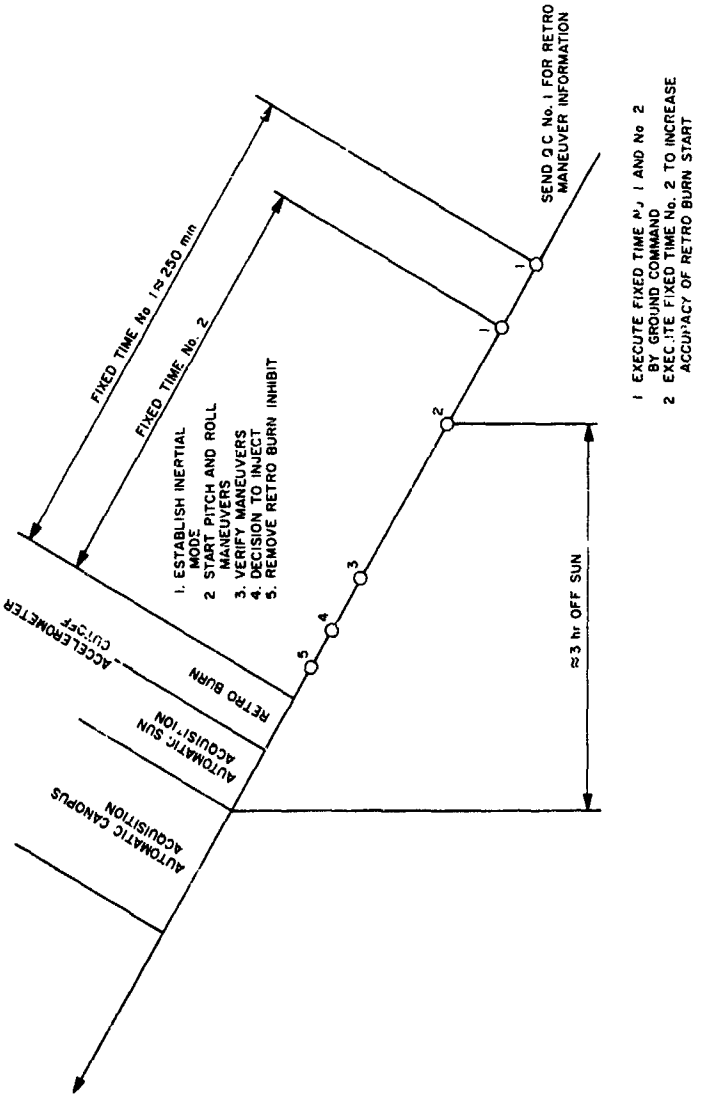


Figure 9-1. Mars 1969 Nominal Retro Maneuver

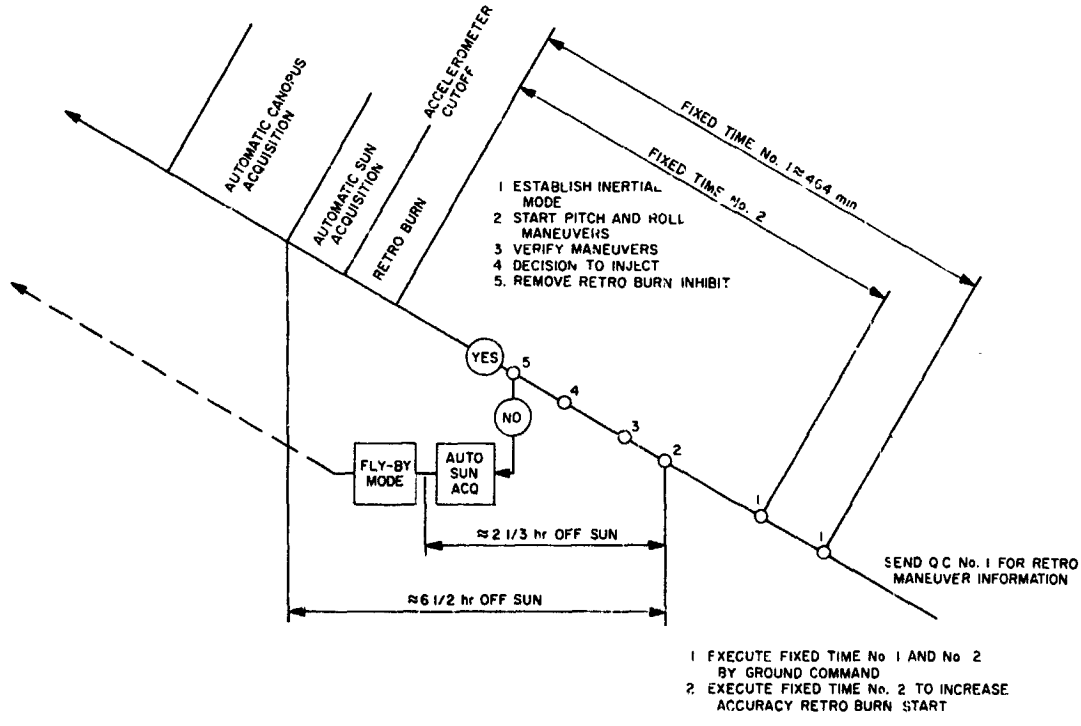


Figure 9-2. Mars 1969 (Maximum Case) Retro Maneuver

for the maximum case and indicates a flyby capability with a penalty of 6 1/2 hours off Sun.

5) The retro burn duration is determined by accelerometer cutoff.

g. Orbit Sequence

The first orbit will provide the necessary information to establish orbit parameters. Earth occultation experiments may be performed during this first orbit. After references reacquisition and one complete orbit a number of quantitative commands are sent (as required) to establish the following:

1) Playback time for the Tape Recorder to coincide with the orbit period minus approximately two hours.
2) Select and sequence the cruise science instruments.
3) Select either the Mars Scanner or TV for the planet science sequence.
4) Select the Mars Scanner Mode.
5) Select the direction of the planet science platform position. This position can be changed once each orbit.

The orbit sequence of events indicates that the spacecraft is initially in data mode No. 2 until D. C. No. 33 is sent to establish data mode No. 3. At this time the planet science goes on and a fixed data mode No. 3 timer is started. This fixed timer is set for approximately two hours. The planet science data is taken until the "end of tape" signal which is the same as for Mariner 1964 spacecraft. After two hours the spacecraft goes into data mode No. 4. During this mode the planet science data is played back. If more than one playback orbit is necessary this may be established by Q. C. No. 2. After playback data mode No. 3 is reestablished automatically thereby not requiring the use of D. C. No. 33. The planet oriented science (i.e., the Mars Scanner and TV) may be cycled automatically or by command each orbit. But, for the nominal case only one of these instruments will be active each orbit. Note that data mode No. 2 is not repeated. The nominal orbit sequence is shown in Figure 9-3.

2. Design Constraints

The mission profile described above reflects the nominal approach to resolve the following design constraints of the Mars 1969 Orbiter study:

1) Two trajectory types were considered:
   a) Type I-B, 1500 x 50,000 km, Inc. = 45 degrees, southerly direct aiming point
   b) Type II-B, 1500 x 50,000 km, Inc. = 50 degrees, southerly direct aiming point
2) The Mars area of interest lies between +10 degrees and -40 degrees latitude.
3) The preferred lighting condition (for TV coverage) lies between +100 degrees and +140 degrees Sun-Spacecraft-Planet angle.

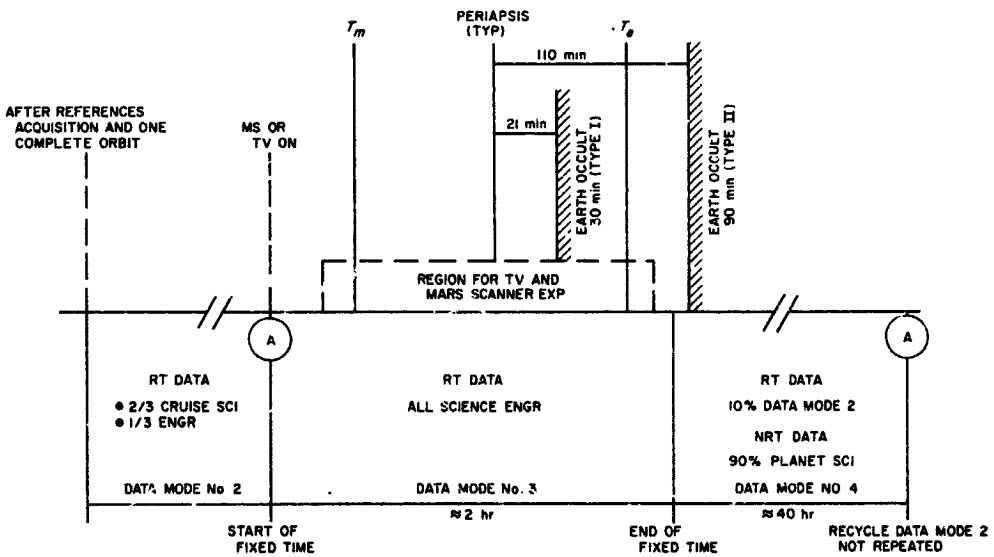


Figure 9-3. Mars 1969 Nominal Orbit Sequence

4) The nominal range limits for planet oriented science data are twice periapsis altitude.
5) The nominal in-orbit mission time is 90 days.
6) The nominal downlink has 10-watt capability with three bit rates. The communications calendar date limit is column (A) and the last arrival dates of the spacecraft to Mars for Type I-B and Type II-B nominal trajectories are shown in column (B).

	A	B	B
bps		Type I-B	Type II-B
133 1/3	12-2-69	10-3-69	11-2-69
66 2/3	2-1-70	10-3-69	11-2-69
8 1/3	full mission duration	10-3-69	11-2-69

7) The planet-oriented science for the nominal case is the Mars Scanner and TV experiment. However, only one experiment is active per periapsis passage.

Figures 9-4, 9-5, 9-6, and 9-7 illustrate diagrammatically what the previous constraints mean in terms of area coverage of Mars by the planet-oriented science. Note that the Type I-B trajectory provides early coverage of the evening terminator. After 90 days, TV coverage is minimal until about 160 days.

The time sequencing and pointing of either the Mars Scanner (MS) or Television (TV) appear not to be a major problem up to approximately 60 days. However, beyond 60 days the areas of interest have shifted sufficiently toward the morning terminator to preclude data optimization without a change in both the time start and pointing of the MS and TV. In the Type I-B orbits it is possible to obtain data at both the evening and morning terminators as shown in Figure 9-4, but not within the nominal 90 day orbit mission time.

The Type II-B orbits preclude all evening terminator science data and require early time sequencing of both MS and TV experiments. The pointing requirements appear critical for the MS experiment. For both Type I-B and Type II-B orbits, the TV experiment does not require drastic pointing change for an orbit mission time of 90 days (i.e., Figures 9-6 and 9-7).

The science platform scan axis is updated once at 80 days for the Type I-B trajectory and updated once at 140 days (for the Maximum Case) for the Type II-B trajectory due to the motion of Mars in its orbit about the Sun and precession of the spacecraft orbit plane.

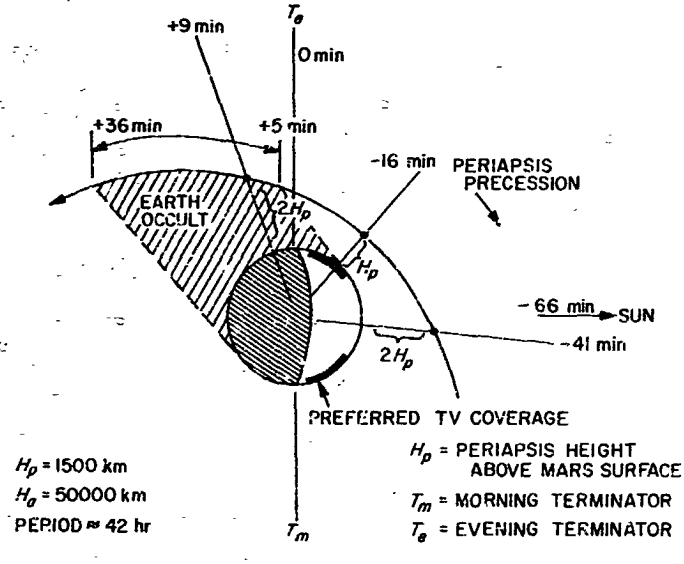


Figure 9-1. Type I-B, Inc. = 45 Degrees, Southerly Direct Aiming Point, Mars Orbit Geometry (0 Day)

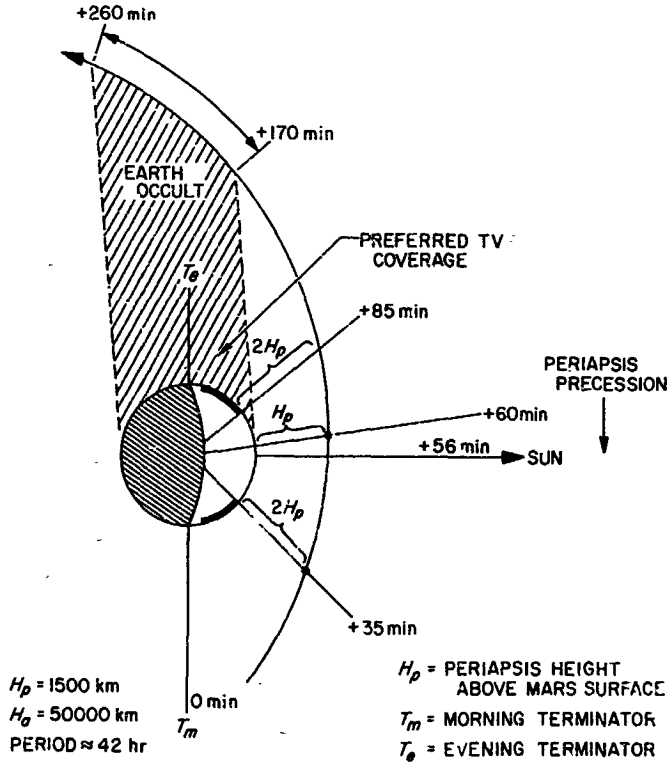


Figure 9-5. Type II-B, Inc. = 50 Degrees, Southerly Direct Aiming Point, Mars Orbit Geometry (0 Day)

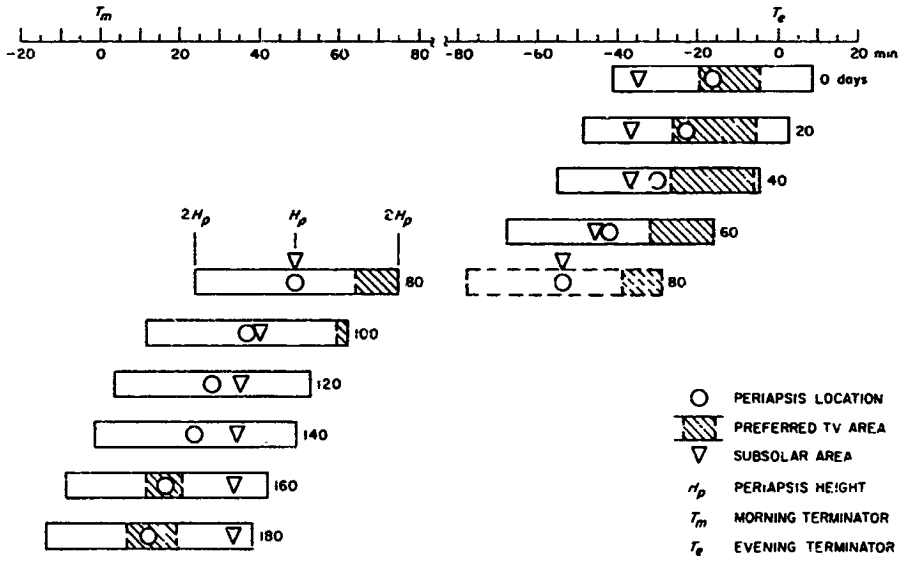


Figure 9-6. Mars 1969 Type I-B, Nominal 1500 x 50,000 km, Inc. = 45 Degrees (Southerly Direct); Time and Event Schedule for 6-Month Orbit Mission

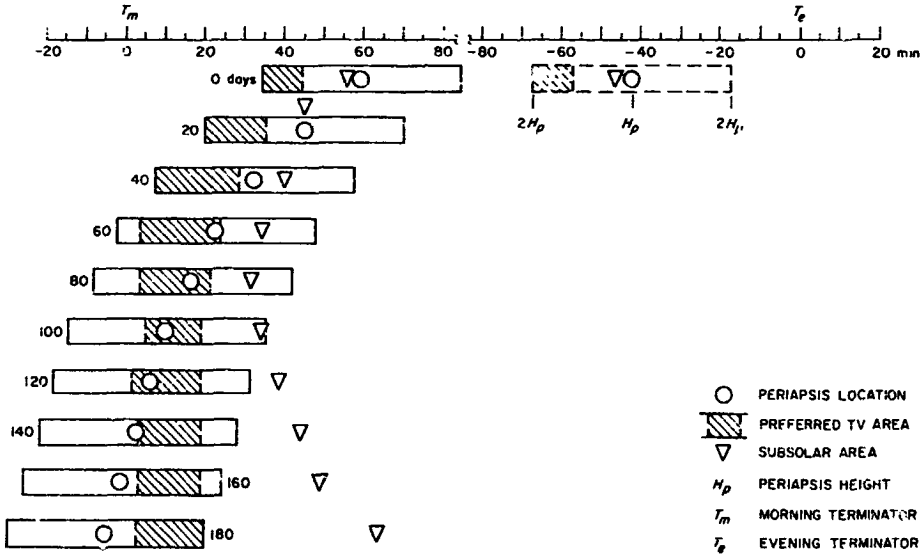


Figure 9-7. Mars 1969 Type II-B, Nominal 1500 x 50,000-km, Inc. = 50 Degrees (Southerly Direct); Time and Event Schedule for 6-Month Orbit Mission

The in-orbit sequencing is closely related to the communications downlink capability. Note that constraint No. 6 shows that we will have 133 1/3 bps capability for a minimum of two months for Type I-B and 1 month for Type II-B Mars orbit. For a nominal 40-hour playback period this corresponds to 19.2×10^6 bits total. The proposed storage capacity is estimated at 15×10^6 bits. The tape recorder has an "advance tape" capability and thereby is considered sufficiently flexible to handle the maximum bits. The tape recorder will be required to playback two orbits at a 66 2/3 bps capability. This capability has also been included.

Where the downlink is 20 watts the bit rates will double. To take full advantage of this additional capability the on-board storage capacity should be doubled also.

Note that with an instrument bit rate of 50,000 bps (i.e., TV) the TV operates five minutes to store 15×10^6 bits. With a 5000 bps for the Mars Scanner this instrument will operate 50 minutes to store 15×10^6 bits. The instrument operating times are compatible with the time it takes the spacecraft to pass over the Mars areas shown in Figures 9-6 and 9-7.

3. Detailed Sequence of Events

Table 9-1 shows a typical flight sequence for the nominal Mariner 1969 case. The table defines in detail the sequence of operations performed by the spacecraft from the period immediately preceding launch until completion of the mission.

Table 9-1. Typical Flight Sequence--Mars 1969 Orbiter
(Nominal Case)

Event	Time	Source	Destination	Comment
A. PRELAUNCH				
1. Insert Retro Maneuver Times	T - 10 min	LCE	CC&S	This is the sequence times for the complete retro maneuver.
2. Tape Recorder to Launch Mode	T - 9 min	LCE	Tape Recorder	Monitor D/E Channel 221, maneuver B.R. output current to determine if the Tape Recorder is in the Launch Mode
3. Switch to Spacecraft Power	T - 5 min	LCE	Power	
4. Start Prelaunch Checkout	T - 3 min	LCE	CC&S	
5. Clear Relay Release	Event 2 + 120 sec			
6. Release Relay Hold	After Event 5	LCE	CC&S	Provided Event 5 occurs within tolerance relative to Event 4
B. LAUNCH EVENTS				
7. Liftoff	T + 0	Event		
8. RF Power Up and Turn On Cruise Science	T + 5 min	Nose Fairing Separation	Power	At nose fairing separation
9. Spacecraft Injection	I (29.2 to 48.0 min)	Event-Centaur		
10. Spacecraft Separation	S = I + 2.6 min	Centaur Timer		
a. RF Power Up and Turn On Cruise Science		Separation Connector	Power	Backup to Event 8.
b. Enable CC&S		Separation Connector	CC&S	

Table 9-1. (cont)

Event	Time	Source	Destination	Comment
c. End Tape Recorder Launch Mode		Separation Connector	Tape Recorder	
d. Remove Plasma 10 kv Inhibit		Separation Connector	Plasma Probe	
e. Arm Pyrotechnics		Pyro-Arming Switch	Pyro	This switch wired in parallel with Separation Initiated Timer for redundancy
f. Centaur Isolation Amplifier Turned Off		Pyro-Arming Switch	D/E	
g. Turn On Attitude Control Subsystem		Pyro-Arming Switch	A/C	Initiate Sun Acquisition. Roll S/C to Calibrate Magnetometer
h. Separation Initiated, Timer Activated				
11. Arm Pyrotechnics	S + 20 sec	Separation Initiated Timer	Pyro	See Comment, Event 10 e.
12. Deploy Solar Panels and Solar Vanes	S + 80 sec	Separation Initiated Timer	Pyro	
13. Deploy Solar Panels and Solar Vanes	T + 50 min	CC&S L-1	Pyro	Backup to Event 12.
C. ACQUISITION EVENTS				
14. Turn On Attitude Control Subsystem	T + 57 min	CC&S L-2	A/C	Backup to Event 10 g. Backup: D.C. 13
15. Sun Acquisition Complete	Event 12 or 13 plus 0 to 20 min			If D.C. 13 was used to turn on A/C, Canopus Acquisition will begin at Event 15

Table 9-1. (cont)

Event	Time	Source	Destination	Comment
16. Turn on Solar Vanes and Canopus Sensor, Initiate Roll Search about the S/C Z-axis	T + 997 min	CC&S L-3	A/C	Backup: D.C. 13 Inhibit magnetometer calibration roll signal.
17. Canopus Acquisition Complete	Event 16 + 0 to 75 min			
D. FIRST MANEUVER EVENTS				
18. Pitch-Turn Duration and Polarity	T + 1 to 10 days	Q.C. 1	CC&S	
19. Roll-Turn Duration Polarity	T + 1 to 10 days	Q.C. 1	CC&S	
20. Motor-Burn Duration	T + 1 to 10 days	Q.C. 1	CC&S	
21. Initiate Maneuver Sequence	M	D.C. 27	CC&S	
22. Maneuver Sequence Start	M + 0			
a. Turns on Gyros for Warmup		CC&S M-1	A/C	
b. Switch to Data Mode 1		A/C	D/E	Backup: D.C. 1
23. Begin Maneuver	M + 59 to 60 min	CC&S M-2	A/C	
a. S/C to Inertial Control (All Axes). Autopilot On, Star Sensor Off				
b. Set Turn Polarity		CC&S M-3 or M-3	A/C	
c. Start Pitch Turn		CC&S M-4	A/C	
24. a. Stop Pitch Turn	Event 23 1000 sec (1 sec resolution)	CC&S M-4	A/C	Magnitude inserted by Q.C. 1 prior to maneuver start
b. Reset Turn Polarity		CC&S M-3	A/C	

Table 9-1. (cont)

Event	Time	Source	Destination	Comment
25. a. Set Turn Polarity	Event 23 + 22 min	CC&S M-3 or M-3	A/C	
b. Start Roll Turn		CC&S M-5	A/C	
26. a. Stop Roll Turn	Event 25 + 1 to 1000 sec (1 sec resolution)	CC&S M-5	A/C	Magnitude inserted by Q.C. 1 prior to maneuver start
b. Reset Turn Polarity		CC&S M-3	A/C	
27. Ignite M/C Motor	Event 23 + 44 min	CC&S M-6	Pyro	Relay pulsed
28. Stop M/C Motor	Event 27 + 0.080 to 102.36 sec (0.040 to 0.080 sec resolution)	CC&S M-7	Pyro	Relay pulsed - magnitude inserted by Q.C. 1 prior to maneuver start
29. a. Commence Automatic Reacquisition of References	Event 23 + 50 min	CC&S M-1 and CC&S M-2	A/C	If L-3 has failed to operate in Event 16, the Canopus sensor and solar vanes will be turned off by this signal. This condition can be corrected by sending Discrete Command 13.
b. Switch to Data Mode 2		A/C	D/E	Backup: D.C. 2
30. Sun Acquisition Complete	Event 29 + to 20 min			
31. Canopus Acquisition Complete	Event 30 + 0 to 75 min			
32. Turn Off Maneuver Counter	Event 23 + 139 min	CC&S	CC&S	Internal function to CC&S which permits subsequent maneuver to be executed

Table 9-1. (cont)

Event	Time	Source	Destination	Comment
E. SECOND MANEUVER EVENTS				
33. Arm Second Propulsion Maneuver		D.C. 23	Pyro	
Complete tracking and Send Trajectory Commands for Second M/C Maneuver				
34. Perform Events 18 to 32				
F. CRUISE EVENTS				
35. Switch Bit-Rate to 8-1/3 bps	R - 192 days	CC&S MT-6	D/E	Backup: D.C. 5
36. Set Canopus Sensor Cone Angle 1	R - 137 days	CC&S MT-1	A/C	Backup: D.C. 17
37. Transmit via High-Gain - Receive via Low-Gain	R - 131 days	CC&S MT-5	Radio	Backup: D.C. 10
38. Set Canopus Sensor Cone Angle 2	R - 103 days	CC&S MT-2	A/C	Backup: D.C. 17
39. Set Canopus Sensor Cone Angle 3	R - 68 days	CC&S MT-3	A/C	Backup: D.C. 17
40. Set Canopus Sensor Cone Angle 4	R - 30 days	CC&S MT-4	A/C	Backup: D.C. 17
G. RETRO MANEUVER EVENTS				
41. Arm Retro Propulsion Maneuver	R - 261 min	D.C. 23	Pyro	
Complete Tracking and Send Trajectory Commands for Retro Maneuver				

Table 9-1. (cont)

Event	Time	Source	Destination	Comment
42. Perform Events 18 to 20				
43. Execute Retro Maneuver	R - 249 min	D.C. 29	CC&S	Coincides with Nominal time sequence for Retro-Motor burn start. This time set prior to launch
44. Execute Retro Maneuver	R - 215 min	D.C. 30	CC&S	This starts second retro-sequence time to improve accuracy of retro-maneuver start if first timer was started inaccurately
45. Begin Retro Maneuver Repeat Events 21 to 26				
46. Decision to Start Retro Burn	R - 92 min			
47. Remove/Insert Retro Inhibit	R - 32 min	D.C. 28	CC&S	Case I: With sterilization requirements D.C. 28 removes inhibit. Case II: Without sterilization requirements D.C. 28 inserts inhibit.
48. Ignite Retro Motor	R + 0	CC&S M-6	Pyro	Relay pulsed Backup: D.C. 31
49. Stop Retro Motor	R + 15 min	Accelerometer	Pyro	Backup: CC&S (M-7). Magnitude inserted by Q.C. 1 prior to retro maneuver start Backup: D.C. 32
50. Begin Automatic Reacquisition of References Perform Events 29 to 31				
51. End of References Reacquisition	R + 110			

Table 9-1. (cont)

Event	Time	Source	Destination	Comment
52. End of One Complete Orbit	Event			Orbit geometry is calculated and orbit period established. Nominal orbit period equal to 42 hours. 1500 by 50,000 km. Nominal Periapsis and Apoapsis.
a. Occultation Experiment		Radio	Radio	For Type I-B trajectories this experiment lasts approximately 30 min. For Type II-B trajectories this experiment lasts approximately 90 min.
53. Select Playback Time	After Event 52	Q.C. 2	CC&S	Selected to match orbit period.
54. Select Cruise Science Instruments	After Event 52	Q.C. 3	CC&S	
55. Select Planet Science Instruments Sequence	After Event 52	Q.C. 4	CC&S	This Q.C. also selects either MS or TV for any one orbit. MS and TV may be cycled each orbit automatically by DAS logic.
56. Select Mars Scanner Mode	After Event 52	Q.C. 5	CC&S	
57. Select Platform Position	After Event 52	Q.C. 6	CC&S	This command changes the platform pointing once per orbit-period.
58. Turn Planet Science On	Event A	D.C. 33	DAS	Timer fixed at a Nominal 2 hours.
a. Data Mode 3 Timer Start				
b. Start Data Mode 3 End Data Mode 2				
c. Science Instrument Cover Removed			Pyro	
d. Turn Off Battery Charger		Power	Power	
e. Turn On Tape Recorder		Power	Tape Recorder	

Table 9-1. (cont)

Event	Time	Source	Destination	Comment
59. Calibrate MS	After Event 58	D.C. 35	DAS	Calibrate MS about 10 min prior to start of MS experiment.
60. Start MS or TV experiment		CC&S	DAS	D.C. 4 selects either MS or TV and determines start time of experiment
61. End MS or TV experiment		Tape Recorder		"End of Tape" signal determines end of experiment. Backup: D.C. 2
62. Start Data Mode 4 End Data Mode 3	Event 58 + 2 hours	CC&S Timer	DAS	Playback begins. Data Mode 2 is not repeated again. Three XTRM bps are available at their max corresponding dates. 1. 133 1/3 bps (12-2-69) 2. 66 2/3 bps (2-1-70) 3. 8 1/3 bps (full mission duration) Note that for the nominal arrival time of the spacecraft is for: 1. Type I-B 10-3-69 2. Type II-B 11-2-69
63. Earth-Occultation Experiment		Radio	Radio	This experiment is performed each orbit if required.
64. End Data Mode 4 Start Data Mode 3	Event 62 + 40 hours	CC&S	DAS	Automatic recycling of Data Mode 4 and Data Mode 3. D.C. 33 is not required to start Data Mode 3 again. It is used only as backup.
65. Advance Playback	Event	D.C. 36	Tape Recorder	Provides playback flexibility
66. Readout Mars RF Noise Experiment	Event	D.C. 37	DAS	
67. Update High-Gain Antenna	Event	D.C. 38	Radio	Update incrementally as required - may include onboard logic for update.
68. End of Mission	R + 90 days			The nominal mission is completed. Experiments may be continued as required.

D. SPACECRAFT BLOCK DIAGRAM

The simplified spacecraft block diagram of Figure 9-8 shows the major subdivisions of the proposed Mars 1969 spacecraft functional mechanization.

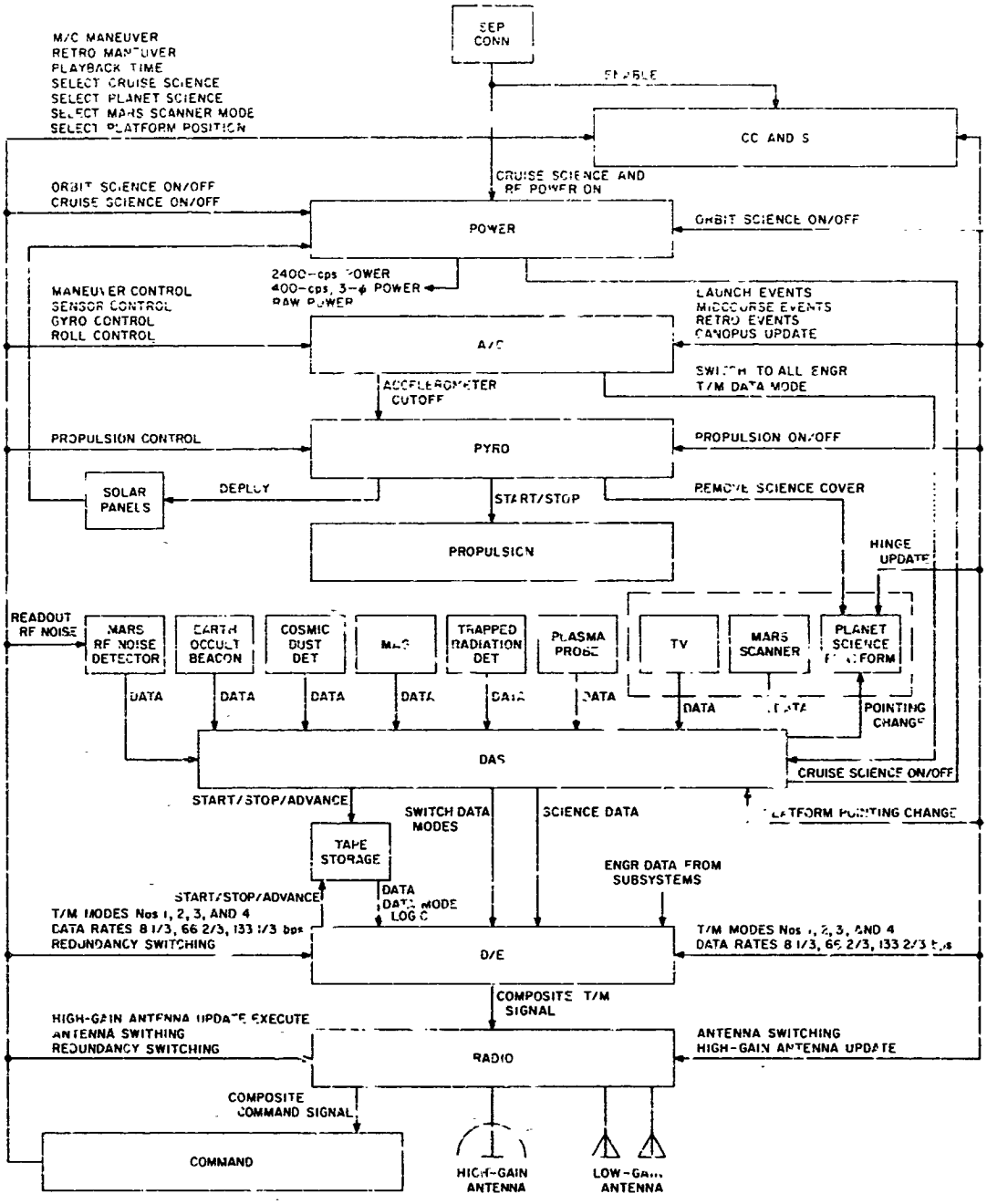


Figure 9-8. Mars 1969 Spacecraft System Block Diagram (Nominal Case)

E. DATA HANDLING, TELEMETRY AND RF COMMAND REQUIREMENTS

1. Description

a. General Capabilities

The Mariner 1969 spacecraft will be equipped with a communications system capable of transmitting spacecraft data to the DSIF. The spacecraft data is divided into engineering data and scientific data. During the maneuver portions of the flight, only engineering data will be transmitted back to Earth. At other than maneuver times, both engineering and scientific data will be transmitted back to Earth in real time, with the scientific data comprising the greater bulk of the total data. While in orbit, much of the data taken at planet encounter will be stored in an on-board magnetic tape storage device. This stored scientific data will be transmitted back to Earth during one or a number of orbits about Mars.

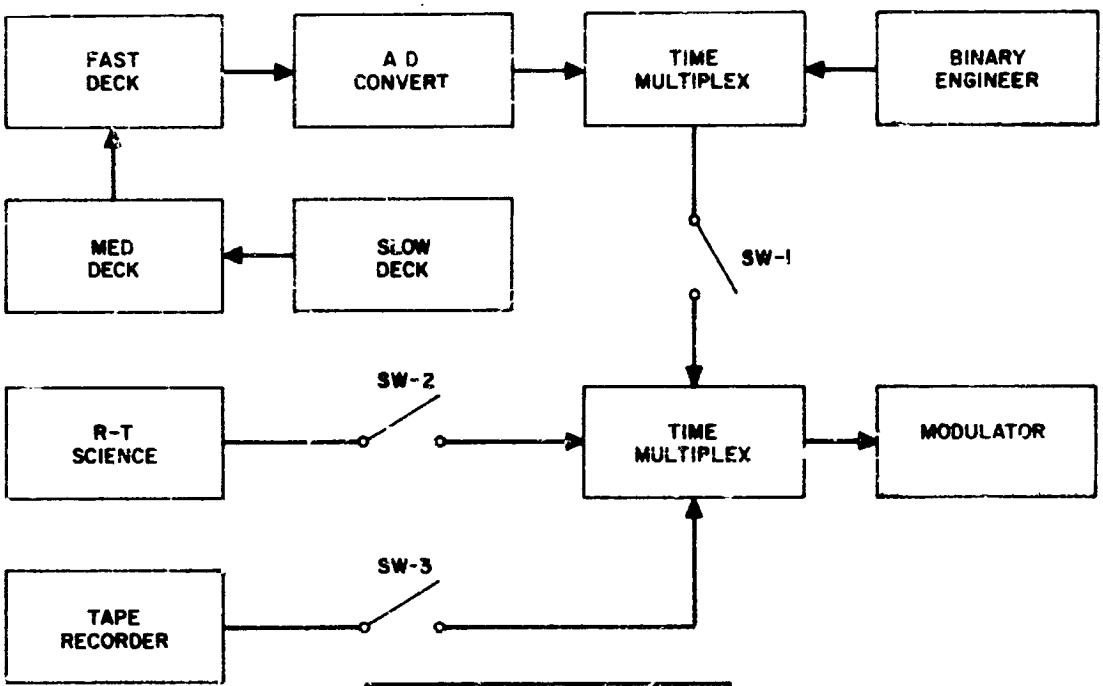
The Mariner 1969 spacecraft will have three transmission rates and four data modes available to allow some flexibility in the spacecraft data telemetry systems. This flexibility is highly desirable because of the large range of communication distance and the several operational modes that take place during the Mariner 1969 mission.

b. General Data Handling

1) Data will be handled in the spacecraft in several ways as shown in Figure 9-9.
2) All analog engineering data will be time shared by the data encoder commutator and converted from analog voltage to 7 bit binary data words by the data encoder analog to digital converter (ADC).
3) All digital engineering data (i.e., data which is in binary form when received by the data encoder) will be time-shared with other measurements of this type and with the output of the ADC.
4) During the launch phase, initial acquisition and cruise, blocks of science data 280 bits long are alternated with blocks of engineering data 140 bits long for real-time transmission.
5) During maneuvers, only engineering data will be transmitted.
6) During planetary encounters a large portion of the science data will be stored in the on-board magnetic tape recorder. The remainder of the science data will be transmitted in real time to the DSIF.
7) The stored science data will be transmitted to DSIF after planetary encounters during a specified portion of an orbit or orbits. During the time the stored science data is being transmitted, both engineering and RT Science will be transmitted,

8) No on-board engineering storage-playback system will be used on the Mariner 1969 spacecraft, except in case of Retro Maneuver verification.

9) The engineering data will be divided into fast, medium and slow speed measurements. The sampling frequency of each is assumed to be compatible with Mariner 1964.



	MODE			
	1	2	3	4
SW-1	CLOSED	CLOSED	OPEN	CLOSED
SW-2	OPEN	CLOSED	CLOSED	CLOSED
SW-3	OPEN	OPEN	OPEN	CLOSED

Figure 9-9. Telemetry Mode Functional Block Diagram

c. Data Modes

(1) General. The purpose of having a number of data modes is to obtain the maximum available sampling rate of the measurements required during a particular period by not transmitting information which is not as useful during that period. Four data modes have been selected for the Mariner 1969 Orbiter.

(2) Data Mode Allocation.

1) Data Mode 1: 100 percent Engineering Data
2) Data Mode 2: 1/3 Engineering, 2/3 Science
3) Data Mode 3: 100 percent Science
4) Data Mode 4: 90 percent Playback, 10 percent Real Time
2/3 Science 1/3 Engineering

(3) Sample Format. A sample format is presented in Figure 9-10.

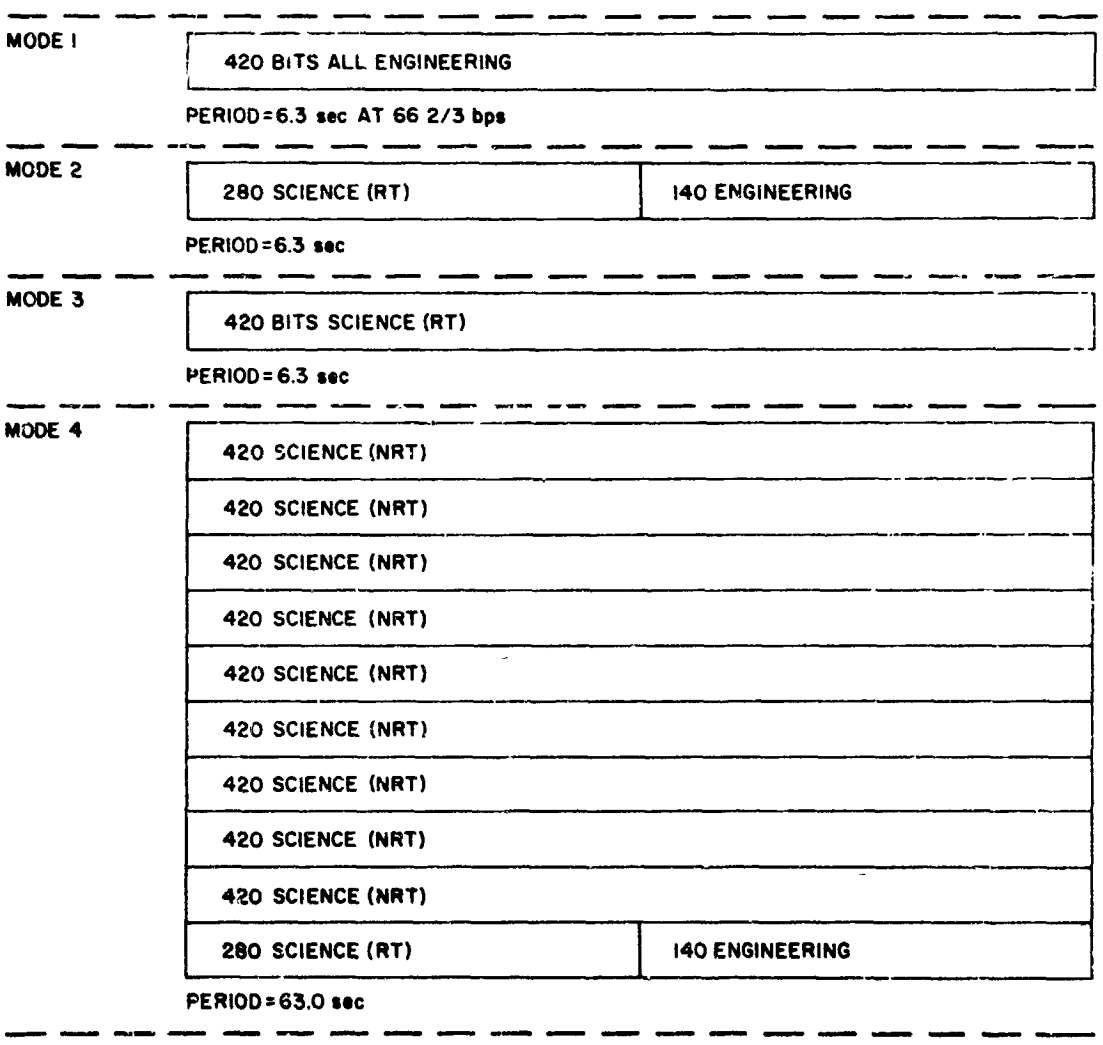


Figure 9-10. Telemetry Mode Sample Format

d. Telemetry Measurements

The following engineering telemetry channel allocations are considered for the Mariner 1969 Orbiter.

Division	Number of Channels
1) 33	12
2) 34	58
3) 35	45
4) 38	15
5) Total	130

The breakdown of the allocated channels for a three-speed commutation system is shown in Table 9-2.

Table 9-2. Nominal Case Commutation Allocations

Division	No. of Low Speed Measurements	No. of Medium Speed Measurements	No. of High Speed Measurements
33	3	5	4
34	13	26	19
35	41	2	2
38	9	3	3
Total	66	36	28

e. Flight Sequence Requirements

(1) Data Mode Switching. At launch the spacecraft will be in Data Mode 2 (cruise). It will normally remain in this mode until the first midcourse maneuver. At that time a command will be sent from the ground causing it to go into Mode 1 (maneuver). After the midcourse sequence is completed a command will be sent from the ground causing it to return to Mode 2. Mode 2 will be used until just before planetary encounter except for additional maneuvers for which the above sequence will be repeated.

After the terminal maneuver, the spacecraft will reacquire the Sun and Canopus, and remain in Data Mode 2 for one complete orbit. This initial orbit will be utilized for determining orbital characteristics. Some time during the second orbit, a quantitative command

will be sent to the spacecraft which will provide an orbital period reference for the spacecraft. At some time later during the second orbit, a ground command will start an orbit timer and will place the spacecraft in an orbit mode of operation. This orbit mode will alternate the spacecraft Data Modes between Mode 3 (planetary science data acquisition) near periapsis, and Mode 4 (playback). The planetary instruments will be so mechanized as to alternate between the Mars Scanner and the Television during consecutive orbits. There will be a ground command to switch planetary instruments. For the purpose of viewing alternate portions of Mars, a platform pointing command will be available and a time delay command for the planetary instrument activation.

(2) Data Rate Switching. Three bit rates will be available on the Mariner 1969 spacecraft. They are 133 1/3 bits per second, 66 2/3 bits per second and 8 1/3 bits per second (see Paragraph 4.).

The spacecraft bit rate will normally be chosen by radio command. A CC&S backup should be provided to switch the data rate to the 8 1/3 bps rate sometime after the completion of the first maneuver.

The 133 1/3 bit rate will be used as long as the signal level from the spacecraft is high enough to allow good data recovery at this rate.

2. RF Command Requirements

The Command Lists as proposed for the Mariner 1969 Orbiter are presented in Table 9-3 (Discrete Commands) and Table 9-4 (Quantitative Commands).

3. Deviations from the Nominal Case

a. Maximum Case

In considering the maximum case, certain assumptions are made (see Section IX. B) which alter the telemetry criteria as discussed in the nominal case. The purpose of this section will be to point out some of the major deviations from the nominal case.

(1) Measurements. The number of measurements considered for the maximum case are as follows:

Table 9-3. Mariner 1969 Orbiter Command List (Discrete Commands)

Discrete Commands (Number)	Event	Source	Destination	Comments
1	Command TLM Mode 1	Gnd	D/E	Backup for Event No. 22B
2	Command TLM Mode 2	Gnd	D/E	Operational command for Event No. 49 and backup for Event No. 29B
	Turn-on Cruise Science			This will also turn Cruise Science back on after Emergency Power conditions
3	Command TLM Mode 3	Gnd	D/E	Backup for Event No. 58
4	Command TLM Mode 4	Gnd	D/E	Backup for Event No. 62
	A. Switch Cruise Science On	D/E	Power	
5	Command Switch Data Rate	Gnd	D/E	Backup for Event No. 35 Switches to alternate data rate
6	Command Switch ADC/PNG	Gnd	D/E	Emergency
7	Switch Power Amplifiers	Gnd	Radio	Emergency
8	Switch Exciters	Gnd	Radio	Emergency
9	Switch Ranging	Gnd	Radio	Operational command to turn ranging off and on
10	Transmit Hi - Receive Lo	Gnd	Radio	Backup for Event No. 37
11	Transmit Hi - Receive Hi	Gnd	Radio	Operational command
12	Transmit Lo - Receive Lo	Gnd	Radio	Emergency
13	Maneuver Command Inhibit	Gnd	A/C	In event of malfunction during maneuver. Inhibits all CC&S maneuver commands to attitude control. Permits normal automatic attitude control operation despite any type of CC&S failure
	Spare Command for Power			
	Turn on Solar Vanes Canopus Sensor and, Turn-on Attitude Control	A/C	A/C	Backup for Event No. 16

Table 9-3. (cont)

Discrete Commands (Number)	Event	Source	Destination	Comments
	Inhibit Prop. Command		Pyro	In event of CC&S malfunction during maneuver which would cause an incorrect maneuver to be performed
14	Remove Maneuver Inhibit	Gnd	A/C	Removes inhibit of D. C. No. 13
	Turn-off Attitude Control	A/C	A/C	If D. C. No. 13 was the method used to turn on A/C
15	Canopus Gate Inhibit Override	Gnd	A/C	Allows star sensor to acquire any celestial object of sufficient brightness to give an output. Provides acquisition gate signal to permit gyro shut-down
16	Science Platform Update	Gnd		
17	Cycle Canopus Cone Angle	Gnd	A/C	Backup for Events No. 36, 38, 39 and 40
18	Gyros on-Inertial Control (Roll Neg. Increment)	Gnd	A/C	This command will be used to provide backup roll stabilization in the event of a Canopus sensor malfunction or if other than normal roll position is required at any time. Place Z (roll) axis under inertial control and command negative increment in roll position. Turns on gyros, turns off Canopus sensor, places roll gyro in position mode, and commands a standard rate turn in negative direction for a fixed time.
19	Gyros off-Normal Control	Gnd	A/C	Return Z (roll) axis to normal automatic optical control - Resets D. C. No. 18, 20, and 15.

Table 9-3. (cont)

Discrete Commands (Number)	Event	Source	Destination	Comments
20	Remove Roll Control	Gnd	A/C	In event of a Canopus sensor failure, the roll axis may be left uncontrolled until orientation is needed, then D. C. No. 18 may be sent. Turns off Canopus sensor and provides acquisition gate signal, thus permitting gyros to turn off.
21	Roll Override - Pos Incr	Gnd	A/C	In the event the Canopus sensor has locked onto a celestial object other than the Canopus. This command turns on the gyros and commands a roll rate until another object meeting the brightness range requirements enters the Canopus sensor field of view. Used in conjunction with D. C. No. 18 for vernier control of roll axis in inertial mode.
22	Arm Next Prop Maneuver	Gnd	Pyro	If a second M/C is desired
23	H. G. Antenna Update	Gnd	Radio	For updating the high gain antenna
24	Turn-on Planet Science	Gnd	Power	Backup to Event No. 58
	Unlatch Cover		Pyro	
	A. Turn-off Battery Charger	Power	Power	
	B. Turn-on Tape Recorder	Power	Power	
25	Turn-off Planet Science		Power	Operational
	A. Switch off Cruise Science	Power	Power	Emergency Power Condition
	B. Switch Battery Charger Off	Power	Power	
26	Initiate M/C Maneuver	Gnd	C&S	Starts M/C maneuver sequence
27	Turn-on Battery Charger	Gnd	Power	In event the battery needs recharging

Table 9-3. (cont)

Discrete Commands (Number)	Event	Source	Destination	Comments
28	Remove Retro Inhibit	Gnd	CC&S	If retro motor in satisfactory position
29	1st Retro Maneuver Start	Gnd	CC&S	To set retro burn timer (Operationally rigid)
30	2nd Retro Maneuver Start	Gnd	CC&S	To set retro burn timer (Operationally rigid)
31	Start Retro Motor	Gnd	Pyro	In the event of CC&S failure
32	Stop Retro Motor	Gnd	Pyro	In the event of CC&S failure
33	Start Orbit Time	Gnd	CC&S	To initiate orbit mode
34	Switch Platform Instruments	Gnd	DAS	For repeating passes
35	Calibrate Science Instruments	Gnd	DAS	
36	Advance Playback	Gnd	T/R	For bypassing stored data
37	Read Out RF Noise Data	Gnd	DAS	
38	Update Canopus Sensor	Gnd	A/C	

Table 9-4. Mariner 1969 Orbiter Command List (Quantitative Commands)

Quantitative Commands (Number)	Event	Source	Destination	Comments
1	Maneuver Command Bits to CC&S Q. C. 1-1 Pitch Turn Duration Q. C. 1-2 Roll Turn Duration Q. C. 1-3 Motor Burn Duration	Gnd	CC&S	Operational Command
2	Set Mode 4 Time	Gnd	CC&S	To set playback time
3	Select Cruise Instruments	Gnd	DAS	To permit the selection of any or all of the cruise instruments
4	Planet Oriented Instrument Delay	Gnd	DAS	To select the proper information retrieval times for the planet oriented instruments (~1 minute resolution)
5	Mars Scanner Coverage	Gnd	DAS	For the selection of the scan amplitude and direction for the Mars scanner (8 cases)
6	Platform Position Command	Gnd	DAS	For the selection of the proper instrument look angle

Division	Number of Channels
1) 33:	13
2) 34:	66
3) 35:	51
4) 38:	20
5) Total:	150

These channels will be commutated as shown in Table 9-5.

Table 9-5. Maximum Case Commutation Allocations

Division	No. of Low Speed Measurements	No. of Medium Speed Measurements	No. of High Speed Measurements
33	3	5	4
34	15	26	20
35	46	2	3
38	12	3	4
Total	76	36	31

(2) Command List. In addition to the nominal command list, the following commands would be necessary for the maximum case (see Table 9-6).

Table 9-6. Additional Maximum Case Commands

Direct Command (Number)	Event	Source	Destination	Comments
39	Start TV Playback	Gnd	Radio	
40	Rewind MS, UV, IR Tape and Stop	Gnd	Radio	For selective playback

In addition to the above commands, the complexity of some of the nominal case commands will increase due to the fact that four instead of two planetary instruments will be affected.

b. Minimum Case

The considerations of the minimum case outlined in Section IX. B would cause a great reduction in both the number of measurements and the number of commands required, as shown in the following paragraphs.

Division	Number of Channels
1) 33:	13
2) 34:	36
3) 35:	36
4) 38:	5
5) Total:	90

(1) Channel Allocations. The allocation of the above channels will be made as shown in Table 9-7.

Table 9-7. Minimum Case Commutation Allocations

Division	No. of Low Speed Measurements	No. of Medium Speed Measurements	No. of High Speed Measurements
33	5	5	3
34	8	17	11
35	35	0	1
38	0	2	3
Total	48	24	18

(2) Command List. The following commands will be deleted from the nominal case:

- Discrete Commands: 16, 24, 25, 34, 35, 36, 37
- Quantitative Commands: 2, 3, 4, 5, 6

4. Twenty-Watt Transmitter Alternate

Although the bulk of the Mariner 1969 Orbiter Feasibility Study was performed with the assumption of having a 10-watt spacecraft transmitter, the possibility of utilizing a 20-watt transmitter in either of the before-mentioned cases has been proposed. The possible bit rates corresponding to this increased available transmitting power would be 224 bps, 112 bps and 14 bps. This in effect would double the total number of bits transmitted per orbit. In order to take advantage of this situation, it is inferred that the storage capacities being considered for the 10-watt case be doubled. Furthermore, the data handling problem would become correspondingly more difficult. Although the detailed problems associated with the 20-watt transmitter case have not been sufficiently analyzed, it is anticipated that most of the perturbations would not be great enough to significantly change the system as outlined in the nominal case.

REFERENCES

1. 292-1787 Mariner 1969 Orbiter System Description
2. 292-1807 Mariner 1969 Orbiter Weight Breakdown and Equipment List
3. 292-1829 Mariner 1969 Orbiter Mission Profile

F. TV, MARS SCANNER, OCCULTATION-PROBABILITY OF SUCCESS

The Mars 1969 Orbiter spacecraft is analyzed to develop the probability of success of the TV, Mars Scanner and Occultation experiments. The general basis of departure assumes that the spacecraft approximates the degree of complexity of the Mariner 1964 spacecraft. This analysis does not include the reliability for the launch vehicle, ground flight operations and for all spacecraft maneuvers. The maneuvers require the successful operation of relatively few electronic components. The dependent subsystems (i.e., attitude control; CC&S) are included in the generalized spacecraft reliability model indicated in Figure 9-11. Additional assumptions are listed in subsequent paragraphs.

The planet oriented science includes both Television and the Mars Scanner. Data are obtained first from one then from the other experiment. Data are never obtained from both at the same time. Playback of data is required prior to switching to the other experiment. The occultation data are desired at least once.

1. Introduction

The reliability analysis evaluates the probability of obtaining:

1) Television
2) Mars Scanner Data
3) Television and Mars Scanner Data
4) Television or Mars Scanner Data
5) Earth Occultation Data

This evaluation was performed for:

6) One spacecraft launch opportunity
7) Two spacecraft launch opportunities

Reliability calculations were made for both Type I-B and Type II-B trajectories at three points in time, i.e.:

8) Transit time and including the first planet oriented science pass at Mars, designated as orbit No. 1 in Table 9-8.
9) Transit time and including the first 50 orbits. This approximates a 90 day orbit mission for a nominal orbit period of 42 hours.
10) Transit time and including the first 100 orbits. This approximates a 180 day orbit mission for a nominal orbit period of 42 hours.

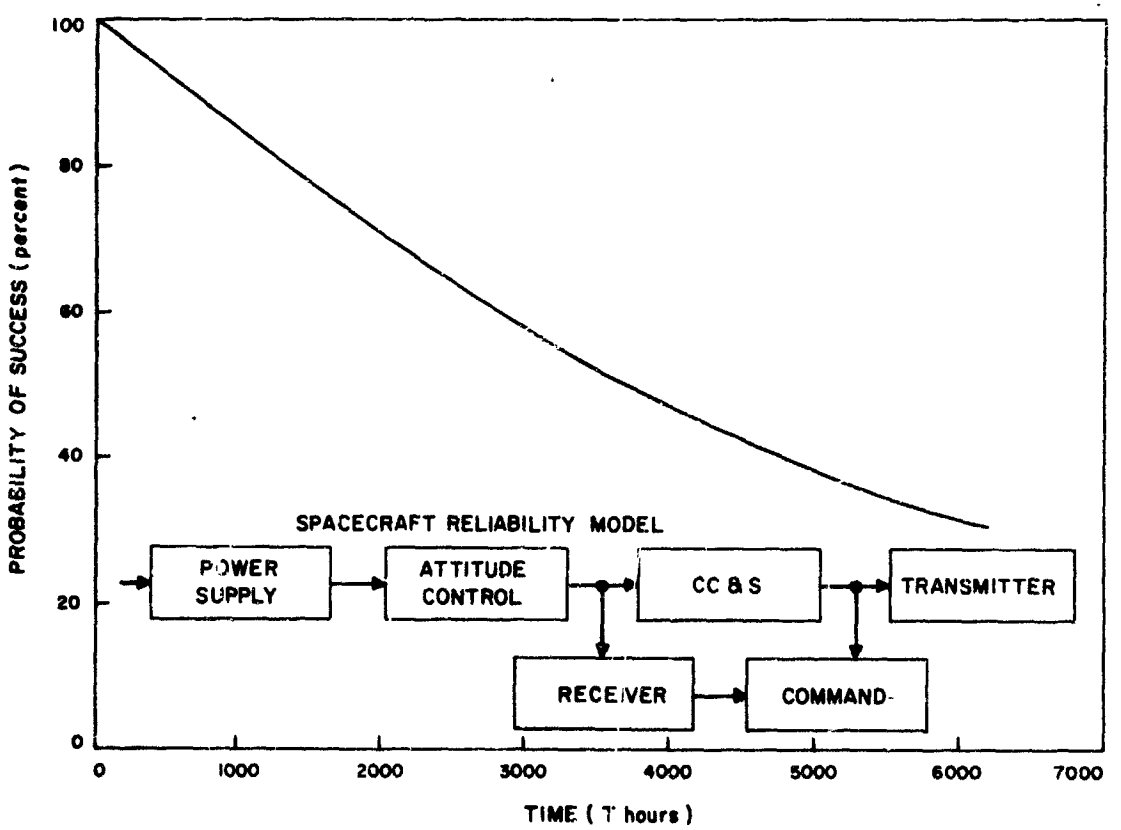


Figure 9-11. Mariner Mars 1969 Probability of One Spacecraft Operating for T Hours

Table 9-8. Probability of Obtaining TV/MS Data (Mars 1969 Spacecraft)



Failure Rate hr^{-1}			$100x10^{-6}$	$50x10^{-6}$	$50x10^{-6}$	$200x10^{-6}$	$100x10^{-6}$	$200x10^{-6}$	$200x10^{-6}$
No. of Orbits	Trajectory Type	Nominal Operating Hours							
1	I-B	4440	4440	2	40	40	40	2	40
1	II-B	6600	6600	2	40	40	40	2	40
50	I-B	6600	6600	100	2000	2000	2000	100	2000
50	II-B	8760	8760	100	2000	2000	2000	100	2000
100	I-B	8760	8760	200	4000	4000	4000	200	4000
100	II-B	11040	11040	200	4000	4000	4000	200	4000
No. of Orbits	Trajectory Type	Reliability Model $P = \exp(-\lambda t)$							
		P_1	P_2	P_3	P_4	P_5	P_6	P_7	P_8
1	I-B	0.822	0.641	0.999	0.998	0.992	0.996	0.996	0.992
1	II-B	0.753	0.516	0.999	0.998	0.992	0.996	0.996	0.992
50	I-B	0.753	0.516	0.995	0.904	0.670	0.818	0.980	0.670
50	II-B	0.691	0.416	0.995	0.904	0.670	0.818	0.980	0.670
100	I-B	0.691	0.416	0.990	0.818	0.449	0.670	0.960	0.449
100	II-B	0.645	0.331	0.990	0.818	0.449	0.670	0.960	0.449

The Earth Occultation Data probability of success was calculated at only the first orbit. Data for this analysis was obtained from IOM 313-1711 "Mariner C Spacecraft Subsystems Reliability Analysis" by P.H. Steinbrook/R.F. Miles, Jr., (8/17/64) and IOM 313-1719 "Reliability Calculation for the Probability of Obtaining Television Data and Occultation Data for the Mariner C Mission" (8/20/64) by the same authors.

2. Restrictive Assumptions

The most restrictive assumption of this analysis is that it is based on random part failures. Part failures are assumed to be catastrophic in nature and degraded operation of parts is not considered. It is assumed that a failed part is completely inoperable and will remain inoperable from time of failure throughout the balance of spacecraft life.

Component failure rates are taken as those shown in PRC-R-433: "Reliability Analysis of the Mariner C Spacecraft" (Planning Research Corporation, 9 December 1963). Not energized components do not degrade during the flight. The data are tenuous and can only be considered as gross estimates.

Spacecraft components failures during the launch period have not been included in this analysis. All spacecraft subsystems are assumed to be operable after injection.

3. Reliability Model

The reliability model is derived by using three basic forms. Components are summed to obtain units, units arranged into subsystems, and finally subsystems combined to form the spacecraft. No redundant component paths assumed in the formation of the unit reliability. The failure rates for all of the components in each unit summed to form unit failure rates. All failures assumed to be random in nature, so the probability that the i^{th} unit remaining operable decreases as:

$$P_i = \exp\{-\lambda_i t\},$$

Where λ_i = The failure rate for the i^{th} unit,

t = Flight-time

The reliability diagrams for the Occultation and TV/MS Missions display all required units as series elements, with redundant units displayed as parallel elements. The spacecraft's probability of success obtained by multiplying together each of the units that appear in series,

$$P = P_a P_b \cdots\cdots ,$$

while redundant units or mission alternates are treated as:

$$P = P_a + P_b - P_a P_b$$

Figure 9-11 represents basically the spacecraft reliability model used to develop the data in Table 9-8 and Table 9-9.

4. Conclusions

Table 9-9 shows the probability of obtaining TV, MS, occultation data for 1 and 2 spacecraft launch opportunities, for Type I-B and Type II-B trajectories at three points in time. Though the calculated results are based upon some gross assumptions it is readily seen the effect time has upon the probability figures for spacecraft success.

Table 9-9. Mars 1969 Spacecraft Probability of Success for TV, MS Occultation Experiments

No. of Orbits	Trajectory Type	Only One Experiment		Only Two Experiments		TV or MS Experiment		Occultation Experiment	
		One S/C	Two S/C	One S/C	Two S/C	One S/C	Two S/C	One S/C	Two S/C
1	I-B	0.514	0.764	0.254	0.444	0.764	0.944	0.822	0.967
1	II-B	0.372	0.606	0.138	0.257	0.606	0.844	0.753	0.939
50	I-B	0.126	0.236	0.016	0.029	0.236	0.417		
50	II-B	0.095	0.181	0.009	0.018	0.181	0.330		
100	I-B	0.030	0.059	0.0009	0.002	0.059	0.115		
100	II-B	0.022	0.043	0.0004	0.001	0.043	0.086		

SECTION X

SPACECRAFT SYSTEM MECHANIZATION DESCRIPTION

A. NOMINAL CONFIGURATIONS

1. Instruments and Subsystems

The nominal Mars orbiter spacecraft is comprised of a set of body fixed science instruments, a set of scanning instruments and the necessary subsystems to support the scientific mission. The spacecraft complement of science instruments and salient subsystems are listed below:

a. Science Instruments

1) Body Fixed Instruments
   a) Micrometeoroid detector
   b) Solar plasma experiment
   c) Energetic particle detector
   d) Magnetometer
   e) RF occultation beacon
   f) Mars RF noise detector
2) Scan Platform Instruments
   a) Mars scanner
   b) TV experiment

b. Principal Spacecraft Subsystems

1) Spacecraft Bus - Octagonal structure which houses electronic subsystems
2) Antenna subsystems having the capability to accommodate Type I and Type II trajectories
3) Power Subsystem - Flay-array solar photovoltaic cells and battery
4) Cold gas/solar vane attitude control subsystem
5) Orbit insertion and midcourse propulsion systems:
   a) Restartable liquid midcourse propulsion system and solid propellant retro engine
   b) Liquid retro propulsion system with integral midcourse capability
6) Thermal control subsystem

2. Basic Configurations

Two basic spacecraft configurations will be discussed. The primary difference between the two configurations is the propulsion systems. One configuration contains a bipropellant liquid propulsion system for all midcourse and the orbit insertion maneuver. The other configuration contains a solid propellant propulsion system for the orbit insertion maneuver and a Mariner 64 type of liquid monopropellant midcourse propulsion system. The other subsystems of the spacecraft are essentially the same for both configurations. The configuration containing the liquid propulsion system will be discussed first and then the differences in the configuration caused by substituting the solid propellant retro and liquid midcourse system will be defined.

Configuration 1 is shown on JPL Drawing J-4300619, Sheet 15 and Configuration 2 is shown on Sheet 16.

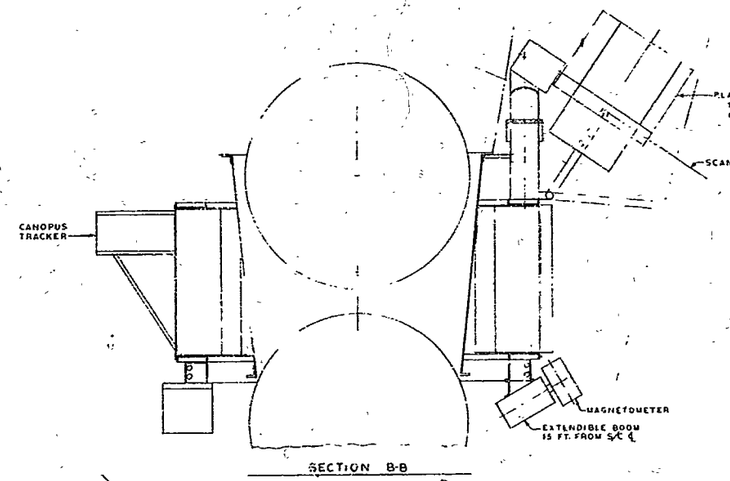
3. Configuration 1 Science Instruments (Figure 10-1)

a. Body-Fixed Instruments

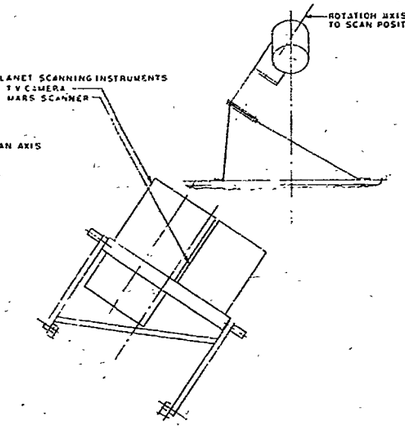
All of the body-fixed science instruments are mounted on the Sun-side of the spacecraft bus in order to satisfy required look angles and positions. Both the magnetometer and the Mars RF noise detector have booms which must extend between the spacecraft solar panels. In order to keep these booms from being within the look angles of the forward spacecraft antennae, the booms are pointed aft (end opposite from the Sun) of the solar panel plane by 30 degrees. Even with this pointing position, the 30-foot boom of the RF noise detector and the 15 foot telescoping boom of the magnetometer cause perturbations to the antenna patterns. Cyclic deployment of these booms may be required to satisfactorily meet the antenna subsystem communication requirements.

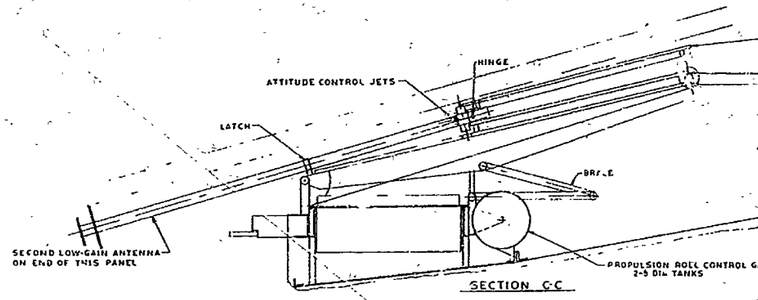
b. Scan Platform Instruments

The Mars Scanner and TV experiments are mounted on a scan platform which attaches to the bottom of the spacecraft on the opposite side from the Canopus sensor. It has 2 degrees of freedom, one degree about the deployment axis and one degree about the scan axis which is nominally perpendicular to the spacecraft orbit plane about Mars. In order to provide adequate structural support, the platform is stowed close to the spacecraft bus. After retro into the Mars orbit, the platform is deployed to position 1 for the first part of the orbital period. Apparent motion of the Sun and Canopus requires that this deployed position be updated to position 2 for the latter part of the orbital period. When the platform is in either of these positions, the scan axis has a capability of nearly 200 degrees of travel. This permits the scan instruments to look at the planet ahead of the morning terminator and past

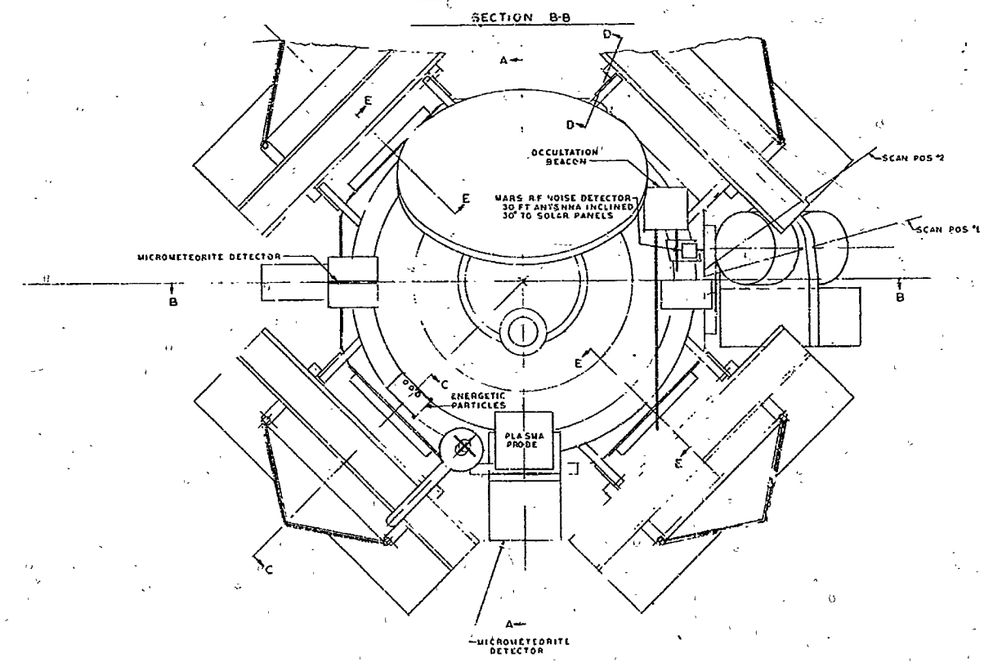


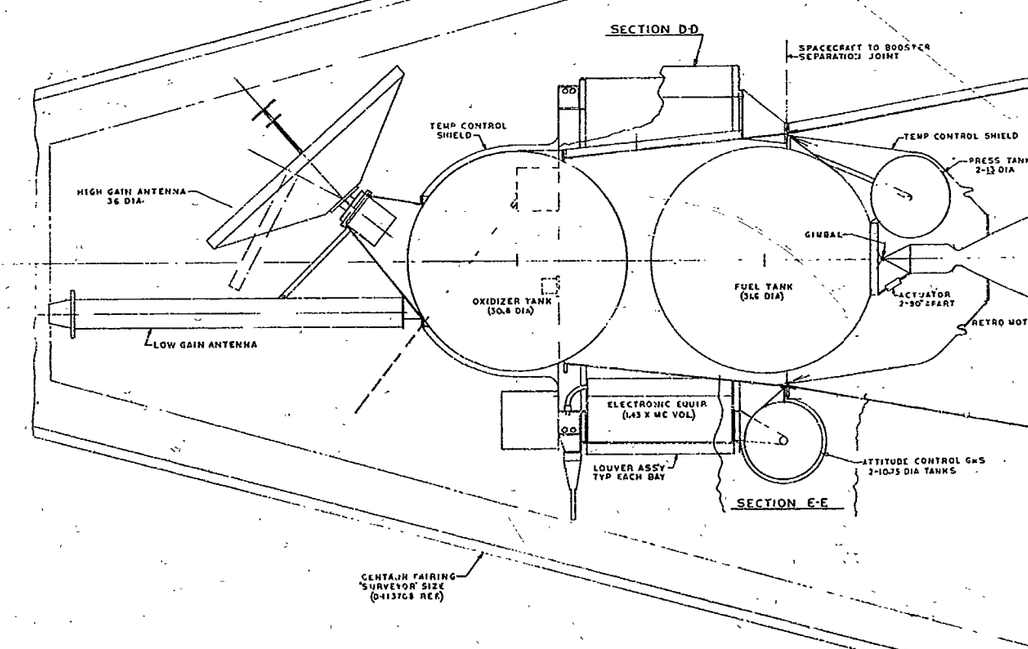
SECTION B-B





SECTION C-C





SECTION A-A

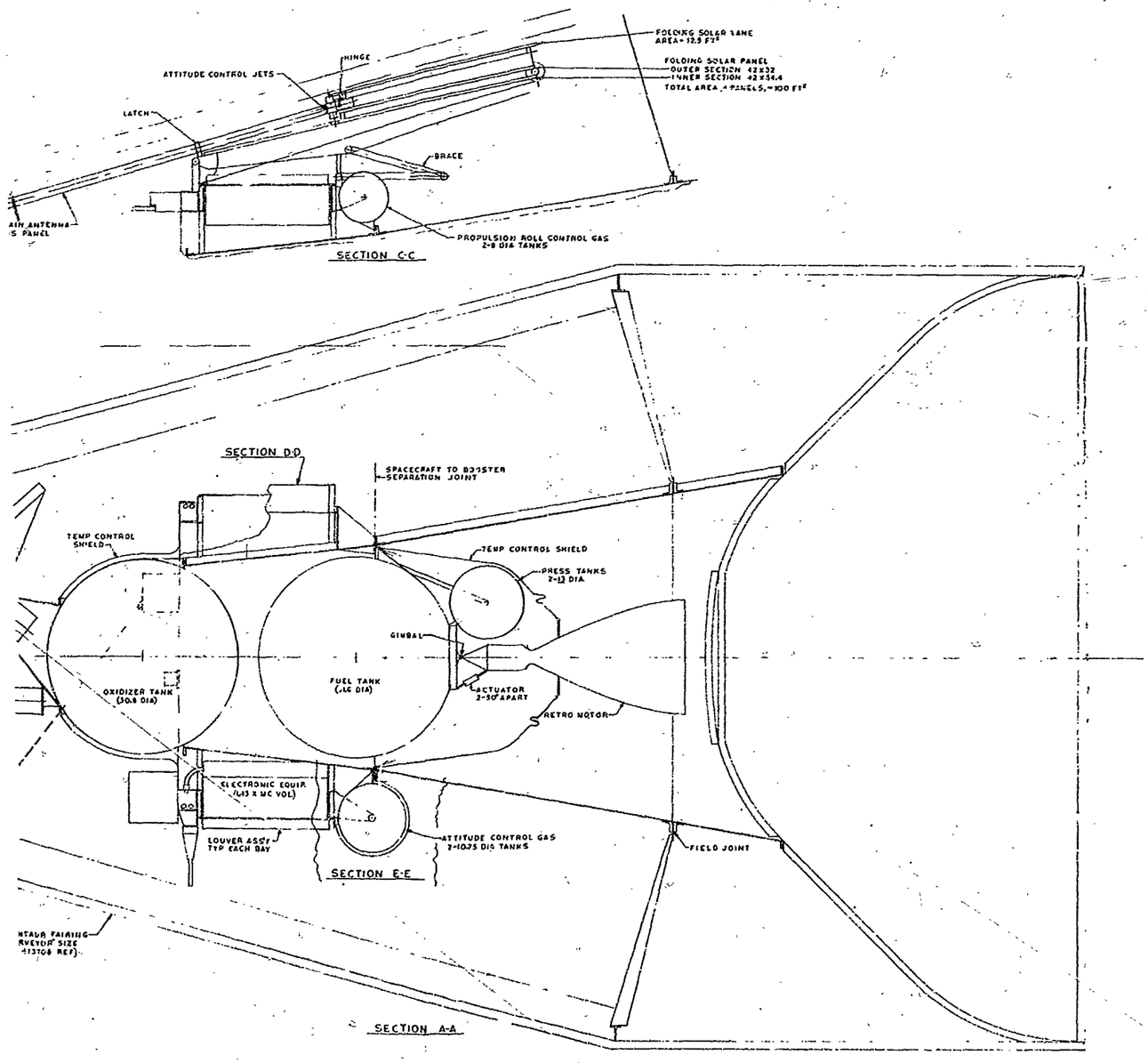


Figure 10-1. Configuration 1 Using a Liquid Retro Propulsion System

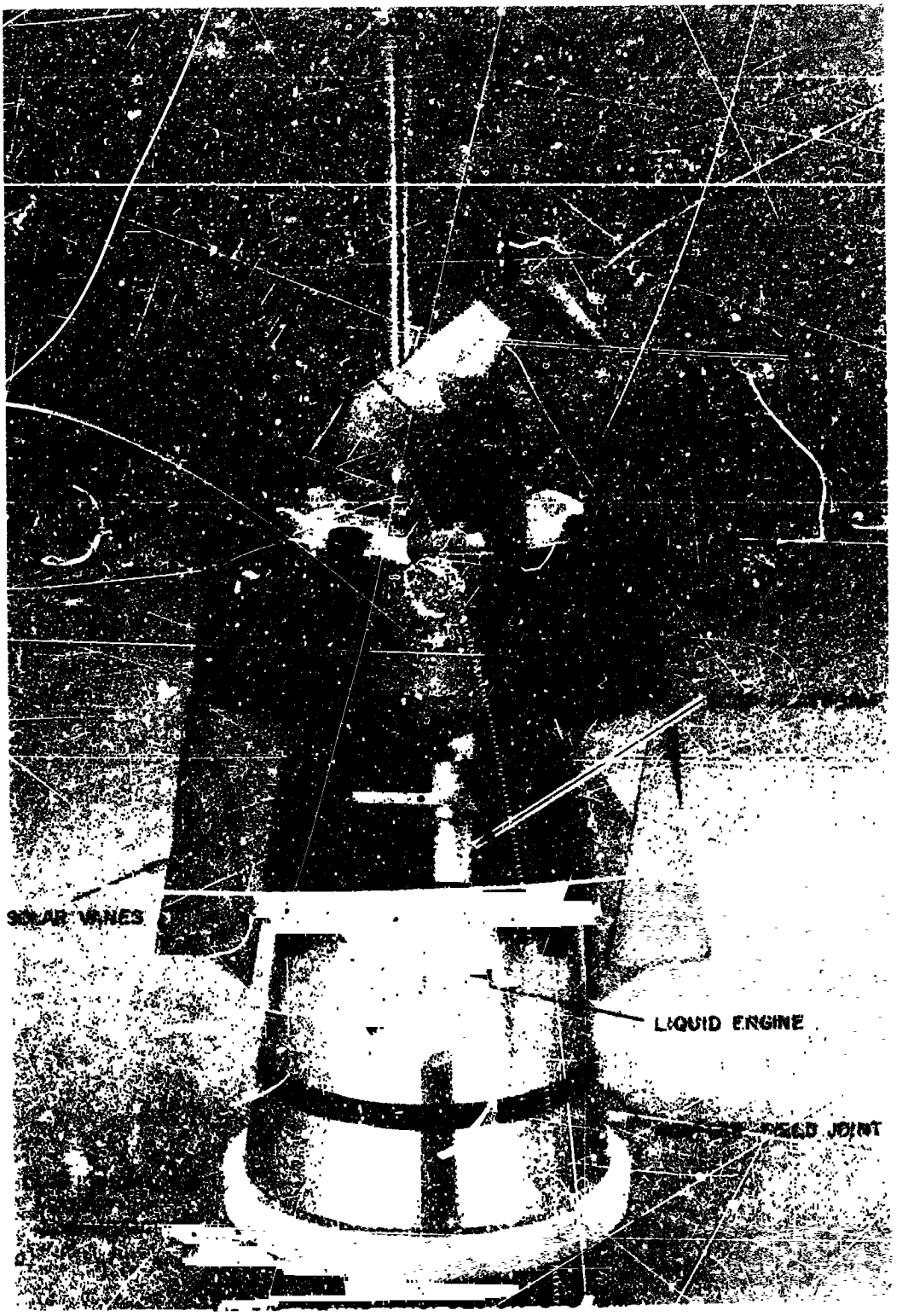


Figure 10-1a. Boost Configuration

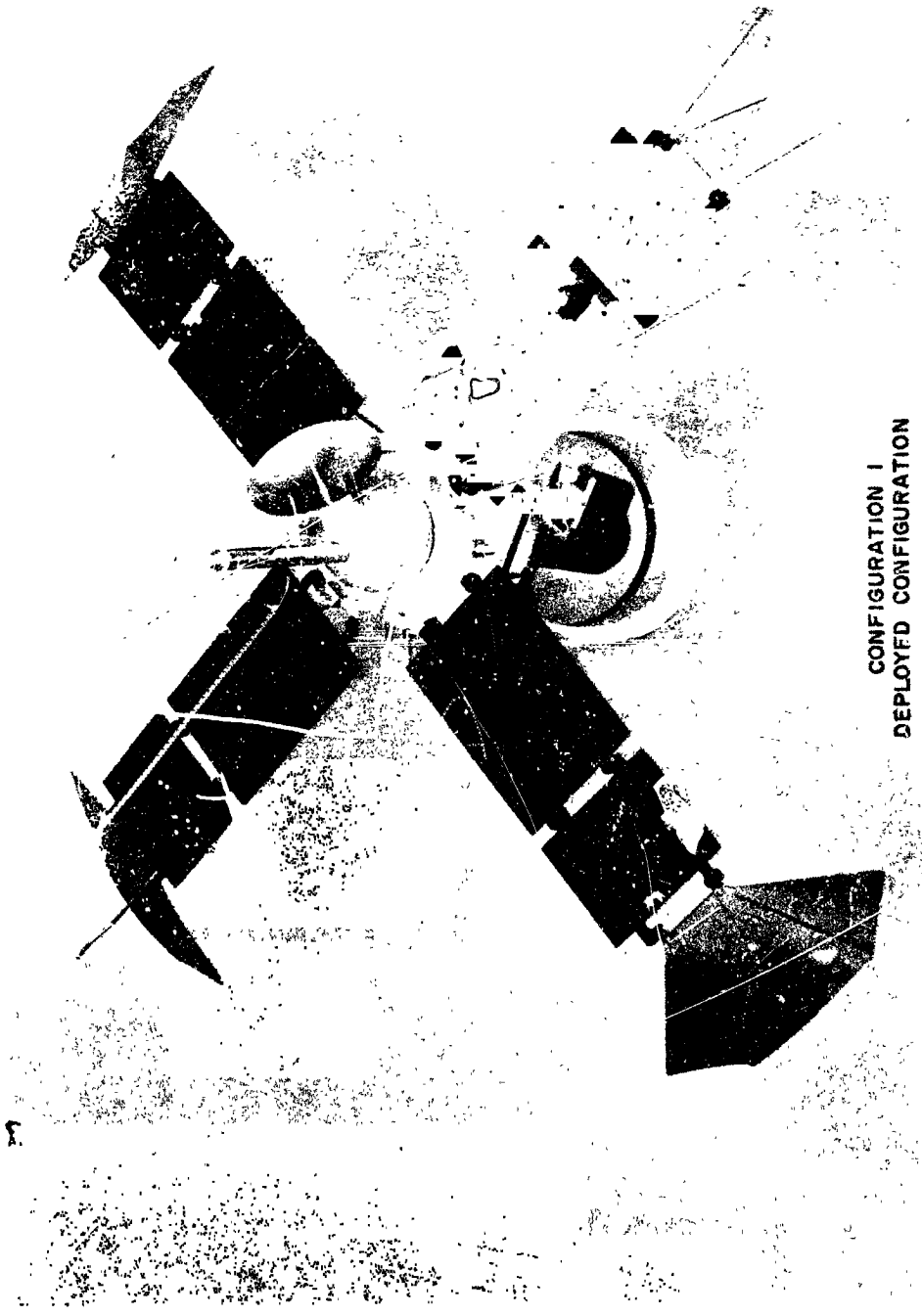


Figure 10-1b. Deployed Configuration

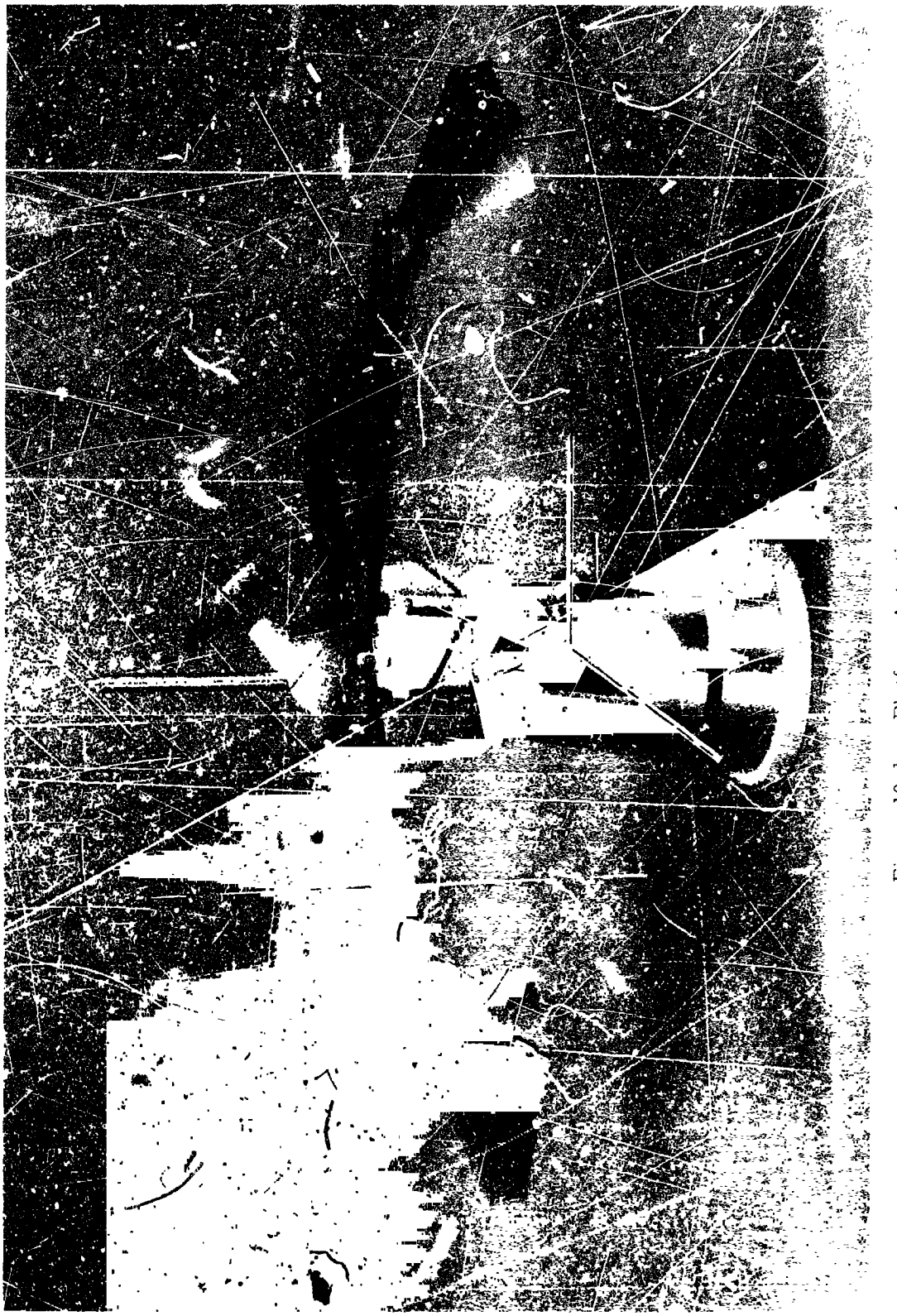


Figure 10-1c Platform Actuation Axes

the evening terminator. The mechanization of the scan axis, however, is such that a given position can be selected for each orbit and by command can be moved to that position and locked there for that orbit.

c. Deployment Positions

The deployment positions 1 and 2 are selected such that the scan axis is nominally normal to the spacecraft orbit plane about Mars throughout the spacecraft's design lifetime. Both Type I-B and Type II-B orbits having 1500 kilometer periapsis and inclinations of 45 degrees and 50 degrees, respectively, were used to select these positions. Position 1 is such that the scan axis has a cone angle of 67 degrees and a clock angle of 195 degrees and position 2 is such that the scan axis has a cone angle of 80 degrees and a clock angle of 215 degrees.

d. Scan Platform Design

The design of the scan platform must integrate the design of the instruments themselves with the structural design of the platform and its support in order to keep the vibration environment of the instruments within acceptable limits. The instruments will probably present the most challenging structural design and thermal design problems of any component on the spacecraft.

4. Spacecraft Bus

The spacecraft bus is conceptually similar to that of the Mariner 64. It is an octagonal structure having the same diametral dimensions as the Mariner 64 but the depth is increased to obtain 1.43 times the Mariner 64 packaging volume. The structure is wrapped around the two propellant tanks of the spacecraft to aid in the thermal control of the spacecraft. The bus support structure attaches to the lower tank and to the forward end of the spacecraft adapter. The inflight separation joint is located at the base of the support structure. As is typical, the spacecraft bus serves as the mounting structure for both the science packages and for the gas bottles used in the attitude control subsystem.

a. Antenna Subsystem

The antenna subsystem consists of two low-gain antennae which will cover both Type I and Type II trajectories during the interplanetary transfer portion of the mission and a high-gain antenna which is used near encounter and during the Mars orbital period after encounter.

(1) Forward Low-Gain Antenna. This antenna is similar to the Mariner 64 low-gain and is used for telemetry during early portions of the flight for Type I trajectories

and also for getting commands into the spacecraft. A requirement for roll symmetry is nearly achieved by locating this antenna just off the roll axis of the spacecraft A 120 degree look angle from the roll axis is achieved, although reflections from the spacecraft structure and science booms present problems. It appears feasible to increase the shroud envelope height by at least one foot; thus it is possible to achieve a slightly larger look angle with this antenna if needed.

(2) Side Low-Gain Antenna. A side looking low gain antenna of the circularly polarized type is required for early Type II trajectory coverage and to cover early midcourse maneuvers. For Type II trajectories which have been considered in this study, the spacecraft passes through perihelion early in the flight. In this case, the spacecraft lies between the Earth and the Sun; thus antenna coverage is required on the aft side of the spacecraft. This antenna is mounted on the solar panel which is located at 45 degree clock angle from the Canopus sensor. To achieve a 120 degree look angle from the antenna peak gain direction it must be mounted on a boom out beyond the solar vane which is attached to the panel tip. Because of shroud constraints this boom must be hinged at the panel tip and latched to the panel support structure.

(3) High-Gain Antenna. The high-gain antenna is a 3-foot circular reflector and operates at S-band. It has a single axis of rotation by updating the actuator position it follows the Earth track at the end of the heliocentric transfer orbit and for an orbiting period greater than 90 days. The actuator axis is oriented at 38 1/2 degrees cone angle and 270 degree clock angle and the antenna RF axis is braced 9 degrees to the actuator axis. Thus the RF axis describes a 9 degree half angle cone as the actuator is rotated 360 degrees. The launch position pointing of the antenna is 45 degrees cone and 270 degrees clock (spacecraft coordinates) which will assure communications at Mars encounter should an actuator failure occur during the cruise phase of the mission.

b. Solar Panels

The configuration drawings show solar panels 42 inches wide by 85 inches long, giving 100 square feet of cell area. The required area is 97 square feet if a 10 watt transmitter is used and 106 square feet if a 20 watt transmitter is used.

The solar panels are hinged on the forward end of the bus structure and are packaged downward in the shroud envelope. A chordal fold is required in order to achieve the required panel area. These panels may be erected either by using a single actuator with the outer panel slaved to the inner or by utilizing two actuators, one at each hinge. The panels will remain erected during the retro maneuver; therefore an outrigger support is required at approximately the quarter point on the panels, so the panels will sustain the g loading caused by retro with minimum weight penalty. Point dampers will be used at the support point for both the launch configuration and for the retro configuration.

c. Attitude Control Subsystem

Canopus/Sun references are used for this subsystem. The Canopus tracker is mounted on the spacecraft bus between two solar panels thus achieving the required look angles for the sensor. Sun sensors locations have not been defined.

Redundant nitrogen gas systems are used for attitude control. These systems consist of two eleven and a half-inch diameter gas bottles with jets mounted on the ends of the panels. The plumbing must cross two solar panel joints.

Solar vanes approximately 13 square feet in area are mounted on the tip of each panel and are used for center of pressure trim and also for active attitude control. These vanes interact with the antenna system and further study of this interface is required.

d. Liquid Propulsion System (Hydrazine-N_2O_4)

The two propellant tanks in the liquid propulsion system are approximately 31 inches in diameter. The tanks, together with the thrust chamber, are on the spacecraft roll axis in a tandem arrangement. Expulsion of the propellant is accomplished by using bladders and pressurized helium gas. A single 600 pound thrust engine having an 80:1 area ratio is used. The engine is gimbaled from the bottom tank and pitch and yaw thrust vector control is achieved by two electromechanical actuators. Roll control is provided by a cold gas system with jets mounted on the tips of the solar panels.

Midcourse corrections will be made by firing the main engine. In order to accomplish very small ΔV midcourse corrections, it is possible that a cold gas system will have to be added.

Alignment of the thrust vector through the experimentally determined center of gravity can be achieved by moving the engine gimbal attach-point on the closure to the lower tank.

This configuration permits the assembly of the propulsion system separate from the spacecraft but does require that they be mated quite early in the final assembly program. The configuration is also not overly sensitive to small changes in the propellant tank diameters.

e. Thermal Control

Thermal control of the spacecraft is accomplished by using both passive and active devices. The propulsion system is cocooned by a thermal insulation shield both forward and aft. This will permit the use of the propellant tanks as a sink or source of heat for the spacecraft when required. Since the thrust chamber will be looking at black space, a heater is

required in the injector to insure that the propellant does not freeze during engine startup. Each of the spacecraft electronic packaging bays will have louvers for active thermal control with a possibility of some louvers being placed on the Sun side of the spacecraft to allow heat to come into the spacecraft as needed. The scan platform which is mounted on the side of the spacecraft is exposed to direct sunlight except for some shadowing caused by the solar panels. It is expected that some heater capability will be required on the scan platform science experiments.

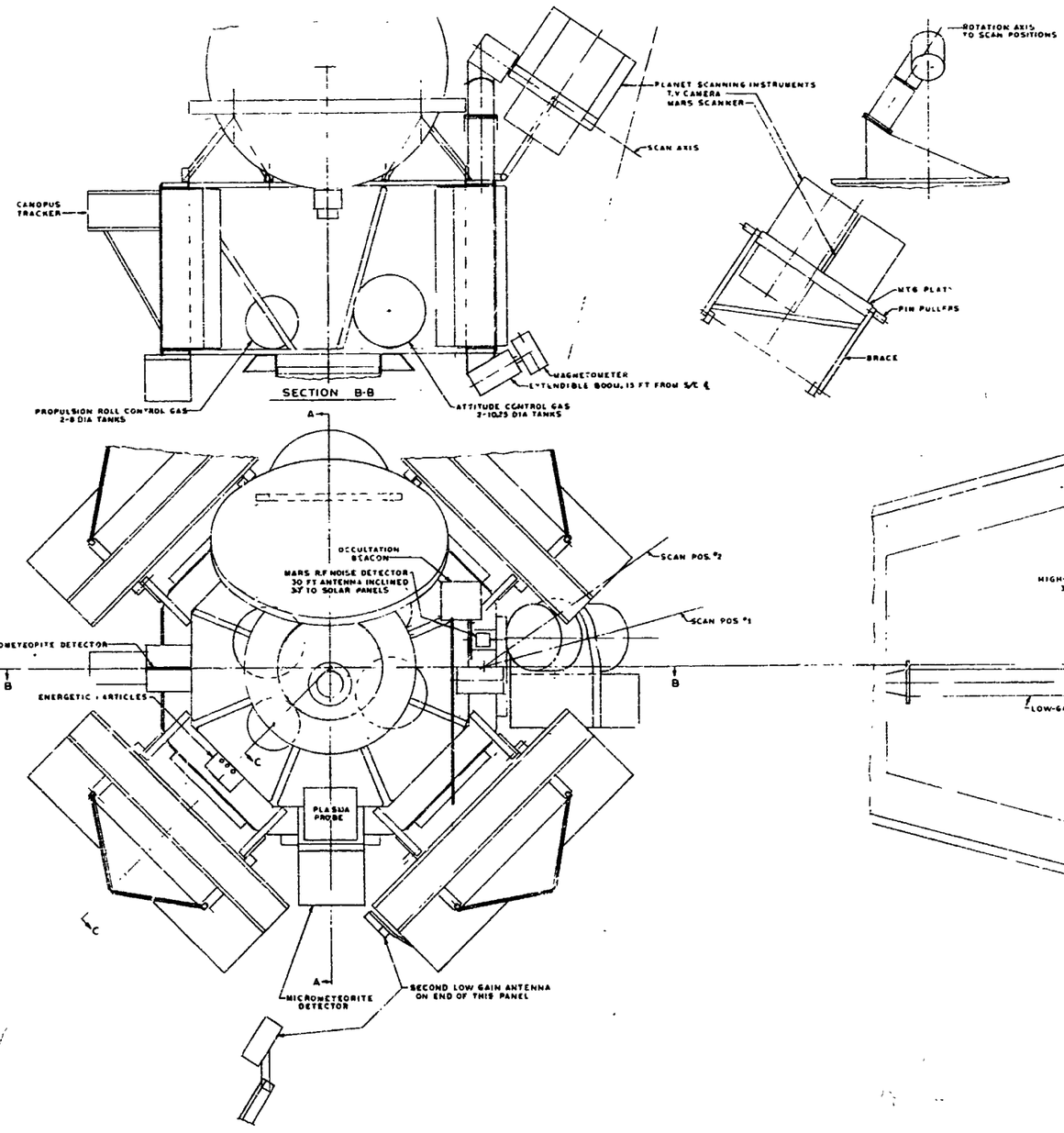
5. Configuration 2 - Solid Rocket Propulsion System (Figure 10-2)

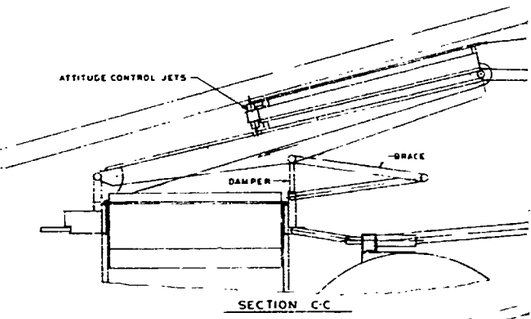
Changing the spacecraft propulsion system from a liquid to a solid system results in very little change to any of the other spacecraft subsystems. Because the midcourse propulsion unit is separate from the retro unit, the depth of the spacecraft bus must be increased to maintain the total packaging volume of 1.43 times that of the Mariner 64. In addition there is a change in the second low gain antenna location because the midcourse propulsion unit will fire normal to the roll axis. The solar panels and the science orientation remain unchanged from that of Configuration 1.

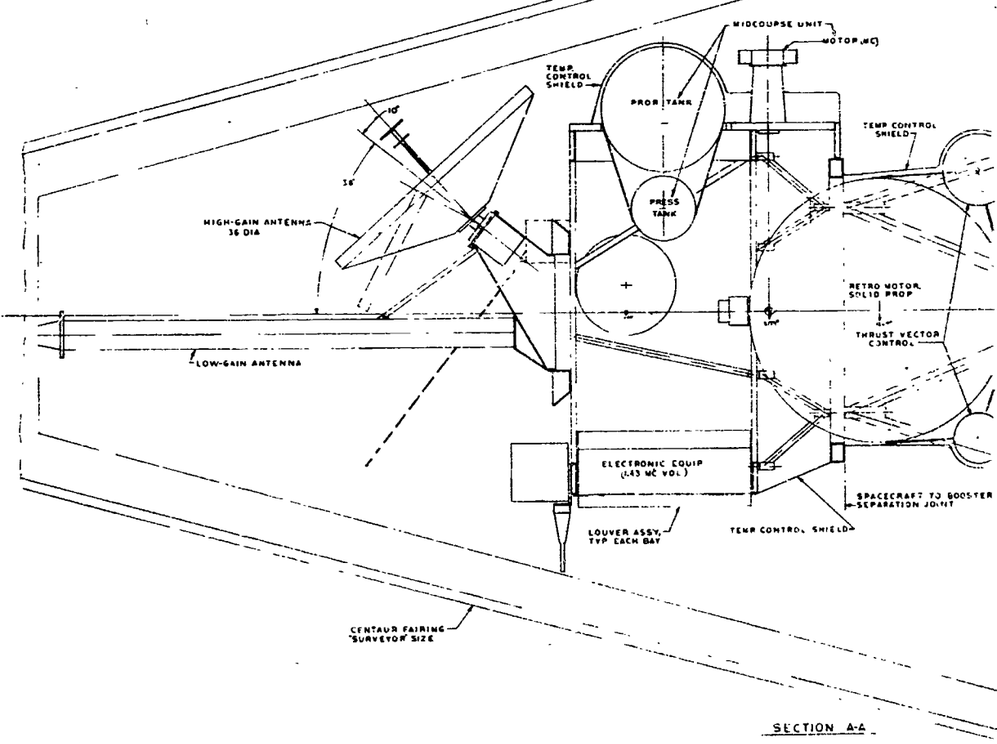
The midcourse propulsion unit is similar to that of Mariner 64 except that it is scaled up to a ΔV capability of 100 meters/second. It mounts in one bay of the spacecraft bus. Since the midcourse propulsion unit has served its function prior to the retro maneuver, it is desirable to jettison the unit before firing the solid rocket. The mechanism for ejecting the unit has not been defined.

The solid retro rocket is a Surveyor type motor and is mounted on the roll axis of the spacecraft. Thrust vector control is achieved by injecting Freon into the nozzle of the rocket. Roll control during retro is obtained by cold gas jets in the same manner as for the liquid retro system. Aligning the thrust vector so it will pass through the experimentally measured c.g. will be more difficult for the solid motor because the entire motor case will have to be moved relative to its support brackets rather than moving just the thrust chamber as is possible in the liquid configuration.

Some changes in the thermal control subsystem are required for this configuration. The spacecraft bus will be isolated by a thermal control blanket from the chamber of the solid rocket. A heater will be required to keep the solid rocket warm in addition to the thermal control blanket around the exterior of the motor case. If the midcourse unit is jettisoned prior to retro, an insulation blanket to cover the resulting hole in the spacecraft bay is required. In addition a heater will be required in the propellant tank as well as on the midcourse motor.


CANOPUS TRACKER
PLANET SCANNING INSTRUMENTS
T.V CAMERA
MARS SCANNER
SCAN AXIS
ROTATION AXIS TO SCAN POSITIONS
MTG PLATE
PIN PULLERS
BRACE
MAGNETOMETER EXTENDIBLE BOOM, 13 FT FROM S/C ℄
PROPULSION ROLL CONTROL GAS 2-8 DIA TANKS
ATTITUDE CONTROL GAS 2-10.25 DIA TANKS
SECTION B-B
OCCULTATION BEACON
MARS R.F NOISE DETECTOR 30 FT ANTENNA INCLINED 37 TO SOLAR PANELS
SCAN POS. #2
SCAN POS #1
MICROMETEOPITE DETECTOR
ENERGETIC PARTICLES
PLASMA PROBE
MICROMETEORITE DETECTOR
SECOND LOW GAIN ANTENNA ON END OF THIS PANEL


ATTITUDE CONTROL JETS
BRACE
DAMPER
SECTION C-C


MIDCOURSE UNIT
MOTOR (MC)
TEMP CONTROL SHIELD
PROP TANK
PRESS TANK
HIGH-GAIN ANTENNA 36 DIA
LOW-GAIN ANTENNA
RETRO MOTOR SOLID PROP
THRUST VECTOR CONTROL
ELECTRONIC EQUIP (143 WC VOL)
SPACECRAFT TO BOOSTER SEPARATION JOINT
LOUVER ASSY, TYP EACH BAY
CENTAUR FAIRING SURVEYOR SIZE
SECTION A-A

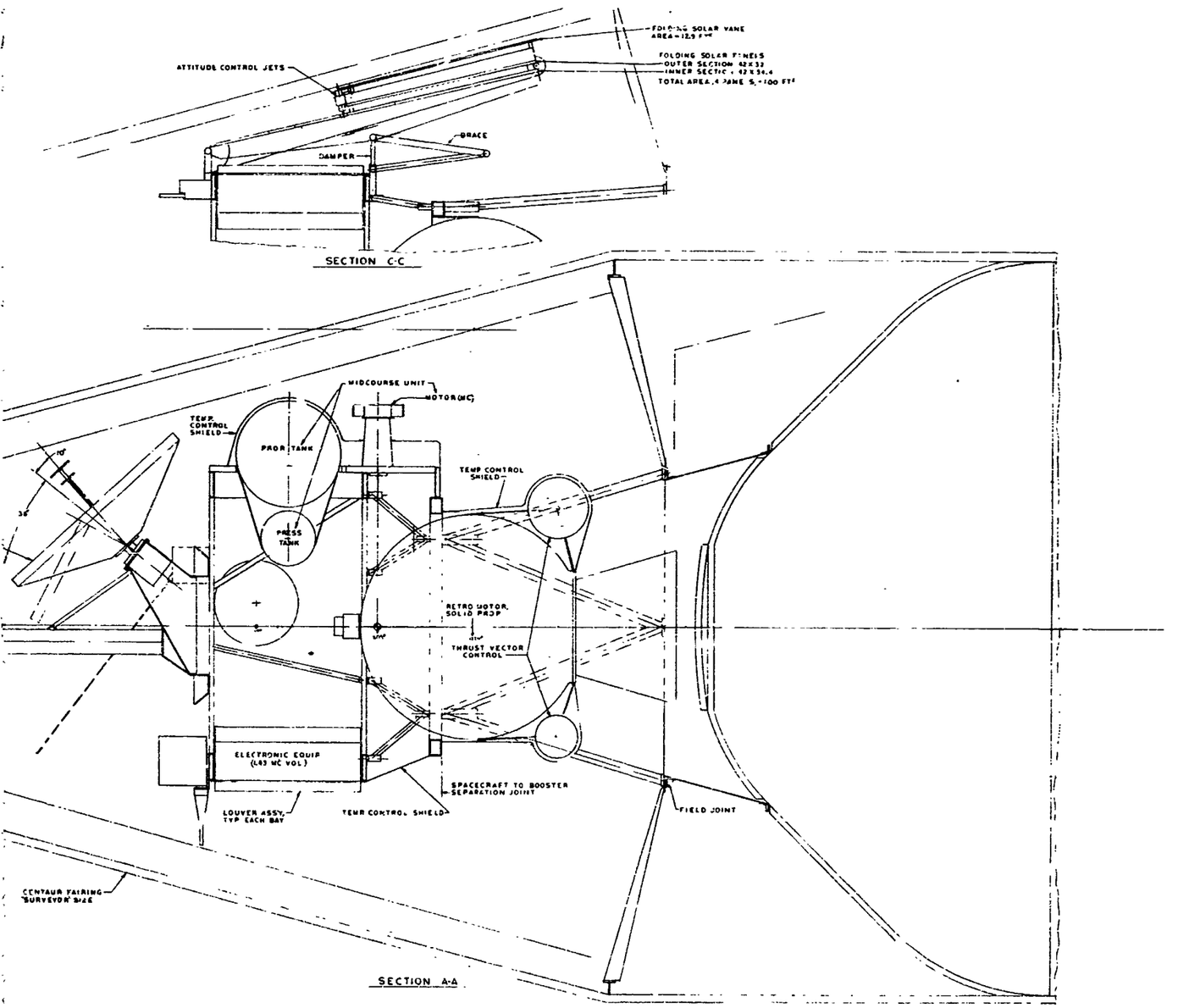


Figure 10-2. Configuration 2 Using a Solid Propulsion Retro System



Figure 10-2a. Boost Configuration



Figure 10-2b. Deployed Configuration

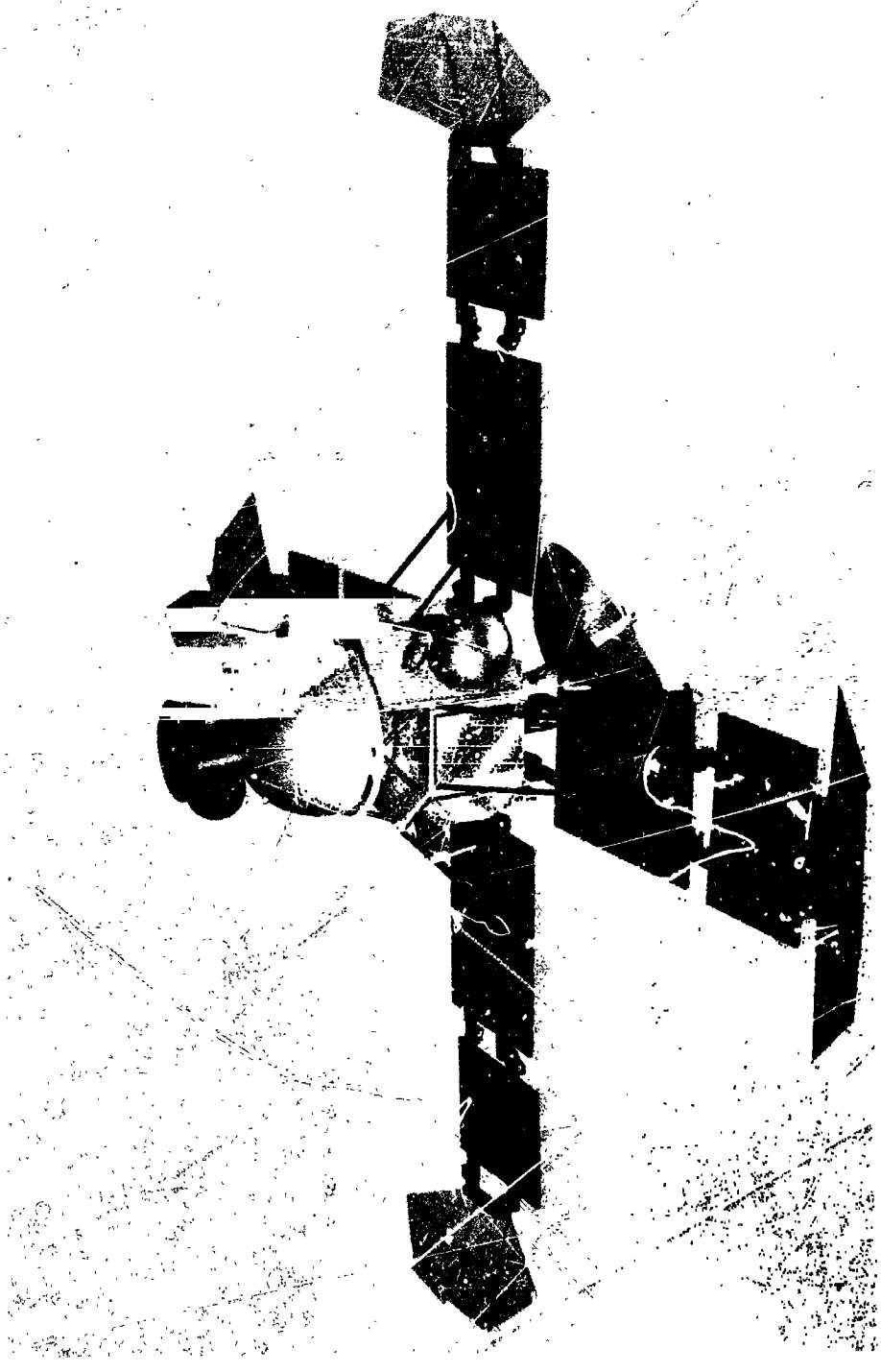


Figure 10-2c. Planet Oriented View

B. WEIGHT SUMMARY

1. Spacecraft Summary

An equipment list is given and a weight summary is indicated for that equipment list. Table 10-1 gives a breakdown of the spacecraft, and Tables 10-2 and 10-3 give the breakdowns for the nominal case propulsion system, liquid bipropellant and solid, respectively. A weight summary is given for three Mariner Mars 1969 Orbiter spacecraft described in Section XI. B, and for the Mariner 64 spacecraft. Section XI provides more detail information concerning subsystem weights and their estimates. The weight of the nominal case spacecraft was estimated by the responsible division. A contingency of 15 percent was added to the total orbiter weight. This increase in the spacecraft weight is to allow for estimate errors of units requiring development and allowance for requirements or constraints that do not become apparent until design work has begun.

2. Cases

The weights for the minimum and maximum cases were usually made by scaling capability from the nominal and sometimes considering the Mariner 64 estimates, especially for the minimum case, (see Table 10-1). The minimum case telecommunications capability is equivalent to Mariner 64.

3. Weight Estimation

The retro propellant loading estimates allow no contingency, (see Tables 10-2 and 10-3). Even though the estimates given are considered accurate within a few percent, unforseen development problems with a motor could possibly require more propellant, or some unexpected inflight difficulties could be solved if more propellant were on board. (See Section XI. G for greater detail.) The propulsion weight estimates are for two periapsis altitudes, 1500 km and 4000 km. Two propulsion systems are considered, the solid and the liquid bipropellant system. The propulsion estimates are for the 995 pound nominal spacecraft. [The 1500 km periapsis orbit velocity increment of 6270 ft/sec (1.91 km/sec), and 7240 ft/sec (2.21 km/sec).] These velocity increments correspond to a Mars approach velocity of 4.2 km/sec and are consistent with incremental variable loading as indicated in Table 11-3.

4. Additional Weight Entries

The equipment list is abbreviated and requires the following explanation. The equipment case structure is the octagonal electronics case. The miscellaneous structure weight includes equipment such as dampers, fasteners, etc. The magnetometer weight estimate

Table 10-1. Mariner Mars 1969 Orbiter Weight in Pounds

Schedule of Events	Minimum		Nominal		Maximum		Mariner 1964	
	Unit	Subsystem	Unit	Subsystem	Unit	Subsystem	Unit	Subsystem
Structure		85		123		135		86.1
Equipment Case Structure	52.0		75.0		87.0		59.8	
Misc. (Dampers, fasteners, etc)	13.0		13.0		13.0		13.2	
Thermal Control	20.0		35.0		35.0		13.1	
Science		None		143		221		71.1
Infrared Interferometer	--				26.0			
UV Spectrometer	--				24.0		24.5	
TV Camera	--		23.0		23.0			
Mars Scanner (IR)	--		13.0		13.0			
Magnetometer	--		14.5		14.0			
Plasma Probe	--		10.0		10.0		21.5	
Energetic Particles	--		2.5		2.5			
Meteoroid Micrometer Detector	--		5.0		5.0			
Two-Frequency Occultation	--		5.5		5.5			
Mars Radio Noise	--		6.5		6.5			
DAS	--		28.0		37.0		11.8	
Platform + Actuator	--		26.2		41.5		10.5	
Science Case & Harness + Mounting Hardware	--		9.0		13.0		2.8	
Telecommunications		101		165		210		100.5
Radio	48.7		65.6		72.5		34.9	
Antenna + Support Structure	15.8		23.6		26.6		9.2	
Data Encoder	25.0		32.6		34.8		26.3	
Command	12.0		24.5		24.7		11.7	
Tape Recorder + Electronics	0		11.6		37.8		18.4	
Actuators +	0		7.0		14.0			

Table 10-1. (cont)

Schedule	Minimum		Nominal		Maximum		Mariner 1964	
	Unit	Subsystem	Unit	Subsystem	Unit	Subsystem	Unit	Subsystem
Power		179		294		384		157.2
Solar Panels (0.7 g's)	85.0		126.0		138.0		74.8	
Conversion Electronics	36.0		55.0		58.0		34.6	
Battery	40.0		78.0		50.0		33.4	
Deployment, support and shock absorbers for panels	18.0		35.4		38.0		14.4	
Guidance and Control		78		104		133		71.2
Cold Gas System and Actuators	22.0		42.0		63.0		26.1	
Solar Vanes, Actuators + Electronics	4.0		6.5		9.7		3.7	
Celestial Sensors	6.4		6.4		6.4		6.3	
Gyros + Electronics System	11.0		11.0		11.0		11.5	
Control System Electronics	6.7		8.7		13.0		10.2	
Midcourse autopilot and control system roll control, insertion autopilot	14.0		15.0		16.0			
CC&S	14.0		14.0		14.0		13.4	
Pyrotechnics		13		16		17		13.0
Cabling (ring harness)		10		20		26		19.8
GRAND TOTAL		466.		865		1126		518.9
Contingency		70		130		169		10.0
Spacecraft (wt less propulsion)		536		995		1295		528.9
Mariner 1964 Propulsion								51.3
Mariner 1964 Spacecraft Weight								580.2

Table 10-2. Weight Breakdown of Nominal Case Using a Bipropellant Liquid Propulsion System for Mariner 1969 Mars Orbiter

Orbit Characteristics	1500 km x 50,000 km	4000 km x 50,000 km
Velocity Increments (ft/sec)		
Retro into Orbit	6270	7240
Midcourse Corrections and gt Losses	330	330
TOTAL	6600	7570
Active Orbiter Weight (lb)	995	995
Propellant Weight (lb)	1085	1380
Propulsion System Weight (lb)		
Residual Propellant	11	14
Pressurant and Tank	49	63
Oxidizer Tank	20	25
Fuel Tank	21	25
Bladders	6	8
Engine	23	29
Components and Plumbing	23	23
Structure	15	19
Gimbal Actuator	10	10
TOTAL	177	216
Design Margin (15%)	26	32
Total Propulsion System Weight (lb)	203	248
Separated Spacecraft Weight (lb)	2283	2323

includes 10 pounds for a boom. The solar panel weight estimates are for 65 square feet for the minimum case, 100 square feet for the nominal case, and 106 square feet for the maximum case. Refer to the detail coverage in Section XI for further information concerning the subsystems.

Table 10-3. Weight Breakdown of Nominal Case Using a Solid Propellant Retro Propulsion System for Mariner 1969 Mars Orbiter

Orbit Characteristics	1500 km x 50,000 km	1000 km x 50,000 km
Velocity Increments (ft/sec)		
Retro into Orbit	6270	7240
Gravity Loss (negligible)	0	0
Total for Retro Motor	6270	7240
Midcourse Correction (Supplied by Separate Monopropellant System)	330	330
Active Orbiter Weight (lb)	995	995
Midcourse System Weight (lb)	155	171
Retro Propellant (I_{sp} = 310) Weight (lb)	1030	1303
Propulsion Hardware Weight (lb)		
Inert Components	118	147
TVC System	47	60
TOTAL	165	207
Design Margin (15%)	25	32
Total Dry Propulsion System Weight (lb)	190	239
Separated Spacecraft Weight (lb)	2370	2713

C. POWER REQUIREMENTS

The total power required by the spacecraft for each phase of the mission is listed in Figure 10-1. Power values are presented in bar chart form with the total unregulated power expressed in watts. The chart is in a general chronological order. More detail is presented in the Electrical Power Subsection of XI. C. The Mission Profile Sequence is explained in Subsection IX. C.

Periapsis refers to the orbit science instrument sample time when all of the science instruments and the platform are "on". Apoapsis refers to the playback and data transmission interval, at which time planet instruments are "off".

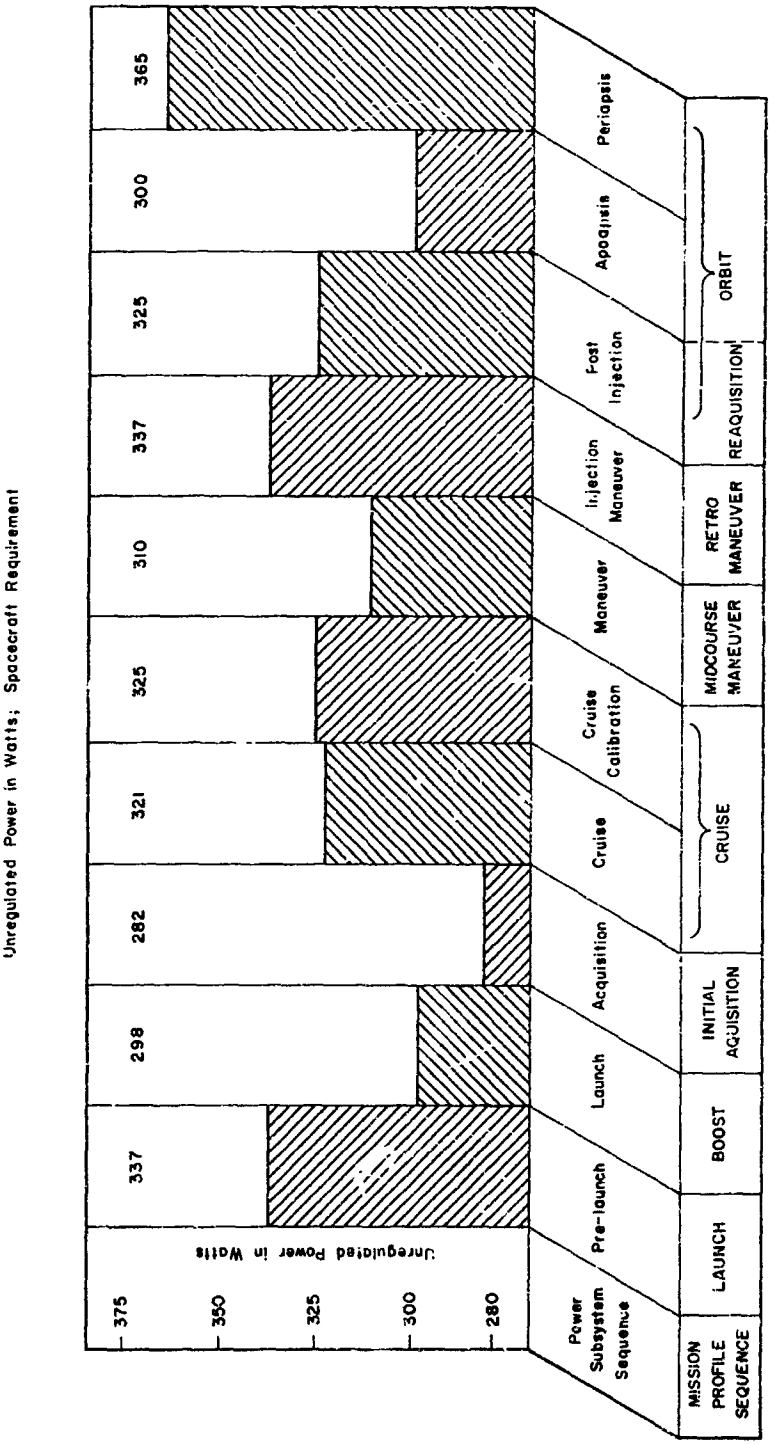


Figure 10-3. Power Profile Nominal Case

D. TEMPERATURE CONTROL

The temperature control subsystem weight breakdown and power requirements are given in Table 10-4.

1. Spacecraft Bus Thermal Considerations

Bus--Mariner 64 technology will be utilized for the Mars 1969 orbiter and the basic approach will be very similar. This approach will be to thermally integrate all parts of the bus into one thermal mass and to isolate from the Sun. The electronics subassemblies will be wrapped around an internal cavity which houses the attitude control gas tanks. Certain areas will be closed with thermal shields and louvers will be used on the external faces of the electronics. These external surfaces form the primary radiators. The influence of the solar panels on louvers capability will be minimized to the greatest extent. All solar panel, antenna, or strut attachments will have insulating inserts to minimize the heat gained or lost by the bus to these external components.

The two propulsion system concepts require essentially different approaches. The all-liquid system will have the tanks located as much as possible within the bus proper. Thermal shields enclosing the bus will completely cover the tanks and roughly one-half of the motor chamber. The motor chamber is located in a position where it does not receive any direct sunlight and is connected to the spacecraft structure by a poor thermal connection, the gimbal joint. The nozzle cannot be plugged with a thermal shield during the entire cruise portion of the mission because the engine will also be used for the midcourse corrections. Due to the large radiating area of the nozzle, the heat loss from the nozzle is larger than the capability of the gimbal structure to supply and yet maintain the injector at an acceptable temperature. Thus, it will be necessary to provide an electric heater of approximately 10 watts on the injector to prevent freezing of the fuel prior to ignition.

The solid retro system will be mechanized by isolating the chamber from the electronics in order to avoid the heat pulse caused by retro firing. The exterior of the motor including the nozzle opening will be insulated during cruise. The nozzle cover will be blown out on motor ignition. An electric (approximately 10 watts) heater will be necessary to maintain the required grain temperature. The liquid midcourse propulsion system, necessary when a solid retro motor is used, will be integrated in the manner of Mariner 64 unless it must be jettisoned. In the case of midcourse propulsion system jettison, additional heaters will be required on the main octagon.

Maneuvers present special problems. Non-Sun oriented periods must be kept to times less than one hour near Earth. At Mars the requirements on non-Sun orientation can be relaxed, and as much as a six-hour period off the Sun at Mars appears to provide no major

Table 10-4. Temperature Control Subsystem Weight Breakdown and Power Requirements

Item	Subsystem	Weight (lbs)
1.	Bus	
	a. Louvers (eight bays)	12.0
	b. Upper Thermal Shield	6.0
	c. Lower Thermal Shield	6.0
	d. Lateral Shields on Bus	5.0
	e. Miscellaneous Insulators	2.0
		31.0
2.	Planet Scan Platform	
	a. Thermal Shield	4.0
		4.0
3.	Contingency	3.0
		3.0
	TOTAL	38.0

Item	Subsystem	Power Watts
1.	Retro Motor (Throughout flight until after retro firing)	
	a. Large Liquid System	10.0
	b. Solid Retro and Liquid M/C	15.0
2.	Planet Scan Platform (Part of cruise and in-orbit)	8.0

thermal problem. Because of the isolation from the Sun there should be no problem associated with solar eclipses.

2. Planet Science Platform Thermal Considerations

The attempt will be made to thermally integrate the package as a unit, separate from the bus. It appears that the major problem is the 100 to 150°F temperature drop during Earth to Mars transit. The in-orbit temperature fluctuations seem to be relatively small (on the order of 20°F). The approach will be to keep the package in the Sun as much as possible during all phases of flight. Active control (heaters or louvers) will probably be required to reduce the temperature drop during transit. The orbits considered are positioned such that at any time at least one face of the platform will not be exposed to solar radiation. This side will be utilized as a cold-plate radiator for the IR instruments. Close cooperation between the experimenter, the packaging engineer, and temperature control engineer will be required.

3. Component Thermal Considerations

External actuators, science, etc. are considered as components. For these types of components, the operating temperature ranges must be large enough to accommodate the 100 to 150°F temperature drop between Earth and Mars. These temperature extremes appear to be within the state-of-the-art as evidenced by Mariner 64.

SECTION XI

SUBSYSTEM FUNCTIONAL DESCRIPTION, INTERFACE REQUIREMENTS AND POSSIBLE MECHANIZATION

A. ATTITUDE CONTROL

The Attitude Control Subsystem is required to achieve and maintain the desired orientation of the spacecraft for the purposes of solar power conversion, antenna pointing, and temperature control. In addition, it is required to perform the midcourse and retro maneuvers necessary to effect trajectory corrections and to accomplish a planetary orbit.

1. Cruise Attitude Control

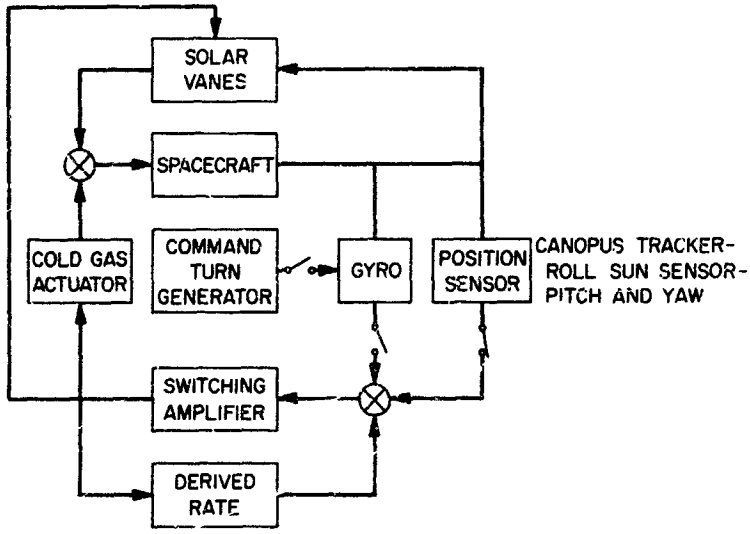
The basic Attitude Control System is shown in Figure 11-1 and consists of Sun sensors, a Canopus tracker, nonlinear controllers, and a cold gas actuation system. The gas system consists of two independent gas supplies and two sets of jets. Orientation of the spacecraft is achieved by using the Sun and the star Canopus as references for the pitch-yaw and roll axes, respectively. During the cruise or transit phase, control is accomplished by using position error signals from the Sun sensors and the Canopus tracker as a measure of the deviation of the spacecraft from the desired references. These signals are processed by the nonlinear Switching Amplifier which establishes a position limit cycle by pulsed operation of the cold gas actuation system. Damping is introduced into the system by means of derived rate feedback.

After the basic control system has established position control, the solar vane control system is used to maintain the spacecraft within the deadband of the cold gas primary Attitude Control System. This objective is accomplished by attaching solar vanes which have a threefold purpose:

1) To make the spacecraft system statically stable
2) To align the stable position of the spacecraft with the null of the primary Attitude Control System
3) To supply retarding forces to damp out any oscillations that may occur.

The spacecraft system is made statically stable by locating the point of application of the resultant solar pressure force so that the center of mass of the spacecraft lies between the Sun and it. This is accomplished by erecting the solar vanes at some nominal angle to the solar panels which are normal to the Sun's rays.

The spacecraft will not be perfectly symmetrical and an adaptive mode of operation will be used to balance it. Unbalanced solar torques acting on the spacecraft during the cruise mode will cause the limit cycle to be biased toward one side of the deadband resulting in a one sided output of the switching amplifier. The amplifier output is used to actuate a stepping motor which in turn drives the solar vanes with respect to the solar panels. This effectively enables the vanes to offset the effect of the solar torque unbalance.



NOTE:

1. BOLD LINES INDICATE BASIC CRUISE SYSTEM
2. GYRO IS SWITCHED INTO CONTROL LOOP DURING ACQUISITION AND AND COMMAND TURNS
3. POSITION SENSORS ARE SWITCHED OUT DURING COMMAND TURNS

Figure 11-1. Basic Roll or Pitch-Yaw Attitude Control Block Diagram

In addition, the control vanes provide damping by means of thermal actuators that operate in series with the stepping motor and control the vane angle with respect to the solar panels. Differential heat input to the thermal actuators causes a rotation of the vanes, thereby providing control-system damping. Thus a near-null condition within the switching amplifier deadband is achieved and no gas will be blown in this condition.

a. Acquisition

Upon reception of the Sun Acquisition Command the switching amplifier and the Sun sensor are turned on. The error voltage driving the switching amplifier is comprised of both positional information (Sun sensor) and rate information supplied by the gyro operating in the rate mode. The closed loop system acts on the spacecraft to minimize the error voltage to the point where the summation of the rate and position-error is within the deadband of the amplifier. At that time the Sun has been acquired.

To accomplish Canopus acquisition, a search-rate generator constant voltage is introduced into the roll switching amplifier. The gas jets act on the system until the spacecraft rate as sensed by the gyro is approximately equal to the search-rate command input. When the Canopus tracker logic indicates Canopus acquisition, the input to the switching amplifier is switched from the search-rate generator to the Canopus tracker. As before, the closed loop system acts on the spacecraft to minimize the error voltage to the point where the summation of the rate and position error is within the deadband of the amplifier. At that time Canopus has been acquired.

b. Commanded Turns

The Attitude Control System is required to orient the thrust axis of the propulsion system in the required direction for trajectory correction. This is accomplished by a sequence of spacecraft roll and pitch maneuvers which reorient the spacecraft at the required attitude. The order of the maneuvers or commanded turns is dependent upon the orientation of the propulsion unit with respect to the vehicle axes. While the first turn may be about an arbitrary spacecraft axis the second turn must be about an axis normal to both the thrust axis and the axis of the first turn. Failure to do so will result in a conical region in space within which it is impossible to orient the motor-thrust axis. One of the propulsion systems under consideration has the midcourse motor axis in the pitch-yaw plane and a separate retro-motor aligned with the roll axis of the spacecraft. Such a configuration requires a pitch-roll commanded turn sequence at midcourse and a roll-pitch sequence for retro-orientation.

The commanded-turn configuration of the Attitude Control System is shown in the block diagram of Figure 11-1. The gyro is switched to the inertial mode providing both rate and position information. At the start of the sequence, the celestial position sensors are switched

out and position control is maintained by the gyro loop. The commanded rate is introduced by a precision current generator which produces a calibrated torque about the precession axis of the gyro. The net precession axis torque is then the sum of the torque proportional to spacecraft rate and the torque produced by the command-current generator. The magnitude of the commanded turn is controlled by adjusting the time duration of the turn and direction is determined by the polarity of the command-current generator. The gyro then retains the position references for the remainder of the maneuver sequence.

The midcourse pitch turn causes Canopus to drift out of the field of view of the tracker so it is necessary to switch all three spacecraft axes to gyro position control at the start of the pitch maneuver. If the propulsion system configuration allows a roll-pitch turn sequence, the effect of pitch and yaw gyro drift can be minimized by retaining celestial position control until the start of the pitch turn.

The gyros also provide rate and position signals to the autopilot for control during the propulsion phase. After maneuvers, the spacecraft reacquires the positional references as in the acquisition sequence.

c. Orbital Attitude Control

During the planetary orbit phase the Attitude Control System maintains the spacecraft orientation with respect to the Sun and Canopus. When there is no occultation of the celestial references the system operates on derived rate control with the gyros off as it does in the transit phase. When the orbit characteristics are such that either the Sun or Canopus is occulted during part of the orbit, an external command switches the Attitude Control System to a gyro stabilized mode. In this inertial mode, the gyros control the spacecraft rate and position continuously throughout the orbit. When the celestial reference is not occulted the position sensor controls the gyro-position signal and orients the gyro to coincide with the position sensor. When the reference body is occulted the position-sensor output goes to zero and the gyro-position signal stabilizes the spacecraft. A block diagram of the orbital attitude control is shown in Figure 11-2. During periods of occultation, the spacecraft accumulates a position error due to gyro drift. The magnitude of this drift error is typically 0.25 degrees per hour so that in an eight-hour occultation a two-degree error can be built up. At the end of the occultation the spacecraft must realign itself with the reference body and the accumulated gyro-drift error must be reset to zero. This is accomplished by applying a torque signal to the gyro which is proportional to the position-sensor output.

Prior to Canopus occultation reflected sunlight from the planet can be indirectly reflected into the Canopus tracker and cause a roll-position error. It is, therefore, necessary to sense this condition and disconnect the roll-position signal before a significant error is built up. Such a switchover signal could be provided by an output from a CC&S orbit-sequence timer, a planet-light detector, or a position signal from the science scan platform.

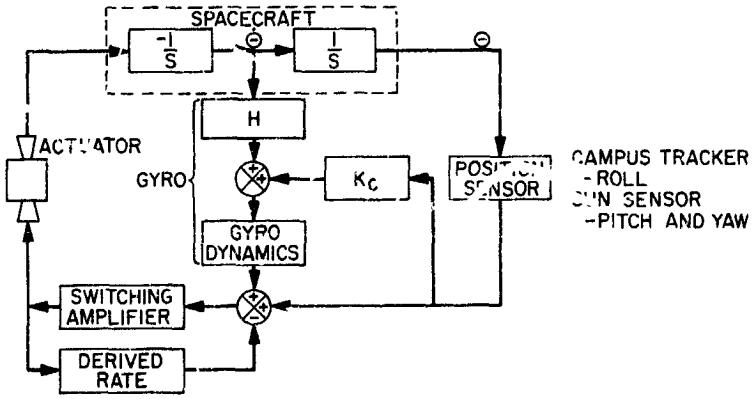


Figure 11-2. Orbital Attitude Control Block Diagram

In orbits where Canopus is the only reference body occulted, it is possible to switch to inertial control on the roll axis only and leave pitch and yaw on the Sun. Such a system conserves power since only one gyro need be operating. Similarly, when only the Sun is occulted the roll gyro need not be used provided the pitch and yaw gyro drift does not cause the loss of Canopus in cone angle. The loss of Canopus is dependent upon the duration of occultation, gyro drift rate, and the cone angle limitation of the star tracker.

The attitude control power can be reduced to a minimum if none of the gyros are operated during occultation. Such a system would drift uncontrolled and reacquire the references at the end of occultation. The total drift accumulated during occultation would depend upon the initial limit cycle rate and the external torques encountered. Typical values of these parameters are:

1) Initial rate of 1 degree/hour, and
2) An external torque of 20 dyne-cm.

With these values the position error and rate after a 2-1/2 hour occultation would be approximately 12 degrees and 10 degrees per hour respectively. These rates and positions are well within the pitch and yaw reacquisition capability when the system is on derived rate control. The problem is more severe in the case of the roll axis due to the problem of acquiring and identifying Canopus. The introduction of RF signal-strength criteria to the Canopus-acquisition logic and the use of ground commands can reduce the acquisition difficulty. In general this method of drifting without inertial control should be used only when power reduction is mandatory and when the reacquisition problem is simple.

d. Attitude Control Gas Requirements

The combined weight of the gas, the gas bottle, and the plumbing hardware associated with the gas system is 42 pounds for the nominal weight spacecraft. This weight total is based

upon what shall here be referred to as the nominal mission case. The breakdown of this weight total is shown in Table 11-1.

Table 11-1. Breakdown of Weight Total

Mode Description	Full Gas System (lb)	Half Gas System (lb)
Separation Removal	8.46×10^{-2}	8.46×10^{-2}
Commanded Turn	1.94×10^{-2}	3.40×10^{-2}
Reacquisition	1.7×10^{-2}	1.83×10^{-2}
Limit Cycle	12.6×10^{-2}	3.2×10^{-2}
Leakage	130.4×10^{-2}	65.2×10^{-2}
Roll Torque Unbalance	14.3×10^{-2}	14.3×10^{-2}
Orbiter:*		
Gravity Gradient	7.52×10^{-2}	7.52×10^{-2}
Limit Cycle	33.25×10^{-2}	8.97×10^{-2}
Total	2.1	1.13
Safety Factor X3	6.3	
Gas + Gas Bottle x 2.7	[illegible]	
Gas + Gas Bottle + Plumbing	42.0	

*Magnetic and Aerodynamic Torque Disturbance are not included in this summation.

The inclusion of the limit-cycle operation in the cruise and orbit modes presumes that the solar vanes were effective in trimming the spacecraft but not effective in arresting the spacecraft within the deadband in a mode where no gas would be blown.

The calculations have been made using the moments of inertia for the spacecraft listed in Table 11-2.

Table 11-2. Spacecraft Moments of Inertia Calculations

	Tanks One on Top the Other	Tanks Side by Side
J_{xx}	320 slug ft^2	340 slug ft^2
J_{yy}	320 slug ft^2	340 slug ft^2
J_{zz}	400 slug ft^2	510 slug ft^2

The difference in gas consumption due to the two different configurations considered here were negligible. Other parameters used were:

α, acceleration constant = $.45\ mr/s^2$

I_{sp}, specific impulse of gas = $70\ \frac{lb_f\ sec}{lb_m}$ (continuous)

= $35\ \frac{lb_f\ sec}{lb_m}$ (pulsing)

L, moment arm = 139 inches

For sizing the gas requirements, the overall mission time considered was 360 days of which the orbit phase is 180 days.

The safety factor of 3 allows for either one of several failure modes or a combination thereof as shown in Figure 11-3. The ordinate of Figure 11-3 is in days elapsed from the beginning of the mission until the half-gas system failure and the abscissa is in average unbalance torque in dyne cm that the spacecraft can tolerate.

The torque unbalance due to a single vane failure is 124 dyne cm. Here a single vane failure refers to a condition where one vane fails to erect but the opposite vane adapts properly. From Figure 11-3, both a half-gas system failure and a single vane failure may be tolerated

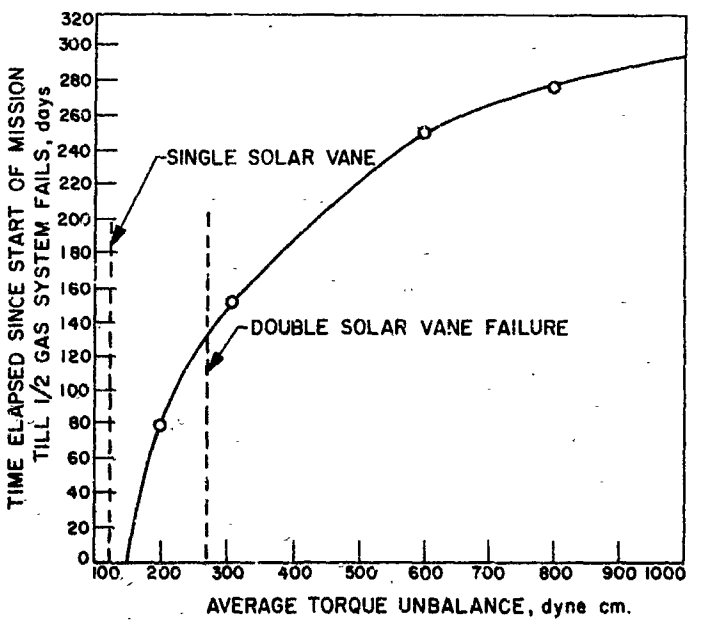


Figure 11-3. Average Torque Unbalance in Dyne-Cm

on the first day of the mission. The torque unbalance due to a double-vane failure is 271 dyne cm. A double-vane failure refers to the worst case where one vane failes to erect and the other van erects but fails to adapt. From Figure 11-3 this type of failure may be tolerated from the 132nd day of the mission onwards.

Nominal power and weight estimates are listed in Table 11-3.

2. The Midcourse Autopilot

A consideration of the retro-propulsion system indicates that for the solid engine configuration a separate midcourse autopilot will be required. This autopilot and propulsion system will be similar to the Mariner 1964 midcourse propulsion system. After the midcourse corrections have been achieved and prior to retro injection it is desirable to jettison the midcourse autopilot and propulsion system in order to provide for more payload capacity.

The function of the autopilot is to maintain a stable and accurate vehicle attitude during the rocket-motor firing. The autopilot uses three gyroscopes to sense motion about the three spacecraft axes, and applies corrective torques by positioning four jet vanes in the exhaust stream of the rocket.

Figure 11-4 shows a functional block diagram of the autopilot system. Three axis disturbing torques arising from misalignment of the rocket-motor thrust vector act through the spacecraft dynamics to produce rotations about the three spacecraft axes. The gyroscopes sense these rotations and provide the autopilot with voltages proportional to the spacecraft angular rates and positions. The gyro signals are processed by a mixing network into signals appropriate to a coordinate system natural to the jet vanes, and the jet-vane actuator amplifiers use these signals to position the four jet vanes. Forces on the jet vanes are resolved into torques about the spacecraft axes by their geometrical placement, represented in the block diagram as the jet-vane torque gain matrix.

The dynamic properties of the spacecraft consist of its rigid body inertia, which is sufficient for a low-frequency description, and the resonances of its structure. The dynamics of the Mariner spacecraft reflect an increased consideration of the effects of dynamics on the autopilot. The products of inertia should be a small percentage (say less than 10 percent) of the moments of inertia; opposite solar panels should be balanced about the center of mass of the spacecraft; and dampers should be provided on all four panels. All other hinged inertias should have a natural frequency well above the range of concern of the autopilot, or be heavily damped.

Figure 11-5 shows the rocket orientation with respect to the spacecraft axes on Mariner 1964. This configuration was selected because the antenna is along the spacecraft Z axis. Mariner 1969 is anticipated as having the retro rocket along the spacecraft Z axis.

Table 11-3. Power and Weight Estimates (Nominal Case)

Item	Power (Watts)			Weight (lbs)
	Cruise	Intermittent	400 ~	
A/C System				
Control System Electronics	11			8.5
Gyro Pkg. and Electronics		.0	21.0	11.1
Canopus Tracker and Shutter	3			5.7
Sun Sensor and Sun Gate	1			0.7
Solar Vane Actuator and Electronics and Vanes	2			6.5
Gas System	4			42.0
Midcourse Autopilot				
Jet Van Actuators and Mounting Ring		18.0		3.5
SUB-TOTAL	21.0	39.0	21.0	78.0
Retro Autopilot				
*Actuators (P & Y)		45.0		
Electronics				2.0
Roll Control		10.0		
SUB-TOTAL	21.0	94.0	21.0	80.0
Science Instrument Platform				
Actuators (Servo)		4.0		5.0
Electronics and Sensors		2.0		2.0
Antenna Pointing				
Actuators		4.0		5.0
Electronics	2.0			1.0
TOTALS	23.0	104.0	21.0	93.0

*Actuator weights are discussed in retro autopilot description and will be tabulated with the various propulsion configuration weights by Propulsion Division.

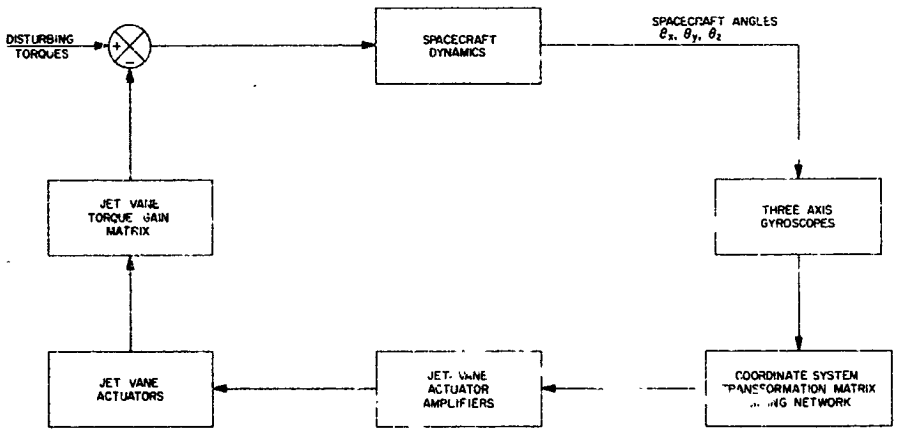


Figure 11-4. Autopilot Block Diagram

Therefore, if there is a separate midcourse motor, it may again be oriented as it is in Mariner 1964. The motor axis is not parallel to X-Y plane in order to point the thrust vector as close as possible through the spacecraft mass center. Figure 11-6 shows the arrangement of the four jet vanes, which are mounted in a plane perpendicular to the rocket thrust and located at the exit of the rocket nozzle. The figure is a view looking directly into the rocket nozzle with the jet vanes in their neutral position, so that the back edge of the four vanes can be seen. The inset shows how a jet vane is mounted in the exhaust stream.

In order that a signal from the X gyro produce an X torque on the spacecraft, all four jet vanes must be moved in their proper ratio, and similarly Y and Z gyro signals must each move all four jet vanes. The mixing of the three gyro signals to command the four jet-vane rotations is tantamount to applying a coordinate transformation to the gyro signals from the spacecraft axes to a coordinate system natural to the jet vanes. This is accomplished electronically by a network of resistors which determine the amount of motion of each jet vane for each gyro signal.

The principal source of autopilot error is proportional to the misalignment of the undeflected thrust vector with the spacecraft center of mass. In order to provide a steady-state signal, which implies a steady-state angular offset of the spacecraft. This steady-state

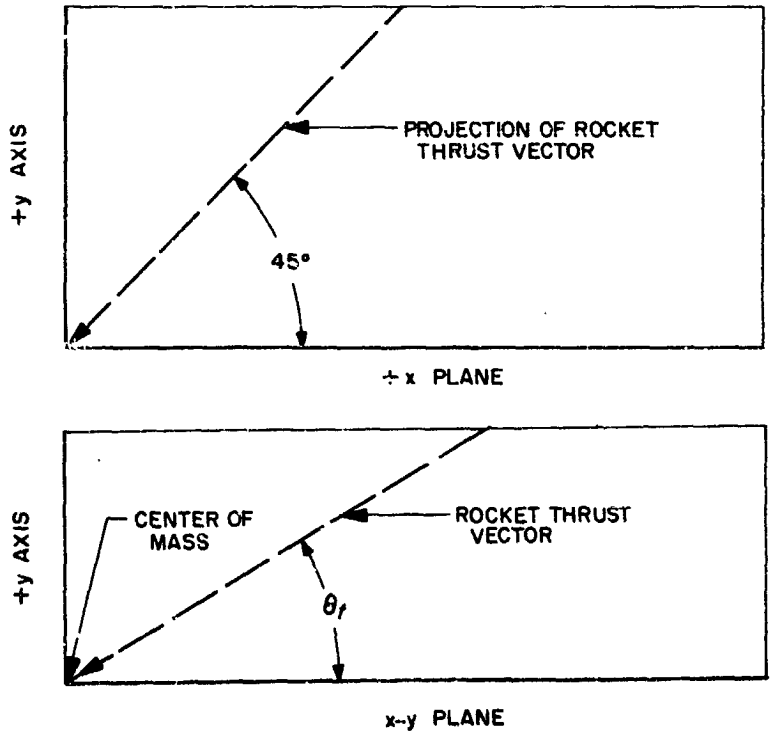


Figure 11-5. Rocket Thrust Vector in Spacecraft Coordinates

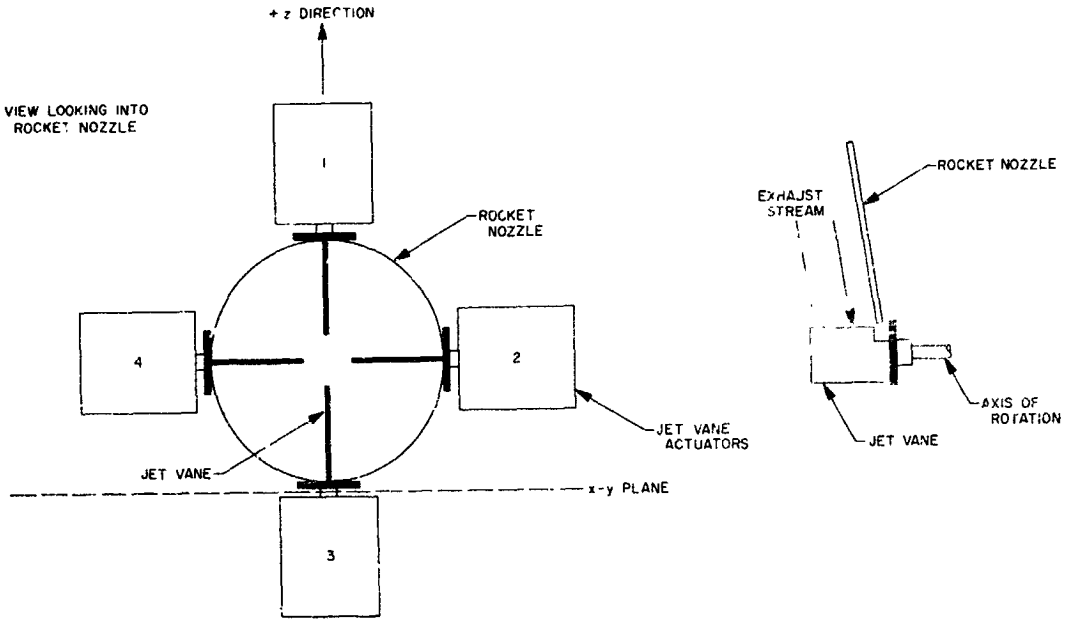


Figure 11-6. Placement of Jet Vanes on Rocket Motor

angular offset of the spacecraft in inertial space, added to the angle of thrust vector deflection with respect to the spacecraft, gives the total difference between the desired and actual thrust-vector direction in inertial space. The angle is designated θe. This error is kept small by calibrating the angle between the undeflected thrust vector prior to launch and compensating for the error in midcourse turns. The calibration uncertainty for Mariner 1964 is a 5 mrad cone. The pointing error can also be reduced by increasing the autopilot gain but this method is limited by stability constraints imposed by the spacecraft dynamics and the gyro loop characteristics. The problem is further complicated because the spacecraft is not a rigid body.

Another contribution to the pointing error results from the thrust motor inclination to all three of the spacecraft principle axes as previously discussed and illustrated in Figure 11-5. To aid in understanding the problem consider a simplified configuration where the motor thrust axis is in the X-Y plane but still at 45 degrees to the X and Y axes. Figure 11-6 shows a view of the jet vanes looking into the exhaust nozzle. In Mariner 1964 all jet-vane lift centers are approximately 2.3 feet from the spacecraft Z axis but opposite jet-vanes lift centers are only .09 feet from the motor axis. These two dimensions are extremely important since they are the lever arms which act with the jet-vane lift to produce torque about the spacecraft axes.

In the simplified example, consider a positive disturbance sensed by the X gyro. This can be corrected by rotating both horizontal jet vanes through an angle θ in the same direction imposing a negative torque about the X and Y axes through the 2.3 foot lever arm. The imposed negative torque on the Y axis must now be balanced by requiring both pairs of opposite jet vanes to rotate in opposite directions through an angle ϕ to create a positive Y and negative X torque through the .09 foot lever arm.

This type of mechanization requires that ϕ be larger than θ by one-half the lever arm ratios $1/2 \left(\frac{2.3}{.09}\right) \approx 13$. This means that the X gyro signal must be precisely proportioned into all four jet-vane actuators so that there is no cross coupling to the Y axis. Any error in the signal proportioning will be reflected as a steady-state Y error. In Mariner 1964 all three gyro signals are mixed at each jet-vane actuator amplifier to produce the necessary control signals. The actual mixing resistors are selected after preflight center-of-mass calibration.

3. The Retro Autopilot

a. Purpose and Requirements

The Mars 1969 orbiter will require a sizeable retro maneuver to transfer the spacecraft from a hyperbolic transit trajectory to an elliptical planetary satellite orbit. The retro autopilot must maintain a stable vehicle attitude and supply accurate control of the thrust-vector direction during this propulsion maneuver. To accomplish these objectives the

autopilot must have information as to both vehicle attitude and velocity vector direction and some means of controlling the forces and torques acting on the spacecraft.

For the Mars 1969 orbiter, vehicle attitude and attitude rate will be supplied by gas bearing gyroscopes. It is anticipated that a single gyroscope will be associated with each axis to supply both vehicle attitude and attitude rate information. Preliminary JPL studies indicate that a satisfactory retro maneuver can probably be accomplished by maintaining the rocket-thrust vector in a constant inertial direction.

Direct measurement of the velocity-vector direction requires the use of accelerometer and the supplemental coordinate conversion and integration equipment. This would imply a fair amount of complex equipment. Indirect velocity-pointing measurements are far simpler and can yield satisfactory performance providing that care is taken in establishing the structural and propulsion configuration in the spacecraft preliminary design phase and careful use of alignment and calibration techniques are employed in the assembly phase of the program.

Control of the spacecraft forces and torques include the problems of reducing the spacecraft torques to zero and directing the rocket thrust so that the net velocity increment imparted to the spacecraft is within a small error angle of the desired velocity correction. In general this can be accomplished by algebraically adding other vernier forces and torques to the spacecraft or by altering the direction or point of action of the propulsive forces with respect to the vehicle center of mass. The type of actuators utilized to accomplish the control is heavily dependent on which of the several propulsion configurations is employed for the Mars orbiter. They will be presented with the propulsion options later in this section.

b. The Interaction of Stability and Pointing Error

The design of autopilots is generally complicated by the conflicting loop-gain requirements introduced by the stability and pointing specifications on the spacecraft. From the point of view of stable autopilot operation, it is generally desirable to maintain a relatively low-loop gain. This is particularly true in the face of some of the destabilizing influences that may be present in the Mars-orbiter retro maneuver. In particular, because of the large change in vehicle mass from the start to the termination of the retro burn, a sizeable decrease in moment of inertia will occur which requires the autopilot to be stable over a large dynamic range of loop gain. There is additionally a tendency for the center of mass to migrate away from the motor point of action during the burn period which also results in an increase in the loop gain due to the increasing control lever arms. Furthermore, the structural resonances of the solar panels, antennae, and articulating appendages can contribute serious destabilizing influences, particularly at high autopilot gains.

On the other hand, accurate pointing of the motor thrusting axis is enhanced by a high loop gain and a fast autopilot. Several of the important components of the total pointing error are inversely proportional to the autopilot gain. Care must be taken during the spacecraft preliminary design, particularly in the choice of propulsion and structural configurations, to prevent these conflicting requirements on autopilot gain from over-constraining the autopilot design.

c. Autopilot Pointing Errors

The purpose of the retro maneuver is to impart a specific velocity increment to the spacecraft. It is the responsibility of the autopilot to maintain the sense of the velocity vector. The component of this vector in the desired direction is defined as the longitudinal velocity, the perpendicular error component is referred to as the transverse velocity. The pointing error of the autopilot is the angle between the resultant and the longitudinal velocity vectors.

Transverse velocity can be accumulated during the retro burn either during the starting and stopping transients or throughout the steady-state portion of the maneuver. The transient errors are the result of the autopilot's inability to instantaneously remove the torques resulting from the misalignment of the motor thrust with the spacecraft center of mass. As a result of these torques the spacecraft and motor rotate away from the desired thrusting direction for as long as it takes the autopilot to restore the thrust axis to the desired direction. During this period some transverse velocity is imparted to the spacecraft. Transient errors can also occur in the shutoff of multiple-engine configuration propulsion systems due to variations in the cutoff characteristics of the engines. In general transient errors can be minimized by maintaining wide autopilot bandwidth and by minimizing the initial disturbing torques produced by the spacecraft structure.

Steady-state errors are characterized by a constant misdirection of the thrusting axis during the steady-state operation of the autopilot. The most important components of the steady-state error are related to the angle ρ. ρ is defined as the angle between the null direction of the motor thrust and the line connecting the center of mass of the spacecraft and the thrust point of action. For autopilots of the Ranger and Mariner type, where thrust-vector control is accomplished by rotating the thrust vector and no lateral accelerometers are employed, the principal component of steady-state error has the form:

$$\text{Pointing error} = \left(1 + \frac{1}{K_{AP}}\right) \rho, \quad K_{AP} = \text{autopilot dc gain}$$

The importance of both having the center-mass as close to the motor line of action as possible and maintaining it there as fuel is depleted becomes apparent.

For a given value of the angle σ, there are several techniques for reducing the pointing error. The most obvious reduction can be achieved by increasing the autopilot gain. From the nature of the expression this reaches a point of diminishing return when the reciprocal of the autopilot gain becomes small with respect to one. Further this tends in the direction of aggravating the stability problem. A related method of increasing the autopilot gain is by the use of integral compensation. This increases the autopilot dc gain significantly which reduces the steady-state error, however, the transient response of the autopilot becomes poorer and the transient errors may become the largest pointing error contribution. A third technique of error reduction is to bias the commanded turns for any known offset of the center of mass. This would mean that only uncertainty in the value of ρ would contribute to pointing error.

The choice of propulsion configuration can be an important aid in controlling the magnitude of the pointing error. If thrust vector control is accomplished by translating the force as opposed to rotating it, the pointing error expression is of the form:

$$\text{Pointing error} = \frac{\rho}{K_{AP}}.$$

Multiple engines having throttling capabilities are examples of this type of propulsion system. It can be seen that for a fixed pointing requirement the constraints on the autopilot gain are considerably relaxed by such a configuration.

As a last resort, pointing accuracy may be improved by the use of lateral accelerometers. It would be necessary to coordinate convert their outputs which could be accomplished by either placing them on the inner element of an inertial platform or by supplying a computer with the gyro and accelerometer signals and having it perform the coordinate conversion. The autopilot would then act to null the integral of transverse accelerometer. This represents more complexity than will probably be required for this mission.

d. Structural Dynamic Effects

The structural dynamic properties of the spacecraft have a considerable effect on the design of the autopilot. During the transient following motor ignition, nonsymmetrical "flapping" of the solar panels can contribute sizeable disturbance torques to the vehicle. Similarly, any flexible booms and antennae are potential sources of trouble.

During the steady-state burn period, the greatest concern is the frequency and damping of the structural resonance. It is probable that the solar panel resonance will be constrained to occur in the 1-5 cps region, preferably at the lower end of that range. In addition, adequate means of damping their resonances will be required. Hopefully the other articulating members can be designed to resonate well above the autopilot frequency range of interest.

To reduce the effects of inertial cross coupling, control must be exercised over the cross products of inertia. Cross product terms greater than 10% of the moments of inertia should be avoided.

e. Propulsion Configurations

There are presently three propulsion configurations being considered for the retro maneuver. They include:

1) A single gimbal liquid engine with approximately 0.3 g initial acceleration.
2) A single solid engine with initial acceleration of 3 g and with secondary injection providing pitch and yaw thrust vector control.
3) A three liquid throttline engine system with one gimbal engine to provide roll control and a 0.3 g starting acceleration.

For the single gimbal engine configuration pitch and yaw control would be provided by swiveling the nozzle with linear or rotational actuators. It is estimated that the actuators could achieve about a 5 cps response consistent with the mass of the rocket thrust chamber and nozzle assembly. This represents the slowest actuation loop of the three configurations and may lead to a more difficult stability problem because of the close proximity of its actuator resonance to some of the spacecraft structural resonances. Since control is accomplished by a rotation of the thrust vector the pointing error is the sum of the angular deviation of the center of mass and the resultant autopilot steady-state gain error, which places more of a constraint on the autopilot gain than the three-engine liquid system. It is estimated that two 5-pound actuators requiring a total of about 45 watts of peak power would be required for this system. Approximately two pounds of electronics would be required for autopilot circuitry. The same propulsion and autopilot would be useable for some midcourse corrections since the system is restartable and has sufficiently low thrust to be accurately controllable for short burns.

The single solid propellant engine propulsion system also obtains its pitch and yaw control by rotation of the thrust vector. Physically this is accomplished by injecting streams of liquid such as Freon or nitrogen tetroxide into the rocket nozzle perpendicular to the rocket thrusting direction. Since the movement of only the small liquid control valve masses are required to produce the thrust vector deflection, frequency responses in the vicinity of 20 cps appear reasonable for the actuator loops. It is estimated that the valves, liquid, tanks and liquid-pressurizing system to accomplish this control might weigh approximately 50 pounds. The lower inert weight of the solid-propellant system might tend to reduce this weight disadvantage. Two pounds of electronics should also suffice for this system and power consumption of approximately 15-watts peak would be typical.

As a result of the higher thrust, and shorter burn time of the solid engine configuration, a higher bandwidth autopilot would be required as compared with the liquid configurations. The higher g thrust also results in heavier structural weight as a result of the more severe environment during motor burn. An inherent advantage of solid propellants is the capability for more precise location and maintenance of the vehicle center of mass. The dynamic problems of fuel slosh are similarly eliminated.

Because of the lack of engine restart capability and the higher acceleration levels, a separate liquid engine midcourse autopilot described earlier would be required to perform midcourse velocity corrections.

The three throttling liquid engine configuration utilizes the technique of translating rather than rotating the thrust vector. As a result, the primary contribution to pointing error is of the form:

$$\text{Pointing error} = \frac{\rho}{K_{AP}}.$$

As a result for the same autopilot gain more accurate pointing can be achieved as compared to the other propulsion configurations. Alternately, if the pointing error is maintained constant, the autopilot gain can be lowered and the structural constraints can be somewhat relaxed.

The actuators for this configuration can be considered the propellant flow control valves. Each of these complete assemblies, of which there are three, weigh approximately 11 pounds. Of this about 2 pounds represents the throttling valves which provide the thrust vector control in pitch and yaw. For a more realistic system comparison, all autopilot actuator weights have been included in the propulsion weight summary. Only the autopilot electronic weight is summarized in the attitude control section. As in the other configurations approximately two pounds will be required for the autopilot electronics. The frequency response of the throttling engines is about 14 cps.

Perhaps the most serious dynamic disadvantage of multiple throttling engine configuration is the transient problem produced by the variation in start up and cutoff times and characteristics of the engines. Typical starting time variation of present state-of-the-art engines do not appear to create serious retro autopilot problems.

The restart capability of this propulsion system will enable its use for the midcourse velocity correction. As in the single liquid engine case, the same autopilot electronics can be used during midcourse maneuvers.

From purely autopilot considerations the three throttling engine system appears to be the most desirable propulsion configuration.

f. Roll Control

The disturbance torques about the motor thrusting axis are at least an order of magnitude greater than the capability of the Roll Attitude Control System. As a result an auxiliary source of roll correcting torque must be supplied during the retro and midcourse maneuvers.

For the single liquid and solid propulsion configurations, it appears most convenient to accomplish roll control with a high level cold gas system. The gas supply can either be combined with the attitude control gas or stored in separate tanks. Assuming that the valves and nozzles can be placed at the solar panel tips for the largest possible lever arms, a roll system weight of approximately 12 pounds should be satisfactory for maintaining roll control. The roll control power requirements will be about 5-watts peak.

For the three throttling engine configuration, roll control can be obtained by gimbaling one of the engines about one axis. A single 4-pound actuator requiring about 10 watts peak should be sufficient for this purpose. One of the inherent advantages of the multiple engine configuration is the convenience with which roll control can be accomplished.

A summary of Retro Autopilot characteristics is presented in Table 11-4.

g. Antenna Control System

The function of the antenna control system is to orient the directional antenna toward the Earth to enable high-gain communications. In the single degree of freedom system under consideration the axis of rotation is at an angle of 9 degrees from the RF axis of the antenna. The rotational axis is inclined 38.5 degrees from the spacecraft Roll axis in a direction which optimizes antenna tracking during the orbit phase. The antenna has unlimited freedom about the rotational axis so the antenna axis lies in a cone of 9-degrees half angle, about an axis 38.5 degrees from the Roll axis. This configuration enables high gain communication between 100 days prior to encounter and 120 days post-encounter. During the transit phase prior to encounter minus 100 days, the antenna is oriented at an angle to optimize communications at encounter so that limited science data transmission is possible in the event of an antenna positioning failure.

Just prior to the switchover to the high-gain antenna, an external signal turns on the antenna control system and the antenna orients to the required angle to establish high-gain communications. Subsequent adjustments of the antenna position are accomplished by periodic "update" commands from the CC&S which advance the positioning system to successive points in a programmed sequence. Redundant control of the angle sequence is achieved by a ground command to update the sequencer. An additional ground command can be implemented to add or subtract a small increment to the stored program should such a correction be desirable.

Table 11-4. Summary Retro Autopilot Characteristics

Propulsion Configuration	Single Liquid Engine	Single Solid Engine	3 Liquid Engines
Technique for P-Y Control	Gimbal Actuator	Secondary Injection	Throttling Capabilities
Technique for Roll Control	High Level Cold Gas	High Level Cold Gas	Single Swiveled Engine
Peak Power Required for P-Y Control	45 W	15 W	20 W
Peak Power Required for Roll Control	10 W	10 W	10 W
Weight for P-Y Thrust Vector Control	10 lbs	53.5 lbs	6 lbs
Weight Required for Roll Control	12 lbs	12 lbs	4 lbs
Weight for A. P. Electronics	2 lbs	4 lbs	2 lbs
Total A. P. Actuator Weights	24 lbs	69.5 lbs	12 lbs
Form of Point Error Magnitude	$(1+\frac{1}{K_{AP}})$	$(1+\frac{1}{K_{AP}})$	$\frac{1}{K_{AP}}$
Frequency Response P-Y Actuator	5 cps	20 cps	14 cps
Need for Separate Midcourse A. P.	No	Yes	No
Relative Bandwidth Required	Medium	High	Medium

A block diagram of the antenna control system is shown in Figure 11-7. The basic control loop is a dc rebalancing system in which a dc input is compared with a signal from a voltage divider on the output shaft and the error drives the output toward a null condition. The prime mover in the antenna actuator is a bidirectional step servomotor that rotates through a fixed angle in response to an input pulse. The control amplifier drives the motor at a constant rate when the input exceeds a predetermined value. The direction of rotation depends upon the polarity of the amplifier input. The angle program is generated by a ring counter in which one or more stages are set at any time. The update pulses from the CC&S advance the state of the counter in a predetermined sequence. When a stage of the counter is in the "set" state a positive reference voltage is gated through a scaling resistor to the input of the motor drive amplifier.

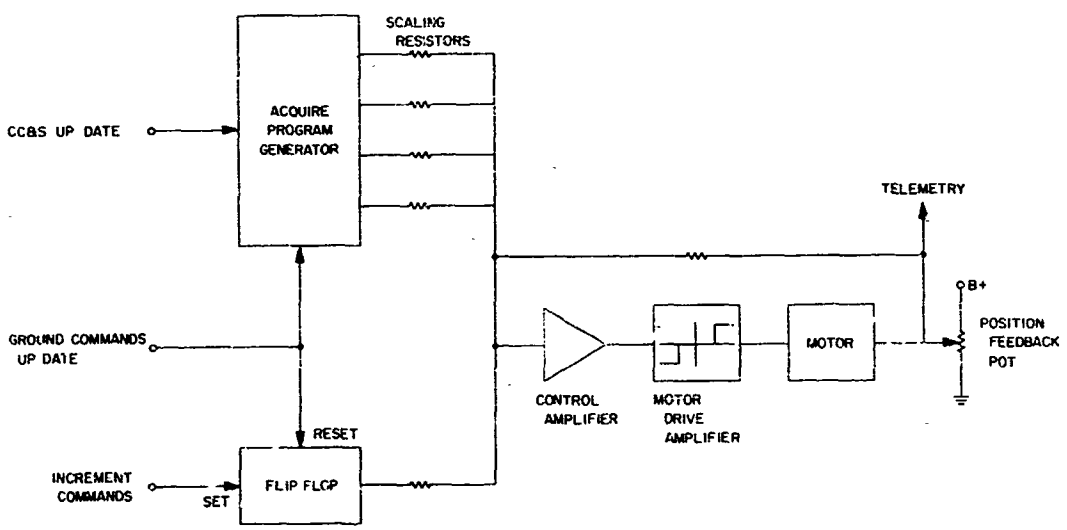


Figure 11-7. Antenna Position Control System

By adjusting the scaling resistors from each stage of the counter any arbitrary program can be generated. Depending upon program complexity, stage-to-stage feedback can increase the capacity of the counter to 2η states for an η state counter. The gated reference signal from the counter is balanced at the amplifier input by the signal fed back from the output-shaft potentiometer.

A small increment can be added to the program by an R-S flip-flop controlled by a ground command. This flip-flop gates the reference voltage to the amplifier to increase the signal from the program generator. The reset input of the flip-flop is connected to remove the increment upon receipt of the next update pulse.

4. Orbital Instrument Pointing

a. Introduction

Several of the planetary science instruments require orientation toward Mars while gathering data. The following discussion presents a nominal case design, possible alternatives and a comparison of how well they satisfy the performance requirements.

b. Desired Performance

The nominal level of performance within the power and weight constraints requires that the planetary instrument payload must:

1) View Mars within ±30° of the normal to the line of sight for at least a portion of each orbit.
2) View Mars from before the morning terminator to past the evening terminator, about 200 degrees total sweep. This could be accomplished over a period of several orbits rather than on every orbit.

The maximum level of performance would require the ability to accurately point to selected portions of Mars on successive orbits. This case, while not greatly affecting the weight and power of the scan platform itself, would require a high order of complexity in the command system and the scan system electronics.

c. Nominal Case Scan Platform

The nominal case scan platform has a degree of freedom permitting 200 degrees of scan motion approximately in the plane of the orbit. A second degree of freedom permits erection of the platform from the stowed position to a position with the above scan axis approximately

perpendicular to the plane of the orbit. The secondary axis also permits one update either programmed or ground commanded of the primary scan axis orientation so as to satisfy the performance requirements over a 6 months orbital life. The single update by means of a spring-latch mechanism would be sufficient for normal dispersions of an orbit with periapsis at 1500 km.

Three modes of operation possible with this scan platform are:

1) Tracking of the planet with a simple visual center of illumination finder. The platform could be controlled to follow continuously or by using a large amount of hysteresis in the electronics to follow discontinuously in perhaps 20 degree steps.
2) Constant rate scan initiated by acquisition of Mars with a narrow angle gate or by ground command. The necessary rate can be preselected before launch to obtain the required performance.
3) Constant angle of platform for one orbit being changed for successive orbits by on-board program or ground command.

Mode 1) continuous tracking of the planet has not been mechanized for the nominal spacecraft configuration. Mode 2) is somewhat risky unless the necessary rate can be revised after achieving orbit. While mode 3) is a low performance mode, it has inherent simplicity and accordingly a high probability of success.

d. Raised Periapsis

If it should become necessary to raise periapsis from 1500 km to 4000 km the nominal case mechanization becomes marginal at best. Several more orientations of the scan axis will be necessary probably requireing an actuator on the deployment axis similar to the one on the scan axis. The scan axis could then be updated by a simple tracker, program or ground command.

Even for the 1500 km periapsis this extra capability for the scan axis could guard against off design orbits and provide extra flexibility in the system at a small cost in weight and power. Additionally, the full second axis would satisfy the mechanization requirements for a maximum case scan platform.

e. Scan Platform Characteristics

(1) Performance. The nominal scan platform meets the requirements of the 1500 km periapsis orbit. The second axis needs to be actuated in a similar fashion if periapsis is raised to 4000 km, if maximum case performance is desired or if an additional safety margin against off design orbits or additional flexibility is desired.

(2) Reliability. The scan platform reliability will be degraded by the addition of the second actuator. However, the overall mission reliability may well be improved by the additional capability and flexibility of the second axis. In the case of the higher periapsis clearly the mission reliability is improved since operation is at best marginal with the nominal scan platform.

(3) Development Needed. No breakthrough or extended developments are needed. The normal development of adapting available devices to the particular system is of course necessary.

(4) Telemetry. Telemetry of the angular positions of the scan platform axes will be required for data reduction and also for ground command operation.

(5) Command Requirements. Command requirements vary depending on the degree of ground control desired. Restricting ground control to backup of on-board programmed and automatic tracking modes would result in higher mission reliability than depending on ground command as the primary operational mode.

f. Conclusion

While the nominal case scan platform will perform the nominal mission for the 1500 km periapsis orbit, it is recommended that strong consideration be given to the more capable two-axis platform and if the small additional weight and power are available.

The two-axis platform will be necessary if periapsis is raised to 4000 km and in any case buys a greatly increased capability and flexibility at a small weight and power penalty.

The modes of operation should be selected to operate primarily on-board and secondarily ground command to achieve high reliability. A fixed angle on-board program backed up by fixed angle ground command would provide the best available combination for the nominal spacecraft configuration.

The development needed for any of the described platforms is nominal.

B. SPACECRAFT CONTROL

1. Central Computer and Sequencer (CC&S) Functional Description

The functions performed by the CC&S are threefold:

1) It provides frequency signals as timing references to other subsystems.
2) It receives from the Command Decoder and stores quantitative commands that are required for the determination of maneuver-turn durations and polarity, midcourse and retro-motor burn durations, retro-maneuver duration and for the sequencing of orbital operations.
3) It provides properly timed outputs to other subsystems in appropriate sequences. The time that any output occurs, the sequence in which it appears and the resolution to which it is timed are changeable at any time until just prior to the occurrence of that output.

An "output" is defined in this discussion as a momentary change, or the initiation of a continuous change, in impedance between a pair of wires connected to another subsystem. The change in impedance may be from a high value to a low one or vice versa as specified by the subsystem requiring it. One or more simultaneous outputs comprise an "event."

Little can be said about function 1) until other subsystems become definitized and their need for reference frequencies is established. Functions 2) and 3) are described in the following paragraphs in terms of the sequences to which they are applicable. At the same time, where functional changes in the interfaces with other subsystems are apparent, a discussion of them is interjected. The sequences may be characterized by the mission functions associated with them. They are Prelaunch, Launch, Cruise, Midcourse, Retro, Flyby, Encounter Backup and Orbit. Each of these is defined and described in the following paragraphs.

a. Prelaunch Sequence

Before launch all CC&S outputs are held in their non-operational states. A program, consisting of an appropriate number of groups of bits, is entered into the CC&S memory. Defining the CC&S functions for a nominal mission, the program's contents vary according to launch date. After a prescribed time has elapsed a signal is returned to the Launch Complex signifying that the CC&S is ready and operating properly.

b. Launch Sequence

This sequence may be identical to that in Mariner 1964. A possible exception, though, depends on the presence of an R-F noise detector experiment. A CC&S output initiating

deployment of the antenna for purposes of calibration may be required after cruise attitude has been attained.

c. Cruise Sequence

The cruise sequence includes those functions which are launch-date dependent. Possible functions comprising this sequence are Canopus sensor cone angle update, Telemetry bit-rate change, switch to High-gain antenna, High-gain antenna step pointing and Planetary Platform position change (in orbit). The times at which these outputs occur are fixed by the program. However, they may be varied in flight after trajectory determination if increased accuracy is desirable. In addition, the number of such outputs may be altered.

d. Midcourse Sequence

At some time prior to the start of a midcourse maneuver, a number of quantitative commands are transmitted to the spacecraft. They specify the duration of the turns and motor burn and the polarity of the former. They are routed to the CC&S for storage. Since the CC&S contains a relatively large number of memory locations, a change from the Mariner 1964 quantitative command format is required. Two alternatives present themselves.

1) The length of the command word may be increased to accommodate the additional address bits required by the CC&S.
2) A quantitative command may consist of two words. The information part of the first word transmitted contains the CC&S address into which the information part of the second word is to be stored.

Upon receipt of the appropriate discrete command, the maneuver which is similar to Mariner 1964 is started. The maneuver may be repeated as often as desired as far as the CC&S is concerned. If the duration and polarity information have not changed, the maneuver may be repeated without transmitting Q. C. No. 1 again.

e. Retro Sequence

Before the Retro Maneuver begins, a number of quantitative commands are transmitted for storage in the CC&S. They specify the duration of the turns and retro motor burn, the polarity of the former and the elapsed time between receipt of the appropriate discrete command and the start of the retro motor. Subsequent to this the discrete command is issued to begin the sequence. If it is observed that the sequence did not start as required, a new quantity for the elapsed time between receipt of the discrete command and start of motor burn is transmitted and the discrete command reissued. This may be repeated as often as time allows until start of the sequence is verified, each time decreasing the interval

to be measured from receipt of the discrete command to start of motor burn. At the start of the sequence, turns to orient the spacecraft for orbit injection are commanded. When the turns are completed and verified as correct, an inhibit on the start of the retro motor is removed or inserted by a discrete command, depending on planetary contamination constraints and at the stored time the CC&S originates the signal to start the retro motor. For the maximum case, in the event that the retro motor inhibit is not removed at a specified time in the sequence the CC&S abandons the Retro Sequence and begins the Flyby Sequence. It should be noted that the maximum motor burn interval for the retro maneuver may be several times longer than that needed for midcourse correction. If the resolutions for both intervals are similar an increase in the number of information bits in the quantitative command may be necessary.

f. Flyby Sequence

The Flyby Sequence is similar to the Mariner 1964 Encounter phase except that it may begin with CC&S commands to reacquire cruise attitude.

g. Encounter Backup

Encounter Backup is a single-event sequence. It is activated before launch and at the proper time it enables the start of the Flyby Sequence if the Retro Sequence has not begun. This furnishes the opportunity to accomplish a flyby mission in the event that command capability is permanently lost during the flight. This sequence is turned off when the retro motor Inhibit is removed. It should be noted that due to uncertainties in the CC&S clock source frequency the Encounter Backup sequence may be in error by ±40 minutes at the end of the trajectory. This capability is only present in the maximum case.

h. Orbit Sequence

Before the start of the second orbit several quantitative commands are transmitted for storage within the CC&S. These commands pertain to the time of periapsis (or other orbital reference point), the orbit period, the times of data-mode changes, instrument turn-on and turn-off times and any other sequenced outputs which may be required. Upon receipt of a discrete command this sequence is begun. It repeats itself thereafter unless interrupted by another discrete command. The following functional options are available:

1) Alternate orbital sequences may be followed during succeeding orbits.
2) Orbital event-times may be corrected or changed.
3) Events may be rearranged in any order.

These options can be chosen by transmission of one or more appropriately addressed quantitative commands.

2. Possible Mechanization

Certain aspects of an orbiter mission sufficiently complicate the implementation of CC&S functions as to make necessary the consideration of alternative mechanizations. Until now, the CC&S has been composed of shift registers and binary dividers or counters. CC&S outputs have been derived from diode decoding matrices which detect the appropriate states of these registers. A one-to-one correspondence exists between the combination of a register state and its associated decoding diode configuration and the time of a CC&S output. This correspondence cannot be altered without rewiring the matrix. Such an approach to a sequencer is characterized as hard-wired and inflexible. In general, the addition of any new function to those already performed necessitates an increase in hardware. The class of mechanizations for which this is true is referred to here as timer-oriented.

a. Timer-Oriented Design

A consideration of the Orbit Sequence options outlined in Subparagraph XI. B. 1. b exemplifies the serious drawback of a timer-oriented sequencer. Those options, while they may not be deemed essential to a minimally successful mission, greatly enhance the prospects for a meaningful mission. The degree of flexibility they require of the CC&S implies inclusion of the following hardware in a timer-oriented design:

1) One storage register for each orbital quantitative command.
2) Logic circuits for loading and circulating these registers.
3) Increased address decoding capability so that quantitative commands can be stored in the correct registers.
4) A counter which is capable of being recycled at an arbitrary time and whose length is adequate to prevent overflow during the longest expected orbit period.
5) A comparator which matches the contents of the counter with those of the registers and supplies outputs when it detects equality.
6) Logic circuits for controlling the comparison process and updating and changing event times, associating the contents of a register with a particular output, and possibly alternating between two sequences.

A functional block diagram of a timer-oriented CC&S incorporating these capabilities is shown in Figure 11-8. It is an extension of the Mariner 1966 CC&S design. The blocks enclosed within the dashed lines are the additions needed to perform the orbital sequencing task. They represent a 35 percent increase in the number of components over the Mariner 1966 CC&S.

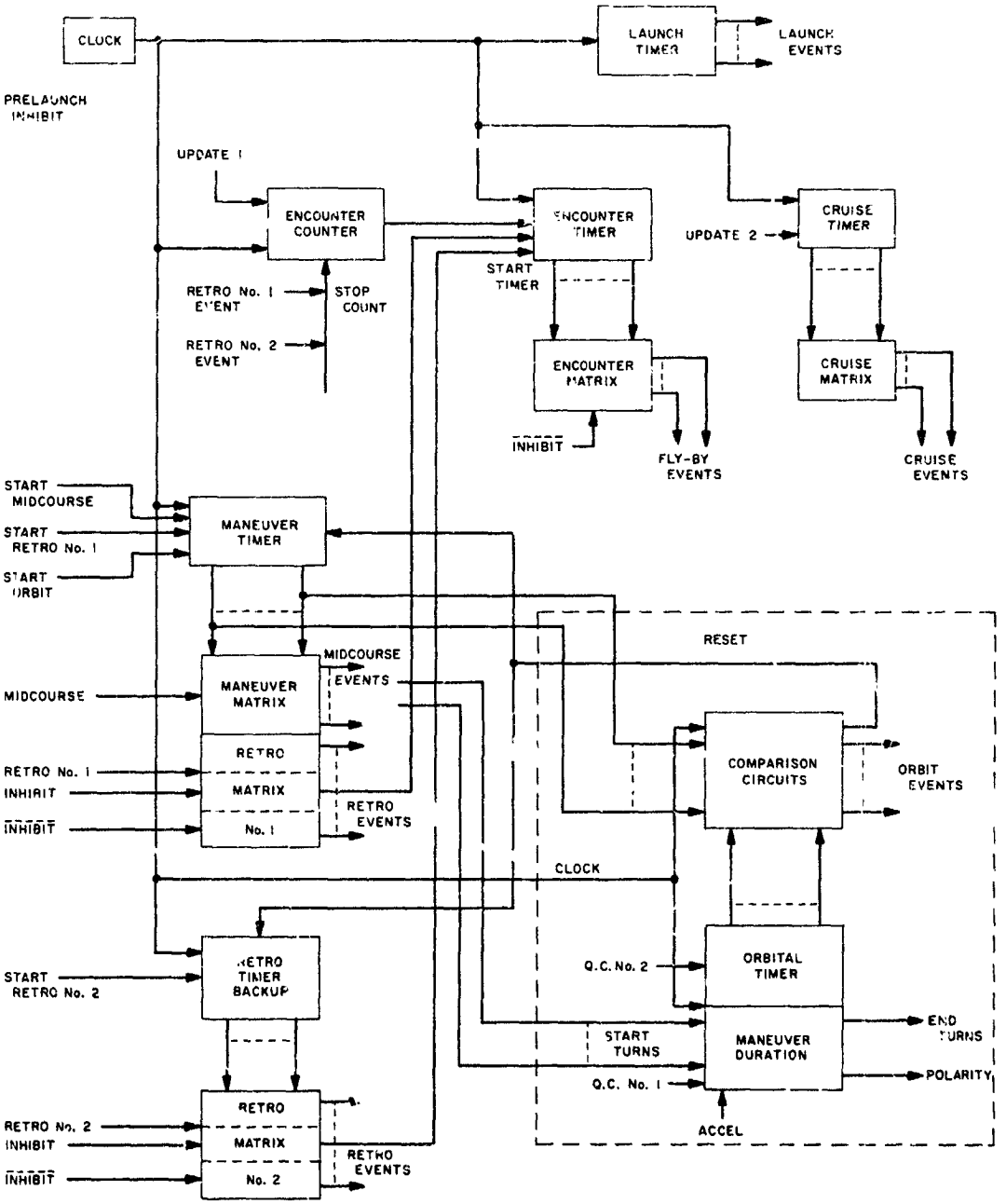


Figure 11-8. Timer-Oriented CC&S, Functional Block Diagram

b. Memory-Oriented Design

Another mechanization which apparently promises a reduction in weight, volume and number of semiconductors, is that of a special-purpose digital "computer." A computer only in that its organization is computer-like, i.e., contains an accumulator, instruction register, random-access memory, etc., it is severely limited in its computing capability. It can perform only addition, magnitude comparison and transfer of program control. The device is designed to carry out only sequencing functions such as those described in Subsection B.1. Its discussion is included here in order to emphasize the characteristics of a generic class of devices of which it is a member. To distinguish it from the "timer-oriented" subsystem, this device is characterized as "memory-oriented." Some of the interesting features of its class are:

1) Mission independence. The identical design can be used in a variety of missions.
2) Places a burden on programming. A large number of programs, one or more for each launch date and as many as possible for predictable non-standard eventualities, should be provided. An executive routine for choosing, loading and transmitting the proper programs may be advisable.
3) Exhibits a high degree of versatility.

Spacecraft control signals are derived within a memory-oriented sequencer by an iterative time-keeping routine. Such a routine in its general form appears in Figure 11-9. The R-F Interrupt subroutine for initial program loading and storage of quantitative commands is wired into the machine. The remainder of the routine is contained in a non-destruct-read-out core memory. Once loaded, this routine is alterable through the R-F Interrupt feature. A functional block diagram of a sequencer capable of executing this routine is shown in Figure 11-10. The design is based on a fast word-parallel/bit-serial associative memory in which the comparison between the current time and all event times is accomplished. Another portion of the central memory contains locations which are directly accessible to the registers and part of the input buffer. They are used for storage of register contents during temporary loss of primary power, and for storing various sense and control bits.

This design, employing for the most part state-of-the-art techniques, demonstrates the advantages which memory-oriented sequencers have over timer-oriented designs. Table 11-5 compares estimated weight, power and volume for the two subsystems considered here.

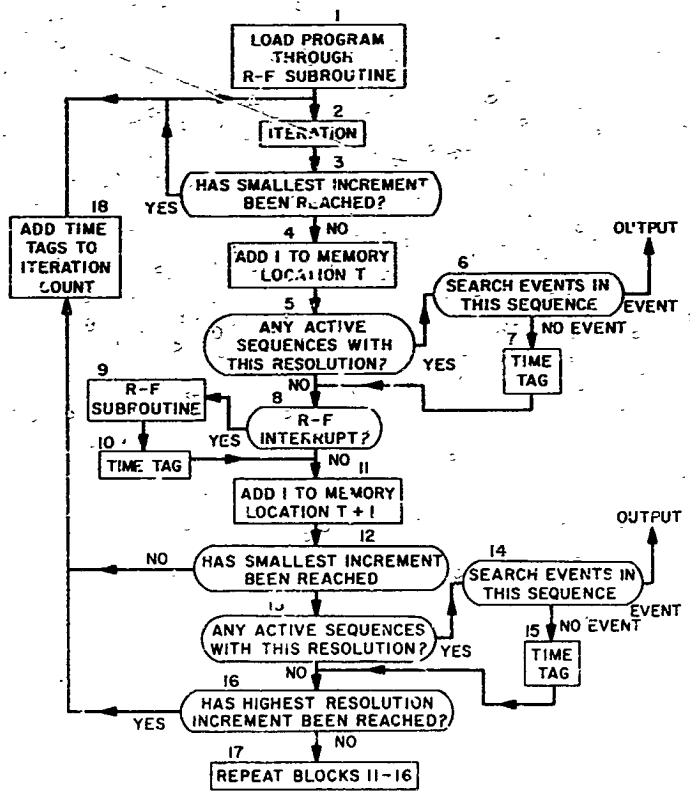


Figure 11-9. Time-Keeping Routine

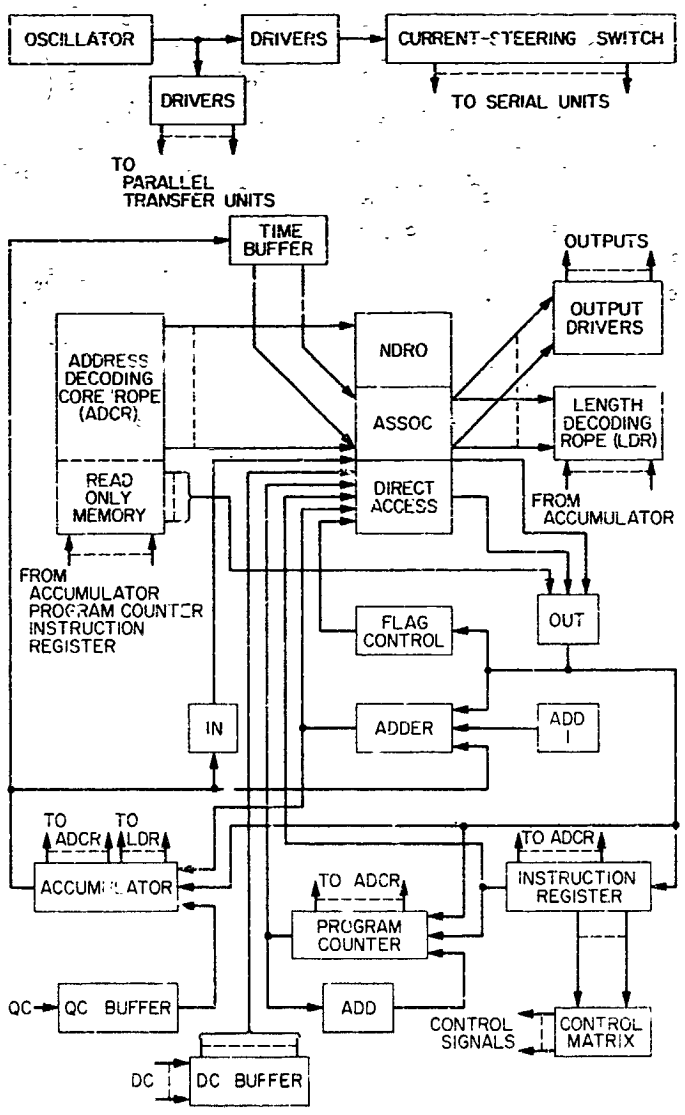


Figure 11-10. Memory-Oriented CC&S, Functional Block Diagram

Table 11-5. Comparison of Weight, Power and Volume

	Timer-Oriented	Memory-Oriented
Weight	22 lb	14 lb
Power	14 w	15 w
Volume	600 cu in.	400 cu in.

On the basis of these figures and in order to take advantage of the more attractive capability of the memory-oriented approach, it is suggested that future Mariner 1969 Orbiter efforts be directed toward utilizing a central memory in the spacecraft sequencer subsystem.

C. ELECTRICAL POWER

The power system is required to maintain the desired operation of the spacecraft by providing electrical energy necessary for all other systems and this energy must be provided in a controlled form and at discrete power levels. In addition, this electrical energy must be obtained from a source which is compatible with other spacecraft systems, provide a maximum power for a minimum size, weight, cost, and development time and a maximum reliability consistent with the flight constraint requirements.

Parametric studies on power systems have been performed to determine their feasibility in satisfying the requirements of the Mariner 1969 orbital mission. From these studies, a selection of power source, storage, and conversion can be made for the mission requirements. A principal objective of the parametric study was to establish operational and design versatility so that, in the event mission constraints or subsystems requirements changed, a reevaluation would produce a power system consistent with the new requirements. A specific design utilizing solar panels and batteries is presented herein indicating the size of a power system using solar panels for a specific set of constraints. It is important to emphasize that any design presented is specific for the constraints given but is not the only mechanization possible. The system can be mechanized differently as will be shown. Changing of certain of the design constraints will require a complete redesign.

1. Study Summary

Solar photovoltaic systems appear to be the most attractive for the Mariner 1969 orbital mission as now conceived. By use of P/N silicon cells, a system designed for 90 days in a Mars orbit can provide a raw power of 600 watts of electrical energy for 127 square feet of active panel area. All of this power is not available to the spacecraft, however. For one mechanization, whereby a period of one hour is set aside for eclipse of the Sun during each 14 hour orbit, 400 watts of power would be available for the spacecraft systems. A specific design is presented for the constraints of this study and will show in detail the effects of variations in the system mechanization and constraints.

Solar thermionic power sources also show promise of providing the required amount of electrical energy. However, certain aspects of this primary source of power negates its use from present considerations. For a specific power level, this system is heavier and less compact in size as compared to photovoltaic systems. The number of developmental problems are numerous and in areas which may affect the reliability and scheduling of the system.

Radioisotopes, used to provide thermal energy for thermoelectric and thermionic devices, have also been studied. Thermoelectric generators developed from this study indicate that they are not feasible at this time. Primarily, the rejection of this power source is

based upon doubtful radioisotope development, radiation shielding and weight per unit of power. The parametric study and the results from the study for a specific design are classified and will not be made a part of this document. Additional information will be contained in a document which will be made available at a later date.

2. Solar Photovoltaic Power System for Mariner 1969

The designed system in this section is a specific mechanization which is applied to determine the size of a solar panel-battery system which will provide the electrical power required to operate the spacecraft within the constraints listed in Table 11-6. In addition, several alternate modes of operation are studied in anticipation of possible growth of communications systems and to show the effects of these alternate modes upon the sizing of the system

Table 11-6. Spacecraft Electrical Power Constraints

Number	Constraints
1.	Orbit life of 90 days.
2.	Science to consist of all proposed cruise science instruments, one TV, and one Mars Scanner as planet science.
3.	Two midcourse maneuvers.
4.	Orbit injection maneuver requiring 3 hours of non-solar orientation including reacquisition time.
5.	Orbital period from 26 to 43 hours.
6.	No science measurements during first orbit.
7.	Maximum Sun-Mars distance is 1.45 a.u. (216×10^6 km).
8.	No Sun or Canopus occultation occuring during 90 day orbital life. (Gyros off in orbit.)
9.	Cruise science on continuously during sunlit portion of orbit.
10.	Required planet science data occurs near periapsis, is 2 hours in duration, and this time is independent of orbital period.
11.	Communications RF power: 10 watts.
12.	Spacecraft raw power requirements are as shown in the power profile.
13.	Maximum solar array area limited to 127 ft^2.

Using the constraints listed in Table 11-6, mission power profiles were developed as shown in Tables B-1 and B-2 in Appendix B and summarized in Table 11-7. These profiles are based on power requirements as presently known to be required by the various systems. The subsystem most likely to require a larger power demand would be communications, which may find it desirable to utilize a 20-watt transmitter. To show the power penalty in this event, the second power profile in Table B is presented and used throughout the study. In any event, these profiles are only representative at this time and the effect of any change can be obtained from the results to be shown here.

In sizing the power subsystem, the two most important events during the mission will be shown to be the Mars injection maneuver and the orbital phase. During the orbital period, the power must be derived from the solar panels as a primary source of electrical power and, therefore, the panels must be designed to provide this power. It is, therefore, necessary that the panels be designed for the amount of solar energy available in Mars space and the variation of this solar energy be recognized and presented as a limiting factor in the panel design. During the injection maneuver, as in all midcourse maneuvers, the spacecraft will not be oriented with a Sun-line angle and the spacecraft power will have to be provided by a secondary energy source. This source will be a battery which will provide the necessary energy required by the spacecraft during the maneuver and until the Sun-line is reacquired. The primary significance of the injection maneuver is the length of time anticipated to perform this maneuver. As pointed out in Table 11-6 this time is assumed to be a maximum of three hours.

The mission power profile summary as shown in Table 11-7 is a breakdown of the raw power requirements for spacecraft operation during critical periods. This power requirement does not reflect the power necessary to recharge the battery nor the additional power required from the primary source to remove the system from a marginal operating condition. The power required from the primary power source to recharge the battery is dependent upon the method of operation of the spacecraft, orbit parameters such as orbital period and length of orbital Sun occultation time, and the type of battery used; this will be enlarged upon later. In addition to designing the primary source for spacecraft raw power requirements and battery recharging, some over capacity is required to prevent marginal operation of the subsystem. To prevent this, a total of 23.4 percent increase in raw power is required. See Appendix B for the derivation of this value.

This overcapacity is utilized expressly to prevent marginal subsystem operation and no contingencies are included or anticipated for other system designs or operational unknowns. In place of overdesigning to anticipate design and operation unknowns, it is preferable to point out to the systems management, alternate operational modes which can be attained to achieve system operation in the event of power level requirements greater than those assumed.

Table 11-7. User Power Requirements (Watts)

	Injection Maneuver	Apoapsis	Periapsis	Eclipse
10 Watt System				
2.4 kc Inverter	192	180	232	192
400 cps Inverter	19	-	-	19
Main Regulator	260	225	286	260
RF Power	47	47	47	47
Heater Power	10	10	10	10
TOTAL	357	300	365	337
20 Watt System				
2.4 kc Inverter	183	182	234	183
400 cps Inverter	19	-	-	19
Main Regulator	250	228	286	250
RF Power	85	85	85	85
Heater Power	10	10	10	10
TOTAL	367	344	405	367

Table 11-8 presents a summary of the raw power requirements from the solar panels for various modes of operation. The Array Power is that power which is required to provide the spacecraft power as called out in the power profile and the additional power required to charge the battery during orbit. The Array Power (margin included) is the total power required from the solar array to provide spacecraft power, to recharge the battery, and to provide the power overcapacity to prevent marginal operation as discussed above. Also indicated in the table are the sizes of the solar panels in area and weight when using P/N cells, N/P cells, and N/P thin cells. In addition, six separate modes of operation are summarized indicating the power and size characteristics for possible variations from the nominal.

Mode I represents the nominal design as specified in the constraints of Table 11-6. For a 26-hour orbit with no Sun eclipse time, the panels must provide 385 watts of raw power of which 300 watts is allocated to the operation of all spacecraft systems in orbit. This power represents the load encountered throughout the orbit without the inclusion of the planet science instruments. The planet science is considered a peak load and this is derived from the energy stored in the battery. Since energy storage is required during transit to Mars for periods of non-solar orientation, the battery should also be utilized in orbit to reduce panel requirements and provide energy for possible failure modes. If the panels were designed to provide for the peak load the array power would increase to 450 watts with margin and the panel area for the P/N cells would increase to 94 square feet. The additional weight would be 18 pounds and no

Table 11-8. Solar Panel Sizing and Power Requirements

Operational Mode		10 Watt System			20 Watt System		
		I	II	III	IV	V	VI
Power at Periapsis	Watts	365			405		
Power at Apoapsis	Watts	300			344		
Power in Eclipse	Watts	337			367		
Peak Load Period	Hours		2			2	
Eclipse Period	Hours	0	1	2	0	1	2
Array Power	Watts	310	339	365	354	383	432
Array Power - Margin Included	Watts	385	421	454	440	477	539
Panel Area P/N	Ft^2	80	88	95	92	100	112
Panel Weight	Pounds	104	114	123	119	130	146
Panel Area N/P	Ft^2	84	92	99	96	104	117
Panel Weight	Pounds	109	119	128	124	135	152
Panel Area N/P Thin	Ft^2	87	96	103	100	108	122
Panel Weight	Pounds	102	107	120	117	127	143

saving would be realized in battery weight so that the area and weight saving justifies the use of the battery for peak loads.

The values obtained in Table 11-8 assume the use of a silver cadmium (Ag Cd) battery with a recharge efficiency of 44 percent (including charge control losses). The derivation of the method of subsystem analysis is contained in Appendix B and indicates a reduced power requirement for silver-zinc (Ag Zn) batteries having a recharge efficiency of 56 percent. However, the value of 44 percent is a worse case efficiency and this value can be expected to be increased. It is significant to stress this point since the array overcapacity required for charging of the battery is a strong function of the battery efficiency and a one percent increase in this value could produce a two and one-half percent decrease in panel area.

Modes II and III also consider the nominal system with the exception that one and two hours of Sun eclipse, respectively, are considered. In the event of Sun eclipse, the full spacecraft load must be carried by the battery power. To reduce this load, the full science complement is switched off and the attitude control gyros are on to stabilize the spacecraft. Although this produces a reduced spacecraft load, Table 11-8 indicates a larger power requirement as the eclipse time increases. This is brought about by a larger power required to replace the charge in the battery which has been drawn upon during the non-Sun period.

Modes IV, V, and VI correspond to the first three except a 20-watt communications transmitter replaces the 10-watt unit. A summary power profile is shown in Table B-2 in the Appendix. Table 11-9 summarizes the various operational modes or variations of operation from the nominal. These are by no means the only variations obtainable and a further study might indicate some operational modes which might reduce the required battery or panel size. As an example: By requiring operation of science on alternate orbits rather than every orbit, the panel area or power required would be reduced.

Figures 11-11 and 11-12 indicate the variation in solar panel area as a function of power and Sun-Mars distance for two types of photovoltaic cells. Superimposed on these graphs are the power levels from Table 11-8. As can be seen from the figures, an increase in solar distance reduces the energy available, thus increasing the area of the array to maintain a given power requirement. On the other hand, for a selected power requirement and array size, the solar distance must be restricted (which in turn limits the operational life of the spacecraft) because the planet eccentricity is great enough to produce a change in the solar distance to a maximum of 1.61 AU after 6 months in orbit from 1.45 AU in a three month orbit. The horizontal line at the 100 square foot level indicates the operating level for Mode V or spacecraft operation using a 20-watt transmitter and allowing one hour of eclipse time using P/N cells. As shown in Figure 11-12 this mode cannot be achieved with N/P cells. From both figures it is obvious the mission as defined in the constraints can be supplied the required power and if 100 square feet of panel area is allotted, additional operational modes can be performed. However, if the panel area is restricted to the values shown in Table 11-8 for Mode I, the nominal can be achieved, but there is no operation to fall back to in the event of system degradation.

As pointed out earlier, no degradation allowance is taken in the system design. It is for this reason that a panel area of 100 square feet is selected for the nominal case. By this selection and if P/N cells are used, referring to Figure 11-11, enough power will be provided by the

Table 11-9. Optional Modes of Operation

Mode Number	Mode
I	Spacecraft Operation with Given Constraints.
II	Occurrence of a 1 Hour Eclipse.
III	Occurrence of a 2 Hour Eclipse.
IV	Use of 20 Watt RF System and 2 Tape Recorders.
V & VI	20 Watt System with 1 and 2 Hours Sun Eclipse.
1-6	Same as All of the Above With No Cruise Science. Loss of Canopus Reference.

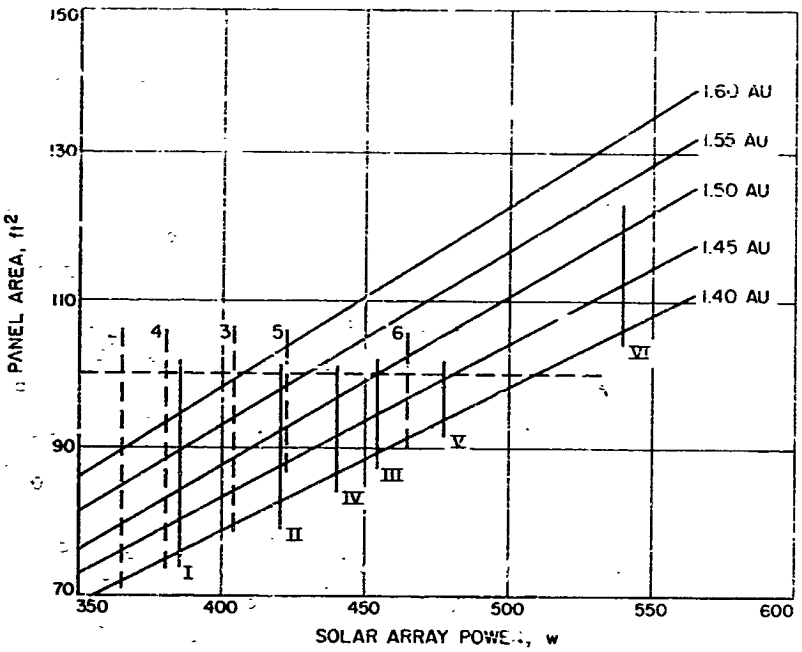


Figure 11-11. Orbital Power Characteristics Using P/N Silicon Cells

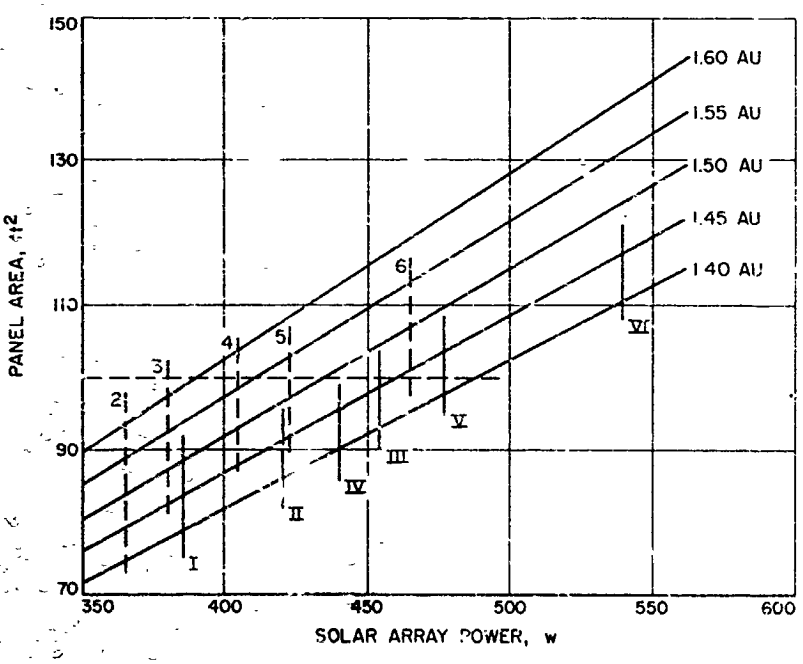


Figure 11-12. Orbital Power Characteristics Using N/P Silicon Cells

panels to operate in a Mode V condition. It has the additional advantages of providing other and lower power-level operational modes in the event of a net power shortage. Because of this operational versatility, no additional contingency factors need be applied to the subsystem sizing for orbital operations.

As shown in Figures 11-11 and 11-12, system deficiencies (by way of orbit injection whereby the solar distance is larger than anticipated) may be compensated by dropping to a lower power mode. In the same operational manner the life of the spacecraft in orbit can be extended past the required three months. The same procedure can be used to determine a secondary mode in the event of panel degradation caused by solar flares, micrometeoroids or shorted cells. In addition, cycling of planet and cruise science can be performed or cycling of the gyros, which are now considered off continuously, would produce additional operational modes between those of I and V on Figures 11-11 and 11-12.

Table 11-10 summarizes the major parameters of a power subsystem which will perform the mission required and specified in the constraints of Table 11-6. The table also includes a recommended set of parameters and some specific reasons for this selection. It is to be noted that the panel sizes are based on the use of F/N silicon solar cells. As will be shown later, these particular cells are not the only ones available. the final selection of the type of silicon cell to be used will rest upon several factors not yet defined.

The sizing of the battery which is stated in Table 11-10 as 2100 watt-hours capacity is based primarily upon the three hour injection maneuver and the power required by the spacecraft during this lengthy maneuver A full discussion on battery sizing is presented in Paragraph 4 and in Appendix B.

A block diagram of the primary elements of the power subsystem is shown in Figure 11-13. The only conversion equipment necessary is that shown. The function of the main regulator is to provide a regulated voltage output to the two inverters from two different source voltages. All system operation is performed by using a 2.4 kc square wave voltage except the gyros which require 400 cycle three phase voltage. The system is provided with complete redundancy for the regulator and 2.4 kc inverter. This is provided through failure sensing circuits which switch to the redundant unit only when the failure is localized to that unit's counterpart. Power switching and synchronization are not shown here, but covered in Paragraph 7.

Table 11-10. Solar Panel-Battery Subsystem Major Parameters

System Size	Panels P/N	80 Ft^2	104 lbs
	Battery Ag Cd	2100 W-H	78
	Electronic Conversion		58
		TOTAL	240 lbs
Spacecraft available power at periapsis:		256 watts @ 1.45 AU	

∴ Proposed system is feasible with 80 Ft^2.

Recommended System:

A Panel Area of 100 Ft^2 is recommended and will provide:

1. Studies of alternate implementation.
2. Contingencies for:
   a. Panel degradation
   b. Turn on of gyros in orbit
   c. Eclipse time operation
   d. Operation for greater than 90 days
   e. Larger RF and data rates

System Size	Panels P/N	100 Ft^2	130 lbs
	Batteries	2100 W-H	78
	Electronic Conversion		58
		TOTAL	266 lbs
Spacecraft available power at periapsis:		326 watts @ 1.45 AU	

3. Sizing of Primary Power Sources

a. Solar Panels

Sizing of the solar panel array, after selection of the photovoltaic cell has been made, is dependent upon the load to be carried during the orbital period if the load is comparable to or greater than the load in Earth space. As the solar distance increases, the solar energy decreases reducing the nominal specific power output of the solar cells. Although the load is the dominant criteria, this can be defined by selection of an optimum operational mode, by limiting distance, and by defining the maximum allowable panel weight. Figure 11-14 shows how the solar intensity falls off as the Sun probe distance increases. After 90 days in orbit, the solar intensity is reduced from 73 mw/cm^2 to 65 mw/cm^2, a reduction of 11 percent.

As shown in Figures 11-11 and 11-12, for a constant power load the panel size is dependent upon the Sun probe distance. As pointed out in the last paragraph, this distance

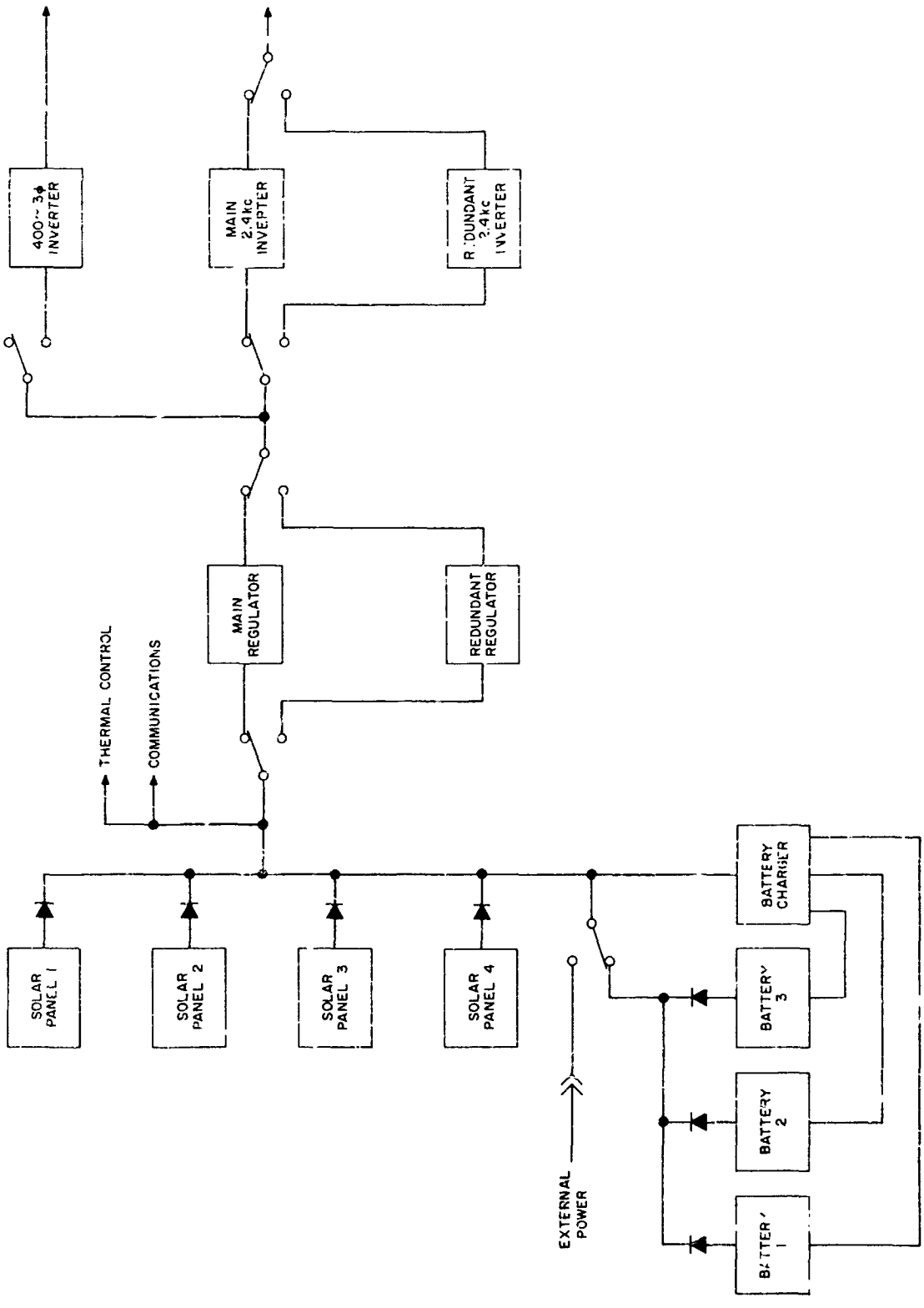


Figure 11-13. Power Block Diagram with Redundant Regulator and Inverter 58 lb (Conversion Plus Case Plus Harness)

must be limited and clearly defined in order to size the panels. If a range of distance is anticipated the panel must be sized for the worst case distance or, if this makes the size prohibitive, reduce the average demand.

The panel weight with respect to the solar cells and the associated hardware is a constant and dependent only upon the panel area. The structural weight of the panel is a variable and dependent upon the method of construction, and the expected stress applied to the panels. For the presently available cells, a figure of 0.45 lbs/ft^2 is to be realized for the solar cells, zener diodes, connectors, and hardware. It may be possible to reduce this value to 0.38 lbs/ft^2 by elimination of the zener diodes (which limit the panel output voltage). This can be done by careful design of circuitry within the conversion equipment. In addition, a new thin N on P photovoltaic cell is in the development stage at JPL which has a potential of providing an array with a weight of 0.32 lbs/ft^2.

Determination of panel size by choice of operational mode has been presented earlier. A significant saving in panel area and weight can be achieved by the use of the secondary source during orbit to provide peak loads for short durations. The total system weight saving may be negligible due to the required increase in battery weight.

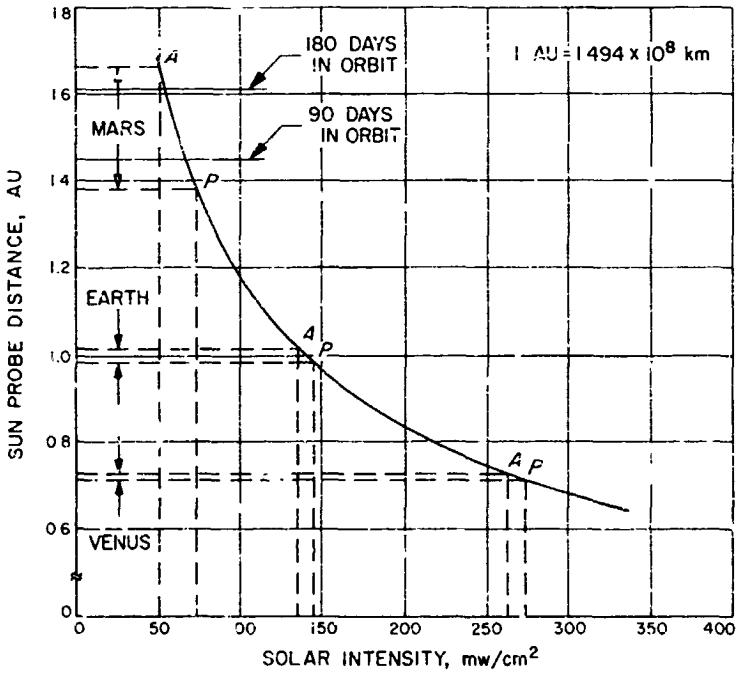


Figure 11-14. Solar Intensity as a Functional Distance From the Sun

Selection of the type of solar cell to be utilized in the design is predicated on system, economic and physical principles. From Figures 11-11 and 11-12, it can be seen that a four percent saving in panel area can be obtained by using P/N rather than N/P cells. However, the N/P cell offers a higher resistance to degradation. In addition, the N/P cell is now being manufactured in quantity whereas the P/N cells are no longer being produced except on special order.

During the 1969 orbit opportunity, the activity of the Sun in producing solar flares is expected to be near a maximum. The magnitude of electron and proton flux will increase, but the amount of this increase is unknown at this time. Figure 11-15 shows a comparison of the effects of electron flux damage to P/N and N/P cells. At low levels of flux the P/N cell provides an efficiency which is higher by more than six percent. As the electron flux rises above 2×10^{12} electrons/cm^2 the P/N cell degrades at a much faster rate than the N/P and the efficiency of the N/P becomes greater by a factor in excess of 25 percent. No information is available on proton flux damage to P/N cells, but it is felt the curves approximate those of Figure 11-15. In any event, the degradation is significant enough that an investigation must be pursued in this area. Although a design margin factor of 11 percent is included in the subsystem design, this may prove to be inadequate if P/N cells are used and if the electron and proton flux from solar flares is large. Because the value of flux is unknown at this time, the design of the solar panels cannot neglect use of N/P cells. Use of P/N cells cannot be negated in view of the reduced panel area which will also provide a reduction in weight (because both cells exhibit the same weight per unit area).

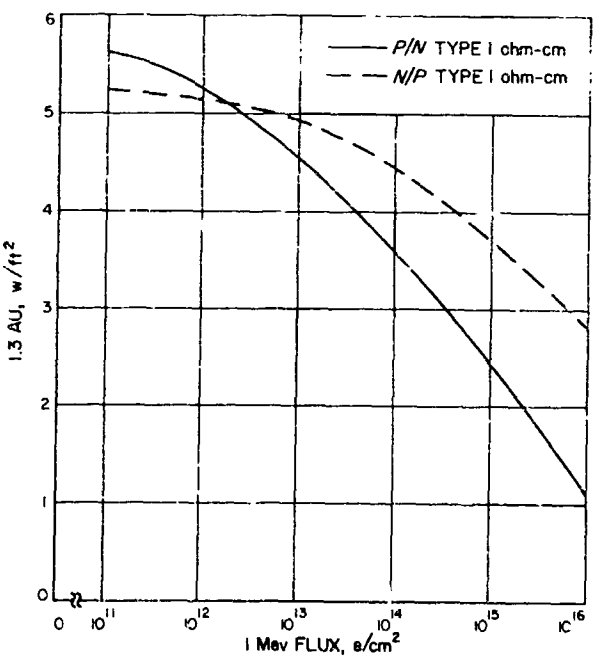


Figure 11-15. Panel Degradation Expected From a Dose of Integrated Electron Flux

In sizing solar arrays, uncertainties must be established so that the minimum power of the array can be clearly defined. Measurement errors and Van Allen belt radiation damage are the primary factors for which a total of 7.1 percent contingency in panel design is taken. This can be broken down as shown in Table 11-11.

The curves shown in Figure 11-16 reflect the minimum specific energy as a function of the available solar intensity. The curves are derived assuming free space radiation and a panel α/ε of 0.50 for panel temperature considerations. The calculation of solar intensity as a function of Sun probe distance assumes the solar intensity at one astronomical unit (Au) is 140 mw/cm^2 and the inverse square law is applicable.

In addition to the standard N/P and P/N cells mentioned above, a new N/P cell is in the development stage which has the potential of providing a reduction of 30 percent in the weight per unit area of solar panels. The main disadvantage to this type of cell is the lower efficiency, 7 percent less than the efficiency of a P/N cell and 3.5 percent less than that for a standard N/P cell. This means that although a weight reduction can be achieved, the panel area would increase (see Table 11-8)

b. Solar Thermionic Systems

The following information is a summary of a parametric study performed to show feasibility of solar oriented concentrators used to collect thermal energy for conversion to electrical energy by thermionic generators. For the study, a range of power levels from 200 to 800 watts were analyzed; however, the lower levels are more pertinent to this study and the discussion will show that serial use of systems will provide the larger powers.

The determination of the required solar concentrator area is based on a specific power of 4 watts/ft^2 and a minimum solar intensity of 54 mw/cm^2 which would occur in Mars space.

Table 11-11. Contingency Factors in Panel Design

Percentage	Factor
1.0%	Solar measurements standardization panel temperature uncertainties
3.0%	a) Accuracy of α/ε measurement
2.0%	b) Non-Isothermo panel temperature in space
3.5%	Table Mountain, California, Sunlight measurements
5.1%	RMS total
2.0%	Van Allen radiation

The power required to operate each converter in a thermionic generator is 350 watts and the number of concentrators is limited to a maximum of four.

Based on these considerations, the total solar collector area can be determined as follows:

$$At = \frac{1.2\ Po}{\text{Specific Power}} = \frac{1.2\ Po}{4} = 0.3\ Po\ ft^2 \qquad (1)$$

where Po is the unregulated power output of the thermionic system.

From the results of this equation, the number of concentrators can be determined for a particular power level and concentrator diameter. For a 400 watt requirement, the total area required would be 120 ft^2 and increases by 30 ft^2 for each 100 watts of additional power.

Mirror sizes, ranging in diameter from 4 feet to 9.5 feet and a rim angle of 45 degrees are used as a basis for selection. The rim angle of 45 degrees is for convenience and existing mirror masters with this rim angle, capable of producing all the above diameters, are in

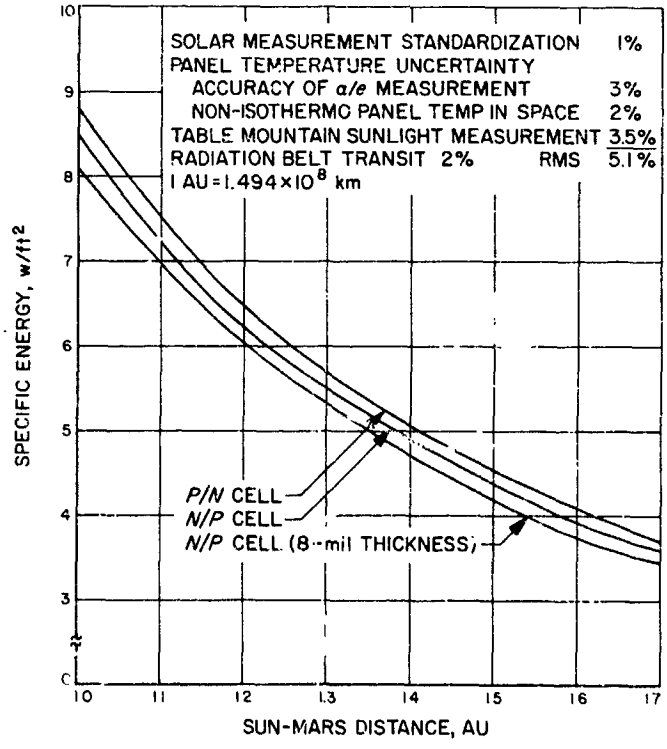


Figure 11-16. Decrease in Solar Panel Specific Energy as a Function of Sun Distance

existence. Figure 11-17 is used to determine the thermal energy available for a specified solar intensity and mirror efficiency. From this, a family of curves are generated as in Figure 11-18 for determining the mirror diameter. Also, a family of curves for determining the optimum diameter of the generator cavity aperature is obtained from the thermal power requirements as shown in Figure 11-19.

For the mirror diameters considered, the 9.0 foot diameter approaches the optimum for power levels of 200 watts or greater. Use of this diameter for a 800 watt system satisfies the limit of four concentrators and utilizes the maximum number of converters (6) per generator. This would provide a generator with two parallel sets of three converters in series for redundancy and reliability or six series converters for high voltage operation.

All mirror sizes less than 8.0 feet are eliminated from this analysis since they would require an excess number of concentrators to provide the power and as the size decreases the number of converters per generator decrease to an undesirable, unreliable number. If, however, the power level is limited to 400 watts or less, it may be significant in spacecraft design if the diameter is reduced and more concentrators are used.

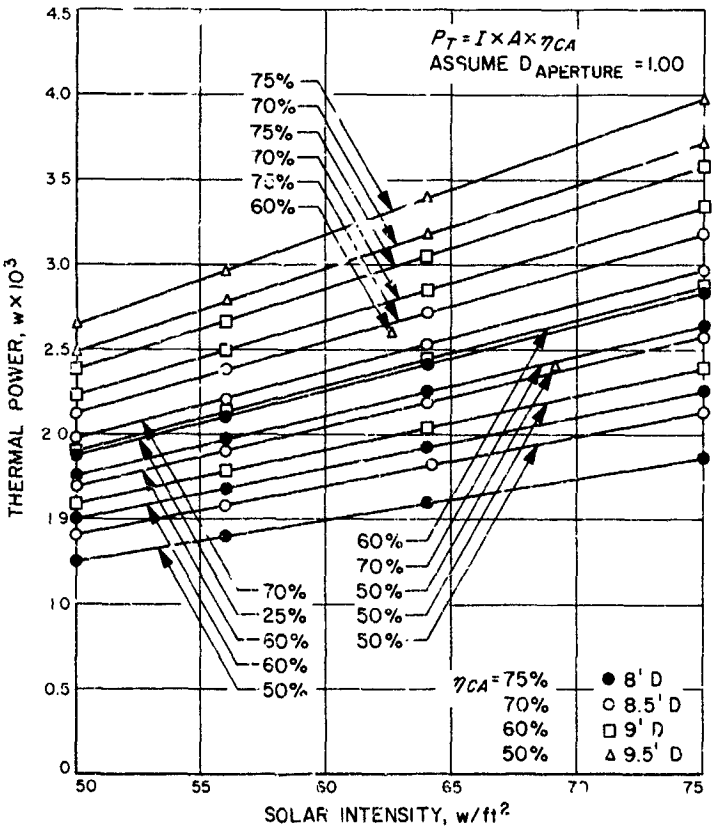


Figure 11-17. Thermal Energy Available Per Unit of Solar Intensity

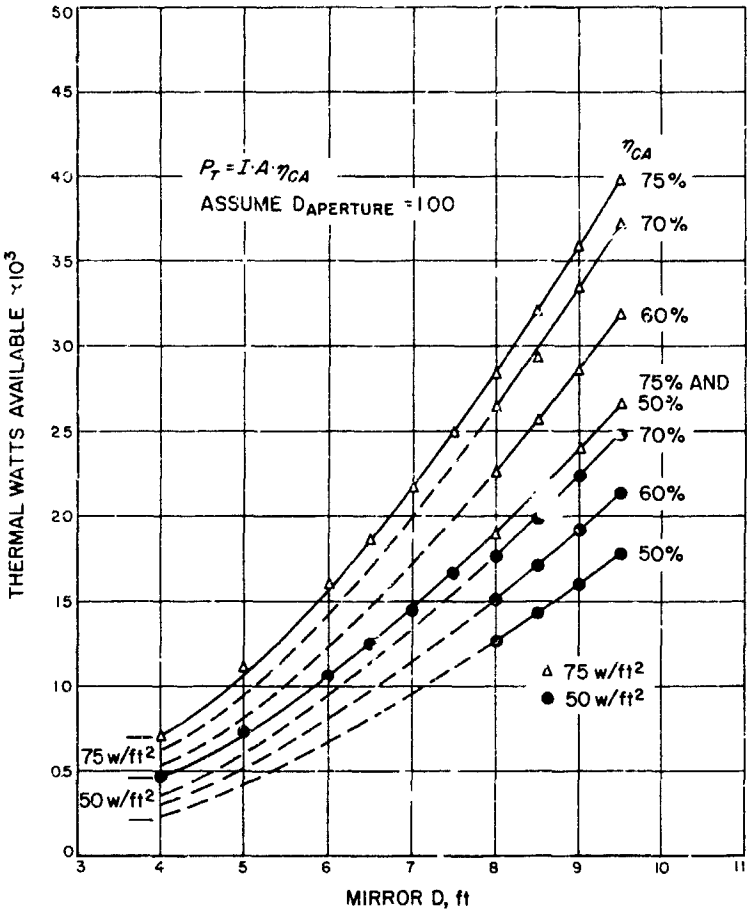


Figure 11-18. Thermal Energy Collected as a Function of Concentrator Diameter

In determining the weight of concentrators, the material used for fabrication must be considered. At present, most concentrators are made with nickel which has a high density. The techniques of manufacturing are well known using this material; however, weight and magnetic requirements dictate the use of a material such as aluminum or berylium. Berylium mirrors are not feasible at this time so that aluminum mirrors are anticipated. From Figure 11-20, a 9.0 foot diameter aluminum mirror would weigh 26 pounds.

The thermionic generator is a low voltage, high current source of energy. Therefore, the use of a single converter, however desirable from some points of view, is impractical for high-power outputs due to all the problems associated with the transport of high currents. It is, therefore, desirable to connect several converters in series to increase the voltage to values between 3 and 6 v. Such voltages will avoid the excessive magnetic fields, the extra heavy conductors, and the excessive voltage losses associated with the high-current, low-voltage conditions, and will alleviate and improve the operation and efficiency of the dc-to-dc conversion equipment.

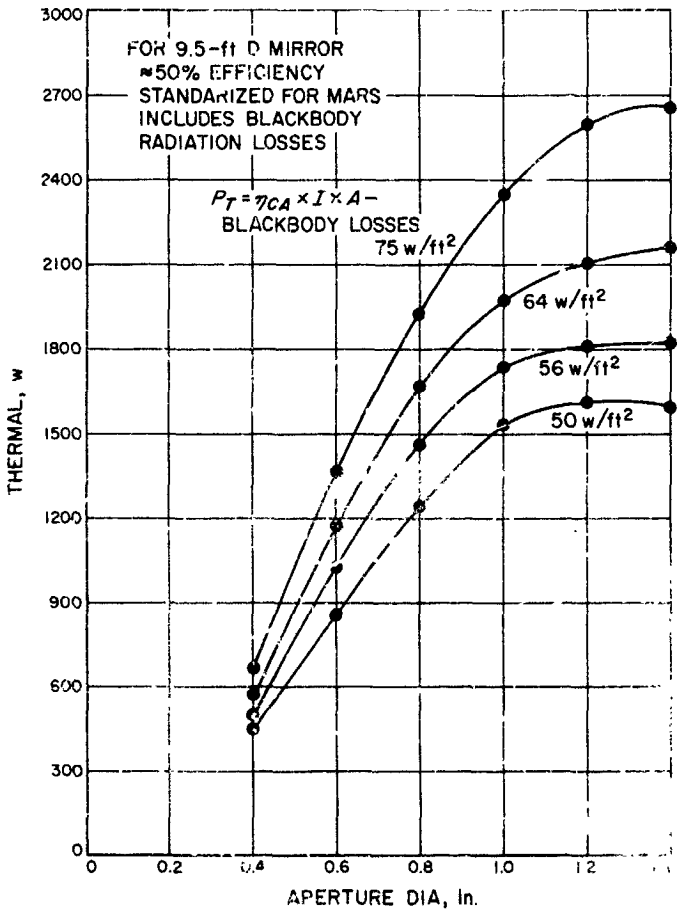


Figure 11-19. Thermal Energy as a Function of Generator Cavity Aperture

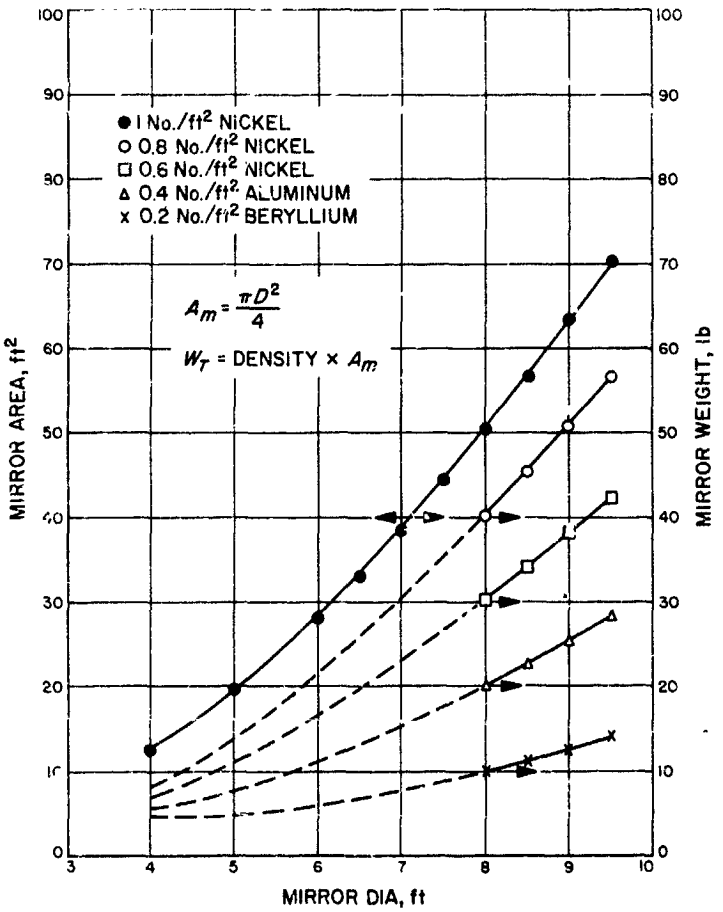


Figure 11-20. Solar Concentrator Weight as a Functior of Diameter

Thermionic converters for the generators are limited to those having an emitter area of 2.5 cm^2. Generators using 4, 5, and 6 converters are used in this analysis to determine the optimum total emitter area to provide a specific generator output power. Since the power density is a function of the generator output power and the emitter area available, this power density can be determined. (See Figure 11-21.) Power density values on the order of 20 w/cm^2 are presently available and higher values are to be expected. As a result, larger power levels for a specific emitter area can be achieved. Selecting 6 converters as optimum, a total emitter area of 15 cm^2 is available. The 6 converters can be connected all in series to provide 4.2 volts and various other configurations dependent upon the voltage and desired current levels required (each converter operates at 0.70 volts). Figure 11-21 indicates that for a six generator converter, 9 foot concentrator and a power demand of 210 watts, a generator with a power density of 14 mw/cm^2 would be adequate. This converter is available today.

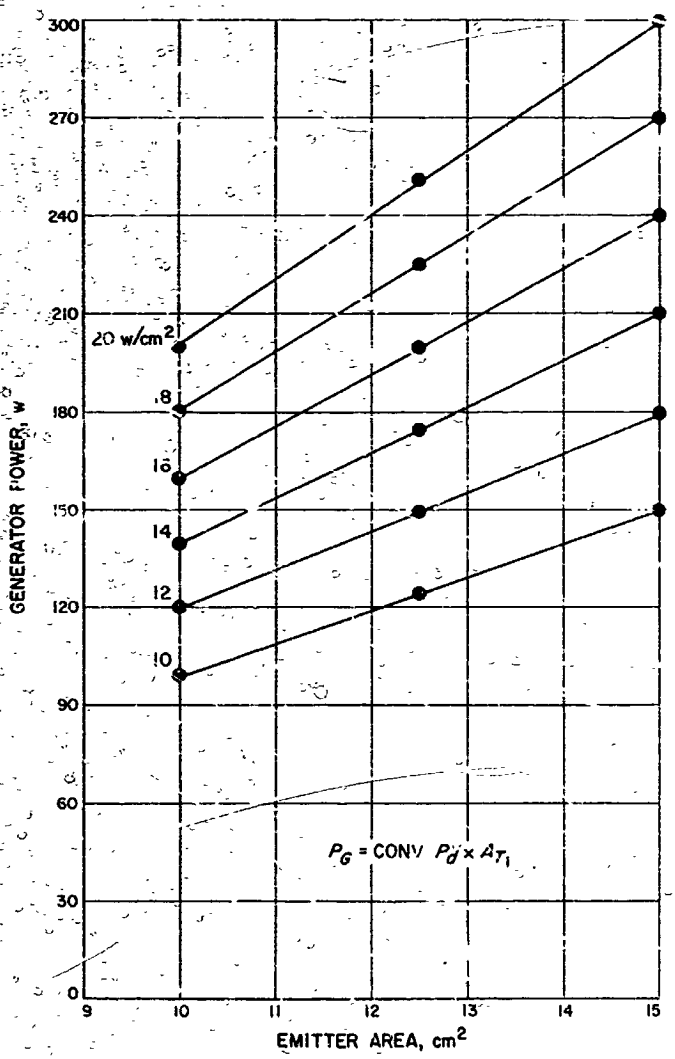


Figure 11-21. Thermionic Generator Power Output as a Function of Energy Density of the Converters and the Total Emitter Area Available

Table 11-12. Summary List of Parameters

Collector		Converter	
Size	9.0 ft diameter	Emitter Area	2.5 cm^2
Reflectivity	90%	Emitter Material	Rhenium
Slope Error	±4 minutes	Collector Material	Molybdenum
Shadow Factor	-5%	Spacing (electrode)	0.003 inch
Density	0.4 lb/ft^2	Temitter	1700°C
Weight	26 lb	Tcesium	345°C
Efficiency	70%	Tradiator	385°C
Material	Aluminum	Vo	0.70 volts
		Efficiency	15%

Generator		Tolerances:	
Aperture Size	1.25 inch	System Efficiency	±10%
Cavity Temperature	2300°K	Orientation Accuracy	±7%
Converters in Series	3		
Vo	2.1 volts		
Total Converters	6		
Efficiency	12%		

Table 11-12 above is a summary list of the various parameters for the components of the solar thermionic system.

As in the case of photovoltaic systems, energy storage is required during periods of non-orientation of the solar concentrator.

A method of thermal energy storage is being investigated whereby the latent heat of fusion of various materials is used to store thermal energy until needed. The material is heated to a molten state during the solar orientation period and the material releases this energy during non-solar periods to provide thermal energy to the emitters of the thermionic converters. The development of this process is proceeding but will not be available for 1969.

Energy storage by electrochemical methods remains the only type of reliable dark time energy. The basis of selection is the same as for the solar cells and the battery discussion is contained in the next section.

Because of the low voltage obtainable from this system, the conversion problem is more extensive. See Paragraph 5 for a discussion on the conversion equipment.

Due to the sensitivity of the thermionic converter emitters to temperature changes and the variation of the output power with this change, it is necessary to ensure correct orientation of the solar concentrator to the Sun. It has been determined that to maintain 90 percent of the electrical energy received for exact orientation, the maximum error in orientation must be ±14 minutes of arc. Figure 11-22 shows the fall-off in power for misorientation of the concentrator to the Sun in minutes of arc. The curve is based on a concentrator having a geometric slope error of less than ±4 minutes of arc and a cavity aperture in the generator with a diameter of one inch.

A three percent reduction in power from misorientation is not significant, so that to maintain no greater loss, the accuracy of orientation would have to be ±7 minutes of arc to the true Sun line. This may be difficult to achieve by attitude control methods, necessitating vernier systems for each concentrator for control. This also requires a high degree of accuracy in concentrator manufacture to keep the geometric slope error minimized.

Finally, a system sized for a requirement of 400 watts would have the characteristics as shown in Table 11-13.

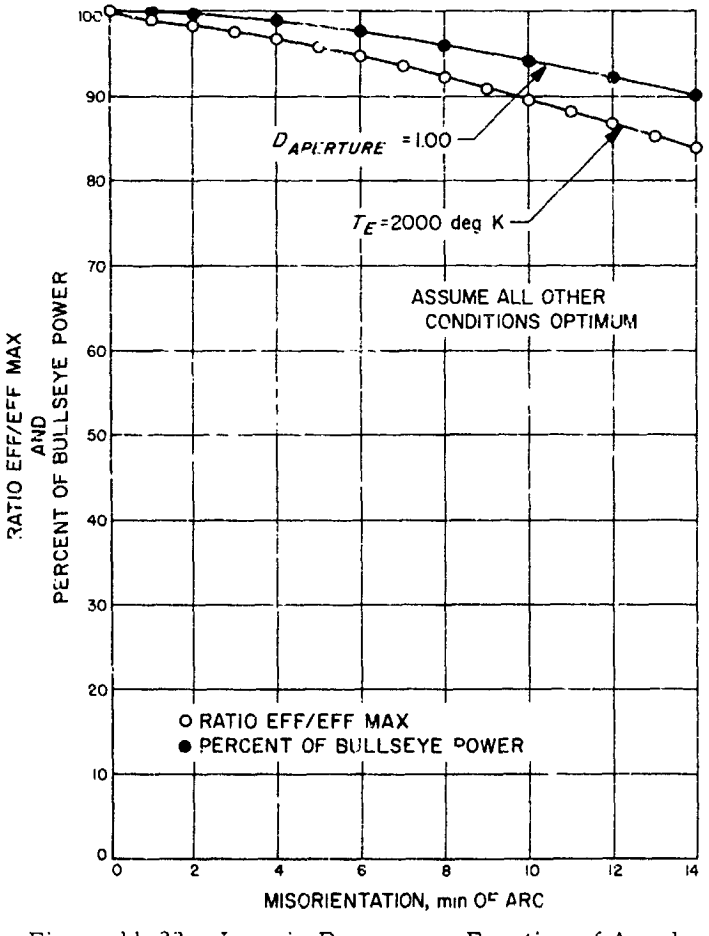


Figure 11-22. Loss in Power as a Function of Angular Deviation from the True Sun Line

Table 11-13. Characteristics of 400-Watt System

Quantity	Equipment	Weight
2	Concentrators	52 lbs
2	Generators	27 lbs
2	Orientation System	20 lbs
2	Support Structure	12 lbs
2	Deployment Mechanisms	15 lbs
	Battery	78 lbs
	Conversion Equipment	125 lbs
	TOTAL	329 lbs
*Total weight is much heavier than the Solar Panel System.		

4. Energy Storage Sources

In determining the minimum initial battery capacity, it must be derived from its dependency upon either the injection maneuver energy requirements or on the orbital energy requirements. Since we are considering no eclipse time and the battery usage in orbit is small compared to the injection maneuver period, the energy requirement in all cases discussed herein are governed by the injection event.

If a Ag Cd battery is used, the depth of discharge for a few (five or less) deep cycles is at least 95 percent. This means that the battery capacity should be 1.05 times the bare energy required. If we assume that recharge of the injection energy occurs during the first planetary orbit, then a minimum of 26 hours are available for recharge, and the charge rate is Cb/27--sufficiently low. A second consideration enters into the calculation of battery capacity; the battery should contain one or more series cells to account for cell shorts. Assuming that a three-cell short must be tolerated, this raises the initial capacity by 10 percent (in a 33 volt system) and decreases the charge rate to Cb/30.

Thus the capacity of a Ag Cd battery is.

$$Cb = 1.15\,(PiTi) = 1160 \text{ watt-hours} \qquad (2)$$

Where Pi, Ti are the injection power level and duration respectively,
Pi = 337 watts,
Ti = 3 hours.

The weight of the Ag Cd battery is given by the capacity and the energy density. If the energy density is 30 watt-hours per pound the battery weight is:

$$Wb = \frac{Cb}{37} = 35.9 \text{ lbs} \qquad (3)$$

In the event 3 parallel batteries are used to provide the same capacity the energy density is reduced because of the added case weight and becomes 27 watt-hours per pound.

The battery weight would then be:

$$Wb = \frac{Cb}{27} = 43 \text{ pounds}$$

If a Ag Zn battery is used, the depth of discharge for a few cycles is 70 percent and the capacity (assuming 10 percent shorted cells as above) would produce a battery of 1.4 times the bare energy requirements or 1400 watt-hours. Since the minimum charge rate for this type of battery is Cb/25, the value of Cb/27 just provides the minimum. The weight of the Ag Zn battery is 48 pounds based on an energy density of 30 watt-hours per pound.

Although the weight of the Ag Zn battery is computed to be more than that of the Ag Cd battery, both of these weights are only provisionally acceptable. It should be noted that actual Ag Zn batteries have achieved lower and higher (80 watt-hours/lb for the Surveyor battery) energy densities. It should also be noted that the higher energy density value of 80 watt-hours/lb is achieved with a very large battery: 250 ampere hours as opposed to approximately 10 ampere-hour cells.

It must be noted that charge methods effect the sizing. If trickle charging is allowed, a loss in total capacity of a Ag Zn battery could amount to 25 percent over the transit period requiring an oversized battery as a penalty.

Another major aspect of battery sizing is that of reliability. It has been assumed heretofore that cell failures result in low impedance short circuits; however, the failure mechanism of Ag Cd and Ag Zn cells in the space environment are not well known. It is possible that cell failures will result in cell voltage reversal, causing eventual rupture of the cell. If thereafter, the electrolyte evaporates, an open circuit condition will occur.

It is important, then, to evaluate the impact of the open circuit failure mode on battery sizing. If this should occur during or prior to the injection maneuver, the minimum power of 337 watts could not be supplied for the total maneuver and the spacecraft would cease to operate. Under these conditions, Sun reacquisition could not be attained and no information would be obtained during the orbital period. For this reason, it is necessary to provide for

this extreme case rather than for the ten percent for a probable cell shortage. Thus, the final design capacity for a Ag Cd battery is:

$$Cb = 2.1 (PiTi) = 2100 \text{ watt-hours}$$

By using three batteries, each with a capacity of 700 watt-hours, true redundancy will be achieved in orbit if none of the batteries fail prior to orbit attainment. During the orbital period any two batteries would supply the required eclipse load energy of 658 watt-hours with only a 50 percent depth of discharge.

The weight now becomes:

$$Wb = \frac{Cb}{27} = \frac{2100}{27} = 78 \text{ lbs}$$

A study now in progress on battery sizing appears to indicate that the specific weight of a battery system including charging, can be minimized by using between four and six batteries in parallel. As an example; if a single battery is used to provide the total energy required, then in order to insure no catastrophic failure a second battery of equal size must be carried. However, if the required energy is placed in two batteries, then a third battery with one-half the total energy required should prevent catastrophic failure since the probability of both required batteries failing is small. This would mean a reduction in total system capacity and weight although some volume increase would be expected. This study is continuing and the results may revise the battery sizing philosophy now used.

It is entirely possible that the proper way to insure battery life is through the use of redundant battery packs. One battery pack being held in a standby condition while the second battery pack is in use. After injection, the two battery packs could be reversed so that each pack is exercised at intervals by ground command. This area will be investigated in terms of weight penalty and battery life versus charge control complexity (reliability).

In sizing the batteries at the beginning of this section no account is taken of the battery design unknowns such as true capacity. There is no known method available in determining a battery's true capacity other than actually discharging the battery. This, of course, is an unexceptable method for a flight battery since this produces wear within the battery and reduces the reliability. Until a method for true capacity measurement can be produced, either a number of test batteries will have to be provided to display repetitive results of the required capacity or a contingency allowance will have to be utilized in sizing the battery to compensate for the unknown quantity. The same is true for determining the allowable number of charge-discharge cycles.

To summarize, Table 11-14 presents the major information on which a choice of battery is made One point which is very important and not very obvious is that for the constraints given in Paragraph 2., it is important to point out that the full charge removed from the battery during the injection maneuver is not replaced during the orbital period. The solar array is designed to provide only enough recharge in the battery to provide for the orbital peak loads.

5. Preliminary Design Study of Power Conversion System

To determine the configuration of the power conversion system suitable for Mariner 1969, a study was performed using the Mariner 64 power conversion system as a basis.

The weight, efficiency and capability of each module used in the Mariner 64 system are tabulated in Table 11-15. A block diagram of the power subsystem is shown in Figure 11-23.

For Mariner 1969 application, some modules required improvements to increase their power handling capability, reduce their power dissipating losses and improve their efficiencies. The improvements proposed were an updating to the present state of the art, utilizing improved components such as transistors with higher power handling capacity and faster switching capability, and microelectronics circuits to reduce weight and power losses.

The proposed improvements are discussed in detail in the write-up of each module and are summarized below.

1) Higher power, faster switching transistor to increase power handling capacity and improve efficiency of the Booster regulator module and 2.4 kc Inverter module.
2) Switching regulator unit recently designed to replace the Booster regulator in order to improve the overall efficiency of the conversion system.
3) Phase control regulator to replace the Booster regulator.
4) Free running capability of the 3 Ø 400 cps Inverter utilizing a magnetic oscillator capable of accepting sync signal and 3 Ø phasing circuits, housed in the Inverter module.
5) Microelectronics circuit to replace transistorized countdown circuit in the synchronizer to reduce weight and power dissipation.

The improvements proposed were introduced and the maximum power handling capability of the modules was established. In order to accommodate the spacecraft power requirements of 200 to 500 watts, parallel arrangement of inverter and regulator was necessary. To obtain sufficient comparable values of the efficiency and weight of the power conversion system, considering the power handling capabilities established for the proposed inverters and regulators, it was decided to perform calculations for the spacecraft power requirements of

Table 11-14. Battery Requirements and Comparisons

Item	Battery Requirements
1.	Size based on length of injection maneuver and power required during maneuver.
2.	Must have recharge capability.
3.	Must provide a minimum of 100 charge-discharge cycles.
4.	Provide 4, or less, discharges to a depth of 95 percent of capacity.
5.	Will be used to provide energy for orbital peak loads. (Planet science considered a peak load.) Longer orbital period reduces high charge rates.
Item	**Ag Cd versus Ag Zn**
1.	Greater shelf life.
2.	Greater cycle life.
3.	Greater depth of discharge.
4.	Lower failure rate.
5.	Less loss of initial charge with deep discharge and temperature.
6.	Better charge characteristics: a) Higher rate b) Stands overcharge
7.	Less efficient.
8.	Less specific energy per pound.

Table 11-15. Weight Efficiency and Capability

Unit	Designation	Weight	Efficiency	Capabilities
Power Distributor	4A11	1.87 lb	1.85 watts	
Synchronizer	4A12	1.65 lb	3.79 watts	
Battery Charger	4A13	2.99 lb	--	
2.4 kc	4A15	2.65 lb	85%	120 watts
2.4 kc	4A16	2.67 lb	85%	120 watts
1 Ø Invert	4A17	2.01 lb	82%	12 watts
3 Ø Invert	4A18	3.44 lb	87%	40 watts
Case 8 PS & L and 2 Booster		20.8 lb		
Booster Capability				160 watts

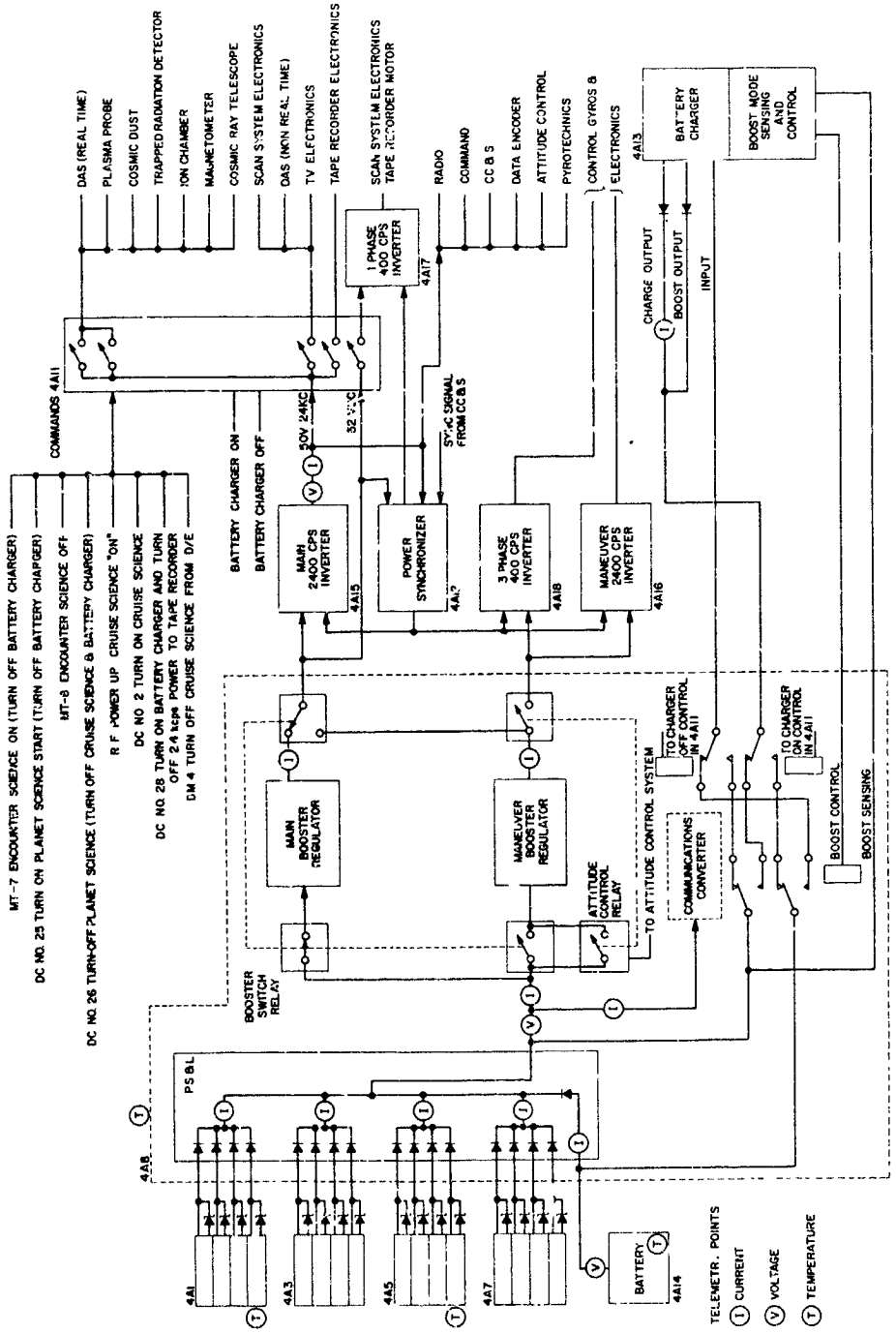


Figure 11-23. Functional Block Diagram for Mariner 1964 Power Subsystem

200, 300, 400, 500 watts. The calculation of the efficiency and weight of the power conversion system proceeded as follows:

a. Photovoltaic and Battery or RTG and Battery Source

(1) Booster Regulator. Determine the efficiency and weight of the power conversion system using Booster regulator to provide the regulated bus lines of 40 to 52 ±1% volts DC to the inverters for the following power requirements:

1) 200 watt peak power demand consisting of:
   a) 2.4 kc 176 watts peak
      150 watts average approximately 85% of peak
   b) 400 cps 1 Ø 4 watts
   c) 400 cps 3 Ø 20 watts
2) 300 watt peak power demand consisting of:
   a) 2.4 kc 267 watts peak
      225 watts average approximately 85% of peak
   b) 400 cps 1 Ø 6 watts
   c) 400 cps 3 Ø 27 watts
3) 400 watt peak power demand consisting of:
   a) 2.4 kc 358 watts peak
      300 watts average approximately 85% of peak
   b) 400 cps 1 Ø 8 watts
   c) 400 cps 3 Ø 34 watts
4) 500 watt peak power demand consisting of:
   a) 2.4 kc 450 watts peak
      375 watts average approximately 85% of peak
   b) 400 cps 1 Ø 10 watts
   c) 400 cps 3 Ø 40 watts

(2) Switching Regulator. Determine the efficiency of the power conversion system using the Switching regulator to provide the regulated bus line of 20 to 30 ±1% volts DC to the inverter for the power requirements mentioned above.

(3) Phase Control Regulator. Determine the efficiency of the power conversion system using the phase control regulator to provide the regulated bus line was not calculated. The system will be similar to the switching regulator except heavier because of the excessive weight of the phase control regulator.

b. Solar Thermionic and Battery

Determine the efficiency and weight of the power conversion system using a low voltage converter-regulator to provide bus line voltage of 35 to 52 ±1% volts DC to the inverters for the power requirements mentioned in the photovoltaic source study.

c. Items Considered for Optimum Design

It was felt that the conversion system configuration should remain the same for either photovoltaic and battery or RTG and battery source. Both sources have an appreciable input voltage variation that will require close regulation. The pulse width modulation method used in the booster regulator or the switching regulator is considered the most efficient known system.

To reduce the weight and power dissipation of the inverters which supply the AC power to the spacecraft users, the regulated supply voltage should be increased to a practical value. The higher the regulated voltage, the lower the current required by the inverter transistors and transformers.

In the Booster regulator system the 52 volts level is considered optimum for the following reasons:

1) The inverter losses are lower (series losses in transistor and transformers). The weight is lower (less copper required).
2) The maximum voltage across the collector diode of the transistor will be 104 volts which is within the rating BVCEO of the fast switching RCA or STC transistors of 150 volts.

In the switching regulator system, the 20 volt level is the maximum value that can be obtained for the minimum input voltage considered of 24 volts.

In the low-voltage converter-regulator system with the Solar Thermionic source, 45 volts or 52 volts can easily be obtained with no excessive loss in efficiency and weight.

d. Proposed Limitation

In the above study, the optimum power conversion system was investigated utilizing the proposed inverters on regulators. With the proposed limitation of the maximum power handling capacity of the power modules the following can be accomplished:

1) The overall dissipation of the module will remain within the power dissipation capability of its housing case.
2) Redundant units will be used for those that are essential.
3) Manufacturing will be eased with present techniques.

e. Power Converter Modules

The capabilities of types of power converter modules are listed in Table 11-16.

(1) P S & L Module. The P S & L module will be similar to Mariner 64 with additional telemetry measurement for the added 2.4 kc inverters and regulator modules.

The weight of the module is expected to be 7.0 pounds. The efficiency or loss in the unit will be approximately 6 percent of the power required by the booster.

(2) Synchronizer. The Mariner 64 basic design will be used with the following modifications and characteristics:

1) Removal of the three phase drive. This section will be incorporated into the 3 ϕ Inverter with the free running circuit.
2) Incorporate the crystal or tuning fork sync circuit as proposed.
3) Utilization of microelectronics technique for countdown and drive circuits.
4) The overall weight of the module will be as follows:

Board & Chassis	0.5 lb	0.5 lb
Crystal	0.3 lb tuning fork	0.6 lb)preliminary info.
Electronics	0.2 lb	0.2 lb
Switch. Traj (F.)	0.4 lb	0.4 lb
	1.4 lbs	1.7 lbs

5) The power dissipation will be approximately 3.2 watts.

(3) Power Distribution Module. The power distribution module will contain all the circuitry presently used to perform the Mariner 64 functions. In addition, there will be circuitry to detect a faulty 2.4 kc inverter or regulator and to switch a standby module.

The weight of the module, including failure protection and switching proposed, will be 2.4 lbs and the loss in the module will be 2.2 watts.

Table 11-16. Capabilities of Power Converter Modules

Module	Weight	Efficiency or Power Dissipation at Peak Power	Capability, Remarks
1) P S & L	7.0	94%	Similar to Ma-64 with additional telemetry
2) Synchronizer	1.3/1.7	3.2 watts	Revised from Ma-64 with the following: a) Crystal Sync circuit b) Microelectronics c) Removal of 3 Ø phasing circuits
3) Power Distributor	2.4	2.2 watts	Similar to Ma-64 with additional switching for redundant circuits
4) 400 cps 1 Ø Invert	2.0	84%	At 10 watts similar to Ma-64
5) 400 cps 3 Ø Invert	3.94	82%	At 40 watts similar to Ma-64 with free running capability
6) 2.4 kc Invert	3.0	See graph	150 w, 200 w, 240 w with 30 v, 40 v, and 52 v input
7) 4.8 kc Invert	3.5, 3.4, 3.3		300 w, 400 w, 500 w with 30 v, 40 v, and 52 v input
8) 2.4 kc Invert	3.0	87%	At 110 watts with 20 volt input
9) 4.8 kc Invert	3.3	84%	At 200 watts with 20 volt input
10) Booster Regulator	5.8	87%	At 260 w 25 v input higher capabilities than Ma-64
11) Booster Regulator	6.4	85%	At 380 w 25 v input higher capabilities than Ma-64
12) Switching Regulator	6.6	89.5%	At 250 watts peak power 25 volt input
13) Switching Regulator	7.2	89%	At 400 watts peak power 25 volt input
14) Phase Control Regulator	7.8	86%	At 260 watts peak power 25 volt input
15) Battery Charger	2.2	-	Charging the battery at all times as long as source power is available

(4) 400 cps Single-Phase Square Wave Module. Same design as Mariner 64, no modifications are anticipated. With the 20 volt regulated line, the design will be similar; no increase in weight or change in efficiency are expected. The efficiency of the model is shown in Figure 11-24.

(5) 400 cps Three-Phase Quasi Square Wave Module. Same basic design as Mariner 64, no modifications are anticipated. With the 20 volt regulated line, the design will be similar; no change in efficiency is anticipated. Free running capability is proposed to be accomplished as follows:

A free running magnetic oscillator similar to the one used to drive the 2.4 kc power amplifiers. This oscillator will provide square wave drive to transistorized countdown and phasing network to provide 3 ∅ drive to 400 cps 3 ∅ amplifier. The circuitry will be housed in the same module and the sync pulse will be similar to the one used for the 2.4 kc system. A similar technique was used in the Mariner R power system.

The overall increase in weight will be approximately 0.8 lbs, with reduction in the synchronizer of approximately 0.4 lbs. The overall efficiency of the free running 400 cps 3 ∅ system will be reduced to the one shown in graph of 3 ∅ inverter. The efficiency of the module is shown in Figure 11-25.

(6) 2.4 kc Inverter. Same basic design as Mariner 64, utilizing new high power and faster switching transistors. The limitation of maximum power handling capacity of the unit will be determined by components other than transistors such as transformers and manufacturing techniques.

Utilizing the present state of the art and considering the recommended size and weight of flight transformer, it is necessary to limit the wire size used in the transformer design to 13 WG or maximum of 5 amperes. Above that value the transformer becomes hard to manufacture, oversized and difficult to support in the flight module for a useful increase in power handling capacity. Bifilar windings can be used which will increase the current capacity to 10 amperes; however, in order to remain within the same workable volume the frequency of operation should increase to 4.8 kc. 4.8 kc frequency can be utilized for the square wave inverter with sufficiently high efficiency. With the above information, the capacity efficiency and weight of the inverter at various input voltages are as follows:

(a) 52 Volt Input. The maximum capacity of the 2.4 kc inverter with 52 volt input should be limited to 240 watts. The efficiency of the unit is shown in Figure 11-26. The weight of the unit will be 3.0 pounds. By increasing the switching frequency of the inverter to 4.8 kc and using bifilar winding for the transformer current capacity, the maximum power output of the inverter can be increased to 500 watts. The efficiency of the unit and weight are shown in Figure 11-26. A more realistic unit will be a 300 watt unit which can be operated on a 2.4 kc or 4.8 kc frequency. The efficiency and weight of the unit are shown in Figure 11-27.

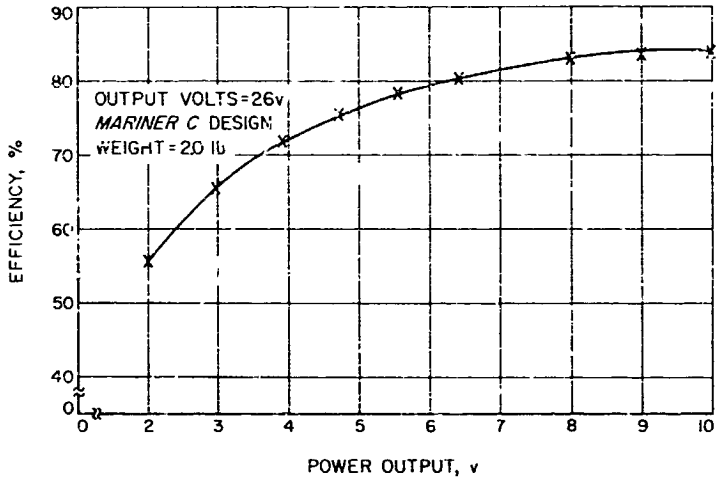


Figure 11-24. 400 cps, Single Phase, Square Wave Inverter

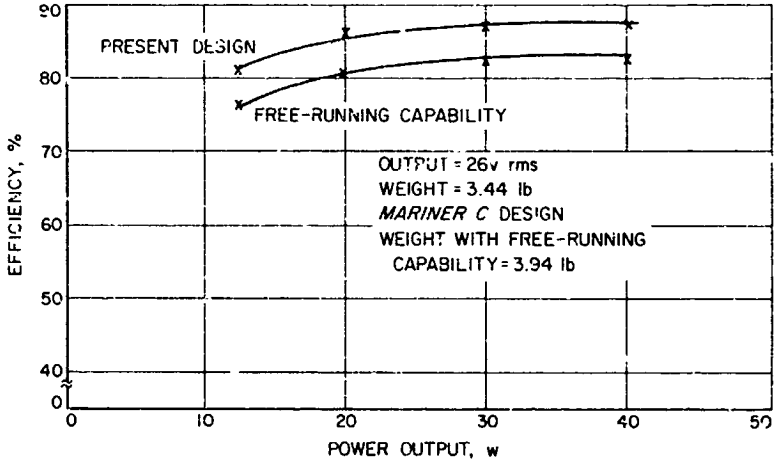


Figure 11-25. 400 cps, Three Phase, Quasi-Square Wave Inverter

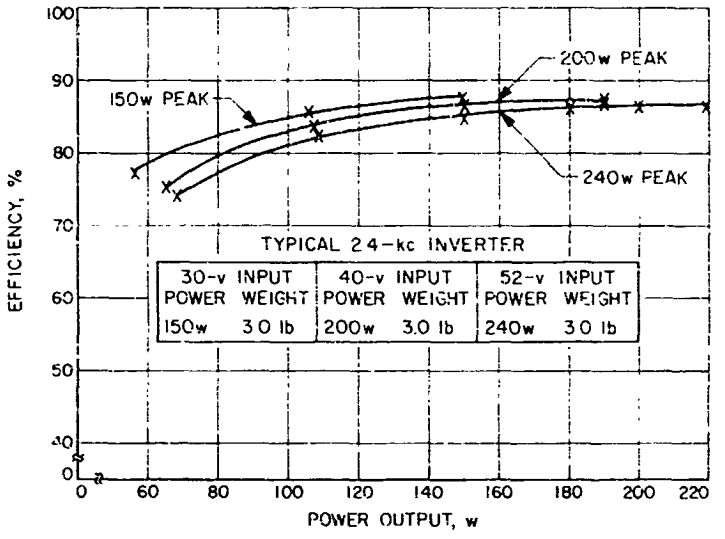


Figure 11-26. 2.4 Kc Square Wave Inverter

(b) 40 Volt Input. The maximum capacity of the 2.4 kc inverter with 40 volt input should be limited to 200 watts. The efficiency and weight of the unit are shown in Figure 11-26. By increasing the frequency to 4.8 kc, the capacity of the unit can be increased to 400 watts. The efficiency of 400 watt and 300 watt units, and the weight of both is shown in Figure 11-27.

(c) 30 Volt Input. The maximum capacity of the 2.4 kc inverter with 30 volt input should be limited to 150 watts. The efficiency and weight of the unit are shown in Figure 11-26 By increasing the frequency to 4.8 kc, the capacity of the unit can be increased to 300 watts. The efficiency and weight of the unit are shown in Figure 11-27.

(d) 20 Volt Input. The maximum capacity of the 2.4 kc inverter with 20 volt input should be limited to 100 watts. The efficiency of the inverter is shown in Figure 11-28. By increasing the frequency to 4.8 kc, the capacity of the unit can be increased to 200 watts. The efficiency and weight of the unit are shown in Figure 11-29.

(7) Booster Regulator. The booster regulator will be based on Mariner R and 64 design with higher power handling and faster switching transistors.

Presently, there are available, transistors from RCA and Minneapolis Honeywell Corporation that can be utilized in the present booster design. The transistor characteristics are as follows:

1) Collect current: 25 amperes peak
2) Collect breakdown voltage: VCEO of 150 volts
3) Faster switching characteristics.

(a). Power Capability. The power capability of the booster will be either 260 watts peak for 200 watts spacecraft power demand or 380 watts peak for 300 watts spacecraft power demand.

The maximum power capability of the booster regulator should be limited to 400 watts because of packaging and maximum power dissipation allowable per spacecraft case. Considering the known spacecraft packaging techniques and temperature control methods, it has been recommended the maximum safe power dissipation per case level be limited to 50 or 55 watts which is the power dissipation of the 400 watts output booster regulator.

If the above limitation is removed, then the maximum power capability of the booster regulator can be increased to 450 watts maximum considering the available high power transistors and the transformer design limitations.

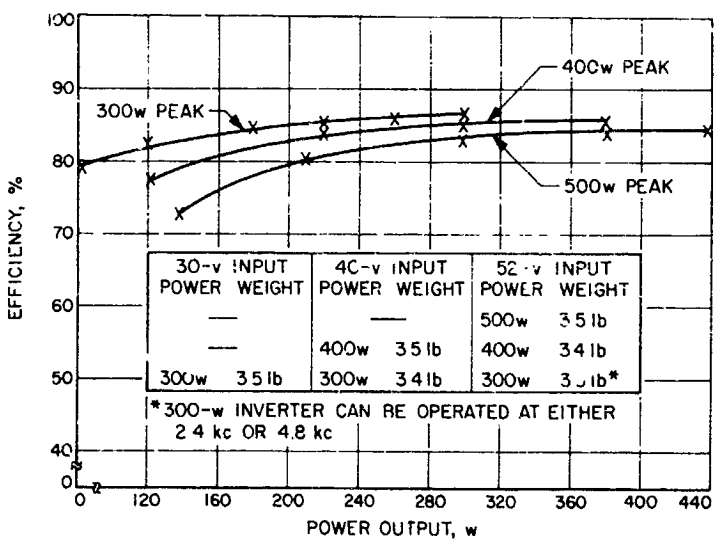


Figure 11-27. 4.8 Kc Square Wave Inverter (400 Watt Peak)

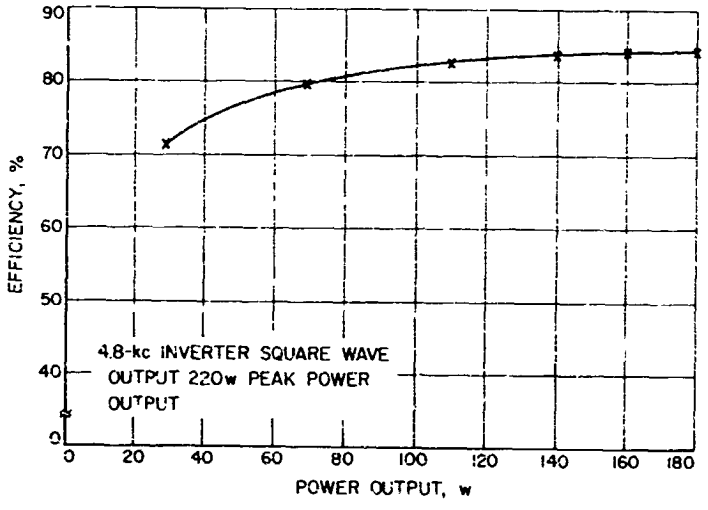


Figure 11-28. 4.8 Kc Square Wave Inverter (220 Watt Peak)

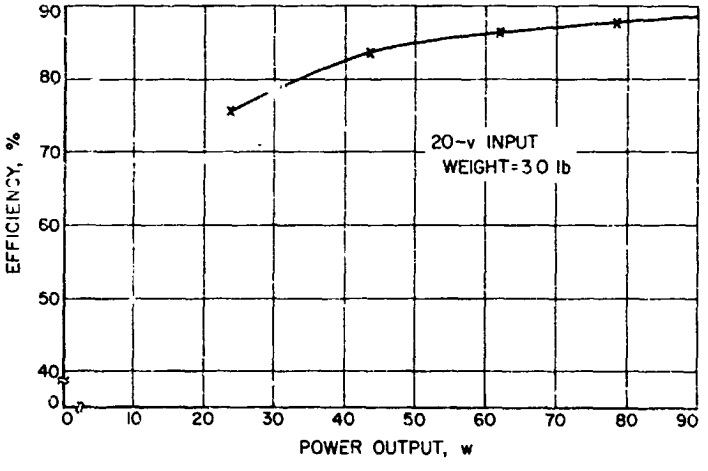


Figure 11-29. 2.4 Kc Square Wave Inverter, Peak Power Capacity 110 Watts

The 260 watt peak power output booster regulator will utilize the same design of Mariner 64 with the faster and higher power transistor and basic higher power transformer.

The 380 watt peak power output booster regulator will utilize the same basic design of Mariner 64 with faster and higher power transistor, redesigned base drive circuit, increased operating frequency of power amplifier stage from 2.7 kc to approximately 4.0 kc to accommodate the transformer design for current handling capacity. The transformer and inductor design will utilize bifilar winding so that the current handling capacity is within the recommended value per wire size. The maximum wire size of No. 13 WG is recommended for flight design for proper sizing and feasible manufacturing.

(b) Efficiency. The efficiency of the booster regulator of 260 watts output is shown in Figure 11-30. The 380 watt output unit is shown in Figure 11-31. The minimum efficiency of the booster, considering limited input voltage variation and higher or lower output, is shown in Figures 11-30 and 11-31. The maximum efficiency of any booster will be within 2 to 3 percent above the minimum value shown.

(c) Comparisons. Booster regulator advantages and disadvantages are as follows:

1) Advantages:

a) The booster regulator can be bypassed so that the system can operate directly from the power source.
b) A momentary short on the output will not destroy the booster, it will merely shut off the oscillator.

2) Disadvantages:

a) Slow response to any load change because of the magnetic amplifier control.
b) Range of only 48 to 52 volts.

(8) Switching regulator. Switching regulator characteristics are based on the recently designed regulator by W. Schubert of JPL.

The power capability of the regulator will be either 260 watts peak for 200 watts spacecraft power demand or 400 watts peak for 300 watts spacecraft power demands.

The maximum power capability of the switching regulator should be limited to 450 watts because of packaging and maximum power dissipation allowable per spacecraft case.

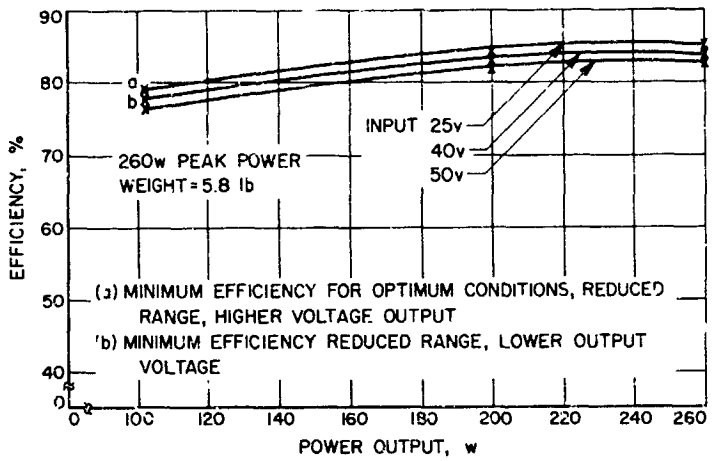


Figure 11-30. Booster Type Regulator

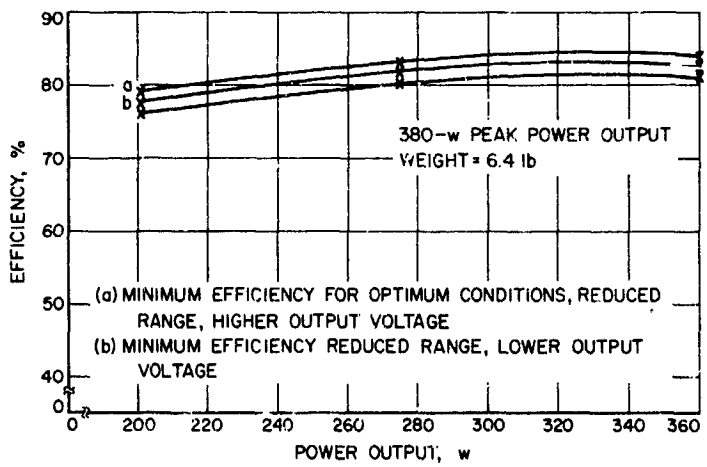


Figure 11-31. Booster Type Regulator (High Output Power)

The switching regulator advantages and disadvantages are:

1) Advantages:

a) Higher efficiency 4 to 6 %.
b) Regulation range 25 to 70 volts.
c) Zener regulators required for higher input range of regulation can be eliminated.

2) Disadvantages:

a) No direct bypass capability.
b) Momentary short will destroy the unit.
c) Probably a slow responding unit to load changes. Data is not available.

The output of the switching regulator is approximately three to four volts below the lower input voltage available. This difference in voltage is the line drop across the switching transistor and inductor. By increasing the output voltage to 30 volts, the minimum input voltage should be 34 to 35 volts. The minimum efficiency of a 260 watt unit is shown in Figure 11-32 and the 400 watt unit is shown in Figure 11-33.

(9) Phase Control Regulator. The phase control regulator utilizes two oscillator power amplifier units which are operating at different frequencies. By mixing the output of each oscillator at different time intervals, regulation can be accomplished.

Because of the nature of regulations utilizing two separate magnetic oscillator amplifiers in addition to the regulator circuits, the overall weight of the unit is estimated to be 7.8 lbs for 260 watt regulator. Because of the weight, the unit is considered undesirable. The 400 watt unit may weigh as much as 10.4 lbs.

(10) Battery Charger. The charger will consist of a DC to DC converter followed with a current limiter and voltage regulator to control the battery maximum voltage. The DC to DC converter will boost the source voltage so that charging will take place at all times even if the source voltage or current are low because of defective source. The battery charge will be connected directly to the source ahead of the diode logic. The battery charger will require a relay disconnect to remove the charger from the battery in case of battery overcharge condition or battery short.

The characteristics of the charger will be similar to Mariner R and the weight will be 2.2 lbs.

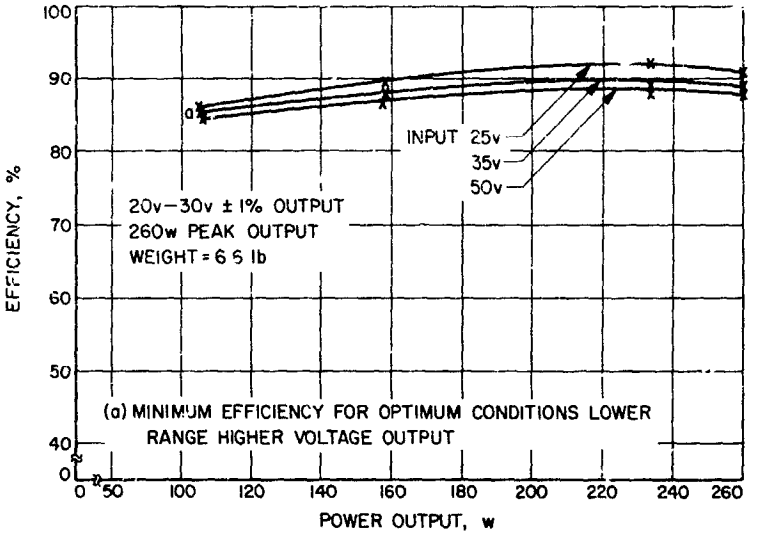


Figure 11-32. Switching Type Regulator (260 Watt Unit)

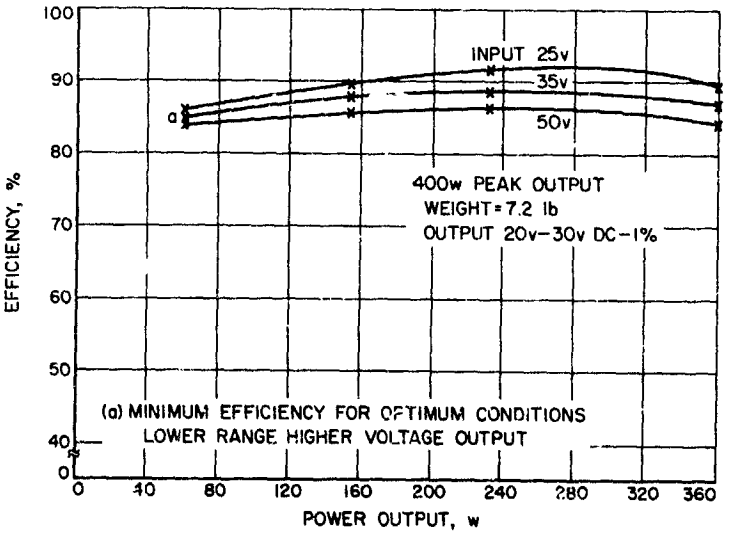


Figure 11-33. Switching Type Regulator (400 Watt Unit)

(11) Photovoltaic or RTG source. The photovoltaic and battery or RTG and battery sources power conversion system will utilize the booster regulator or switching regulator to provide regulated power to the square wave inverter 2.4 kc or 4.8 kc and 400 cps 1 Ø and 3 Ø ac square wave and quasi square wave units.

Considering the available

1) 2.4 kc and 4.8 kc inverters
2) Booster regulator maximum capacity units, and
3) Switching regulator maximum capacity units,

and utilizing them to their maximum capability and best combination, the conversion system has been analyzed. The efficiency and weight for 200, 300, 400 and 500 watts spacecraft power as proposed have been calculated and the results are tabulated in Tables 11-17 through 11-24. Battery charging has been considered but will require special attention when the final selection of source has been established. The basic block diagram of the conversion system with either photovoltaic and battery or RTG and battery is shown in Figure 11-34.

No boost mode or means of eliminating power sources sharing has been considered since proper design of the source and critical selection of battery voltage will make this unnecessary.

To understand the conversion system tables, an example of the calculation performed to determine the efficiency and weight of the conversion system is given below:

Example: Booster Regulator System Case No. 1 peak spacecraft power requirement of 200 watts consisting of:

2.4 kc Peak	176 watts	Average	150 watts
400 cps 1 Ø	4 watts	Average	4 watts
400 cps 3 Ø	20 watts	Average	0

Table 11-20: The number of 2.4 kc inverters required is established as two, one for the system, one for standby. The amount of regulated power required by the inverter is: Peak 204 watts, average 178 watts.

Table 11-19: The regulated power for 2.4 kc, 1 Ø 400 cps, 3 Ø 400 cps is calculated and the total regulated power is established: Peak 234.2 watts, average 183.5 watts. In this case, only one regulator is required.

Table 11-17. Raw Power Requirement, Photovoltaic or RTG Source Booster Regulator System

a) 26[illegible]ts peak power b) 360 watts peak power

Spacecraft Power Requirement Watts)Peak)Aver.	Regulated Power Required (watts)	Regulated Power Requirement Per Boost		Raw Power Requirement Calculated from Booster Efficiency		Total Raw Power Required Watts to PS&L	Eff. 94 Percent Raw Power) No Charger (watts)	Total Eff. No Charger	Total Weight System 100 Percent Redundancy (lbs)
		No. 1 Peak Average (watts)	No. 2 Peak Average (watts)	25 V 50 V (watts)	25 V 50 V (watts)				
				276	-	276	294	68.1	
200	234.2	234.2	-	286	-	286	304	65.7	27.64
1)				220	-	220	234	65.7	
154	183.5	183.5	-	226	-	226	240	64.2	36.44
				421	-	421	448	67.0	
300	351.0	351.0	-	434	-	434	461	65.0	28.54
2)				327	-	327	348	66.2	
231	271.5	271.5	-	340	-	340	362	63.8	38.24
				273	279	552	586	68.2	
400	468.8	232.0	236.8	282	288	570	608	65.8	37.04
3)				273	169	442	471	65.5	
308	367.6	232.0	135.6	282	173	455	484	63.7	55.24
				351	352	703	747	66.9	
500	584.4	292	292.4	363	364	727	773	64.8	38.24
4)				351	220	571	608	63.6	
385	453.9	292	161.4	363	226	589	626	61.5	57.64

Table 11-18. Weight Calculation Photovoltaic or RTG Source Booster Regulator System

Module	Weight Per Unit (lbs)	Case 1		Case 2		Case 3		Case 4	
		Amount	Weight (lbs)	Amount	Weight (lbs)	Amount	Weight (lbs)	Amount	Weight (lbs)
PS&L	7.0	1	7.0	1	7.0	1	7.0	1	7.0
400 cps 1Ø	2.0	1	2.0	1	2.0	1	2.0	1	2.0
400 cps 1Ø	3.94	1	3.94	1	3.94	1	3.94	1	3.94
Synchronizer	1.3	1	1.3	1	1.3	1	1.3	1	1.3
Booster Regulator									
1) 260 watt	5.8	1	5.8			2	11.6		
2) 380 watt	6.4	-	-	1	6.4	-	-	2	12.8
Square Wave Inverter									
2.4 kc 240 watt	3.0	1	3.0	-	-	-	-	-	-
4.8 kc or 2.4 kc 300 watt	3.3	-	-	1	3.3	2	6.6	2	6.6
Power Distribution	2.4	1	2.4	1	2.4	1	2.4	1	2.4
Battery Charger	2.2	1	2.2	1	2.2	1	2.2	1	2.2
Total Per System			27.64		28.54		37.04		38.24
Square Wave Inverter		1	3.0	1	3.3	2	6.6	2	6.6
Regulator		1	5.8		5.4	2	11.6	2	12.8
System +100 Percent Redundancy			36.44		28.24		55.24		57.64

Table 11-19. Regulated Power Requirements

Booster Regulator
1) 260 watts peak capacity
2) 360 watts peak capacity

1) 2.4 kc or 4.8 kc Inverter
2) 400 1 Ø and 3 Ø Inverter

Load Requirement Assumed as Follows					Regulated Power for 2.4 kc (watts)	Regulated Power for 1 Ø 400 cps (watts)	Regulated Power for 3 Ø 400 cps (watts)	Total Regulated Power (watts)	Output Power per Regulator		
Spacecraft Power		2.4 kc (watts)	1 Ø 400 cps (watts)	3 Ø 400 cps (watts)					No. 1 (watts)	No. 2 (watts)	No. 3 (watts)
1)	peak 200	176	4	20	204	5.5	24.7	234.2	234.2	-	-
	average 154	150	4	-	178	5.5	-	183.5	183.5	-	-
2)	peak 300	267	6	27	310	7.5	33.5	351.0	351.0	-	-
	average 231	225	6	-	264	7.5	-	271.5	271.5	-	-
3)	peak 400	358	8	34	418	9.6	41.2	468.8	232.0	236.8	-
	average 308	300	8	-	358	9.6	-	367.6	232.0	135.6	-
4)	peak 500	450	10	40	524	11.9	48.5	584.4	292	292.4	-
	average 385	375	10	-	442	11.9	-	453.9	292	161.9	-

Efficiency of Spacecraft Power to Regulated Power 2.4 kc and 400 cps 3 Ø and 1 Ø

Case	Peak %	Average %
1	85.2	84.4
2	85.5	85.5
3	85.5	84.0
4	85.8	85.0

Table 11-20. Square Wave 2.4 kc, 4.8 kc Regulated Power Requirement

Booster Regulator 1) 360 watts peak power
2) 260 watts peak power

1) 2.4 kc or 4.8 kc 300 watts peak power capacity
2) 2.4 kc 220 watts peak power capacity
3) 4.8 kc 500 watts peak power capacity

	Spacecraft Load Requirement Assuming 85% Peak to Average Watts	Number of Inverters Required	Number of Inverters As Standby	Number of Inverters Used	Load Distribution Between Inverters						Total DC Regulated Power Required (watts)	
					Inverter No. 1		Inverter No. 2		Inverter No. 3			
					Load Peak Average (watts)	Eff. %	Load Peak Average (watts)	Eff. %	Load Peak Average (watts)	Eff. %		
1)	peak 176 average 150	2 2.4 kc 240 watt peak	1	1	176 150	86.0 84.5	-	-	-	-	204.0 178	
2)	peak 267 average 225	2 2.4 or 4.8 kc 300 watt peak	1	1	267 225	86.0 85.5	-	-	-	-	310 264	
3)	peak 358 average 300	4 2.4 or 4.8 kc 300 watt peak	2	2	200 200	86.0 86.0	158 100	85.0 79.5	-	-	418 358	232 186 232 126
4)	peak 450 average 375	4 2.4 or 4.8 kc 300 watt peak	2	2	250 250	86.0 86.0	200 125	86.0 83.0	- -	- -	524 442	292 232 292 150

Overall efficiency and weight

Case	Peak %	Average %	Weight lbs
1	86.0	84.5	6.6
2	86.0	85.5	6.6
3	85.5	82.8	13.2
4	86.0	84.5	13.2

Table 11-21. Raw Power Requirement, Photovoltaic or RTG Source Switching Regulator System

a) 260 watts peak power b) 360 watts peak power

Spacecraft Power Requirement (watts)	Regulator Power Requirement (watts)	Regulated Power Requirement Per Regulator		Raw Power Requirement Calculated from Regulator Efficiency		Total Raw Power Required (watts)	PS&L Efficiency 94 Percent Raw Power (watts)	Total Eff.	Total Weight System 100 Percent Redundancy (lbs)
		No. 1 Peak Average (watts)	No. 2 Peak Average (watts)	No. 1 25 v 50 v (watts)	No. 2 25 v 50 v (watts)				
				254	-	254	270	74.1	28.74
200	240.2	204.2		279		279	297	67.3	
1)				205	-	205	218	70.7	38.64
154	185.5	185.5		215		215	229	67.2	
				406		406	432	69.4	
300	362	362.0		431		431	460	65.2	32.64
2)				310		310	330	70.0	
231	285.5	285.5		331		331	352	65.5	46.54
				237	290	527	560	71.5	
400	477.8	218	259.8	252	298	550	585	68.4	38.64
3)				237	160	397	422	72.7	
308	369.6	218	141.6	252	165	417	445	69.0	58.44
				437	229	666	709	70.6	
500	600.4	389	210.4	466	240	706	752	67.3	42.54
4)				437	88	525	559	68.8	
385	462.9	389	73.9	466	90	556	593	65.0	66.24

Table 11-22. Weight Calculations, Photovoltaic or RTG Source Switching Regulator System

Module	Weight Per Unit (lbs)	Case 1		Case 2		Case 3		Case 4	
		Amount	Weight (lbs)	Amount	Weight (lbs)	Amount	Weight (lbs)	Amount	Weight (lbs)
PS&L	7.0	1	7.0	1	7.0	1	7.0	1	7.0
400 cps 1Ø	2.0	1	2.0	1	2.0	1	2.0	1	2.0
400 cps 3Ø	3.94	1	3.94	1	3.94	1	3.94	1	3.94
Synchronizer	1.3	1	1.3	1	1.3	1	1.3	1	1.3
Switching Regulator									
1) 260 watt	6.6	1	6.6	-		2	13.2	1	6 6
2) 400 watt	7.2	-		1	7.2			1	7.2
4.8 kc In. 200 watts	3.3	1	3.3	2	6.6	2	6.6	3	9.9
Charger	2.2	1	2.2	1	2.2	1	2.2	1	2.2
Power Distributor	2.4	1	2.4	1	2.4	1	2.4	1	2.4
Total Per System			28.74		32.64		38.64		42.54
4.8 kc Invert		1	3.3	2	6.6	2	6.6	3	9.9
Regulator		1	6.6	1	7.2	2	13.2	2	13.8
Total System +100 Percent Redundancy			38.64		46.44		58.44		66.24

Table 11-23. Regulated Power Requirement, Switching Regulator System

1) 260 watt peak 2) 400 watt peak

Load Requirement Assumed as Follows					Regulated Power For 2.4 kc (watts)	Regulated Power For 1 Ø (watts)	Regulated Power For 3 Ø (watts)	Total Regulated Power (watts)	Regulated Power per Regulator		
		2.4 kc	1 Ø	3 Ø					No. 1 (watts)	No. 2 (watts)	No. 3 (watts)
1)	peak	176 w	4 w	20 w	210	5.5	24.7	240.2	240.2	-	-
	average	150 w	4 w	-	180	5.5	-	185.5	185.5	-	-
2)	peak	267 w	6 w	27 w	321	7.5	33.5	362.0	362.0	-	-
	average	225 w	6 w	-	278	7.5	-	285.5	285.5	-	-
3)	peak	358 w	8 w	34 w	427	9.6	41.2	477.8	218	259.8	-
	average	300 w	8 w	-	360	9.6	-	369.6	218	141.6	-
4)	peak	450 w	10 w	40 w	540	11.9	48.5	600.4	389	210.4	-
	average	375 w	10 w		451	11.9	-	462.9	389	73.9	-

Table 11-24. Raw Power Requirement, Photovoltaic or RTG Source, Switching Regulator System

Switching Regulator 260 watts 4.8 kc 200 watts peak
360 watts 2.4 kc 100 watts peak

	Load Requirement Assuming 85% Peak to Average (watts)		Number of Inverters Required	Number of Inverters on Standby	Number of Inverters Used	Load Distribution Between Inverters						Total DC Regulated Power Required (watts)	
						Inverter No. 1		Inverter No. 2		Inverter No. 3			
						Peak Average (watts)	Eff. %	Peak Average (watts)	Eff. %	Peak Average (watts)	Eff. %		
1)	Peak	176	2	1	1	176	84	-		-		210	
	Average	150	4.8 kc 200 watt			150	83.5	-		-		180	
2)	Peak	267	4	2	2	150	83.5	117	83	-		321	180 141
	Average	225	4.8 kc 200 watt			150	83.5	75	77.0	-		278	180 98
3)	Peak	358	4	2		183	84	175	84	-		427	209 218
	Average	300	4.8 kc 200 watt			183	84	117	83	-		360	209 151
4)	Peak	450	6	3		175	84	150	83.5	125	83	540	186 151
	Average	375	4.8 kc 200 watt			175	84	150	83.5	50	80.5	451	209 180 62

Efficiency and Weight	Case	Peak %	Average %	Weight lbs
	1	84	83.5	6.6
	2	83.2	80.0	13.2
	3	84.0	83.5	13.2
	4	83.5	82.3	19.8

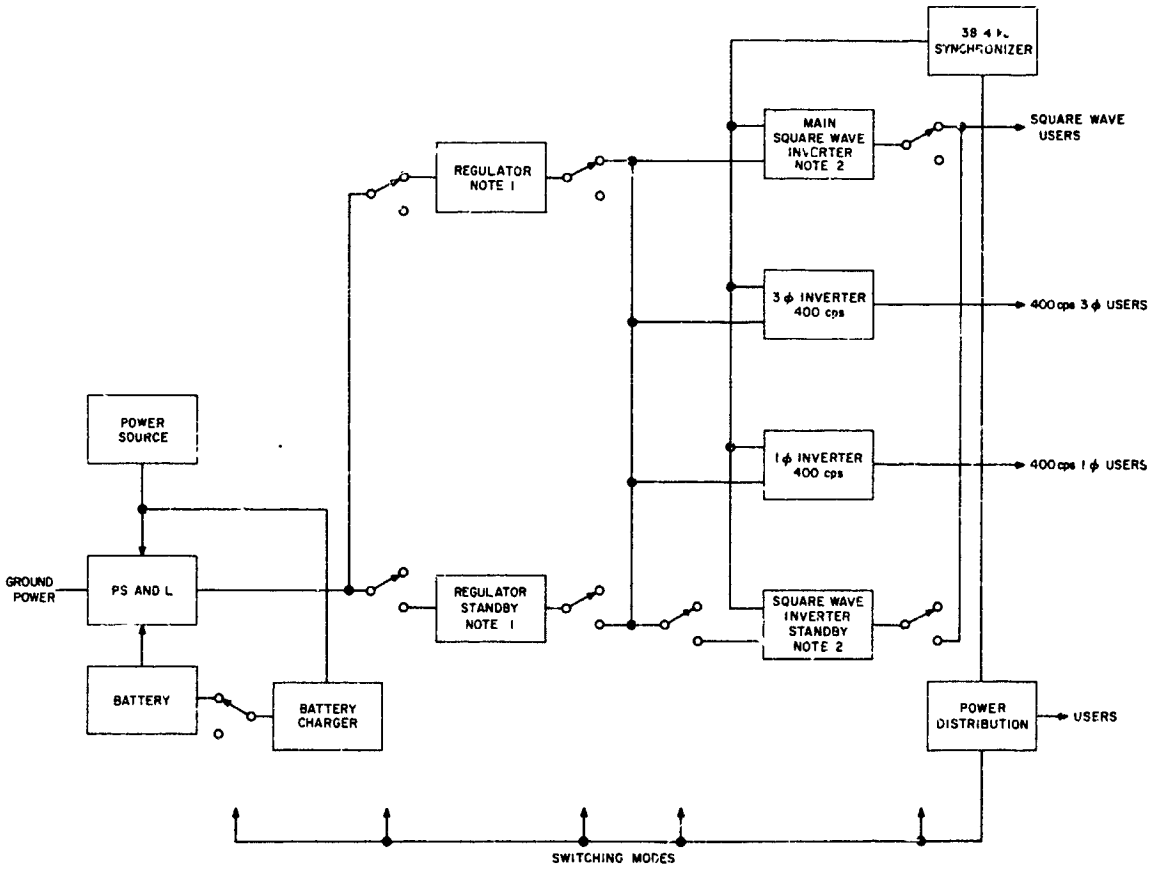


Figure 11-34. Simplified Block Diagram for Mariner 1969 Electrical Conversion (For use with Photovoltaic or RTG Power Sources)

Table 11-17: The Raw power requirements at the booster regulator are calculated considering the efficiency of the booster regulator for 25 volts and 50 volts input, the extreme input voltage anticipated. The Raw power requirements at the source are calculated considering the efficiency of the P S & L. The Raw power requirements for the conversion system excluding battery charging are: Peak 304 watts, average 240 watts. The total weight of the conversion system is calculated in Table 11-17. The weight of the system without redundancy is 27.64 pounds; with 100 percent redundancy, 35.44 pounds. The total efficiency of the conversion system excluding battery charging is: Peak 68.1 percent, average 64.2 percent. The same steps are followed through Tables 11-21, 11-23 and 11-24, for the calculation performed to determine the efficiency of the conversion system using the switching regulator in place of the booster regulator.

f. Solar Thermionic and Battery

The Solar Thermionic and Battery System will utilize a low voltage converter regulator unit to provide usable regulated bus line from the Solar Thermionic source of 1.6 to 4.0 volts. The regulated bus line proposed will be 40 to 52 volts (±1 percent). A Booster regulator will be utilized to provide the regulated bus line from the Battery source of 20 to 35 volts.

The P S & L module will contain the diode logic which is required only for the low voltage converter regulator. In addition, there will be a regulated voltage applied to the magnetic amplifier of the booster regulator to control the sharing mode of booster regulator and low voltage converter regulator.

The booster regulator operates on the principle of adding power to the source. The additional power is provided by a power amplifier stage and the amount of voltage provided is controlled by a magnetic amplifier in the base of the power amplifier. Supplying a separate winding to the magnetic amplifier which will unsaturate the magnetic amplifier and provide no base drive to the power amplifier, the output voltage of the booster will drop to the power source voltage. This scheme will remove the booster regulator output from the bus line and will provide a standby voltage of the battery source for emergency condition. When the thermionic source drops below the regulated bus level, the Booster regulated magnetic amplifier will return to the regulator control path and provide regulated power to the bus line. Failing to accomplish this, the bus line will be supplied directly from the battery at the battery voltage level.

The low voltage converter regulator is feasible with the efficiency characteristics shown in Figure 11-35. However, the unit utilizes germanium transistors which require a good temperature control ambient. The maximum ambient temperature of the unit operating should be limited to +145°F.

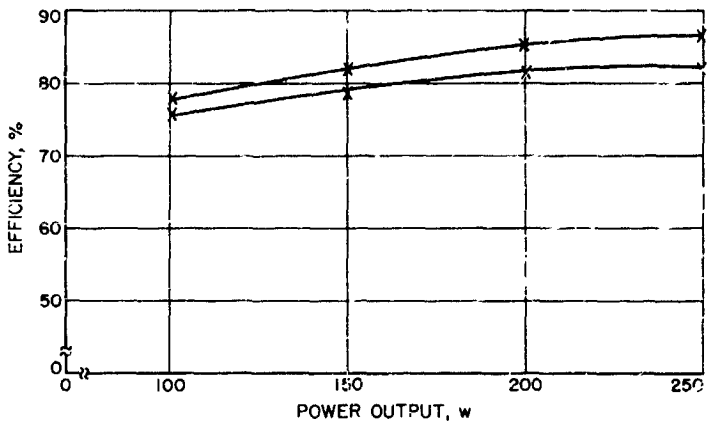


Figure 11-35. Low Voltage Input Converter-Regulator

The Electro Optical System Corporation is presently working on low voltage converter regulators using an inverter and pulse width switching regulator unit to accomplish the output regulation of ±1 percent. The weight estimated for a 260 watt unit is 18 lbs. The weight estimated for a 400 watt unit is 54 lbs. It seems from the standpoint of the power source generation that the 260 watt unit will be the most practical for the system proposed.

Using the available 2.4 kc or 4.8 kc units and a booster regulator with 260 watt peak power output and utilizing them to their maximum capacity and best combination, the conversion system has been analyzed. The efficiency and weight for 200, 300, 400, and 500 watts spacecraft power as proposed has been calculated and the results are tabulated in Tables 11-25 through 11-30. Using the same steps as in the photovoltaic and battery system, one can follow the calculations performed for the efficiency and weight of the conversion system. The battery charger will not require the converter boost proposed and, therefore, the battery charger weight will be 1.4 lbs.

The basic block diagram of the conversion system is shown in Figure 11-36.

No boost mode has been considered.

Table 11-25. Raw Power Requirements, Thermionic Battery Source
Low Voltage Converter Regulator System

Spacecraft Power Requirements		Regulated Power			Raw Power Requirement Calculated for Low Voltage Converter Regulator Unit			Total Raw Power To PS&L	PS&L Efficiency 96% Total Raw Power	Total Efficiency	Total Weight Per System
Case	Watts	No. 1	No. 2	No. 3	4.0 v 1.6 v	4.0 v 1.6 v	4.0 v 1.6 v				System + 100% Redundancy
1)	200	234.2			272	-	-	272	284	73	44.84
					286	-	-	286	298	69.2	
					219	-	-	219	228	67.6	71.64
	154	183.5			227			227	237	64.9	
2)	300	178	132	-	212	217		429	446	67.3	
					220	225		445	464	64.7	66.44
					212	135		347	362	63.9	
	231	178	105	-	220	138		358	373	62.0	114.84
3)	400	231	237.8	-	269	286		555	579	69.2	
					283	289	-	572	596	67.2	71.64
					269	155		424	442	69.6	
	308	231	123.6	-	283	161	-	444	463	66.5	125.24
4)	500	178	189.9	226.5	212	225	264	701	732	68.3	98.44
					220	233	275	728	759	66.0	
					212	155	182	549	572	65.5	178.84
	385	178	123	143.9	220	160	184	564	587	63.8	

Table 11-26. Raw Power Requirements, Thermionic Battery Source
Booster Regulator System

Case	No. 1 Regulator (Watts)	No. 2 Regulator (Watts)	No. 3 Regulator (Watts)	Raw Power Requirement Calculated from Booster Efficiency (Watts)			Total Raw Power Requirement (Watts)	PS&L Efficiency 96% Raw Power	Total Weight System 100% Redundancy (Lbs)	Total Efficiency	Total Load Requirement (Watts)
				25 v 50 v	25 v 50 v	25 v 50 v					
1)	234.2	-	-	)277.0		-	)277	288	Given in the low voltage Converter Regulator Page 11-89	69.5	200
				)289			)289	301		66.7	
	183.5			)225		-	)225	234		65.8	154
				)232			)232	242		63.5	
2)	360			)446		-	)446	464		64.8	300
				)456			)456	475		63.2	
	283			)371		-	)371	386		59.8	231
				)380			)380	396		58.4	
3)	231	237.8	-	)273	)280	-	553	575		69.5	400
				)285	)293		578	603		66.4	
	231	123.6	-	)273	)169	-	442	461		66.7	308
				)285	)175		460	479		64.5	
4)	178	189.9	226.5	)221	)232	)270	723	753		66.5	500
				)226	)239	)277	742	773		64.6	
	178	123	143.9	)221	)168	)188	577	596		64.5	385
				)226	)174	)193	593	617		62.3	

Table 11-27. Weight Calculations, Solar Thermionic Source
Low Voltage Converter Booster Regulator

Module	Weight Per Unit (lbs)	Case 1		Case 2		Case 3		Case 4	
		Amount	Weight (lbs)	Amount	Weight (lbs)	Amount	Weight (lbs)	Amount	Weight (lbs)
PS&L	7.0	1	7.0	1	7.0	1	7.0	1	7.0
Synchronizer	1.3	1	1.3	1	1.3	1	1.3	1	1.3
400 cps 1Ø	2.0	1	2.0	1	2.0	1	2.0	1	2.0
400 cps 3Ø	3.94	1	3.94	1	3.94	1	3.94	1	3.94
Power Distributor	2.4	1	2.4	1	2.4	1	2.4	1	2.4
2.4 kc Inverter	3.0	1	3.0	2	6.0	2	6.0	3	9.0
Low Voltage Converter Regul.	18.0	1	18.0	2	36.0	2	36.0	3	54.0
Booster Regulator	5.8	1	5.8		6.4	2	11.6	3	17.4
Charger	1.4	1	1.4		1.4	1	1.4	1	1.4
Total per System			44.84		66.44		71.64		98.44
2.4 kc Inverter			3.0		6.0		6.0		9.0
Regulator Unit			23.8		42.4		47.6		71.4
Total System and 100% Redundancy			71.64		114.84		125.24		178.84

Table 11-28. Regulated Power Requirement, Low Voltage Converter Regulator or Booster Regulator System, 260 Watt Peak Power

	Load Requirement Assumed as Follows				Regulated Power For 2.4 kc (Watts)	Regulated Power For 1 Ø (Watts)	Regulated Power For 3 Ø (Watts)	Total Regulated Power (Watts)	Regulated Power per Regulator		
		2.4 kc	1 Ø	3 Ø					No. 1 (Watts)	No. 2 (Watts)	No. 3 (Watts)
1)	peak	176 w	4 w	20 w	204.0	5.5	24.7	234.2	234.2	-	-
	average	150 w	4 w	-	178.0	5.5	-	183.5	183.5	-	-
2)	peak	267 w	6 w	27 w	319.0	7.5	33.5	360.0	178	182	-
	average	225 w	6 w	-	278.5	7.5	-	286.0	178	105.0	-
3)	peak	358 w	8 w	34 w	418	9.6	41.2	468.8	231	237.8	-
	average	300 w	8 w	-	355	9.6	-	354.6	231	123.6	-
4)	peak	450 w	10 w	40 w	534.0	11.9	48.5	594.4	178	189.9	226.5
	average	375 w	10 w	-	423.0	11.9	-	434.9	178	123	143.9

Table 11-29. 2.4 kc Regulator Power Requirements

Regulator Unit - 260 Watts Peak Power. 2.4 kc 220 Watt Peak Power Capacity.											
Spacecraft Load Requirement Assuming 85% Peak to Average Power	Number of Inverters Required	Number of Inverters On Standby	Number of Inverters Used	Load Distribution Between Inverters						Total DC Regulated Power Required	
				Inverter No. 1		Inverter No. 2		Inverter No. 3			
				Load Peak Average (Watts)	Eff. %	Load Peak Average (Watts)	Eff. %	Load Peak Average (Watts)	Eff. %		
1) peak 176	2	1	1	176	86.0	-	-	-	-	204.0	
1) average 150				150	84.5	-	-	-	-	178.0	
2) peak 267	4	2	2	150	84.5	117	83.0	-	-	319.0	
2) average 225				150	84.5	75	77.0	-	-	278.5	
3) peak 358	4	2	2	200	86.5	158	84.5	-	-	418	231 187
3) average 300				200	86.5	100	81.0	-	-	355	231 124
4) peak 450	6	3	3	150	84.5	150	84.5	150	84.5	534.0	
4) average 375				150	84.5	100	81.0	100	81.0	423.0	

Overall efficiency and weight

Case	Peak %	Average %	Weight Lbs
1	86.0	84.5	6.0
2	81.0	81.0	9.0
3	85.5	83.8	9.0
4	84.2	82.4	12.0

Table 11-30. Power Conversion System Weight Efficiency

Source	Spacecraft Power Demands											
	200 Watt			300 Watt			400 Watt			500 Watt		
	Weight (lbs)	Efficiency* Peak	Efficiency* Average	Weight (lbs)	Efficiency* Peak	Efficiency* Average	Weight (lbs)	Efficiency* Peak	Efficiency* Average	Weight (lbs)	Efficiency* Peak	Efficiency* Average
1) Photovoltaic Battery or RTC and Battery												
a) Booster Regulator System 100% Redundancy of square wave inverter and regulator	27.64	68.1	64.2	28.54	67.0	63.8	37.04	68.2	63.7	38.24	66.9	61.5
	36.44			38.24			55.24			57.64		
b) Switching Regulator 100% Redundancy of square wave inverter and regulator	28.74	74.1	67.2	32.64	69.4	65.5	38.84	71.5	69.0	42.54	70.6	65.0
	38.64			45.44			58.44			65.24		
2) Solar Thermionic and Battery 100% Redundancy of square wave and regulator	44.84	73.0	64.9	66.44	67.3	62.0	71.64	69.2	66.5	98.44	68.3	63.8
	71.64			114.84			125.24			178.84		

*The efficiency figure does not include battery charging.

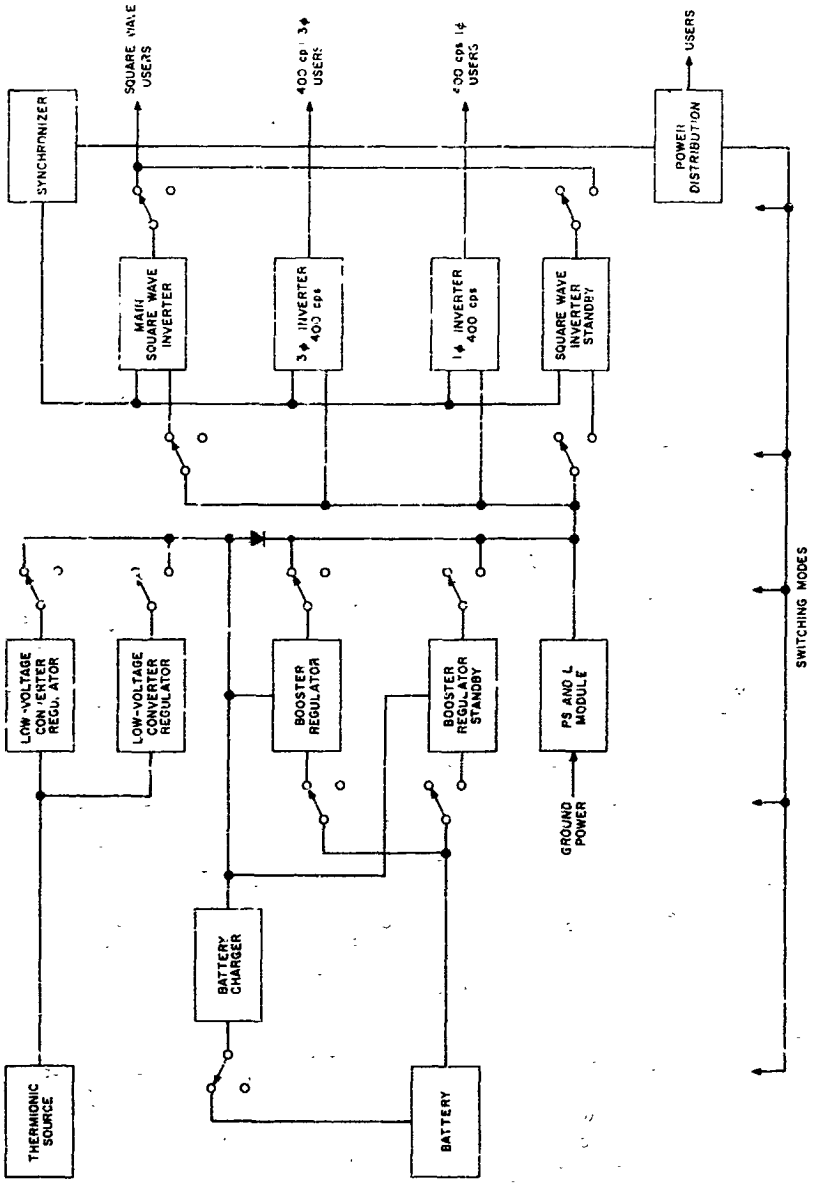


Figure 11-36. Simplified Block Diagram for Mariner 1969 Electrical Conversion (For use with Thermionic Power Source)

6. Electrical Power System Problem Areas

Before any subsystem can be selected for a mission or set of constraints, information in addition to the parametric data must be known. It is the purpose of this section to define some of the problem areas which will be encountered within the power subsystem. Early recognition of these problems and their complexity may help in the system selection and, it is hoped, provide enough scheduled time for solution of the problems for that system.

1) Solar Photovoltaic Power Sources
   a) Design of lightweight deployable, nonmagnetic, arrays.
   b) Electron and proton flux damage to cells.
   c) Deployment and retraction methods.
   d) Temperature cycling of arrays made of nonmagnetic materials.
   e) Availability of silicon cell types whenever procurement is required.
2) Solar Thermionic Power Sources
   a) Materials and methods of eliminating magnetic interference problems and maintaining lightweight structures.
   b) Deployment of generator support structures and concentrators
   c) Converter matching.
   d) Metal to ceramic seals for converters.
   e) Cesium and other impurities attack on converter internal surfaces.
   f) Flux control techniques.
   g) Heat rejection mechanisms.
   h) Method of maintaining accurate sunline orientation.
   i) Thermal energy storage has not been developed to a degree necessary to include it in this study.
3) Radioisotope Thermoelectric Generators
   a) For systems of 200 watts electrical and greater, availability of usable radioisotopes is paramount.
   b) Method and size of shielding to prevent radiation damage.
   c) Containment materials.
   d) Heat rejection methods and mechanization.
   e) Test methods.
4) Electrochemical Energy Storage
   a) Degradation of battery under trickle charge or open circuit conditions. Favorable data will determine the minimum initial capacity of the battery.
   b) Overcharge capability for short periods at a rate up to 2 times the normal capacity.
   c) Operation on the second discharge plateau for 200 cycles. Recharge efficiency will determine the overcapacity of the primary source for recharge. The mode of recharge will determine the charge control requirements.

5) Electrical Conversion Equipment
   a) Low voltage converter - regulator design.
   b) Availability and screening of proposed high power and faster switching transistors.
   c) Transformer design and fabrication of high-current transformers and inductors for reduced weight and volume.
   d) Fabrication of high-current terminal and circuit boards.
   e) Power dissipation per module to remain within the case capability of spacecraft.
   f) Microelectronics manufacturing techniques.
   g) Evaluation of crystal or tuning fork units.
   h) Constant voltage or constant current charging, depending on the best method of charging the battery.
   i) Development of failure protection devices.
   j) Development of monitoring devices having no subsystem failure modes (no method of failure which degrades system operation, but results in loss of telemetry only).

D. SCIENTIFIC MEASUREMENTS

The scientific measurements considered in this feasibility study are based on the following configurations:

1) Planetary Scan (see Figure 11-37):
   a) Infrared Spectroscopy (Interferometer or Spectrometer).
   b) Ultraviolet Spectroscopy.
   c) TV Pictures.
   d) Mars Scanner (Visual, Thermal and Water Vapor).
2) Spacecraft Body (see Figure 11-38):
   a) Magnetometer
   b) Plasma Probe
   c) Energetic Particles
   d) Micrometeorite Detector
   e) Two-Frequency Occultation Beacon
   f) Mars Radio Frequency Noise Detector

Data acquisition requirements for planet oriented science instruments are shown in Figure 11-39.

1. Planetary Scan Experiments General Characteristics and Requirements

Scan considerations are specific to each mode of operation of each instrument. Typical considerations are aiming point, surface coverage, seasonal coverage, altitude and lighting angle. General characteristics and requirements for planetary scan experiments are listed below:

1) High bit rates.
2) Large block of data bits per operation cycle.
3) Time storage requirement
4) Intermittent operation capabilities:
   a) Sequencing
   b) Command
   c) Control

2. Television Measurements

Specific television measurement considerations are listed as follows:

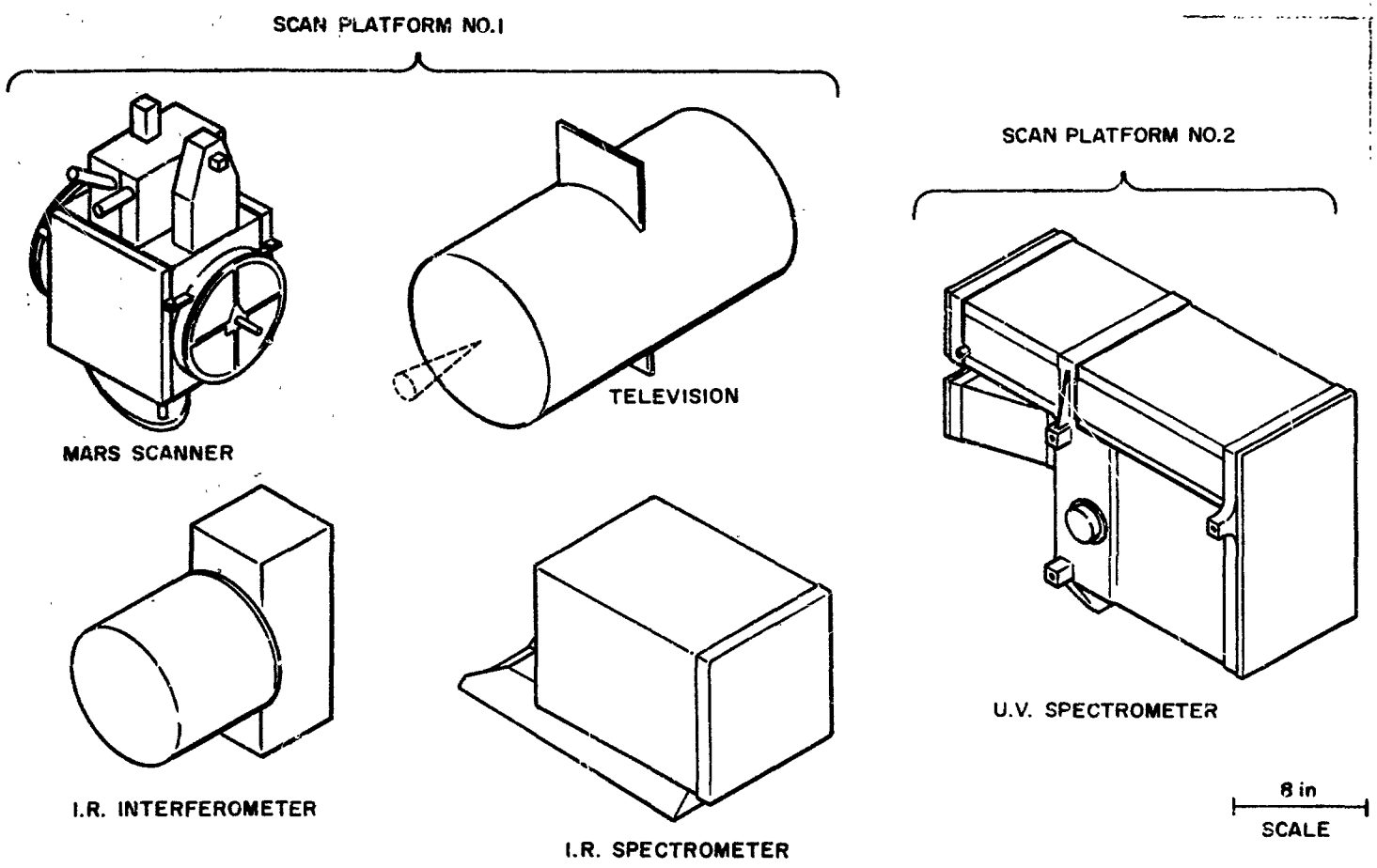


Figure 11-37. Scan Platform Instruments

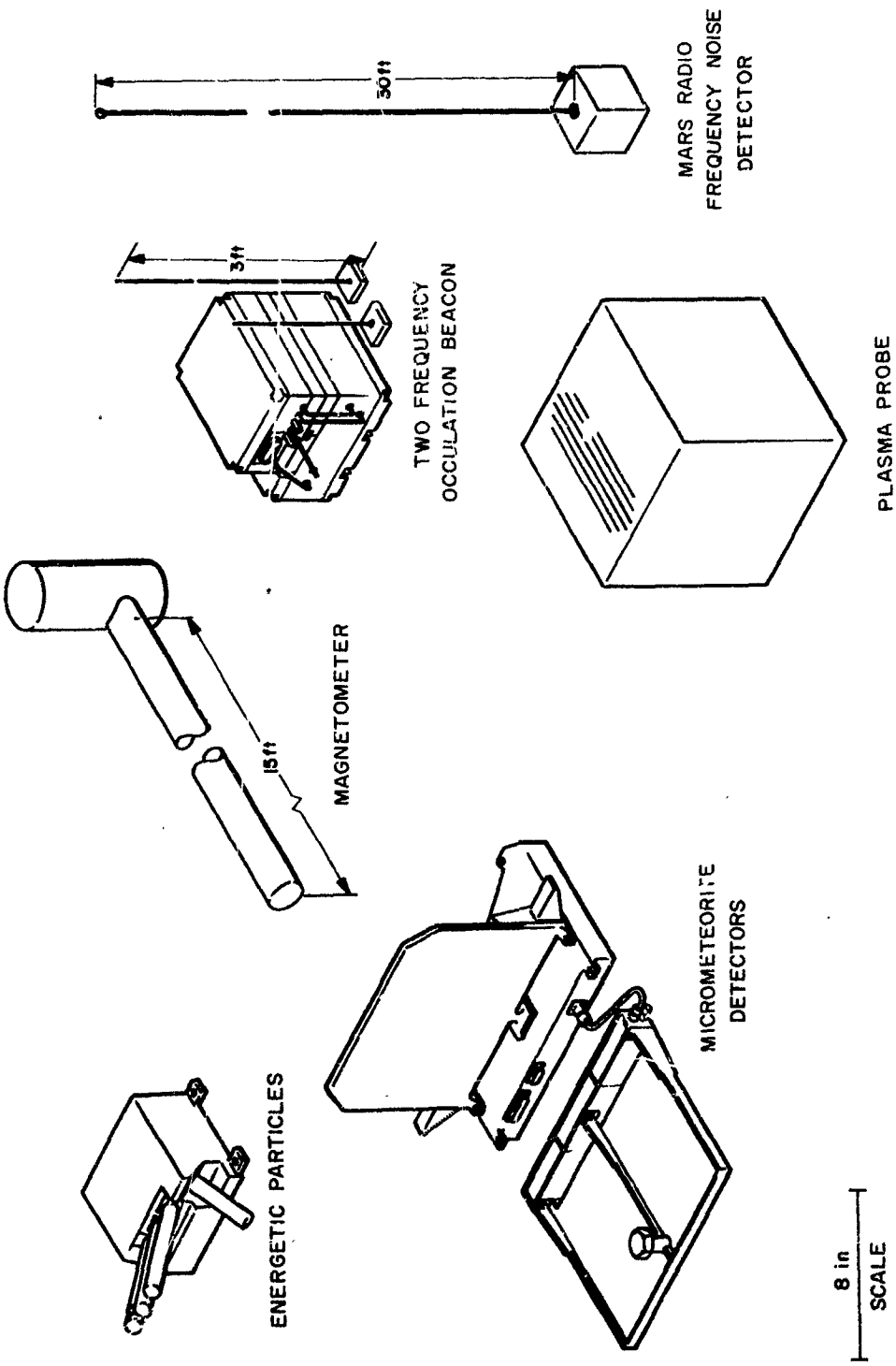


Figure 11-38. Spacecraft Bus Instruments

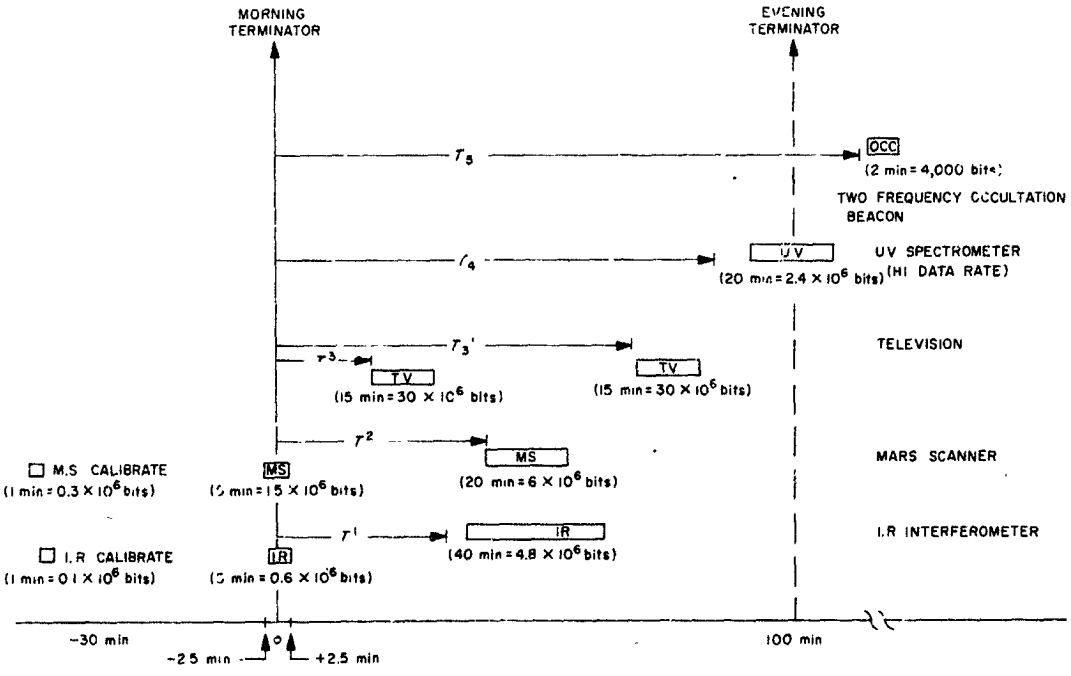


Figure 11-39. Data Acquisition Requirements for Planet-Oriented Science Instruments

1) Purpose:
   a) Topographic: 10 to 50 degrees lighting angle requirement
   b) Color: High spatial resolution, high illumination (near local noon).
   c) Subsolar point: Reflection measurement
2) Operation cycle:
   a) Highest bit rate
   b) Largest bit block
   c) Practically unlimited total bits
3) Pointing direction and altitude:
   a) Nearly normal desired (up to 30 degrees deviation at surface usable)
   b) Up to 3 h_p altitude usable (special cases beyond 3 h_p)
4) Surface coverage:
   a) Entire illuminated planet available (subject to 1) above)
   b) Middle-to-south latitudes (+10 to -40°) chosen as preliminary goal
   c) Repeat of areas for temporal changes

3. Infrared Interferometer Measurements

Specific Infrared Interferometer measurement considerations are listed below:

1) Purpose: Very high wavelength resolution (5 cm^{-1}) spectra at relatively low spatial resolution (100's km sq) for surface and atmospheric feature interpretation.
2) Operation cycle:
   a) 10-second continuous operation for each interferogram
   b) All data bits required for data reduction
3) Pointing direction and altitude:
   a) Nearly normal desired (up to 45-degree deviation at surface usable)
   b) Up to 2 h_p altitude usable
4) Surface coverage: Entire illuminated planet and up to 10 degrees beyond terminator (morning terminator, equatorial regions, light and dark areas, prepared)

NOTE

For an infrared spectrometer experiment, the requirements would be, in general, similar to those listed above.

4. Mars Scanner

Specific Mars Scanner measurement considerations are as follows:

1) Purpose: Overlaid pictures of the planet surface in three wavelengths; visible, near infrared for water vapor content and far infrared for temperature interpretation.
2) Operation cycle:
   a) Saw-tooth motion of mirror pair produces a facsimile scan of the surface.
   b) Continuous operation for minimum time increments of five minutes required.
3) Pointing direction and altitude:
   a) Normal to surface desired, up to 30-degrees deviation usable.
   b) Constant velocity and altitude desired, internal instrument adjustment provided for large change.
4) Surface coverage:
   a) Entire illuminated planet and up to 10 degrees beyond terminator (morning terminator preferred).
   b) Repeat of areas for temporal changes.

5. Ultraviolet Spectrometer

Specific ultraviolet spectrometer measurement considerations are listed below:

1) Purpose: Very high wavelength resolution (1 Angstrom) as follows:
   a) With tangential viewing of atmospheric layers during passage of lighted limb.
   b) With normal viewing at passage of terminator and into shadow.
   c) During passage of lighted planet between a) and b).
2) Operation cycle:
   a) 10-second cycle continuously repeated during a) and b) of 1) above.
   b) Intermittent operation sufficient during c) of 1) above.
3) Pointing Direction and Altitude:
   a) Low altitude (close approach) desired.
   b) Fixed pointing direction possible.
   c) Special requirements for rotation about optic axis of instrument for all but ecliptic orbits.
4) Surface coverage: Orbit inclination within 30 degrees of ecliptic is probably required.

6. Planetary Environment-Cruise Experiments

The general characteristics and requirements listed below apply to the Planetary Environment-Cruise experiments:

1) Fixed spacecraft mounting:
   a) Look angles
   b) Antennas
   c) Booms
2) Contaminations:
   a) Magnetic
   b) Electromagnetic
   c) Radioactive
   d) Vibration
3) Bit rates:
   a) Low bit rates
   b) Low total bits
4) Operation cycle:
   a) Minimal: Continuous operation at low bit rate that permits real-time transmission during cruise.
   b) Desirable: Intermittent operation at high bit rate for flare operation.
5) Special: Occultation, sequencing and storage

7. Tabular Data

Additional data utilized in establishing requirements for scientific measurements are presented in tabular form as listed below:

1, Weight/Power/Volume Summary (Table 11-31)
2) Temperature Control Requirements (Table 11-32)
3) Science System Command Requirements (Table 11-33)
4) Science System Functional Design Parameters, Case A (Table 11-34)
5) Science System Functional Design Parameters, Case B (Table 11-35)
6) Power Profile Science Instruments, Case A (Table 11-36)
7) Power Profile Science Instruments, Case B (Table 11-37)

Table 11-31. Weight/Power/Volume Summary

Weight	Case I (2 Scan Instruments)	Case II (4 Scan Instruments)
Scan Platform Instruments	36 lbs.	86 lbs.
Scan Platform	24 lbs.	42 lbs.
Bus Instruments	44 lbs.	44 lbs.
Data Automation System	28 lbs.	37 lbs.
Cables	6 lbs.	8 lbs.
TOTAL	138 lbs.	217 lbs.

Power	Case I (2 Scan Instruments)	Case II (4 Scan Instruments)
Scan Platform Instruments	20 watts	43 watts
Bus Instruments	21 watts	21 watts
Data Automation System	18 watts	22 watts
TOTAL	59 watts	86 watts

Volume	Case I (2 Scan Instruments)	Case II (4 Scan Instruments)
Scan Platform Instruments	11 inches	19 inches
Bus Instruments	7 inches	7 inches
Data Automation System	18 inches	25 inches
TOTAL	36 inches	51 inches

Table 11-32. Temperature Control Requirements

	Operating Thermal Conditions (Sensor)		
	Minimum Temp (°C)	Maximum Temp (°C)	Maximum Temp Change (°C/Min)
IR Instruments			
Mars Scanner	-40°C	-20°C	2°C/Min
IR Spectrometer	-80°C	+10°C	2°C/Min
IR Interferometer	- 8°C	- 5°C	0.1°C/Min
Television	-10°C	+55°C	2°C/Min

Table 11-33. Science System Command Requirements

Number	Function	Requirement
1.	Power On-Off	Independent control for each instrument
2.	Boom/Antenna Extension	Magnetometer Mars Radio Frequency Noise Detector
3.	Protective Cover Removal	Scan Platform instruments
4.	Calibrate	All instruments
5.	Data Acquisition On-Off	Independent control for each planet oriented instrument
6.	Data Playback On-Off (Stored Data)	Independent Control for: 1) Each planet oriented instrument's data 2) Flare data 3) Occultation data
7.	Data Playback Advance (Stored Data)	Advance Television data fixed increments
8.	Instrument Setting Update	Television Mars Scanner

Table 11-34. Science System Functional Design Parameters, Case A

Totals based upon nominal case (Television No. 1 and Mars Scanner plus all F and P)

Instrument	Volume (Bus) (Chassis) (cu in.)	Total Weight (lb)	Weight		Electrical Power (Bus)				Electrical Power (Sensor)				Total Power (w)	Power Source (kc)	Operating Thermal Conditions (Sensor)			Nonoperating Thermal Condition (Sensor)		Data	
					Input Power		Dis. Power		Input Power		Dis. Power										
			Bus (lb)	Plat. Sensor (lb)	Avg (w)	Peak (w)	Avg (w)	Peak (w)	Avg (w)	Peak (w)	Avg (w)	Peak (w)			Min Temp (°C)	Max Temp (°C)	Max Temp Change (°C/min)	Min Temp (°C)	Max Temp (°C)	Bits/ sec	Total Data/ Orbit (bits)
Television No. 1	7.5	23.0	8.0	15.0	10.0	10.0	9.0	9.0	-	-	1.0	1.0	10.0	2.4	-10	+55	2	-50	+80	9k-64k	10.0×10^6
Mars Scanner	3.0	13.0	4.5	8.5	9.5	9.4	5.0	5.0	-	-	4.4	4.4	9.4	2.4	-40	+20	2	-50	+70	3,500	7.6×10^6
Magnetometer	4.0	4.5	4.5	-	5.0	5.0	4.7	4.7	-	-	0.3	0.3	5.0	2.4	-10	+55	2	-50	+80	4	
Plasma Probe	NA	10.0	10.0	NA	NA	NA	NA	NA	12.0	12.0	12.0	12.0	12.0	2.4	-10	+55	2	-50	+80	1	
Energetic Particles (Trapped Radiation Detector)	NA	2.5	2.5	NA	NA	NA	NA	NA	0.5	0.5	0.5	0.5	0.5	2.4	-10	+55	2	-30	+60	2	
Micrometeorite Detector (Cosmic Dust Detector)	NA	5.0	5.0	NA	NA	NA	NA	NA	0.5	0.5	0.5	0.5	0.5	2.4	-10	+55	2	-50	+80	3	
Two Frequency Occulation Beacon	NA	5.5	5.5	NA	NA	NA	NA	NA	1.6	1.6	1.6	1.6	1.6	2.4	-10	+55	2	-50	+80	2	
Mars RF Noise Detector	3.0	4.5	4.5	NA	NA	NA	NA	NA	2.0	2.0	2.0	2.0	2.0	2.4	-10	+55	2	-50	+80	1	
DAS (Nominal)	18.5	28.0	28.0	NA	18.5	18.5	18.5	18.5	NA	NA	NA	NA	18.5	2.4	-10	+55	2	-50	+80	-	
Scan Platform	NA	23.5	23.5	-	-	-	-	-	-	-	-	-	-	-	-	-	-	-	-	-	
Magnetometer Boom and Sensor	NA	10.0	10.0	-	-	-	-	-	-	-	-	-	-	-	-10	+55	2	-80	+80	-	
Mars RF Noise Antenna	NA	2.0	2.0	NA	NA	NA	NA	NA	NA	NA	0.5	0.5	0.5	2.4	-10	+55	2	-50	+80	NA	
Science Case Harness	NA	6.0*	6.0*	-	-	-	-	-	-	-	-	-	-	-	-	-	-	-	-	-	
Total	36.0	137.5	144.0	23.5	42.9	42.9	37.2	37.2	16.6	16.6	22.3	22.3	59.5	-	-	-	-	-	-	-	37.8×10^6

*Includes mounting hardware

Table 11-35. Science System Functional Design Parameters, Case B

Totals based upon Television No. 1, IR Interferometer, and Mars Scanner mounted on Scan Platform and UV Spectrometer bus mounted (Maximum Case)

Instrument	Volume (Bus) (Chassis) (cu. in.)	Total Weight (lb)	Weight		Electrical Power (Bus)				Electrical Power (Sensor)				Total Power (w)	Power Source (kc)	Operating Thermal Conditions (Sensor)			Nonoperating Thermal Condition (Sensor)		Data	
					Input Power		Dis. Power		Input Power		Dis. Power				Min Temp (°C)	Max Temp (°C)	Max Temp Change (°C/min)	Min Temp (°C)	Max Temp (°C)	Bits/ sec	Total Data/ Orbit (bits)
			Bus (lb)	Plat. Sensor (lb)	Avg (w)	Peak (w)	Avg (w)	Peak (w)	Avg (w)	Peak (w)	Avg (w)	Peak (w)									
IR Experiment Multi-Detector Spectrometer	3.0	20.0	8.0	12.0	5.0	5.0	2.5	2.5	-	-	2.5	2.5	5.0	2.4	-80	+10	2	-80	+60	7	42,000
IR Interferometer	4.0	26.0	6.0	20.0	8.0	8.0	6.0	6.0	-	-	2.0	2.0	8.0	2.4	-8	-5	0.1	-50	+60	1,730	5.5×10^6
					-	-	-	-	3.5	7.0	3.5	7.0	3.5	28 vdc							
UV Spectrometer	4.0	24.0	24.0	NA	12.0	12.0	6.0	6.0	-	-	6.0	6.0	12.0	2.4	-10	+40	2	-30	+60	2,000	2.4×10^6
Television No. 1	7.5	23.0	8.0	15.0	10.0	10.0	9.0	9.0	-	-	1.0	1.0	10.0	2.4	-10	+55	2	-30	+80	8k-64k	30.0×10^6
Television No. 2	7.5	16.0	8.0	8.0	10.0	10.0	9.0	9.0	-	-	1.0	1.0	10.0	2.4	-10	+55	2	-30	+80	8k-64k	10.0×10^6
Mars Scanner	3.0	13.0	4.5	8.5	9.4	9.4	5.0	5.0	-	-	4.4	4.4	9.4	2.4	-40	-20	2	-50	+70	3,500	7.8×10^6
Magnetometer	3.0	4.5	4.5	-	5.0	5.0	4.7	4.7	-	-	0.3	0.3	5.0	2.4	-10	+55	2	-50	+80	4	-
Plasma Probe	NA	10.0	10.0	NA	NA	NA	NA	NA	12.0	12.0	12.0	12.0	12.0	2.4	-10	+55	2	50	+80	1	* -
Energetic Particles Trapped Radiation Detector)	NA	2.5	2.5	NA	NA	NA	NA	NA	0.5	0.5	0.5	0.5	0.5	2.4	-10	+55	2	-30	+60	2	
Micrometeorite Detector (Cosmic Dust Detector)	NA	5.0	5.0	NA	NA	NA	NA	NA	0.5	0.5	0.5	0.5	0.5	2.4	-10	+55	2	-50	+80	3	
Two Frequency Circulation Beacon	NA	5.5	5.5	NA	NA	NA	NA	NA	1.6	1.6	1.6	1.6	1.6	2.4	-10	+55	2	-50	+80	2	
Mars RF Noise Detector	3.0	4.5	4.5	NA	NA	NA	NA	NA	2.0	2.0	2.0	2.0	2.0	2.4	-10	+55	2	-50	+80	1	
DAS (Maximum)	25.0	37.0	37.0	NA	22.0	22.0	22.0	22.0	NA	NA	NA	NA	22.0	2.4	-10	+55	2	-50	+80	-	
Scan Platform	NA	41.5	41.5	-	-	-	-	-	-	-	-	-	-	-	-	-	-	-	-	-	
Magnetometer Boom and Sensor	NA	10.0	10.0	-	-	-	-	-	-	-	-	-	-	-	-10	+55	2	-50	+80	NA	
Mars RF Noise Detector Antenna and Preamplifier	NA	2.0	2.0	NA	NA	NA	NA	NA	NA	NA	0.5	0.5	0.5	2.4	-	-	-	-	-	-	
Science Case Harness*	NA	8.0	8.0	-	-	-	-	-	-	-	-	-	-	-	-	-	-	-	-	-	
Total	50.5	216.5	173.0	43.5	66.4	66.4	52.7	52.7	20.1	23.6	33.8	37.3	86.5	-	-	-	-	-	-	-	45.7×10^6

*Includes mounting hardware

Table 11-36. Power Profile Science Instruments (Case A)

Nominal Case (All power values in watts)

Instrument	On Pad Tests	Launch	Acquisition	Cruise	Cruise Calibrate	Injection Maneuver	Post Injection	Apoapsis ±90°	Periapsis ±90°
Television No. 1	10.0	-	-	-	-	-	-	-	10.0
Mars Scanner	9.4	-	-	-	9.4	-	-	-	9.4
Magnetometer	5.0	5.0	5.0	5.0	5.0	-	5.0	5.0	5.0
Plasma Probe	12.0	-	-	12.0	12.0	-	12.0	12.0	12.0
Energetic Particles (Trapped Radiation Detector)	0.5	0.5	0.5	0.5	0.5	-	0.5	0.5	0.5
Micrometeorite Detector (Cosmic Dust Detector)	0.5	0.5	0.5	0.5	0.5	-	0.5	0.5	0.5
Two Frequency Occulation Beacon	1.6	-	-	1.6	1.6	-	1.6	1.6	1.6
Mars RF Noise Detector	2.0	-	-	2.0	-	-	2.0	2.0	2.0
DAS (Nominal)	18.5	8.0	8.0	8.0	18.5	-	8.0	18.5	18.5
Total	59.5	14.0	14.0	29.6	47.5	0	29.6	40.1	59.5

Table 11-37. Power Profile Science Instruments (Case B)

(All power values in watts)

Instrument	On Pad Tests	Launch	Acquisition	Cruise	Cruise Calibrate	Injection Maneuver	Post Injection	Apoapsis ±90°	Periapsis ±90°
Infrared Experiment Multi-Detector Spectrometer	5.0	-	-	-	5.0	-	-	-	5.0
IR Interferometer	11.5	-	-	3.5	11.5	-	3.5	3.5	11.5
UV Spectrometer	12.0	-	-	-	-	-	-	12.0	12.0
Television No. 1	10.0	-	-	-	-	-	-	-	10.0
Television No. 2	10.0	-	-	-	-	-	-	-	10.0
Mars Scanner	9.4	-	-	-	9.4	-	-	-	9.4
Magnetometer	5.0	5.0	5.0	5.0	5.0	-	5.0	5.0	5.0
Plasma Probe	12.0	-	-	12.0	12.0	-	12.0	12.0	12.0
Energetic Particles (Trapped Radiation Detector)	0.5	0.5	0.5	0.5	0.5	-	0.5	0.5	0.5
Micrometeorite Detector (Cosmic Dust Detector)	0.5	0.5	0.5	0.5	0.5	-	0.5	0.5	0.5
Two Frequency Occulation Beacon	1.6	-	-	1.6	1.6	-	1.6	1.6	1.6
Mars RF Noise Detector	2.0	-	-	-	-	-	2.0	2.0	2.0
DAS (Nominal)	22.0	8.0	8.0	8.0	22.0	-	8.0	22.0	22.0
Total*	86.5	14.0	14.0	31.1	62.5	0	33.1	59.1	86.5

*Based on (5) Scan Platform Instruments & UV Spectrometer (Body Mounted)

E. SPACECRAFT DATA HANDLING

1. Science System Data and Command Requirements

a. Instrument Sequence and Data Requirements

Figure 11-40 illustrates the data requirements for the planet oriented science instruments, based on preliminary estimates. The morning terminator is a good reference point for science and it is assumed that this point can be determined accurately (within < 1 min.) through trajectory information. All other times, if held to a tolerance of one (1) minute, will be within acceptable limits. Times T_1 through T_5 are to be estaolished by means of Real Time Quantitative Commands.

The following assumptions are made with respect to the data acquisition modes for the IR Interferometer, Mars Scanner, Television and UV Spectrometer instruments:

1) A calibration will be required for the Mars Scanner and IR Interferometer just prior to the taking of planet data.
2) The dark and light areas adjacent to the morning terminator will be of interest to the Mars Scanner and IR Interferometer.
3) The Mars Scanner and IR Interferometer will operate for some period about periapsis.
4) The television instrument will take data when closest approach is achieved with good lighting conditions.
5) The UV Spectrometer will obtain data at the planet limb and terminator.

The information provided above only describes the data acquisition for the high data rate instruments; comments relative to some of the other instruments are listed below:

(1) IR Spectrometer. In one possible version, data would be transmitted, in real time, from morning terminator to evening terminator.

(2) Two-Frequency Occultation Beacon. Between 2000 and 10,000 bits will be stored at occultation and then transmitted at some time later in the orbit.

(3) Mars Radio Frequency Noise Detector. Several spectrum (5000 bits/spectrum) may be stored during an active period and transmitted at some time later in orbit.

(4) Fields and Particles Instrument. Flare mode data of up to 1×10^6 may be stored and transmitted at some time later in the orbit.

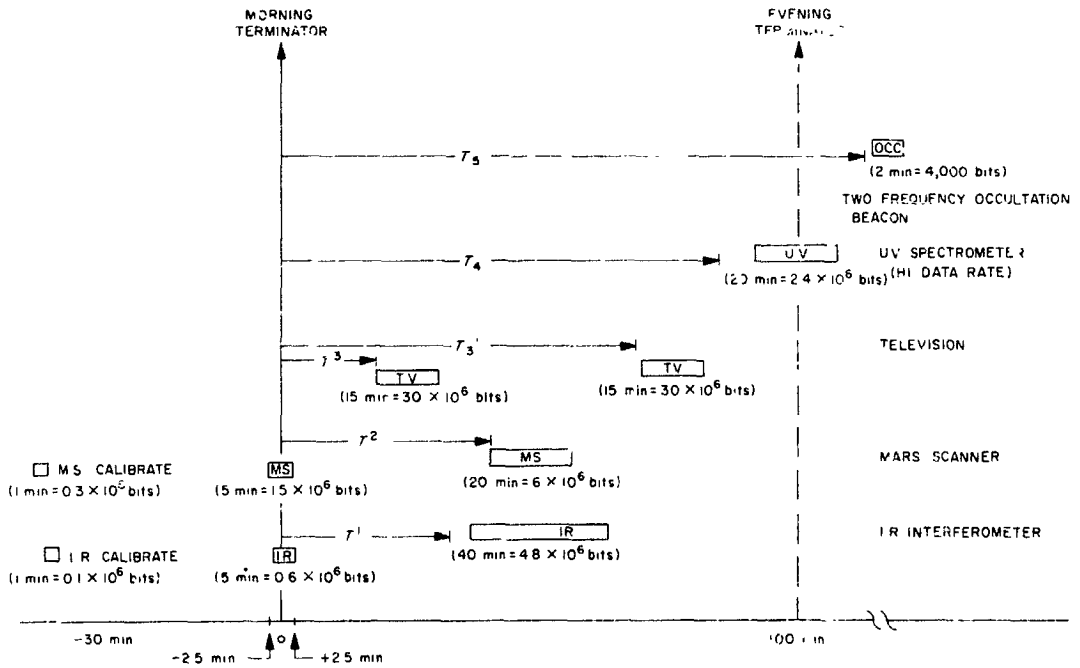


Figure 11-40. Data Requirements for Planet-Oriented Science Instruments

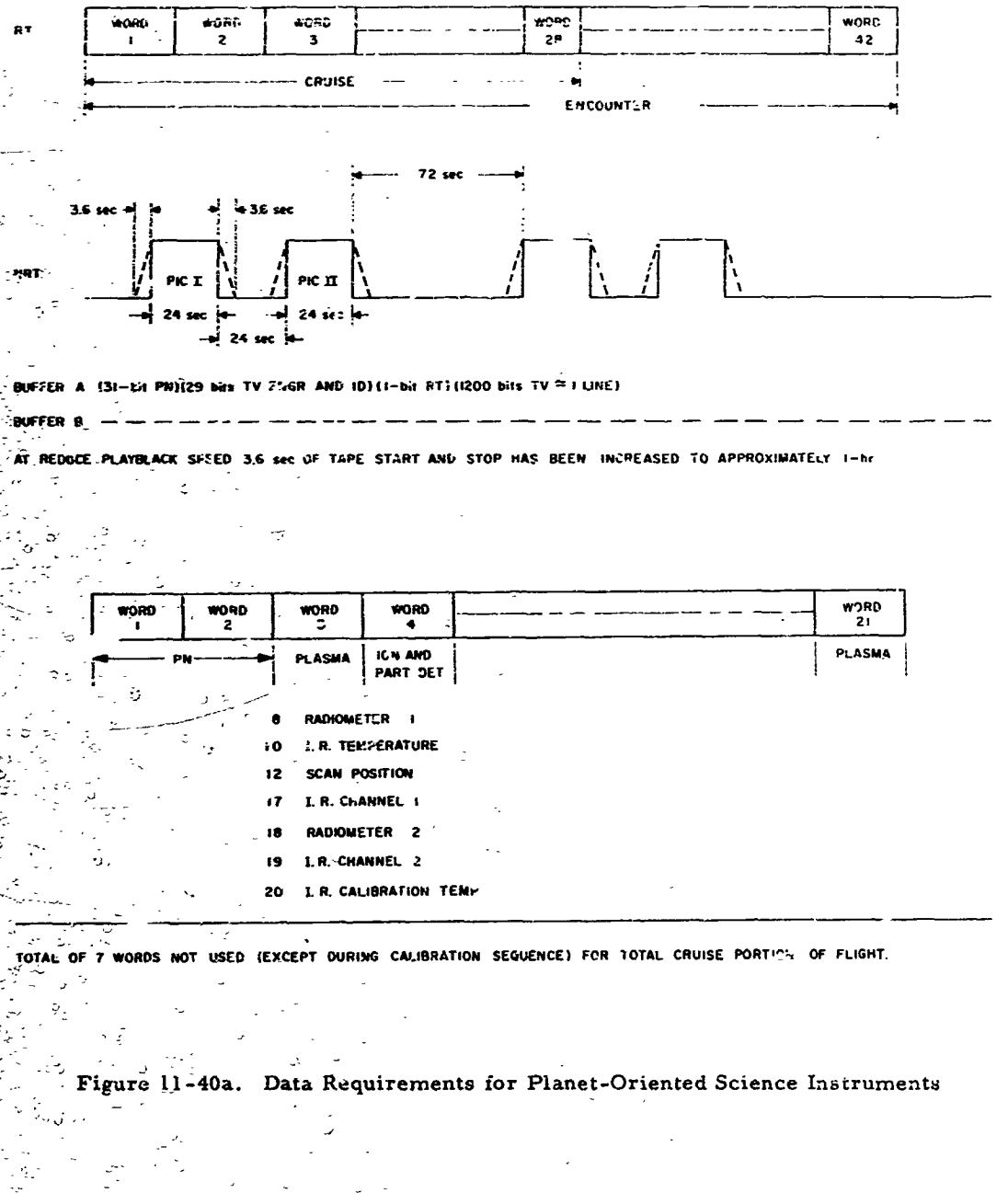


Figure 11-40a. Data Requirements for Planet-Oriented Science Instruments

(5) UV Spectrometer. Low rate (4 b/s) data will be gathered during the entire orbit for several orbits for later playback.

From apoapsis to approximately ±90 degrees from apoapsis, power may be turned off for the IR Interferometer, Mars Scanner, and Television instruments with the exception that heater power must be maintained on the IR Interferometer.

b. Data Storage

(1) Nominal Case. The nominal case (Mars Scanner/Television) data and storage requirements are listed below:

1) Data
   a) Mars Scanner: 15×10^6 bits at 5000 bits/second
   b) Television: 15×10^6 bits at 8000 to 64,000 bits/second
2) Storage

   Tape Storage: 15×10^6 bits, alternate storage of Mars Scanner and Television data (1 orbit Mars Scanner Data, 1 orbit Television data).

   Although Diagram 1 only indicates 7.8×10^6 bits of Mars Scanner Data being acquired each orbit, the instrument is by no means constrained to this amount. For the nominal case, the total Mars Scanner data acquisition about periapsis would be expanded from 20 minutes to approximately 40 minutes. This would bring the total data acquired per orbit up to 15×10^6 bits.

   To simplify the data storage device, the total Television data would be limited to 15×10^6 bits. It should be noted that the data taking rate of the Television instrument is higher than that of the Mars Scanner and is dependent on the characteristics of the TV instrument. For example:

   a) 200 line picture (64 levels), 30 second readout = 240,000 bits/30 seconds = 8,000 bits/second.
   b) 200 line picture (64 levels), 15 second readout = 240,000 bits/15 seconds = 16,000 bits/second.
   c) 400 line picture (64 levels), 30 second readout = 960,000 bits/30 seconds = 32,000 bits/second.
   d) 400 line picture (64 levels), 15 second readout = 960,000 bits/15 seconds = 64,000 bits/second.

   For the nominal case, 15×10^6 bits of storage is consistent with the requirement to have adequate storage for continuous transmission of

data, at the maximum bit rate throughout the orbit having the longest possible period.

2) Four Instrument Case. The maximum case (IR Interferometer, Mars Scanner, Television, UV Spectrometer) requirements are listed below:

1) Data
   a) IR Interferometer: 5.5×10^6 bits at 2000 bits/second
   b) Mars Scanner: 7.8×10^6 bits at 5000 bits/second
   c) Television: 30.0×10^6 bits at 8000 to 64,000 bits/second
   d) UV Spectrometer: 2.4×10^6 bits at 2000 bits/second
   e) Total: 45.7×10^6 bits
2) Storage
   Tape storage: 50×10^6 bits, all instruments having the capability of acquiring data during each orbit as indicated on Figure 11-41.

One possible mechanization would be a system having the following characteristics:

Recorder 1 (20×10^6 bits, one speed)
  Channel 1 - IR Interferometer
  Channel 2 - UV Spectrometer
  Channel 3 - Mars Scanner

Recorder 2 (30×10^6 bits, one speed)
  Channel 1 - Television

3) Data Readout
   The capability for selecting the recorded data to be played back (e.g., UV Spectrometer, Television, etc.) is required. The capability of stopping the playback of one instrument's data and switching to the start of another instrument's data is also required. Television data are to be capable of being stopped and then advanced. This advance may be, for example, in increments of 5×10^6 bits throughout the stored TV data.

Once the information is stored, the capability should exist to rerecord new data from each instrument independent of the other instruments (e.g., record new UV data without disturbing the IR Interferometer, Mars Scanner and Television data recorded on previous orbits).

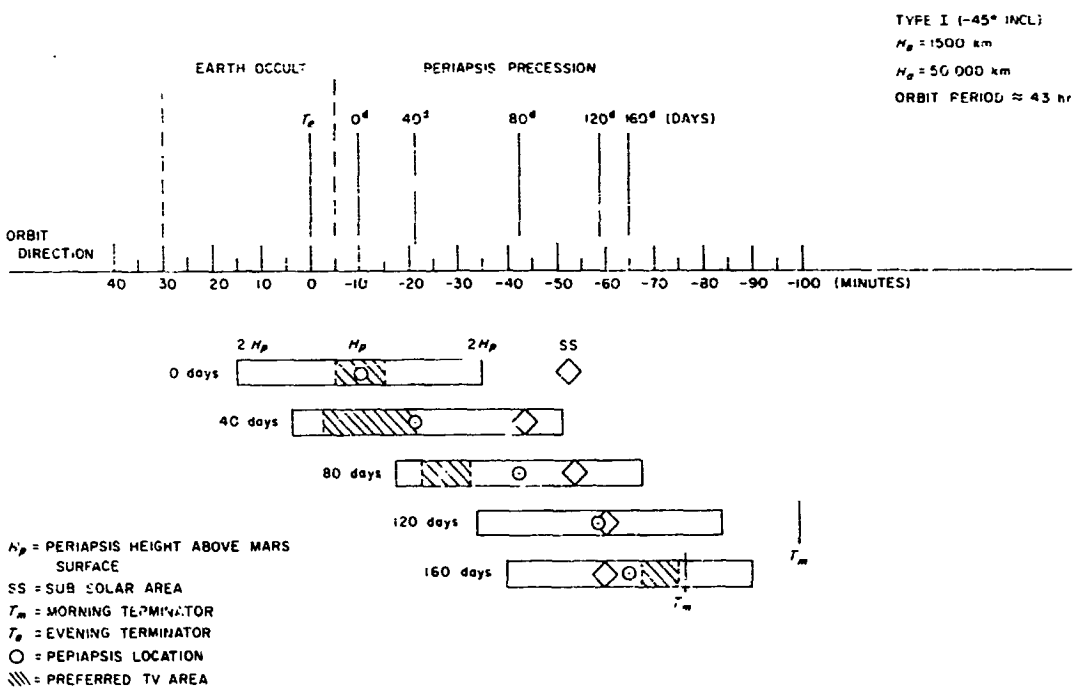


Figure 11-41. Tape Storage Capabilities

4) Scan Platform

The proposed Scan Platform requirements are based on a two (2) degree of freedom platform which can be incrementally updated in both directions. In the direction perpendicular to the plane of the orbit, a nominal latitude is to be chosen and then updated periodically throughout the life of the mission (every 10 to 20 days), or whenever any special coverage by the Scan Platform instruments is required.

It would be desirable to reposition the Scan Platform in the plane of the orbit approximately ten times during the 180 degree lit portion of the planet. These ten positions would not necessarily be equal increments apart. This capability has not been provided in the nominal case.

The UV Spectrometer is not to be mounted on the Scan Platform and can be considered mounted on the spacecraft bus. This can be accomplished if the mounting structure on the bus is designed to rotate the Spectrometer about its pointing axis. The position of the Spectrometer will be set so that the Spectrometer slit is parallel to the limb of the planet. The spectrometer is to be rotated so that the slit is parallel to the terminator when the terminator is scanned: this may be done between orbits if necessary.

5) Communications Rate

The Communications Rate in orbit is to be capable of being changed so as to provide the maximum information for the life of the mission. The probability of mission failure versus life in orbit should be considered in arriving at these communications rates. For the purposes of this mission three (3) communications rates in orbit are considered although many more are possible.

6) Commands

Both the Real Time and Stored Time commands are listed in Table 11-38.

Table 11-38. Science System Command Requirements (Mariner 1969)

Instrument	RT Commands		Stored Commands	
IR Spectrometer	1*	Power On	1	To** = Minus 2 Hours IR Spectrometer Power On
	2*	Power Off	2*	To = 100 Min. IR Spectrometer Power Off
IR Interferometer	3*	Power On		To = Minus 2 Hours IR Interferometer Power On
			3*	To = Minus 29.5 Min. Remove IR Interferometer Black Body
	4*	Power Off	4*	To = T1 + 40 Min. (a) IR Interferometer Power Off (b) Replace IR Interferometer Black Body
Mars Scanner	5	Power On		To = Minus 2 Hours Mars Scanner Power On
			5	To = T2 + 20 Min. Mars Scanner Power Off
	6	Power Off		
	7	Scan Amplitude 1		
	8	Scan Amplitude 2		
	9	Scan Amplitude 3		
	10	Scan Position 1		
	11	Scan Position 2		
	12	Scan Position 3		
	13	Scan Position 4		
	14	Scan Position 5		
Television	15	Power On		To = Minus 2 Hours Television Power On
	16	Power Off	6	To = T3 + 15 Min. Television Power Off
	17	Update Settings		
UV Spectrometer	18*	Power On		
	19*	Power Off		
	20*	Update Slit Angle		

Table 11-38. (cont)

Instrument	RT Commands		Stored Commands	
Two Frequency Occultation Beacon	21	Power On	7	T = Time = Solar Panel Extension Extend Antenna
	22	Power Off		
Mars RF Noise Detector	23	Power On		T = Time = Solar Panel Extension Extend Antenna
	24	Power Off		
Magnetometer	25	Power On		T = Time = Solar Panel Extension Extend Boom
	26	Power Off		
Plasma Probe	27	Power On		
	28	Power Off		
Energetic Particles	29	Power On		
	30	Power Off		
Micrometeorite Detector	31	Power On		
	32	Power Off		
DAS	33*	Start Playback of IR Interferometer Data	8*	To = 0 Start Transmission of IR Spectrometer Data
	34*	Stop Playback of IR Interferometer Data		To - 100 Min. Stop Transmission of IR Spectrometer Data
	35	Start Playback of Mars Scanner Data	9	To = Minus 30 Min. IR Interferometer/Mars Scanner/IR Spectrometer Calibrate
	36	Stop Playback of Mars Scanner Data		
	37	Start Playback of Television Data	10	To = Minus 2.5 Min. Record IR Interferometer/Mars Scanner Data
	38	Stop Playback of Television Data		
	39	Advance Television Data	11	To = Plus 2... Min. Stop Recording IR Interferometer/Mars Scanner Data
	40*	Start Playback of UF Spectrometer Data		

Table 11-38. (cont)

Instrument	RT Commands		Stored Commands	
DAS	41*	Stop Playback of UV Spectrometer Data		
	42	Readout Occultation Data		
	43	Readout Mars RF Noise Detector Data	12*	To = T1 Record IR Interferometer Data
	44	Readout Fields and Particles Flare Data		To = T1 + 40 Min. Stop Recording IR Interferometer Data
	45	Calibrate Science		
	46	Cruise Data Rate (Backup)		
	47	Orbit Data Rate 1 (Backup)		
	48	Orbit Data Rate 2 (Backup)		
	49	Orbit Data Rate 2 (Backup)	13	To = T2 Record Mars Scanner Data
				To = T2 + 20 Min. Stop Recording Mars Scanner Data
			14	To = T3 Record Television Data
				To = T3 + 15 Min. Stop Recording Television Data
			15*	To = T4 (a) Switch UV Spectrometer to High Data Rate (b) Record UV Spectrometer Data
				To = T4 + 20 Min. (a) Switch UV Spectrometer to Low Data Rate (b) Stop Recording UV Spectrometer Data
			16	To = T5 Store Occultation Data

Table 11-38. (cont)

Instrument	RT Commands		Stored Commands	
IRAS			17	To = T5 + 2 Min. Stop Storage of Occultation Data
			18	T = Time = Cruise Science Power On + 1 Min. Cruise Data Rate
			19	To = Time = Injection Orbital Data Rate 1
			20	To = Time = Injection + 60 Days Orbital Data Rate 2
			21	To = Time = Injection + 120 Days Orbital Data Rate 3
			22	T = 1/week Calibrate
Scan Platform	50	Scan Platform Update (Plane of Orbit) (Backup)		To = Minus 2 Hours Scan Platform Update
	51	Scan Platform Update (Perpendicular to Plane of Orbit)	23 thru 32	To = T_{p1} through T_{p10} Scan Platform Update
General	52	Cruise Science On	33	To = Minus 2 Hours Remove Encounter Instrument Sensor Covers
	53	Cruise Science Off		
	54	Encounter Science On		
	55	Encounter Science Off		
	56	Remove Encounter Instrument Sensor Covers (Backup)	34	T = Time = Solar Panel Extension Cruise Science Power On

Table 11-38. (cont)

Instrument		RT Commands		Stored Commands	
General		57	Set $T_1 = 0$		
		58*	Set T_1		
		59	Set T_2		
		60	Set T_3 Quantitative		
		61*	Set T_4		
		62	Set T_5		
TOTAL	Nominal	49 RT COMMANDS		28 STORED COMMANDS	
	Maximum	62 RT COMMANDS		34 STORED COMMANDS	

*Commands not required for the Nominal Case (Mars Scanner and Television)

**Definitions:

T = Cruise time

To = Orbital times (referenced from the Morning Terminator)

F. PROPULSION SYSTEMS

1. Introduction

Since the propulsion system(s) of an orbiting vehicle comprise 50 percent or more of the injected spacecraft mass, it is more important in a time-limited feasibility study to characterize the performance (payload) capabilities of prime candidate systems in some detail rather than to make more general parametric comparisons of a wide variety of systems. The approach taken in this study has therefore been to focus attention on two systems which appeared to be quite suitable for the mission. The basis on which these systems were selected will be discussed subsequently. The candidate systems were:

1) A solid retro motor for the insertion-into-orbit maneuver combined with a monopropellant liquid system for the midcourse corrections.
2) A liquid bipropellant liquid system which, operating at a single thrust level, would provide both the course-correction and injection maneuvers.

The chosen systems were selected on two bases, as discussed below in a. and b.

a. Projected Schedule

A rough projected schedule for the 1969 mission was considered. This schedule showed that very little time was available for advanced development directed toward the 1969 mission. It is doubtful that a new system concept could be incorporated unless its feasibility had been demonstrated by the start of CY 1965. Advancements in component areas which did not alter the basic system concept might be incorporable if they became available during the succeeding six months. Since these dates left very little time for advanced development (compared with typical propulsion development schedules), interest was focused on systems which are representative of or close to the current state-of-the-art. The liquid monopropellant, high performance solid propellant and storable liquid bipropellant systems fall into this category as, indeed, do several liquid propulsion systems employing cryogenic propellants. The choice was then further limited on the basis of the following considerations.

b. Voyager Propulsion Studies

Results from JPL's Voyager propulsion studies were considered. As shown in the studies documented in JPL EPD-139, Volumes I and II, use of the more highly developed cryogenic systems (e.g., $F_2 - N_2H_4$) for Mars orbiting Voyager missions yielded only a 10-15 percent increase in the payload over the solid/liquid-vernier system or the bipropellant liquid system. Comparison of the Voyager mission with the current Mariner mission shows that the spacecraft injection mass has decreased by a factor of three and the velocity

increments have decreased by 30 percent due respectively to the smaller vehicle and more elliptical orbits which are currently being studied. Both of these factors reduce the performance advantage of the cryogenic system with the result that it is improbable that the high impulse system would deliver more than a 5 percent increase in payload over the selected systems for the Mariner mission. In view of the substantially greater development risk associated with the cryogenic system, it was concluded that it should not be considered a primary candidate for this study. As time permits, this system will be considered in some detail in follow-on phases of the Mariner 1969 studies.

2. Mission Considerations

a. Velocity Requirements

Figure 11-42 shows the impulsive velocity requirements for the two orbits considered in detail in this report, namely, a periapsis of 4000 km and apoapsis of 50, 000 km and a periapsis of 1500 km and apoapsis of 50, 000 km. The figure shows that, for the range of approach velocities of interest (3.5 - 4.5 km/sec), the velocity decrement requirements range from about 4750 - 8000 ft/sec.

b. Propellant Variation Concept

As shown in Section VIII (Mission Analysis), there is a substantial variation in the achievable orbiter mass if the propellant loading for the retro-into-orbit maneuver may be varied during the launch period. As a typical example, from Figure 8-34 one may observe a difference of 0.0296 in orbiter-to-injected-spacecraft mass ratio over a 30-day launch period. For an injected spacecraft mass of 2300 lbm, this represents a difference of 68 lbm between the case where the retro propellant may be varied continuously during the launch period and the case where this loading is fixed throughout the period. It is therefore important to state the concept which has been adopted with regard to retro propellant variations during the launch period.

Preliminary considerations have indicated that it is feasible to consider daily variation of the loading of a liquid retro propulsion system. However, the methods for accomplishing this variation are not attractive. Either additional ground lines (probably at least four) would have to be added to the umbilical or external lines would have to be connected. The latter in turn requires gaining access to the spacecraft inside the shroud. It is believed that both methods (the latter in particular) might produce deleterious effects on the mission reliability. On the other hand, the performance penalty of the fixed loading case, which is of particular interest for the solid retro alternative, was so large that the feasibility of the mission was

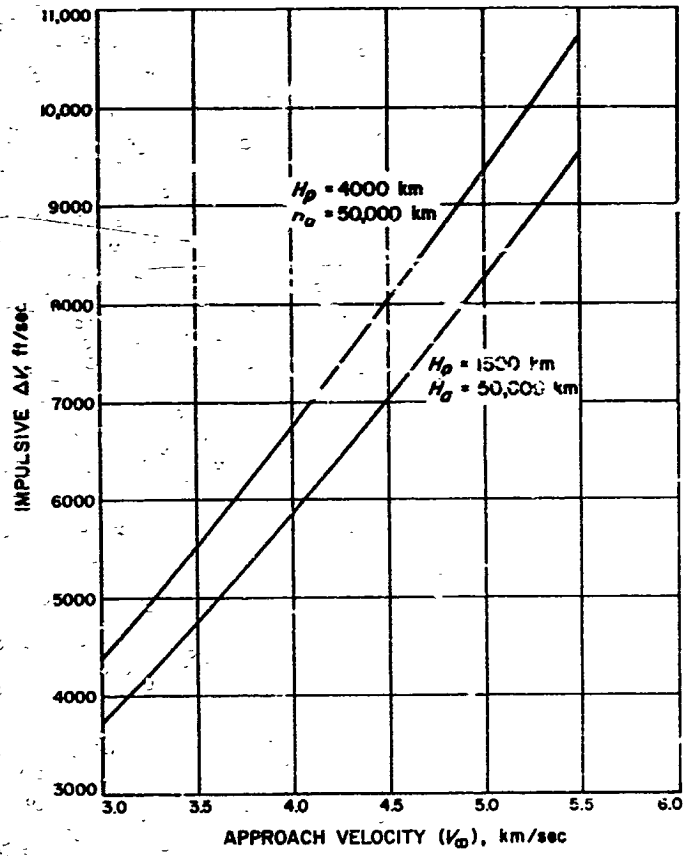


Figure 11-42. Impulsive Velocity Increment for Martian Orbits

questionable. For these reasons, a system of varying the retro propellant loading once or perhaps twice during the launch period was selected as the proposed concept. In this way, the launch period is broken up into two or three discrete intervals. For the liquid system, the variation would be accomplished either by attaching lines while the spacecraft was on the launch pad or destaging and accomplishing the propellant transfer in the ESA. While the latter would not at first appraisal appear to be attractive, there are other components on the spacecraft, such as batteries, for which a recycle requirement exists. Thus it is possible that variation of the propellant loading at the established recycle times might incur little penalty. For the solid system, the variation in propellant loading would be accomplished by substitution of a different retro motor which would be identical in all respects except for the amount of propellant loaded. Two or three flightworthy solid motors would then have to be available to support each launch.

A rigorous analysis to define the optimum times and amounts of propellant variation has not as yet been accomplished. This remains as a prime task for the Launch Operations Analysis in subsequent studies. However, preliminary results indicate that one or two propellant variations during the launch period will allow use of a payload which is close to the daily-variable maximum. Combination of these results and the foregoing remarks on launch operations have led to the selection of the stepwise loading concept for this study. It is clear that further studies in this area will be required.

c. Meteorite Impact

No allowance for meteoric damage has been made in this study. While it is recognized that such a problem potentially exists, it was felt that the available crude estimates of the puncture probability preclude selection of an impact design criteria on a rational basis. This is another area which should be firmed up in subsequent studies. It is noted that the meteorite impact consideration might tend to favor the use of aluminum instead of titanium for tankage applications.

3. Solid Propellant Retro Motor

a. Propellant

The propellant is a composite solid propellant containing beryllium (Be) as a high energy fuel ingredient. Predicted propellant characteristics are shown in Table 11-39. These values are nominal and typical of the propellants currently being screened and evaluated for advanced motor programs.

Table 11-39. Solid Propellant Retro Motor Characteristics for a Mariner 1969 Mars Orbiter Mission

Specific Impulse:	310 lbf-sec/lbm
Expansion Ratio:	50 : 1
Burning Rate at 500 psi:	0.30 in/sec
Temperature Sensitivity of Chamber Pressure (π_K):	0.10%/°F
Pressure Exponent (N):	0.28
Propellant Density:	0.06 lbm/in^3

b. Motor Design Parameters

The primary design parameters of the motor are the following:

1) A total motor weight range of 1000 to 1500 lbm.
2) A thrust level consistent with maximum accelerations of 2 to 5 g's.
3) An expansion ratio of 50.
4) A case-bonded grain design.

The motor inert weights are based on the use of titanium for case material and a composite, ablative nozzle with a hard throat insert. The motor mass fraction is 0.90, which does not include any weight for thrust vector control.

c. Thrust Vector Control System Design Parameters

The primary design characteristics of the motor thrust vector control system which provides pitch and yaw capability are the following:

1) The total system weight is approximately 44.0 to 56.0 lbm for the range of motor weights being considered.
2) These weights are based on a nominal thrust vector excursion of 0.5 degrees for the larger motor.
3) The working fluid for the secondary injection system is Freon.
4) The driving force is provided by a blow-down, cold-gas (N_2) pressurized system at a final pressure of 500 psi.

When the thrust vector control system is included with the rocket motor, the overall subsystem mass fraction is reduced to 0.86.

d. System Performance

The ratio of orbiter mass to injected spacecraft mass for a solid propellant retro system is shown in Figure 11-43. These calculations are based on the following:

1) Use of a monopropellant midcourse system described in paragraph 4. to perform a maneuver of 100 meters/second.
2) A solid propellant specific impulse of 310 ibf-sec/lbm and a motor mass ratio of 0.86 which includes thrust vector control. Mass ratio is defined as the ratio of propellant weight to retro propulsion system weight.

The mass fraction above provides for the nozzle, the motor case, the ignition system, attachment on the case, and thrust vector control in pitch and yaw (actuator, fluid supply, high pressure regulation and valves). The mass fraction does not provide for structure beyond the case attachment fittings, cabling beyond the ignition pigtails, power supply for the igniter and thrust vector control, thermal control and for roll control during the retro maneuver.

Two performance curves are shown in Figure 11-42. The lower curve is based on carrying the midcourse propulsion system through the orbit retro maneuver. The upper curve is based on jettisoning the midcourse system prior to the orbit retro maneuver. Jettisoning of the midcourse propulsion unit provides for significantly higher payload weight in orbit. It is recognized that development of the system to jettison the midcourse unit may be a difficult problem, particularly in the face of a requirement that the probability of the ejected unit impacting the planet must be less than 10^{-4}. Some consideration has been given to packaging the midcourse unit in the nozzle of the solid motor, a proposition which is attractive from the volume requirements standpoint, but not too attractive from the standpoint of thermal control. Detailed study in the follow-on phases is required to establish the feasibility of jettisoning the midcourse unit.

4. Midcourse Propulsion System

The propulsion system for the midcourse trajectory-correction is a monopropellant hydrazine fueled unit similar to that utilized in the Ranger and Mariner C spacecrafts. It consists of a small constant thrust rocket capable of providing variable total impulse. The fuel is pressure-fed from the bladdered tank by pressure regulated compressed nitrogen gas. The engine contains a spontaneous catalyst bed to decompose the hydrazine. The system schematic is presented in Figure 11-44.

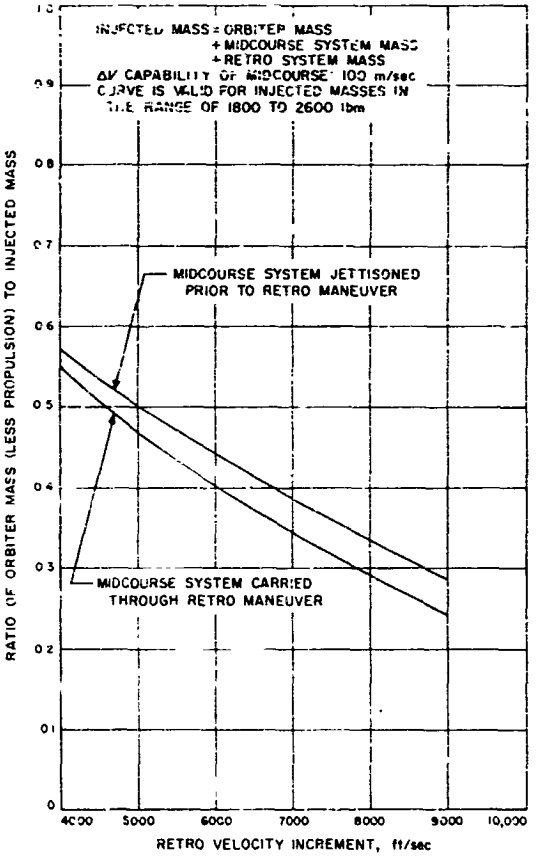


Figure 11-43. Ratio of Orbiter Mass to Injected Spacecraft Mass for Solid Propellant Retro System

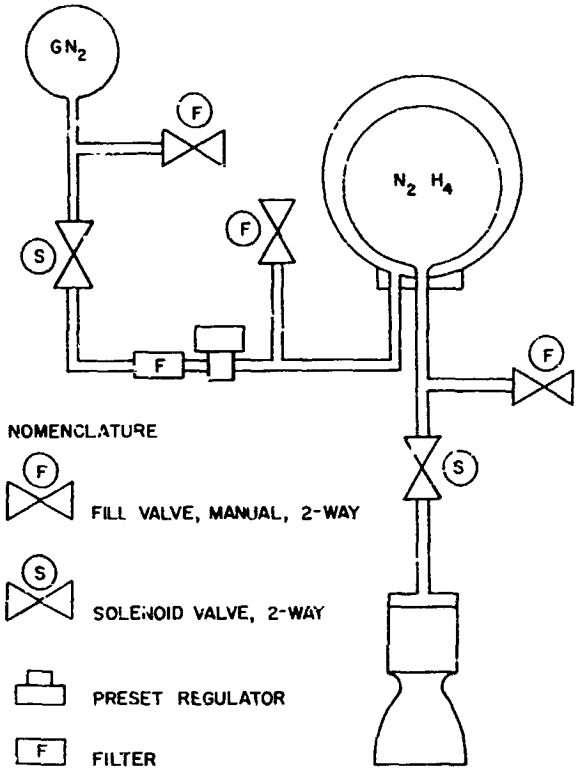


Figure 11-44. Regulated-Gas-Pressure-Fed Constant Thrust Spacecraft Propulsion System Monopropellant Hydrazine

The delivered vacuum specific impulse of hydrazine is 235 lbf-sec/lbm for an engine nozzle expansion ratio of 44:1 and chamber pressure of 190 psia. Jet vanes are installed at the nozzle exit plane to provide thrust vector control during engine firing. The propulsion system is capable of operating between +35°F and 125°F. The nominal engine performance and propulsion design features are summarized in Table 11-40. The propulsion system mass for total velocity increments in the range between 50 and 200 meters per second with an injected spacecraft mass between 1400 and 2800 pounds is shown in Figure 11-45.

The modifications to the Mariner C propulsion unit incorporated for the 1969 mission are larger tanks, three-start capability, replacing of the explosives valves with solenoid valves to alleviate the packaging problems associated with a three-start capability, and use of the spontaneous catalyst. The spontaneous catalyst has been developed under NASA contract NAS 57-9 and is at the stage where it can be considered for flight use.

Table 11-40. Monopropellant Midcourse Propulsion System Characteristics For Mariner 1969 Mars Orbiter Mission

Propellant:	N_2H_4 Monopropellant
Specific Impulse:	235 lbf-sec/lbm
Thrust Vector Control:	Jet Vanes
Thrust:	50 lbf
Chamber Pressure:	190 psia
Expansion Ratio:	44:1
Temperature Range:	35°F to 125°F
Number of Starts:	3
Tank Pressurization:	Gaseous Nitrogen
Propellant Tank Operating Pressure:	310 psia
Initial Nitrogen Tank Pressure:	3300 psia

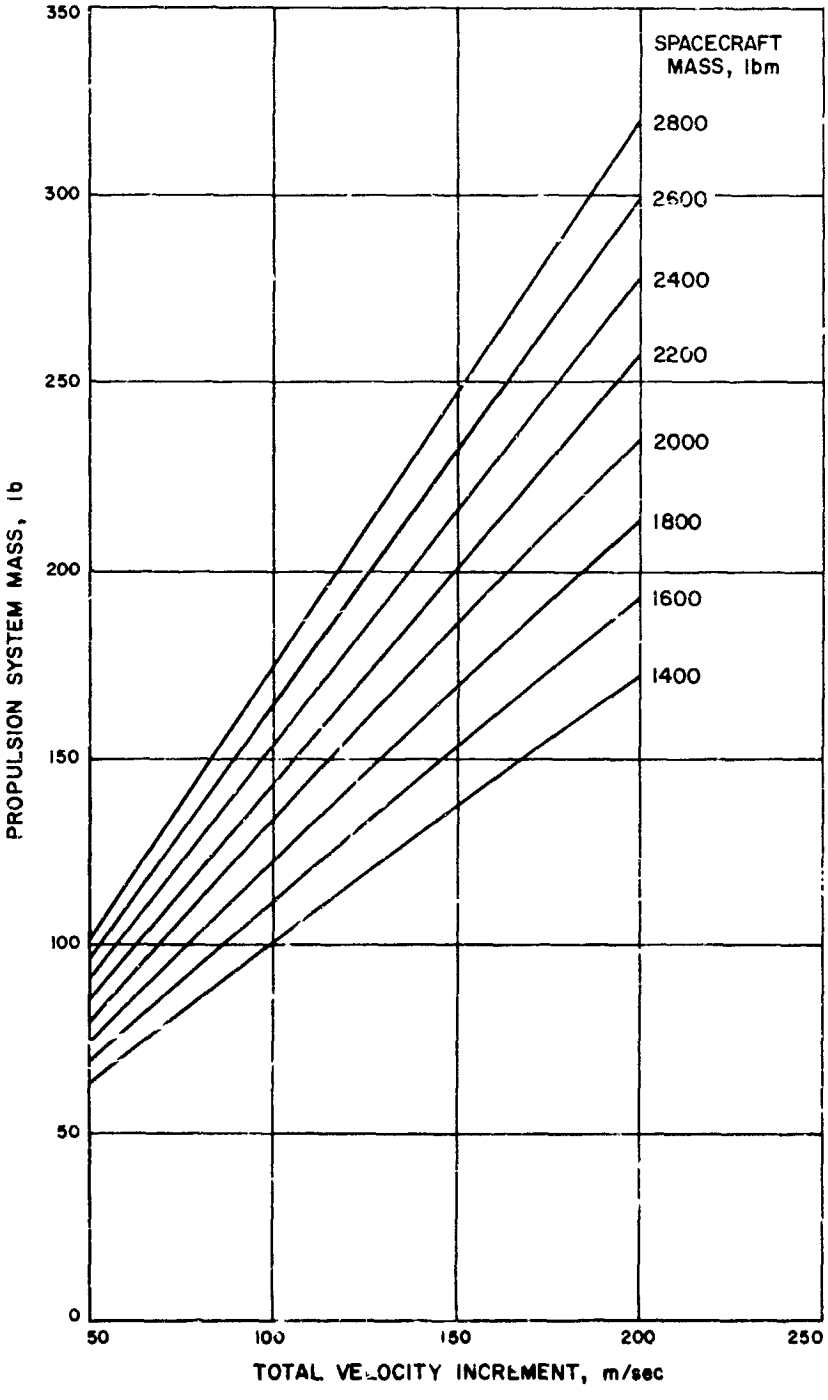


Figure 11-45. Monopropellant Propulsion System Mass

5. Bipropellant Liquid System

a. Propellants

The propellants chosen for this application were hydrazine (N_2H_4) and nitrogen tetroxide (N_2O_4). These were chosen because they yield the highest performance of any of the hydrazine, hydrazine-derivative, or hydrazine-blend family of fuels with the nitrogen tetroxide oxidizer. The specific impulse of this system is 317 lbf-sec/lbm at the 96 percent efficiency level for both the combustion and expansion processes, at a mixture ratio of 1.2 and an expansion ratio of 80:1. A major influencing factor in the choice of N_2H_4/N_2O_4 was the extent of the development work which has been accomplished. Also, both propellants have flown previously in other systems. The thermal control limitations are dictated by the freezing point of hydrazine and the vapor pressure of nitrogen tetroxide. Under the expected operating pressures, these limits are 35°F to 125°F.

b. Components

Figure 11-46 shows a schematic of the storable liquid bipropellant system. As shown in this figure, the system features cold gas-helium pressurization and positive expulsion bladders for the propellant tanks. The helium and propellant tanks are titanium, while the bladder material is teflon with a 10 percent aluminum powder dispersion. Solenoid type pressurizing valves are incorporated to prevent mixing of propellant vapors which might permeate the bladders during the coast phase of flight. The thrust chamber is composed of a refrasil phenolic material with a hard throat insert (JTA graphite) and a metallic nozzle extension.

Figure 11-47 shows the estimated mass of such a thrust chamber as a function of thrust and is plotted parametrically with chamber pressure and expansion ratio as variables. This figure shows that the estimated mass of the thrust chamber can be from about 21-45 lbm depending upon the chosen design parameter trade-off. It should be noted that this curve was derived for a total impulse requirement o 360,000 lbf-sec. The proposed injector is a doublet type with a regeneratively cooled injector plate.

Thrust vector control for this system is provided by gimballing the chamber for pitch and yaw control with auxiliary cold gas jets provided for roll control.

An alternative system concept is to utilize three smaller motors of the same construction, but with a lower thrust level. Single oxidizer and fuel tanks would feed propellants to the three motors. All three motors would have throttling capabilities to effect pitch and yaw control and one motor would be hinged to allow roll control. The mass of this system is roughly equivalent to the single motor system with cold gas roll control.

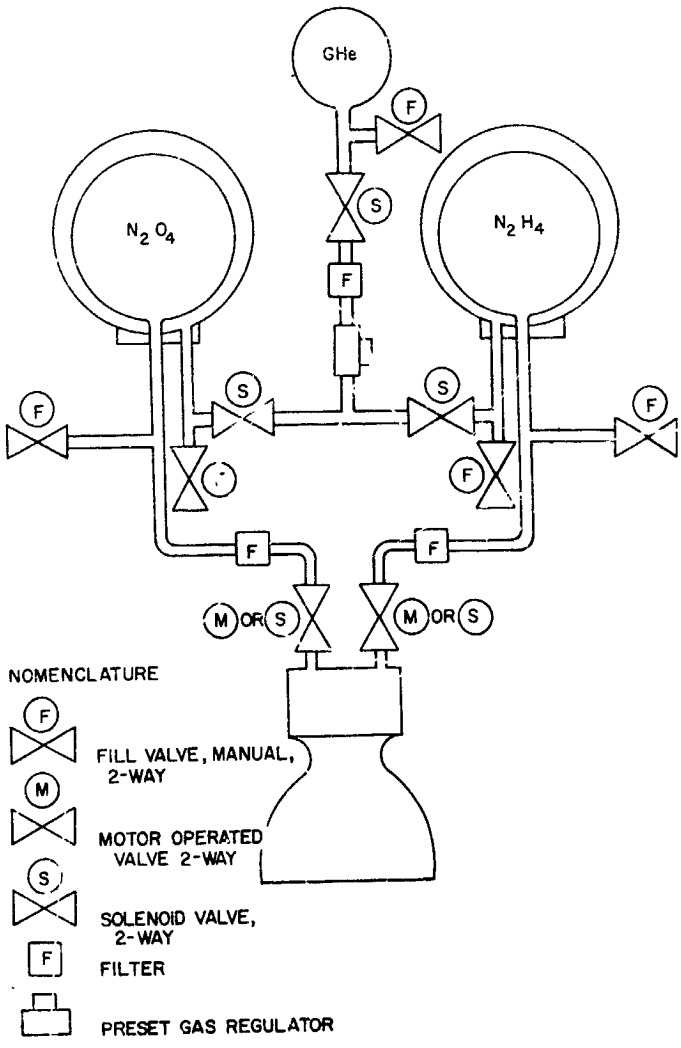


Figure 1-46. State of the Art Bipropellant System Schematic Cold Gas Pressurization System

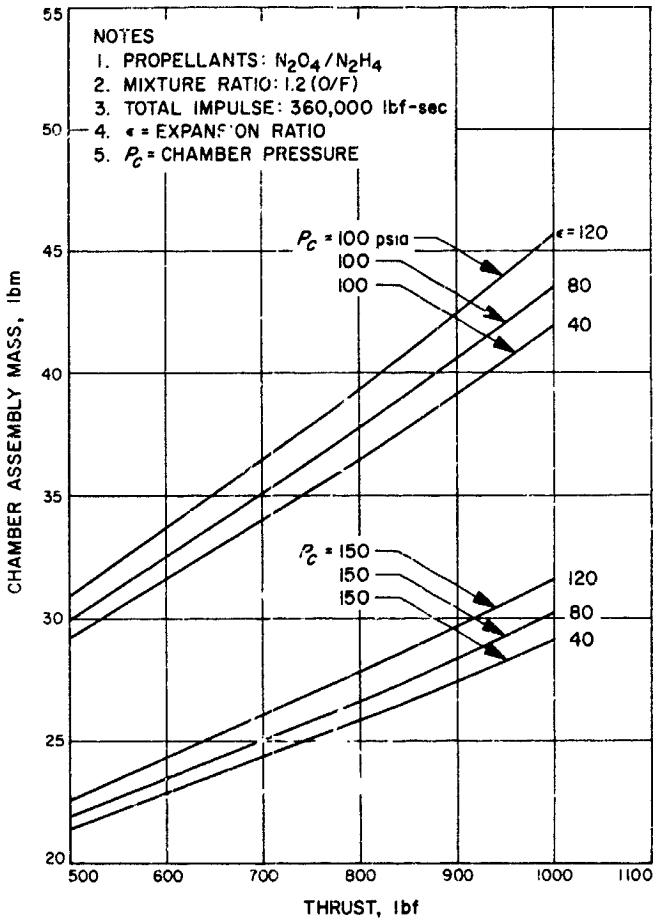


Figure 11-47. Mass of State-of-the-Art Ablative Thrust Chamber Assemblies

c. Design Parameters

Some of the pertinent design parameters which have been chosen for the single motor system are listed below:

Thrust	600 lbf
Chamber Pressure	150 psia
Expansion Ratio	80:1
Mixture Ratio	1.2
Propellant Tank Operating Pressure	250 psia
Helium Tank Initial Pressure	4000 psia

d. System Performance

Figure 11-48 shows the ratio of orbiter mass to total spacecraft mass as a function of total velocity increment required of the propulsion system. This curve is drawn for injected spacecraft masses between 1800 and 2600 lbm for the bipropellant storable liquid system.

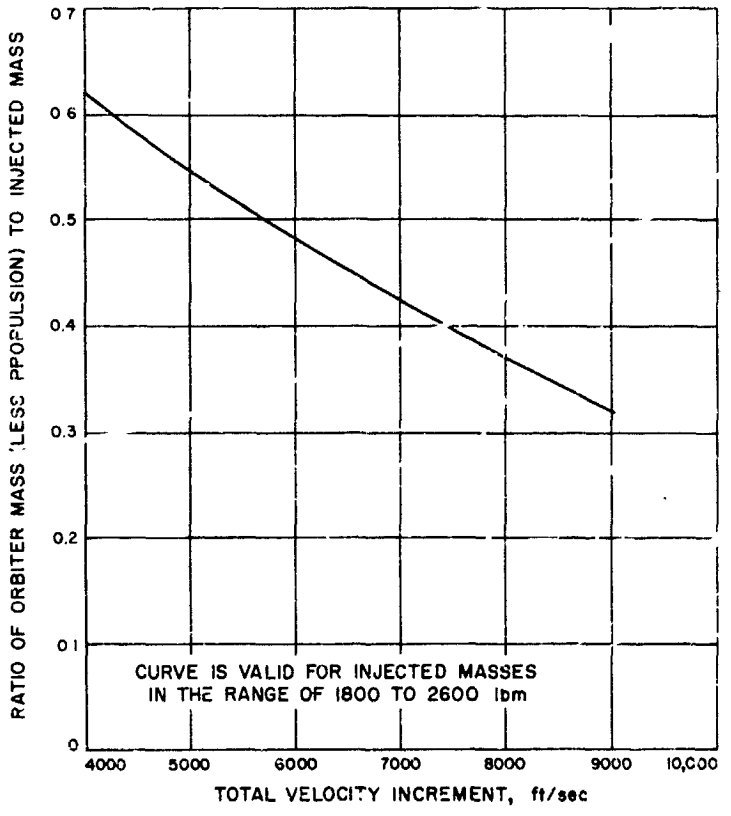


Figure 11-48. Ratio of Orbiter Mass to Injected Spacecraft Mass for Liquid Bipropellant Retro System

e. Configuration and Variation

The configuration for the storable liquid bipropellant is envisioned as having both the oxidizer and fuel tanks in-line, the oxidizer tank being forward of the fuel tank, with the helium supply being stored in two tanks as shown on Figure 10-1. A variation of the above concept would have the propellant tanks side by side with the helium supply stored in a single tank mounted on the spacecraft roll axis. This configuration is shown in Figures 11-78, 11-79, and 11-80. The single gimballed engine would, in both of the above cases, be mounted

on the nominal spacecraft roll axis. The alternate three-engine system would have the motors mounted at the vertices of an equilateral triangle. This variation could be utilized with either of the above mentioned propellant tank mounting concepts.

6. Small Correction Vernier System

As discussed in Section VIII. D, it may be desirable to be able to perform accurately very small final midcourse corrections. The range of maneuvers under consideration is from several tenths of a meter per second to several meters per second. These requirements must be compared with the minimum ΔV capability of the propulsion system used for midcourse correction. For the monopropellant system of the proposed solid/monopropellant combination, the predicted value for ΔV_{min} was about 0.15 m/sec. Thus, this system would be capable of completing the smallest maneuvers which might ever be attempted. On the other hand, the ΔV_{min} capability predicted for the 600 lbf thrust bipropellant system was about 0.6 m/sec. Therefore, it appeared desirable to determine the approximate mass of a system which would be capable of providing velocity increments in the range of 0.1 to approximately 4 or 5 m/sec. The upper end of the range was extended beyond the ΔV_{min} capability of the bipropellant system on the basis that the small thrust system would be used for these maneuvers because of its inherently smaller system errors. Further analysis of nominal midcourse velocity increment requirements will have to be made before a decision is made to incorporate such a system.

Three types of propulsion systems have been considered to determine their capability of accurately providing very small velocity increments. These were:

1) A cold nitrogen gas system similar to those commonly used for attitude control.
2) The Curtiss-Wright cap pistol concept which is currently being developed under NASA contract and is to be used on future Tiros spacecraft as an experiment. It is noted that this system will be a strong contender for other propulsive applications such as attitude control provided it is demonstrated satisfactorily in the forthcoming tests. Its state of development was not far enough advanced that it could be considered for such use in the Mariner 1969 spacecraft, however. Its proposed application as a vernier correction unit is justified because this is in a sense a backup or redundant system for the main propulsion unit.
3) A monopropellant hydrazine system utilizing Mariner C technology with a scaled-down engine of approximately five pounds thrust.

The cap pistol unit provides approximately three pounds of thrust. The three propulsion system masses are shown in Figure 11-49 for total velocity increments from 0.1 to 10 meters per second and spacecraft masses between 2200 and 2500 pounds. The propellant masses were determined based on specific impulses of 60, 200, and 235 lbf-sec/lbm for the

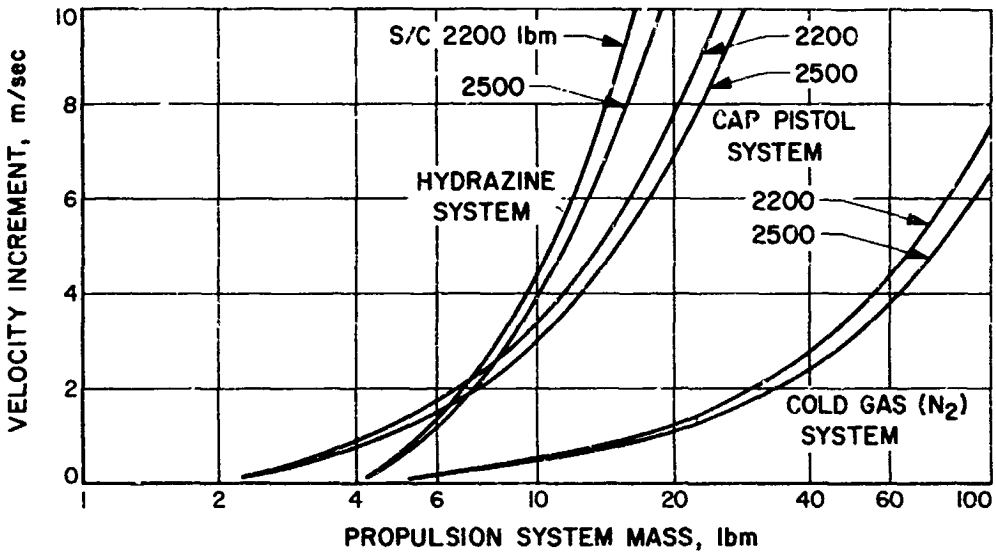


Figure 11-49. Small Correction Propulsion System Mass

cold gas, cap pistol, and hydrazine systems, respectively. It appears that the minimum velocity increment capability of any of the systems from a propulsion standpoint would be $\leq 1 \times 10^{-3}$ m/sec. Thus the accuracy of the maneuver would probably not be governed by the propulsion system performance limitations.

7. Nominal Case Propulsion System Conceptual Designs

a. Trajectory Data

To complete the conceptual design, a "baseline" propulsion system was required. This in turn led to a reexamination of the trajectory requirements in view of the assumed concept for variation of the retro propellant loading. A comparison of the spacecraft injection capabilities from the two launch-vehicle curves with the different energy requirements of the two periapses altitudes led to the selection of two missions as feasible alternates (ones for which the launch vehicle capability exceeded the injected mass requirement). These missions are summarized in Table 11-41. One may observe that the resultant trade-off is essentially periapsis altitude against launch vehicle capability. Since the time of this selection, the combination of an increasing nominal-case spacecraft mass and changes in the design margin philosophy have pushed the injected spacecraft mass up to the point where the mission with the 1500 x 50,000 km orbit and the "original" injection capability is no longer feasible. However, these numbers are of interest at least in a parametric sense and they have therefore been included.

Table 11-41. Summary of Parameters for Selected Trajectories and Orbits

Propellant Loading Concept: 1 or 2 Variations During Period	
Launch Vehicle Capability: 30% Flox "Original" Curve	Launch Vehicle Capability: 30% Flox "Revised" Curve
Max Hyperbolic Excess Velocity Allowable During Period: 4.2 $\frac{km}{sec}$	Max Hyperbolic Excess Velocity Allowable During Period: 4.2 $\frac{km}{sec}$
Orbit Periapsis 1500 km Apoapsis 50,000 km	Orbit Periapsis 4000 km Apoapsis 50,000 km
Approximate Total Launch Period: 45 Days Type II: 30 Days Type I: 15 Days (DLA > -50°)	Approximate Total Launch Period: 45 Days Type II: 30 Days Type I: 15 Days (DLA > -50°)
Maximum Orbiting Velocity Increment: 6270 fps	Maximum Orbiting Velocity Increment: 7240 fps

To obtain a satisfactory payload fraction, it appeared necessary to restrict the maximum allowable planetary approach velocity to 4.2 km/sec. This value determines the launch periods for the two types of trajectories (Table 11-41). The listed periods are labeled "approximate" because the rigorous analysis has not been completed (see 2-b, above). Specification of the approach velocity allows computation of the velocity increment for the retro-into-orbit maneuver, the governing parameter in propulsion system design.

b. Solid Retro/Monopropellant Midcourse System

A mass breakdown is given for the solid/monopropellant system in Table 11-42. No allowance is added for gravity loss since the thrust level of the retro system is sufficiently large that the transfer is essentially impulsive with respect to energy considerations. The monopropellant system is sized to provide a correction capability of 100 m/sec. Although this is essentially a 6 or 7σ allowance, it is usually wise to carry a capability of this magnitude in order to handle certain non-standard errors (in addition to the expected random errors) (see Section IX). In other words, the additional capability over the 3σ allowance is carried to be able to correct errors which are essentially non-stochastic. Further study of the likelihood of occurrence of these non-stochastic variations will have to be made to ensure that the 60 lbm penalty in spacecraft mass (see Figure 11-45) is justified.

Table 11-42. Mass Breakdown of Solid Propellant Retro Propulsion Systems for Mariner 1969 Mars Orbiter

Orbit	1500 km x 50, 000 km	4000 km x 50, 000 km
Velocity Increments (fps)		
Retro Into Orbit	6270	7240
Gravity Loss	0	0
Total for Retro Motor	6270	7240
Midcourse Correction (Supplied by separate monopropellant system)	330	330
Orbiter Mass (Payload)	995	995
Midcourse System Mass	155	171
Retro Propellant	1030	1303
Propulsion Hardware		
Inert Components	118	147
TVC System	47	60
Total	165	207
Design Margin (15%)	25	32
Total Dry Mass	190	239
Injected Spacecraft	2370	2713
Mass Ratio (W/O Margin)	0.86	0.86
Sensitivity Coefficients: $\frac{lbm^2}{lbf\text{-}sec}$		
$\frac{\partial M_{orbiter}}{\partial 2 I_s}$ $M_{injected}$ = const	3.0	3.8
$\frac{\partial M_{injected}}{\partial 2 I_s}$ $M_{orbiter}$ = const	-6.3	-8.8

Note: The Monopropellant Midcourse System is assumed to be jettisoned prior to the initiation of the retro maneuver.

The nominal case orbiter mass is assumed to be the payload. A breakdown of this 995 lbm may be found in Section X. A design margin of 15 percent has been added to the propulsion hardware mass to be consistent with the philosophy which has been followed elsewhere in the spacecraft. No margin has been added for under-nominal specific impulse and therefore the value used should be regarded as a "guaranteed minimum." To assess the penalty of specific impulse below this value, derivatives have been computed and are included in Table 11-43. For example, if the specific impulse was one lbf-sec/lbm below the 310 nominal in the case of 1500 x 50,000 orbit, the orbiter mass (payload) would have

Table 11-43. Mass Breakdown of Bipropellant Liquid Propulsion Systems for Mariner 1969 Mars Orbiter

Orbit	1500 km x 50, 000 km	4000 km x 50, 000 km
Velocity Increments (fps)		
Retro Into Orbit	6270	7240
Course Corrections	165	165
Gravity Loss	165	165
Total	6600	7570
Orbiter Mass (Payload)	995	995
Propellant Mass	1085	1380
Propulsion System Components		
Residual Propellant	11	14
Pressurant and Tank	49	63
Oxidizer Tank	20	25
Fuel Tank	21	25
Bladders	6	8
Engine	23	29
Components and Plumbing	23	23
Structure	15	19
Gimbal Actuators	10	10
Total	177	216
Design Margin (15%)	26	32
Total System Components	203	248
Injected Spacecraft	2283	2623
Mass Ratio (W/O Margin)	0.860	0.865
Sensitivity Coefficients: $\frac{lbm^2}{lbf\text{-}sec}$		
$\frac{\partial M_{orbiter}}{\partial 2\, I_s}$ M injected = const	2.9	3.5
$\frac{\partial M_{injected}}{\partial 2\, I_s}$ M orbiter = const	-6.9	-9.5

to be decreased 3 lbm if the injected mass (gross) was constant. Alternatively, if the payload were to be constant at 995 lbm, the gross mass would have to increase 6.3 lbm for every 1 lbf-sec/lbm the specific impulse was below nominal.

An idea of the solid motor size may be observed in Figure 11-50. The dimensions on this figure correspond to the 1500 x 50,000 km case. Comparison of these dimensions with ones which are presented in the following section point out one of the great advantages of the solid, namely compact size.

c. Liquid Bipropellant System

Table 11-43 contains the corresponding breakdown for the liquid system. In this case, the lower thrust level requires an allowance for gravity losses. Recent results have indicated that the assumed value of 50 m/sec is quite conservative. The gt_b loss rarely exceeds 15 m/sec or about 1/3 of the assumed value. The midcourse-correction allowance for the liquid system was 50 m/sec. While it may appear that a different philosophy is being followed with the solid/monopropellant system, it was assumed that the few cases which required more than 50 m/sec could be handled by slightly shorting the main propellant loading. Since this option of combining the maneuver allowances did not exist with the solid/monopropellant system, the apparent discrepancy was justified. The remaining parameters in Table 11-43 are analogous to those of Table 11-42. A characteristic specific impulse of 315 lbf-sec/lbm was used to compute the propellant masses which are given in Table 11-43.

Comparison of the total injected spacecraft masses for the solid/monopropellant and bipropellant liquid systems shows an excess of approximately 4 percent for the former. This is mostly due to the fact that the monopropellant system is a somewhat less efficient system than either of the others. The dimensions of a typical stage layout for the bipropellant system (1500 x 50,000 km case) are given in Figure 11-51. The greater volume of this system is readily apparent by comparison with Figure 11-50 which shows the solid motor of the solid/monopropellant system. (The monopropellant system would be mounted separately in a bay of the bus.) Since length appears to be a greater restriction than diameter, an alternate tankage arrangement is sketched in Figure 11-52. While this arrangement reduces the length of the bipropellant system to a more competitive value with respect to the solid system, it is somewhat less desirable for reasons of c.g. control. The alternative arrangements for the bipropellant liquid system will have to be studied in much greater detail before a rational choice may be made between them.

8. Summary

Two systems have been described which appear attractive for the 1969 Mariner Mars Orbiter Mission. While the performance of one was slightly better there was not a great enough performance difference that a system could be selected on this basis alone. A comparison of the individual advantages of the two systems is contained in Table 11-44.

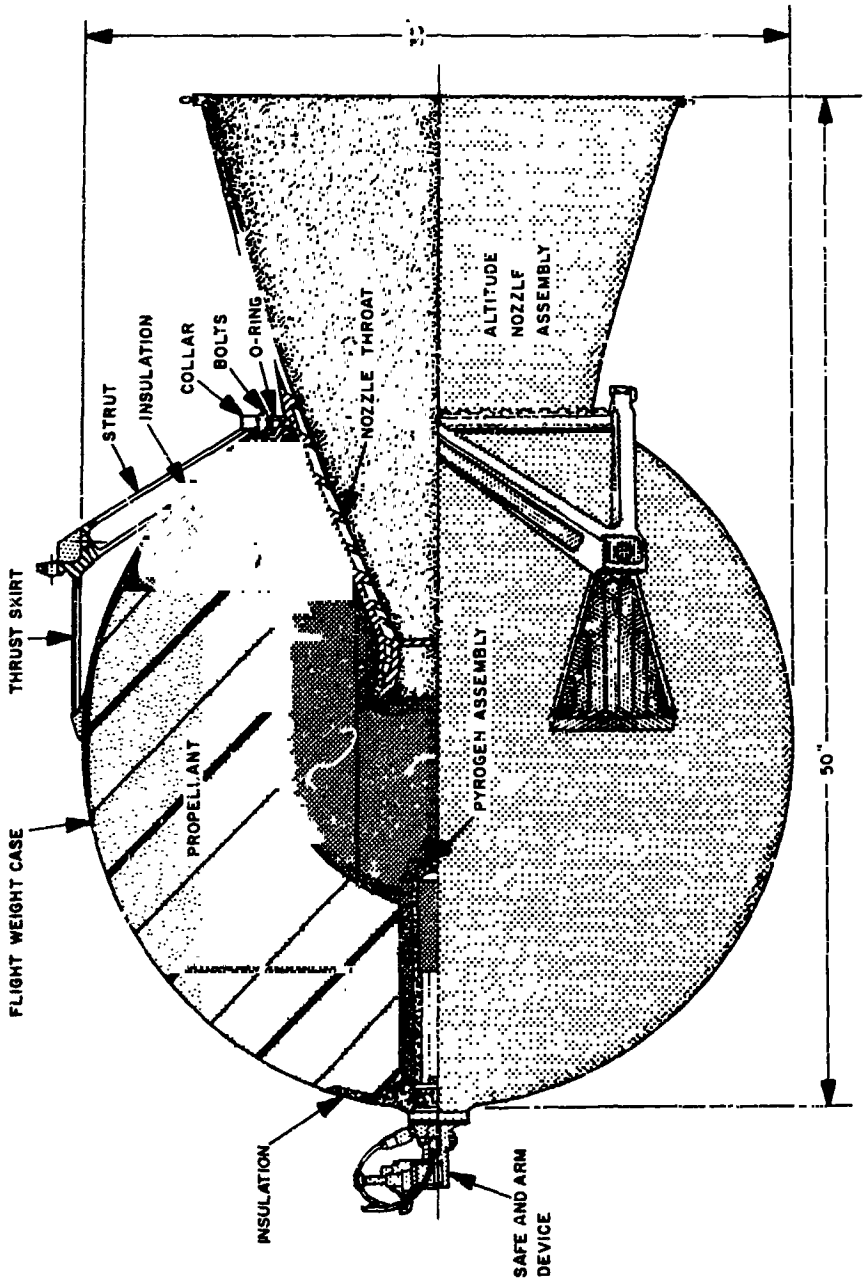


Figure 11-50. Typical Configuration for Solid Propellant Retro Motor

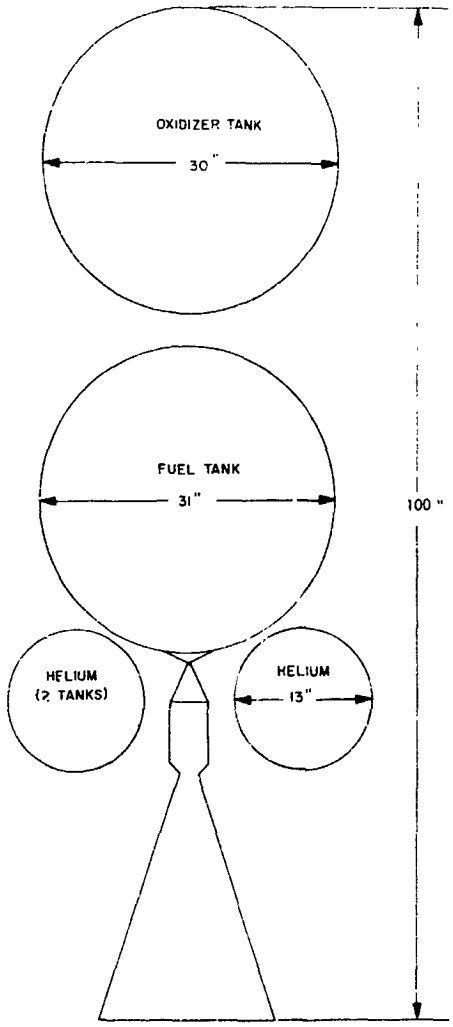


Figure 11-51. Bipropellant Liquid Stage Layout In-Line Tankage

Table 11-44. Summary Comparison of Candidate Systems

Advantages of Solid/Monopropellant System

- More compact system
- Shorter development time for new system
- Less flexible solar panels ease autopilot design
- Capable of making very small correction-maneuvers accurately without a separate system

Advantages of Liquid Bipropellant System

- Flexibility in use of propellant
- Slightly higher payload
- System to jettison monopropellant system is not needed
- Lower solar panel mass because of lower thrust
- More advanced TVC system development
- Lower thrust level eases autopilot design. Only one autopilot needed

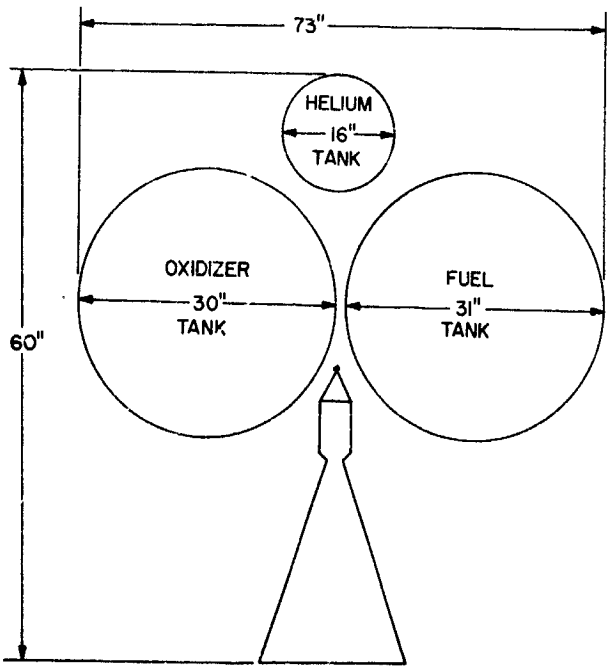


Figure 11-52. Bipropellant Liquid Stage Layout Side-by-Side-Tankage

G. STRUCTURES AND DYNAMICS

The launch environment of the floxed Atlas/Centaur is not expected to be very different from the Atlas-Agena. However, it has been the policy at JPL to perform slow-sweeping sinusoidal vibration tests as part of the qualification requirements for the Proof Test Model (PTM) vehicle. This has historically been the governing design condition for most structural components of any spacecraft even though matching of the input by force limiting has been incorporated into the Design Criteria.

In the light of this requirement several observations can be made. The spacecraft configurations required for this mission are large in mass and their centers of gravity are relatively high. Any meaningful vibration testing should certainly include the long adapter structure and large amplifications in the low-frequency test range can be expected. Structural components which will require special development attention include the solar panels, planet-scan platform, the support structure for the many pressure bottles and the propulsion system.

The scan platform in particular must be an integrated design of the science actuators and the support structure. Very likely, point dampers will be required as is planned in the solar panel supports. The high-gain antenna actuator, since it also will carry structural loads, must be designed integrally with the support structure.

The requirement that the solar panels remain erected during the retro maneuver imposes a requirement for a support at about the quarter point of the panel. The 3/4-g loads caused by the liquid retro should not be a problem, but the nearly 6 g caused by the solid retro will require that the solar panels be reinforced.

The above comments are based on the continuation of the present spacecraft testing requirements which are generally accepted as being conservative. During the early design phase of the project, however, a dynamic loads analysis will be made on the total spacecraft launch vehicle configuration to obtain better low frequency loads data for which the spacecraft should be designed and tested. If this analysis can be implemented and accepted early enough in the program, it will make the structural design problem easier to solve within the weight allocation. This will be because the loads will be based on the total vehicle response to transient excitations coupled with quasi-steady state loads rather than the assumption that the spacecraft may experience sinusoidal vibrations at all frequencies.

H. SPACECRAFT MECHANISMS

The possible mechanisms that are considered compatible with the feasibility study configurations, exclusive of the mechanisms which are part of the guidance and control system are described herein.

The components which are deployed after launch such as solar panels, planet platform, and high-gain antenna will require some degree of latching to the spacecraft structure to limit dynamic excursion and loads during boost and (possibly) injection into Mars orbit. Multi-model components, specifically the solar panels and possibly others will require damping to limit the structural gains during this dynamic loading. This damping can easily be incorporated in the latch link in the form of viscous dampers similar to those successfully used on Ranger spacecraft. These dampers can be completely sealed to avoid possible fluid leakage which may occur with dynamic seals (the Ranger design). Although the roll-axis symmetric low-gain antenna mast will probably not be deployed, similar point dampers may be required in the support members.

Pyrotechnic powered pin pullers similar to those used on Ranger and Mariner spacecraft could be used to release the launch latches. These devices are redundant in terms of firing signal and pyrotechnics, but are not mechanically. Although the pin pullers have demonstrated extreme mechanical reliability, consideration should be given to providing mechanical redundancy. The use of two bolt cutters in series in order to separate the launch tie would give such redundancy and could have the added desirability over pin pullers, in some applications, of eliminating "slop" and releasing against higher residual loads.

The double-hinged solar panel configuration is considered feasible. The two sections could be latched together at two places in the launch position utilizing a single launch damper and release mechanism at each point. A spring (or two for redundancy) at the inboard panel hinge would provide deployment with the outboard panel slaved to the inboard for a reasonably coordinated deployment of all panels. A viscous damper in series with the OUT position strut could absorb the deployment spring energy near the end of travel. This spring/damper could probably also satisfy the solar panel autopilot loop dynamic requirements.

Considerable weight and space is saved with the antenna supported directly on the output shaft of the actuator together with some probable advantages in terms of pointing accuracy, less "slop" and greater reliability (through simplicity and without space-exposed bearings). This actuator would have a hollow shaft to pass the required coaxial RF cable.

Similarly, the planet platform should be directly supported from the "in-orbit-plane" actuator shaft. It may be necessary to introduce damping to this rotation to achieve the

required planet smear limits. The two discrete position-actuators used to orient the above actuator in the orbit plane, could be spring-driven to index points and released with a pyrotechnic or a solenoid device.

The separation-actuated mechanical backup timer for initiating spacecraft functions could be either a temperature compensated fluid dash-pot type or a clock mechanism.

I. TELECOMMUNICATIONS

1. Introduction

a. Objectives

In the area of telecommunications, this study has been directed toward an analysis of radio tracking, telemetry, and command functions for an orbiting spacecraft. The two principal objectives of the study were:

1) Determine by estimation and assumptions the feasibility of a telecommunications system capable of supporting a Mars orbiter space-probe to be launched during the 1969 opportunity using a floxed Atlas/Centaur. Feasibility for the purpose of this study will refer to the technical considerations of the proposed mission.
2) Determine the communication capabilities of three alternate mission concepts in terms of the functional requirements imposed by the missions.

It should be understood that the mechanizations presented here do not preclude the feasibility or development of alternative schemes or designs.

b. Definitions

For this discussion relating to the telecommunications area, a number of terms are defined. See definitions (1) through (5) below.

(1) Telemetry Subsystem. The telemetry subsystem includes all the circuits that (a) sample, transduce, condition and convert spacecraft engineering measurements into binary waveforms for time multiplexing with scientific measurements, (b) accept the telemetry data in a serial binary waveform and combine them with synchronizing information into a composite signal for modulating the RF carrier.

(2) Command Subsystem. The command subsystem includes the non RF circuits which detect and decode signals which convey control information from Earth.

(3) Radio Subsystem. The radio subsystem includes all of the receivers, transmitters and associated RF transmission circuits required for the tracking, telemetry, and command functions.

(4) Antennas. All S-Band antennas common to the telecommunications system are treated as part of the radio subsystem.

(5) Link. A link is a radio frequency transmission circuit between pairs of transmitters and receivers from Earth to orbiter and vice versa.

c. Telecommunication System Functional Requirements

The telecommunication system of the considered Mariner 1969 orbiter mission to be discussed in this chapter must satisfy the functional requirements of (1) through (3).

(1) Tracking. Track the relative angular position, radial velocity, and range of the spacecraft with respect to designated coordinate systems to enable the computation of the spacecraft trajectory.

(2) Telemetering. Telemeter certain engineering parameters and scientific observations from the spacecraft to the Deep Space Net stations.

(3) Command Communication. Communicate commands from the Deep Space Net Stations to the recipient spacecraft subsystems.

d. Detailed Subsystem Requirements

The respective subsystem functional requirements for the telemetry, command, and radio subsystems are presented in (1) through (3).

(1) Telemetery Subsystem. The functions of the spacecraft portion of the telemetry system are:

1) To accept serial binary data measurements or to transduce analog engineering measurements into appropriate electrical signals,
2) Condition and convert analog engineering samples into binary words.
3) Time multiplex (commutate) engineering and scientific measurement signals.
4) Phase shift key (PSK) a square wave subcarrier with the binary signal.
5) Phase shift key (PSK) a second square wave subcarrier with a binary pseudorandom (PN) sequence for synchronizing the encoding and decoding of the digital telemetry data.
6) Generate a binary pseudorandom (PN) sequence.
7) Combine the two PSK subcarriers into a composite telemetry signal which will phase modulate the RF carrier of the spacecraft to Earth channel.

(2) Command Subsystem. The function of the spacecraft command subsystem is to:

1) Detect a phase-shift keyed synchronization subcarrier from the output of the spacecraft receiver.
2) Detect and digitally store command words.
3) Decode the digital command words and channel direct commands to recipient spacecraft subsystems and qualitative commands to the CC&S.

(3) Radio Subsystem. The function of the spacecraft radio subsystem is to:

1) Receive the RF signal transmitted to the spacecraft from the DSIF.
2) Coherently translate the frequency and phase of the received RF signal by a fixed ratio.
3) Demodulate the received RF signal and send a composite command signal to the spacecraft command subsystem.
4) Demodulate the ranging code transmitted to the spacecraft from the DSIF.
5) Modulate the transmitted signal with a composite telemetry signal.
6) Modulate the transmitter with the demodulated ranging signal from the turnaround ranging channel.
7) Transmit a modulated RF signal to the stations of the DSIF.

2. Constraints, Assumptions, and Philosophy

The most complex single constraint on the telecommunications system is the requirement for compatibility with the Deep Space Network's RF system. Therefore, a brief description of the RF system of the DSN is included. A number of other lesser constraints also appear.

The fundamental assumption of the telecommunications study was that the Mariner Mars 1964 telecommunications system could be adapted and extended to serve the 1969 mission without appreciable extension as a minimum design.

The philosophy of the study has been to build up the 1969 system from the 1964 design, allowing for changes of mission conditions and requirements, and considering state-of-the-art progress conservatively, but opportunistically.

a. DSN Configuration as a Constraint

For the purpose of this study a particular configuration for the Deep Space Net (DSN) has been assumed. The assumptions are based on information supplied by the DSN Project Office.

The configuration of the DSIF subsystem of the DSN is detailed below. The RF portion consists of antenna reflectors, feeds, feed lines, diplexers, low noise amplifiers, receivers, exciters, data extractors, transmitters, and acquisition equipment all operating at S-band.

The subsystem will provide angle-of-arrival error data to the tracking servo, wide-band and narrow-band telemetering outputs, one-way and two-way doppler outputs, ranging detection, ranging and command modulation capability, frequency synthesizers and exciters, and highpower RF generation. This subsystem will also include equipment necessary for subsystem test and calibration.

The standard Deep Space Stations (see Figure 11-53) for support of Mariner 1969 will be located at the DSN tracking and communications sites at Goldstone, California; Canberra, Australia; Johannesburg, South Africa; and Madrid, Spain. The Spacecraft Monitor Station at Cape Kennedy will have similar equipments.

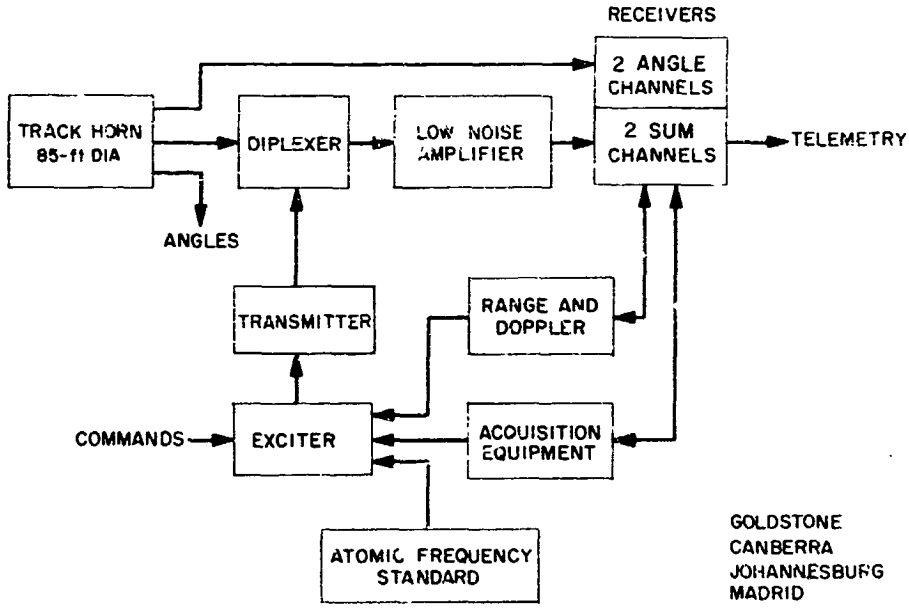


Figure 11-53. Standard Deep Space Station for Mariner 1969 Support

(1) Antenna Reflectors. Antenna reflectors employed in the DSN are steerable paraboloids, and will use Cassegrain feeds. At present, the standard DSIF antennas are HA-Dec 85-ft reflectors; by the time Mariner 1969 is launched, three AZ-EL 210-ft reflectors (the Low Noise Listen Station shown in Figure 11-54) may also exist.

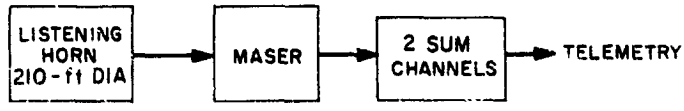


Figure 11-54. Low Noise Listening Station Configuration

(2) Receivers. Double superheterodyne receivers which phase-lock with the incoming RF carrier are employed. Angle-of-arrival tracking is accomplished by deriving angle-error signals from the output of the simultaneous lobing feeds. The S-Band receiver incorporates coherent AGC and ranging system reference loops. The basic S-Band maximum RF bandwidth is 3.3 Mc/s. Automatic Phase Control (APC) loop noise bandwidth is selectable from 12 cps to 150 cps at threshold. The receivers provide demodulated subcarriers to the ground telemetry subsystem. The receiver VCO output and the necessary reference signals are supplied to the doppler extraction equipment. Dynamic signal level range is from -65 dbm to threshold (typically -160 to -170 dbm). The S-Band receivers are tunable to 2295 ±5 Mc with crystal selection, each crystal being voltage tunable over a ±75 kc range about the received carrier frequency. Rapid change of frequencies will be available.

(3) Transmitters and Exciters. The S-Band transmitters use 10 kw klystron amplifiers. Typical gain is 45 db, and the minimum BW is 6 Mc. The 100 kw klystron amplifier will be available at Goldstone and possibly several other sites. Low-power transmitters will be employed for the Launch Station. An exciter provides the stable frequency source, tuning capability, multipliers, and phase modulators for both the command and ranging system. Atomic-supervised oscillators provide ground transmitter frequency stability of better than 1 part in 10^{10} over a 15 minute period. Transmitter frequency tuning is provided in 1 cps steps at the carrier frequency throughout the transmitter channel (2115 ±5 MC), with a voltage controlled crystal oscillator (VCO) locked to a synthesizer output.

(4) Dual Probe Coverage. In the event of two probes simultaneously occupying the same antenna beamwidth, it will be possible to receive telemetry from one probe, and two-way doppler, and telemetry from the other. The period to switch two-way doppler and command from one spacecraft to the other would take about one hour at planetary distances. For a complete discussion of DSN availability, see Appendix A.

(5) Microwave Parameters. The nominal parameters of the Standard Deep Space Station are given in Table 11-45. Characteristics of the Low Noise Listening Station (210-foot antenna) are given in Table 11-46.

b. Additional Constraints

Factors which constrain the design and feasibility but were not explicitly prescribed include system weight and engineering state-of-the-art. The telecommunications system weight must be compatible with sensible spacecraft weight distribution and the capability of the Atlas/Centaur vehicle in launching to Mars. The state-of-the-art can be expected to surpass that expressed in the Mariner Mars 1964 flight equipment.

Table 11-45. Standard Deep Space Station Parameters

Parameter	Receiver	Transmitter
Antenna Gain	53.0 $^{+1.0}_{-0.5}$ db	51.0 ±1 db
Antenna Beamwidth	~0.4°	~0.4°
Axial Ratio	0.75 ±0.25 db	0.75 ±0.25 db
Feed Line Loss to Transmitter		0.5 ±0.1 db
Antenna Temperature (zenith)	16° ±3° k	
Maximum Feed Power		10 kw
Polarization	LC & RC	LC & RC
Diplexer Loss (Included in Item 4)		
Paramp System Temperature (referenced to paramp input)	270° ±50° k	
Maser System Temperature	55° ±10° k	
Transmitter Power		to 100 kw
Transmitter Noise Contribution	5° ±3° k	

Table 11-46. Low Noise Listen Station Parameters

Parameter	Value
Antenna Gain	61.0 ±1 db
Antenna Beamwidth	0.1
Axial Ratio	< 0.5 db
Feed Line Loss to LNA	0.02 ±0.01 db
Antenna Temperature	10° ±2° k
Polarization	RC & LC
Masser T_{excess}/2nd Stage	20° ±3° k

(1) Physical Size. Antenna configuration, particularly the size of the high-gain reflector is constrained by the dimensions of the Atlas/Centaur Surveyor nose fairing.

(2) Interplanetary Geometry. Both the communication distance and the look angles are imposed by the 1969 Earth/Mars geometry. The antenna configuration must be compatible with Type I and Type II transit trajectories.

(3) Thermal control. Present heat-dissipation techniques limit transmitter power to about 50 watts.

(4) Electrical Power. With a solar-powered Mars mission the spacecraft is somewhat power-limited; therefore, transmitter power suffers a secondary constraint.

c. Assumptions

The Mariner Mars 1964 telecommunications system was developed for a mission not radically different from that under study here. Therefore, that system may be used as the baseline or minimum system for the 1969 study. Such a system, with no provision for scientific data, is sketched in Figure 11-55.

The nature of the orbiter mission imposes an increase of 90 to 180 days upon spacecraft operational lifetime, thus doubling the expected orbital phase. The telecommunications system must, therefore, exhibit a reliability commensurate with a 360 to 450 day lifetime.

The technology supporting telecommunication systems is presently advancing, and the probability of developments applicable in the design of Mariner 1969 telecommunications system is reasonable. Without compromising reliability, it is a valid assumption that some such opportunities will exist.

d. Philosophy

The basic philosophy in studying a Mariner Mars 1969 telecommunications system has been to build up from the 1964 flight equipment with a view to accommodating the changed conditions, increasing the reliability for a longer duration mission, and making use of such advances as the new art can provide. The principle of using the advanced state-of-the-art without being dependent upon it has been applied.

3. Functional Description and Mechanization

The telecommunications system considered for the Mariner 1969 orbiter mission (see Figure 11-56) is an extension of the Mariner 1964 design. Reliability studies conducted for the Mariner Mars 1966 project recommended redundancy in receivers, exciters, power

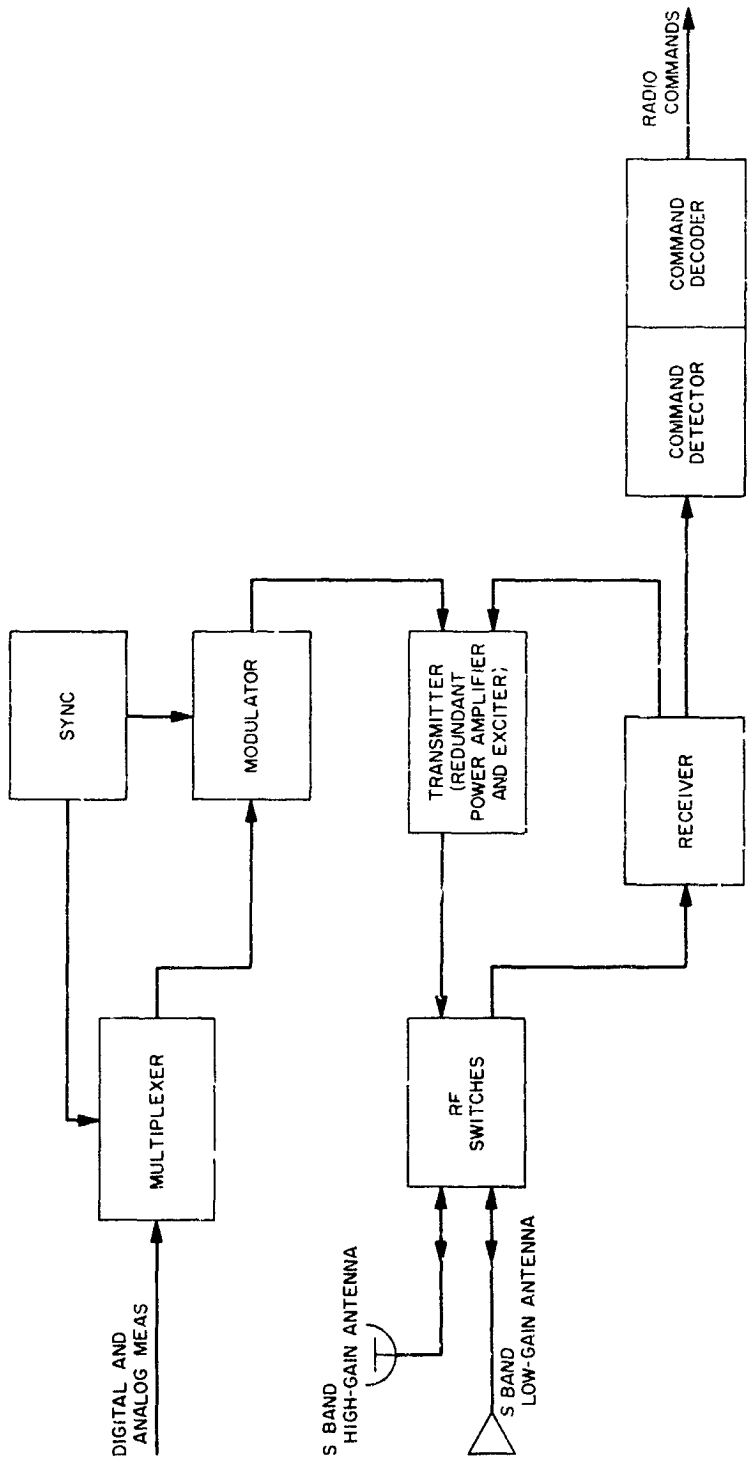


Figure 11-55. 1969 Orbiter Telecommunications (Minimum Case) Block Diagram

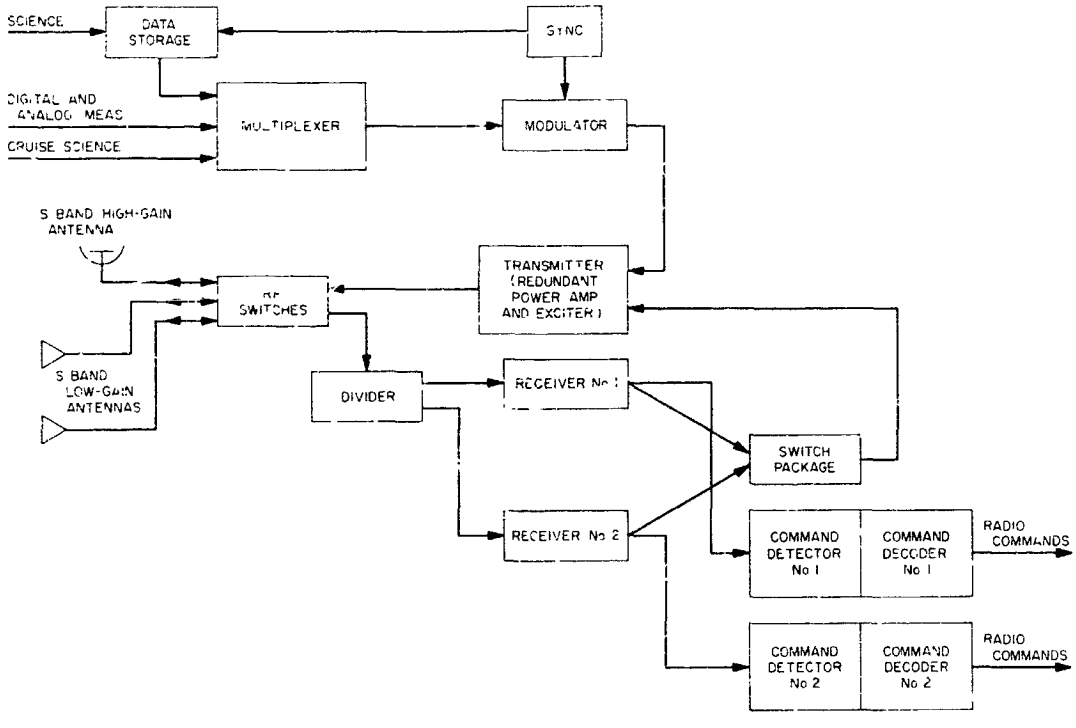


Figure 11-56. 1969 Orbiter Telecommunications (Nominal & Maximum) Block Diagram

amplifiers, and command subsystems. The Mariner 1964 system has redundant exciters and power amplifiers as shown in Figure 11-55. One of the major factors affecting the command and two-way doppler tracking functions is the receiving equipment; therefore, improving the reliability of the receiving equipment increases the overall reliability of these functions. Command reliability can be further increased by redundancy of the command detector and decoder. Thus, the Mariner 1969 telecommunications system incorporates duplicate receivers and command subsystems.

To connect either receiver to any antenna without additional switching complexity a passive divider is used due to the inherently high reliability of such devices.

Mission geometry requires the use of two low-gain antennas in addition to a directional high-gain antenna. (For explanation see Spacecraft Antenna Subsystem description.)

a. Spacecraft Antenna Subsystem

One of the major elements of the spacecraft system design is a three-axis attitude stabilization system. Sun seeking devices will first orient the roll axis of the probe in the direction of the Sun and subsequently an optical sensor will establish stabilization around the roll axis with respect to the star Canopus. The successful establishment of the three-axis attitude stabilization is also essential for eventual pointing of a high-gain antenna toward the Earth. It must be realized, however, that following a certain period after launch due to trajectory considerations and during midcourse maneuvers when the spacecraft is not in its cruise attitude, communications must be maintained through omni-directional antennas. One of the design ground rules requires that one spacecraft configuration should satisfy both Type I and Type II trajectories.

(1) Low-Gain Antenna Orientation. Calculation of the telemetry channel performance requirements for three Type I trajectories (early, nominal and late) indicated that a Mariner Mars 1964 type low-gain antenna oriented with its axis of symmetry parallel to spacecraft -Z axis would guarantee communications coverage for at least 55 days after launch. Figure 11-57 shows the radiation pattern of a Mariner Mars 1964 type low-gain antenna as a function of spacecraft cone angle along with the antenna gain requirements for the two limiting Type I trajectories. In this figure the solid line indicates the worst-case antenna pattern. The dashed line on the plot indicates the required antenna gain for days after the (late) launch date. A ten watt spacecraft transmitter, an 8-1/3 bits per second data rate, and an 85-foot diameter ground receiving antenna are assumed. Where the solid line exceeds the other curves, an excess performance margin exists and communications can be guaranteed.

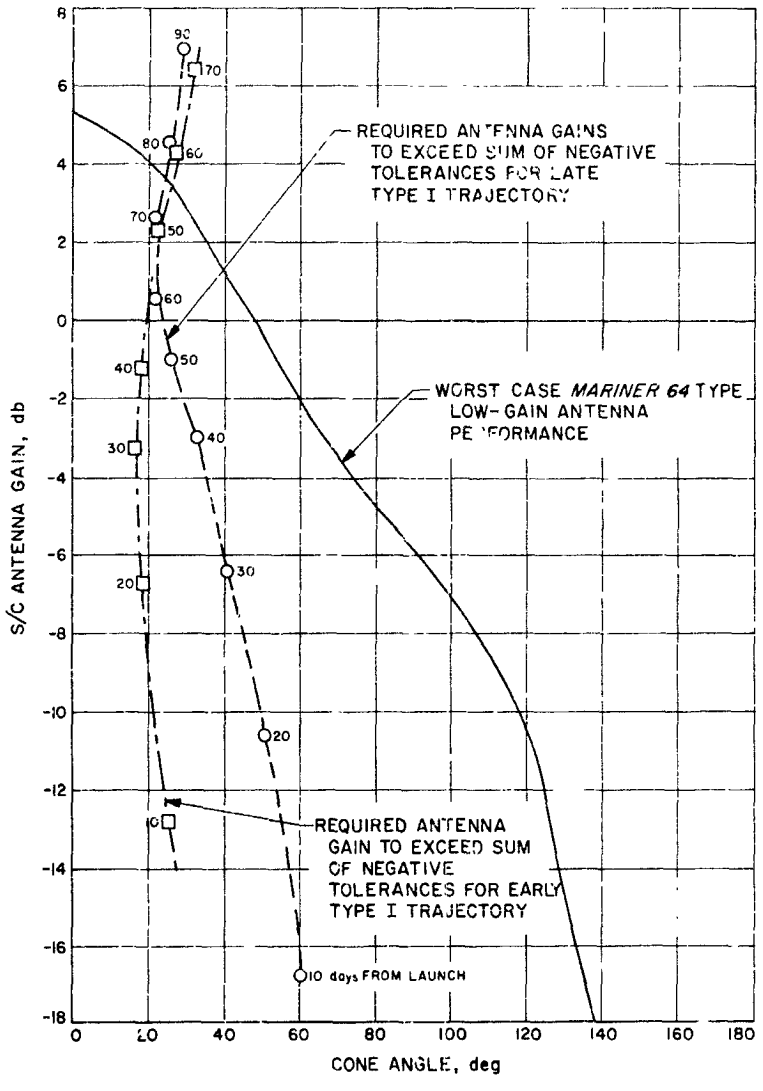


Figure 11-57. Type I Trajectory Low-Gain Antenna Coverage vs Cone Angle with Mariner Mars 1964 Low-Gain Antenna

High-gain antenna coverage, to be detailed later, will be initiated at 103 days after launch for the early and 74 days after launch for the late Type I trajectories. Consequently, if no additional provisions were made a communications "gray out" period of 28 days maximum would have to be accepted. A communications "gray out" is defined as a condition where the communication system performance margin is positive, but less than the sum of the negative tolerances. Performance margin: Versus days after launch for the early, nominal and late Type I trajectories are shown in Figures 11-58, 11-59, and 11-60 respectively. A similar examination of the Type II trajectories indicates that the communication "gray out" periods would be much more severe, namely from the 7th to the 150th days after launch for an early, and from the 24th to the 87th days after launch for a late Type II trajectory. The Type II trajectory low-gain antenna coverage with the same Mariner 64 type low-gain antenna is shown in Figure 11-61. The telemetry channel performance margins versus days after launch for the three Type II trajectories are given in Figures 11-62, 11-63, and 11-64.

To commit a mission without reliable telemetry coverage for such extended periods of time as would be encountered with a single Mariner 64 type low-gain antenna during a Type II trajectory mission is most undesirable. Consequently, the use of an additional rear-mounted Mariner 64 type low-gain antenna was investigated. The results are plotted in Figure 11-65 which shows that this solution would still result in telemetry "gray out" periods of 90 days for the early and 60 days for the late Type II trajectories. Since this solution still remains unacceptable, the performance of a side-mounted low-gain antenna was investigated. Figure 11-66 shows the antenna coverage which can be obtained using a roll-axis-symmetrical Mariner 64 low-gain antenna and an additional low-gain antenna oriented at a 90 degree cone angle with respect to the first one. This approach appears to be the most desirable, not only because it would provide the best telemetry coverage, but it would also allow constant communications from spacecraft to Earth during midcourse maneuvers. The above condition is accomplished with an additional roll maneuver which keeps the spacecraft to Earth vector in the forward hemisphere of the side looking low-gain antenna while the motor mounted along the roll axis assumes any arbitrary direction.

(2) Low-gain Antenna Description. Both low-gain antennas would provide right-hand circularly polarized radiation. The first low-gain antenna will be considered the prime antenna and will provide hemispherical coverage with its axis parallel to the spacecraft roll (-z axis) axis. This antenna would be similar to the one used on Mariner Mars 1964. That is, it would consist of a combination waveguide and structure which would support the antenna at a sufficient distance above the spacecraft so that the pattern will neither be obstructed nor reflected by the spacecraft (120 degree cone angle). The antenna itself will be a shaped open end of an ultra low loss circular waveguide with a coaxial-to-circular-polarization transition at the base of the waveguide. The antenna pattern coverage will be symmetrical about its axis with gain of +5 db on axis and -6 db at 90 degrees from this axis.

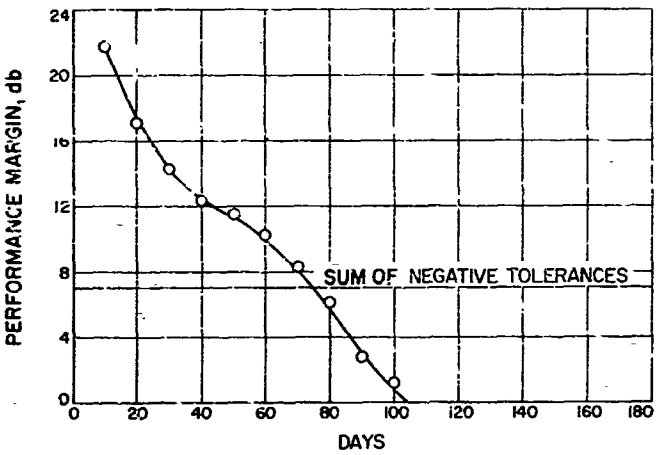


Figure 11-58. Performance Margin vs Days After Launch (Mariner Mars 1964 Low-Gain Antenna, 10 w Spacecraft Transmitter, 85-Foot Diameter Ground Antenna, Communication Rate 8 1/3 bps, Launch 3-7-69)

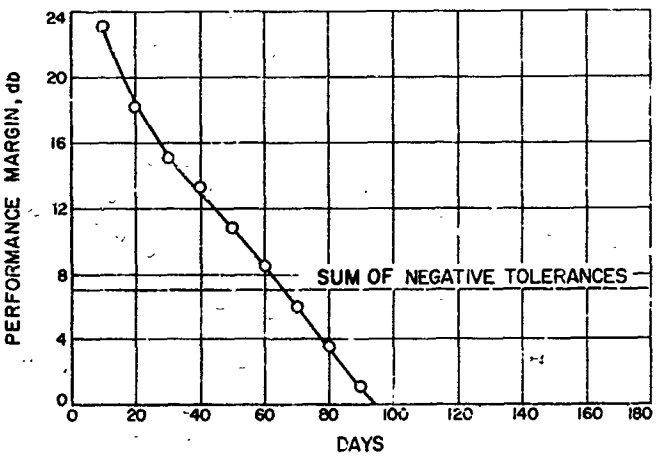


Figure 11-59. Performance Margin vs Days After Launch (Mariner Mars 1964 Low-Gain Antenna, 10 w Spacecraft Transmitter, 85-Foot Diameter Ground Antenna, Communication Rate 8 1/3 bps, Launch 3-20-69)

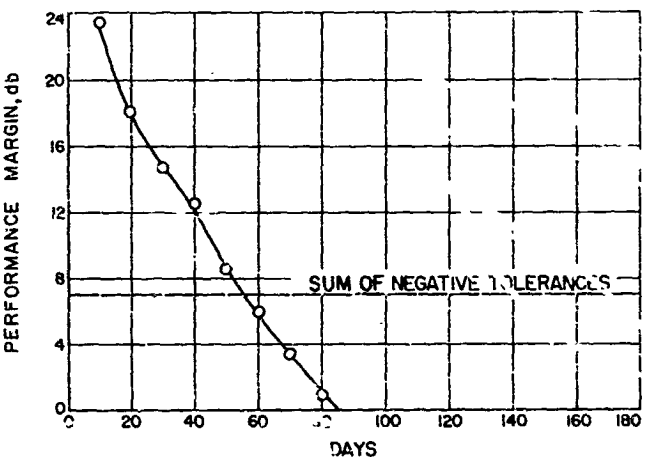


Figure 11-60. Performance Margin vs Days After Launch (Mariner Mars 1964 Low-Gain Antenna, 10 w Spacecraft Transmitter, 85 oot Diameter Ground Antenna, Communication Rate 8 1/3 bps, Launch 4-4-69)

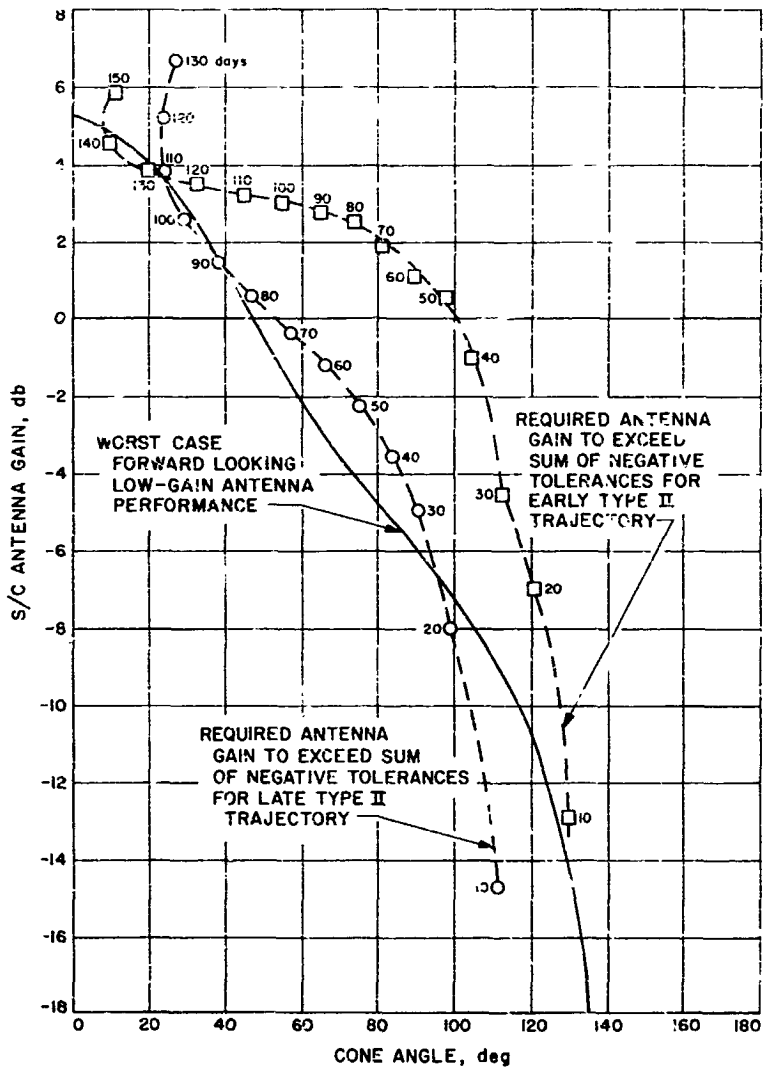


Figure 11-61. Type II Trajectory Low-Gain Antenna vs Cone Angle with Mariner Mars 1964 Low-Gain Antenna

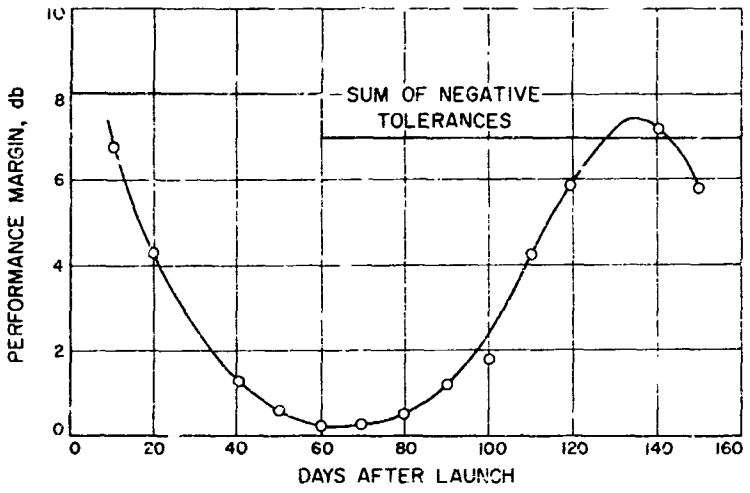


Figure 11-62. Performance Margin vs Days After Launch (Mariner Mars 1964 Low-Gain Antenna, 10 w Spacecraft Transmitter, 85-Foot Diameter Ground Antenna, Communication Rate 8 1/3 bps, Launch 1-9-69)

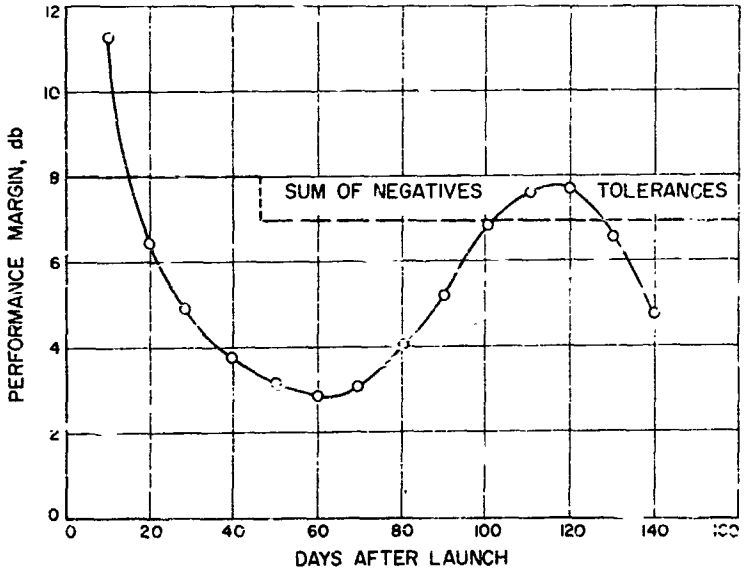


Figure 11-63. Performance Margin vs Days After Launch (Mariner Mars 1964 Low-Gain Antenna, 10 w Spacecraft Transmitter, 85-Foot Diameter Ground Antenna, Communication Rate 8 1/3 bps, Launch 1-24-69)

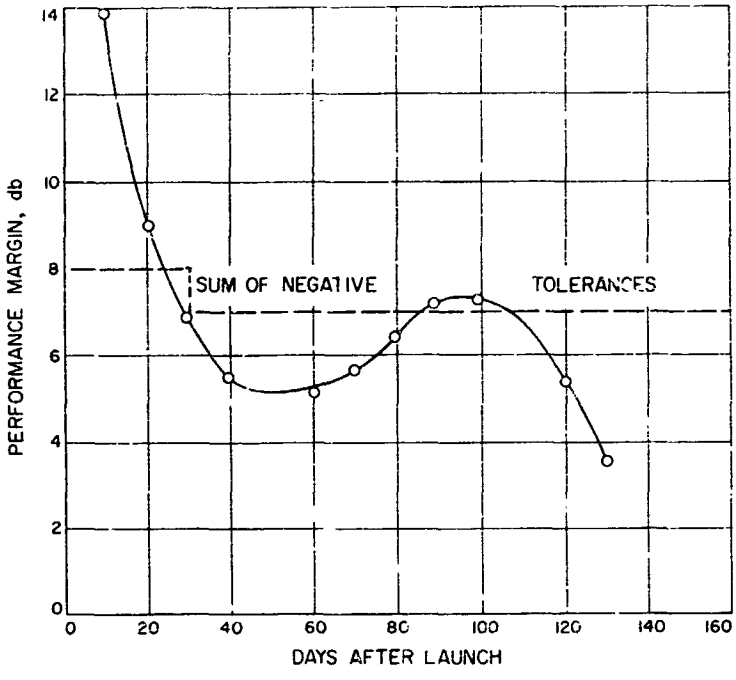


Figure 11-64. Performance Margin vs Days After Launch (Mariner Mars 1964 Low-Gain Antenna, 10 w Spacecraft Transmitter, 85-Foot Diameter Ground Antenna, Communication Rate 8 1/3 bps, Launch 2-7-69)

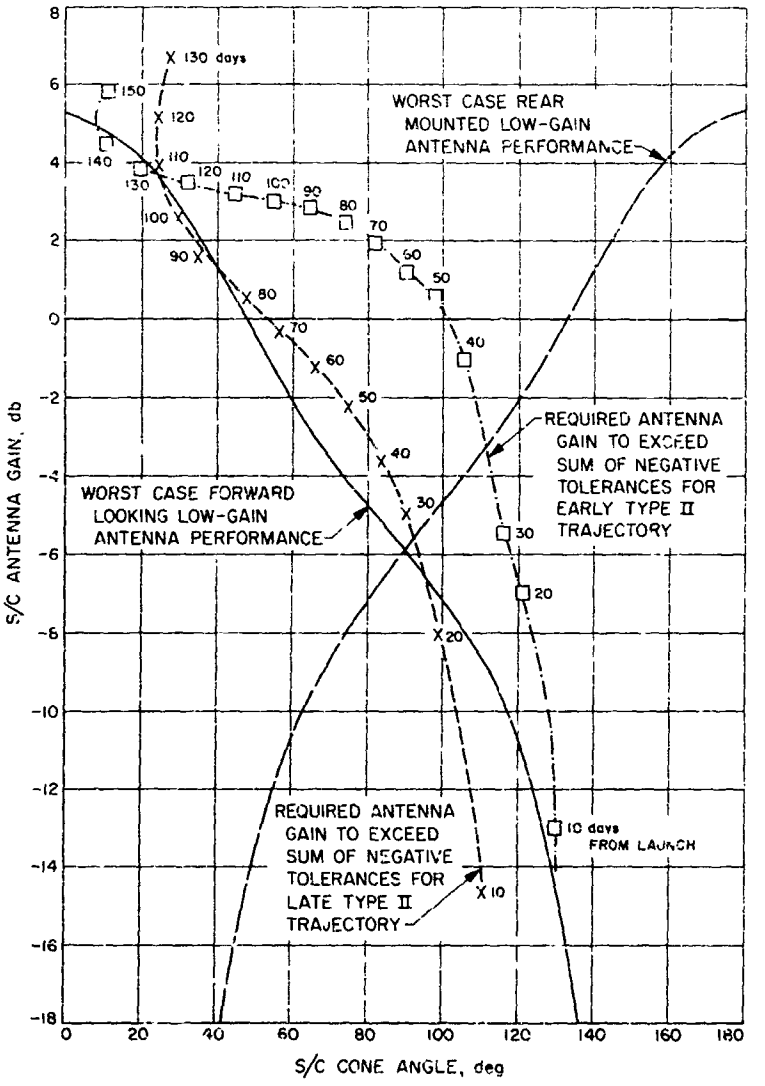


Figure 11-65. Type II Trajectory Low-Gain Antenna Coverage vs Cone Angle with Forward and Rear Looking Low-Gain Antennas

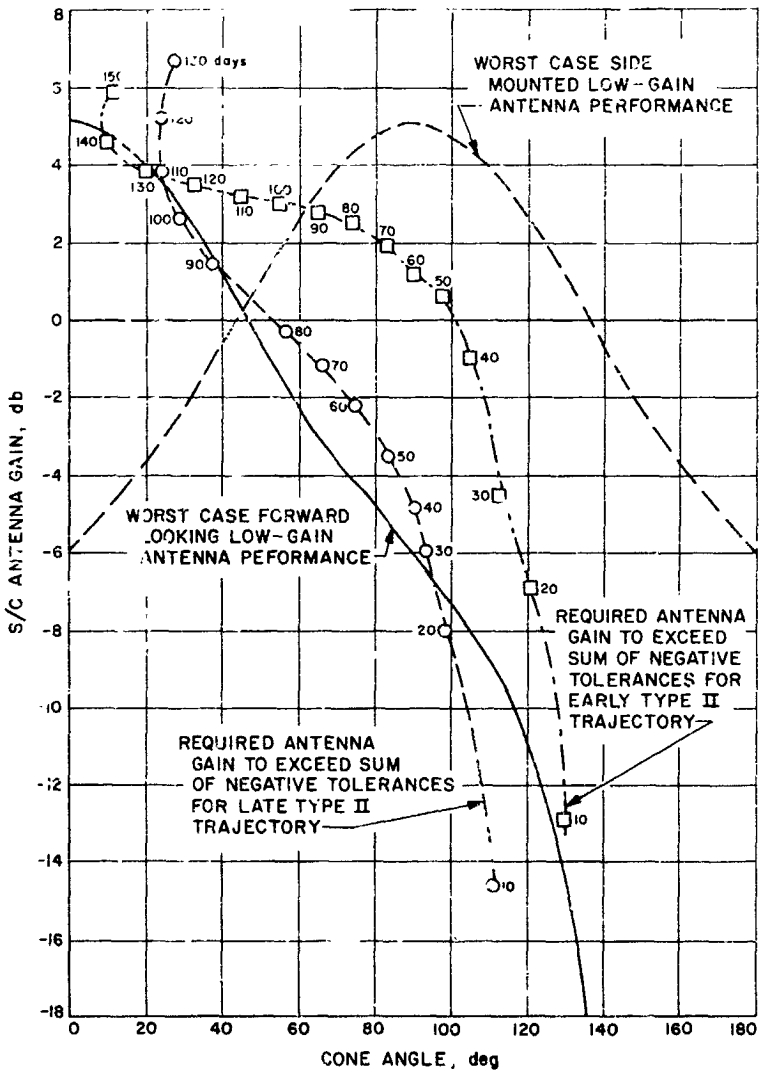


Figure 11-[illegible]. Type II Trajectory Low-Gain Antenna Coverage vs Cone Angle with Forward and Side Looking Low-Gain Antennas

The second low-gain antenna would also give hemispherical coverage, but with its axis in the roll plane at a 45-degree clock angle to the Canopus sensor. This would orient the second low-gain antenna axis at a 90-degree angle to that of the prime omni-antenna thus allowing for telemetry coverage during midcourse maneuvers when the motor is mounted along the roll axis. It would also greatly reduce the "grey out' problem discussed earlier (see Figure 11-66) with respect to the Type II trajectory Earth track. This side-mounted secondary low-gain antenna would be a coaxial cable-fed circular radiating aperture. Its pattern coverage would be symmetrical about the antenna axis with +5 db gain on axis and -6 db at 90 degrees from the axis

The weight of the primary low-gain antenna is estimated to be 7 lbs and the associated coaxial cabling weight about 0.5 lbs. The weight of the secondary or side-mounted low-gain antenna is estimated at 0.3 lbs, its coaxial cabling 3 lbs and the associated rotary joint at 1.0 lbs.

(3) High-Gain Antenna. In selecting the high-gain antenna configuration for the 1969 Mars opportunity, the following factors were taken into consideration:

1) The state-of-the-art of unfurlable or erectable antennas.
2) Packaging capacity under the Surveyor nose fairing.
3) Parabolic antennas versus arrays.
4) Reliability tradeoffs as a function of the relative complexity of each alternative configuration.

Reliability considerations at this time indicate the advisability of rejecting unfurlable or erectable antennas because of the mechanization complexity of the antenna-deploying system and the flexible reflecting surfaces required for most of these antennas. The Surveyor nose fairing dimensions and the spacecraft placement under the nose fairing limits the high-gain antenna to a maximum of four feet in diameter. The half-angle, half-power beamwidth of a four-foot diameter antenna is only 3.5 degrees. In order to avoid excessive performance loss during the planetary orbit phase and in order to avoid communications blackout during transit, a two-axis of freedom actuation system is required. Communications blackout is defined as the condition existing when the predicted performance margin is negative.

If a two-axis antenna pointing system is to be considered the utilization of antenna arrays versus parabolas should also be considered. Antenna arrays with somewhat higher gain performance could also be packaged under the Surveyor nose fairing at the expense of some penalty in weight. By this means, higher telemetry bit rates could be obtained. On the other hand, parabolic antennas are preferred, especially if a single degree of freedom actuation system is used because of their inherent simplicity, reasonable efficiency (60 to 65 percent) and higher gain to weight ratio.

If a finite period of "gray out" is acceptable, a three foot diameter (4.5 degree beamwidth), high gain antenna is recommended on the basis of its relative simplicity and consequently high reliability. If the antenna is mounted with a single degree of freedom and oriented as shown in Figure 11-67, the "gray out" would be from 8 to 25 days duration depending on the trajectory. Figures 11-68a, b, c and d show the relationship between the look angles of such a single axis high-gain antenna relative to both early and late Type I and Type II trajectories.

The study examined the pointing ability of this three-foot, single-axis, parabolic antenna, disregarding such error sources as attitude-control dead zone, RF boresight, and mechanical alignment tolerances. The antenna would follow the Earth track (namely the spacecraft cone and clock look angles to Earth) during the Mars orbit period to within 1.0 degree or better from 7 days after the earliest Type I trajectory encounter to 108 days after the latest Type II trajectory encounter. Consequently, the minimum orbit communication period for the earliest arrival Type I orbit could be 164 days.

The axis of rotation of the high-gain antenna would be oriented at 270-degrees clock angle in the roll plane from the Canopus sensor reference and at 38.5 degrees in cone angle from the Sun-oriented spacecraft axis. The RF axis of the antenna subtends a 9.0 degree angle from the axis of rotation. Refer to Figure 11-67 for coordinate representation.

The antenna polarization would be right-hand circular with less than 0.5 db on axis ellipticity. The weight of this antenna is estimated to be 3 lbs, in addition to an estimated 1 lb for cabling and 0.5 lbs for a rotary joint.

b. Radio Subsystem

(1) Transmitter. The spacecraft S-Band transmitter that was examined for this study was sized to 10 watts of output, but to illustrate the possible tradeoffs available, the capabilities of a 20 watt system also were included (see Figure 11-69). A 50 watt system is highly desirable for the mission, and appears to represent the practical limit based on other constraints.

The first choice configuration would be a solid-state exciter followed by a traveling wave tube (TWT) power amplifier. The desirability of solid-state circuitry is obvious; development experience and reliability data from Mariner 1964 reinforce this choice. The traveling wave tube is more advanced in development than, for instance, the amplitron or the klystron for long life in the 10 to 20 watt range. A 10 watt TWT is used on Mariner 1964; larger units are under development. The exciter would contain the basic crystal controlled oscillator, phase modulator, amplifiers and frequency multipliers to produce an output in the 50 to 250 milliwatt range, depending on TWT drive requirements and RF losses between the exciter and TWT. The presently available efficiency for this unit, and its associated power supply, is on the order of 10 percent.

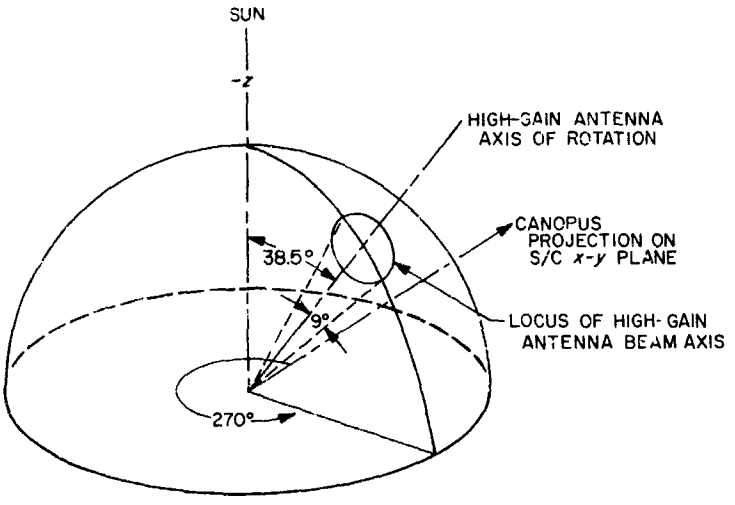


Figure 11-67. Single Axis of Freedom High-Gain Antenna Spacecraft Orientation

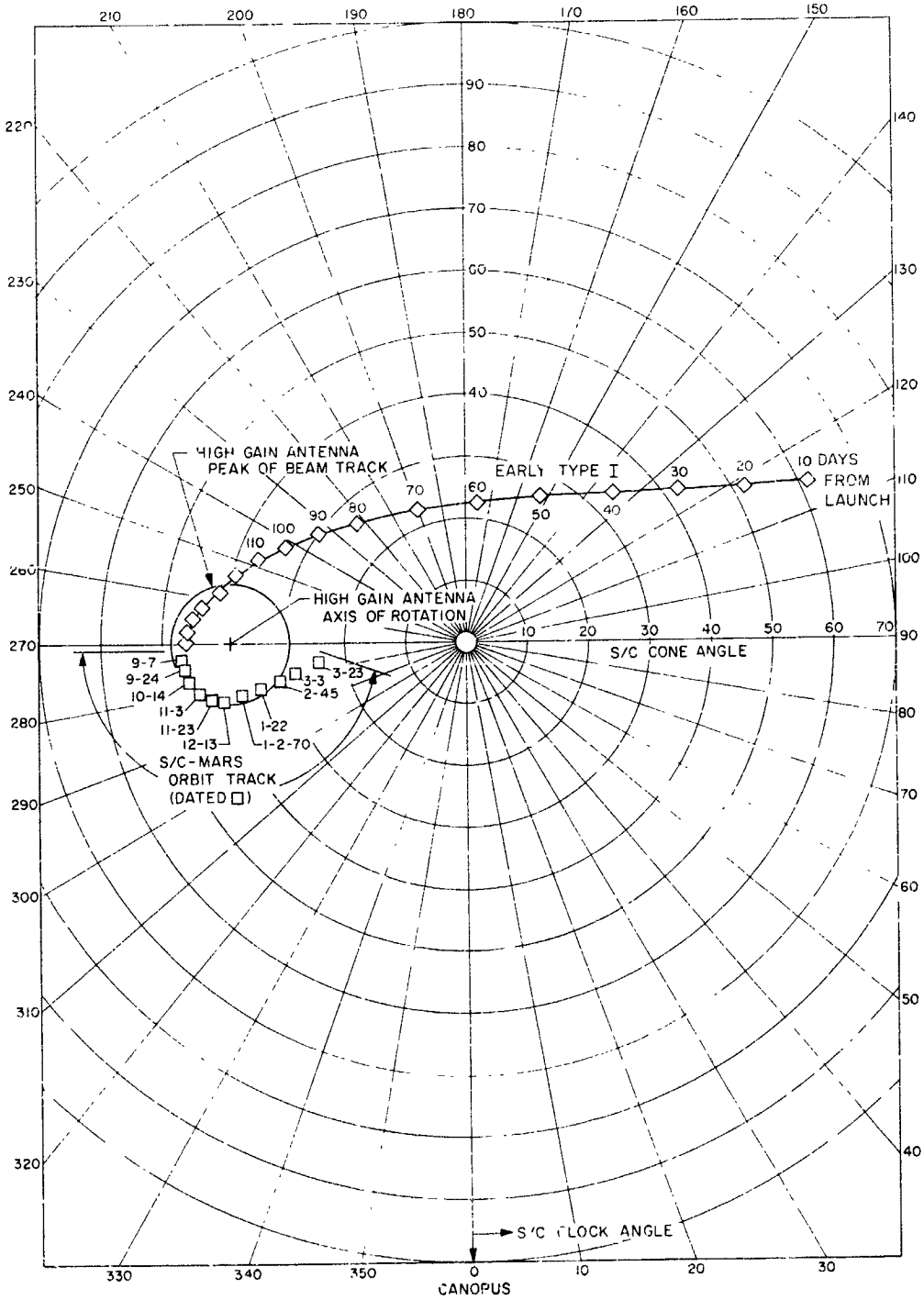


Figure 11-68a. Earth Look Angles Relative to Spacecraft Coordinates for Early Type I Trajectory

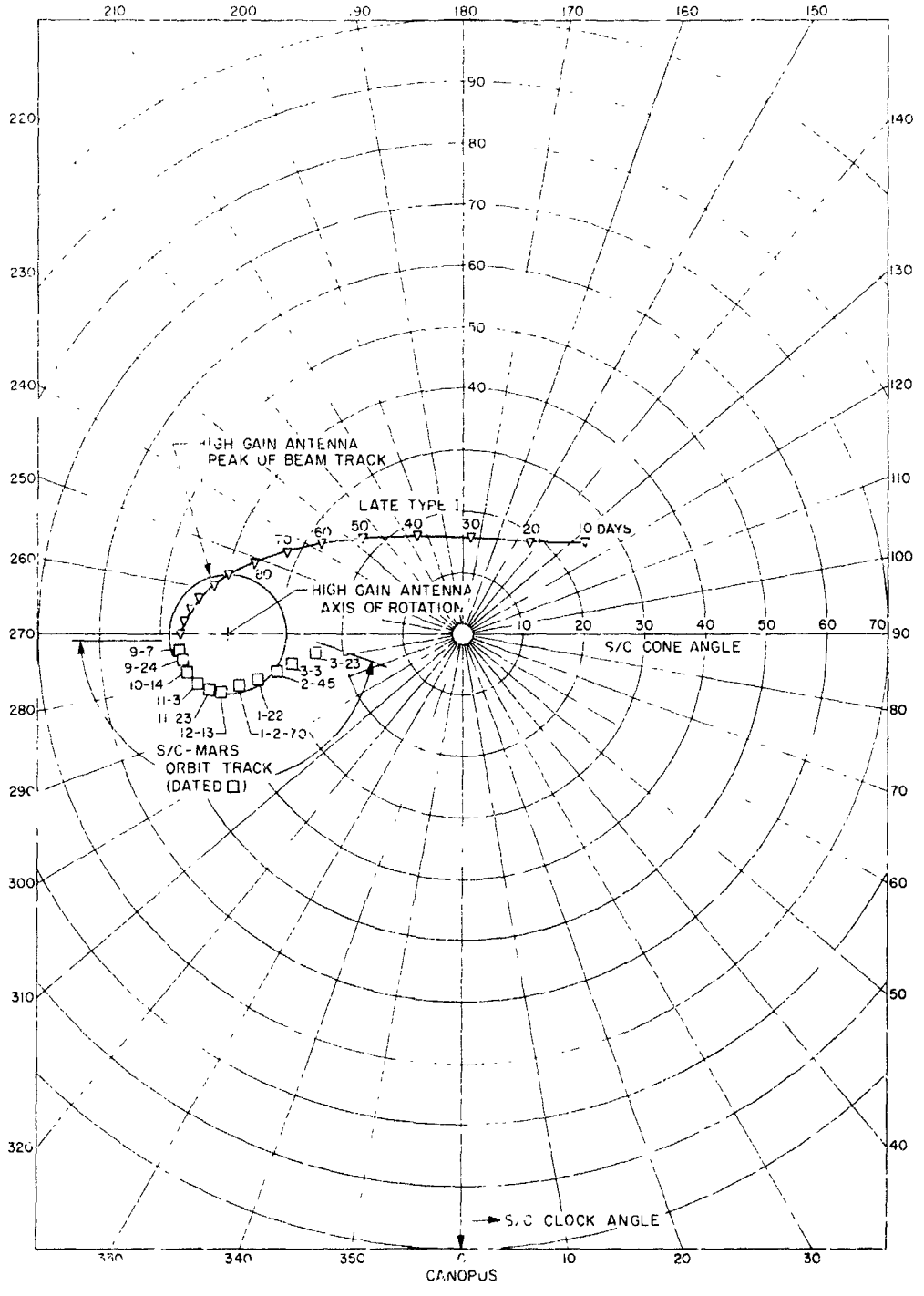


Figure 11-68b. Earth Look Angles Relative to Spacecraft Coordinates for Late Type I Trajectory

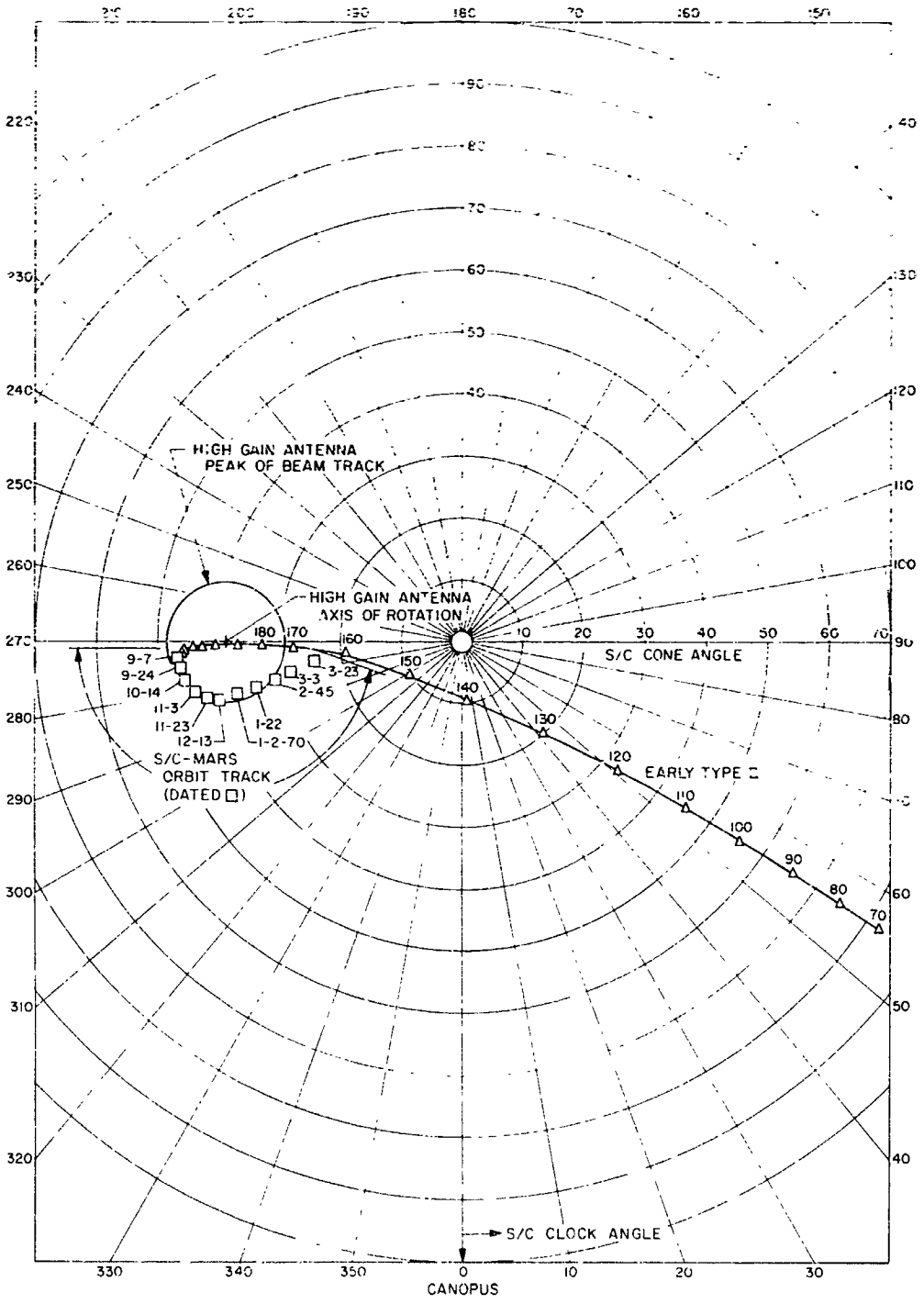


Figure 11-68c. Earth Look Angles Relative to Spacecraft Coordinates for Early Type II Trajectory

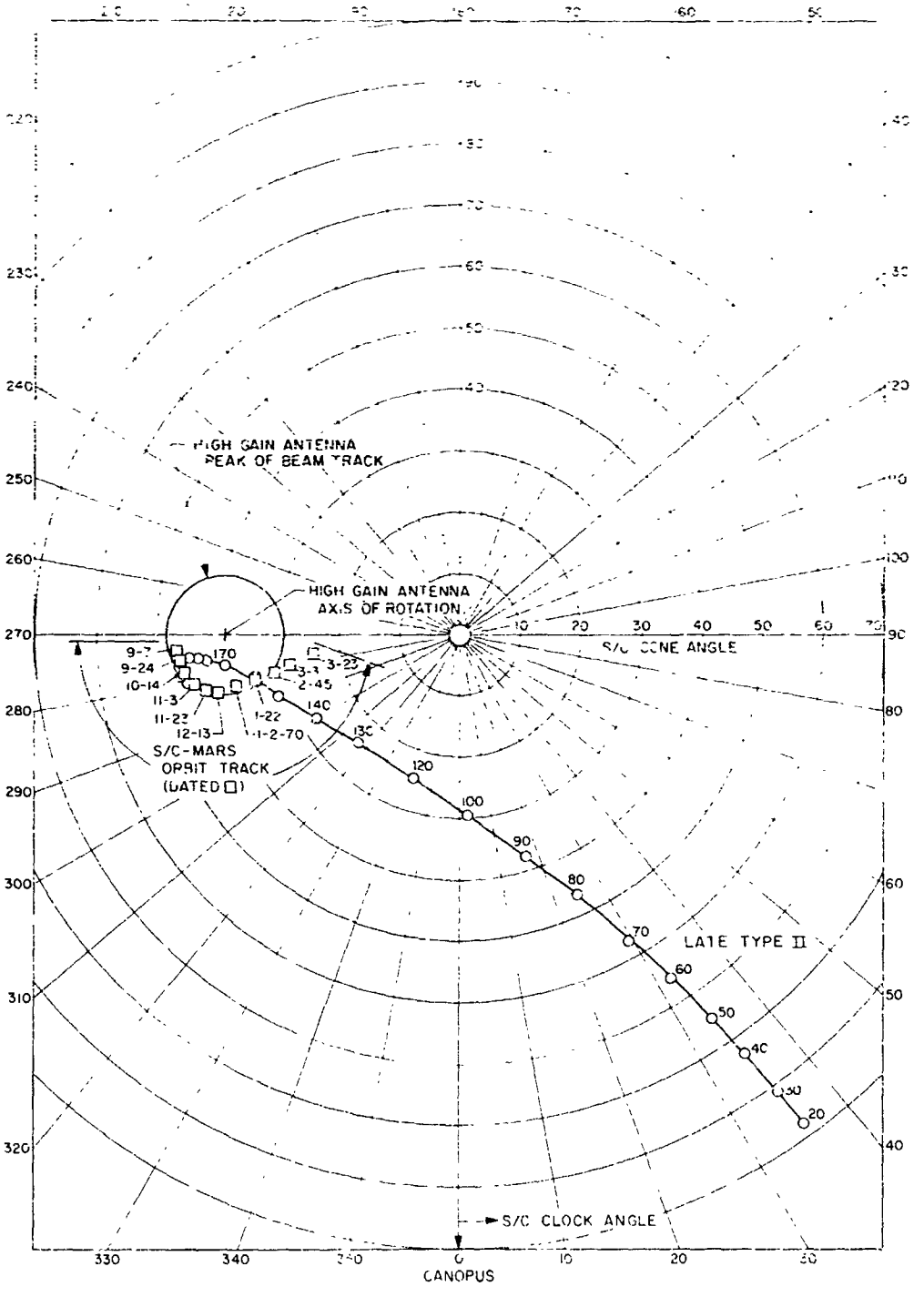
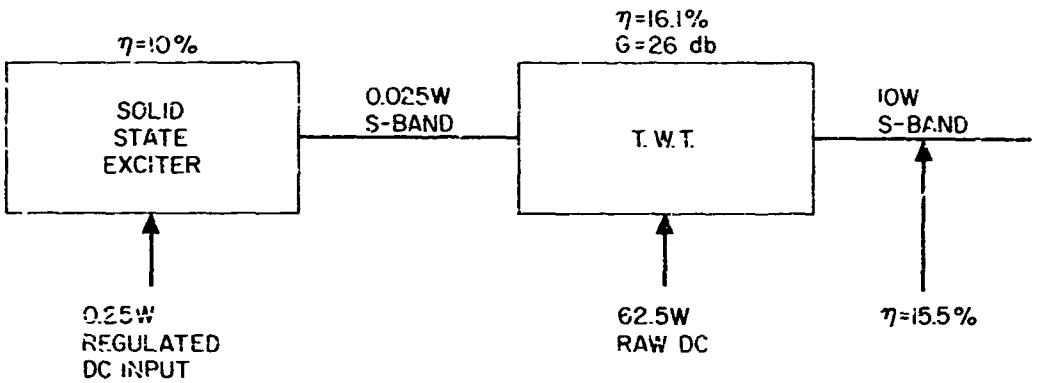
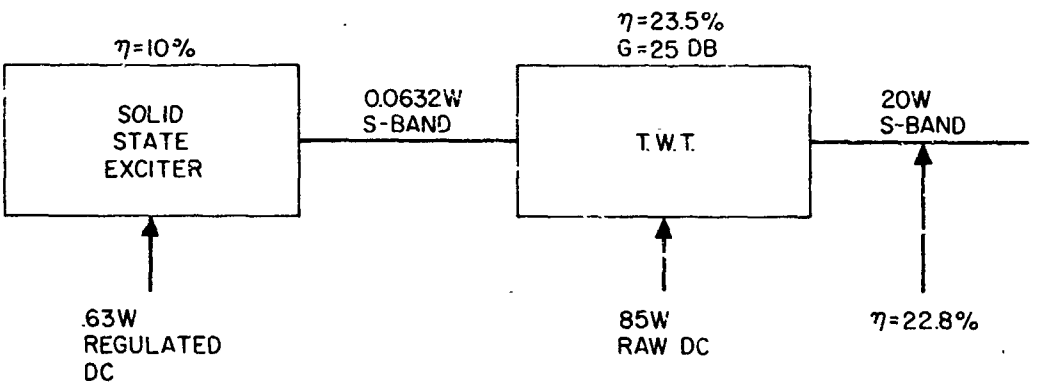


Figure 11-68d. Earth Look Angles Relative to Spacecraft Coordinates for Late Type II Trajectory



10 WATT TRAVELING WAVE TUBE



20 WATT TRAVELING WAVE TUBE

Figure 11-69. Orbiter S-Band Transmitters

A flight quality TWT is available that can provide 10 watts of output power at 26 db of saturated gain. The TWT, with its power supply, is 16.1 percent efficient. The overall efficiency of the exciter, TWT, and power supplies would be 15.5 percent. A TWT and integral power supply should be available within the next year that will have 20 watts of output power, 25 db of saturated gain and be 23.5 percent efficient, including associated power supply. The overall exciter, TWT, and power supply efficiency would be 22.8 percent.

The problem of dc and RF breakdown, as the unit passes through critical pressure, will have to be studied and solved if the unit is to remain ON during the launch phase. An alternate solution to the breakdown problem would be a separate launch-mode exciter with sufficient power output to be used directly as the transmitter. Then the TWT would not have power applied during the launch phase. The dc and RF voltages for this mode could be kept below the values necessary to cause ionization breakdown. For the purpose of a consistent system design a separate launch mode exciter will be included in the weight and power estimates.

The transmitter would contain two redundant exciters and two redundant power amplifiers. The exciters would be connected to the power amplifiers by a nonswitching power splitting device so that either exciter could drive both power amplifiers. The active exciter power amplifier combination would be selected by appropriate power supply switching. A cavity filter would be required in each TWT output circuit.

A circulator switch network will be employed to select either amplifier output, either antenna and receiver input to give the following modes of operation:

1) Receive HI - Transmit HI
2) Receive LO - Transmit LO
3) Receive LO - Transmit HI

An additional switching function would allow the selection of either low-gain antenna. (See Figure 11-70.)

(2) Spacecraft Receiver. The system uses a continuously operating narrow-band, double-superheterodyne, automatic phase-tracking receiver with a turnaround ranging channel.[1]

The receiver operates in the coherent mode when the receiver is locked to a signal transmitted from the ground. In this mode the phase and frequency of the carrier transmitted

[1]Turnaround ranging is discussed in detail in Reference 2.

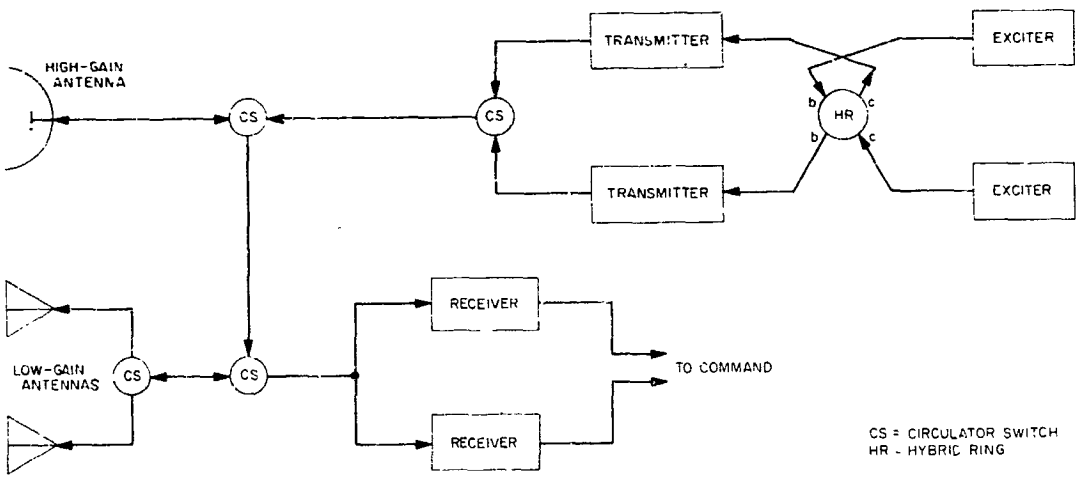


Figure 11-70. Radio and Antenna System Switching Arrangement

from the spacecraft is a rational multiple of the received signal, because the carrier frequency is controlled by the receiver. When no signal is received, the receiver operates in the noncoherent mode, and the carrier transmitted from the spacecraft is controlled by a fixed-frequency crystal-controlled oscillator.

For the minimal mission, a single receiver will be employed (see Figure 11-55). For the nominal and maximal mission, two redundant receivers will be employed. The two receivers will be passively interconnected at the input and will be frequency addressed. The possible use of tunnel-diode amplifiers should be considered, if the 3 db signal-to-noise ratio loss in the interconnection cannot be tolerated. The receivers will supply two demodulated command outputs, one from each receiver. When utilizing frequency addressing of the two receivers (for command transmission to one of the two command systems), about 350 kc carrier separation will be required.

c. Telemetry and Modulation Subsystem

The telemetry system for the purpose of this discussion will be divided into the digital telemetry data processing, (not described in this section), storage, multiplexing and the telemetry modulation subsystems.

(1) Storage. The data storage requirement for the nominal mission could be met by an isoelastic transport, multitrack, 15×10^6 bit capacity, buffered input, buffered output, reel-to-reel tape recorder. The primary users of the tape recorder will be the television and the Mars Scanner experiments. Television data recording will take place on four parallel tracks in addition to a clock recording at a 10^3 bit per inch density. The television recording speed is estimated at 4 ips and the TV bit rate at 8×10^3 to 1.6×10^4 bps. Recording of the Mars Scanner data will be 5×10^3 bps on a single track and a clock recording channel at 4 ips recording speed with a density of 1250 bits per inch.

The estimated tape length is 400 feet and the playback speed is 0.5 to 1.0 ips. The input/output core buffer would have a capacity of about 1320 bits corresponding to the storage of one TV line.

(2) Recording Capability. The maximum mission concept requires recording capability of TV, Infrared, Ultraviolet and Mars Scanner experimental data. Because of the high data rate and bit storage requirements such as:

1) TV rates up to 64×10^3 bps and a maximum total of 30×10^6 bit storage capacity
2) Infrared experiment bit rates up to 2×10^3 bps and a maximum total of 4.8×10^6 bit storage capacity

3) Ultraviolet experiment bit rates up to 2×10^3 bps and a maximum total of 4.8×10^6 bit storage capacity.
4) Mars Scanner experiment bit rates of 5×10^3 bps and a maximum of 12×10^6 bit storage capacity.

Because of reliability consideration the use of three separate tape recorders is recommended. All three tape recorders should be buffered input, buffered output machines with playback speeds of 0.5 to 1.0 ips. One of the three tape recorders will store TV data only, on four parallel data tracks and a clock recording track. Assuming 8 to 12 inches per recording speed this machine will require 300 to 500 feet of tape capacity for 30×10^6 bits. The second tape recorder will store the data of the Mars Scanner experiment on two parallel tracks at 2.5 ips recording speed requiring 500 feet of tape capacity to record 40 minutes worth of data per orbit. The ultraviolet and infrared experiments will use a data and a clock recording track. The recording bit rate will be 200 bps at a recording speed of 2 ips. A 40 minute recording time per orbit will require a 400 foot tape capacity. The UV and IR data recording must either be coincident or time sequenced, they cannot be partially overlapping in time.

All three tape recorders would be provided with the capability for command initiated playback and new data recording without the possibility of destroying previously recorded data.

(3) Recorder Interface. The tape recorder provides one of the severest interface problems that occur within the telecommunication system. With either a single tape recorder or multiple tape recorders the storage systems must interface with the data encoder, data automation system and the command subsystem. The interfaces are anticipated to consist of:

1) With the data encoder:
   a) Data to the data encoder
   b) End of tape signal to the data encoder
   c) Temperature and pressure transducer outputs to the data encoder
   d) Bit sync from the data encoder
2) With the command decoder:
   a) Playback command or playback backup command
   b) Stop playback command
   c) Track change backup for Mars Scanner playback
3) With the data automation system:
   a) Data and sync from DAS
   b) Record TV and MS from DAS
   c) Stop record from DAS
   d) End of tape to DAS

(4) Multiplexing. It is assumed that the nominal and the maximum mission concepts will require the use of four data modes. These modes are associated with certain events of the flight, such as midcourse maneuver and stored data playback. When the requirement for changing data mode arises this means that certain measurements must be deleted from, and others added to the multiplexer input. This is accomplished through the switching in or out of data "decks" of the multiplexer. For the minimum mission 90, for the nominal mission 130 and for the maximum mission 150 engineering measurements are necessary. In addition, both the nominal and the maximum mission concepts require the use of three data rates. The design philosophy of the three different capacity data encoders would follow the basic Mariner 1964 data encoder design.

(5) Telemetry. The telemetry modulation design must accommodate science and engineering measurements in a reliable yet flexible manner. Recognizing the limitations imposed by available bandwidth, a synchronous two channel PCM/PSK/PM telemetry system is recommended. The reasons for this recommendation are:

1) The coherent PSK system is the most efficient presently known technique.
2) A Synchronous system provides relatively fast data synchronization and consequently more real time telemetry data.
3) There is no need for inserting word sync information in the data stream and hence the system efficiency is higher.

(6) Synchronization. Synchronization is accomplished by a pseudonoise (PN) code of length 63 cycling at the word rate. This method conveniently supplies both bit and word synchronization and also allows changing of data rates by factors of two. The reason for utilizing subcarriers is that the DSN receiving system is a phase-locked receiver which requires that:

1) The carrier should not be completely suppressed by the modulation, and
2) The modulation spectrum should not extend into the tracking bandwidth of the phase locked loop near dc.

Since biphase modulation (PSK) does suppress the carrier, and the relatively low bit rates do have appreciable energy near dc, the use of subcarriers is necessary.

d. Command Subsystem

There are two types of ground based commands that will be transmitted to the orbiter.

1) Direct Commands (DC) are the types of commands which will be executed by the spacecraft immediately upon receipt, such as, begin midcourse maneuver, turn on power for television subsystem, etc.
2) Quantitative Commands (QC) are first stored by the spacecraft and used later in conjunction with a real time command. Such quantitative commands are, for example, midcourse velocity increment, midcourse maneuver, pitch, yaw and roll duration.

The command subsystem of the minimum mission would basically follow the present Mariner 1964 design. This command system is capable of handling thirty commands (29 DC/1 QC). For the two higher complexity missions considered, the nominal mission requires 45 commands (40 DC/5 QC) and the maximum mission requires 50 commands (45/5). The total number of commands quoted above will be divided between the two command decoders; however, 15 of the most important commands (10/5) will be redundant so that either command system can accept them. This requires that each command decoder shall be capable of accepting a total of 30 commands and that the address of the command must contain a few bits designating the command decoder to which the command is sent.

As an additional reliability improvement all command addresses should be unique with the possible exception of the redundant commands. The command word structure will consist of a start of word sync code, a command decoder designating code, a command address code (and its parity) identifying the nature (DC/QC) and the recipient subsystem of the command, and additional bits for designating the magnitude of the command in case of a QC only. The word sync code will consist of a 7 bit maximal length shift-register (PN) sequence.

The spacecraft receiver through which the command word is to enter the spacecraft will be frequency addressed. Subsequently, the command detector associated with the "addressed" receiver phase locks to the received synchronization signal, provides the command decoder with an in-lock signal which serves as an alert for accepting valid command signals only. The command decoder performs the command signal demodulation and bit detection also. The recommended command bit rate is one bit per second.

The command modulation scheme (see Reference 1) recommended for this mission is a two-channel PCM/PSK/PM system. The basis of this technique is a coherent system employing a correlation and matched filter detection technique. This technique for an encounter distance of 2.7×10^8 km and a bit error probability of 1×10^{-5} will give a probability of correctly receiving a command word of less than 50 bits long as 99.9 percent. In addition, the coding distance will be so mechanized that a one bit error will not cause a false command to be issued.

4. Performance Capabilities

a. Earth-to-Orbiter Link

Tables 11-47 and 11-48 list the assumed parameters and estimates of the tolerances for the Earth-to-orbiter communications link for both low-gain antennas and the three-foot single degree of freedom high-gain antenna. A 1-bps command data rate is considered. The performance of the command link for both the low gain and high-gain antennas at 1 bps is shown in Figure 11-71. A 0.0 db low-gain spacecraft antenna mode will support command transmission to about 101×10^6 km, while use of the spacecraft high-gain antenna will enable command transmission to 12×10^8 km or more than the maximum Mars range.

b. Orbiter-to-Earth Data Link

Tables 11-49 and 11-50 list the assumed parameters and estimates of the tolerances for the 85-foot and 210-foot diameter receiving antennas and the orbiter antennas parameters.

Estimates of orbiter data rate capability versus range for both the 85-foot and 210-foot diameter antennas and the various spacecraft high-gain antenna configurations are presented in Figures 11-72, 11-73, and 11-74. The parameter used is the spacecraft transmitter power. The performance of the telemetry link during maneuvers is shown in Figures 11-75 and 11-76. Assumed is a spacecraft transmitter power of 10 watts and a data transmission rate of 8-1/3 bps, and that the spacecraft-to-Earth vector is kept in the forward hemisphere of the respective low-gain antenna. Under these conditions the maximum transmission range is about 7.6×10^6 km for the 85-foot diameter receiving antenna and 23×10^6 km for the 210-foot receiving antenna.

5. Weight, Power and Volume

Weight, volume and power estimates for the three mission concepts are given in Tables 11-51 and 11-52.

Assumptions are listed below:

1) Two 10-watt TWT's and a third exciter for launch mode telemetry.
2) Single receiver with turnaround ranging.
3) Two receivers, each with turnaround ranging.
4) Data encoder with 90 channels, 2 data rates and one data mode.
5) Data encoder with 130 channels, 3 data rates and 4 data modes.
6) Data encoder with 150 channels, 3 data rates and 4 data modes.
7) M/C command system with 30 command capability

Table 11-47. DSIF Transmitting Parameters

Item	Value	Tolerance
1. Transmitter Power Output	100 kw	$^{+0.5}_{-0.0}$ db
2. Transmitting Circuit Loss	0.5 db	±0.1 db
3. Antenna Axial Ratio	-	-
4. Antenna Gain	+51.0 db	±1.0 db
5. Frequency	2115 Mc	-

Table 11-48. Orbit Parameters, Earth to Orbiter Link

Item	Forward Looking S/C Omni-Antenna		Side Look S/C Omni-Antenna		3-Foot S/C High-Gain Antenna	
	Value	Tolerance	Value	Tolerance	Value	Tolerance
1. Antenna Gain	-5.0 db	±2.0 db	+5.0 db	±2.0 db	23.5	±1.0 db
2. Antenna Axial Ratio	Variable		Variable		7.0 db	±1.0 db
3. Antenna Pointing Loss (±90°)	-11.0 db	$^{+11.0}_{-0.0}$ db	-11.0 db	$^{+11.0}_{-0.0}$ db	1.5 db	$^{+0.0}_{-1.5}$ db
4. Receiving Circuit Loss	4.0 db	±1.0 db	4.0 db	±1.0 db	4.0 db	±1.0 db
5. Noise Spectral Density (10 db N.F.)	-164.0 $\frac{\text{dbm}}{\text{cps}}$	$^{+1.0}_{-2.0}$ db	-164.0 $\frac{\text{dbm}}{\text{cps}}$	$^{+1.0}_{-2.0}$ db	-164.0 $\frac{\text{dbm}}{\text{cps}}$	$^{+1.0}_{-2.0}$ db
6. Carrier APC Noise B.W.	20 cps	-	20 cps	-	20 cps	-
7. Required Carrier SNR in $2B_{LO}$ for command reception	8.0 db	±1.0 db	8.0 db	±1.0 db	8.0 db	±1.0 db
8. Required command ST/N/B for 1 bps (P_e^b 1 x 10^{-5})	15.7 db	±1.0 db	+15.7 db	±1.0 db	+15.7 db	±1.0 db

Table 11-49. Orbiter Communication Parameters, High-Gain Antennas

Item	Minimum		Nominal		Maximum	
	Value	Tolerance	Value	Tolerance	Value	Tolerance
1. Total Transmitter Power	Variable	±1.0 db	Variable	±1.0 db	Variable	±1.0 db
2. Transmitting Circuit Loss	1.0 db	±0.5 db	1.0 db	±0.5 db	1.0 db	±0.5 db
3. Transmitting Antenna Gain	24.70 db	±1.0 db	24.70 db	±1.0 db	27.1 db	±1.0
4. Transmitting Antenna Pointing Loss	1.0 db maximum	-	1.5 db	-	1.7 db	-
5. Antenna Axial Ratio*	1.5 db	$^{+0.5}_{-1.5}$ db	1.0 db	±1.0 db	0.5 db	±0.5 db
6. Frequency	2295 Mc		2295 Mc		2295 Mc	

*Maximum ellipticity at maximum off axis earth look angle

Table 11-50. Orbiter Communications Parameters, Low-Gain Antennas

Parameter	Forward Looking S/C Low-Gain Antenna		Side Looking S/C Low-Gain Antenna	
	Value	Tolerance	Value	Tolerance
1. Antenna Gain	+5.0 db	2.0 db	+5.0 db	±2.0 db
2. Antenna Axial Ratio-Forward Hemisphere	<6.0 db		<6.0 db	
3. Antenna Pointing Loss-Forward Hemisphere	-11 db Max	$^{+11}_{-0.0}$ db	-11 db Max	+11 db 0.0
4. Circuit Losses to Communications Pan	0.25 db	±0.1 db	1.75 db	$\pm^{0.25}_{0.50}$ db
5. Frequency	2295 Mc		2295 Mc	

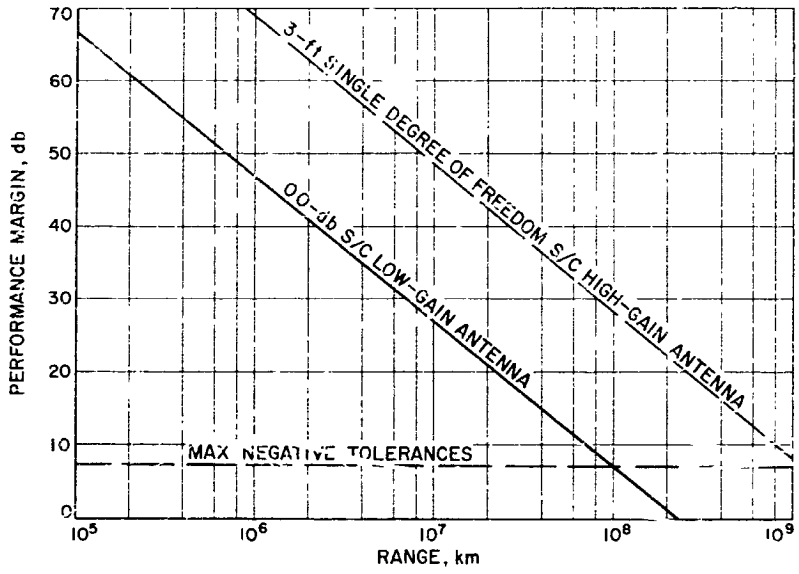


Figure 11-71. Command Performance Margin vs Range (Transmitter Power 100 kw, Transmitting Antenna 85-Foot Diameter)

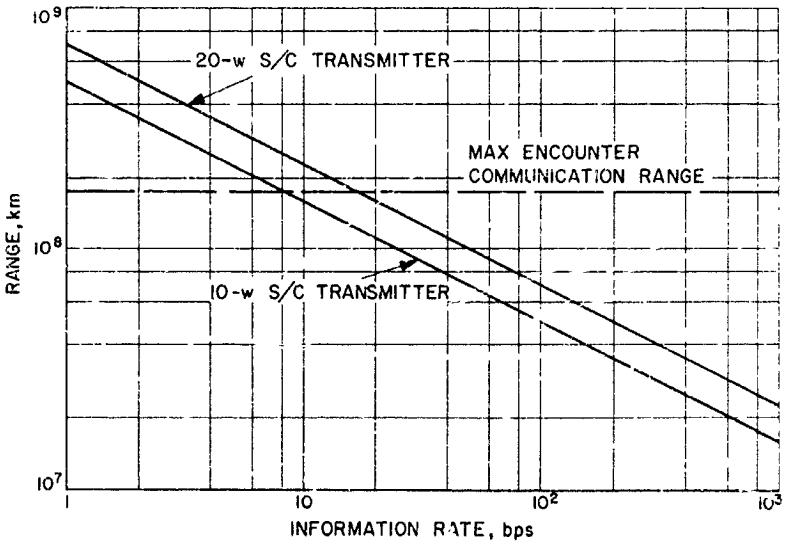


Figure 11-72. Information Rate vs Range (85-Foot Diameter Ground Antenna, 36-Inch Diameter Spacecraft Single Degree of Freedom High-Gain Antenna)

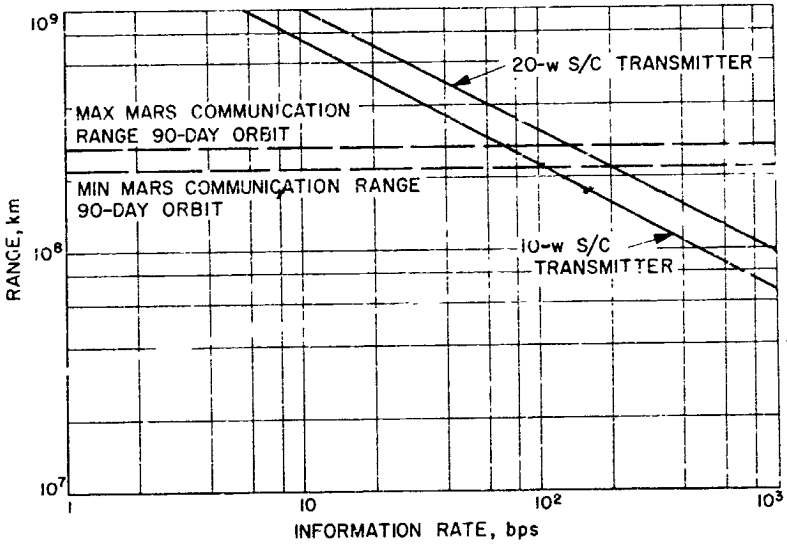


Figure 11-73. Information Rate vs Range
(210-Foot Diameter Ground Antenna,
36-Inch Diameter Spacecraft
Single Degree of Freedom
High-Gain Antenna)

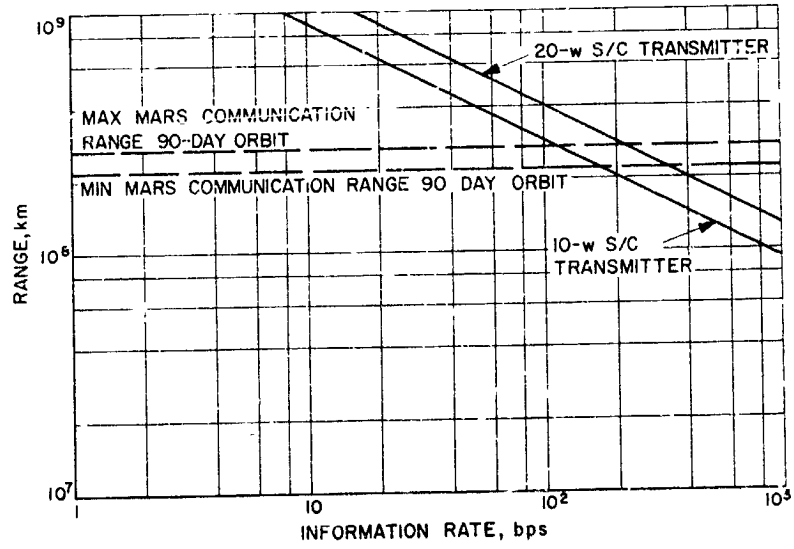


Figure 11-74. Information Rate vs Range
(210-Foot Diameter Ground Antenna,
48-Inch Diameter Spacecraft
Two Degree of Freedom
High-Gain Antenna)

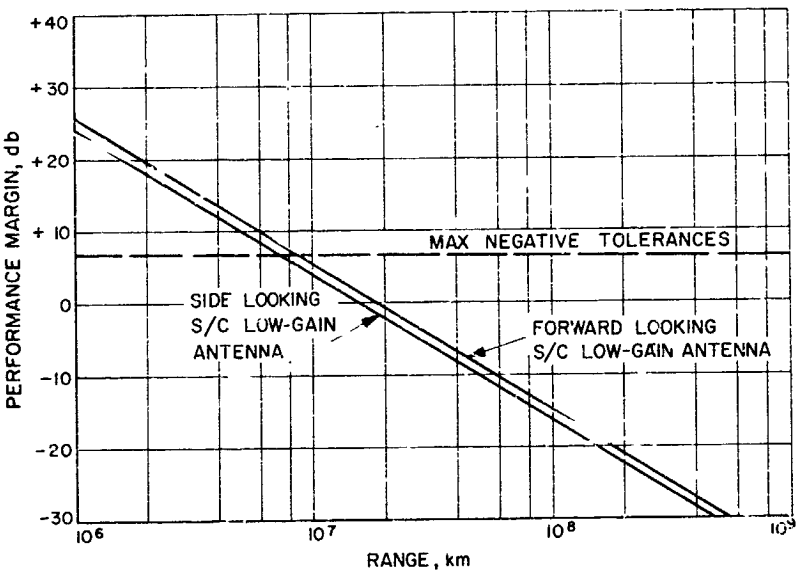


Figure 11-75. Maneuver Telemetry Performance Margin vs Range (10 w Spacecraft Transmitter, 85-Foot Diameter Ground Antenna, 8 1/3 bps Information Rate)

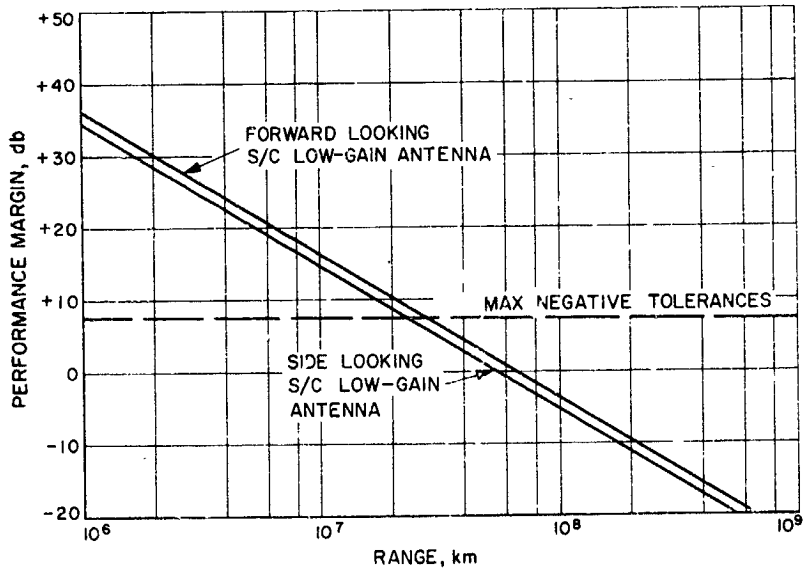


Figure 11-76. Maneuver Telemetry Performance Margin vs Range (10 w Spacecraft Transmitter, 210-Foot Diameter Ground Antenna, 8 1/3 bps Information Rate)

Table 11-51. Spacecraft Telecommunication Weight and Volume Estimates

SUBSYSTEMS		Minimum		Nominal		Maximum	
		Weight Lbs.	Volume $(in)^3$	Weight Lbs.	Volume $(in)^3$	Weight Lbs.	Volume $(in)^3$
Transmitter		(1) 31.80	(2) 2992.0	(1) 38.75	(1) 3580.0	(1) 38.75	(2) 3580.0
Receiver		(2) 16.89	(2) 1360.0	(3) 33.78	(3) 2720.0	(3) 33.78	(3) 2720.0
Data Encoder		(4) 24.79	(4) 869.0	(5) 32.6	(5) 908.5	(6) 34.8	(6) 948.0
Command		(7) 11.70	(7) 328.0	(8) 24.50	(8) 749.0	(9) 24.70	(9) 749.0
Tape Recorder		None		(10) 11.6	(10) 401.0	(11) 37.5	(11) 1353.0
Antenna (Without actuation system)		(12)		(13)		(14)	
	High-Gain	3.0		3.0		5.2	
	High-Gain Coaxial Cables	1.0		1.0		1.0	
	High-Gain Rotary Joints	-		0.5		1.0	
	Low-Gain	5.5		7.0		7.0	
	Low-Gain Coaxial Cables	0.5		0.5		0.5	
	Side Mount Low-Gain	-		0.3		0.3	
	Side Mount Coaxial Cables	-		3.0		3.0	
	Side Mount Low-Gain Rotary Joints	-		1.0		1.0	
	Total	10.0		16.3		19.0	
TOTAL		95.18	5549.0	157.53	8359.03	188.83	9,350

All Weight estimates include wiring harnesses.

Table 11-52. Spacecraft Telecommunications Power Estimates

	Minimum			Nominal			Maximum		
	Raw DC Watts	Regulated AC	Launch Only	Raw DC Watts	Regulated AC	Launch Only	Raw DC Watts	Regulated AC	Launch Only
		(1)			(1)			(1)	
A) Transmitter									
a) Power Amplifier	62.0			62.0			62.0		
b) Exciter TR		2.5			2.5			2.5	
c) Launch Mode Exciter			10.00			10.00			10.00
		(2)			(7)			(3)	
B) Receiver		8.25			17.00			17.00	
		(4)			(5)			(6)	
C) Data Encoder		9.65			14.00			14.50	
		(7)			(8)			(9)	
D) Command		3.60			8.0			8.0	
E) Tape Recorder									
a) Record		None			10.5 (10)			31.5 (11)	
b) Playback					8.5 (10)			27.5 (11)	

8) Two command systems with 45-command capability 15 redundant commands.
9) Two command systems with 50-command capability 15 redundant commands.
10) Tape storage for 15×10^6 bits.
11) Tape storage for 50×10^6 bits.
12) Three foot fixed high-gain and Mariner Mars 1964 type low-gain antenna.
13) Three foot single degree of freedom high-gain and two low-gain antennas.
14) Four foot two degree of freedom high-gain and two low-gain antennas.

REFERENCES

1. J. C. Springett, "Telemetry and Command Techniques for Planetary Spacecraft," Technical Report No. 32-495, Jet Propulsion Laboratory, Pasadena, Pending.

2. R. P. Mathison, "Tracking Techniques for Interplanetary Spacecraft," Technical Report No. 32-284, Jet Propulsion Laboratory, Pasadena, August 1, 1962.

J. ENVIRONMENTAL CONTROL

1. Functional Requirements for the Mars Orbiter Temperature Control System

a. Temperature Control System Capabilities

The temperature control system for the orbiter shall provide all parts of the spacecraft with tolerable operating temperatures during all phases of operation, including:

1) Complete spacecraft system testing
2) Launch pad operations
3) Launch
4) Cruise
5) Midcourse maneuvers
6) Orbit injection
7) Orbit

Primary emphasis will be placed on the cruise and orbiting portions of flight, wherein a temperature environment will be provided which enhances the operating lifetime of the electronic components. Variations from this optimum temperature environment will be allowed during all other phases of operation, due to their transient nature compared with the cruise or orbiting portions. Temperature control of the spacecraft requires cognizance of thermal design at all levels of design, i.e., component, subassembly, assembly, and stem.

b. Passive Techniques

Passive techniques shall be used to the maximum extent possible.

c. Active Controls Reliability

Active controls, when required, shall be proven reliable to the maximum extent consistent with the launch schedule.

d. Active Temperature Control

Active temperature control continuous electric power requirements shall not exceed 23 watts.

2. Description

a. General Description

The temperature control system for the orbiter consists of:

1) All the external surfaces of the vehicles which are utilized as primary radiator surfaces;
2) Any attachments, finishes, or mechanisms applied to the primary radiator surfaces which are used for varying the radiating ability of these surfaces;
3) Any electrical power dissipating devices and their controls utilized specifically for temperature control;
4) The radiative and conductive paths between the operating components of the spacecraft and the primary radiator surfaces.

Final control of the bulk temperature of all parts of the spacecraft is obtained by the treatments and attachments or mechanisms applied to the external surfaces. Control of the temperatures at any point inside the outer surface is provided by regulating the electrical power dissipation and the radiative and conductive paths connecting the point of interest to the primary radiators.

3. Temperature Limits

1) The nominal temperature environment during cruise for operating components located in the main octagon will be between 50°F and 120°F. Exceptions to this range shall be held to a minimum.
2) Equipment mounted in locations other than the main octagon will be controlled on an individual basis and nominal temperature environments cannot be defined.

4. Influence of Meteoroids on Propellant Tank Wall Thickness

In addition to the uncertainties described in Section V. C. regarding the interplanetary meteoroid flux, there is an additional uncertainty associated with the interaction of the meteoroid with the target material. Very little experimental data is available at meteoroid impact velocities in the range 15 to 20 km/sec Whipple[1] uses the correlation developed by Hermann and Jones to estimate the depth of penetration. Whipple then compares this correlation with other penetration equations of Bjork, Whipple, Bruce, and Öpik. The analysis presented here is based on the penetration equations of Summers and Charters. The analytical results are then compared to thick target experimental results obtained by N. Scully at North American Aviation. In Scully's experiments, he utilized 0.002-inch diameter glass projectiles (ρ = 2.3 gm/cc) to bombard aluminum, stainless steel, copper, and beryllium at velocities

to 20 km/sec. This data indicates that for impact velocities greater than 10 km/sec the depth of penetration is equal to or greater than the impact particle diameter.

In order to compare the results presented herein with those of Whipple, the penetration parameter $t/m^{1/3}$ used by Whipple is shown in Table 11-53 for the equation of Summers and Charters and the data of N. Scully, as well as the values given in Whipple's papers. These values are for an aluminum target, an impact velocity of 22 km/sec, a meteoroid density of 0.44 gm/cc (except for the data of Scully) and a thin target factor of 1.5. The results in Table 11-53 indicate that the analysis of Summers and Charters are somewhat optimistic compared to other analyses.

The nominal meteoroid flux-mass distribution used in the analysis is that given in Reference 2. The nominal flux-mass relationship developed in Reference 2 is lower than the "best estimate" suggested by Whipple in Reference 1 by approximately a factor of 3. Therefore, the results of the analysis are not conservative on a total probability of puncture basis.

By combining the penetration equation of Summers and Charters with the flux-mass law given in Reference 2, the resulting penetration equation is

$$t = K \left[\frac{\tau}{1-P(o)}\right]^{1/3b} (A_v)^{1/3b} \qquad \text{(Equation 1)}$$

Table 11-53. Aluminum Target Comparisons

Author	Aluminum Target $P/m^{1/3}$ $cm/gm^{1/3}$
Hermann and Jones*	1.94
Bjork*	4.58
Whipple*	6.04
Bruce*	5.34
Öpik*	3.19
Summers and Charters	1.56
Scully	2.82

*Obtained from Reference 1

where:

t = penetration thickness, cm

$K = Fk(a)^{1/3b}$

F = thin target factor (1.5 or 2.0)

$k = 4.0\left(\frac{\rho_m V^2}{\rho_\tau E g_c}\right)^{1/3}$

ρ_m = meteoroid density, gm/cc

V = meteoroid velocity, ft/sec

ρ_t = target density, gm/cc

E = modulus of target, lb/ft^2

g_c = 32.2 lbm ft/lbf sec^2

A_v = vulnerable area, m^2

τ = time of exposure, seconds

$P(o)$ = probability of no punctures during mission

and the meteoroid flux is given by

$$\Phi = a\, m^{-b} \qquad \text{(Equation 2)}$$

where:

Φ = meteoroid flux, particles/m^2sec

a = 1.3×10^{-15} $gm^{4/3}$ /m^2sec (coefficient in flux mass law)

b = 4/3 (exponent in flux mass law)

m = mass of meteoroid, gm

First, the inherent protection associated with the tank wall thickness based on a design internal pressure of approximately 400 psia is considered. The minimum tank wall thickness has been estimated to be 0.024 inches. The tank wall is assumed to be titanium (ρ = 4.4 gm/c , E* = 16×10^6 psi). The vulnerable tank area is approximately 1 m^2 (two tanks of approximately 31-inch diameter with a total propellant capacity of 1100 lb.) An average meteoroid velocity** of 30 km/sec has been assumed rather than 22 km/sec as assumed by Whipple and a total interplanetary flight time of 270 days (type II trajectory) is utilized.

The results of the calculations for an 0.024-inch wall thickness are shown in Table 11-54. Assuming a cometary origin meteoroid density of 0.4 gm/cc and a thin target factor of 1.5, the probability of no punctures during the mission is 99 percent. For the same meteoroid density and a thin target factor of 2.0, the probability of no punctures during the mission is 98 percent. If the flux of meteoroids is indeed 100 times greater than predicted by Equation 2 (See Section V. C.), the probability of no punctures during the mission is 21 percent for a

*E must be converted to lb/ft^2 before substituting in the equation for k.

**By utilizing a meteoroid velocity of 30 km/sec, the $P/m^{1/3}$ using the penetration equation of Summers and Charters is equivalent to the Hermann and Jones equation used by Whipple.

Table 11-54. Mission Probabilities of No Punctures

Thin Target Factor	Density of Impacting Meteoroid (gm/cc)	
	Cometary Origin ρ = 0.4	Asteroidal Origin ρ = 3.0 (Same Flux-Mass Distribution as Cometary Meteoroids)
1.5	P (0) = 0.99	P (0) = 0.86
2.0	P (0) = 0.98	P (0) = 0.58
100 Times Nominal Flux-Mass Distribution		
	ρ = 0.4	
1.5	P (0) = 0.21	
2.0	P (0) = 0	

thin target factor of 1.5 and approximately 0 percent for a thin target factor of 2.0. If it is assumed that the same nominal flux-mass law used above pertains to asteroidal origin meteoroids (ρ = 3 gm/cc) and that this flux is present throughout the heliocentric phase of the mission, the probability of no puncture during the mission is 86 percent for a thin target factor of 1.5 and only 58 percent for a thin target factor of 2.0.

The mass of importance for ρ = 0.4 gm/cc particles is approximately 10^{-4} gm, and the particle diameter is approximately 0.030 inch. If the depth of penetration is 1.5 to 2.0 times the particle diameter depending on the degree of penetration of titanium compared to steel or aluminum (on the basis of the experimental data of Scully), the tank wall thickness should be 0.045 to 0.060 inches. Thus, even if the nominal flux-mass distribution pertains and the particles have a density of 0.4 gm/cc, the tank walls are not conservatively designed on the basis of internal pressurization. These results indicate that it is important to define the meteoroid environment in Earth-Mars space.

There is an additional factor which has not been included in this analysis. If smaller meteoroids impact the tanks, they will not penetrate as deeply. However, considering that nonfatal meteoroid "spall" may occur at a number of locations on the tanks during the interplanetary flight and that maximum tank pressure occurs at orbit injection, the probability of a meteoroid causing a failure is greater than has been calculated. It seems appropriate to give additional thought to this problem prior to committing to specific propulsion system weight estimates.

One last consideration is the degree of protection inherent in the temperature control insulation blanket. The "thickness" of the blanket is approximately 0.2 lb/ft^2 compared to a thickness of approximately 1.0 lb/ft^2 required to stop 10^{-4} gm meteoroids assuming an impact velocity of 30 km/sec. The insulation blanket will tend to shield the tanks from smaller meteoroids, although the degree of shielding has not been evaluated. However, in the case of meteoroids in the 10^{-5} to 10^{-4} gm size range, the insulation blanket may cause the meteoroid to do more damage to the tank walls. Hypervelocity testing performed at Boeing indicates that the bumper may be spalled to such a degree to inflict more damage on the target if the projectile impacts directly on the target even though the maximum penetration depth is less. A complete review of test conditions, etc., has not been performed to determine whether this data is applicable in the flight situation.

In summary, the meteoroid flux in Earth-Mars space is likely to determine the required propellant tank wall thickness for a Mars orbiter mission.

REFERENCES

1. F. L. Whipple, "Meteoroids and Penetration," Journal of Geophysical Research. Vol. 68 No. 17, pp. 4929-4939, September 1, 1963.

2. K. O. Parker and R. A. Stone, "Spur High-Temperature Space Radiator" ARS Paper 2549-62.

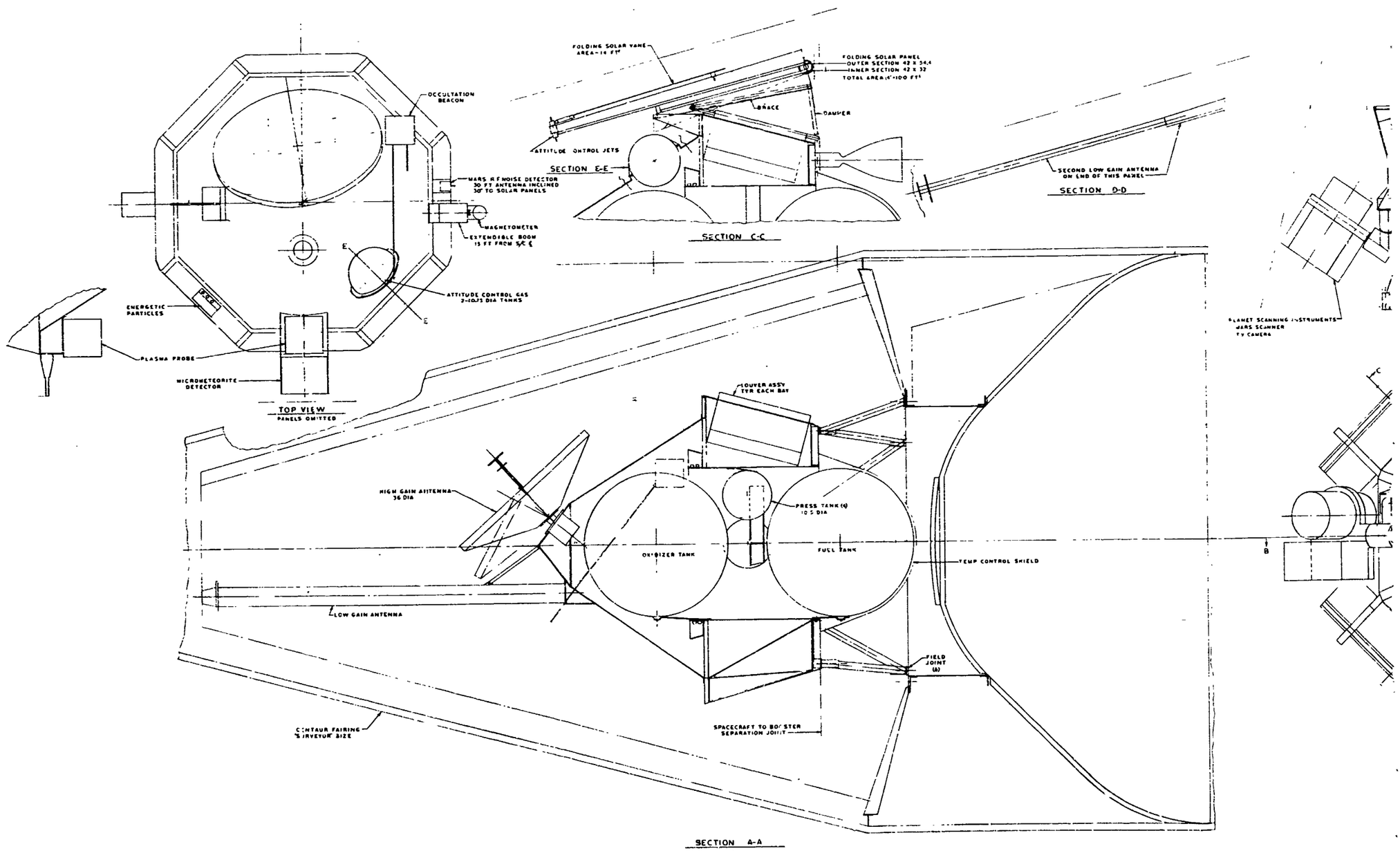
K. ALTERNATE SPACECRAFT CONFIGURATIONS

Figures 11-77, 11-78, 11-79 and 11-80 show other spacecraft configurations incorporating different methods for packaging the spacecraft subsystems, all with liquid propulsion systems.

Figure 11-77 shows a three engine retro system. Pitch and yaw thrust vector control is achieved by throttling three engines and the roll control is accomplished by gimbaling one of the engines.

The spacecraft bus has tilted sides to reduce interaction of infrared radiation emitted from the solar panels with the spacecraft electronic packaging thermal control subsystem.

Figures 11-78, 11-79 and 11-80 show early configuration studies that were based on the ground rule that a Mariner 1964 type bus be used. These studies indicated that the propulsion system and the solar panels strongly affected the total configuration. It is desirable to have the spacecraft center of gravity as low in the Centaur fairing as possible. Generally this means that the propulsion system be consolidated in the lower portion of the envelope and that the spacecraft must be packaged around the propulsion system rather than in a stacked manner. This tight packaging improves thermal control and also permits the retro-motor to be located perpendicular to the roll axis. Some adapter weight savings results and the solar panels can be packaged upward with the undesirable folded joint eliminated.


OCCULTATION BEACON
MARS R F NOISE DETECTOR 30 FT ANTENNA INCLINED 30° TO SOLAR PANELS
MAGNETOMETER
EXTENDIBLE BOOM 15 FT FROM S/C ℄
ATTITUDE CONTROL GAS 2-10.75 DIA TANKS
ENERGETIC PARTICLES
PLASMA PROBE
MICROMETEORITE DETECTOR
TOP VIEW
PANELS OMITTED
FOLDING SOLAR VANE AREA-16 FT²
FOLDING SOLAR PANEL
OUTER SECTION 42 X 54.4
INNER SECTION 42 X 32
TOTAL AREA (4)100 FT²
BRACE
DAMPER
ATTITUDE CNTROL JETS
SECTION E-E
SECOND LOW GAIN ANTENNA ON END OF THIS PANEL
SECTION D-D
SECTION C-C
LOUVER ASSY TYP EACH BAY
HIGH GAIN ANTENNA 36 DIA
PRESS TANK (4) 10.5 DIA
OXIDIZER TANK
FUEL TANK
TEMP CONTROL SHIELD
LOW GAIN ANTENNA
FIELD JOINT (A)
CENTAUR FAIRING 3 RIVETOR SIZE
SPACECRAFT TO BOOSTER SEPARATION JOINT
SECTION A-A
PLANET SCANNING INSTRUMENTS
MARS SCANNER
TV CAMERA

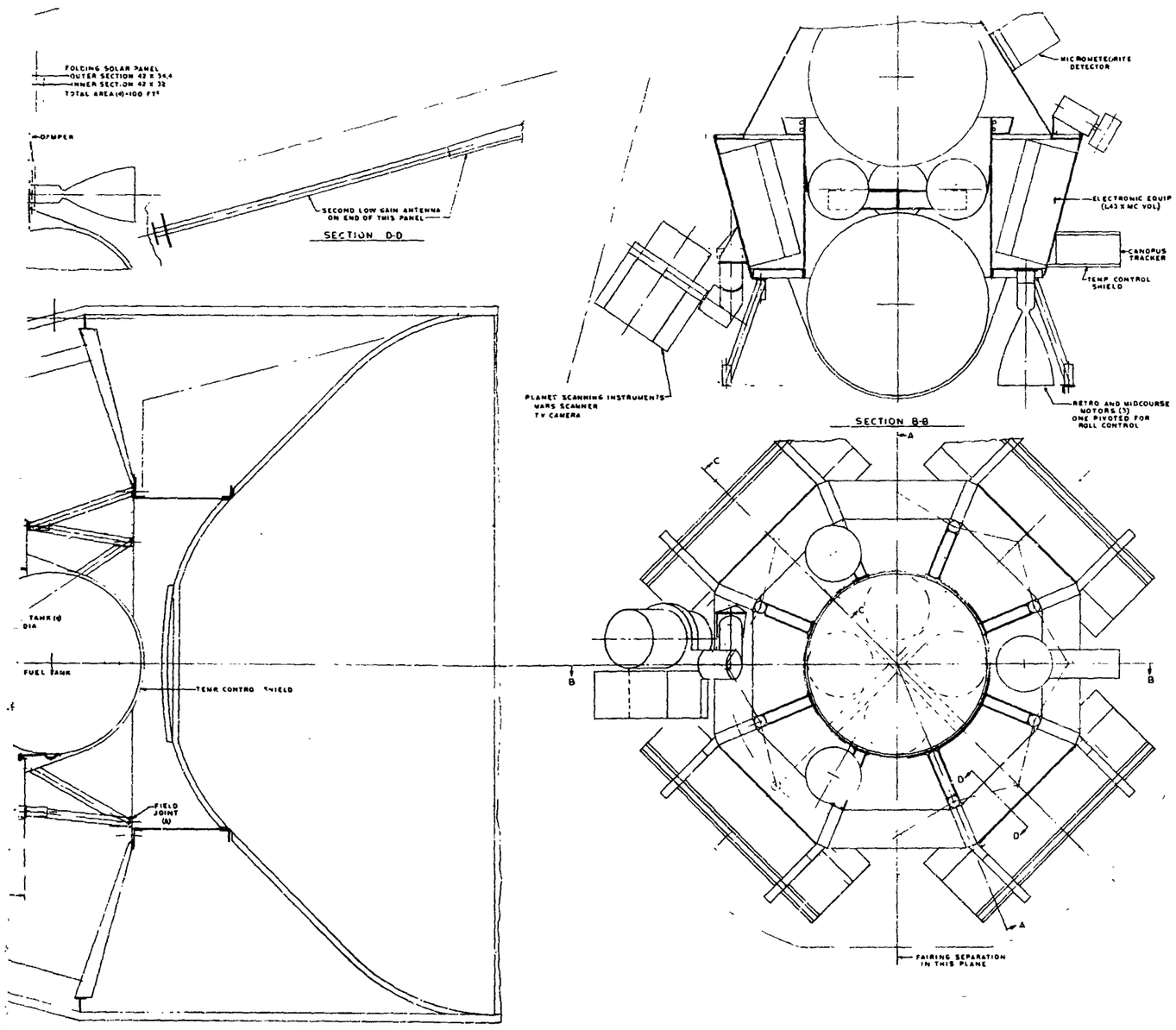


Figure 11-77. Spacecraft Mars Orbiter, JPL Drawing 4300619, Sheet 17

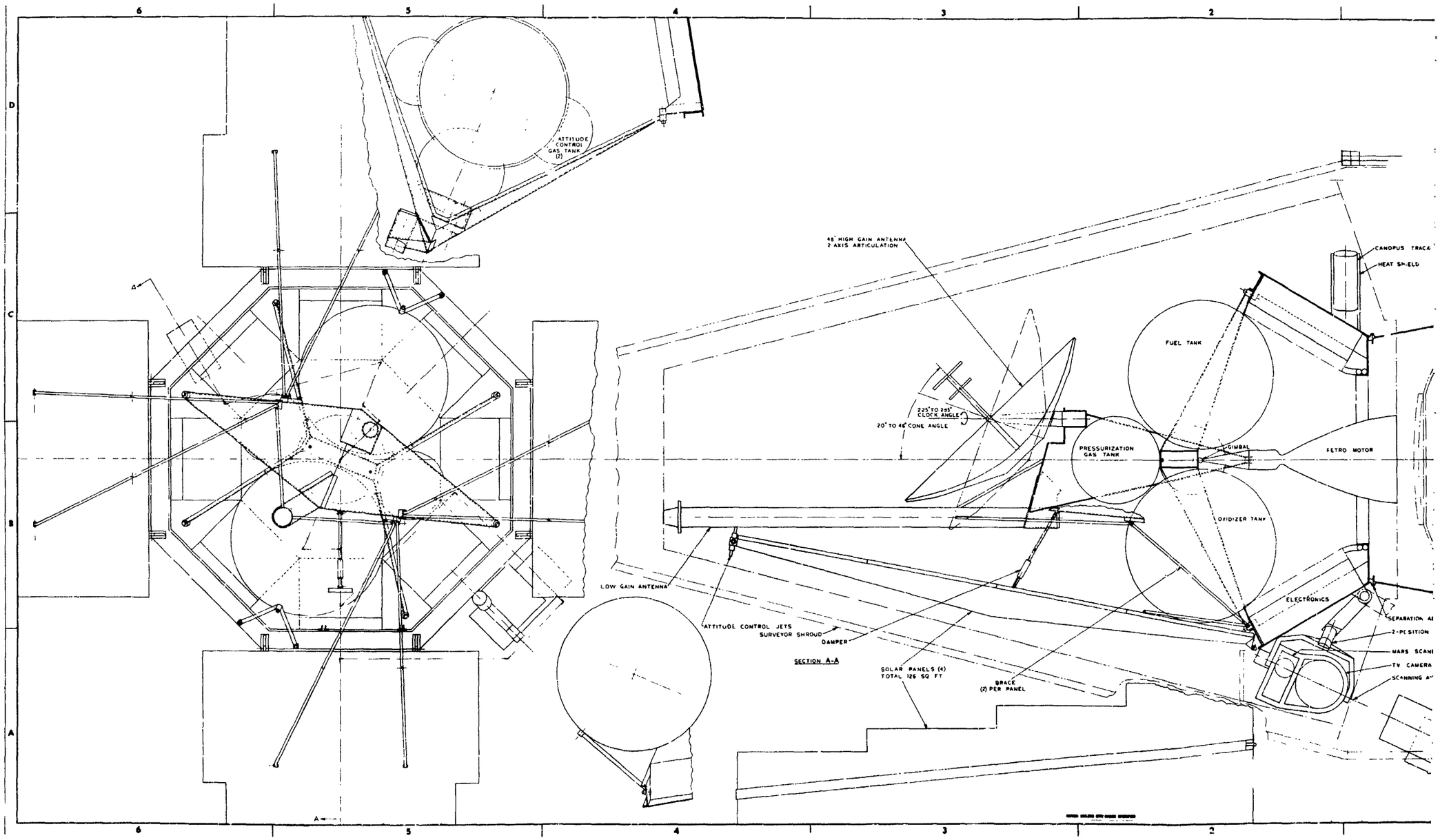


Figure 11-78. Spacecr
JPL Drawing 43006.

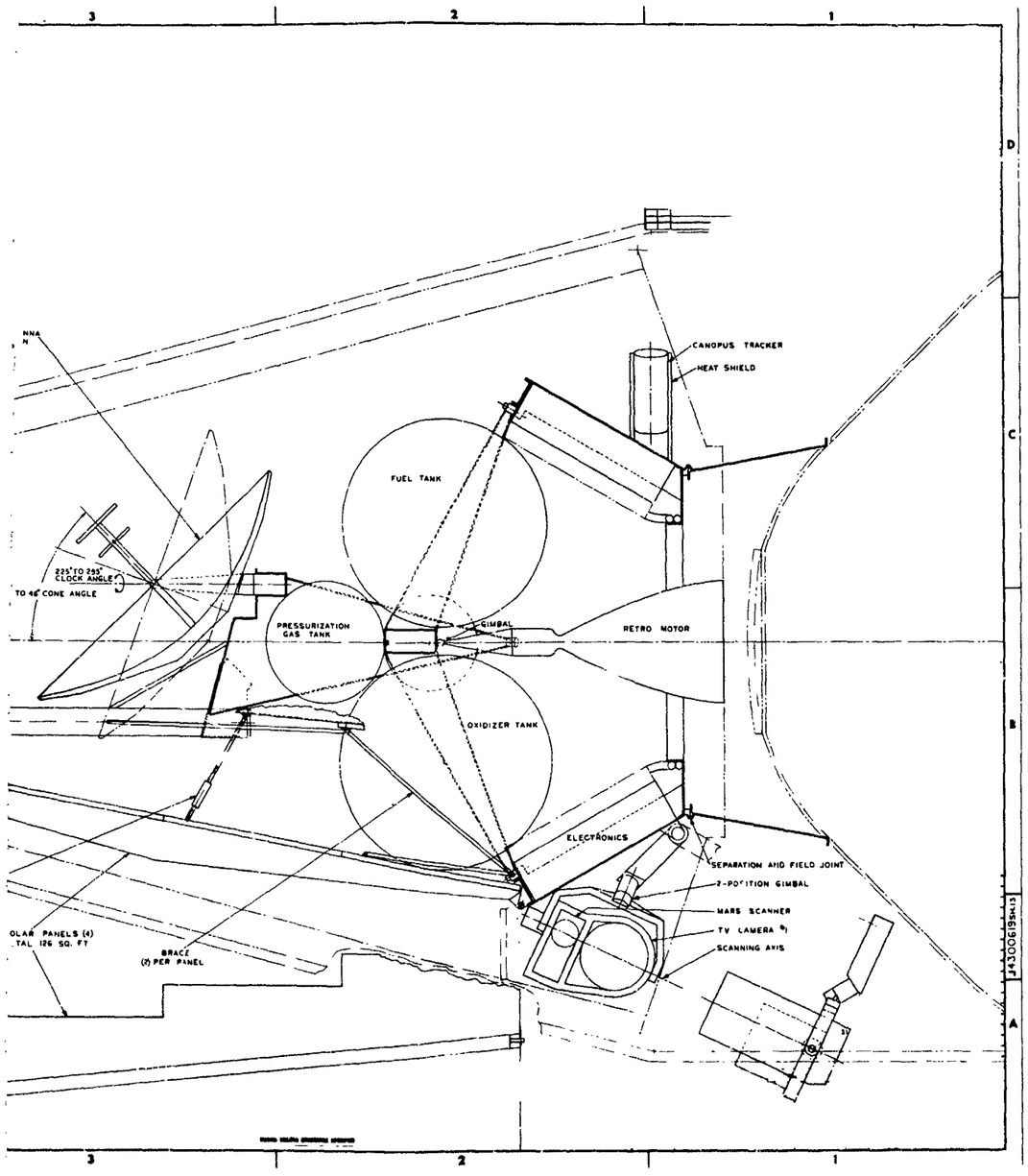


Figure 11-78. Spacecraft Mars Orbiter, JPL Drawing 4300619, Sheet 13

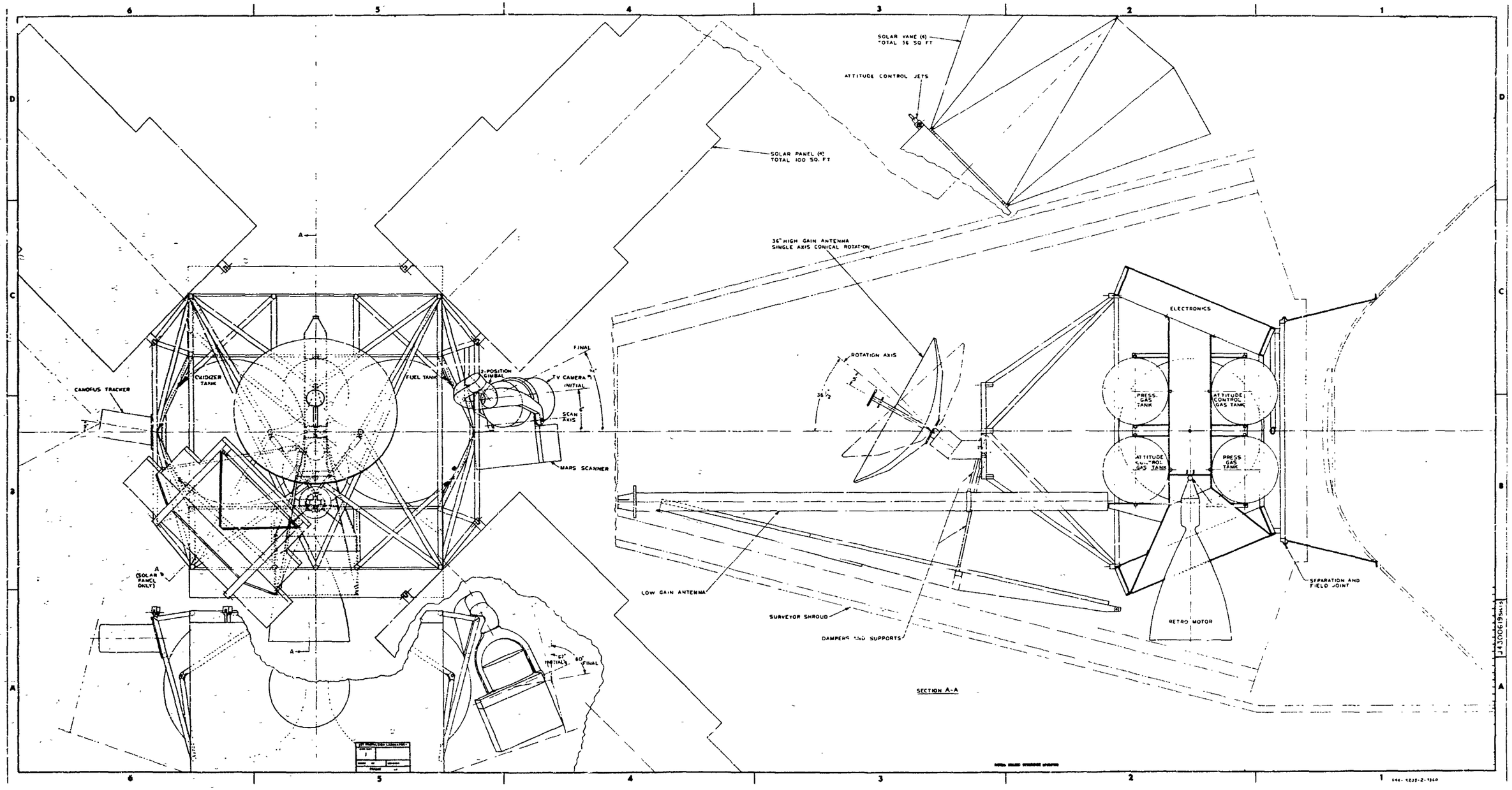


Figure 11-79. Spacecraft Mars Orbiter, JPL Drawing 4300619, Sheet 19

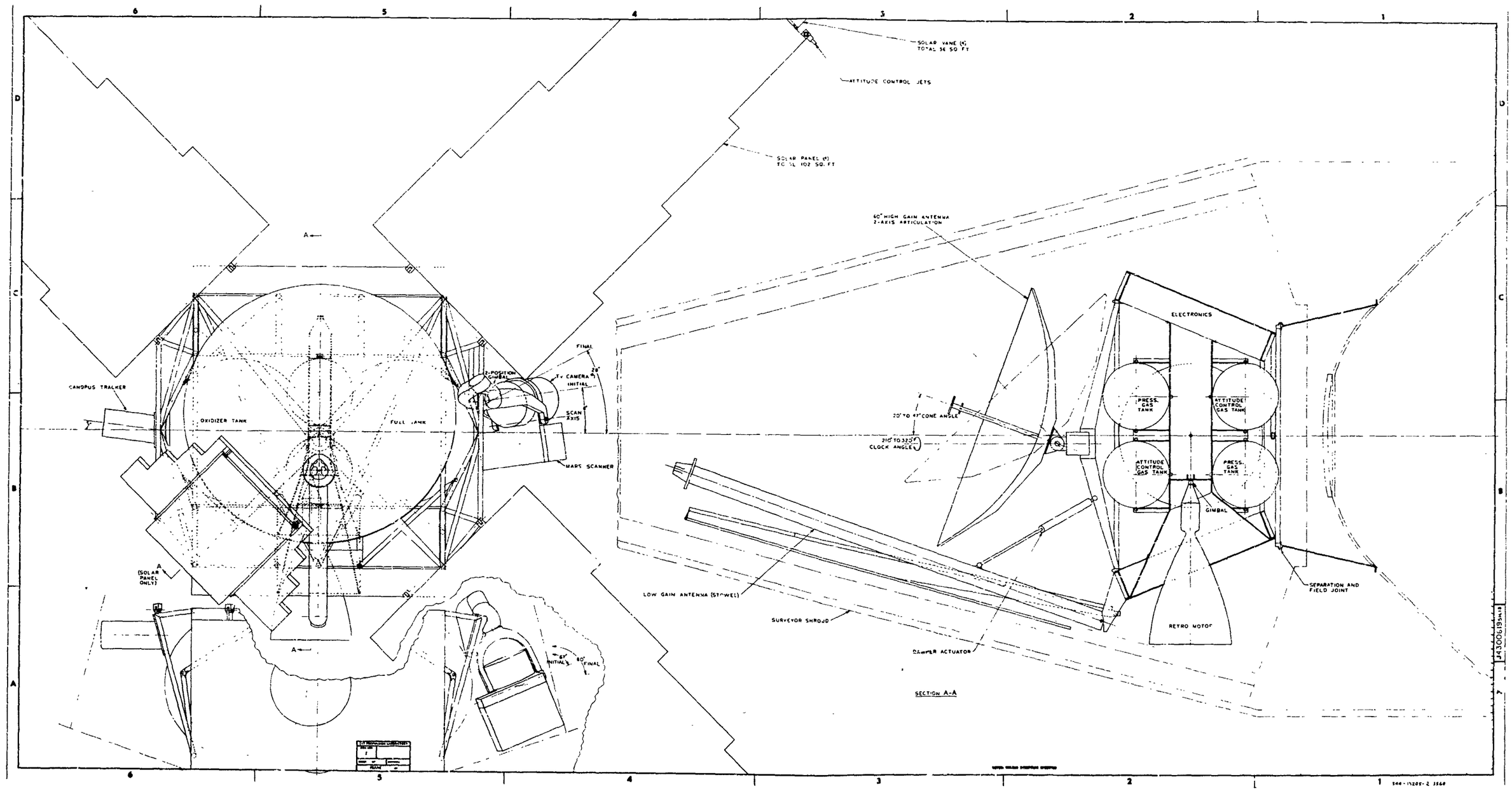


Figure 11-80. Spacecraft Mars Orbiter, JPL Drawing 4300619, Sheet 18

APPENDIX A

DEEP SPACE NETWORK CONFIGURATION MARS '69 ORBITER STUDY

1. General DSN Configuration and Availability

This section discusses the general configuration and availability of the Deep Space Network for the Mars 1969 Orbiter. The suggested network is based on the use of a spacecraft monitoring station at Cape Kennedy to provide pre-launch spacecraft-DSN compatibility, checkout and telemetering from lift-off to local horizon; a three-station 85-ft HA-Dec antenna network; and the Space Flight Operations Facility (SFOF) at JPL.

Locations of the Deep Space Stations are approximately 120 degrees apart in longitude and between 40 degrees north and 40 degrees south latitude so that a spacecraft which is more than 10, 000 miles away from earth will be under continuous surveillance.

All stations of the Deep Space Instrumentation Facility (DSIF) system will be operational on S-Band frequencies for the Mars 1969 Orbiter. Implementation of the S-Band system frequencies (2110-2120 Mc from earth to spacecraft and 2290-2300 Mc from spacecraft to earth) at Goldstone (Pioneer and Echo), Johannesburg, Canberra, Madrid and Woomera is planned for completion during Calendar 1965.

2. 85-Foot HA-Dec Antenna Network

The three-station 85-ft HA-Dec antenna network is proposed for Mars 1969 Orbiter use from launch up to encounter or as reasonably close to there as possible This network may be available 24 hours per day during critical phases of the mission and a nominal 10 hours per day or one station view period per day for the cruise phase. General network configuration and performance will be as follows:

1)	Gain:	
	a) Listen/track:	53 db
	b) Transmit:	51 db
2)	S-Band Receiver:	2295 ±5 Mc
3)	S-Band 10 kw Transmitter:	2115 ±5 Mc
4)	Antenna Beamwidth:	0. 35 degrees
5)	Receiver Threshold @ BW of 12 cps:	-170. 4 dbm
6)	Effective System Noise Temperature:	
	a) Listen only:	55° ±10°K
	b) Two-way track, listen and transmit simultaneously:	60° ±10°K

Use of the 100 kw transmitter at the Goldstone (Venus) station is also proposed for command and two-way doppler backup in conjunction with either the Goldstone Pioneer and Echo stations during the entire mission. This backup capability would be similar to that available for the Mariner 1964 mission.

3. 210-Foot Az-El Antenna

A 210-ft Az-El antenna located at the Goldstone Mars site is proposed for use during the orbiting phase of the Mars 1969 mission. Upon successful completion of the construction schedule, this antenna will be available on a nominal 10-hour per day basis (or one station view period) during the orbiting phase, with the exception of one two-week period of non-availability due to a possible support committment to an Apollo mission.

The general configuration and performance of the 210-ft antenna will be as follows:

1)	Gain:	
	a) Listen/track:	61 db
	b) Transmit:	60.3 db
2)	S-Band Receiver:	2295 ±5 Mc
3)	S-Band 10 kw Transmitter:	2115 ±5 Mc
4)	Antenna Beamwidth:	0.1 degrees
5)	Receiver Threshold @ 12 cps BW:	-170.4 dbm
6)	Effective System Noise Temperature:	
	a) Listen only:	30° ±5°K
	b) Two-way track, listen and transmit simultaneously:	45° ±5°K

4. Tracking Capability

a. Tracking

The automatic angle tracking systems used in the DSIF are of the simultaneous-lobing type. The 85-ft HA-Dec antennas have a maximum tracking rate capability of 0.7 deg/sec about each axis, depending on tracking system bandwidth requirements. During the periods in which angle tracking accuracy is most significant (e.g., when data for an initial ephemeris calculation are required), the strong signal levels available result in a root-mean-square angle tracking error from 0.01 to 0.02 degrees. The rms tracking error at receiver threshold increases to approximately 0.05 degrees. Bias errors lie in the range of -0.1 to ±0.1 degrees. However, optical calibration techniques such as star tracking have led to the accurate determination of certain bias errors, and these are removed from the observed data at the computational facility (SFOF). Resolution of the angle encoders is 0.002 degrees. The 85-ft Az-El mount antenna at the Goldstone (Venus) site is capable of tracking rates up to 2.0 deg/sec and has rms tracking errors comparable to the polar-mount 85-ft antennas.

Expected performance of the 210-ft altazimuth-mount DSIF antenna includes maximum tracking rates of 0.5 deg/sec and maximum acceleration rates of 0.2 deg/sec in azimuth and elevation. Tracking errors and bias data will be determined upon completion of the antenna installation.

b. Doppler

One- and two-way doppler measurement capability is included at all stations in the DSIF. Two-way doppler requires a ground transmitter in the vicinity of the DSIF receiver to achieve frequency control by a single exciter. The distance at which the DSIF stations can obtain doppler data is, of course, dependent on the sensitivity of the spacecraft receiver and the power output of the spacecraft transponder; if the carrier can be tracked in phase, doppler data can be made available. One-way doppler accuracy is 30 m/sec, and two-way accuracy is expected to be 0.003 m/sec. The latter accuracy is based upon a minimum of 5 hours of tracking using correlation periods of 60 sec. The accuracy of one-way doppler data is limited primarily by the average frequency instability of the spacecraft oscillator. The detected doppler in either the one- or two-way system is equal to the doppler shift at the receiver RF frequency with the addition of a 1 Mc bias. The 1 Mc bias is derived from the station's ultrastable oscillator.

c. Precision Ranging

A ranging system presently under development by JPL is planned for installation at all DSIF stations upon implementation of S-Band frequency capabilities. The system measures the time difference between two identical, separately generated, pseudo-random noise codes one generated at the transmitter for modulation, and the other generated at the receiver for correlation detection) to represent range. The transponder in the spacecraft receives the code-modulated transmitted signal and retransmits the same modulation back to the ground. The transponder is called a "turnaround" transponder, and normal signal-to-noise ratios available with this type of system limit the measurement of range to less than 800,000 km. The resolution of the ranging system is 0.007 microseconds round-trip time, which is approximately equivalent to 1.05 meters one way. However, worst-case estimates of the unknown time delays in the receiving system are expected to limit the accuracy of the ranging system to ±0.1 microsecond round-trip time, which is approximately equivalent to ±15 meters one way. This system will probably be extended to planetary ranges with comparable resolution and with no change in the spacecraft (from Mariner 1964 transponder).

The ranging system is operable as long as carrier phase coherence is maintained in the two-way system. The general mode of operation will be to initiate range modulation, establish range lock, and then remove range modulation and count carrier doppler cycles to maintain a range tally.

d. Tracking Data Hardling

Tracking data handling equipment is operational at all Deep Space Stations. This equipment automatically punches out, on paper tape and in standard Baudot Teleprinter five-hole code, characters which represent carriage return, line feed, figures, spaces and the following technical information:

1) Station identification number
2) Spacecraft identification number
3) Data condition
4) Greenwich Mean Time (GMT)
5) Antenna hour or azimuth angle
6) Antenna declination or elevation angle
7) Doppler frequency
8) Range data including "range condition" code (A)
9) Transmitter frequency (A)
10) Day of year

The format is designed so that one complete set of information is printed on one or two lines of a teleprinter page printer, which will accept a nominal 60 characters per line, including spaces. The system is capable of punching at a rate of 60 characters per second, using two punches connected to operate singly or in parallel. A control is available so that both punches can operate in parallel but with one punch set to punch at 1/1, 1/2, 1/3, 1/4, 1/5, 1/6, 1/7, 1/8, 1/9, or 1/10 the rate of the other punch. Since the normal maximum teletype speed is 6 characters per second (60 words per minute), it is possible to use one punch to punch out data for real time teleprinter transmission while the other punch is punching out data at the maximum rate. The tracking data sampling rate is generally determined by project requirements and varies considerably over the period of a mission.

5. Communications

a. Receiver Subsystem

The S-Band phase-lock loop receiver is a double conversion superheterodyne receiver with a 50 Mc first IF and a 10 Mc second IF. The output of the 10 Mc IF passes through a bandpass filter which can be selected to have any one of four different bandwidths: 3.3 Mc, 420 kc, 20 kc, and 4.5 kc. When required, this filter may be replaced with one designed to meet particular characteristics. The bandpass filter has two outputs. One output feeds an IF amplifier with a 3.3 Mc, 420 kc, 20 kc, and 4.5 kc. When required, this filter may be replaced with one designed to meet particular characteristics. The bandpass filter has two

outputs. One output feeds an IF amplifier with a 3.3 Mc bandwidth input to the filter which furnishes signal voltages to the input of the down converter associated with the FR-700 video tape recorder. The other output feeds a wideband phase detector which in turn has two outputs. One of these outputs is a video amplifier with a bandwidth of 300 cps to 1.65 Mc; the other is a dc amplifier with a bandwidth of dc to 250 kc. The latter is called the narrow-band telemetry output and would be the output used to provide inputs to the various discriminators when standard IRIG telemetry channels are used. Some stations are equipped with standard phase-lock IRIG discriminators and channel selectors for channels 1 through 8. If necessary, arrangements can be made to furnish an output from the 50 Mc IF amplifier with a bandwidth of 10 Mc.

b. Telemetry Data Handling

The data handling and instrumentation capability available at the DSIF sites for the 1969 Orbiter mission will be centered around the use of general purpose digital computers. The processing of telemetry data for real time display and recording at the station, as well as transmission to the SFOF, will be accomplished by the DSIF On-Site Data Processing System (OSDP). Two Scientific Data Systems SDS-920 computers will comprise the OSDP. This system offers a total memory capacity of 8192 words. Telemetry demodulators and input buffers for the system will still be classed as special-purpose equipment and therefore be supplied by the Spacecraft Project Office to the DSN. These equipments will be designed such that they can be operated independently of as much other mission-dependent equipment as possible. The OSDP will be capable of the following functions during the mission if programs for this purpose are supplied by the project:

1) Selective editing of spacecraft telemetry data
2) Decommutation
3) Generation of alarms
4) Telemetry monitoring
5) Formatting telemetry data messages
6) Verification of spacecraft command data both as received and as transmitted
7) Generation and verification of command tapes
8) Permissive and limit checking of commands

The telemetry data recording equipment installed or programmed for installation at each DSIF site is designed to allow recording of a variety of signals from spacecraft and station sources. Signal-conditioning equipment of various types is also provided. The types of available recording equipment and a listing of their capabilities is included in the referenced DSIF capabilities document.

The standard magnetic tape recording capability for telemetry data at each station will consist of two Ampex FR-1400 recorders, and they will normally be used to record the detected telemetry output from the phase-lock receivers. The FR-1400 recorders have direct FM, and digital record and reproduce capability at six standard speeds varying from 3 3/4 to 120 in./sec and use 1/2 inch tape. This recorder is capable of recording a bandwidth of 400 cps to 1.5 Mc and is normally used in a post-detection capacity.

Oscillograph recorders are used primarily for real-time system evaluation. In most cases where the spacecraft data rate is low, oscillographic recordings duplicate magnetic tape recordings of the ground system parameters.

c. Television

The capability of recording television pictures is provided in the receiver at two points. For signals having a very wide band, an output 10 Mc wide is available from the 50 Mc first IF. A detection bandwidth of 300 cps to 1.65 Mc is also available from the output of the video amplifier which follows the wideband phase detector. Television recording capability is provided by an FR-800 magnetic tape recorder. The FR-800 is capable of recording a bandwidth of 10 cps to 4 Mc. The FR-800 is a special-purpose recorder using a transverse rotating head and is intended for use with signals having an extremely wide band such as video. It ca be used for predetection recording of the 10 Mc second IF, by down conversion to a lower frequency, whenever the demodulation method is unknown or when demodulation on site will destroy some of the received data.

d. Ground Command and Control

Presently planned JPL projects use a digital command and control system with a transmission rate of one bit per second. A ground command subsystem which is designed to meet the requirements of the Mariner communication system and is adaptable to other systems of a similar design is installed at all DSIF stations and is authorized for Madrid and Canberra.

Three successive identical commands (26 bits long for Mariner) are sent by teleprinter circuits to the station and received on punched paper tape. This tape is placed in the tape reader of the ground command subsystem; then it is read into the system where the command is verified, displayed, and recorded on punched paper tape. Initiation of actual command-modulated RF transmission can be done manually or automatically by insertion of a given time of day. During transmission to the spacecraft, the RF signal is detected and compared bit by bit with the stored command. Transmission is inhibited when an error is detected by this monitor. Actual transmissions are recorded on punched paper tape for future reference. A nearly universal ground command and control system using a general purpose computer is under design and should be available for the Orbiter mission.

e. Frequency and Time Standards

The basic frequency standards at the stations consist of two stable crystal oscillators (one for redundancy). In 1964 these oscillators will be supplemented with two atomic standard (rubidium vapor) oscillators per station. Using the crystal oscillators for the timing standard, the drift is stable to 2 parts in 10^{10} over 24 hours, and the initial frequency setting error is less than 5 parts in 10^{9}. Local time readout can be synchronized to WWV or WWVH to at least 10 milliseconds. Using the atomic standard oscillators, the drift error is not greater than 2 parts in 10^{11}. Using VLF receivers and WWVL it is anticipated that local time settings can be made to 3 milliseconds or less.

f. Interstation Communications

A NASA-operated full duplex teleprinter (TTY-FD) communications net presently exists which links the Goldstone, Woomera, Canberra, Madrid and Johannesburg Deep Space Stations to the JPL Space Flight Operations Facility in Pasadena. Voice circuits between the Deep Space Stations and the SFOF are also available. The primary function of the TTY-FD and voice circuits are to transmit tracking and telemetry data and to permit operational control of the DSIF net.

A microwave link between Goldstone and the SFOF at JPL was made operational in 1964 and would be available for the Mars Orbiter mission. The link is capable of transmitting real time telemetry, tracking, and video data from Goldstone to JPL. It has the following capabilities:

1) One 6 Mc video channel, Goldstone to JPL only.
2) One 240 Kc full duplex communication channel which provides the following capabilities:
   a) Full duplex teletype
   b) Simplex voice circuits (2 wire with signaling)
   c) Full duplex voice/data circuit (4 wire with signaling)
   d) Full duplex voice/data circuit (4 wire without signaling)
   e) 3 kc data circuit for 600 and 1200 bit/sec data transmission, Goldstone to JPL only.
   f) 96 kc full duplex data circuit for analog data.

6. Space Flight Operations Facility

The SFOF consists of a three-story building which houses the operations control center, data displays, control consoles, digital computers and associated input/output equipment, data reduction equipment, and the communications center, and provides areas for

scientific and engineering spacecraft data analysis teams. It has facilities for the reception and reduction of tracking data, the generation of trajectory, prediction, acquisition and command information, and the reduction of telemetry data for use by cognizant engineering and scientific experimenters. The SFOF will exercise control over the 1969 Mars Orbiter mission.

REFERENCES

1. Technical Memorandum 33-83, Revision 1, 24 April 1964

APPENDIX B

ELECTRICAL POWER DATA

1. Preliminary System Sizing Analysis (Revised 9/17/64)

The material presented in this Appendix is supplementary to Section XI, Subsection C. The mission profiles for 10 and 20 watt systems (referenced in XI. C) are presented as Tables B-1 and B-2.

a. General

Block diagrams of power subsystems using each of the three types of regulators discussed in Reference 4 are shown in Figures B-1, B-2, and . 3. The block diagrams of the subsystem using a Boost Regulator or a Series-Switching Regulator may be analyzed in exactly the same fashion with respect to solar array, battery, and charge control sizing. For brevity, the three subsystem components: solar array, battery, and charge control will be referred to herein as the "system." This Appendix discusses various aspects of system sizing.

The mission is assumed to be a Mars orbiter as outlined in Reference 5. Power requirements during launch, maneuver, and cruise modes are not discussed. It is presently thought that a system capable of supporting a Mars orbiting mission is sized sufficiently large so that it would be capable of supporting all other phases of the mission. A check of this statement will be the subject of a future study.

b. Summary

A specific energy balance technique is developed, whereby a minimum size power system is derived for a particular power profile. Results of this sizing calculation are then utilized in computing power system weight for various electrochemical systems. The system weight crossover loci are calculated as a function of orbital period for various battery parameters.

A general energy balance technique is developed for a power profile which varies in a continuous fashion. Results of this calculation are used solely to visualize the minimizing process occurring at the energy balance condition.

c. Conclusions

1) Array, battery, and charge control sizing is independent of the kind of regulator used.
2) Although array overcapacity is maximum for the AgCd (70%) system, system weight is not necessarily so, but depends on the mission parameters: Orbit period, T_o, and eclipse fraction α.
3) AgZn batteries produce minimum system weight for extremely short orbits (less than approximately 4 hours), and AgCd (70%) batteries produce minimum system weight for long orbits.

Table B-1. Mariner Block IV Power Profile (10 Watt RF System)

Subassembly	Prelaunch	Launch	Acquire	Cruise	Cruise Calibrate	Maneuver	Encounter	Injection Maneuver	Post Injection	Apoapsis	Eclipse	Periapsis
Science	58.5	14.0	14.0	27.6	51.0		58.5		27.6	27.6		58.5
Planetary Scan Electronics							15.0					15.0
Tape Recorder Electronics							10.5		8.5	10.5		10.5
Data Encoder	14.0	14.0	14.0	14.0	14.0	14.0	14.0	14.0	14.0	14.0	14.0	14.0
Command Decoder	8.0	8.0	8.0	8.0	8.0	8.0	8.0	8.0	8.0	8.0	8.0	8.0
CC&S	16.0	16.0	16.0	16.0	16.0	16.0	16.0	16.0	16.0	16.0	16.0	16.0
Control System Electronics	40.0	4.0	40.0	39.0	39.0	28.0	36.0	50.0	31.0	43.0	50.0	43.0
Pyro Control			2.0	2.0	2.0	2.0	2.0	2.0	2.0	2.0	2.0	2.0
Receiver TR	17.0	17.0	17.0	17.0	17.0	17.0	17.0	17.0	17.0	17.0	17.0	17.0
Control Unit	2.1	2.1	2.1	2.1	2.1	2.1	2.1	2.1	2.1	2.1	2.1	2.1
Exciter TR	11.0	11.0	11.0	11.0	11.0	11.0	11.0	11.0	11.0	11.0	11.0	11.0
Power Distribution	2.0	2.0	2.0	2.0	2.0	2.0	2.0	2.0	2.0	2.0	2.0	2.0
Relay Hold TR	15.0	15.0										
Control Gyro & Electronics	10.0	30.0	30.0	10.0	10.0	30.0	10.0	30.0	15.0		30.0	
Control System Electronics						12.0		12.0			12.0	
Total From 2.4 kc	193.6	133.1	120.1	168.7	172.1	142.1	202.1	164.1	154.2	153.2	164.1	199.1
Total Into 2.4 kc	224	159	145	198	201	169	244	192	181	180	192	232
Total From 400~3ϕ	16	16	16			16		16	16		16	
Total Into 400~3ϕ	19	19	19			19		19	19		19	
Power Synchronizer	5	5	5	5	5	5	5	5	5	5	5	5
Total From Regulator	248	183	169	202	206	193	249	216	205	185	216	237
Total Into Regulator	297	223	208	245	249	234	298	260	248	225	260	286
RF Power Amplifier	10	47	47	47	47	47	47	47	47	47	47	47
Heater Power (Retro Motor)	10	10	10	10	10	10	10	10	10	10	10	10
Total From PS&L	317	280	265	302	306	291	355	317	305	282	317	343
TOTAL POWER SOURCE DEMAND	337	298	282	321	325	310	378	337	325	300	337	365

Table B-2. Mariner Block IV Power Profile
(20 Watt RF System)

Subassembly	Injection Maneuver	Post Injection	Apoapsis	Eclipse	Periapsis
Science	-		27.6	-	58.5
Planetary Scan Electronics	-		-	-	15.0
Tape Recorder Electronics	-		21.0	-	21.0
Data Encoder	14.0		14.0	14.0	14.0
Command Decoder	8.0		8.0	8.0	8.0
CC&S	16.0		16.0	16.0	16.0
Control System Electronics	50.0		43.0	50.0	43.0
Pyro Control	2.0		2.0	2.0	2.0
Receiver TR	17.0		17.0	17.0	17.0
Control Unit	2.1		2.1	2.1	2.1
Exciter TR	2.5		2.5	2.5	2.5
Power Distribution	2.0		2.0	2.0	2.0
Relay Hold TR	-		-	-	-
Control Gyro & Electronics	30.0		-	30.0	-
Control System Electronics	12.0		-	12.0	-
Total From 2.4 kc	155.6		155.2	155.6	202.1
Total Into 2.4 kc	183		182	183	234
Total From 400 3	16		-	16	-
Total Into 400 3	19		-	19	-
Power Synchronizer	5		5	5	5
Total From Regulator	207		187	207	239
Total Into Regulator	250		228	250	286
RF Power Amplifier	85		85	85	85
Heater Power	10		10	10	10
Total From PS&L	345		323	345	381
TOTAL POWER SOURCE DEMAND	367		344	367	405

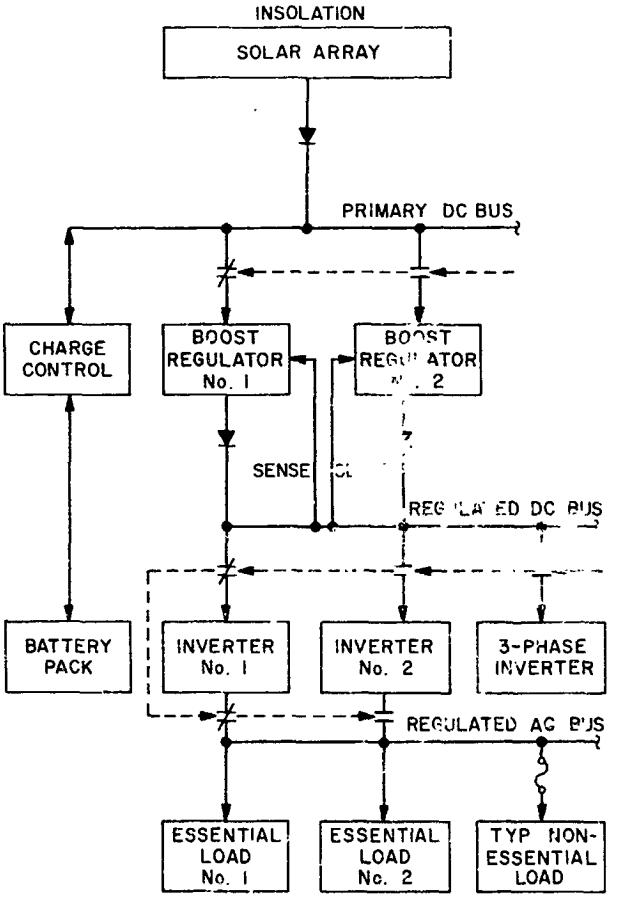


Figure B-1. Boost Regulator Block Diagram

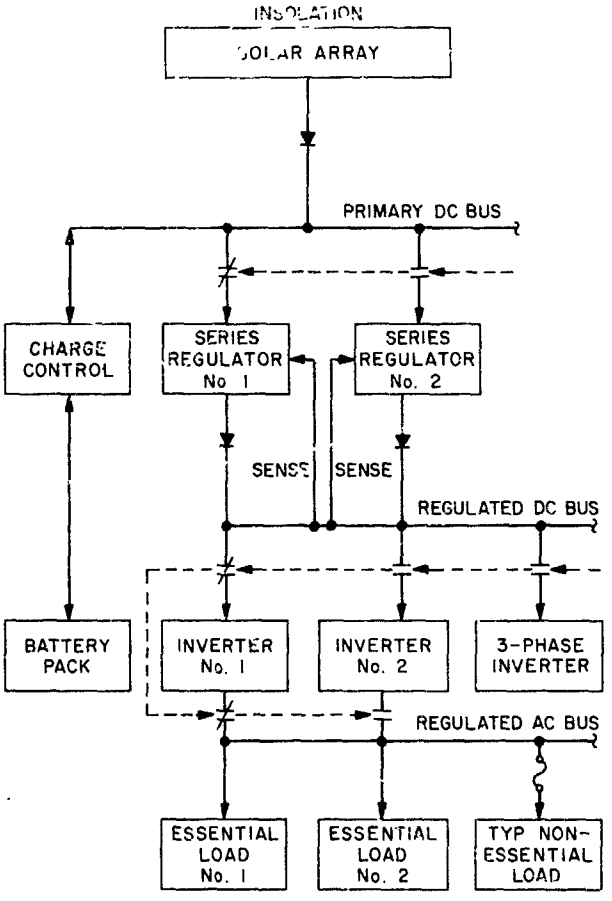


Figure B-2. Series Regulator Block Diagram

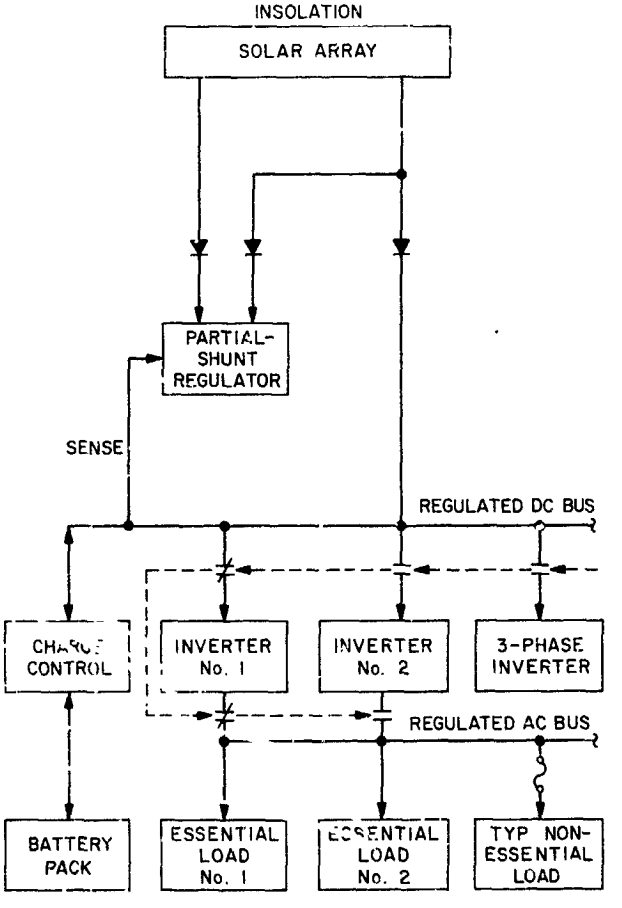


Figure B-3. Partial-Shunt Regulator Block Diagram

d. Power Calculations

(1) Energy Balance - Array Power. An energy balance equation may be written which relates solar array, battery, and charge control parameters. The relation must ensure that sufficient energy is available during the sunlit portion of the orbit to supply all load power as well as battery recharge power.

A typical orbital power profile has been assumed. The profile and a list of symbols are shown in Figure B-4. Energy balance is achieved when: Energy from Array - Energy to Loads = Recharge energy. Symbolically:

$$(P_a - P_l)\, T_l = P_e T_e/h + (P_p - P_a)\, T_p/h \qquad (1)$$

Where P_l is the average load power in sunlight excluding the peak load, and h is the overall battery recharge efficiency ($h = h_w \cdot h_e$). It should be noted that all parameters and variables are referred to the Primary System Bus.

Solving equation (1) for the required solar array power gives:

$$P_a = \frac{(P_e T_e + P_p T_p)/h}{T_l + T_p/h} + P_l \frac{T_l}{T_l + T_p/h} \qquad (2)$$

On a unit power basis, equation (1) became:

$$\frac{P_a}{P_l} = \frac{P_e}{hP_l} \cdot \frac{T_e/T_o}{f(t)} + \frac{P_p}{hP_l} \cdot \frac{T_p/T_o}{f(t)} + \frac{1 - T_e/T_o - T_p/T_o}{f(t)} \qquad (3)$$

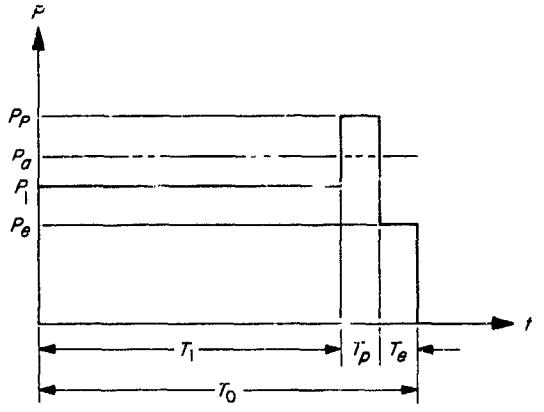
where $f(t) = 1 - T_e\ T_o + (1/h - 1)\, T_p\ T_o$.

The additional array power fraction required (in excess of P_l) may now be calculated for two cases:

I; $T_p/T_o = 0$, which means no peak loading in sunlight

II; $T_p/T_o = 0.10$, which is the case illustrated in Figure B-4.

The additional array power fraction (array overcapacity) is plotted as a function of eclipse fraction ($T_e\ T_o$) for various electrochemical systems. Figure B-5(a) is a plot of array overcapacity for Case I ($T_p/T_o = 0$):



T_0 = ORBITAL PERIOD = $T_l + T_p + T_e$, hr

T_e = ECLIPSE TIME, hr

T_p = PEAK LOAD TIME, hr

P_e = AVERAGE LOAD DURING ECLIPSE, w

P_l = AVERAGE LOAD DURING SUNLIGHT, w

P_p = AVERAGE PEAK LOAD, w

P_a = ASSUMED ARRAY CAPACITY, w

$T_e / T_p \equiv \alpha$

$\frac{P_a}{P_l} - 1 \equiv \mu$

Figure B-4. Typical Orbital Power Profile and List of Symbols

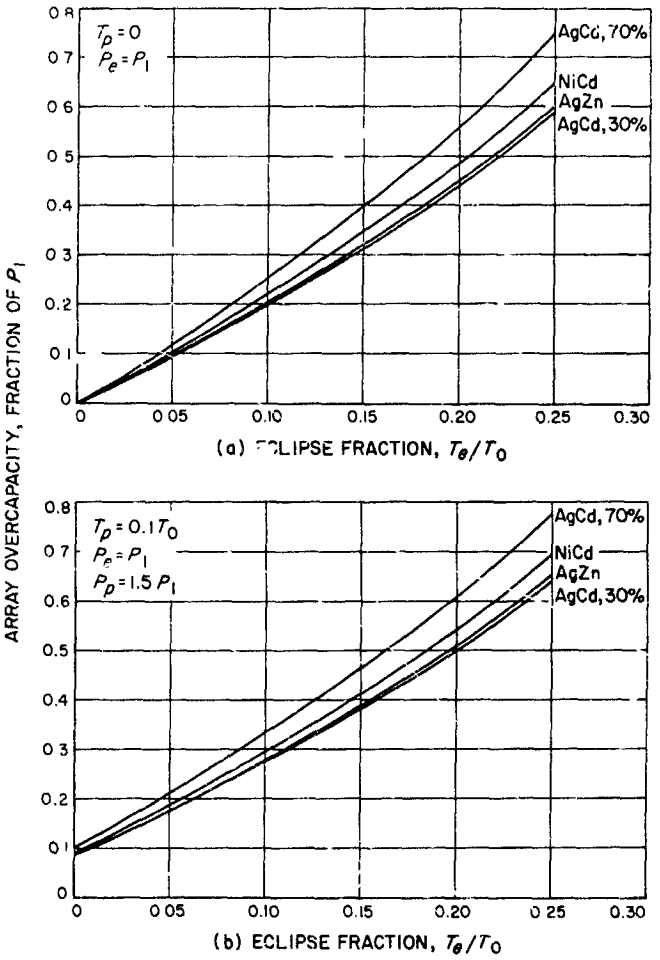


Figure B-5. Array Overcapacity for Cases I and II

$$\frac{P_a}{P_l} - 1 + \mu_I = \frac{P_e}{hP_l} \cdot \frac{T_e/T_o}{1 - T_e/T_o} \tag{3a}$$

Figure B-5(b) is a plot of array overcapacity for Case II ($T_p/T_o = 0.10$):

$$\frac{P_a}{P_l} - 1 = \mu_{II} = \frac{P_e}{hP_l} \cdot \frac{T_e/T_o}{f(t)} + \frac{P_p}{hP_l} \cdot \frac{T_p/T_o}{f(t)} - \frac{T_p/T_o\, h}{f(t)} \tag{3b}$$

The set of equations (3a, 3b) are further reduced by substitution of the assumed power profile values; $P_e/P_l = 1.0$, $T_p/T_o = 0.10$, and $P_p/P_l = 1.50$:

$$\text{Case I;} \quad \mu_I = \frac{1}{h} \cdot \frac{\alpha}{1 - \alpha} \tag{4a}$$

$$\text{Case II;} \quad \mu_{II} = \frac{1}{h} \cdot \frac{0.5 + 10\alpha}{9 - 10\alpha + 1/h} \tag{4b}$$

$$\text{where} \quad \alpha = T_e/T_o \tag{4c}$$

$$\text{The total array power required;} \quad \overline{P}_a = 1 + \mu_{II}, \text{ watts per watt} \tag{4d}$$

(2) Battery Capacity, Cb. The energy drain from the battery (corresponding to the power profile of Figure B-4) is a function of the absolute values of (peak and eclipse load) time;

$$E_o = P_e T_e + (P_p - P_a)\, T_p \tag{5}$$

On a unit power basis and in terms of the orbital period:

$$\overline{E} = E_o/P_l = \left(\frac{P_e}{P_l} \cdot \frac{T_e}{T_o} + \frac{P_p}{P_l} \cdot \frac{T_p}{T_o} - \frac{P_a}{P_l} \cdot \frac{T_p}{T_o}\right) T_o \tag{6}$$

Substituting for P_e/P_l, P_p/P_l, P_a/P_l and T_p/T_o gives:

$$\overline{E}_o = (0.15 + \alpha - 0.1\, \overline{P}_a)\, T_o \tag{7}$$

For a given depth of discharge allowable, d (based on cycle life),

$$\overline{Cb} = \overline{E}_o/d, \text{ watt hours per watt} \tag{8}$$

(3) Charge Control Rating, P_c. The rated power level, P_c, of the charge control converter - regulator is taken as the average recharge power; recharge energy:

$$\bar{E}_p = \bar{E}_o/h_w = \bar{P}_c (T_o - T_e - T_p) \text{ where } \bar{P}_c = P_c/P_l \quad (9)$$

Substituting equation (7) into equation (9) and solving for $\bar{P}_c$, gives;

$$\bar{P}_c = \frac{1.5 + 10\alpha - \bar{P}_a}{(9 - 10\alpha)h_w}, \text{ watts per watt} \quad (10)$$

e. Weight Calculations

(1) Array Weight, W_a. Solar array weight is given by a constant 4.5 watts per lb. This factor is approximately 5 percent higher than the present Mariner array It is assumed that the lower specific weight is achievable with improved packing factor and higher initial minimum efficiency. No weight allowance is made here for any increase in structure which may be caused by any increased folding mechanism requirement.

Solar array specific weight, $\bar{W}_a = \frac{1}{4.5}\bar{P}_a$. Substituting equation (4d) yields:

$$\bar{W}_a = 0.222 (1 + \mu_{II}), \text{ lb per watt} \quad (11)$$

(2) Battery Weight, W_b. Battery weight is a function of the energy density available (ρ, watt hours per lb) and the depth of discharge allowable (d, fraction).

Battery specific weight, $\bar{W}_b$ is given by:

$$\bar{W}_b = E_o/\rho d, \text{ lb per watt} \quad (12)$$

Substituting equation (7) into equation (12) yields:

$$\bar{W}_b = \frac{T_o}{\rho d} (0.15 + \alpha - 0.1 \bar{P}_a) \quad (13)$$

Figure B-6 is a plot of battery specific weight for various electrochemical systems as a function of eclipse fraction (α) for a 10 hour orbit.

(a) Battery Parameters. Table B-3 lists the various assumed battery parameters.

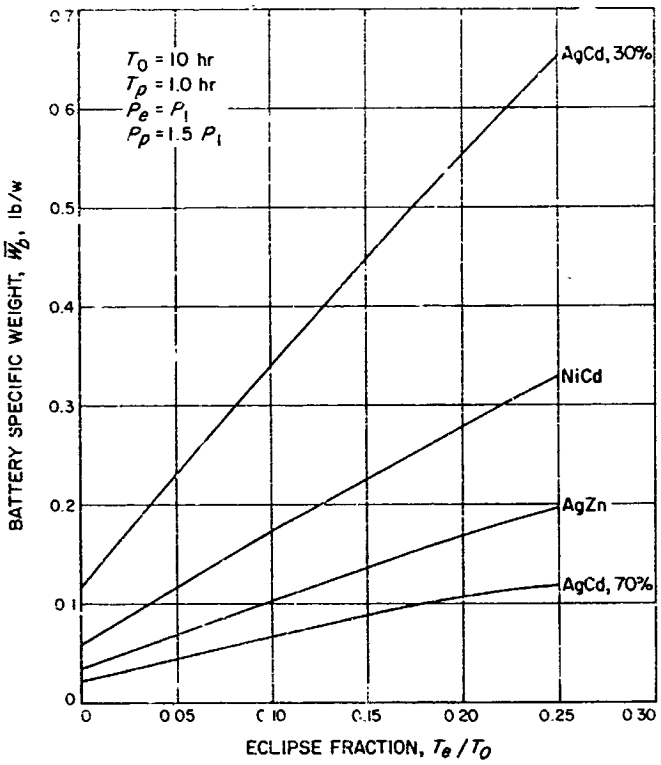


Figure B-6. Battery Specific Weight
(10 Hour Orbit)

Table B-3. Battery Parameters

Parameter	Symbol	Parameter Value				Units
Cell System	-	AgZn	AgCd	AgCd	NiCd	-
Depth of Discharge (1)	d	0.20	0.30	0.70	0.70	-
Energy Density	p	60	12	30	10	watt-hours/lb
Upper Charge Plateau	V_c	1.95	1.65	1.55	1.45	volts
Lower Discharge Plateau	V_d	1.45	1.30	1.00	1.20	volts
Voltage Efficiency (2)	h_v	0.75	0.79	0.64	0.83	-
Current Efficiency (2)	h_i	0.98	0.95	0.92	0.82	-
Energy Efficiency (2)	h_w	0.73	0.75	0.59	0.68	-
Charge Control Efficiency	h_c	0.75	0.75	0.75	0.75	-
Overall Recharge Efficiency	h	0.55	0.56	0.44	0.51	

(1) Delco-Remy experience with sealed AgZn is that a discharge depth of less than 25% is required for a life of 400 cycles.

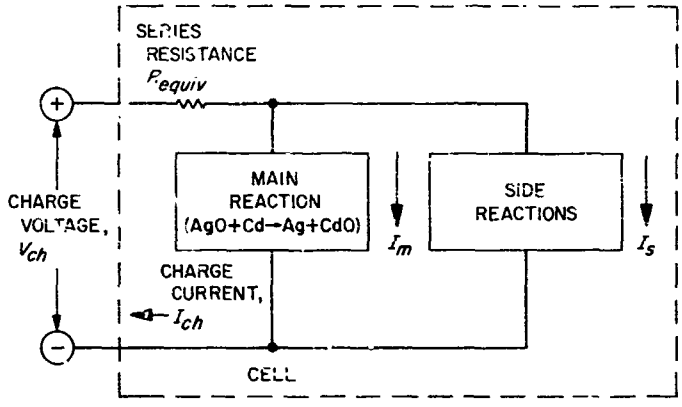
STL experience with sealed AgCd is that a 70% depth of discharge is reasonable for several hundred cycles.

(2) Efficiencies vary from 99% to 20% (or less) depending on charge and discharge rates, amount of overcharging, stand time, and temperature. The figures shown are a practical first estimate of average charge efficiency for a Mars orbit of 14 to 50 hours.

Table B-3 assumed values of parameters used to derive curves of Figures B-5, B-6, B-7 and B-8. Values are representative and are used to illustrate the sizing technique only.

(5) Battery Efficiency. Cell current efficiency, to convert metal back to its oxide, is 100 percent. However, parallel reactions within the cell also require some current. This additional parallel current appears at the cell terminals as a current efficiency, h_i. This parallel reaction also includes the self-discharge reaction of a given cell. A block diagram of the cell is shown in Figure B-7.

Voltage efficiency of the cell, h_w, is determined by the emf at each pole plus the (equivalent) IR drop caused by the resistivities of all the components in the cell system (e.g., separator, plate, solution, and connections).



CURRENT EFFICIENCY, $h_I = I_m/(I_m+I_s)$

$h_I = I_m/I_{ch}$, $I_{ch} = I_m+I_s$

VOLTAGE EFFICIENCY, $h_v = V_{disch}/V_{ch}$

ENERGY EFFICIENCY, $h_w = (h_I)(h_v)$

Figure B-7. Battery Cell Efficiency

(3) Charge Control Weight, W_c.

(a) Charging Equipment. Although the specific weight of charge control equipment does vary with power level (for a constant efficiency), this variation was not included in this analysis. The reason for the omission being that charge control weight forms a small portion of the system weight. A value of 0.040 lb per watt is assumed and used throughout.

$$\text{Charge control specific weight, } \overline{W}_c = 0.04\,\overline{P}_c \tag{14}$$

Substituting equation (10) into equation (14) for $\overline{P}_c$, yields:

$$\overline{W}_c = (0.040)\,\frac{1.5 + 10\alpha - \overline{P}_a}{h_w\,(9 - 10\alpha)}\ \text{, lb per watt} \tag{15}$$

(b) Discharge Equipment. The weight of discharge control equipment has also been omitted on the basis that it is small in comparison to the weight of charge control equipment. It is assumed that the discharge equipment will consist of a series controlled rectifier along with its sensing and triggering circuits. The total weight of such circuitry, packaged, should be less than 0.25 lb.

(4) System Weight, W. Total system specific weight is given by:

$$\overline{W} = \overline{W}_a + \overline{W}_b + \overline{W}_c\text{, lb per watt} \tag{16}$$

Substituting for the various component specific weights from equations (11), (13), and (15) yields:

$$\overline{W} = 0.222\left(1 + \frac{k_1}{A}\right) + \frac{hT_o}{10\,\rho d}\cdot\frac{k_1 k_2}{A} + 0.03\,\frac{k_1}{A}\text{, lb per watt} \tag{17}$$

where $k_1 = 0.5 + 10\alpha$, $k_2 = 9 - 10\alpha$, and $A = 1 + hk_2$.

Equation (17) is plotted for various electrochemical systems as a function of the eclipse fraction for a 10 hour orbit. This plot is shown in Figure B-8. Because of the proximity of the AgZn and the AgCd, 70% characteristics, it was postulated that there would be a cross-over of these characteristics were some lower value of orbital period (T_o) used. A calculation of T_o, derived from the relation:

$$\overline{W}\ (\text{AgZn}) = \overline{W}\ (\text{AgCd, 70\%}) \tag{18}$$

was made. This calculation led to the following expression for T_o:

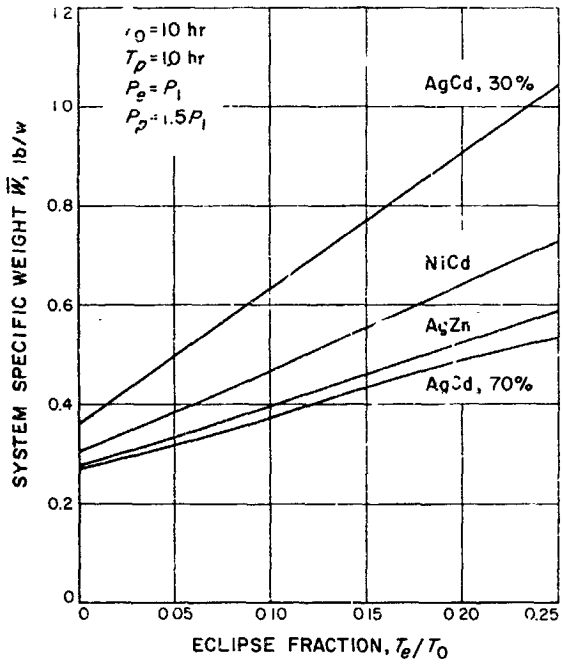


Figure B-8. System Specific Weight

$$T_o = \frac{2.52\,(h_1 - h_2)}{\frac{h_1 A_2}{\rho_1 d_1} - \frac{h_2 A_1}{\rho_2 d_2}}, \text{ hours} \tag{19}$$

where the subscripts 1, 2 refer to systems using AgZn and AgCd, 70% batteries respectively.

A plot of the eclipse function (α) as a function of T_o for the condition of equal weights is shown in Figure B-9. A normalized version is shown in Figure B-10. It should be emphasized here that all of the above equations reflect only minimum requirements. No margin or redundancy requirements are included in the sizing calculations. These will be treated in a separate section.

f. General Expression for Energy Balance

Given the general power profiles shown in Figure B-11, an expression may be derived for the required source output power.

Because they are easier to visualize and understand, the relationships involved are initially written in terms of the variable time (t). After the calculation is complete, the results are rewritten in terms of the variable power (p) to facilitate computation.

It is assumed that the power profile of Figure B-11 repeats every orbit for the life of the spacecraft.

Two cases are considered; a photovoltaic power source and a radioisotope thermoelectric (RTG) power source. The case of a RTG source is considered first, because the added complication caused by eclipse is not present. The case of a photovoltaic power source is then treated as an extension.

(1) Case I, RTG Source. In general: Energy available $\geq$ energy required, and as a minimum, energy available = energy required.

Symbolically:
$$\int_o^{t_1} (P_a - p)dt = \frac{1}{h}\int_{t_1}^{T_o} (p - P_a)dt \tag{20}$$

By normalizing and rewriting equation (20), we obtain:

$$\left[\frac{1}{1-h} - \alpha_1\right] f(\alpha_1) - \int_{\alpha_1}^{1} f(\alpha)d\alpha = \frac{h}{1-h}\,\bar{P}_L \,, \tag{21}$$

where $\bar{P}_L = \int_o^1 (\alpha)d\alpha$ = average load.

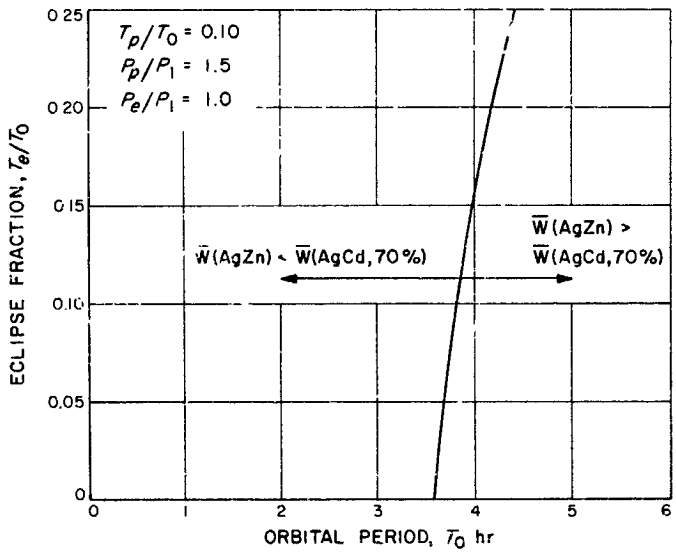


Figure B-9. Plot of Eclipse Function
(Condition of Equal Weights)

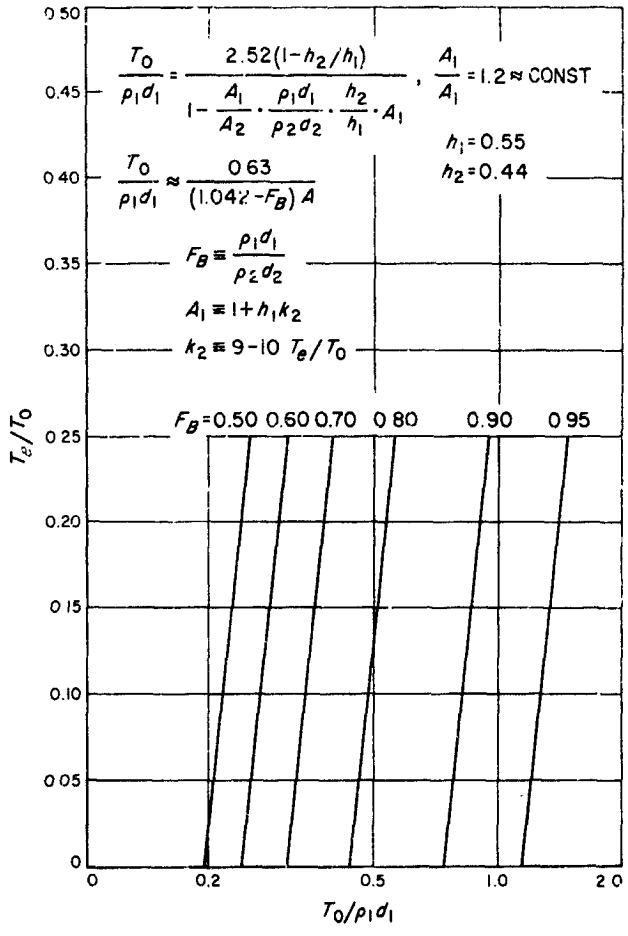
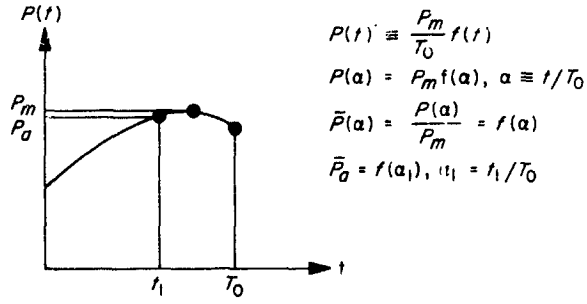
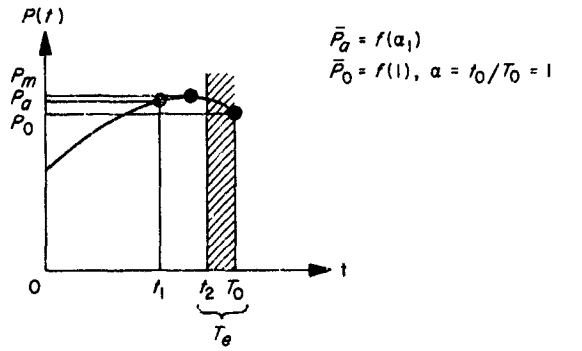


Figure B-10. Plot of Eclipse Functions (Normalized Versions)



(a) POWER PROFILE – RTG SOURCE



(b) POWER PROFILE – PHOTOVOLTAIC SOURCE

Figure B-11. General Power Profile

Given the periodic load function, $f(\alpha)$, explicitly, the integral equation (21) may be solved for α_1 in terms of the overall recharge efficiency, h. Power required may then be found by calculating, $P_a = f(\alpha_1)$. P_a may be calculated directly:

$$\frac{1}{1-h}\,\bar{P}_a + \int_{\bar{P}_a}^{\bar{P}_o} g(\bar{p})d\bar{p} = \frac{1}{1-h}\,\bar{P}_L + \bar{P}_o \tag{22}$$

where $\bar{P}_o = f(1)$

A simple case may be used for an example: Assume $\alpha = g(\bar{p}) = \bar{p}$, then equation (22) becomes:

$$\frac{1}{1-h}\,\bar{P}_a + \int_{\bar{P}_a}^{\bar{P}_o} \bar{p}d\bar{p} = \frac{h}{1-h}\left(\frac{1}{2}\right) + 1, \tag{23}$$

where $\bar{P}_L = \int_o^1 \alpha d\alpha = \frac{1}{2}$, and $\bar{P}_o = 1$

Performing the integration indicated in equation (23) and rewriting gives:

$$(\bar{P}_a)^2 - \frac{2}{1-h}\,\bar{P}_a + \frac{1}{1-h} = 0 \tag{24}$$

Solving equation (24) for $\bar{P}_a$, in terms of h, yields:

$$\bar{P}_a = \frac{1}{h}\left(1 - \sqrt{h}\right) \tag{25}$$

(2) Case II, Photovoltaic Source. Case II relationships analogous to those presented for Case I are given below:

$$\int_o^{t_1} (P_a - P)dt = \frac{1}{h}\int_{t_1}^{t_2} (P - P_a)dt + \frac{1}{h}\int_{t_2}^{T_o} pdt \tag{26}$$

In terms of α_1:

$$\left[\frac{1}{1-h}\alpha_2 - \alpha_1\right] f(\alpha_1) - \int_{\alpha_1}^{1} f(\alpha)d\alpha = \frac{h}{1-h}\overline{P}_L \qquad (27)$$

where α_2 is the sunlit fraction of the orbital period, T_o.

In terms of $\overline{P}_a$:

$$\frac{\alpha_2}{1-h}\overline{P}_a + \int_{\overline{P}_a}^{\overline{P}_o} g(\overline{p})d\overline{P} = \frac{h}{1-h}\overline{P}_L + \overline{P}_o \qquad (28)$$

An obvious limiting case results as α_1 approaches α_2. That is, the fraction of time in which the source is required (α_1) approaches the available sunlight time (α_2). Substituting α_2 for α_1 in equation (27) gives:

$$\frac{h}{1-h}\alpha_2 f(\alpha_2) - \int_{\alpha_2}^{1} f(\alpha)d\alpha = \frac{h}{1-h}\overline{P}_L \qquad (29)$$

Given the explicit function $f(\alpha)$ and solving equation (29) for α_2 yields the minimum value of sunlight time (as a fraction of the orbital period, T_o) as a function of the efficiency, h, and the average load, $\overline{P}_L$.

2. Justification for Array Overcapacity

a. Summary

The recharge function μ_r is reviewed, starting with a general case which includes duty-cycling by orbit. Several particular cases are derived. Computing functions for Ag-Cd and Ag-Zn battery systems are given. Figures B-12, B-13 and B-14 show the computed recharge function (overcapacity) for several cases.

A specific mathematical model of the array IV characteristic is assumed. The model is normalized with respect to unity maximum power point and unity maximum power voltage (and current). All subsequent calculations are based on the normalized model.

Parameter variations of the battery and of the regulators are assumed, and their effect on array overcapacity is calculated. Figures B-15, B-16, B-17, B-18, B-19 and B-20 show the results in terms of the IV characteristics and in terms of overcapacity (μ_m) as a function of the assumed variation (δ). A discussion of several operating modes between the battery and array is presented.

An example of the calculation is carried out for a typical set of values of the variations, δ.

Overcapacity needed for decrease of array output as a function of electron flux and proton damage is calculated on the basis of an arbitrarily selected current and voltage degradation.

b. Conclusions

Array overcapacity for battery recharge is a function of these parameters:

$$\mu_r = f(\alpha, \phi, \overline{P}_e, \overline{P}_p, h, n)$$

where

$\alpha = Te/To$	= eclipse (time) fraction,
$\phi = Tp/To$	= peak load (time) fraction,
$\overline{P}e = Pe/P_l$	= eclipse load to nominal Sunlight load ratio,
$\overline{P}p = Pp/P_l$	= peak load to nominal Sunlight load ratio
h	= overall battery recharge efficiency (includes charge control converter-regulator efficiency)

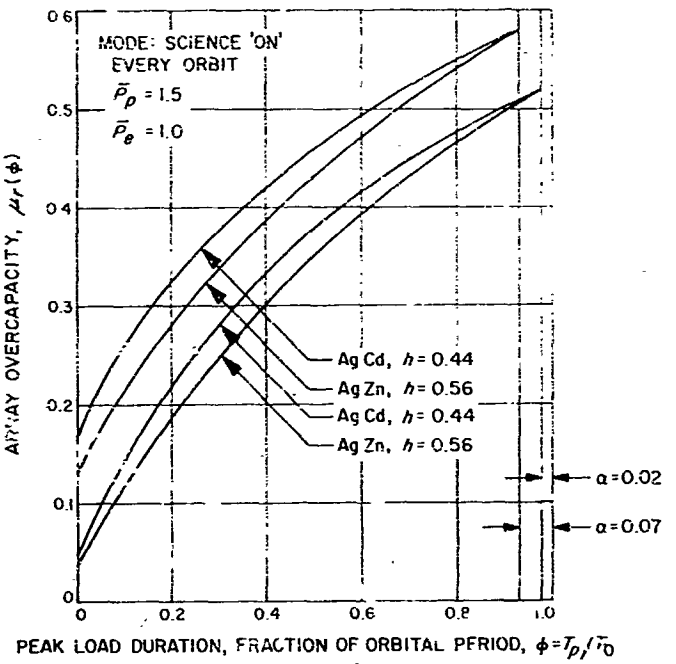


Figure B-12. Array Overcapacity for 14-Hour (α = 0.07) and 50-Hour (α = 0.02) Orbits as a Function of Peak Load Duration

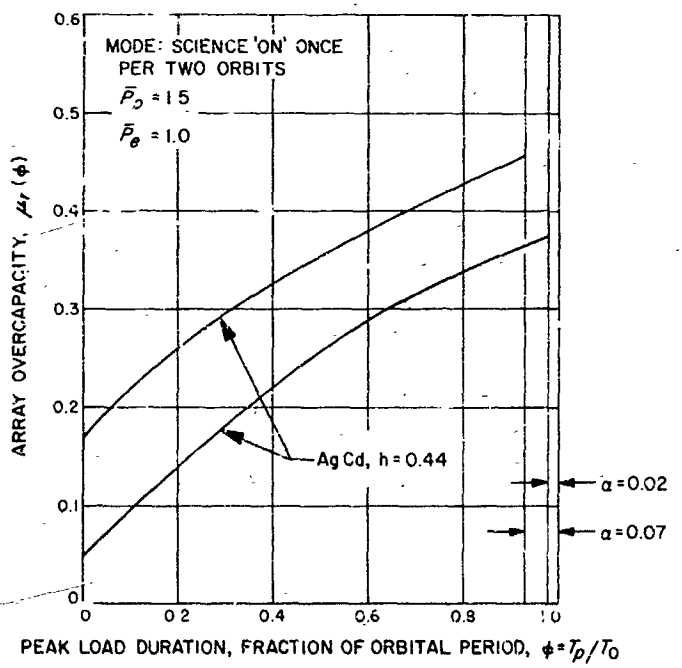


Figure B-13. Array Overcapacity as in Figure B-12, Except Science (Peak) Loads are Turned Off For Every Other Orbit

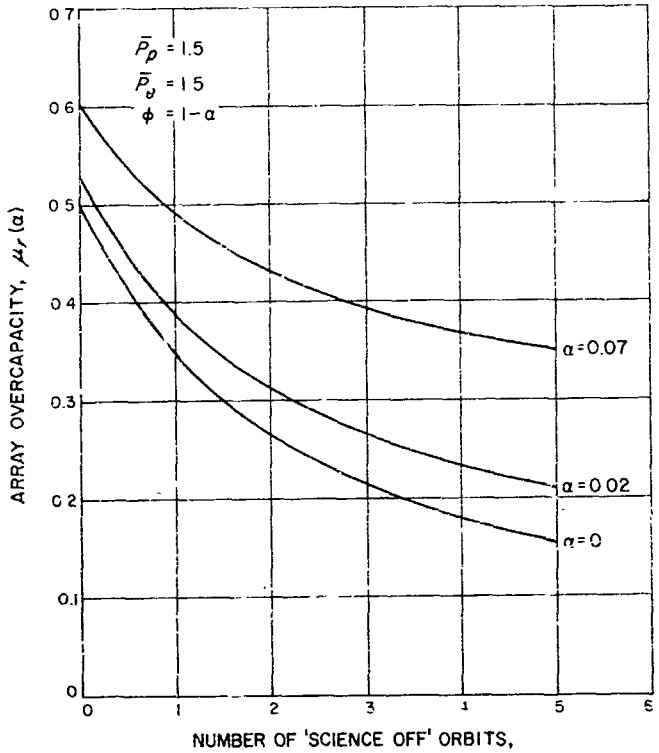


Figure B-14. Effect of Duty-Cycling by Orbit for a System Using Ag Cd Batteries

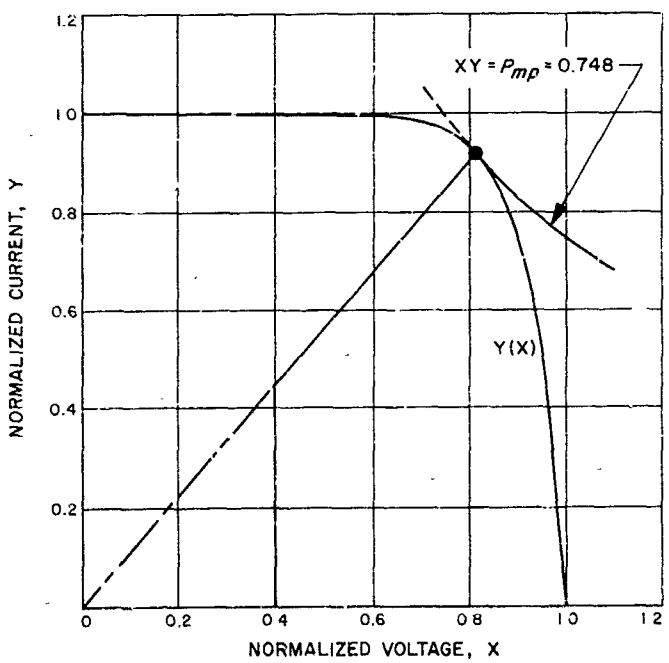


Figure B-15. Normalized Voltage X Maximum Theoretical Array Requirement

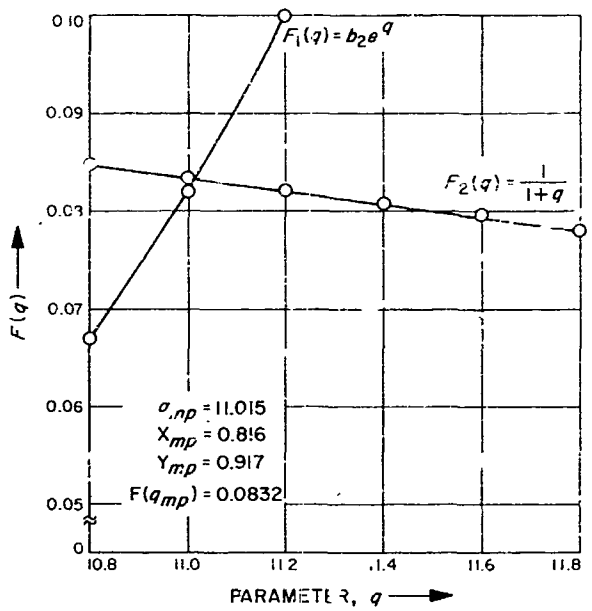


Figure B-16. Solution to Transcendental Equation (14)

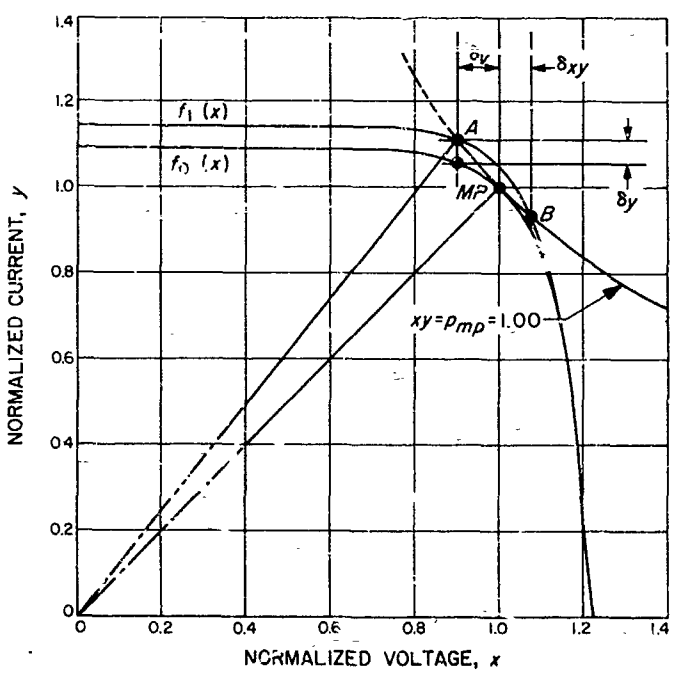


Figure B-17. Current Capacity Increase Due to Peak-Point Voltage Variation

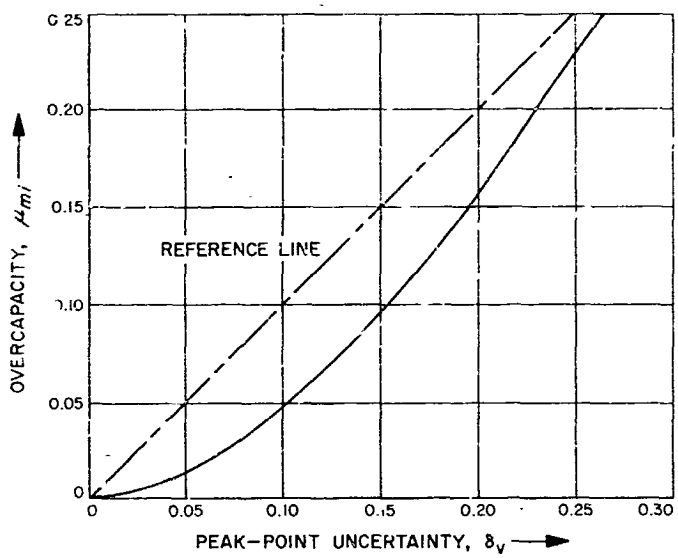


Figure B-18. Array Overcapacity Caused by Variation in the Regulation Start Voltage

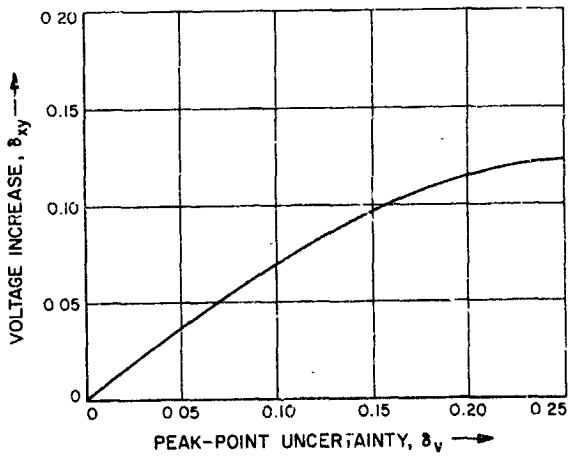


Figure B-19a. Increase in Operating Voltage Caused by Variation of the Regulation-Start Voltage

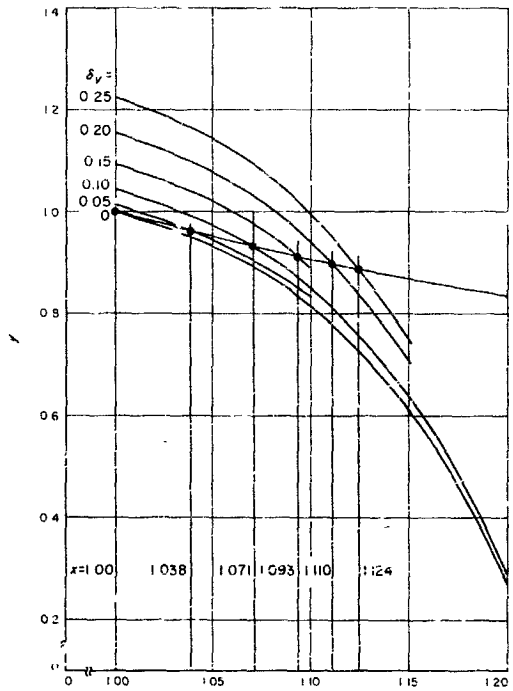


Figure B-19b. Intersection of F(x) with 1/x for Various δ_v

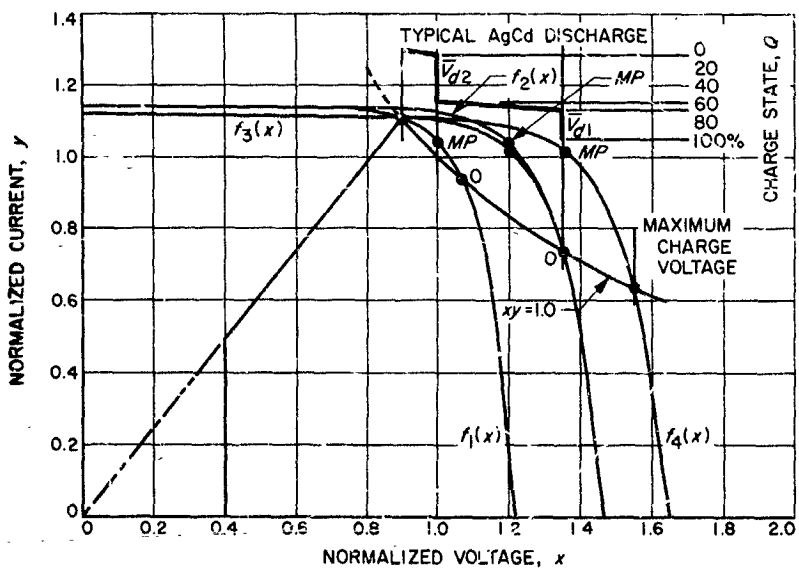


Figure B-20. Array and Load Characteristics in Relation to Battery Discharge

and

n = a numeric defining duty-cycle by orbit--the number of orbits with no peak load.

Operating margins are in some instances capable of providing for more than one parameter variation: Regulation-start (peak-point) voltage, battery voltage (cell failure in short-circuit mode), and solar distance (temperature-intensity effects) voltage variations are redundant. Thus the largest voltage variation will determine the overcapacity.

Operating margin for peak ripple current is simply added to the basic load.

Voltage Tolerances relating to the battery discharge circuit ON and OFF levels result in increased array capacity (μ_{m4}) but are partly offset by the overcapacity necessitated by one of the above-mentioned voltage variations.

Degradation overcapacity is arbitrary in value, but is given by the product of the voltage and current array capacities.

c. Margin Calculations

Three kinds of array overcapacity (capacity beyond the direct Sunlight load) may be defined:

1) Battery recharge overcapacity -- μ_r,
2) Operating Margin overcapacity -- μ_m,
3) Degradation overcapacity -- μ_d.

Recharge overcapacity--once calculated--becomes a portion of the load and is so treated. Thereafter operating margin and degradation overcapacity become factors of the total array power required, thus:

$$\overline{P}a = (1+\mu d)\ (1+\mu m)\ (1+\mu r) \qquad (1)$$

The three overcapacities are discussed in some detail below.

(1) Battery Recharge Overcapacity - μ_r. Battery recharge overcapacity, μ_r, is a function of the recharge efficiency, peak and eclipse load energy, and orbital parameters. A general form of the recharge function is given by equation (2) below on the basis of the power profile of Figure B-15, Reference 9:

$$\mu_r = \frac{(n+1)\ \alpha \bar{P}e + \phi\ (\bar{P}p-1)}{h\ (n+1)\ (1-\alpha) + \phi\ (1-h)} \tag{2}$$

Where α, Pe, Pp, h are as defined in Reference 9 and n is the number of cycles during which the peak load is off (i.e., science off).

Several particular cases are of interest:

1) No duty-cycling by orbit:

$$(\mu r) = \frac{\alpha \bar{P}e + \phi\ (\bar{P}_p - 1)}{h\ (1-\alpha) + \phi\ (1-h)}, \quad n = D \tag{3}$$

2) As in 1) above and no peak load:

$$(\mu r) = \frac{\alpha\ \bar{P}_e}{h\ (1 - \alpha)}, \quad \phi = 0 \tag{4}$$

3) As in 1) above and no eclipse orbits:

$$(\mu r) = \frac{\phi\ (\bar{P}_p - 1)}{h + \phi\ (1 - h)}, \quad \alpha = 0 \tag{5}$$

4) Peak load ON during whole sunlit period: This case reduces to case 2) above except that the reference level P_1 changes to P_p (that is, P_p for values of $\phi < 1 - \alpha$).

Figure B-12 shows the array overcapacity as a function of the peak load duration for two electrochemical systems and for two orbital periods. Figure B-12 assumes that the peak load (science) is on once per orbit and is off during the eclipse period. Equation (3) was used to derive the computing functions, and $\bar{P}_e = 1.0$, $\bar{P}_p = 1.5$ is assumed for all cases:

Ag Cd System, h = 0.44

$$(\mu r) = \frac{0.02 + 0.5\ \phi}{0.43 + 0.56\ \phi}, \quad \alpha = 0.02 \tag{6}$$

$$(\mu r) = \frac{0.07 + 0.5\ \phi}{0.41 + 0.56\ \phi} \quad \alpha = 0.07 \tag{7}$$

Ag Zn System, h = 0.56

$$(\mu r) = \frac{0.02 + 0.5\ \phi}{0.55 + 0.44\ \phi}, \quad \alpha = 0.02 \tag{8}$$

$$(\mu r) = \frac{0.07 + 0.5\,\phi}{0.52 + 0.44\,\phi}, \quad \alpha = 0.07 \tag{9}$$

Figure B-13 shows the effect of duty-cycling by orbit, it is similar to Figure B-12, but assumes that the peak load is only on every other orbit. Figure B-14 also shows the effect of duty-cycling by orbit, but assumes that the peakload occurs both during sunlight and during eclipse. Thus, from Figure B-14, it can be seen that if $\alpha = 0.07$, and the peak load is off one orbit out of two (n=1), the array overcapacity is somewhat less than that required for $\alpha = 0$ (no eclipse orbits) and no duty cycling (n=0).

Computing functions similar to equations (6) through (9) were derived for the cases presented in Figure B-13 and Figure B-14.

(2) Operating Margin Overcapacity - μ_m. The overcapacity discussed here is not to be construed as a safety margin or array failure mode margin. This operating margin is required in order for the system to operate stably when no battery is on the line and to insure that the nominal array operating voltage is greater than the maximum battery discharge voltage. For the system to be as reliable as possible, the batteries must not be required except for those times when the system design calls for load sharing. Reference 4 touched on this subject and described an operating mode which obviates the requirement for a battery solely for purposes of operating stability. To emphasize this point, we repeat; if the peak-point load current is less than the minimum array output (at the corresponding voltage), then sharing is not possible and unstable operation becomes no consideration.

Regarding the battery; for compatibility it is only necessary that the minimum battery discharge voltage be greater than the peak-point voltage. Thus the input voltage range of the regulator, be it a Booster or a Series-Switching type, is much more restricted than, for instance, the Mariner 1964 design. Hypothetically it would be sufficient if the peak-point voltage, the maximum-power-point voltage, and the battery discharge voltage were coincident. Figure B-15 shows the theoretical minimum requirements. Unfortunately, transient, product variation, measurement uncertainties, and system stability and reliability requirements all combine to increase the source capability beyond this theoretical minimum. Figure B-13 of Reference 4 showed the possible intersections of the array IV characteristic with the load IV characteristic (assuming an essentially constant power load). Of all the intersections possible, only intersection A is desirable as an operating point. Thus, it is necessary to calculate the power increase required of the array for each of the appropriate variations which could result in undesired intersections.

(3) Basis for Margin Calculations. It should be noted that all of the array characteristics used herein are based on the following mathematical model:

$$Y = 1 - b_2 \left(e^{b_1 X} - 1\right) \tag{10}$$

Where

$$X = V/Voc, \qquad Y = I/I_{sc},$$

$$b_1 = 13.5, \; b_2 = 1.37 \times 10^{-6}$$

These values of b_1 and b_2 were obtained from Reference 1; a plot of Y (X) is shown in Figure B-15. To obtain the power out of the array, we multiply current and voltage to obtain:

$$P = X\,Y \tag{11}$$

Differentiating P with respect to X yields:

$$\frac{d\,P}{d\,X} = X\frac{d\,Y}{d\,X} + Y \tag{12}$$

and differentiating equation (10):

$$\frac{d\,Y}{d\,X} = -b_1\,b_2\,\epsilon^{b_1 X} \tag{13}$$

Substituting equations (10) and (13) into equation (12) and allowing $\frac{d\,P}{d\,X}$ to vanish gives:

$$b_2\,\epsilon^{b_1 X} = \frac{1}{1 + b_1 X} \tag{14}$$

The solution to the transcendental equation (14) was obtained graphically by obtaining the intersection of $F_1(q)$ with $F_2(q)$; where $q = b_1 X$,

$$F_1(q) = b_2\,\epsilon^{q}, \text{ and } F_2(q) = \frac{1}{1+q}$$

From Figure B-16 we have that $X_{mp} = 0.816$,

$$Y_{mp} = 0.917, \text{ and } P_{mp} = 0.816 \times 0.917 = 0.748$$

To further simplify calculation, the array characteristics were normalized again with respect to P = 1 (unity power instead of unity I_{sc}, V_{oc}). The new coordinates x, y are given as:

$$x = \frac{x}{X} = 1.224\ X,$$

$$y = \frac{Y}{Y_{mp}} = 1.089\ Y,$$

$$p = 1.336\ P$$

and

$$y = f_0(x) = 1.09\ (1 - 1.37 \times 10^{-6}\ \epsilon^{11x}) \tag{15}$$

(4) Peak-Point Voltage Uncertainty. Figure B-17 shows the way in which array current capacity must be increased to accommodate a possible decrease in the "regulation-start," or peak-point, voltage of a pulse-width-modulated regulator.

From the figure shown:

$$y_1 = f_1(x) = \left.\frac{f_1(x)}{f_0(x)}\right|_{x_A} f_0(x) \tag{16}$$

From equation (15) we see that the maximum power occurs at the same value of voltage, x, for both $f_1(x)$ and $f_0(x)$. If we let x_{mp} be the voltage at the maximum power point of the array, and let μ_{m1} be the excess array capacity required, then:

$$\mu m_1 = \frac{P_{mp\ 1}}{P_{mp\ 2}} - 1 = \frac{x_{mp} \cdot f_1(x_{mp})}{x_{mp} \cdot f_0(x_{mp})} - 1 \tag{17}$$

but $\dfrac{f_1(x)}{f_0(x)} = \left.\dfrac{y_1}{y}\right|_{x_A}$ from equation (15). (18)

Substituting equation (17) into (16) yields:

$$\mu m_1 = \left.\frac{y_1}{y_0}\right|_{x_A} - 1 = \left.\frac{P_{mp/x}}{f_o(x)}\right|_{x_A} - 1 \tag{19}$$

Now let

$$\delta_v = 1 - X_A = \text{Uncertainty in peak-point voltage,} \tag{20}$$

and

$$\mu m_1 = \frac{1}{(1 - \delta_v) f_0 (1 - \delta_v)} - 1 \qquad (21)$$

Given $f_o(x)$, μ_{m1} can be calculated and plotted as a function of δ_v. Figure B-18 shows μ_{m1} as a function of δ_v, assuming the model for the array described above in Paragraph 2.c.(1). Referring to Figure B-17 again, it is also evident that if the array current is increased to satisfy the requirement of peak-point voltage variations, the array must also provide a slight voltage increase at B, the operating point. This voltage increase due to current increase, δ_{xy} is plotted in Figure B-19a as a function of the peak-point uncertainty, δ_v. Figure B-19b is the graphical solution for δ_{xy}.

(5) Battery/Array Voltage Compatibility. The requirement that the battery with one or more cells shorted, must remain compatible with the system, and the requirement that the system be stable with respect to peak-point voltage uncertainty, result in the same constraint on the array. Essentially this constraint is an increase in the value of δ_v. Whichever of the two variations above is the greater, will govern the increase in array size. Thus the minimum battery discharge voltage, with one or more cells shorted, is selected to be equal to the minimum value of the "regulation-start" voltage.

Many battery-array relative voltage combinations are possible. Of these, three combinations are considered:

1) As shown in Figure B-20, IV characteristic $f_3(x)$. This situation necessitates the use of an active sensing and discharge circuit in order to fully utilize the array and the battery. For instance, if an SCR discharge path is provided (as shown in Figure B-21) and if the trigger level used to turn on the SCR is the maximum power point voltage, then as the load increases, the bus voltage drops from $\overline{V}_o$ to $\overline{V}_{mp}$, the SCR turns on, and the bus voltage rises to the first discharge plateau ($\overline{V}_{dl}$) of the battery.

   As the load subsequently decreases, the battery voltage remains at $\overline{V}_{dl}$ or at some value less than $\overline{V}_{dl}$, but the array voltage tends to return to V_o. Then the current through the SCR goes to zero, thus turning the SCR off and resetting the circuit for the next peak load or load transient. This arrangement also limits the input voltage design range required of the regulator to approximately 1.5:1.

2) The array may be designed as shown in Figure B-20, IV characteristic $f_4(X)$. An advantage of this scheme is that an active discharge circuit

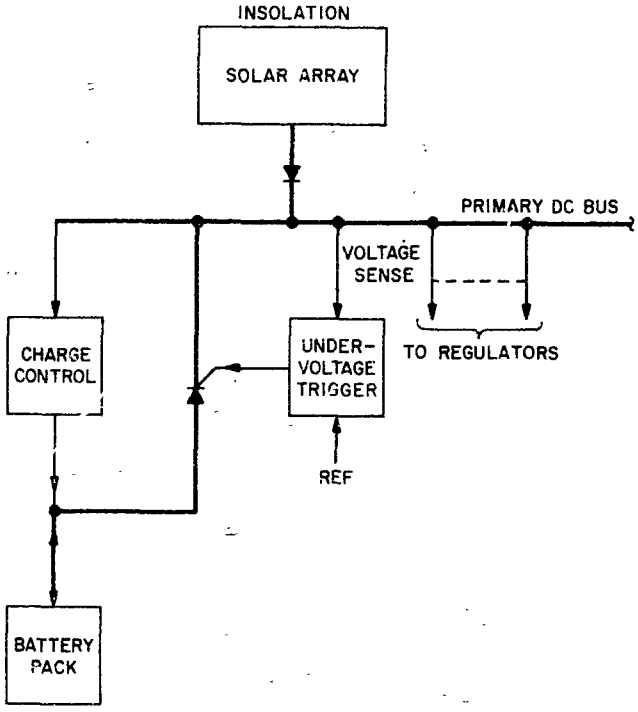


Figure B-21. Discharge Circuit (Undervoltage) Implementation

is not required--a simple rectifier will connect the battery to the bus. However, two penalties are incurred:

a) The array weight and size increase by approximately 33 percent.

b) The input voltage range is increased to approximately 1.75:1.

Because of the penalties this system will not be considered further.

3) If it is feasible, in terms of capacity, to utilize only the second discharge plateau of Paragraph (5) 1) above, then the input voltage range during the orbital phase of the mission is narrowed to approximately 1.2:1. The obvious penalty for this is a possible increase in battery weight. Not so obviously, the system weight decreases for the following reasons:

a) The array size necessary to provide load current at the second discharge plateau is lower by approximately 15 percent (assuming that the reversible potential for the first discharge plateau is 1.35 volts/cell and for the second plateau is 1.15 volts/cell).

b) The battery watt-hour efficiency is higher for the first charge plateau, corresponding to the second discharge plateau, increasing the recharge efficiency from $h = 0.44$ to $h = 0.52$. This increase in recharge efficiency decreases the overcapacity of the array (μ_r) in the following way: For example, for a power profile which consists of a constant load, the overcapacity required for recharge is changed by an amount; $\Delta\mu/\mu$. in this simple, illustrative case,

$$\Delta\mu/\mu = -\Delta h/h = -0.08/0.44 = -0.18.$$

c) The weight of the charge control equipment also decreases by the same amount; $\Delta\mu/\mu$.

If the system described in (5) 3) above is utilized, then the following sequence of events occur:

d) The spacecraft (s/c) is launched with the SCR turned on and

$$V_b \begin{matrix} < 1.35 \\ > 1.00 \end{matrix} \text{ volts/cell.}$$

e) During launch sequence the battery discharges to the minimum,

$$V_b = 1.00 \text{ volts/cell.}$$

f) When the sun is acquired the solar array (s/a) voltage increases so that the voltage difference across the SCR decreases (in the

forward direction) and the forward current through the SCR tends to zero. When the forward current drops below the holding current, the SCR automatically recovers its forward blocking characteristics and resets (turns off).

g) During cruise between Earth and Mars, the s/a provides all of the s/c power. the s/a will also provide battery recharge power. The battery will be recharged to approximately 1.55 volts/cell.

h) Subsequent trajectory correction and/or orbit injection maneuvers will cause the system to follow the same sequence (d), e), f), g)).

i) After the injection maneuver, the first planetary orbit is used solely for battery recharge.

j) During a "normal" orbit, the battery is sized so that battery energy, for the peak load and for eclipse load discharge, is returned to the battery at approximately 1.35 volts/cell during the sunlight period (less the peak load period). This cycle repeats for the life of the spacecraft.

(6) Solar Distance Variations. Another possible constraint on the array is given by the Earth-space output voltage decrease. The array voltage decrease is caused by the increased array temperature. However, this is somewhat offset by the high illumination intensity (relative to Mars-space). Figures B-18 and B-22 may be used to calculate the array overcapacity required as a function of the expected open-circuit voltage difference between Earth and Mars-space.

If the ratio of open-circuit voltage at Earth to open-circuit voltage at Mars, $(V_E/V_M)_{oc} = 0.75$, then the regulator must operate to a lower voltage limit than that assumed previously (0.9). The new lower voltage limit is 0.86 (Linear interpolation of Figure B-22). The voltage difference between the original limit and the new limit (0.04) thus causes another increase in array size. Entering Figure B-18 with $\delta_v = 1 - 0.86 = 0.14$, we have that $\mu_{m3} = 0.085$, compared with the value $\mu_{m1} = 0.048$ for $\delta_v = 0.10$. The increase in capacity, caused by the additional 0.04 voltage variation, is $\Delta\mu m/\mu_{m1} = 0.037$. The regulator input voltage range must increase to approximately 1.57:1 to operate within its range at Earth-space. On the other hand, if the array temperature gradient between Earth and Mars-space is of the same order as that given in Reference 2, then the open-circuit voltage ratio is 0.83 and no additional array voltage or increased regulator input range is required.

Because operation at Earth is on the voltage side of the IV characteristic, an increase in array voltage could provide automatic SCR reset. The increase in voltage must be sufficiently great so that array voltage, after resumption of the average sunlight load (peak loads off) will return to a value greater than the maximum second discharge plateau voltage. In the case of a Ag Cd battery this is taken to be 1.05 volts/cell. At this battery voltage the load

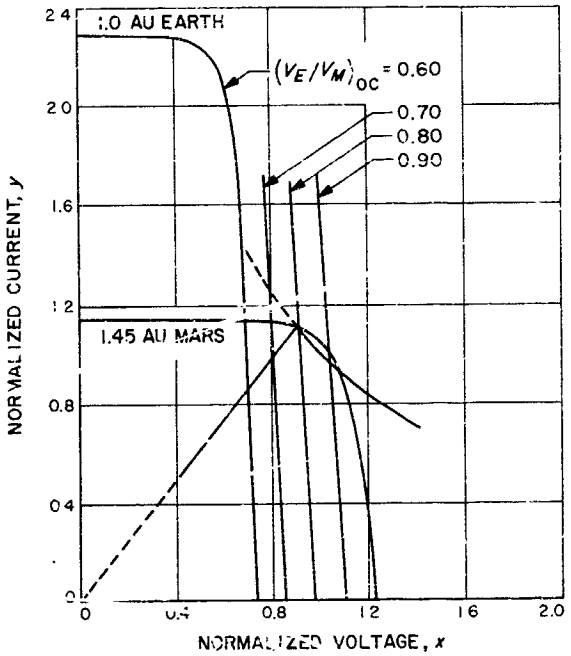


Figure B-22. SCR Turn-On Circuit

current is $y = 1/1.05 = 0.953$, and at this load current the array voltage in Earth-space is $x = 0.96$. The increase in array voltage, and therefore power, is: $\mu_{m3} = 1.05/0.96 - 1 = 0.092$. This voltage margin will insure that the SCR discharge circuit will reset automatically both in Earth and Mars space. The 9.2 percent penalty is, however, not acceptable. To circumvent this overcapacity requirement, a ground initiated command may be used to reset the SCR. Such a command would also provide operational margin (or redundancy) in Mars-space in terms of SCR or undervoltage trigger circuit failure.

(7) Ripple Consideration. The ripple current caused by the gating action of a pulse-width-modulated regulator is generally minimized by means of a regulator input low-pass filter. However, a small fraction of ripple current is demanded from the array. The simplest way in which to account for the ripple current is to consider the peak ripple current as part of the load. Because ripple currents occur both in the regulator and in the charge control, the calculation for array overcapacity should proceed as follows:

$$\overline{P}_a = 1 + \frac{I_p}{I_{dc}} (1 + \mu_r) \qquad (22)$$

where I_p = peak ripple current, and

I_{dc} = average regulator current.

(8) Undervoltage Circuit Tolerance. Assuming that an active discharge circuit is used, an allowance must be made for variations and hysteresis in turn-on and turn-off voltages. Simple SCR turn-on may be accomplished by the circuit shown in Figure B-23. From Figures B-17 and B-19 we see that δ_{xy} would serve as the undervoltage tolerance, provided δ_v is sufficiently large. In the particular instance illustrated, $\delta_v = 0.10$, $\delta_{xy} = 0.085$. Thus δ_t is accounted for, and no additional capacity is required. If δ_v or δ_t were such that $\delta_{xy} < \delta_t$, then the curves of Figure B-34 may be used to calculate the additional array capacity, μm_4, imposed by δ_t (Replace abcissa δ_x by δ_t and ordinate μm_2 by μm_4). Thus if δ_v and δ_t were 10 percent, enter Figure B-34 at 0.10 on the abcissa to the intercept with the $\delta_v = 0.10$ line, yielding $\mu m_4 = 0.0075$ (0.75 percent).

Generally, δ_t is relatively small so that little or no additional array capacity is required.

(9) Degradation Margin - μ_d. Aside from the normal degradation, random failure, and measurement uncertainties which are taken care of in the detail array design, integrated electron flux and proton damage due to solar flares must be considered. Because no environmental data is available, an arbitrary degradation of array current of 6 percent, and

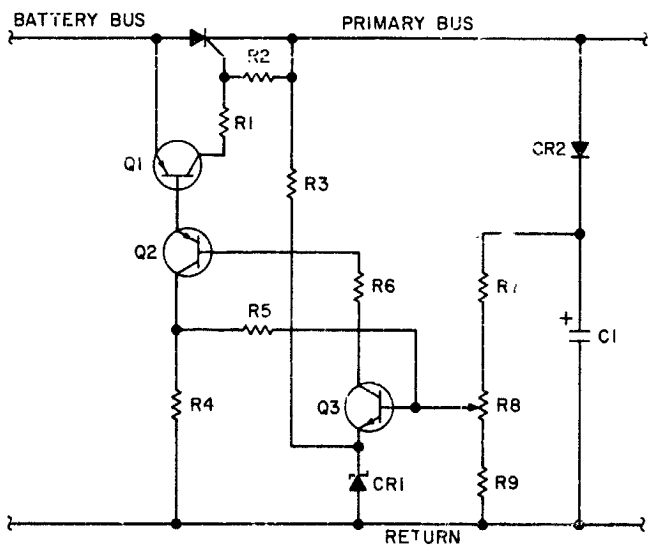


Figure B-23. Undervoltage Trigger Circuit

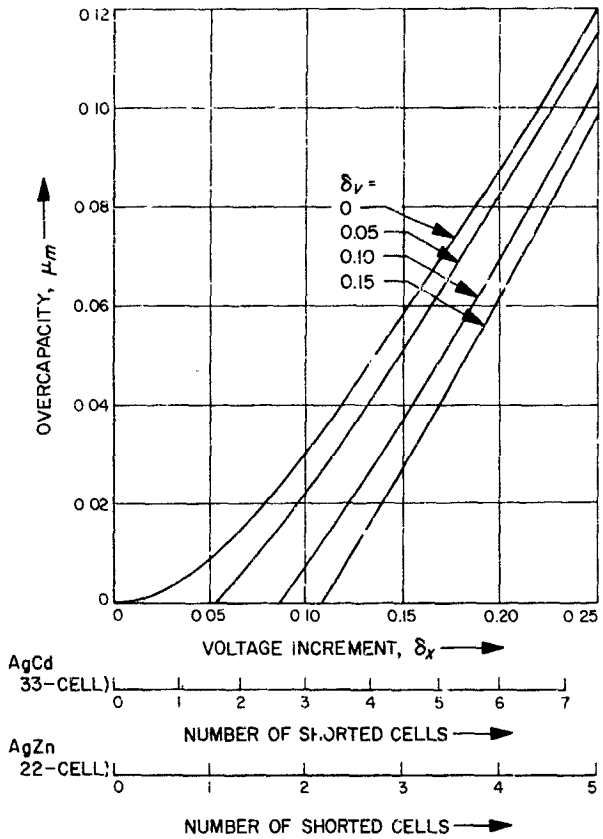


Figure B-24. Array Overcapacity Required as a Result of Battery Discharge Voltage Range or Undervoltage Trigger Level Range

voltage of 5 percent have been assumed. These assumed values correspond approximately to an electron dose of 10^{14}, Reference 1, and result in a degradation overcapacity of,

$$\mu_d = (1.06)\,(1.05) - 1 = 0.113$$

(10) Margin Requirements Summary. Let P_L be the load power required at any step in the array size calculation, and let $\overline{P}_L = P_L/P_1$: Table 1 below summarizes the calculation.

An example of the calculation is given below using typical values of the variations:

Step 1. Ripple current, Ip = 0.050 I_{dc}, peak; $I_p/Idc = 0.050$

Step 2. Peak-point voltage, $\Delta Vpp = 1.0$ volts; $\delta_v = 0.030$

(33 cell, Ag Cd system)

or Cell Failure, three cell failures allowed: $\delta_v = 0.10$

or Solar Distance, $\Delta T = 65°C$, -2.2 mv/°C,

$V_{oc} = 590$ mv;

Table B-4. Margin Calculation Requirements Summary

Overcapacity	Cumulative Power Level	Reference Paragraph
A) Battery Recharger (μ_r)	$\overline{P}_L = 1 + \mu_r$	2.c.(1)
B) Operating Margin		2.c.(2)
1. Ripple Current (I_p/I_{dc})	$\overline{P}_{L_1} = (1+ I_p)\ \overline{P}_L$	2.c.(7)
2. Peak-Point Voltage (μ_m) (1)	$\overline{P}_{L_2} = (1+ \mu_{m1})\ \overline{P}_{L_1}$	2.c.(4)
3. or Cell Failure (μ_{m2}) (1)	$\overline{P}_{L_2} = (1+ \mu_{m2})\ \overline{P}_{L1}$	2.c.(5)
or Solar Distance (μ_{m3}) (1)	$\overline{P}_{L_2} = (1+ \mu_{m3})\ \overline{P}_{L_1}$	2.c.(6)
3. Undervoltage Tolerance (μ_{m4})	$\overline{P}_{L_3} = (1+ \mu_{m4})\ \overline{P}_{L_2}$	2.c.(8)
C) Degradation (μ_d)	$\overline{P}_{L_4} = (1+ \mu d)\ \overline{P}_{L3}$	2.c.(9)
(1) The selection of μ_m to use in step (B2) depends on which of the three variations δ_v, δ_b, or δ_t is largest.		

From Figure B-22:

$$(V_E/V_M)_{oc} = 0.83 \text{ and thus } \delta_v = 0.050$$

Thus for the assumed values, the three-cell failures (shorts) allowed govern the overcapacity:

$$\delta_v = 0.10 \text{ yields } \mu_{m2} = 0.048$$

Step 3 U/V Tolerance, Trigger voltage tolerance ±2 percent, and hysteresis 10 percent gives $\delta_t = 0.140$

but from $\delta_v = 0.10$ and Figure B-19, $\delta_{xy} = 0.084$

Thus $\delta_t > \delta_{xy}$ and using Figure B-23, we obtain $\mu_r = .008$

Step 4. Calculation of the total array capacity required proceeds as outlined in Table B-4 above:

$$\bar{P}_{L1} = 1.05\,\bar{P}_{L_0}, \qquad \text{where } \bar{P}_{L_0} = (1 + \mu_r)$$

$$\bar{P}_{L2} = 1.048 \times 1.05\,\bar{P}_{L_0} = 1.100\,\bar{P}_{L_0}$$

$$\bar{P}_{L3} = 1.008\,\bar{P}_{L2} = 1.109\,\bar{P}_{L_0}$$

$$\bar{P}_{L4} = (1.113)(1.109\,\bar{P}_{L_0}) = 1.234\,\bar{P}_{L_0}$$

and finally:

$$\bar{P}_a = \bar{P}_{L4} = 1.234\,(1 + \mu_r) \tag{23}$$

REFERENCES

1. Spacecraft Electric Power Systems Sizing and Analysis Computations - TRW/STL 8584--6001-RU000
2. Mariner C Solar Panel IV and PV Curves - IOM Goldsmith to Dawson, 8/[illegible]/64
3. Analog Computer Analysis of the Voltage Booster Regulator - G & C Technical Memorandum No. 343-43
4. Preliminary Design Considerations for Spacecraft Regulators - IOM Wilner to Fredrickson Fredrickson, 8/5/64
5. Mariner 1969 Technical Feasibility Study - IOM Ivanoff to Sweetnam, [illegible], 64
6. The Silver Oxide-Cadmium Secondary Battery - AIEE Conference Paper No. CP61-346 - P. L. Howard
7. Electrochemical Cells for Space Power - AFS Conference Paper [illegible]165-61 - R. C. Shair
8. The Sealed Silver-Cadmium Battery - Electrochemical Technology, Vol. I, No. 9 - 10, 1963 - P. L. Howard
9. Preliminary System Sizing Analysis - Revised 9/17/64 IOM Wilner to Fredrickson.